

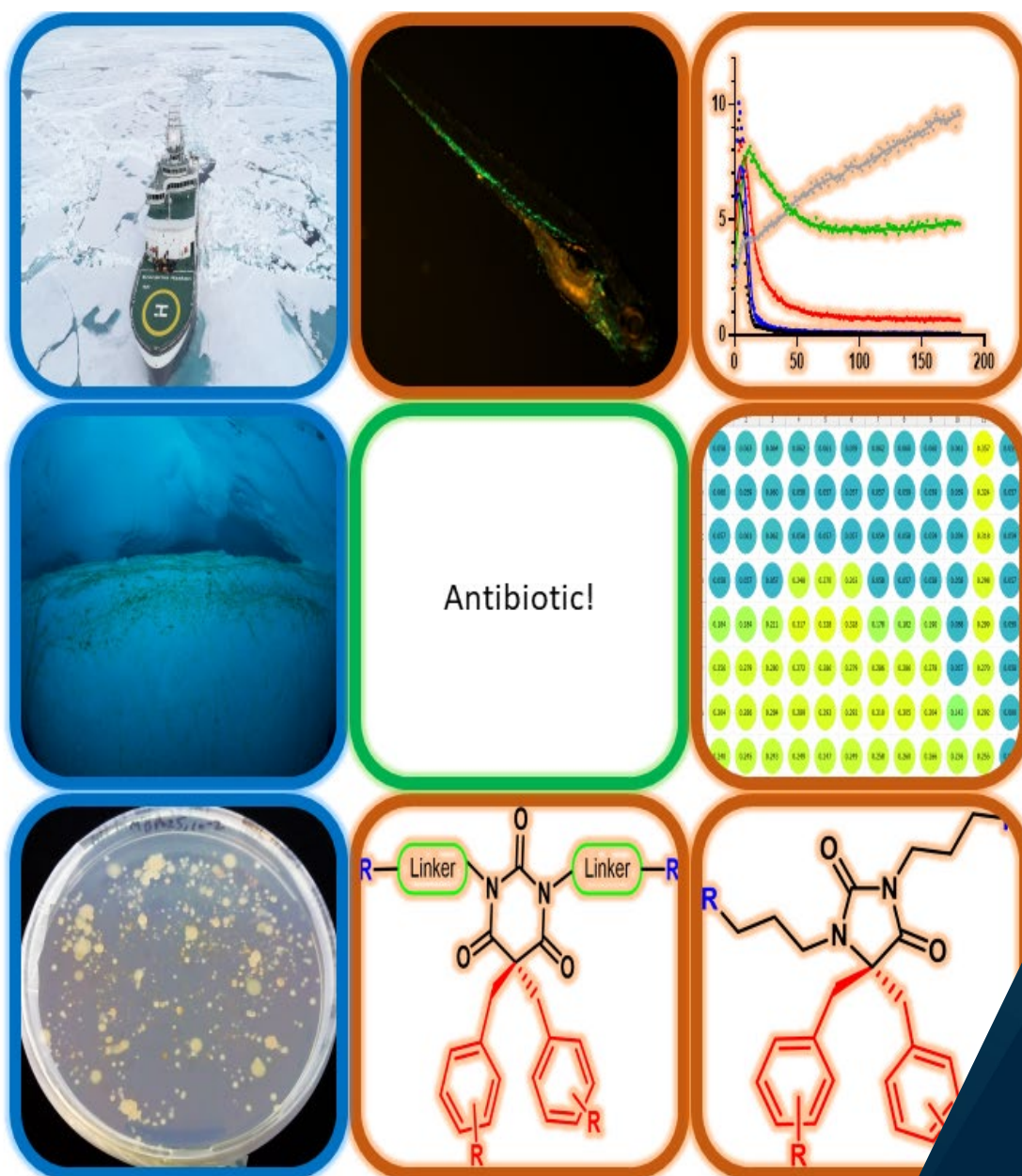
Faculty of Biosciences, Fisheries and Economics
Norwegian College of Fishery Science

Bioactivity profiling and mode of action studies of antibacterial and antibiofilm agents of marine origin

Ataur Rahman

A dissertation for the degree of Philosophiae Doctor

January 2024



A dissertation for the degree of Philosophiae Doctor

**Bioactivity profiling and mode of action studies of antibacterial and
antibiofilm agents of marine origin**

Ataur Rahman



November 2023

The work for this thesis was carried out from May 2019 to November 2023 at the Marine Bioprospecting research group, Norwegian College of Fishery Science, Faculty of Biosciences, Fisheries and Economics, UiT The Arctic University of Norway. The work was part of the AntifoMar project funded by UiT The Arctic University of Norway.

Table of Contents

ACKNOWLEDGMENTS	I
ABSTRACT	II
LIST OF PAPERS.....	IV
ABBREVIATIONS.....	VI
1 INTRODUCTION.....	1
1.1 THE CHALLENGES	1
1.1.1 <i>Infectious diseases</i>	1
1.1.2 <i>Antimicrobial resistance</i>	1
1.1.3 <i>Bacterial biofilm</i>	2
1.1.4 <i>Antibacterial discovery void</i>	3
1.2 SOLUTIONS	4
1.2.1 <i>Marine environment as a source of natural products (NPs)</i>	5
1.2.2 <i>Marine bacteria as a source of NPs</i>	6
1.2.3 <i>Eusynstyelamides, a novel scaffold from marine invertebrates</i>	9
1.2.4 <i>Synthetic mimics of antimicrobial peptides (SMAMPs)</i>	11
1.2.5 <i>AntifoMar</i>	13
2 RESEARCH OBJECTIVES	15
3 RESEARCH DESIGN	16
4 SUMMARY OF THE MAIN RESULTS	18
4.1 PAPER I.....	18
4.2 PAPER II.....	19
4.3 PAPER III	20
4.4 PAPER IV	21
5 GENERAL DISCUSSION.....	22
5.1 PIPELINE AND CHALLENGES ASSOCIATED WITH THE ANTIFOMAR PROJECT	22
5.2 SOURCE OF NOVEL ANTIBACTERIAL COMPOUNDS	23
5.2.1 <i>Synthetic mimics of antimicrobial peptides (SMAMPs)</i>	24
5.2.2 <i>Marine bacterial secondary metabolites (MBSMs)</i>	25
5.3 <i>IN VITRO</i> ACTIVITY ASSESSMENTS.....	26
5.3.1 <i>Barbituric acid derivatives – a potential scaffold</i>	26
5.3.2 <i>Hydantoin derivatives – another potential scaffold</i>	27
5.3.3 <i>Antibiofilm activity of barbiturate and hydantoin derivatives</i>	28
5.3.4 <i>Potential BGCs from marine bacterial isolates</i>	29
5.4 <i>IN VIVO</i> ACTIVITY ASSESSMENTS	29
5.5 POTENTIAL OUTCOMES OF THIS ANTIFOMAR PROJECT	30
6 FUTURE PERSPECTIVE.....	32
7 CONCLUSIONS.....	34
8 REFERENCES.....	35

PAPER I, II, III and IV

Acknowledgments

I stand on the cliff of a monumental personal and professional milestone, completing a journey that has been as challenging as it has been rewarding, fulfilling my doctoral studies. It is a journey I have not walked alone; its chapters are infused with the wisdom, support, and encouragement of numerous individuals to whom I owe immense gratitude. With a deep sense of appreciation, I take this opportunity to acknowledge those whose contributions have been instrumental in pursuing and attaining my PhD.

First and foremost, I extend my heartfelt thanks to my principal supervisor, Prof. Klara Stensvåg, whose expertise and insight have been my guiding light throughout this process. Her patience and unwavering belief in my capabilities have strengthened and inspired me. The intellectual rigour she demanded of me and the generosity with which she shared her profound knowledge have shaped this thesis and my entire approach to scientific inquiry. Her mentorship extends beyond academic guidance; it has been a personal growth experience for which I am profoundly grateful.

I am equally thankful to my co-supervisors, Professor Johanna U Ericson, Professor Morten B. Strøm, Professor Annette Bayer, Associate Professor Hans-Matti Blencke, Associate Professor Gabriel Magno de Freitas Almeida and Dr. Ekaterina Mishchenko, for their wise critiques and valuable suggestions that have greatly enhanced the quality of my research. Their perspectives and association with CANS, Centre for New Antibacterial Strategies, have added a valuable layer of depth to my work.

My sincere appreciation goes to the faculty and staff of the UiT The Arctic University of Norway. Each interaction has added a stone to the edifice of my learning. I would like to acknowledge my colleagues, especially Manuel Karl Langer, Andrea Iselin Elvheim, Christoffer Sivertsen, Hymonti Dey, and Jonathan Hira, for their companionship and for the thought-provoking discussions that have often led to significant breakthroughs in my research. Collaborating with them has been both a pleasure and an enriching experience.

I am grateful to the engineers (Ida Kristine Østnes Hansen, Hege Devold, Frode Jacobsen Øyen) and administrative and technical staff whose support has allowed me to focus on my research without distraction. Their contributions, often behind the scenes, have been invaluable.

This thesis would not have been possible without my family's constant support and patience. To my wife, Wasifa Kabir, I owe a special debt of gratitude. Her understanding, love, and encouragement, even when sacrifices were required, have been a source of personal peace and confidence. Her ability to endure the ups and downs alongside me has been nothing short of extraordinary. To my son, Rihanur Rahman, a bundle of joy and boundless energy, who has brought laughter and light into my toughest days - his hugs have been my haven.

Parents (my and my wife's) and siblings deserve special mention for their unwavering faith and prayers. They instilled in me the value of perseverance and hard work, which have been my companions on this academic voyage.

Finally, I would like to thank UiT The Arctic University of Norway, for the financial assistance and belief in the importance of my research.

Each of you mentioned here, many not named but remembered, have my deepest gratitude. This thesis stands as a testament to your collective support and belief in my potential. Thank you.

Ataur Rahman

Abstract

The emergence of drug-resistant strains and new pathogens intensifies the need for new antimicrobials. Additionally, bacterial biofilms, which contribute to persistent infections, further complicate treatment efforts. The increasing difficulty in discovering and developing new antimicrobials adds to this challenge. However, marine environments, with their vast biodiversity, offer a promising avenue for antibiotic discovery, particularly through natural products synthesized by marine microorganisms. These organisms are a rich source of novel bioactive secondary metabolites with potential therapeutic applications. Additionally, synthetic mimics of antimicrobial peptides represent another promising direction in the quest for new antimicrobials.

Paper I elucidate the structure-activity relationship of cationic amphipathic N,N'-dialkylated-5,5-disubstituted barbiturates as marine eusynstyelamide mimics, investigating their potential as antimicrobial agents. The library of 58 compounds, synthesized through a strategic approach, demonstrated the significance of cationic groups, hydrocarbon linkers, and lipophilic side chains on antimicrobial and haemolytic activities. Notably, guanidyl and amine groups showed broad-spectrum activity, while trimethylated quaternary amines were more selective for Gram-positive bacteria. The compounds, especially 11IG, 13jA, and 13jG, showed potent antimicrobial effects with low haemolytic activity, with the guanidine derivative 11IG significantly disrupting bacterial membranes.

In **paper II**, the investigation into tetrasubstituted, cationic, amphipathic heterocycles as antimicrobial peptide (AMP) mimics identified hydantoin as a favourable scaffold, influencing haemolytic activity and antimicrobial potency. Among the hydantoin derivatives studied, three leads (2dA, 6cG, and 6dG) exhibited promising broad-spectrum activity, with 6dG showing notably low minimum inhibitory concentration values. The mode of action studies revealed a pronounced membranolytic effect on the inner and outer bacterial membranes, emphasizing the importance of structural arrangement in AMP mimics.

In **paper III**, the antibiofilm capabilities and *in vivo* efficacy of these peptidomimetics were explored using a zebrafish model, discovering that 13iA and 2cA presented remarkable biofilm inhibition and eradication potentials, along with moderate activity against resistant clinical isolates. Their lack of toxicity, immunogenicity, and promising *in vivo* antibacterial activity in the zebrafish model up to 16 mg/kg dose showcases their potential as templates for new antibiotics against antimicrobial resistance (AMR).

In **paper IV**, the bioprospecting work focused on Arctic marine bacterial isolates from various habitats near Tromsø and towards the North Pole indicated the presence of biosynthetic gene clusters (BGCs) with antimicrobial activity. Of the 158 isolates, 65 exhibited antibacterial activity, and 37 confirmed the presence of nonribosomal peptide synthetase (NRPS) or polyketide synthase (PKS) BGCs, with genome sequencing and mining unveiling multiple BGCs. Seven of these isolates displayed activity against both Gram-positive and Gram-negative pathogens and contained NRPS or PKS BGCs, advancing them as promising sources of novel antimicrobial agents.

These combined efforts contribute valuable insights into the design and discovery of new antimicrobials, addressing the urgent global challenge of AMR with innovative solutions derived from marine bioprospecting and synthetic peptidomimetic chemistry.

List of papers

This thesis comprises two published articles and two manuscripts, denoted by Roman numerals.

Paper I

Title: A concise SAR-analysis of antimicrobial cationic amphipathic barbiturates for an improved activity-toxicity profile.

Authors: Manuel K. Langer*, **Ataur Rahman***, Hymonti Dey, Trude Anderssen, Francesco Zilioli, Tor Haug, Hans-Matti Blencke, Klara Stensvåg, Morten B. Strøm, Annette Bayer

* The authors contributed equally to this work.

Journal: European Journal of Medicinal Chemistry, available online on 5 August 2022

Paper II

Title: Investigation of tetrasubstituted heterocycles reveals hydantoins as a promising scaffold for development of novel antimicrobials with membranolytic properties.

Authors: Manuel K. Langer, **Ataur Rahman**, Hymonti Dey, Trude Anderssen, Hans-Matti Blencke, Tor Haug, Klara Stensvåg, Morten B. Strøm, Annette Bayer

Journal: European Journal of Medicinal Chemistry, available online on 24 January 2023

Paper III

Title: Peptidomimetic tetrasubstituted barbiturates and hydantoins: Investigation of their antibiofilm, in vivo toxicity and antimicrobial activity.

Authors: **Ataur Rahman**, Manuel Karl Langer, Bartosz Michno, Gabriela Żyłka, Jonathan Hira, Hege Devold, Ida Kristine Østnes Hansen, Ekaterina Mishchenko, Morten B. Strøm, Annette Bayer, Johanna U Ericson, Tomasz Prajsnar, Klara Stensvåg

Manuscript

Paper IV

Title: Antimicrobial potential of marine bacteria from the Arctic and sub-Arctic regions.

Authors: **Ataur Rahman***, Andrea Iselin Elvheim*, Christoffer Ågnes, Ida Kristine Østnes Hansen, Hege Devold, Frode Jacobsen Øyen, Gabriel Magno de Freitas Almeida, Hans-Matti Blencke, Bjarne Landfald, Tor Haug, Klara Stensvåg

* The authors contributed equally to this work.

Manuscript

Authors contribution

	Paper I	Paper II	Paper III	Paper IV
Concept and idea	MKL*, AR*, TH, HMB, KS, MBS, AB	MKL, AR, HMB, TH, KS, MBS, AB	AR, MKL, EM, MBS, AB, JUE, TP, KS	AR*, AIE*, CÅ, HMB, BL, TH, KS
Study design and methods	MKL*, AR*, HDY, TA, FZ, TH, HMB, KS, MBS, AB	MKL, AR, HDY, TA, HMB, TH, KS, MBS, AB	AR, MKL, EM, JUE, TP, KS	AR*, AIE*, CÅ, HMB, BL, TH, KS
Data gathering and interpretation	MKL*, AR*, HDY, TA, FZ, TH, HMB, KS, MBS, AB	MKL, AR, HDY, TA, HMB, TH, KS, MBS, AB	AR, MKL, BM, GŽ, JH, HDD, IKØH, EM, JUE, TP, KS	AR*, AIE*, CÅ, IKØH, HDD, FJØ, HMB, BL, TH, KS
Manuscript preparation	MKL*, AR*, HDY, TA, FZ, TH, HMB, KS, MBS, AB	MKL, AR, HDY, TA, HMB, TH, KS, MBS, AB	AR, MKL, BM, GŽ, JH, HDD, IKØH, EM, MBS, AB, JUE, TP, KS	AR*, AIE*, CÅ, IKØH, HDD, FJØ, GMDFA, HMB, BL, TH, KS

MKL - Manuel K. Langer, AR - Ataur Rahman, HDY - Hymonti Dey, TA - Trude Anderssen, FZ - Francesco Zilioli, TH - Tor Haug, HMB - Hans-Matti Blencke, KS - Klara Stensvåg, MBS - Morten B. Strøm, AB - Annette Bayer, BM - Bartosz Michno, GŽ - Gabriela Žyřka, JH - Jonathan Hira, HDD - Hege Devold, IKØH - Ida Kristine Østnes Hansen, EM - Ekaterina Mishchenko, JUE - Johanna U Ericson, TP - Tomasz Prajsnar, AIE - Andrea Iselin Elvheim, CÅ - Christoffer Ågnes, FJØ - Frode Jacobsen Øyen, GMDFA - Gabriel Magno de Freitas Almeida, BL - Bjarne Landfald.

Abbreviations

AMP(s)	Antimicrobial peptide(s)
AMR	Antimicrobial resistance
BGC(s)	Biosynthetic gene cluster(s)
CANS	Centre for New Antibacterial Strategies
EC ₅₀	Effective concentration to produce 50% of the maximum response
FICI	Fractional inhibitory concentration index
hpi	Hour(s) post-infection
IM	Inner membrane
IY	Intrayolk
MBSM(s)	Marine bacterial secondary metabolite(s)
MIC	Minimum inhibitory concentration
MNP(s)	Marine natural product(s)
MoA	Mode of action
NPN	1-N-phenylnaphthylamine
NP(s)	Natural product(s)
NRPS	Nonribosomal peptide synthetase
OM	Outer membrane
OSMAC	One strain many compounds
PCR	Polymerase chain reaction
PKS	Polyketide synthase
RBC	Red blood cell
RNA-seq	RNA sequencing
SAMP(s)	Synthetic antimicrobial peptide(s)
SAR	Structure-activity relationship
SI	Selectivity index
SMAMP(s)	Synthetic mimic of antimicrobial peptide(s)
TLR(s)	Toll-like receptor(s)
WHO	World Health Organization

1 Introduction

The development of new antibiotics is essential to combat the growing threat of infectious diseases and antibiotic resistance. However, traditional drug discovery approaches have faced several challenges and development of new antibiotics is slow. Natural products (NPs) discovery and synthetic biology are promising approaches to antibiotic drug development¹. This thesis focuses on identifying producers of antimicrobial secondary metabolites and their link to biosynthetic gene clusters (BGCs) from marine bacteria. Additionally, evaluation of the structure-activity relationship (SAR) of synthetic mimics of antimicrobial peptides (SMAMPs) inspired from marine natural products (MNPs).

1.1 The challenges

1.1.1 Infectious diseases

Infectious diseases remain a significant global health challenge^{2,3}, spreading rapidly due to globalization and interconnectedness, posing a serious public health concern⁴. They contribute significantly to the global burden of diseases, particularly in low-resource settings with inadequate infrastructure and poor healthcare access². The availability of healthcare can prevent disease progression and improve health outcomes. Inadequate investment in public health infrastructure and disease surveillance, particularly in resource-limited countries, hinders effective response and management of infectious diseases⁵.

The rise of drug-resistant strains and new pathogens underscores the need for effective infectious disease management⁶. Key challenges include developing diagnostic devices for the real-time detection of multiple disease markers⁷ and establishing robust surveillance systems to identify outbreaks and monitor disease spread. The irrational use of antibiotics further complicates disease control, fostering multidrug-resistant pathogens⁸. Global trade and intensive livestock systems create opportunities for the transmission of disease between species, perpetuating the emergence of infectious agents and posing an economic challenge to the global economy⁹. Globalization, overpopulation, and the movement of people and goods across borders exacerbate the spread of the disease, making containment difficult¹⁰⁻¹². The persistent threat of infectious diseases highlights the need for effective treatment and management¹³.

1.1.2 Antimicrobial resistance

Antimicrobial resistance (AMR) is a pressing global health issue¹⁴⁻¹⁶. AMR is not limited to specific countries or income levels; it is a substantial problem worldwide¹⁷. The clinical and financial burden imposed by AMR is significant and affects healthcare systems globally¹⁷. The economic impact of AMR is predicted to cost more than \$105 billion annually worldwide, with Africa being the region most affected¹⁸. AMR is a complex issue that arises when microorganisms evolve and develop resistance to drugs designed to kill them (**Figure 1**)^{19,20}. AMR spread can occur through several mechanisms, such as the acquisition of AMR genes through horizontal gene transfer or mutation of existing genes (**Figure 1**).

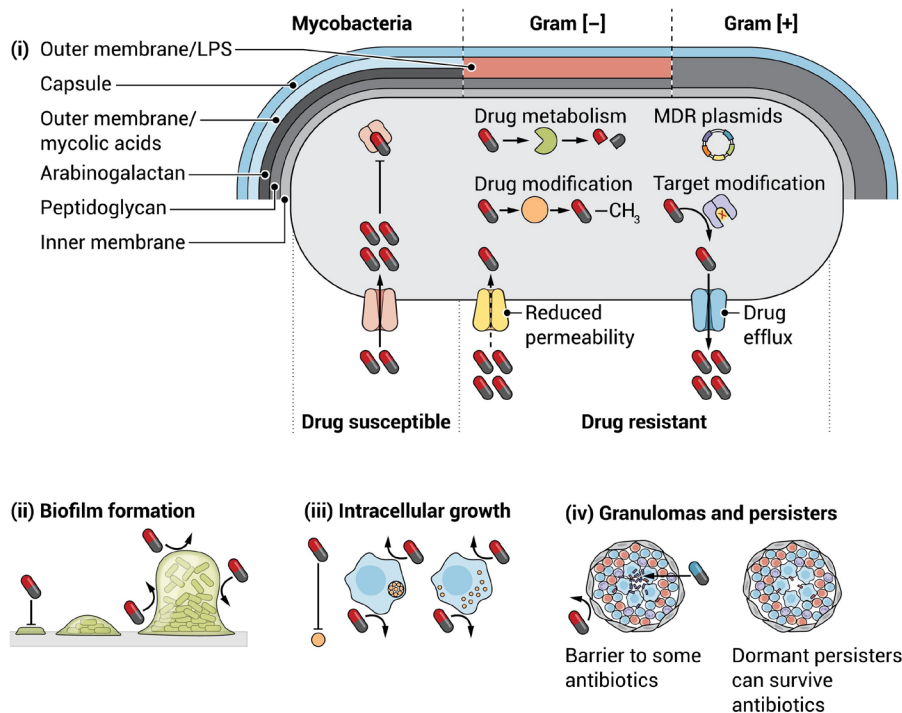


Figure 1. AMR takes many forms, from (i) the intrinsic physical barrier of the cell envelope; direct interventions by different resistance genes; modification in the physical compartmentalization of (ii) biofilms, (iii) intracellular environments, and (iv) granulomas; to persistent states of low metabolic activity. Permission from American Association for the Advancement of Science (AAAS). Based on Cook et al. (2022)¹⁹.

Society's failure to protect antibiotics, a precious resource, has contributed to the emergence of antibiotic-resistant bacteria²¹. Various factors, including the misuse and overuse of antibiotics without rational prescription or reason in human medicine, veterinary medicine, and agriculture^{22,23}, inadequate infection control practices and lack of effective surveillance systems contribute to antibiotic resistance development and spread. This issue of antibiotic resistance is further exacerbated by the lack of national guidelines for antibiotic use and the limited access to laboratory facilities for antimicrobial drug susceptibility tests²⁴⁻²⁶. The World Health Organization (WHO) has identified 12 bacteria or bacterial families that pose the greatest threat to human health and for which new antibiotics are desperately needed²⁷. These challenges highlight the urgent need to discover new antibiotics to continually combat multidrug-resistant bacterial strains.

1.1.3 Bacterial biofilm

Bacterial biofilms pose significant problems in various contexts, including healthcare settings and industrial systems. These biofilms, formed by a community of microorganisms embedded within an extracellular matrix, can cause persistent infections and make treatment challenging (**Figure 2**)^{28,29}. Biofilms are frequently associated with infections in implanted medical devices. These infections can be challenging to resolve and cause significant morbidity in patients. Additionally, bacteria that grow in biofilms are more resistant to antibiotics and host immune responses, making infections chronic and difficult to manage³⁰. The increased prevalence of drug-resistant microorganisms that form biofilms

during treatment or after surgery further complicates the challenges in combating biofilm-related infections³¹.

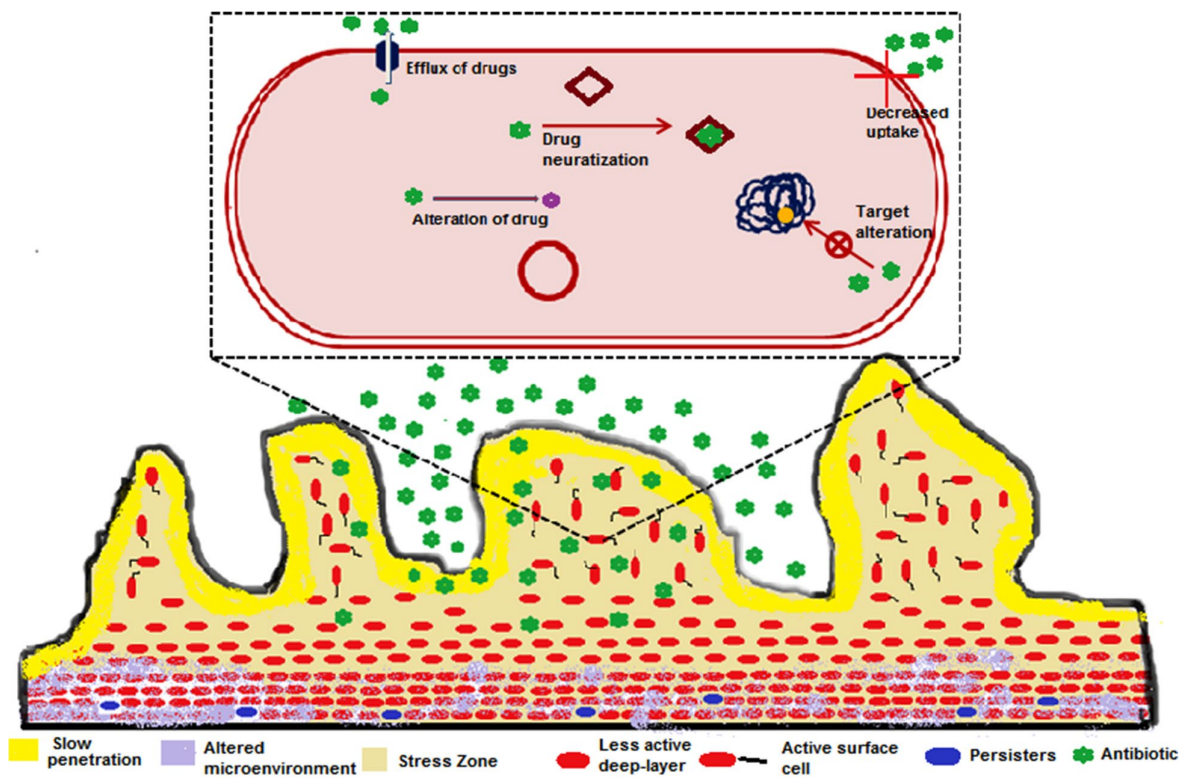


Figure 2. Biofilm and possible mechanisms of antibiotic resistance in biofilm communities; Sharma et al. (2019)³².

In addition, bacterial biofilms exhibit an increased tolerance to antibiotics compared to planktonic bacteria (Figure 1ii and Figure 2)^{32,33}. This increased tolerance is a multifactorial problem arising from the physical and genetic characteristics of biofilms (Figure 2). Extracellular polymeric substances in the biofilm matrix create a physical barrier that hinders the diffusion and penetration of antibiotics into the biofilm (Figure 2). In addition to the physical barrier, bacterial biofilms also possess inherent genetic resistance mechanisms (Figure 2). These mechanisms can include the production of enzymes that can inactivate antibiotics, alterations in the target sites of antibiotics, and up-regulation of efflux pumps that can actively pump antibiotics out from bacterial cells (Figure 1 and Figure 2)^{19,32}.

1.1.4 Antibacterial discovery void

The first antibiotic, salvarsan, was developed and used in 1910³⁴. Antibiotics gained widespread use to treat infections with the discovery of penicillin in 1928^{19,34}. The mid-20th century marked the golden age of antibiotic discovery, introducing many new classes, such as cephalosporins, tetracyclines, and aminoglycosides (Figure 3)³⁴. These antibiotics revolutionized the treatment of infectious diseases against an extensive range of bacteria¹⁹. The current void in discovery and development is a pressing issue because of increasing antimicrobial resistance. Investing in prospective research to discover new antimicrobial substances has become crucial, as many of the current therapies will no longer be effective in the future, even for common infections, if no new agents are discovered.

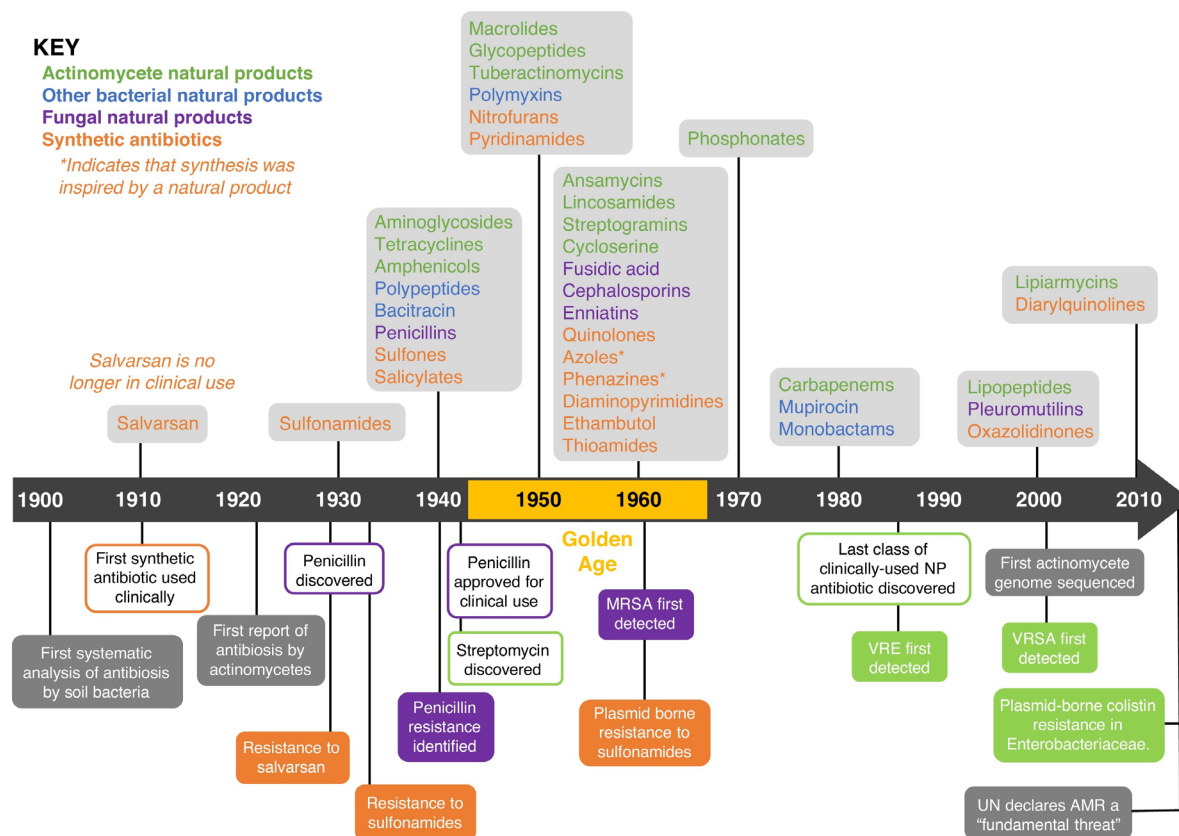


Figure 3. The timeline shows the decade in which new classes of antibiotics entered the clinic. Antibiotics are colored according to their source: green = actinomycetes, blue = other bacteria, purple = fungi, and orange = synthetic. Permission by Elsevier: Hutchings et al. (2019)³⁴.

The lack of discovery of new antimicrobials can be attributed to several factors³⁵. First, the over-reliance on existing antibiotics due to their success has led to reduced funding and research efforts for new compounds³⁵. Additionally, alternative approaches like combinatorial chemistry have not adequately enriched the drug pipeline. Large pharmaceutical companies, facing regulatory, scientific, and financial challenges, lack motivation for new antimicrobial development³⁵. The prolonged research timelines exacerbate this void, leaving the responsibility mainly to small start-ups and academic laboratories^{35,36}. The paucity of new antibiotics in the past five decades underscores the need for innovative approaches, as traditional methods produce diminishing returns³⁷.

1.2 Solutions

This gap in new antibiotics has created a pressing need for alternative approaches to antibiotic discovery. To solve the issue mentioned above, a number of non-traditional/novel/innovative sources (1.2.1, 1.2.2), structures (1.2.2, 1.2.3, 1.2.4), and discovery approaches/workflows (1.2.5) are suggested and discussed in this work.

1.2.1 Marine environment as a source of natural products (NPs)

The marine environment is one potential source to discover new antimicrobial compounds³⁸⁻⁴⁰. Exploring and exploiting vast and largely underexplored marine environments as a potential source of new antimicrobial compounds is a promising strategy. The unique conditions of the marine environment, especially the Arctic, such as high salinity, high pressure, and low temperatures, provide a habitat for organisms that have evolved unique biochemical and physiological adaptations (**Figure 4**)⁴¹⁻⁴³. These adaptations often result in the production of bioactive natural products (NPs) with potent antimicrobial properties.

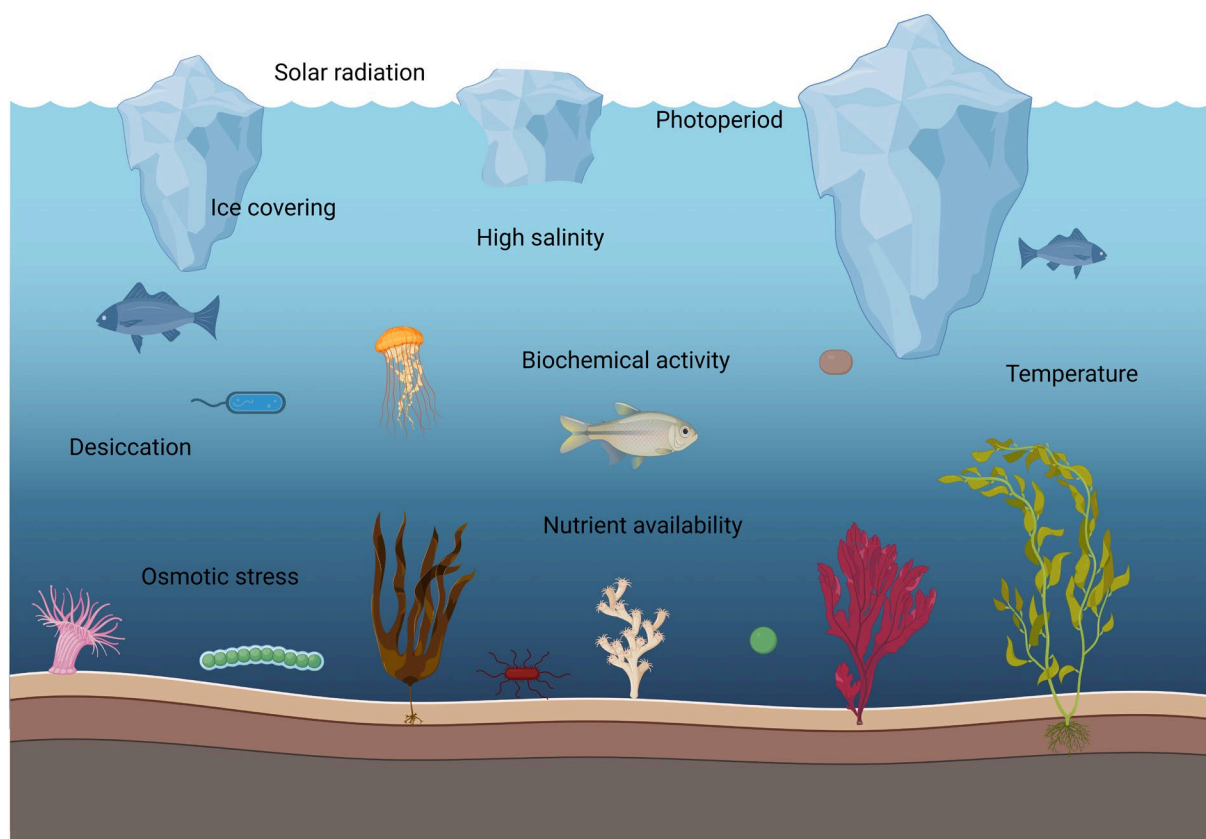


Figure 4. Illustration of stress factors in Arctic marine environments.

Marine bioprospecting, the exploration of marine organisms for bioactive compounds, offers a rich source of novel molecules for drug development, particularly antimicrobials. This approach is enhanced when combined with peptidomimetics (**Figure 5**), where natural peptide structures are mimicked and modified to improve their stability, bioavailability, and specificity. They might be candidates for LEAD compounds for further innovative development if they are found active in bioassays. Thus, the constructive integration in bioprospection leverages the vast chemical diversity of marine natural products and the versatility of peptidomimetics, allowing for the creation of novel compounds with potential therapeutic applications, including combating antimicrobial resistance. Altogether, this integrated strategy enables overcoming the limitations inherent in natural compounds and peptides, paving the way for innovative lead and drug development.

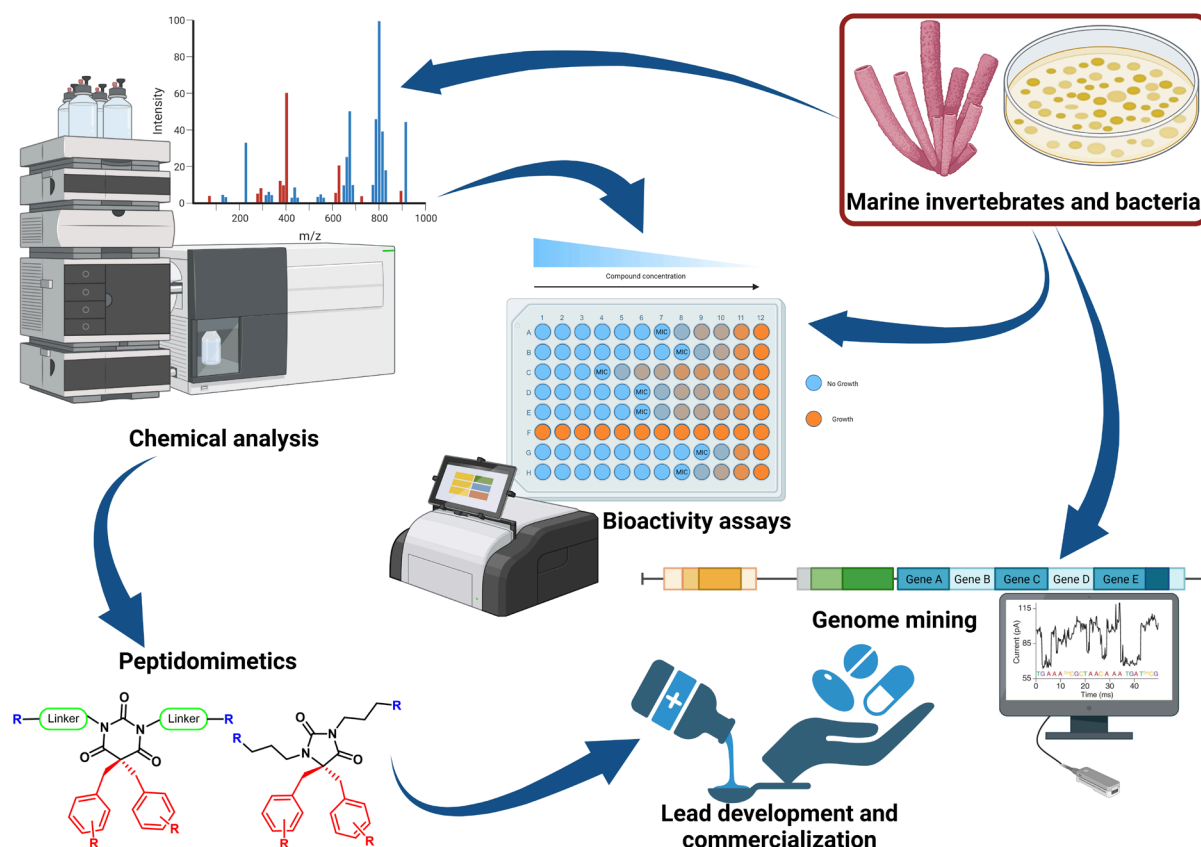


Figure 5. Marine bioprospecting approach, which can be combined with peptidomimetics for drug development.

1.2.2 Marine bacteria as a source of NPs

Most clinically relevant classes of antibiotics derived from NP are of terrestrial origin^{34,44,45} (Figure 6). However, one potential solution to find new antibiotics lies in the vast biodiversity of marine environments. Marine microorganisms have been found to be a rich source of novel bioactive secondary metabolites with potential for therapeutic applications^{38,46}.

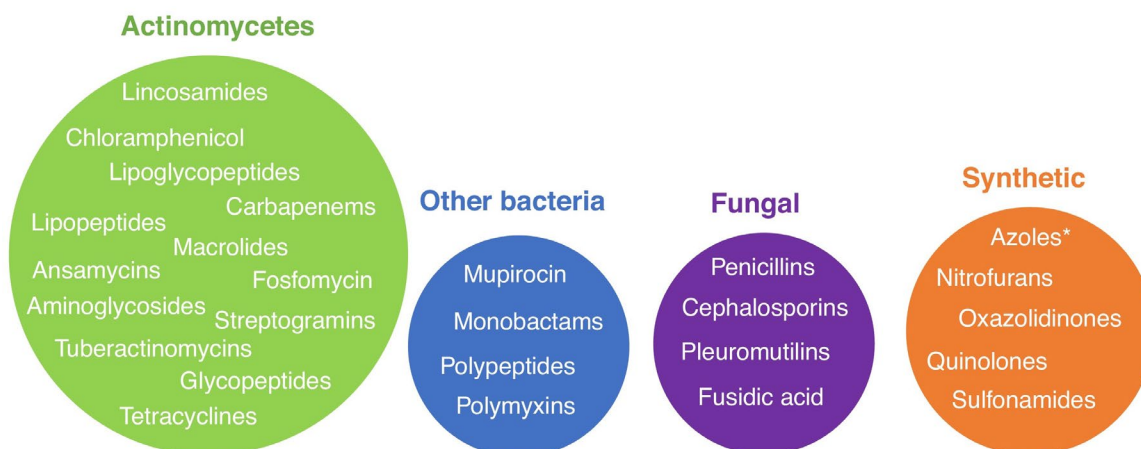


Figure 6. The most relevant class of antibiotics in clinical practice comes from natural products. Permission by Elsevier: Hutchings et al. (2019)³⁴.

The isolation and testing of microorganisms for their ability to produce antibiotically active compounds is a prospective approach⁴⁷. This innovative strategy involves exploring uncharted microbial territories and investigating their potential as sources of new antimicrobial compounds. By venturing beyond the well-known sources of antimicrobials, researchers can discover novel structures and mechanisms of actions. Using high-throughput screening and innovative screening techniques can also aid in the discovery of new antimicrobials. Advances in bioprospection technologies have allowed the collection of samples from deep sea, thermal vents, and polar regions, allowing the discovery of potential secondary metabolites with strong antibiotic activity against drug-resistant pathogens⁴¹. Furthermore, the application of advanced technologies and techniques, such as metagenomics and genome mining, can accelerate the discovery process by allowing researchers to screen large volumes of marine microorganisms and analyse their genetic potential for producing antimicrobial compounds. BGCs, encompassing polyketide synthase (PKS) and nonribosomal peptide synthetase (NRPS), and their derivatives underpin life-saving drugs for acute and chronic diseases (**Figure 7**)^{44,48}. Notable antibiotics include nonribosomal penicillin and polyketide erythromycin A⁴⁸. This prompted investigations into the machinery of these systems, seeking to understand nature's utilization of large proteins for small molecule synthesis⁴⁸. Furthermore, this knowledge aids the genetic engineering of these enzymes to create potentially valuable analogs⁴⁸.

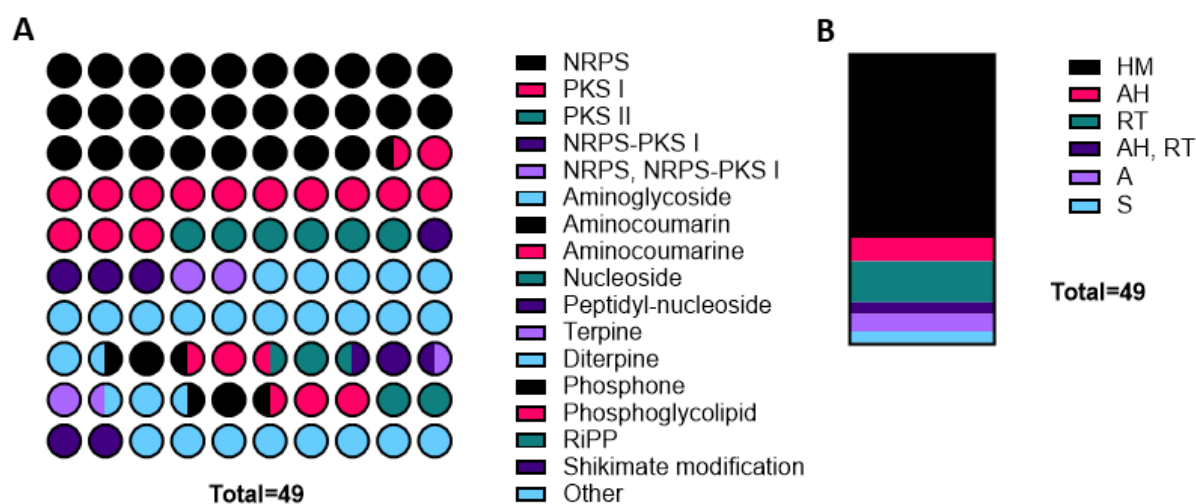


Figure 7. Natural products with antimicrobial activity are produced as secondary metabolites by bacteria or fungi. Data from Katz et al. (2016)⁴⁴. A. Dot plot showing the distribution of their biosynthetic origin, where NRPS - nonribosomal peptide synthetase, PKS - polyketide synthase, RiPP - ribosomally synthesized and post-translationally modified peptide. B. Major uses as antibacterial, where HM – human medicine, AH - animal health, RT - research tool, and S - scaffold for chemical semi-synthesis.

The discovery of NPs with antimicrobial activity from marine bacteria dates back to the 1950s, but it was not until the 1970s that antibiotic properties of marine bacterial metabolites were first reported⁴⁹. Since then, numerous studies have been conducted to investigate the antibiotic potential of marine bacteria. These studies have led to the isolation and characterization of novel NPs with diverse chemical structures and potent antimicrobial activity. Various studies have highlighted the potential of marine bacteria as a source of new antibiotics. For example, a study by Schinke et al. isolated a marine bacterium from deep-sea sediments that produced a compound with potent antibacterial activity against methicillin-resistant *Staphylococcus aureus*⁵⁰.

Marine bacteria, including Cyanobacteria, Actinobacteria, Roseobacter clade, and *Pseudoalteromonas* genus, have been found to produce NPs with interesting pharmacological properties³⁸. Not limited to these genera, other marine bacteria from various marine sources have been investigated for producing antimicrobial compounds, including sponges, seaweeds, sediments, thermal vents, and symbiotic associations with marine invertebrates⁴² (**Table 1**).

Table 1. Antimicrobial activities associated with the main phyla of marine bacteria. Reprinted by permission of Informa UK Limited, trading as Taylor & Taylor & Francis Group: Stincone et al. (2020)⁴², modified.

Source	Antimicrobial producing bacteria	Target microorganism
Aquaculture system	<i>Bacillus velezensis</i>	As
Cephalopod	<i>Leisingera</i> sp.	Vf, Va, Vp
Coral	<i>Micromonospora</i> , <i>Brachybacterium</i> , <i>Nocardia</i> , <i>Micrococcus</i> , <i>Arthrobacter</i> , <i>Rhodococcus</i> and <i>Streptomyces</i>	Sa, Bs, Ec
Coral	<i>S. variabilis</i>	Ec, Vc, Kp, Pa, <i>Enterobacter</i> sp., <i>Streptococcus</i> sp.
Chordate	<i>Streptomyces</i> sp. ZZ338	Sa, Ec, Ca
Gastropod	<i>Pseudomonas aeruginosa</i>	<i>Alteromonas</i> sp., <i>Pseudomonas</i> sp.
Mixture of invertebrate	<i>Streptomyces</i> sp.	Pa, Ca, Sa, Ef, Ec, Lm
Mussel	<i>Bacillus licheniformis</i>	Vh, Pa
Nudibranch	<i>Vibrio</i> and <i>Pseudoalteromonas</i>	Ap, Ec, Sa
Seaweed	<i>B. subtilis</i> MTCC 10407	Vp
Seaweed	Mixture	Sa, Ec, Ca
Sediment	<i>Verrucosipora</i> sp. MS100047	Sa, Mt, Bs, Pa, Ca
Sediment	<i>Micromonospora harpali</i>	Bs
Sediment	<i>Staphylococcus saprophyticus</i> SBPS 15	Ec, St, Sp, Kp, Vp, Vp, Pm, Spn, Bs, Bc, Sa
Sediment	<i>Rhodococcus</i> sp.	Bc, Bs, Ec, Pa, St, Sma, Sf, Sa, Ca
Sediment	<i>Streptomyces</i> sp. NIOT-Ch-40	Bs, Ml, Sa, Se, MRSA
Sediment	<i>Streptomyces</i> , <i>Micromonospora</i> , <i>Nocardiopsis</i> , <i>Saccharomonospora</i> , <i>Actinomadura</i> , <i>Glycomyces</i> , and <i>Nocardia</i>	Kp, Bs, Sa, Ec, <i>Enterococcus</i> sp.
Sediment	<i>Rheinheimera japonica</i> KMM 9513	Ec, Sa, Se, Bs
Sediment	<i>Streptomyces</i> sp. WU20	Sa, Bs, Ec
Sediment	<i>Streptomyces</i> sp. H-KF8	Sa, Lm, Se Ec, Pa
Sediment	<i>Streptomyces</i> sp., <i>Kocuria</i> sp., <i>Dietzia</i> sp., and <i>Nocardiopsis</i> sp.	Bs, Sa, Pa, Ca
Sediment	<i>Streptomyces</i> sp., and <i>Nocardia</i> sp.	St, Kp, Pa, Pm, Sa, Ec, <i>Shigella</i> sp.
Sediment	<i>Variovorax</i> sp.	Sw, Pv, MRSA, VRE
Sediment	<i>Streptomyces</i> sp.	Ab, Ec, Ef, Kp, Pa, Pm, Sa, VRE
Sediment	<i>Aequorivita</i> sp.	MRSA
Shellfish	<i>Lactobacillus</i> sp.	Sa, Vp, Ec, Kc
Sponge	<i>Streptomyces</i> sp.	Bs, Bc, Ca, Ec, Sa, Pa,
Sponge	<i>Acinetobacter</i> , <i>Bacillus</i> , <i>Photobacterium</i> , <i>Shewanella</i> , and <i>Vibrio</i>	Ec, Kp, Pa, Sa, Sh, Ef, Kp, Pa, Sa, MRSA, VRE
Sponge	<i>Vibrio</i> , <i>Pseudomonas/Marinobacter</i> and <i>Bacillus</i>	Bs, Ec, Vp, Vh, Ca
Sponge	<i>Vibrio</i> , etc	Pa, Sa, Bs, Ec, Ca
Sponge	<i>Rhodococcus</i> sp.	Sa
Sponge	<i>B. zhangzhouensis</i> , <i>B. pumilus</i> , <i>Psychrobacter alimentarius</i> , and <i>Arthrobacter citreus</i>	Bc, Se, Ms, Bc, Sen

Source	Antimicrobial producing bacteria	Target microorganism
Sponge	Mixture	Sa, Pa, Ec, St
Water	<i>Bacillus</i> sp., <i>Arthrobacter</i> , and <i>Brevundimonas</i>	Ec, Sa, Pa
Water	<i>Pseudoalteromonas haloplanktis</i> TAC125	Ec
Water	<i>Bacillus</i> sp. and <i>Pseudomonas</i> sp.	Ec, Sa
Water/ Sediment	<i>Pontibacter korlensis</i> SBK-47	Sm, Sa, Ec, St, Sp, Vp, Vc, Bs, Ml, Ef, Kp
Collection of marine bacteria	<i>Bacillus pumilus</i>	Sa, Lm

Ab: *Acinetobacter baumannii*; As: *Aeromonas salmonicida*; Ap: *Arthrobacter psychrolactophilus*; Bc: *Bacillus cereus*; Bs: *Bacillus subtilis*; Ca: *Candida albicans*; Ec: *Escherichia coli*; Ef: *Enterococcus faecalis*; Kp: *Klebsiella pneumoniae*; Lm: *Listeria monocytogenes*; Ml: *Micrococcus luteus*; Ms: *Mycobacterium smegmatis*; Mt: *Mycobacterium tuberculosis*; Pa: *Pseudomonas aeruginosa*; Pm: *Proteus mirabilis*; Pv: *Proteus vulgaris*; Sa: *Staphylococcus aureus*; Se: *Staphylococcus epidermidis*; Sh: *Staphylococcus hominis*; Sw: *Staphylococcus warneri*; Sf: *Shigella flexneri*; Sen: *Salmonella enterica*; Sp: *Salmonella paratyphi*; St: *Salmonella typhi*; Spn: *Streptococcus pneumoniae*; Sm: *Streptococcus mutans*; Sma: *Serratia marcescens*; Va: *Vibrio anguillarum*; Vc: *Vibrio cholerae*; Vf: *Vibrio fischeri*; Vh: *Vibrio harveyi*; Vp: *Vibrio parahaemolyticus*; MRSA: methicillin-resistant *Staphylococcus aureus*; VRE: vancomycin-resistant *Enterococcus*.

1.2.3 Eusynstyelamides, a novel scaffold from marine invertebrates

Not only marine bacteria, but also marine invertebrates and their associated microorganisms are rich sources of bioactive compounds^{51,52}. The main phyla of marine invertebrates explored include sponges, cnidarians, molluscs, echinoderms, and ascidians^{51,52} (Figure 8). However, cold-water bryozoans (moss animals, phylum Ectoprocta) contain many bioactive metabolites and have produced 35 published natural products^{53,54}.

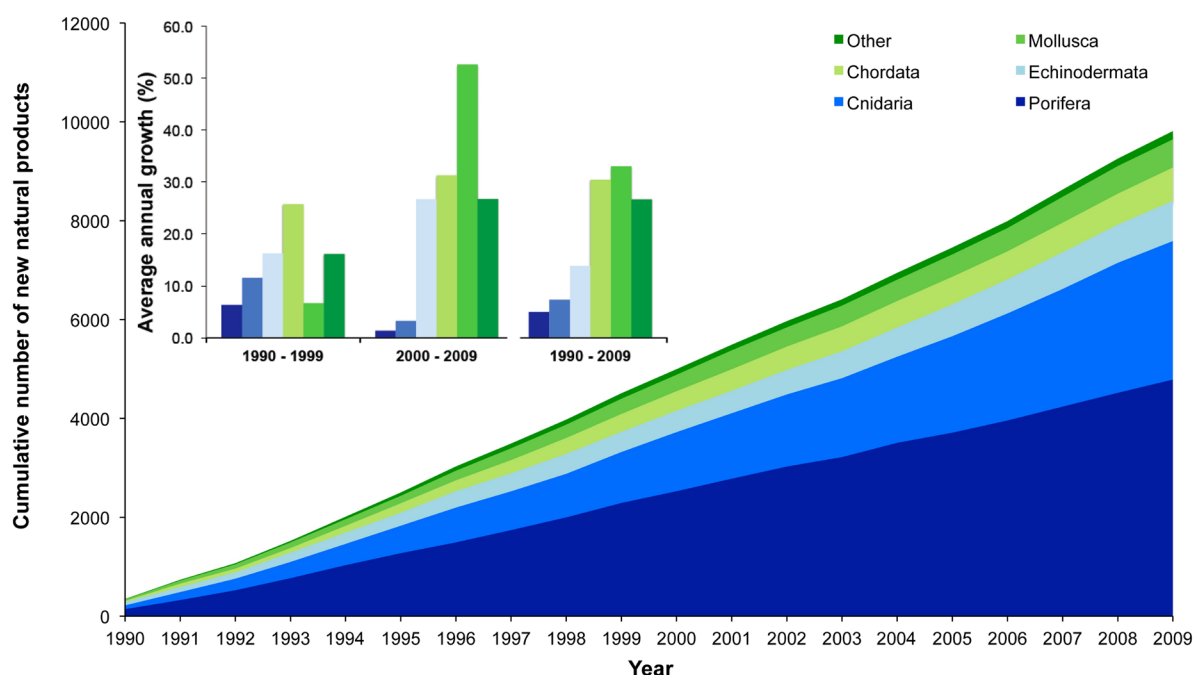


Figure 8. The phyla of marine invertebrates as a source of new natural products. The cumulative number of new natural products discovered from different marine invertebrate phyla between 1990 and 2009 (Group "Other phyla" include Annelida, Arthropoda, Brachiopoda, Hemichordata, Platyhelminthes, and Bryozoa). Inset: The annual growth of the number of new marine natural products from different marine invertebrates discovered in the 1990s, 2000s and during both decades; Leal et al. (2012)⁵².

In a study investigating the chemistry of the Arctic bryozoan *Tegella cf. spitzbergensis*, researchers isolated and determined the structures of ent-eusynstyelamide B and several new derivatives, including eusynstyelamides D, E and F⁵⁵ (**Figure 9**). These compounds exhibited antibacterial activity and were characterized using high-resolution mass spectrometry and NMR techniques⁵⁵. This is the first report on bioactive metabolites of *Tegella* species⁵⁵. Eusynstyelamide B, a brominated tryptophan metabolite, was previously isolated from the ascidian *Eusynstyela latericius*⁵⁶. Eusynstyelamides A, B, and C have inhibition of neuronal nitric oxide synthase and modest anticancer and antibacterial activities⁵⁶. Eusynstyelamide A was later found to contain an open central motif instead of the five-membered ring and an additional hydroxy group⁵⁶.

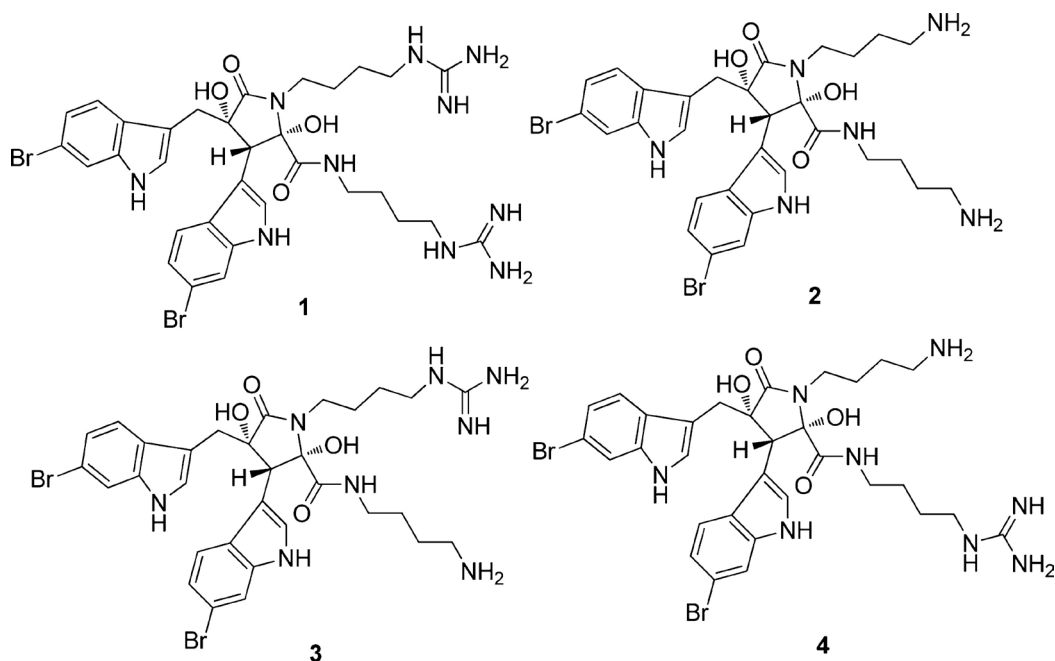


Figure 9. Eusynstyelamides from the Arctic Bryozoan *Tegella cf. spitzbergensis*. 1. ent-eusynstyelamide B, 2. eusynstyelamides D, 3. Eusynstyelamides E, and 4. Eusynstyelamides F. Permission of the American Chemical Society (ACS): Tadesse et al. (2011)⁵⁵.

Overall, these findings highlight the potential of cold-water bryozoans and ascidians as sources of bioactive metabolites. The discovery of new compounds with antibacterial activity from *Tegella spitzbergensis* expands our understanding of the chemical diversity of these organisms. Furthermore, identification of eusynstyelamide B and its isomers in different ascidian species suggests the widespread occurrence of these metabolites in marine environments. More research is needed to explore the therapeutic potential of these compounds and understand their mechanisms of action.

1.2.4 Synthetic mimics of antimicrobial peptides (SMAMPs)

Antimicrobial peptides (AMPs) are naturally occurring molecules that play a crucial role in innate immune defence against microbial pathogens^{57,58}. AMPs typically have 12 to 100 amino acid residues and show rapid and effective antimicrobial activity against various pathogens^{59,60} (**Figure 10**). However, the development of AMPs as therapeutics has been hindered by challenges such as high production costs, limited stability, and potential toxicity⁶¹. Researchers have turned to synthetic antimicrobial peptides (SAMPs) and synthetic mimics of antimicrobial peptides (SMAMPs) to overcome these challenges. SAMPs and SMAMPs are artificially designed peptides that mimic the structure and function of natural AMPs. SMAMPs have earned attention as a crucial solution amid the growing threat of antibiotic resistance^{58,62}. A decline in antibiotic discoveries in recent decades (**Figure 3**) has led to a shortage of effective antibiotics, necessitating innovative approaches to combat resistant bacterial infections⁶³. These SMAMPs can be modified to enhance their activity, stability, and selectivity against specific bacteria⁶¹.

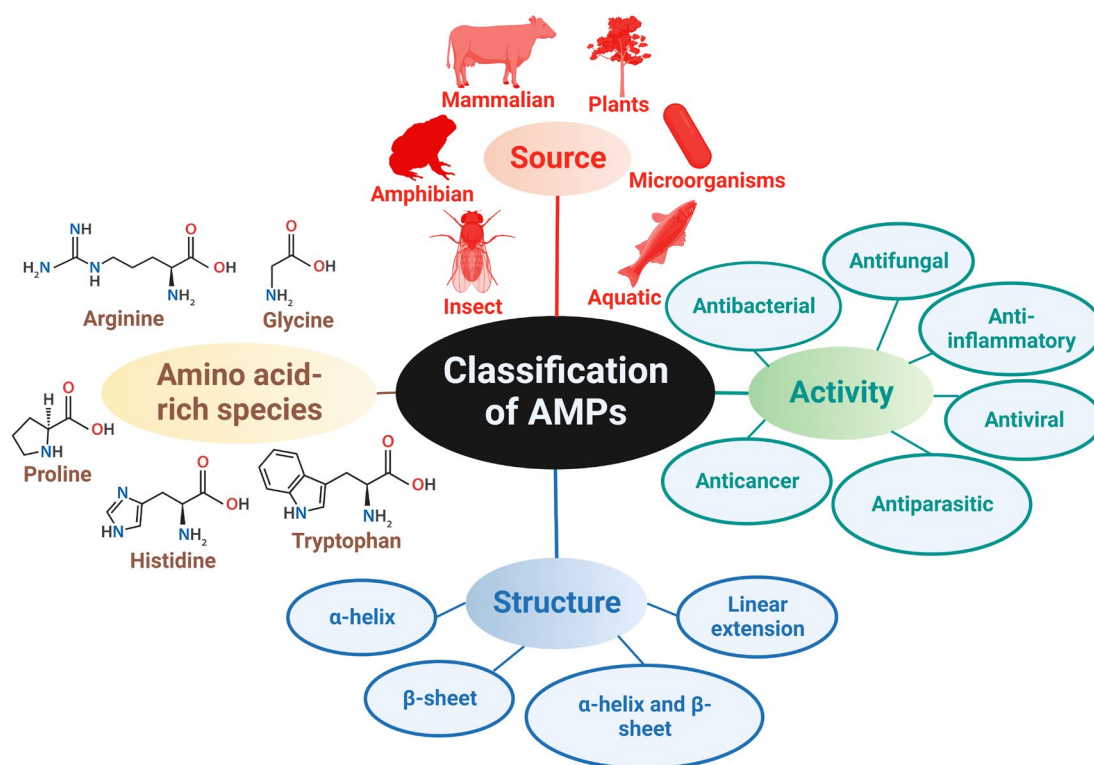


Figure 10. Classification of antimicrobial peptides (AMPs); Huan et al. (2020)⁶⁴, modified.

SMAMPs offer several advantages as a potential solution for new antibiotics. Firstly, SMAMPs have a broad spectrum of activity against various bacterial strains, including drug-resistant ones⁵⁸. Therefore, SMAMPs have the potential to target a wide range of bacteria, making them effective against different types of infections (**Figure 11**) with different modes of action.

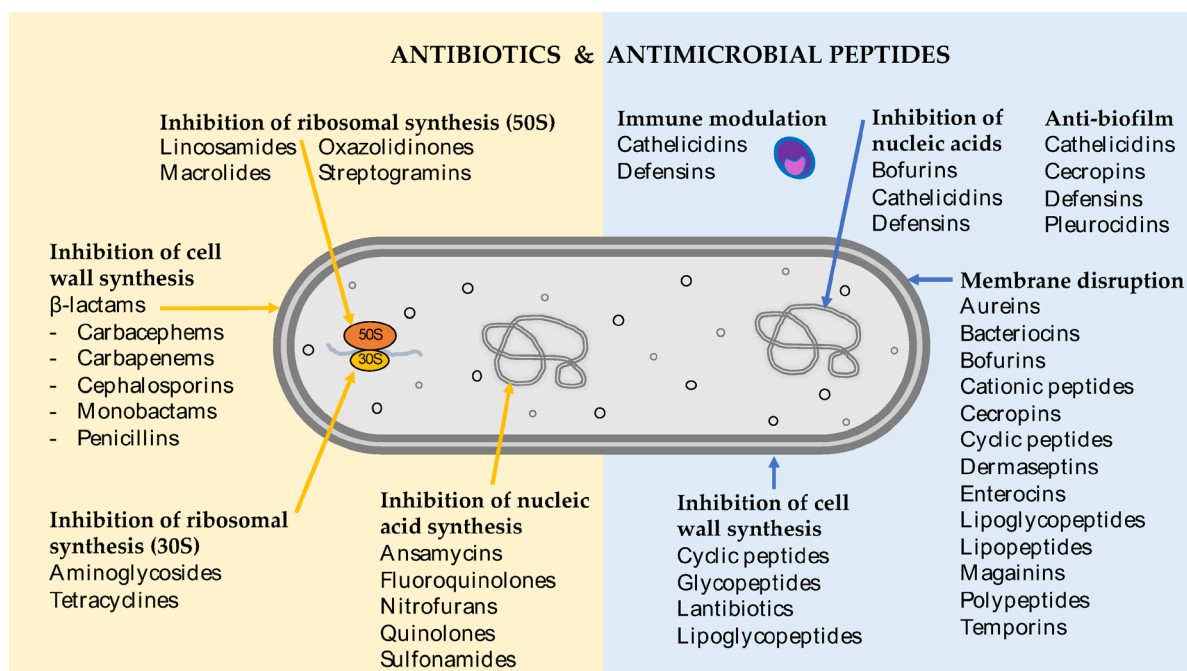


Figure 11. The mechanistic targets of antibiotics and antimicrobial peptides (AMPs); Browne et al. (2020)⁵⁸.

Additionally, bacteria have been shown to have a low tendency to develop resistance toward SMAMPs. This is because SMAMPs target multiple bacterial structures and pathways, making it difficult for bacteria to develop resistance⁵⁸. Furthermore, SMAMPs have been found to have a rapid bactericidal effect. Thus, they can kill bacteria quickly, which is crucial in treating severe bacterial infections⁵⁸. Another advantage of SMAMPs is their potential to enhance the activity of other antimicrobial agents. For example, studies have shown that SMAMPs can enhance the activity of traditional antibiotics, making them more effective in combating bacterial infections⁵⁸. Another benefit of SMAMPs is their potential to be customized and optimized⁵⁸.

Additionally, SMAMPs offer the advantage of being less prone to being toxic compared to traditional antibiotics⁶⁵. SMAMPs also provide a cost-effective and easily synthesized alternative to naturally occurring antimicrobial compounds. Several commercially available AMPs of natural and synthetic origin (**Table 2**) represent a promising solution for the development of new antibiotics.

Table 2. Commercially available peptide-based antibiotics; Browne et al. (2020)⁵⁸, modified.

Active Ingredient	Origin	Target Organism	Class	Mechanism of Action	Indication	Route of Administration
Bacitracin	Bacteria (<i>Bacillus subtilis</i>)	Gram-positive bacteria	Cyclic peptide	Inhibits cell wall synthesis	Skin infections	Topical Ophthalmic Intramuscular
Dalbavancin	Teicoplanin derivative	Gram-positive bacteria	Lipoglycopeptide	Inhibits cell wall synthesis	Skin infections	Intravenous
Daptomycin	Bacteria (<i>Streptomyces roseosporus</i>)	Gram-positive bacteria	Lipopeptide	Membrane lysis	Skin infections	Intravenous
Colistin	Bacteria (<i>Bacillus polymyxa</i>)	Gram-negative bacteria	Cyclic peptide	Membrane lysis	Gram-negative infections resistant to multi-drugs	Intravenous
Gramicidin D	Bacteria (<i>Bacillus brevis</i>)	Gram-positive bacteria, some Gram-negative bacteria	Mix of three polypeptides	Membrane poration/lysis	Skin and eye infection	Topical Ophthalmic
Oritavancin	Vancomycin derivative	Gram-positive bacteria	Lipoglycopeptide	Membrane lysis and inhibits cell wall synthesis	Skin infections	Intravenous
Polymyxin B	Bacteria (<i>Bacillus polymyxa</i>)	Gram-negative bacteria	Polypeptide	Membrane lysis	Urinary tract and bloodstream infections	Ophthalmic Topical Intravenous
Teicoplanin	Bacteria (<i>Actinoplanes teichomyceticus</i>)	Gram-positive bacteria	Glycopeptide	Inhibits cell wall synthesis	Serious Gram-positive infections	Intramuscular Intravenous
Telavancin	Vancomycin derivative	Gram-positive bacteria	Lipoglycopeptide	Membrane lysis and inhibits cell wall synthesis	Skin infections	Intravenous
Vancomycin	Bacteria (<i>Amycolatopsis orientalis</i>)	Gram-positive bacteria	Glycopeptide	Inhibits cell wall synthesis	Serious Gram-positive infections	Oral Intravenous

1.2.5 AntifoMar

The UiT supported ongoing bioprospection research activity at the University by funding the multidisciplinary strategic project AntifoMar associated to CANS. The project is a collaboration between three faculties at UiT and the Nord University. The primary objective of the AntifoMar project was to develop biofilm-inhibiting and -eradicating compounds for therapeutic and industrial purposes. This is achieved by an intensive four PhD collaboration using marine invertebrates, including genes and associated microbial symbionts, as sources for model compounds. Methods for the isolation, characterization, and bioevaluation of model compounds are established and will be complemented with the synthesis of optimized derivatives and bioinformatics. Marine organisms are a rich source of biofilm-inhibiting compounds. Isolated compounds and improved synthetic derivatives will lead to innovative solutions for biofilm inhibition with relevance in preventing marine biofouling and improving public health.

Milestones of the AntifoMar project (see **Figure 12** for WPs):

- 1) Identify biofilm-inhibiting molecules from unexploited marine organisms.
- 2) Identify the actual producer (host or associated microorganisms).
- 3) Synthesize and optimize identified antibiofilm molecules and derivatives.
- 4) Provide innovative lead compounds for therapeutic/industrial applications.
- 5) Provide interdisciplinary R&D education for four PhDs.

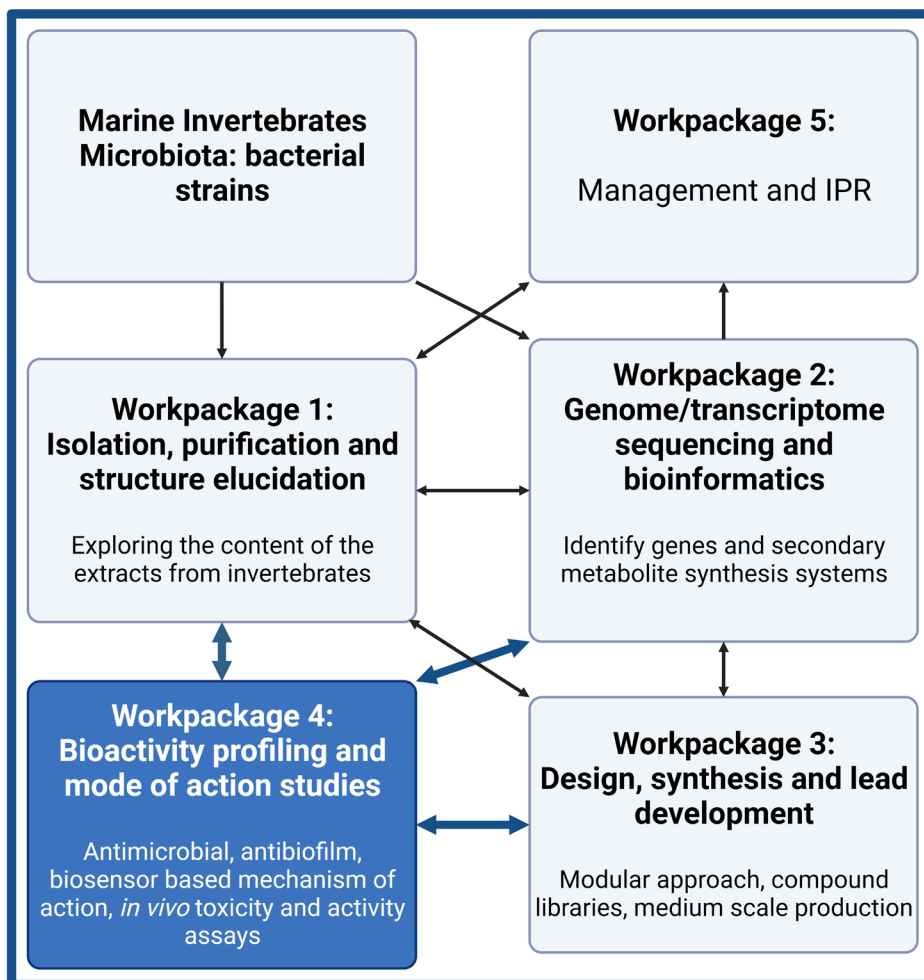


Figure 12. Outline of the AntifoMar project's different work packages and indicated information flow.

2 Research objectives

This project was done in the Marine Bioprospecting group at the Norwegian College of Fishery Science within the WP 4 of the project AntifoMar.

The main aim of the research project was to evaluate the development and characterize antimicrobials, biofilm inhibitors, and biofilm-eradicating compounds of marine origin for therapeutic purposes.

The project was divided into two approaches with the following sub-goals to achieve the goal. The sub-goals of the approaches were as follows:

Approach A: Evaluation of synthetic analogues based on natural products

- Identify candidate antimicrobials, biofilm-inhibitors, and -eradicators from a library of designed and chemically synthesized compounds by evaluating the antibacterial and antibiofilm activities.
- Determine the mode of action of the most promising candidates using optimized *in vitro* test systems.
- Evaluate *in vitro* and *in vivo* toxicity and activity of the most promising candidates.

Approach B: Natural products (NPs) from marine bacteria

- Identify and evaluate producers of antimicrobials, biofilm-inhibitors, and -eradicators of natural origin, with a specific focus on marine bacteria.
- Evaluate the selected marine bacteria as a potential source of antimicrobials, biofilm-inhibitors, and -eradicators.

3 Research design

The research design of this project is based on the sub-goals of the two approaches (**Figure 13** and **Figure 14**) that address the main aim. This research design is formed to identify and characterize biofilm-inhibiting and eradicating compounds of marine origin.

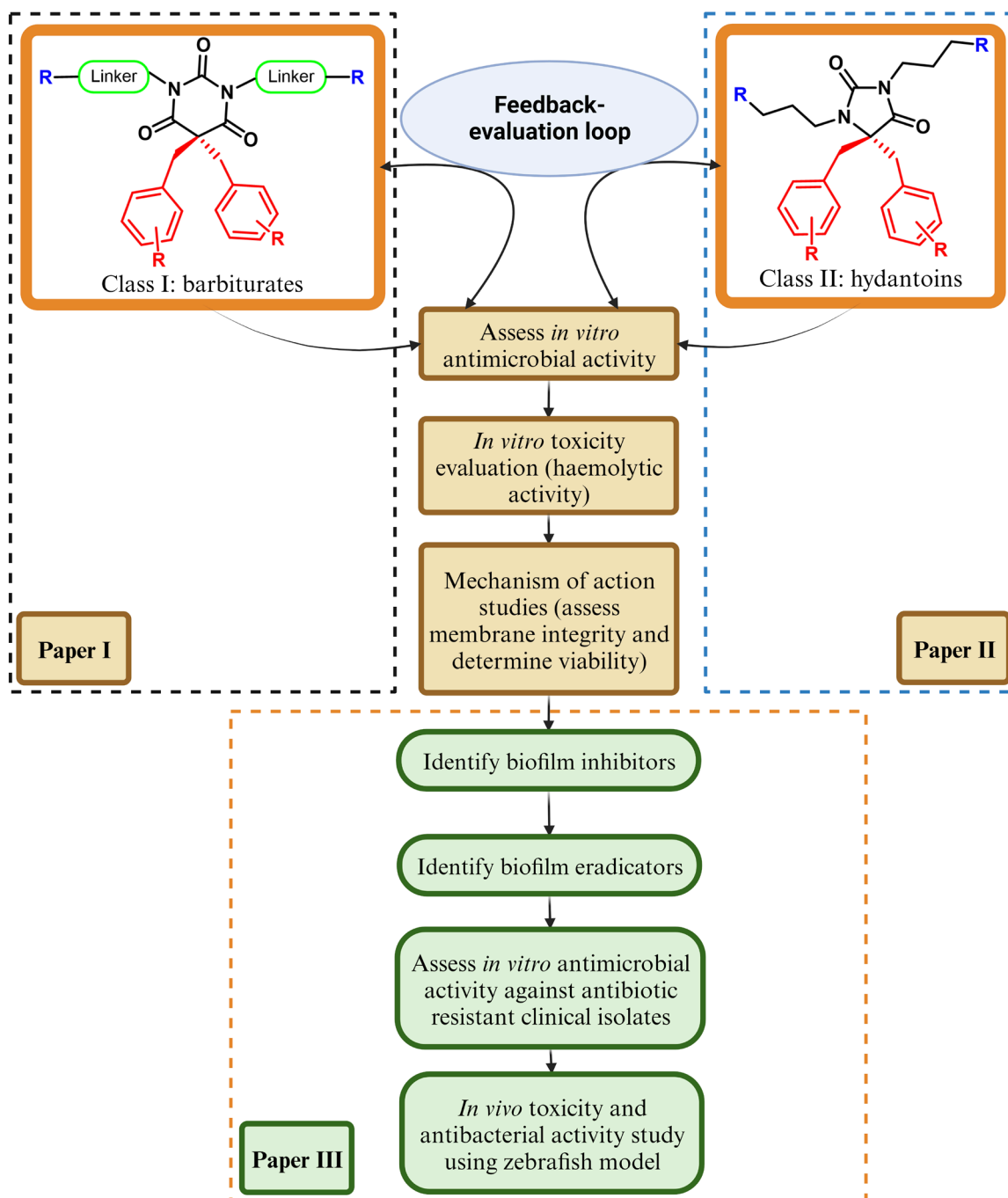


Figure 13. Approach A: Characterization of synthetic analogues based on natural products.

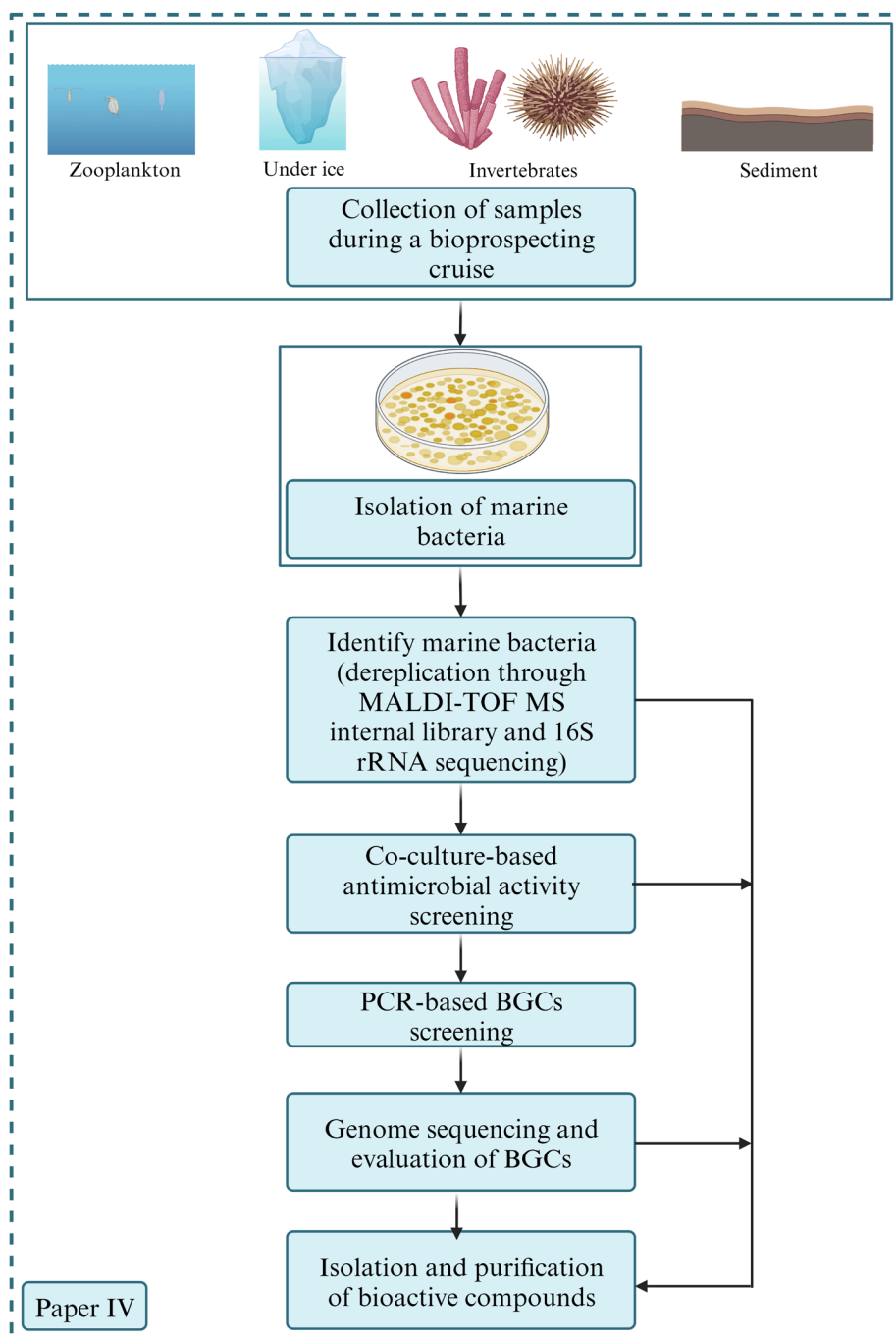


Figure 14. Approach B: Natural products (NPs) of marine bacteria.

4 Summary of the main results

4.1 Paper I

Title: A concise SAR-analysis of antimicrobial cationic amphipathic barbiturates for an improved activity-toxicity profile.

Highlights (Figure 15):

- An efficient synthesis of tetrasubstituted barbiturates with diverse cationic and lipophilic side chains is established.
- The careful choice of structural components provides a good balance of antibacterial and haemolytic activity.
- Guanidyl head groups combined with n-butyl linkers give the highest potency.
- The n-Propyl linkers provide the best balance between antibacterial and haemolytic activity.
- Disruption of membrane integrity is the main mode of antibacterial action.

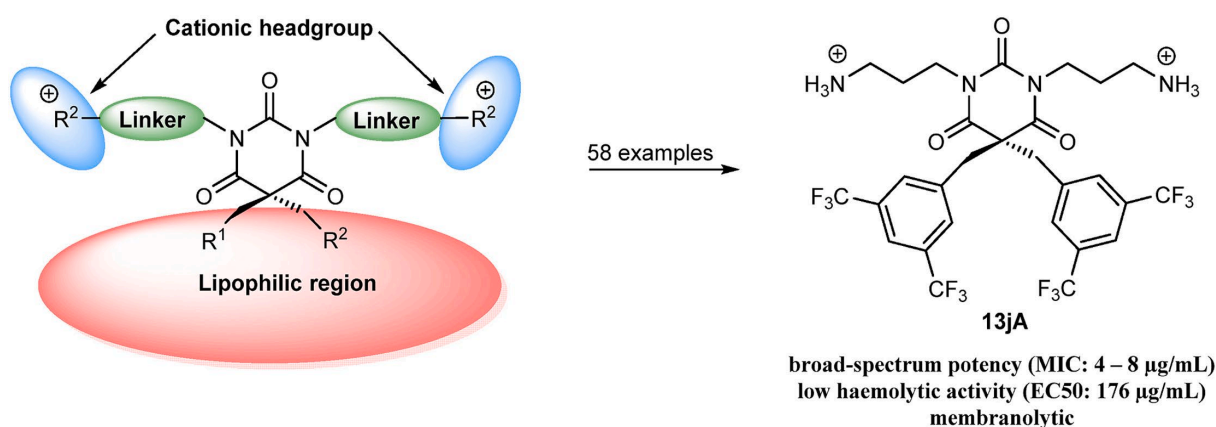


Figure 15. Graphical abstract of antimicrobial cationic amphipathic barbiturates.

Conclusions:

The qualitative influence of the individual structural components of *N,N*-dialkylated-5,5-disubstituted amphipathic barbiturates on their bioactivity was investigated. Studies on membrane integrity and viability of bacterial cells suggest that compounds exert their bactericidal activity by disrupting the bacterial cell wall of Gram-positive *B. subtilis* in a concentration-dependent manner, as exemplified by barbiturate 11IG. In Gram-negative *E. coli* both the inner and outer membranes were supposedly rapidly disrupted at higher compound concentrations, but a second mechanism of action might also be present. This detailed analysis can help to devise new amphipathic cationic mimics of antimicrobial peptides.

4.2 Paper II

Title: Investigation of tetrasubstituted heterocycles reveals hydantoin as a promising scaffold for development of novel antimicrobials with membranolytic properties.

Highlights (Figure 16):

- The hydantoin scaffold was the most promising AMP mimetic of the five heterocycles studied.
- n-Butyl linkers combined with guanidine head groups delivered the highest antimicrobial potency.
- Lead structures 6cG and 6dG delivered high selectivity indices.
- Disruption of the bacterial cytoplasmic membrane was their main mode of action.

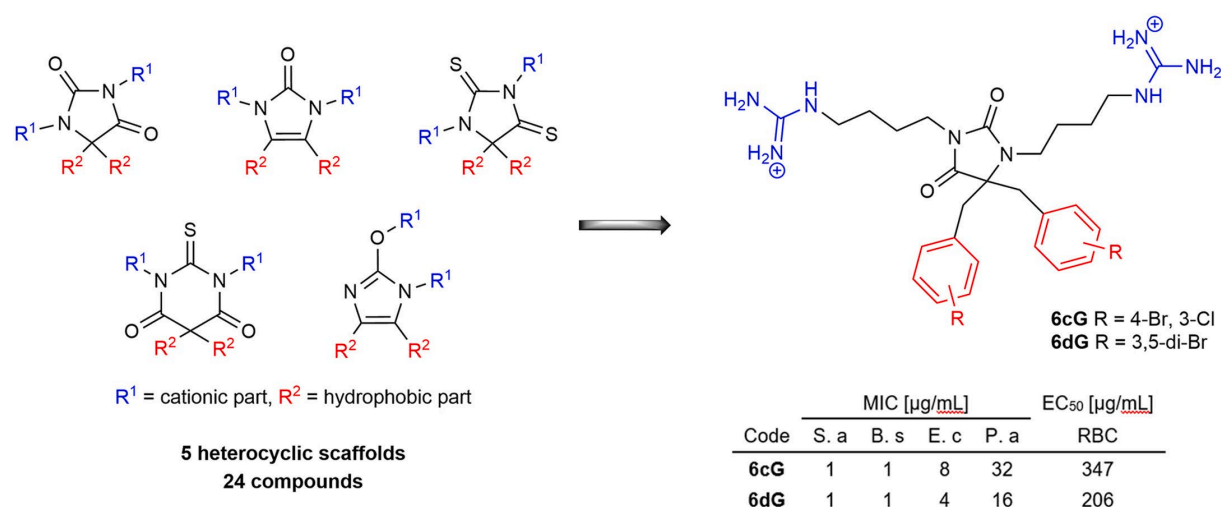


Figure 16. Graphical abstract of hydantoin as a promising scaffold for development of novel antimicrobials.

Conclusions:

We investigated five scaffolds for their suitability for developing novel tetrasubstituted, amphipathic SMAMP antimicrobials, revealing the hydantoin structure as a promising template for antibacterial drug lead development. The results obtained from the viability and membrane integrity assays suggested a rapid membranolytic effect, as demonstrated for hydantoin 6cG in *B. subtilis* and *E. coli*. Interestingly, both the inner and the outer membranes in *E. coli* appeared to be disrupted at a similar speed. We believe that our findings on the qualitative contribution of the scaffold structures can help the development of novel small-molecule analogues of AMPs or SMAMPs.

4.3 Paper III

Title: Peptidomimetic tetrasubstituted barbiturates and hydantoin derivatives: Investigation of their antibiofilm, in vivo toxicity and antimicrobial activity.

Highlights (Figure 17):

- Several biofilm inhibitors and -eradicators from barbiturates and hydantoin derivatives were identified.
- The lead compounds 13iA of barbiturates and 2cA of hydantoin derivatives showed outstanding biofilm inhibition and eradication against *Staphylococcus epidermidis* RP62A.
- With broad spectrum activity of 13iA, it also showed excellent biofilm inhibition and eradication against *Pseudomonas aeruginosa* PAO1.
- Both lead compounds showed promising antimicrobial activity against antimicrobial resistant clinical isolates.
- Compounds 13iA and 2cA did not show toxicity at a dose of 16 mg/kg, similar to the positive control, tetracycline.
- Compound 2cA showed significant antimicrobial activity against *S. aureus*, and compound 13iA was against *S. epidermidis*, better than the positive control, tetracycline.

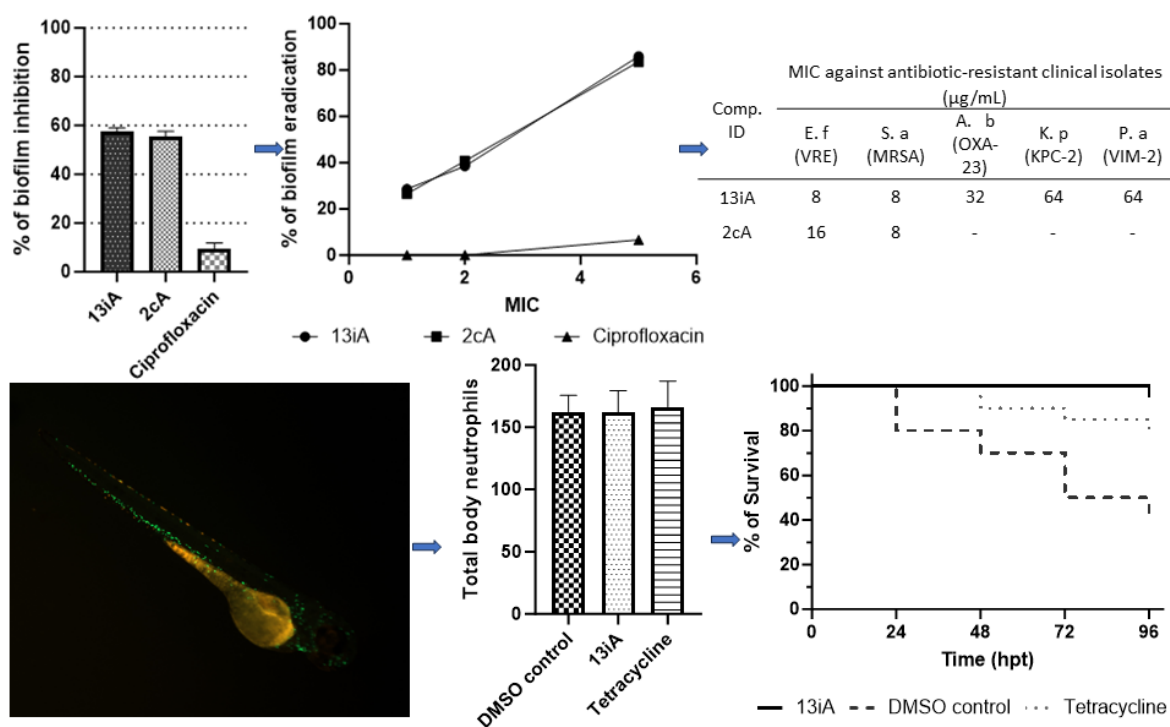


Figure 17. Graphical abstract of in vivo toxicity and activity of barbituric acid and hydantoin derivatives with antibacterial and antibiofilm activity.

Conclusions:

Barbituric acid and hydantoin derivatives showed excellent antibiofilm potential to inhibit biofilm formation and eradicate formed biofilm. They showed dose-dependent inhibition and eradication of biofilms against *S. epidermidis* RP62A, *S. epidermidis* 5179-R1, and *P. aeruginosa* PAO1. The lead compounds showed promising antibacterial activity against both antibiotic-resistant Gram-positive and negative bacteria, almost the same as the activity against reference bacteria. Compounds 13iA and 9 showed excellent in vivo antibacterial activity against *S. epidermidis* RP62A and *S. aureus*.

4.4 Paper IV

Title: Antimicrobial potential of marine bacteria from the Arctic and sub-Arctic regions.

Highlights (Figure 18):

- 158 marine bacteria were isolated in the Arctic regions during a bioprospecting cruise in 2019.
- *Moritella*, *Psychromonas*, and *Shewanella* cover almost half of the identified genera.
- 65 marine bacterial isolates showed antimicrobial activity against at least one strain of the panel of human pathogen-related bacteria.
- 37 isolates indicated the presence of NRPS or PKS gene clusters.
- From genome mining and screening, *Shewanella sp.* MBP011.13.1 and *Pseudomonas sp.* MBP027.4 was the most promising marine bacterial isolates with antibacterial activity and positive for NRPS or PKS and several other BGCs.

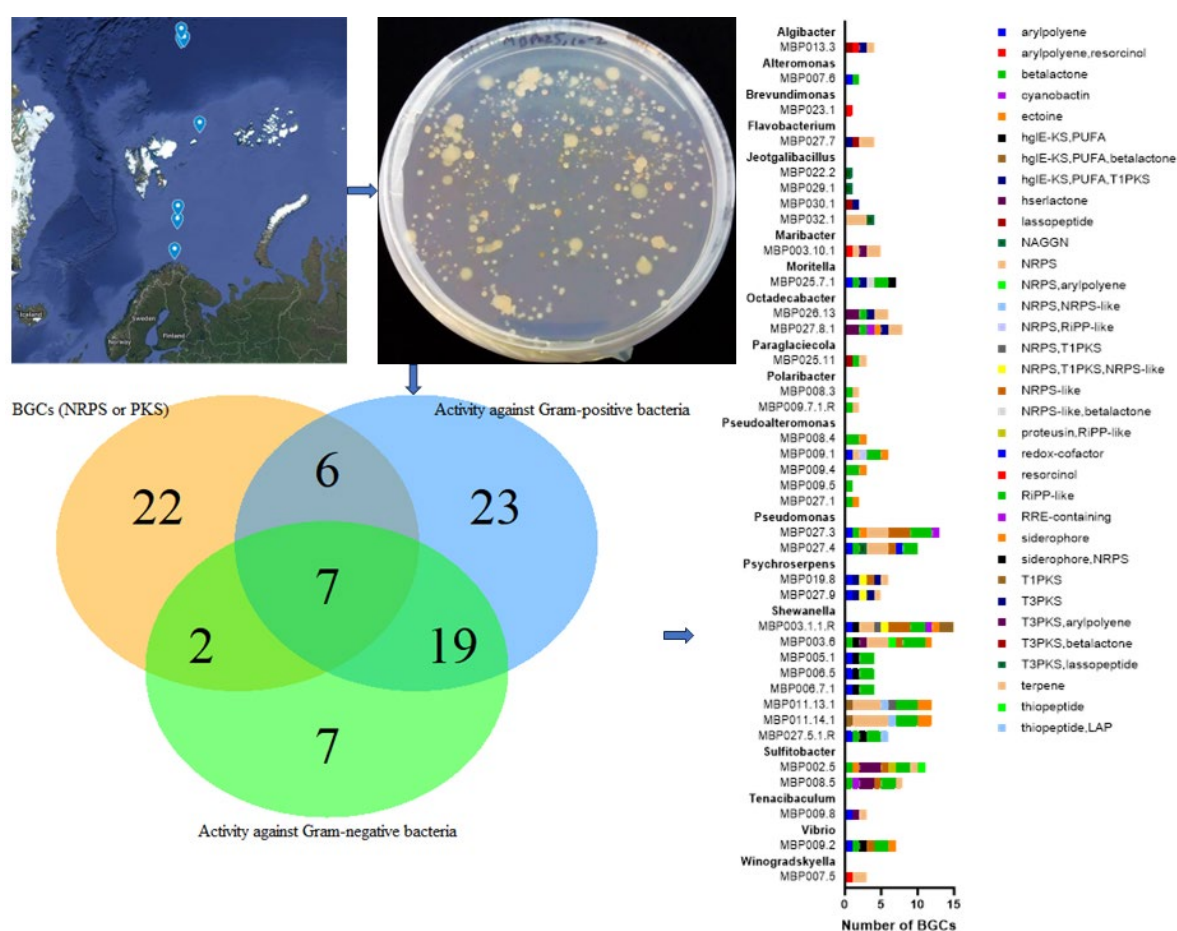


Figure 18. Antimicrobial potential of marine bacteria from the Arctic regions during a bioprospecting cruise in 2019.

Conclusions:

This bioprospecting study of Arctic marine bacterial isolates demonstrates how co-culture and genome mining can be used to identify bioactive marine bacteria as a potential source of antimicrobial compounds. Two marine invertebrates (Porifera), zooplankton, samples from under the ice, and sediments of 452 m deep were the source of the isolates with the most potent antibacterial activity. Genome mining also facilitated the identification of potential BGCs that could encode the antimicrobial compounds.

5 General discussion

Antibiotics have greatly impacted modern medicine, but the rise of antibiotic resistance poses a significant global health concern. The imperative to counteract this threat necessitates the complex and challenging task of discovering and developing novel antibiotics. Multiple factors, such as the complexity of bacterial physiology and a high candidate failure rate, complicate this process¹⁹. However, promising antibiotic candidates are emerging from diverse sources, underscoring the ongoing efforts in this critical field.

This study was part of the larger multidisciplinary project, AntifoMar. The goal was to identify the producer of antimicrobial compounds of marine origin by collaborating with all other work packages involved in the AntifoMar project. Also, to identify and develop biofilm-inhibiting and eradicating compounds. Additionally, this project evaluated the mode of action, toxicity, and antimicrobial activity both *in vitro* and *in vivo*.

Screening of the SMAMPs library resulted in several promising lead compounds with antimicrobial activity against antibiotic-resistant clinical isolates and antibiofilm properties against Gram-positive and Gram-negative bacteria. Furthermore, *in vivo* toxicity and antibacterial activity were assessed using the zebrafish model. This part of the study resulted in three **papers (I-III)**. Moreover, the screening of marine bacteria as producers of NPs with antimicrobial activities resulted in one **paper (IV)**.

5.1 Pipeline and challenges associated with the AntifoMar project

The flow of information between different work packages in the AntifoMar project (**Figure 12**) facilitated productive collaboration from various angles, creating constructive interaction between these packages. Since the work packages of the AntifoMar project started simultaneously, they cannot follow a bioprospecting flow as outlined in **Figure 5**. The bioprospecting pipeline involves identifying lead compounds from marine natural sources like invertebrates or bacteria and then employing a peptidomimetic strategy based on the identified scaffolds (**Figure 5** and **Figure 12**). In the AntifoMar project, on the other hand, we had to use the previously identified scaffold, eusynstyelamide, from the Arctic bryozoan, (**Paper I and II**), as the starting point for the peptidomimetics.

For the development of synthetic mimics of antimicrobial peptides (SMAMPs or peptidomimetics), a feedback evaluation loop was essential to optimize their structure and increase their activity. SMAMPs were synthesized in various batches, with each batch undergoing evaluations of antibacterial and haemolytic activities, followed by SAR analysis. This analysis informed the synthesis of subsequent batches. Ultimately, the SMAMPs library consisted of several series of derivatives, encompassing all these batches (**Paper I and II**). Selected derivatives were then subjected to further testing to pinpoint the most promising candidates. This included MOA analysis (as detailed in **Papers I and II**), evaluation of antibacterial activity against antibiotic-resistant clinical isolates, and antibiofilm studies (discussed in **Paper III**). This process of SAR and MOA investigation is crucial in the drug discovery pipeline (**Figure 5**), shaping the future stages of development.

The search for animal models to study *in vivo* toxicity and antibacterial activity efficiently, cost-effectively, and without regulatory barriers was challenging in a short period of time. The zebrafish model was opted to assess the toxicity and activity of the shortlisted lead compounds. However, there was a lack of expertise in Norway regarding this infection model. The search extended to Europe to find a suitable group to learn the techniques and conduct the necessary studies. Fortunately, the connection with a group at Jagiellonian University in Poland was experienced in the infection model, where toxicity and activity studies were conducted on compounds using the zebrafish model (**Paper III**), supported by a Research Stay Abroad grant.

Both culture-dependent bioprospecting⁶⁶ (as depicted in WP4 and WP2 of **Figure 12**) and culture-independent metagenomics⁶⁷ (WP2 of **Figure 12**) have their respective merits and demerits. Classical cultivation techniques are limited in that they can isolate only a small percentage of all microbial species^{66,68}. Meanwhile, metagenomic approaches face challenges due to limitations in the availability of microbial DNA⁶⁹. This issue becomes particularly pronounced in low-biomass environments or when dealing with microbiomes of low abundance⁶⁹. Similar problems can occur during the separation of microbial cells from host tissues, especially if the host organisms harbor's low densities of associated microbes or if the separation process yields low quantities⁶⁹. Nevertheless, advancements in cultivation techniques are broadening the scope of cultivable isolates, allowing for more extensive phenotypic screening using cell-based assays⁷⁰.

In the marine bioprospecting pipeline (**Figure 5**), numerous biosynthetic gene clusters of marine bacteria remain unexpressed under conventional laboratory conditions, leading to the frequent isolation of already known compounds⁷¹. Over the last decade, the 'one strain many compounds' (OSMAC) approach has been employed to activate these BGCs⁷², primarily encoding enzymes for secondary metabolite biosynthesis⁷³. Various culture conditions, such as aeration rate, temperature, and nutrient composition, were modified to successfully activate these BGCs⁷³. However, applying the OSMAC approach to psychrophilic bacteria from the Arctic marine environment presented difficulties. Most of these bacteria only thrive at temperatures between 4-10 degrees Celsius and grow in specific media such as marine broth and modified half-strength marine broth (FMAP) medium (**Paper IV**). An alternative strategy involved co-culturing these bacteria with human pathogen relatives, simulating the complex ecological interactions of microbial life^{66,71}. This ecology-driven method aimed to activate silent gene clusters to explore the metabolic potential for novel bioactive secondary metabolites⁷¹. Yet, challenges persisted due to temperature constraints and media compatibility, as Arctic marine bacteria prefer temperatures of 4-10 degrees Celsius (some between 10-20 degrees), and human pathogen relatives exhibit limited growth in marine broth, particularly at lower temperatures. To overcome these obstacles, the co-culture method underwent optimization (**Paper IV**).

5.2 Source of novel antibacterial compounds

Novel antimicrobial compounds can come from various sources, including marine bacteria and synthetic antimicrobial peptides. Marine bacteria, such as those from Streptomyces, are known to produce unique secondary metabolites with antimicrobial properties⁷⁴. Furthermore, synthetic antimicrobial peptides, designed through rational peptide engineering, exhibited promising antimicrobial activity against various pathogens^{75,76}. These sources provide attractive opportunities for the discovery of new antimicrobial compounds.

5.2.1 Synthetic mimics of antimicrobial peptides (SMAMPs)

Papers I and II describe the SMAMPs library as a source of novel antimicrobials, taking inspiration from the eusynstyelamide NP class^{55,56}. After previous demonstration of the efficacy of new tetrasubstituted barbiturates⁷⁷, the **paper I** aimed to enhance their therapeutic index by designing a second generation of derivatives, retaining the barbituric acid core and methodically examining the effects of cationic groups, linkers, and lipophilic side chains on antimicrobial and haemolytic activities, as shown in **Figure 19**.

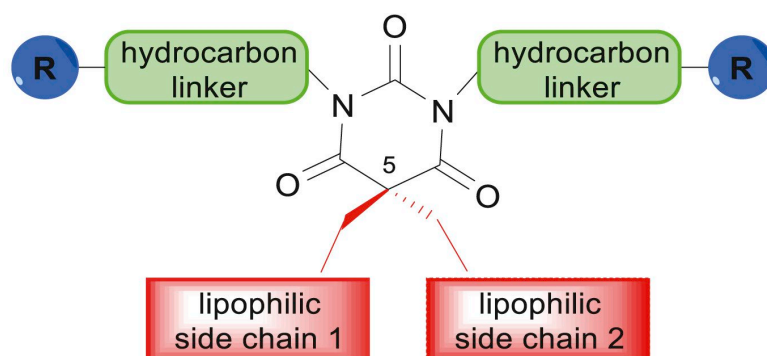


Figure 19. The general structure of the barbituric acid derivatives, mimics of eusynstyelamide.

The derivatives were categorized into five series, each of which alters one moiety while sustaining the rest of the molecular structure. The emphasis of each series was on 1) cationic groups, 2) new lipophilic side chains, 3) a combination of two different lipophilic side chains based on the results of the previous study⁷⁷ and series 2 of this **Papers I**, 4) various hydrocarbon linkers, and 5) the most efficient combinations from series 1-4.

Paper II explored how different central scaffolds affect biological activity after investigating the structural components of amphipathic barbiturates in Paper I. The substitution pattern was applied from earlier studies to five heterocycles structurally similar to barbituric acid (**4bA**, **Paper I**), as shown in **Figure 20**. In **Paper II**, imidazolidine-2,4-dione (**2**, **Paper II**), known as hydantoin, which is acknowledged in medicinal chemistry but seldom in antimicrobials, and 4-imidazolidin-2-one (**3**, **Paper II**) for its unique geometry and increased lipophilicity, were chosen. Taking into account the relevance of sulfur in drugs, including antimicrobials such as penicillins and cephalosporins, we investigated its impact within an amide (**4**, **Paper II**) and urea-type bond (**5**, **Paper II**). Unexpectedly, 2-(hydroxy)-1H-imidazole (**15**, **Paper II**) emerged as a byproduct during synthesis, prompting its inclusion. Having assessed each structure, **Paper II** focused on hydantoin for a targeted library, forming the basis for the third generation of derivatives.

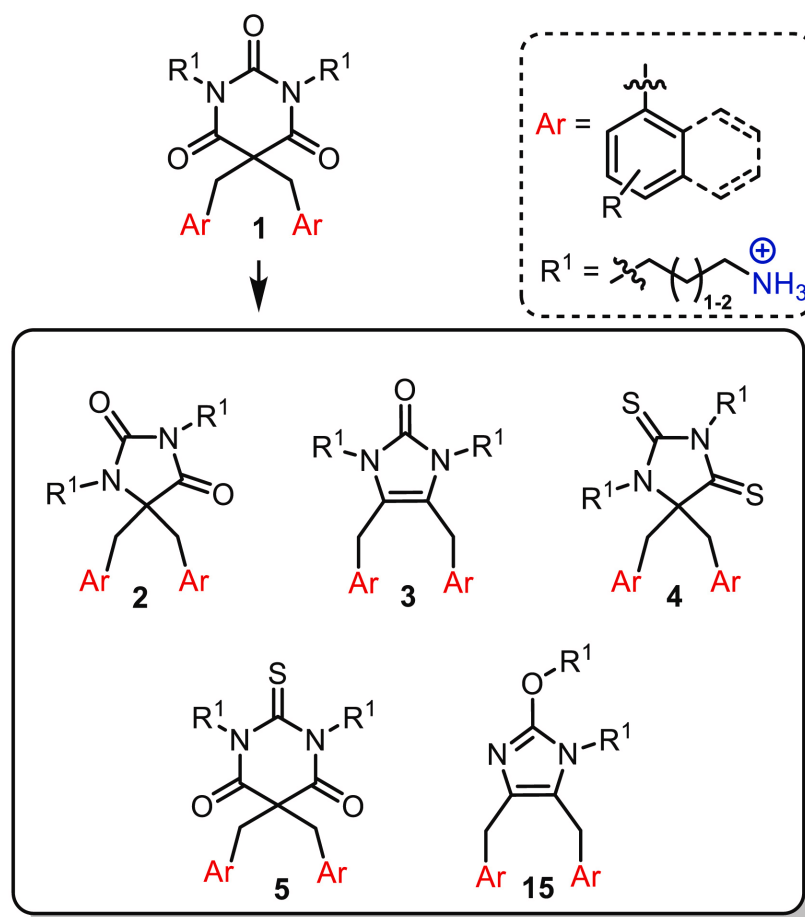


Figure 20. Previously utilized barbituric acid **1**⁷⁷ and core structures **2–5** and **15** were used in this study. *Ar* = lipophilic side chain, *R1* = *n*-alkyl linker with a cationic head group. Red: lipophilic part; blue: cationic part.

5.2.2 Marine bacterial secondary metabolites (MBSMs)

The diversity of marine bacteria and the unique chemical and biological properties of marine bacterial secondary metabolites (MBSMs) make them attractive candidates for the development of new antimicrobials against a wide range of pathogens⁷⁴. In **Paper IV**, 158 marine bacterial isolates were isolated (**Figure 21**) and assessed for their antimicrobial activity against a panel of Gram-positive and -negative human pathogen-related bacteria, including ESKAPE relatives. Additionally, polymerase chain reaction (PCR) screening for NRPS and PKS BGCs and genome mining revealed that at least seven of these marine bacterial isolates should be further investigated for their potential of containing antimicrobial compounds (**Figure 24**).

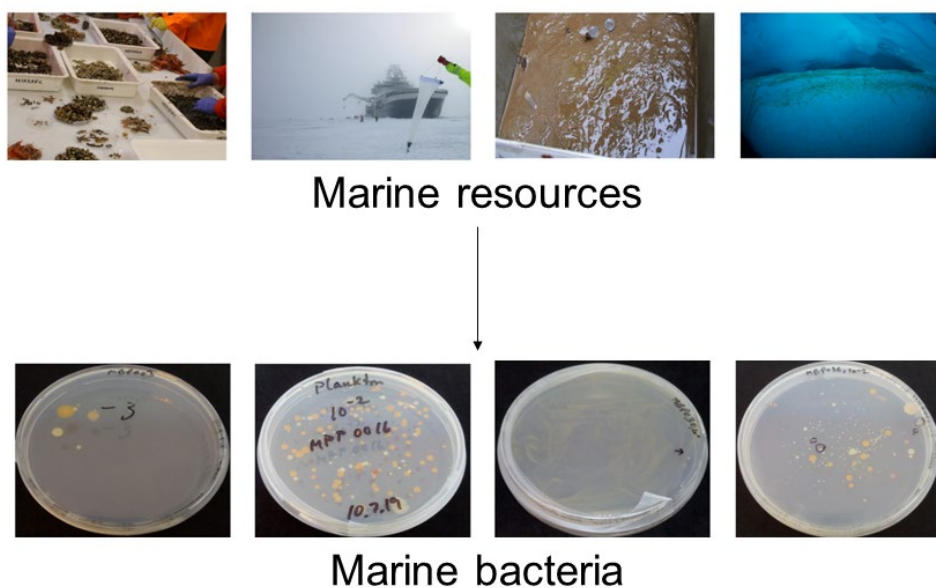


Figure 21. Collection of marine bacteria during a bioprospecting cruise in 2019 in the Arctic region.

5.3 *In vitro* activity assessments

5.3.1 Barbituric acid derivatives – a potential scaffold

Fifty-eight compounds were assessed for antimicrobial potency, indicated by MIC values, and systemic toxicity, reflected in EC_{50} values for haemolysis in the RBC assay. Among the compounds tested, some demonstrated selective activity against Gram-positive strains, while others were effective against both Gram-positive strains and *E. coli*, or against all strains examined. Key trends are highlighted below and in **Figure 22**. Complete MIC data are available in Tables 1-5 in **Paper I**.

In Series 1, (poly)-methylation of primary amines reduced activity against *P. aeruginosa*, likely due to a decreased effective charge on the cationic groups. Previously used amine and guanidine head groups yielded the most comprehensive broad-spectrum activity.

In Series 2 and 3, the antimicrobial potency and haemolytic activity were predominantly affected by the side chains' lipophilicity; greater lipophilicity increased both potency and haemolysis. Side chains with CLogP values over 4.50 resulted in high haemolytic activity and poor solubility. Combining two distinct lipophilic side chains effectively moderated overall lipophilicity.

In Series 4, linkers such as N-pentyl, n-hexyl, cyclobutyl, and cyclohexyl showed high antimicrobial potency but also high haemolytic activity. The n-propyl linker combined with a guanidine head group was the least haemolytic, followed by an ethyl linker with guanidine.

In Series 5, the n-propyl linker and guanidyl cationic group emerged as the optimal combination for broad-spectrum activity. This configuration enabled the creation of barbiturates with identical or diverse lipophilic groups, yielding promising candidates with reduced haemolytic toxicity.

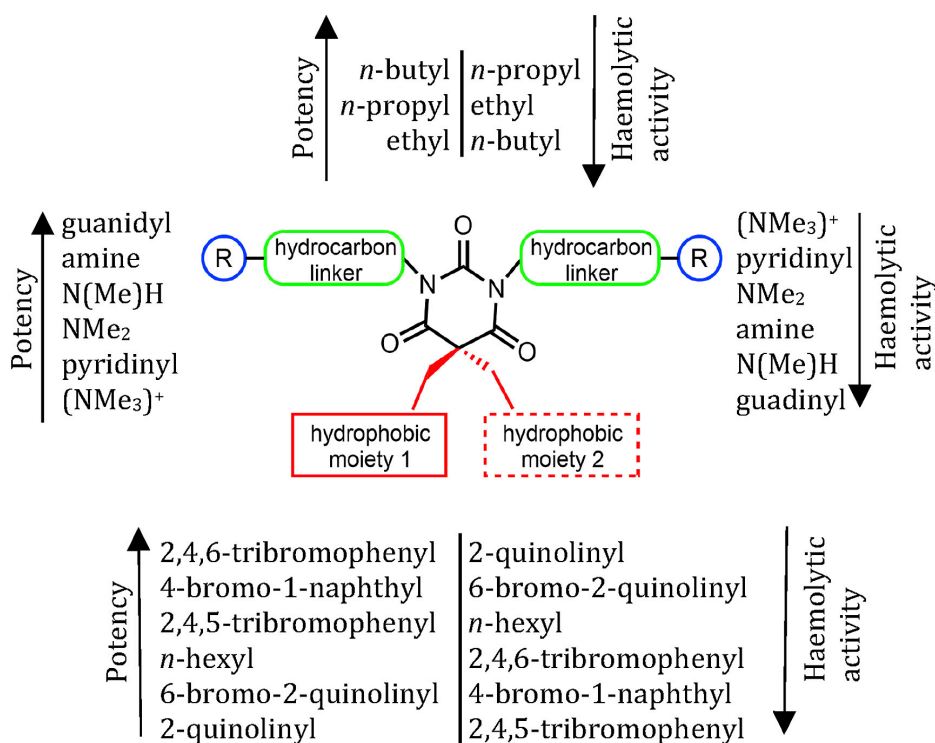


Figure 22. Overview of the general trends observed during the SAR investigation. The trends for haemolytic activity were assessed for the average between the respective amines and guanidines.

Paper I examined 17 narrow-spectrum barbiturates against Gram-positive bacteria and 14 broad-spectrum derivatives against Gram-positive and Gram-negative bacteria. Utilizing the luciferase-based biosensor assays, **paper I** confirmed the concentration-dependent membrane disruption for all tested compounds on *B. subtilis* and *E. coli* cytoplasmic membranes. Additionally, a broad-spectrum barbiturate, 111G (**Paper I**), was assessed using the 1-N-phenyl-naphthylamine (NPN) fluorescent probe to examine its impact on *E. coli*'s outer membrane (OM). Low concentrations (0.8x MIC) increased OM permeability without affecting cell viability. However, at higher concentrations (6.4-12.8x MIC), OM disruption occurred at rates comparable to the inner membrane (IM). These findings indicate a concentration-dependent OM and IM disruption mechanism as the primary antibacterial action.

5.3.2 Hydantoin derivatives – another potential scaffold

Twenty-four compounds were tested for antimicrobial efficacy and haemolysis using assays described in **Paper I** and **II** and a comprehensive data set in **Paper II**, Tables 1 and 2. Thioamides and thioureas rendered compounds less haemolytic and less effective against Gram-negative *P. aeruginosa* or led to instability, as with 5A (**Paper II**). Hydantoin derivatives were generally less haemolytic than 4-imidazolidin-2-ones (3A, **Paper II**) and 2-(hydroxy)-1H-imidazol (15A, **Paper II**). In the hydantoin series, guanidine derivatives were more potent and haemolytic than amine derivatives with an *n*-butyl linker but less so with an *n*-propyl linker, aligning with trends from **Paper I**. All compounds, except 2eA (EC₅₀: 69 µg/mL), had EC₅₀ values over 200 µg/mL.

The investigation into tetrasubstituted amphipathic hydantoin derivatives confirmed their membranolytic properties using a biosensor assay. Thirteen hydantoin derivatives were studied in *B. subtilis*, and six with broad-

spectrum activity in *E. coli*, showing concentration-dependent effects on viability and membrane integrity, with a faster action observed in Gram-positive *B. subtilis*. OM permeability in *E. coli* was assessed with NPN fluorescence, where 6cG (4-Br, 3-Cl) at 0.4x MIC increased OM permeability without affecting viability. At 1.6-3.2x MIC, reduced fluorescence suggested possible rapid OM disruption or an intact OM while viability was reduced. These results imply that OM disruption may occur as swiftly as IM disruption, but further research is required to determine whether high concentrations facilitate translocation across the OM without its disruption.

5.3.3 Antibiofilm activity of barbiturate and hydantoin derivatives

The selection of 44 (**Paper III**) out of 82 synthesized compounds from barbiturate (**Papers I**) and hydantoin (**Papers II**) derivatives for biofilm inhibition studies was addressed on a balance of antimicrobial efficacy, low haemolytic activity, and high selectivity index (SI). Evaluating these compounds on biofilm formation by *S. epidermidis* RP62A and *P. aeruginosa* PAO1 at sub-MIC concentrations showed that six compounds were effective against *S. epidermidis* by inhibiting biofilm formation above 50%. Besides, three compounds inhibited the biofilm formation of *P. aeruginosa* by over 50% (Table S1, **Paper III**).

The data indicated that seven out of eleven compounds achieved over 80% eradication of *S. epidermidis* RP62A biofilms, and four out of ten compounds were effective against *P. aeruginosa* PAO1 biofilms at 5x MIC concentrations (Table S1, **Paper III**).

The lead compounds 13iA and 2cA (**Figure 23**) notably demonstrate exceptional biofilm inhibition at sub-MIC concentrations and eradication capabilities at 5x MIC concentrations against *S. epidermidis* RP62A. Compound 13iA also showed excellent biofilm eradication potential (more than 90%) against *P. aeruginosa* PAO1 at 5x MIC concentrations. These findings suggest a potent therapeutic potential of these compounds in resolving established biofilm infections, which is a critical aspect of treating chronic and device-related infections.

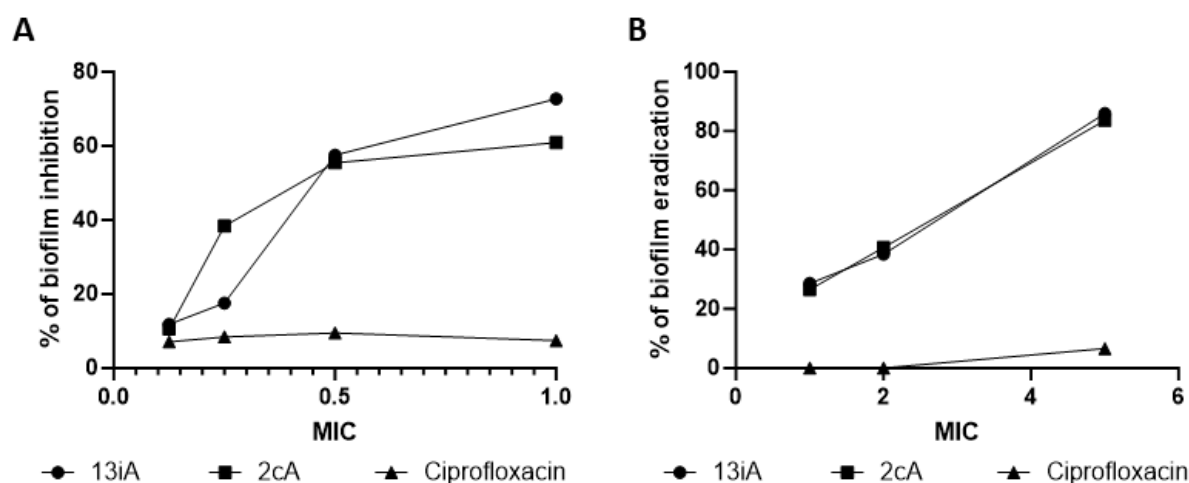


Figure 23. Dose-dependent biofilm inhibition and eradication of compounds 13iA and 2cA against *S. epidermidis* RP62A.

5.3.4 Potential BGCs from marine bacterial isolates

In **Paper IV**, 158 marine bacteria were isolated from various Arctic samples during a 2019 bioprospecting cruise. Co-culture and PCR-based screenings, supplemented by genome sequencing, assessed the potential of BGCs for antimicrobial activity. These bacteria, harvested from benthic invertebrates, sediment from the ocean floor, zooplankton, and biomass from under the sea ice across seven Arctic locations (Figure 9, Figure S1, and Table S1 of **Paper IV**), were evaluated for antimicrobial properties.

Sixty-five isolates inhibited at least one pathogenic strain in a ten human pathogen-related bacteria panel (Tables 1 and Table S3 of **Paper IV**) and five biofilm-forming marine strains (Tables 1 and Table S4 of **Paper IV**). PCR screening using literature-sourced primers (Table S5 of **Paper IV**) identified NRPS or PKS gene clusters in 37 isolates (Table 1 and Table S2 of **Paper IV**). The seven most promising, which contain NRPS or PKS gene clusters and exhibit activity against both Gram-negative and Gram-positive pathogens, belonged to genera *Shewanella* (three isolates), *Pseudomonas* (two), and one each from *Paraglaciecola* and *Pseudoaltermonas* (**Figure 24**).

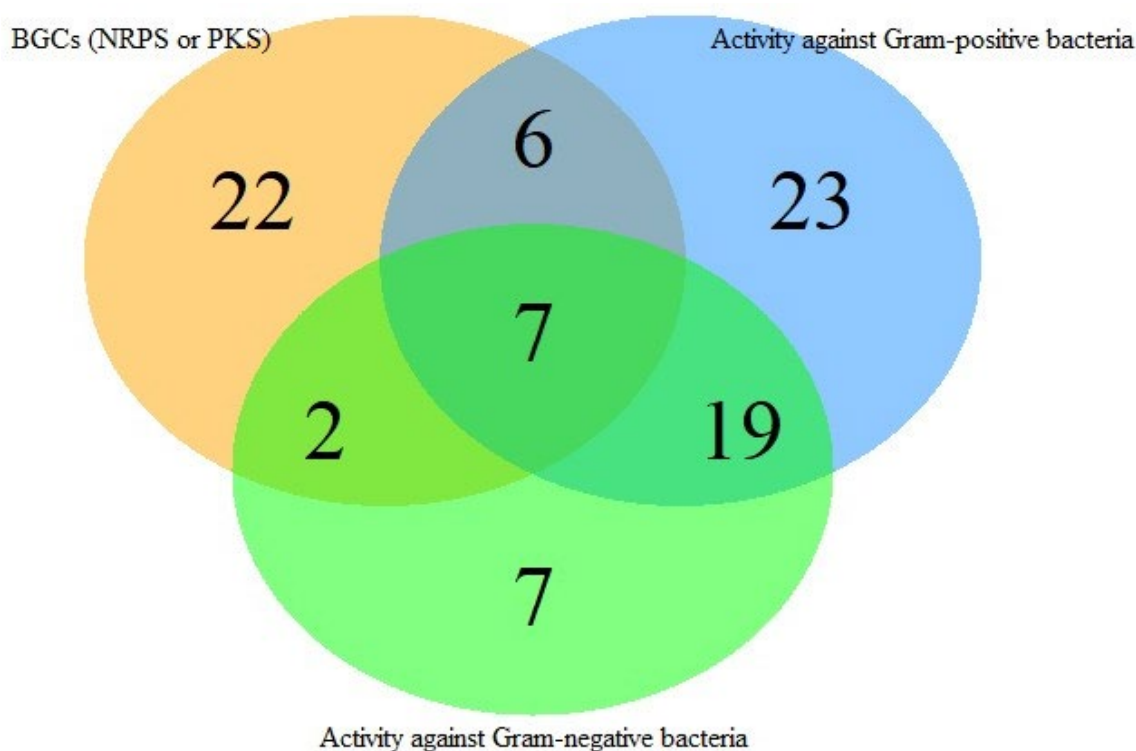


Figure 24. Marine bacterial secondary metabolites (MBSMs) are a potential source of new antimicrobials.

5.4 *In vivo* activity assessments

In **Paper III**, 31 barbiturate and hydantoin derivatives, discussed in **Papers I** and **II**, were selected for zebrafish embryo toxicity studies. Despite the high toxicity observed with the immersion method (Tables S4-S6 of **Paper III**), intrayolk (IY) microinjections of five compounds were non-toxic at 2-8 mg/kg (Table S7 of **Paper III**), aligning with the preclinical dose for this model⁷⁸.

Zebrafish-absorbed molecules tend to be more lipophilic than known drugs, and in most cases, their physiochemical properties fall within a narrow range of values compared to the Lipinski rules⁷⁹. Although the physiochemical properties of our compounds do not fall within a narrow range of values compared to the Lipinski rules (Table S8 of **Paper III**), the amphipathic nature of our compounds could hamper gaseous exchange, which could suffocate the fish, thus explaining our observed toxicity in the immersion method. Consequently, IY injections were employed for subsequent in vivo toxicity and antibacterial efficacy studies⁷⁸.

Zebrafish possess toll-like receptors (TLRs) with high homology to their counterparts in other vertebrates, including humans^{80,81}, and bacterial and viral infections upregulate these TLRs^{81,82}, making zebrafish an excellent infection model. Compounds 13iA and 9 demonstrated significant antibacterial effects against *S. epidermidis* RP62A (Figure 6A and Table S8 of **Paper III**) and 2cA against *S. aureus* (Figure 6B and Table S8 of **Paper III**). Repeated daily dosing proved necessary for infection control, as seen with enhanced survival in *S. aureus*-infected zebrafish treated with compound 9 (**Figure 25**).

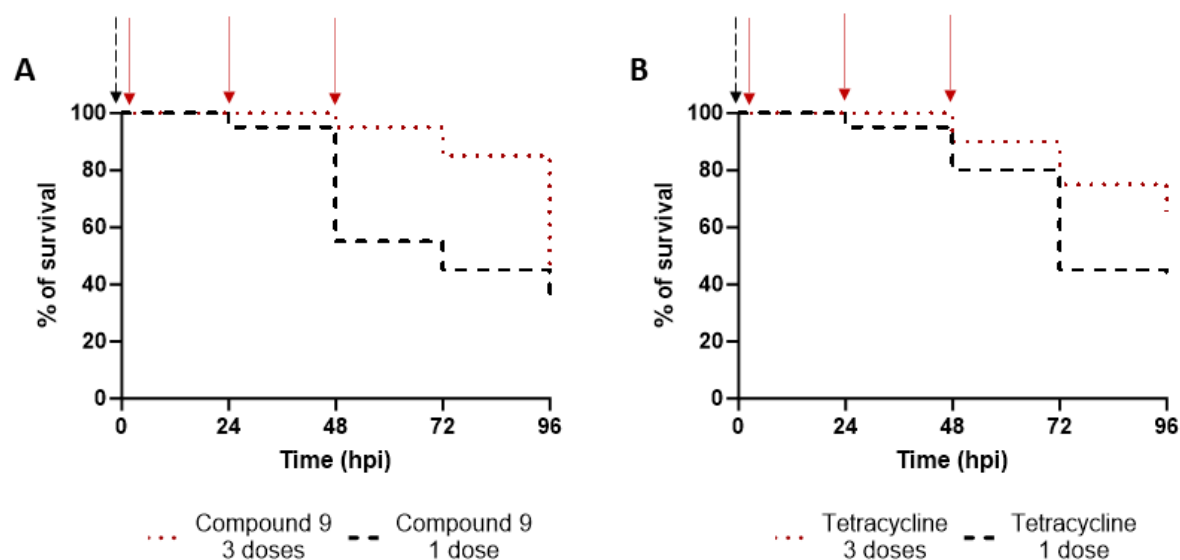


Figure 25. Improved antibacterial activity against *Staphylococcus aureus* when administered in repeated doses daily through IY. **A)** Compound 9. **B)** Positive control, tetracycline.

5.5 Potential outcomes of this AntifoMar project

SMAMPs outperform natural AMPs, displaying increased stability, reduced toxicity, and a broader spectrum of antibacterial action. Researchers are focusing on novel peptidomimetics to tackle diverse and resistant bacterial strains, a critical front against antimicrobial resistance⁸³. Antimicrobial activity against clinical isolates (**Paper III**) highlights that barbiturate (**Paper I**) and hydantoin (**Paper II**) derivatives have the potential to fight resistant bacteria.

SMAMPs can enhance or complement the efficacy of traditional antibiotics. Pt5-1c, for instance, synergistically improved the efficacy of oxacillin against *S. aureus* USA500 and azithromycin against *K. pneumoniae* 2182, with a fractional inhibitory concentration index (FICI) of 0.5 or less, signifying superior bacterial growth inhibition compared to individual treatments⁸⁴. Additionally, Pt5-1c showed

additive effects with vancomycin against *S. aureus* USA500 and with streptomycin against *E. coli* 577, indicated by fractional inhibitory concentration index (FICI) values above 0.5 but at or below 1.0, reflecting a modestly enhanced bacterial growth reduction when used in combination⁸⁴.

Paper III highlights the efficacy of barbiturate (**Paper I**) and hydantoin (**Paper II**) derivatives in targeting biofilm-related infections. In **Paper III**, the compounds 13iA and 2cA significantly inhibit biofilm formation by *S. epidermidis* RP62A at sub-MIC concentrations and can eradicate biofilms at concentrations five times the MIC. Furthermore, 13iA demonstrates over 90% eradication of *P. aeruginosa* PAO1 biofilms at 5x MIC concentrations. Other SMAMPs have similar antibiofilm activity; for example, Pt5-1c exhibits potent antibiofilm activity against three tested MDR bacteria (*S. aureus* USA500, *E. coli* 577, and *K. pneumoniae* 2182)⁸⁴.

AMPs and SMAMPs are increasingly used to coat biomedical implants, with preclinical and clinical research demonstrating their efficacy in preventing implant-associated infections across various animal models⁸⁵.

AMPs and SMAMPs exhibit immunomodulatory effects, such as recruiting and activating immune cells, modulating cytokine production, and promoting wound healing^{86,87}. They recruit various immune cells, including neutrophils, macrophages, and dendritic cells, to infection sites and enhance the bactericidal capabilities of immune cells, like stimulating neutrophils to produce reactive oxygen species⁸⁶. They can also regulate cytokine production, increasing pro-inflammatory cytokines for immune response coordination and anti-inflammatory cytokines to resolve inflammation and prevent tissue damage⁸⁶. Additionally, they support wound healing by stimulating angiogenesis and tissue formation⁸⁶.

There are other applications of AMPs and SMAMPs, such as Pexiganan for diabetic foot ulcers, LL-37 for leg ulcers and rosacea, and iseganan for ventilator-associated pneumonia exemplify peptidomimetics that have progressed to clinical trials, signifying their potential as therapeutic agents⁸³.

On the other hand, marine bacteria, including actinobacteria, streptomyces, and bacillus, are prolific producers of bioactive secondary metabolites^{58,88}. These MBSMs display a spectrum of biological activities—antimicrobial, antifungal, anti-parasitic, anti-cancer, anti-inflammatory, and immunosuppressive—showcasing their potential in diverse therapeutic applications^{58,88}.

Exploiting SMAMPs⁸⁹ and MNPs⁹⁰ as antifouling agents indeed represents a promising avenue toward developing environmentally benign antifouling coatings. Their broad biological activity spectrum, lower environmental impact, and reduced toxicity to non-target marine species enhance their appeal^{89,90}. Continued research and development in this field could yield advanced coatings for a range of marine infrastructure, significantly mitigating biofouling while aligning with environmental sustainability goals^{89,90}.

6 Future perspective

The results obtained in this project should be followed up in further detail, and some of the work is already in progress.

- The assessment of synergistic effects between SMAMPs and antibiotics is a pivotal area of investigation, especially considering increasing antibiotic resistance^{84,91}. Exploring these interactions may reveal effective combination therapies that reduce the required doses of antibiotics, limit toxicity, and mitigate the development of resistance⁹¹. Incorporating these findings into **Paper III** will significantly enhance the paper's contribution to the field, potentially offering new insights into combinatorial treatment strategies.
- Studying the adaptive resistance to SMAMPs and comparing it with that of traditional antibiotics is critical for understanding the long-term efficacy of these compounds. This research will clarify whether SMAMPs retain their effectiveness over time and how quickly bacteria can develop resistance to them compared to conventional antibiotics⁹². Adding these findings to **Paper III** will enrich the discussion on the sustainability of using SMAMPs as a viable alternative or adjunct to existing antimicrobial therapies. Additionally, these findings can be combined with bacteriophage treatment, for example, if there are any resistant bacteria against these SMAMPs or biofilm-related infections, which can be treated with bacteriophage alone or as a combination therapy⁹³⁻⁹⁵.
- In **Papers I and II**, the membranolytic mode of action of these SMAMPs has been demonstrated. However, the possibility of a dual mode of action for SMAMPs is an intriguing aspect that merits further investigation. As seen with the N-terminal fragment of Bac7, concentration-dependent behaviour could reveal alternative intracellular targets at sub-membranolytic levels, such as interactions with proteins like DnaK or ribosomes, which could lead to additional or even more specific antimicrobial mechanisms⁹⁶⁻⁹⁹.
- Certainly, confocal microscopy and flow cytometry offer advanced methodologies to distinguish the effects of SMAMPs on planktonic versus biofilm states of bacteria. Confocal microscopy can provide detailed, three-dimensional images of biofilms, allowing for visualization of the penetration and distribution of SMAMPs within the biofilm matrix^{100,101}. Flow cytometry, conversely, can yield quantitative data on the viability and physiological state of individual bacterial cells within a population, whether in biofilms or planktonic form^{102,103}. Together, these techniques in **Paper III** can elucidate the distinct responses of bacteria in different states to SMAMP treatment, potentially identifying unique susceptibilities of biofilm-associated bacteria that could be exploited for more effective treatment strategies.
- RNA sequencing (RNA-seq) is a powerful tool to study the overall transcriptional response of bacterial cells to SMAMPs, allowing for a thorough assessment of gene expression changes associated with biofilm inhibition and eradication¹⁰⁴⁻¹⁰⁹. By comparing the transcriptomic profiles of biofilm-forming bacteria before and after SMAMP treatment, it is likely to identify which genes and pathways are differentially regulated, thus offering an understanding of the molecular mechanisms supporting the mode of action of SMAMPs¹⁰⁴⁻¹⁰⁹. This evidence can guide the development of targeted strategies to improve the efficacy of SMAMPs and could be a valuable addition to the outcomes of **Paper III**.

- Specific marine bacteria, such as *Shewanella* sp. MBP011.13.1, should be explored to pinpoint antimicrobial compounds and their respective BGCs is an insightful strategy (**Paper IV**). A combination of bioassay-guided fractionation and high-throughput sequencing techniques could be utilized to elucidate these compounds and to identify the gene clusters involved in the biosynthesis of these compounds¹¹⁰. This information can then be exploited for heterologous expression, optimization of production conditions, or even synthetic modification to enhance antimicrobial activity¹¹¹⁻¹¹³. Integrating such findings into the broader context of MBSMs research could significantly advance the field.

7 Conclusions

This project aimed to characterize SMAMPs as antimicrobial and antibiofilm agents and identify the producer of antimicrobial compounds from marine bacteria as MBSMs. Four papers were generated from this part of the project in AntifoMar.

Evaluation of synthetic analogues

Firstly, it was identified how N,N-dialkylated-5,5-disubstituted amphipathic barbiturates' structural components affected the bioactivity (**Paper I**). N-propyl linkers balanced antibacterial potency and haemolytic activity well (*in vitro* toxicity), while n-butyl linkers increased the potency. Guanidyl head groups enhanced the antimicrobial potency, and trimethylated amines were suited for narrow-spectrum use. Notably, compounds 13aG, 13jG, and 13jA outperformed the starting compound 1aG in selectivity.

Secondly, five scaffolds were explored for the antibacterial activity of tetrasubstituted, amphipathic SMAMPs and identified the hydantoin structure as a promising basis for antibacterial leads (**Paper II**). Analysis of derivatives of these hydantoins with various lipophilic side chains, n-alkyl linkers, and cationic groups, and the tetrahalogenated hydantoins demonstrated that 2dA, 6cG, and 6dG were found to be promising leads.

Membrane integrity and bacterial viability studies indicated that compounds like 111G (**Paper I**) disrupted *B. subtilis* cell walls and affected both *E. coli* membranes, suggesting a primary bactericidal mechanism at high concentrations, with a possible secondary mechanism.

Viability and membrane integrity assays indicated an immediate membranolytic effect on *B. subtilis* and *E. coli*, with 6cG rapidly disrupting both *E. coli* membranes simultaneously (**Paper II**).

Both the barbituric acid and hydantoin derivatives demonstrated strong antibiofilm activity, inhibiting formation and clearing established biofilms in a dose-dependent manner against *S. epidermidis* RP62A, *S. epidermidis* 5179-R1, and *P. aeruginosa* PAO1 (**Paper III**). They were effective against antibiotic-resistant Gram-positive bacteria, showing similar MIC values to those for susceptible strains, while for resistant Gram-negative bacteria, MICs were up to four times higher.

The *in vivo* toxicity and antibacterial activity were evaluated using a zebrafish model (**Paper III**). Intrayolk injection at 2-8 mg/kg dose in zebrafish was non-toxic and showed promising *in vivo* antibacterial activity. Compounds 13iA and 9 were notably effective against *S. epidermidis* RP62A, and 2cA against *S. aureus* *in vivo*. For some compounds (9), repeated doses enhanced survival in *S. aureus*-infected zebrafish, indicating a need for consistent treatment for infection control.

Natural products (NPs) from marine bacteria

The study on Arctic marine bacterial isolates (**Paper IV**) identified bioactive marine bacteria for antimicrobial compound discovery using co-culture techniques and genome mining. The most bioactive isolates were obtained from two marine invertebrates (Porifera), zooplankton, under-ice, and sediments (452 m deep).

8 References

- 1 Boyd, N. K., Teng, C. & Frei, C. R. Brief overview of approaches and challenges in new antibiotic development: a focus on drug repurposing. *Frontiers in cellular and infection microbiology* **11**, 684515 (2021).
- 2 Hierink, F., Okiro, E. A., Flahault, A. & Ray, N. The winding road to health: A systematic scoping review on the effect of geographical accessibility to health care on infectious diseases in low-and middle-income countries. *Plos one* **16**, e0244921 (2021).
- 3 Van Der Meer, J. W. The infectious disease challenges of our time. *Frontiers in Public Health* **1**, 7 (2013).
- 4 Kumar Kulabhusan, P., Hussain, B. & Yüce, M. Current perspectives on aptamers as diagnostic tools and therapeutic agents. *Pharmaceutics* **12**, 646 (2020).
- 5 Lee, H.-A., Kung, H.-H., Lee, Y.-J., Chao, J. C., Udayasankaran, J. G., Fan, H.-C., Ng, K.-K., Chang, Y.-K., Kijsanayotin, B. & Marcelo, A. B. Global infectious disease surveillance and case tracking system for COVID-19: development study. *JMIR Medical Informatics* **8**, e20567 (2020).
- 6 Wang, P.-W., Lee, W.-T., Wu, Y.-N. & Shieh, D.-B. Opportunities for Nanomedicine in Clostridioides difficile Infection. *Antibiotics* **10**, 948 (2021).
- 7 Archibald, M. M., Rizal, B., Connolly, T., Burns, M. J., Naughton, M. J. & Chiles, T. C. A nanocoaxial-based electrochemical sensor for the detection of cholera toxin. *Biosensors and Bioelectronics* **74**, 406-410 (2015).
- 8 Cui, F., Zhou, Z. & Zhou, H. S. Molecularly imprinted polymers and surface imprinted polymers based electrochemical biosensor for infectious diseases. *Sensors* **20**, 996 (2020).
- 9 Halasa, T. & Dürr, S. Modeling disease spread and control. **4**, 199 (2017).
- 10 Wang, Y. & Liu, G. Dynamics Analysis for a Stochastic SIRI Model Incorporating Media Coverage. *Mathematical Problems in Engineering* **2022** (2022).
- 11 Smith, K. F., Goldberg, M., Rosenthal, S., Carlson, L., Chen, J., Chen, C. & Ramachandran, S. Global rise in human infectious disease outbreaks. *Journal of the Royal Society Interface* **11**, 20140950 (2014).
- 12 Baker, R. E., Mahmud, A. S., Miller, I. F., Rajeev, M., Rasambainarivo, F., Rice, B. L., Takahashi, S., Tatem, A. J., Wagner, C. E. & Wang, L.-F. Infectious disease in an era of global change. *Nature Reviews Microbiology* **20**, 193-205 (2022).
- 13 Kim, J., Mohamed, M. A. A., Zagorovsky, K. & Chan, W. C. State of diagnosing infectious pathogens using colloidal nanomaterials. *Biomaterials* **146**, 97-114 (2017).
- 14 Chioro, A., Coll-Seck, A. M., Høie, B., Moeloek, N., Motsoaledi, A., Rajatanavin, R. & Touraine, M. Antimicrobial resistance: a priority for global health action. *Bull World Health Organ* **93**, 439-439 (2015).
- 15 Murray, C. J., Ikuta, K. S., Sharara, F., Swetschinski, L., Aguilar, G. R., Gray, A., Han, C., Bisignano, C., Rao, P. & Wool, E. Global burden of bacterial antimicrobial resistance in 2019: a systematic analysis. *The Lancet* **399**, 629-655 (2022).
- 16 Marathe, N. P., Grevskott, D. H., Salva-Serra, F., Nimje, P. S., Svanevik, C. S., Lunestad, B. T. & Moore, E. R. Seawater from Bergen harbor is a reservoir of conjugative multidrug-resistance plasmids carrying genes for virulence. *International Journal of Hygiene and Environmental Health* **248**, 114108 (2023).

- 17 Collignon, P., Beggs, J. J., Walsh, T. R., Gandra, S. & Laxminarayan, R. Anthropological and socioeconomic factors contributing to global antimicrobial resistance: a univariate and multivariable analysis. *The Lancet Planetary Health* **2**, e398-e405 (2018).
- 18 Codjoe, F. S. & Donkor, E. S. Carbapenem resistance: a review. *Medical Sciences* **6**, 1 (2017).
- 19 Cook, M. A. & Wright, G. D. The past, present, and future of antibiotics. *Science Translational Medicine* **14**, eabo7793 (2022).
- 20 Nadeem, S. F., Gohar, U. F., Tahir, S. F., Mukhtar, H., Pornpukdeewattana, S., Nukthamna, P., Moula Ali, A. M., Bavisetty, S. C. B. & Massa, S. Antimicrobial resistance: more than 70 years of war between humans and bacteria. *Critical Reviews in Microbiology* **46**, 578-599 (2020).
- 21 Carlet, J., Collignon, P., Goldmann, D., Goossens, H., Gyssens, I. C., Harbarth, S., Jarlier, V., Levy, S. B., N'Doye, B. & Pittet, D. Society's failure to protect a precious resource: antibiotics. *The Lancet* **378**, 369-371 (2011).
- 22 Llor, C. & Bjerrum, L. Antimicrobial resistance: risk associated with antibiotic overuse and initiatives to reduce the problem. *Therapeutic advances in drug safety* **5**, 229-241 (2014).
- 23 Marshall, B. M. & Levy, S. B. Food animals and antimicrobials: impacts on human health. *Clinical microbiology reviews* **24**, 718-733 (2011).
- 24 Phillips, C. J., Wisdom, A. J., McKinnon, R. A., Woodman, R. J. & Gordon, D. L. Interventions targeting the prescribing and monitoring of vancomycin for hospitalized patients: a systematic review protocol. *Infectious Diseases and Therapy* **6**, 557-563 (2017).
- 25 Ayukekbong, J. A., Ntemgwa, M. & Atabe, A. N. The threat of antimicrobial resistance in developing countries: causes and control strategies. *Antimicrobial Resistance & Infection Control* **6**, 1-8 (2017).
- 26 Iskandar, K., Molinier, L., Hallit, S., Sartelli, M., Hardcastle, T. C., Haque, M., Lugova, H., Dhingra, S., Sharma, P. & Islam, S. Surveillance of antimicrobial resistance in low-and middle-income countries: a scattered picture. *Antimicrobial Resistance & Infection Control* **10**, 1-19 (2021).
- 27 Wu, Y., Wang, B., Lu, H., Zhao, H., Yang, B., Li, L., Lu, Y., Zhang, D., Sun, N. & Huang, H. Identification of novel tricyclic benzo [1, 3] oxazinyloxazolidinones as potent antibacterial agents with excellent pharmacokinetic profiles against drug-resistant pathogens. *Journal of Medicinal Chemistry* **64**, 3234-3248 (2021).
- 28 Reid, G. Biofilms in infectious disease and on medical devices. *International journal of antimicrobial agents* **11**, 223-226 (1999).
- 29 Fisher, L. E., Yang, Y., Yuen, M.-F., Zhang, W., Nobbs, A. H. & Su, B. Bactericidal activity of biomimetic diamond nanocone surfaces. *Biointerphases* **11** (2016).
- 30 Iseppi, R., Di Cerbo, A., Aloisi, P., Manelli, M., Pellesi, V., Provenzano, C., Camellini, S., Messi, P. & Sabia, C. In vitro activity of essential oils against planktonic and biofilm cells of extended-spectrum β -lactamase (ESBL)/carbapenemase-producing gram-negative bacteria involved in human nosocomial infections. *Antibiotics* **9**, 272 (2020).
- 31 Torres, M. D. T. & de la Fuente-Nunez, C. Reprogramming biological peptides to combat infectious diseases. *Chemical Communications* **55**, 15020-15032 (2019).
- 32 Sharma, D., Misba, L. & Khan, A. U. Antibiotics versus biofilm: an emerging battleground in microbial communities. *Antimicrobial Resistance & Infection Control* **8**, 1-10 (2019).
- 33 Hall, C. W. & Mah, T.-F. Molecular mechanisms of biofilm-based antibiotic resistance and tolerance in pathogenic bacteria. *FEMS microbiology reviews* **41**, 276-301 (2017).
- 34 Hutchings, M. I., Truman, A. W. & Wilkinson, B. Antibiotics: past, present and future. *Current opinion in microbiology* **51**, 72-80 (2019).

- 35 Wasan, H., Singh, D., Reeta, K. & Gupta, Y. K. Landscape of Push Funding in Antibiotic Research: Current Status and Way Forward. *Biology* **12**, 101 (2023).
- 36 Regen, S. L. Improving the cellular selectivity of a membrane-disrupting antimicrobial agent by monomer control and by taming. *Molecules* **26**, 374 (2021).
- 37 Zhu, Y., Cleaver, L., Wang, W., Podoll, J. D., Walls, S., Jolly, A. & Wang, X. Tetracyclic indolines as a novel class of β -lactam-selective resistance-modifying agent for MRSA. *European journal of medicinal chemistry* **125**, 130-142 (2017).
- 38 Vynne, N. G., Mansson, M. & Gram, L. Gene sequence based clustering assists in dereplication of *Pseudoalteromonas luteoviolacea* strains with identical inhibitory activity and antibiotic production. *Marine Drugs* **10**, 1729-1740 (2012).
- 39 Karthikeyan, A., Joseph, A. & Nair, B. G. Promising bioactive compounds from the marine environment and their potential effects on various diseases. *Journal of Genetic Engineering and Biotechnology* **20**, 1-38 (2022).
- 40 Ameen, F., AlNadhari, S. & Al-Homaidan, A. A. Marine microorganisms as an untapped source of bioactive compounds. *Saudi Journal of Biological Sciences* **28**, 224-231 (2021).
- 41 Wibowo, J. T., Bayu, A., Aryati, W. D., Fernandes, C., Yanuar, A., Kijjoa, A. & Putra, M. Y. Secondary Metabolites from Marine-Derived Bacteria with Antibiotic and Antibiofilm Activities against Drug-Resistant Pathogens. *Marine Drugs* **21**, 50 (2023).
- 42 Stincone, P. & Brandelli, A. Marine bacteria as source of antimicrobial compounds. *Critical reviews in biotechnology* **40**, 306-319 (2020).
- 43 Lo Giudice, A. & Rizzo, C. Bacteria associated with marine benthic invertebrates from polar environments: unexplored frontiers for biodiscovery? *Diversity* **10**, 80 (2018).
- 44 Katz, L. & Baltz, R. H. Natural product discovery: past, present, and future. *Journal of Industrial Microbiology and Biotechnology* **43**, 155-176 (2016).
- 45 Newman, D. J. & Cragg, G. M. Natural products as sources of new drugs over the nearly four decades from 01/1981 to 09/2019. *Journal of natural products* **83**, 770-803 (2020).
- 46 Needham, J., Andersen, R. J. & Kelly, M. T. Biosynthesis of oncorhyncolide, a metabolite of the seawater bacterial isolate MK 157. *Journal of the Chemical Society, Chemical Communications*, 1367-1369 (1992).
- 47 Oberhofer, M., Wackerlig, J., Zehl, M., Büyük, H., Cao, J. J., Prado-Roller, A., Urban, E. & Zotchev, S. B. Endophytic *Akanthomyces* sp. LN303 from Edelweiss produces emestrin and two new 2-hydroxy-4 pyridone alkaloids. *ACS omega* **6**, 2184-2191 (2021).
- 48 Weissman, K. J. The structural biology of biosynthetic megaenzymes. *Nature Chemical Biology* **11**, 660-670 (2015).
- 49 Wang, W., Park, K.-H., Lee, J., Oh, E., Park, C., Kang, E., Lee, J. & Kang, H. A New Thiopeptide Antibiotic, micrococcin P3, from a marine-derived Strain of the bacterium *Bacillus stratosphericus*. *Molecules* **25**, 4383 (2020).
- 50 Schinke, C., Martins, T., Queiroz, S. C., Melo, I. S. & Reyes, F. G. Antibacterial compounds from marine bacteria, 2010–2015. *Journal of natural products* **80**, 1215-1228 (2017).
- 51 Romano, G., Almeida, M., Varela Coelho, A., Cutignano, A., Gonçalves, L. G., Hansen, E., Khnykin, D., Mass, T., Ramšak, A. & Rocha, M. S. Biomaterials and bioactive natural products from marine invertebrates: From basic research to innovative applications. *Marine Drugs* **20**, 219 (2022).
- 52 Leal, M. C., Puga, J., Serodio, J., Gomes, N. C. & Calado, R. Trends in the discovery of new marine natural products from invertebrates over the last two decades—where and what are we bioprospecting? *PLoS One* **7**, e30580 (2012).

- 53 Lebar, M. D., Heimbegner, J. L. & Baker, B. J. Cold-water marine natural products. *Natural Product Reports* **24**, 774-797 (2007).
- 54 Sharp, J. H., Winson, M. K. & Porter, J. S. Bryozoan metabolites: an ecological perspective. *Natural Product Reports* **24**, 659-673 (2007).
- 55 Tadesse, M., Tabudravu, J. N., Jaspars, M., Strøm, M. B., Hansen, E., Andersen, J. H., Kristiansen, P. E. & Haug, T. The antibacterial ent-eusynstyelamide B and eusynstyelamides D, E, and F from the Arctic bryozoan *Tegella* cf. *spitzbergensis*. *Journal of natural products* **74**, 837-841 (2011).
- 56 Tapiolas, D. M., Bowden, B. F., Abou-Mansour, E., Willis, R. H., Doyle, J. R., Muirhead, A. N., Liptrot, C., Llewellyn, L. E., Wolff, C. W. & Wright, A. D. Eusynstyelamides A, B, and C, nNOS inhibitors, from the ascidian *Eusynstyela latericius*. *Journal of natural products* **72**, 1115-1120 (2009).
- 57 Diamond, G., Beckloff, N., Weinberg, A. & Kisich, K. O. The roles of antimicrobial peptides in innate host defense. *Current pharmaceutical design* **15**, 2377-2392 (2009).
- 58 Browne, K., Chakraborty, S., Chen, R., Willcox, M. D., Black, D. S., Walsh, W. R. & Kumar, N. A new era of antibiotics: the clinical potential of antimicrobial peptides. *International journal of molecular sciences* **21**, 7047 (2020).
- 59 Ganz, T. & Lehrer, R. I. Antibiotic peptides from higher eukaryotes: biology and applications. *Molecular medicine today* **5**, 292-297 (1999).
- 60 Hof, W. v. t., Veerman, E. C., Helmerhorst, E. J. & Amerongen, A. V. N. Antimicrobial peptides: properties and applicability. *Biological Chemistry* **382**, 597 – 619 (2001).
- 61 Chen, C. H. & Lu, T. K. Development and challenges of antimicrobial peptides for therapeutic applications. *Antibiotics* **9**, 24 (2020).
- 62 Guo, X., Yan, T., Rao, J., Yue, X., Pei, X., Deng, J., Sun, W., Yang, W., Zhang, B. & Xie, J. Potent Antimicrobial and Antibiofilm Activities of Feleucin-K3 Analogs Modified by α -(4-Pentenyl)-Ala against Multidrug-Resistant Bacteria. *Biomolecules* **11**, 761 (2021).
- 63 Alves Ferreira, D., Martins, L. M., Fernandes, A. R. & Martins, M. A tale of two ends: repurposing metallic compounds from anti-tumour agents to effective antibacterial activity. *Antibiotics* **9**, 321 (2020).
- 64 Huan, Y., Kong, Q., Mou, H. & Yi, H. Antimicrobial peptides: classification, design, application and research progress in multiple fields. *Frontiers in microbiology* **11**, 2559 (2020).
- 65 Laverty, G., Gorman, S. P. & Gilmore, B. F. The potential of antimicrobial peptides as biocides. *International journal of molecular sciences* **12**, 6566-6596 (2011).
- 66 Marcoléfas, E., Leung, T., Okshevsky, M., McKay, G., Hignett, E., Hamel, J., Aguirre, G., Blenner-Hassett, O., Boyle, B. & Lévesque, R. C. Culture-dependent bioprospecting of bacterial isolates from the Canadian high Arctic displaying antibacterial activity. *Frontiers in microbiology* **10**, 1836 (2019).
- 67 Kodzius, R. & Gojobori, T. Marine metagenomics as a source for bioprospecting. *Marine genomics* **24**, 21-30 (2015).
- 68 Ward, D. M., Weller, R. & Bateson, M. M. 16S rRNA sequences reveal numerous uncultured microorganisms in a natural community. *Nature* **345**, 63-65 (1990).
- 69 Elvheim, A. I., Li, C. & Landfald, B. Conservation of Genomic Information in Multiple Displacement Amplified Low-Quantity Metagenomic Material from Marine Invertebrates. *Marine Drugs* **21**, 165 (2023).
- 70 Vartoukian, S. R., Palmer, R. M. & Wade, W. G. Strategies for culture of ‘unculturable’ bacteria. *FEMS microbiology letters* **309**, 1-7 (2010).

- 71 Peng, X.-Y., Wu, J.-T., Shao, C.-L., Li, Z.-Y., Chen, M. & Wang, C.-Y. Co-culture: Stimulate the metabolic potential and explore the molecular diversity of natural products from microorganisms. *Marine Life Science & Technology*, 1-12 (2021).
- 72 Romano, S., Jackson, S. A., Patry, S. & Dobson, A. D. Extending the “one strain many compounds”(OSMAC) principle to marine microorganisms. *Marine drugs* **16**, 244 (2018).
- 73 Schwarz, J., Hubmann, G., Rosenthal, K. & Lütz, S. Triaging of culture conditions for enhanced secondary metabolite diversity from different bacteria. *Biomolecules* **11**, 193 (2021).
- 74 Srinivasan, R., Kannappan, A., Shi, C. & Lin, X. Marine bacterial secondary metabolites: A treasure house for structurally unique and effective antimicrobial compounds. *Marine Drugs* **19**, 530 (2021).
- 75 Cardoso, P., Glossop, H., Meikle, T. G., Aburto-Medina, A., Conn, C. E., Sarojini, V. & Valery, C. Molecular engineering of antimicrobial peptides: Microbial targets, peptide motifs and translation opportunities. *Biophysical reviews* **13**, 35-69 (2021).
- 76 Torres, M. D., Pedron, C. N., Higashikuni, Y., Kramer, R. M., Cardoso, M. H., Oshiro, K. G., Franco, O. L., Silva Junior, P. I., Silva, F. D. & Oliveira Junior, V. X. Structure-function-guided exploration of the antimicrobial peptide polybia-CP identifies activity determinants and generates synthetic therapeutic candidates. *Communications biology* **1**, 221 (2018).
- 77 Paulsen, M. H., Engqvist, M., Ausbacher, D., Anderssen, T., Langer, M. K., Haug, T., Morello, G. R., Liikanen, L. E., Blencke, H.-M. & Isaksson, J. Amphipathic barbiturates as mimics of antimicrobial peptides and the marine natural products eusynstyelamides with activity against multi-resistant clinical isolates. *Journal of Medicinal Chemistry* **64**, 11395-11417 (2021).
- 78 Guarin, M., Ny, A., De Croze, N., Maes, J., Léonard, M., Annaert, P. & de Witte, P. A. Pharmacokinetics in zebrafish embryos (Zfe) following immersion and intrayolk administration: A fluorescence-based analysis. *Pharmaceuticals* **14**, 576 (2021).
- 79 Long, K., Kostman, S. J., Fernandez, C., Burnett, J. C. & Huryn, D. M. Do zebrafish obey lipinski rules? *ACS Medicinal Chemistry Letters* **10**, 1002-1006 (2019).
- 80 Jault, C., Pichon, L. & Chluba, J. Toll-like receptor gene family and TIR-domain adapters in *Danio rerio*. *Molecular immunology* **40**, 759-771 (2004).
- 81 Meijer, A. H., Krens, S. G., Rodriguez, I. A. M., He, S., Bitter, W., Snaar-Jagalska, B. E. & Spaik, H. P. Expression analysis of the Toll-like receptor and TIR domain adaptor families of zebrafish. *Molecular immunology* **40**, 773-783 (2004).
- 82 Phelan, P. E., Mellon, M. T. & Kim, C. H. Functional characterization of full-length TLR3, IRAK-4, and TRAF6 in zebrafish (*Danio rerio*). *Molecular immunology* **42**, 1057-1071 (2005).
- 83 Molchanova, N., Hansen, P. R. & Franzyk, H. Advances in development of antimicrobial peptidomimetics as potential drugs. *Molecules* **22**, 1430 (2017).
- 84 Duan, H., Zhang, X., Li, Z., Yuan, J., Shen, F. & Zhang, S. Synergistic effect and antibiofilm activity of an antimicrobial peptide with traditional antibiotics against multi-drug resistant bacteria. *Microbial Pathogenesis* **158**, 105056 (2021).
- 85 Drexelius, M. G. & Neundorff, I. Application of antimicrobial peptides on biomedical implants: Three ways to pursue peptide coatings. *International Journal of Molecular Sciences* **22**, 13212 (2021).
- 86 Anbarasu, A. Antimicrobial peptides as Immunomodulators and Antimycobacterial agents to combat *Mycobacterium tuberculosis*: a critical review. *Probiotics and Antimicrobial Proteins*, 1-28 (2022).

- 87 Skovbakke, S. L., Holdfeldt, A., Forsman, H., Bylund, J. & Franzyk, H. The role of formyl peptide receptors for immunomodulatory activities of antimicrobial peptides and peptidomimetics. *Current pharmaceutical design* **24**, 1100-1120 (2018).
- 88 Al-Shaibani, M. M., Radin Mohamed, R. M. S., Sidik, N. M., Enshasy, H. A. E., Al-Gheethi, A., Noman, E., Al-Mekhlafi, N. A. & Zin, N. M. Biodiversity of secondary metabolites compounds isolated from phylum actinobacteria and its therapeutic applications. *Molecules* **26**, 4504 (2021).
- 89 Saha, R., Bhattacharya, D. & Mukhopadhyay, M. Advances in modified antimicrobial peptides as marine antifouling material. *Colloids and Surfaces B: Biointerfaces*, 112900 (2022).
- 90 Liu, L.-L., Wu, C.-H. & Qian, P.-Y. Marine natural products as antifouling molecules—a mini-review (2014–2020). *Biofouling* **36**, 1210-1226 (2020).
- 91 Wu, X., Li, Z., Li, X., Tian, Y., Fan, Y., Yu, C., Zhou, B., Liu, Y., Xiang, R. & Yang, L. Synergistic effects of antimicrobial peptide DP7 combined with antibiotics against multidrug-resistant bacteria. *Drug design, development and therapy*, 939-946 (2017).
- 92 Som, A., Vemparala, S., Ivanov, I. & Tew, G. N. Synthetic mimics of antimicrobial peptides. *Peptide Science* **90**, 83-93 (2008).
- 93 Li, X., He, Y., Wang, Z., Wei, J., Hu, T., Si, J., Tao, G., Zhang, L., Xie, L. & Abdalla, A. E. A combination therapy of Phages and Antibiotics: Two is better than one. *International Journal of Biological Sciences* **17**, 3573 (2021).
- 94 Osman, A.-H., Kotey, F. C., Odoom, A., Darkwah, S., Yeboah, R. K., Dayie, N. T. & Donkor, E. S. The potential of bacteriophage-antibiotic combination therapy in treating infections with multidrug-resistant bacteria. *Antibiotics* **12**, 1329 (2023).
- 95 Akturk, E., Melo, L. D., Oliveira, H., Crabbé, A., Coenye, T. & Azeredo, J. Combining phages and antibiotic to enhance antibiofilm efficacy against an in vitro dual species wound biofilm. *Biofilm* **6**, 100147 (2023).
- 96 Graf, M., Mardirossian, M., Nguyen, F., Seefeldt, A. C., Guichard, G., Scocchi, M., Innis, C. A. & Wilson, D. N. Proline-rich antimicrobial peptides targeting protein synthesis. *Natural product reports* **34**, 702-711 (2017).
- 97 Podda, E., Benincasa, M., Pacor, S., Micali, F., Mattiuzzo, M., Gennaro, R. & Scocchi, M. Dual mode of action of Bac7, a proline-rich antibacterial peptide. *Biochimica et Biophysica Acta (BBA)-General Subjects* **1760**, 1732-1740 (2006).
- 98 Scocchi, M., Lüthy, C., Decarli, P., Mignogna, G., Christen, P. & Gennaro, R. The proline-rich antibacterial peptide Bac7 binds to and inhibits in vitro the molecular chaperone DnaK. *International Journal of Peptide Research and Therapeutics* **15**, 147-155 (2009).
- 99 Mardirossian, M., Grzela, R., Giglione, C., Meinel, T., Gennaro, R., Mergaert, P. & Scocchi, M. The host antimicrobial peptide Bac71-35 binds to bacterial ribosomal proteins and inhibits protein synthesis. *Chemistry & biology* **21**, 1639-1647 (2014).
- 100 Reichhardt, C. & Parsek, M. R. Confocal laser scanning microscopy for analysis of *Pseudomonas aeruginosa* biofilm architecture and matrix localization. *Frontiers in microbiology* **10**, 677 (2019).
- 101 Schlafer, S. & Meyer, R. L. Confocal microscopy imaging of the biofilm matrix. *Journal of microbiological methods* **138**, 50-59 (2017).
- 102 Gelle, M., Jacquelin, L. & Choisy, C. in *Annales Pharmaceutiques Françaises*. 243-252.
- 103 Khomtchouk, K., Weglarz, M., Bekale, L., Koliesnik, I., Bollyky, P. & Santa Maria, P. Quantitative assessment of bacterial growth phase utilizing flow cytometry. *Journal of microbiological methods* **167**, 105760 (2019).

- 104 Zhao, X., Liu, Z., Liu, Z., Meng, R., Shi, C., Chen, X., Bu, X. & Guo, N. Phenotype and RNA-seq-Based transcriptome profiling of *Staphylococcus aureus* biofilms in response to tea tree oil. *Microbial Pathogenesis* **123**, 304-313 (2018).
- 105 Abouelhassan, Y., Zhang, Y., Jin, S. & Huigens III, R. W. Transcript profiling of MRSA biofilms treated with a halogenated phenazine eradicating agent: a platform for defining cellular targets and pathways critical to biofilm survival. *Angewandte Chemie International Edition* **57**, 15523-15528 (2018).
- 106 Tan, X., Qin, N., Wu, C., Sheng, J., Yang, R., Zheng, B., Ma, Z., Liu, L., Peng, X. & Jia, A. Transcriptome analysis of the biofilm formed by methicillin-susceptible *Staphylococcus aureus*. *Scientific reports* **5**, 11997 (2015).
- 107 Qin, N., Tan, X., Jiao, Y., Liu, L., Zhao, W., Yang, S. & Jia, A. RNA-Seq-based transcriptome analysis of methicillin-resistant *Staphylococcus aureus* biofilm inhibition by ursolic acid and resveratrol. *Scientific reports* **4**, 5467 (2014).
- 108 Song, Z.-M., Zhang, J.-L., Zhou, K., Yue, L.-M., Zhang, Y., Wang, C.-Y., Wang, K.-L. & Xu, Y. Anthraquinones as potential antibiofilm agents against methicillin-resistant *Staphylococcus aureus*. *Frontiers in Microbiology* **12**, 709826 (2021).
- 109 She, P., Luo, Z., Chen, L. & Wu, Y. Efficacy of levofloxacin against biofilms of *Pseudomonas aeruginosa* isolated from patients with respiratory tract infections in vitro. *Microbiologyopen* **8**, e00720 (2019).
- 110 Pfeiffer, F., Schneider, Y. K.-H., Hansen, E. H., Andersen, J. H., Isaksson, J., Busche, T., Rückert, C., Kalinowski, J., Zyl, L. v. & Trindade, M. Bioassay-Guided Fractionation Leads to the Detection of Cholic Acid Generated by the Rare *Thalassomonas* sp. *Marine Drugs* **21**, 2 (2022).
- 111 Baiden, N., Gandini, C., Goddard, P. & Sayanova, O. Heterologous expression of antimicrobial peptides S-thanatin and bovine lactoferricin in the marine diatom *Phaeodactylum tricorutum* enhances native antimicrobial activity against Gram-negative bacteria. *Algal Research* **69**, 102927 (2023).
- 112 Zhan, N., Zhang, L., Yang, H., Zheng, Y., Wei, X., Wang, J. & Shan, A. Design and heterologous expression of a novel dimeric LL37 variant in *Pichia pastoris*. *Microbial Cell Factories* **20**, 1-13 (2021).
- 113 Hoelscher, M. P., Forner, J., Calderone, S., Krämer, C., Taylor, Z., Loiacono, F. V., Agrawal, S., Karcher, D., Moratti, F. & Kroop, X. Expression strategies for the efficient synthesis of antimicrobial peptides in plastids. *Nature communications* **13**, 5856 (2022).

Paper I



Contents lists available at ScienceDirect

European Journal of Medicinal Chemistry

journal homepage: www.elsevier.com/locate/ejmech

A concise SAR-analysis of antimicrobial cationic amphipathic barbiturates for an improved activity-toxicity profile

Manuel K. Langer^{a,1}, Aatur Rahman^{b,1}, Hymonti Dey^b, Trude Anderssen^c, Francesco Zilioli^a, Tor Haug^b, Hans-Matti Blencke^b, Klara Stensvåg^b, Morten B. Strøm^{c,**}, Annette Bayer^{a,*}

^a Department of Chemistry, UiT The Arctic University of Norway, NO-9037, Tromsø, Norway

^b The Norwegian College of Fishery Science, Faculty of Biosciences, Fisheries and Economics, UiT The Arctic University of Norway, NO-9037, Tromsø, Norway

^c Department of Pharmacy, Faculty of Health Sciences, UiT The Arctic University of Norway, NO-9037, Tromsø, Norway

ARTICLE INFO

Keywords:

Antibacterial
Barbiturates
Peptidomimetics
SMAMPs
Synthetic mimics of antimicrobial peptides

ABSTRACT

An amphipathic barbiturate mimic of the marine eusynstyelamides is reported as a promising class of antimicrobial agents. We hereby report a detailed analysis of the structure-activity relationship for cationic amphipathic *N,N'*-dialkylated-5,5-disubstituted barbiturates. The influence of various cationic groups, hydrocarbon linkers and lipophilic side chains on the compounds' antimicrobial potency and haemolytic activity was studied. A comprehensive library of 58 compounds was prepared using a concise synthetic strategy. We found cationic amine and guanidyl groups to yield the highest broad-spectrum activity and cationic trimethylated quaternary amine groups to exert narrow-spectrum activity against Gram-positive bacteria. *n*-Propyl hydrocarbon linkers proved to be the best compromise between potency and haemolytic activity. The combination of two different lipophilic side chains allowed for further fine-tuning of the biological properties. Using these insights, we were able to prepare both, the potent narrow-spectrum barbiturate **8a** and the broad-spectrum barbiturates **111G**, **13jA** and **13jG**, all having low or no haemolytic activity. The guanidine derivative **111G** demonstrated a strong membrane disrupting effect in luciferase-based assays. We believe that these results may be valuable in further development of antimicrobial lead structures.

1. Introduction

Since the golden age of antibiotics, the developing rate of new agents has decreased notably, while antimicrobial resistance (AMR) has been rising to a global threat [1]. The prominence of this problem is well demonstrated by the World Health Organization (WHO) enacting a global action plan on fighting antimicrobial resistance [2]. While the action plan is focusing on a framework at many different levels, the need for potent antimicrobials stays. As the antibiotics employed for decades start to lose activity against resistant bacteria, several alternative approaches have been investigated. Among these are combination therapy [3,4], bacteriophage therapy [5], photodynamic therapy [6], antibacterial antibodies [7], phytochemicals [5], nanoparticles [8] and antimicrobial peptides [9,10].

From the above stated list, the short, cationic antimicrobial peptides (AMPs) are an intriguing class of compounds. They constitute the first

line of host defense in virtually all eukaryotic species including plants, mammals, insects, etc. [11] They generally feature between 20 and 50% hydrophobic residues and have an overall positive charge (+2 to +9) at neutral pH [12–14]. Their amphipathic nature is the basis of their most common mode of action, to permeabilize bacterial membranes. AMPs attach to the negatively charged cytoplasmic membrane by electrostatic interactions and subsequently disrupt the apolar bilayer with their hydrophobic part [15]. It is believed that due to these non-specific interactions, bacterial resistance is less likely to be induced [16]. This makes AMPs a promising group of compounds despite their generally lower activity compared to marketed antibiotics [17].

Despite these promising properties, the clinical application of peptide based drugs is often limited by their poor oral uptake and proteolytic instability [18]. Therefore, considerable efforts towards the development of synthetic AMP analogues have been made, cumulating in the development of a variety of different groups of analogues [19–27].

* Corresponding author.

** Corresponding author.

E-mail addresses: Morten.strom@uit.no (M.B. Strøm), Annette.bayer@uit.no (A. Bayer).

¹ Authors contributed equally to this work.

<https://doi.org/10.1016/j.ejmech.2022.114632>

Received 20 May 2022; Received in revised form 15 July 2022; Accepted 24 July 2022

Available online 5 August 2022

0223-5234/© 2022 The Authors. Published by Elsevier Masson SAS. This is an open access article under the CC BY license (<http://creativecommons.org/licenses/by/4.0/>).

Focusing on small molecules, we have recently reported substituted barbituric acid derivatives [28], inspired by a family of marine natural products, the *eusynstyelamides*, [29,30] as peptidomimetics of AMPs. The lead structure **1aG** (Fig. 1) from our previous study [28] demonstrated good *in vitro* and *in vivo* activity as a proof of principle.

Encouraged by the *in vivo* activity of **1aG** we herein describe an in-depth SAR investigation to improve the potency and selectivity of these peptidomimetics. Several series of amphipathic barbiturates with systematically varying substituents were designed and synthesized. Our aim was to assess the qualitative influence of each structural component aside from the barbituric acid on the antimicrobial and haemolytic activity. Once the impact of each component is identified, improved narrow- and broad-spectrum compounds may be prepared. All new compounds were screened for activity against a panel of antibiotic susceptible strains to determine their minimal inhibitory concentration (MIC) values. Cytotoxicity was assessed by determining the EC₅₀ values for the lysis of human red blood cells (RBC). Promising candidates were investigated for their antibacterial mode of action (MoA), using three luciferase-based assays of the viability and integrity of the cytoplasmic inner and outer membrane of bacterial cells.

2. Results and discussion

2.1. Design of the study

To systematically study the influence of structural components of **1aG** [28] (Fig. 1) on the antibacterial and haemolytic activity, we devised several series of compounds based on the general structure shown in Fig. 2. All structures consisted of a central barbituric acid core, which was kept constant. Three structural parts were varied in the design of the compound library: (i) the cationic head groups (blue placeholder in Fig. 2) attached to the nitrogen atoms of the barbiturate core by (ii) a hydrocarbon linker chain (green placeholder) and (iii) the two lipophilic side chains (red placeholders) connected to the barbiturate C-5 carbon.

The influence of the cationic head groups (R; Fig. 2) was investigated by including 1° amines, methylated 2°, 3° and 4° amines and imine derivatives containing guanidino or pyridinium groups in the library design. The cationic groups were chosen based on the prospect of varying the interactions with bacterial membranes and their ability to cross the latter and accumulate in Gram-negative *Escherichia coli* (*E. coli*) [31,32]. Compounds with varying cationic groups are found in compound series 1.

The lipophilic side chains (Fig. 2) were hypothesized to influence the compounds' ability to insert into the hydrophobic lipid bilayer of the bacteria. In our library design haloaryls, hetero-aryls, and linear and cyclic hydrocarbons were chosen as lipophilic side chains. The selection was based on results from our previous study [28] and commercial availability. Two different compound series were included in the study; in series 2 the two lipophilic side chains were identical, while in series 3 two different lipophilic side chains were combined resulting in

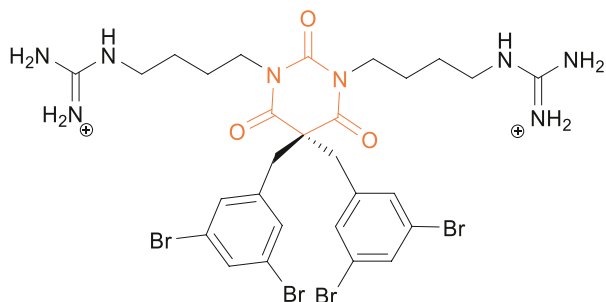


Fig. 1. Lead structure **1aG** from our previous study [28] with the barbituric acid core highlighted in orange.

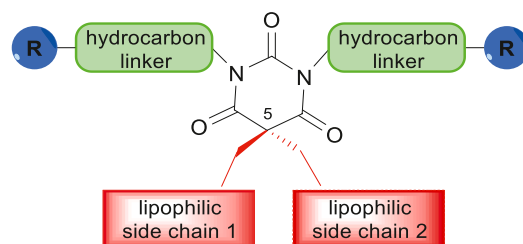


Fig. 2. General structure of the tetrasubstituted barbituric acids used in this study. R = cationic group. The individual parts were evaluated in five series, namely screening of the cationic moieties (series 1), lipophilic side chains (series 2 side chain 1 = side chain 2 and series 3 side chain 1 ≠ side chain 2), hydrocarbon linker chains (series 4) and optimized structures (series 5).

derivatives with mixed side chains.

The hydrocarbon linkers (Fig. 2) were chosen on the premises of investigating the influence of the flexibility and distance of the cationic groups relative to the barbiturate core. Linear hydrocarbon chains of 2–6 carbons length gave flexible linkers, while cyclic hydrocarbon linkers (cyclobutyl and cyclohexyl) gave more restricted analogues. Compounds with varying linkers are included in series 4.

Based on the results from series 4 we prepared a range of compounds included in series 5, having *n*-propyl linkers.

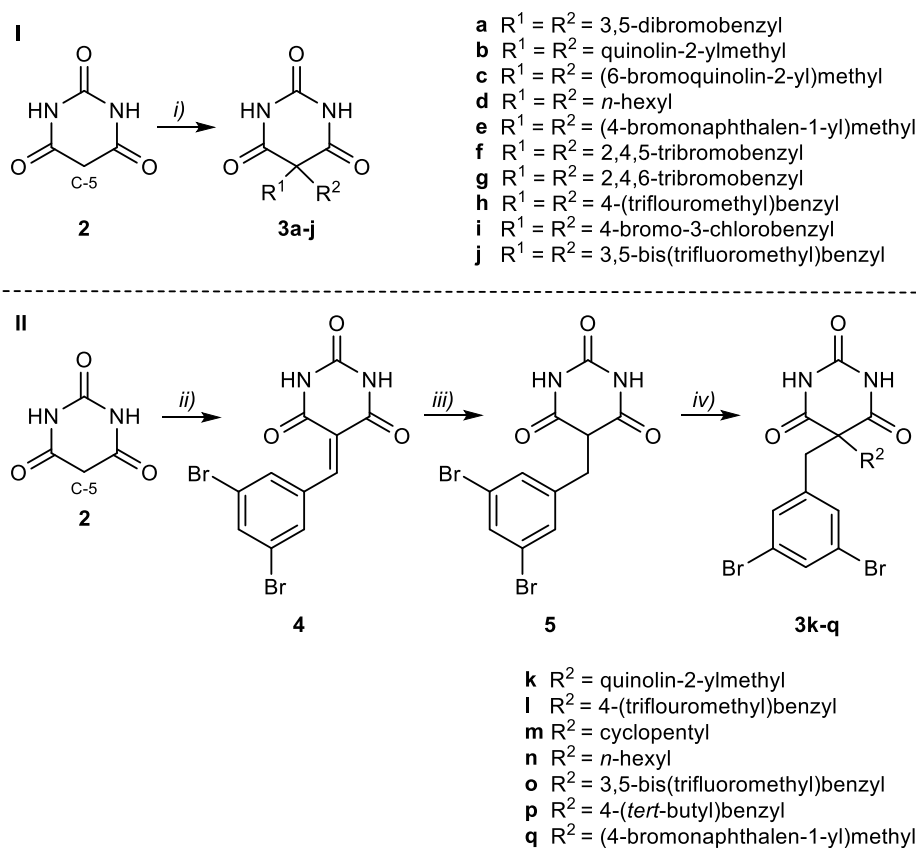
2.2. Synthesis

Our previously reported synthesis of 5,5-dialkylated barbiturates provided amine and guanidine analogues in six or eight synthetic steps, respectively [28]. In the present study, the demand for a large library of compounds prompted us to develop a shorter synthetic approach. Both amines and guanidines were successfully obtained in three steps from barbituric acid.

The synthetic strategy started with the preparation of symmetrical (**3a-j**) or unsymmetrical (**3k-q**) 5,5-dialkylated barbituric acid (Scheme 1). For the preparation of identically dialkylated compounds, barbituric acid **2** could be di-substituted at the C-5 carbon using organohalides to give **3a-j** in 5–92% yield in the presence of NaHCO₃ in PEG-400 (Scheme 1-I). Low yields (5–35%) were obtained for primary alkyl halides and heteroaryls, whereas haloaryls delivered good to excellent yields (70–92%). PEG-400 served as a green solvent alternative and phase transfer catalyst [33]. Commonly applied conditions [34] employing an inorganic base such as K₂CO₃ and benzyltriethylammonium chloride (BTEAC) in CHCl₃ performed worse. Weak electrophiles, such as alkyl halides posed an inherent problem. Harsher conditions were needed, which inevitably led to additional *N*-alkylation due to the acidity of the *N*-H protons (pK_a = 7–9 [35,36] compared to the pK_a (H-C5) = 3–4 [36, 37]).

To obtain unsymmetrically 5,5-dialkylated barbituric acids **3k-q** a different approach was needed, since mono-alkylation enhances the nucleophilicity of the barbiturate C-5 carbon leading to inevitable dialkylation [37]. We investigated several reported methods for selective monoalkylation and *in situ* reductions [37–39], which did not work well in our hands. We therefore decided to use a stepwise approach as shown in Scheme 1-II. Barbituric acid **2** and 3,5-dibromobenzaldehyde were condensed [40] to give compound **4** and subsequent reduction with NaBH₄ in EtOH [41] gave the C-5 mono-substituted derivative **5** in 80% yield. We found **5** being an approximate 2:1 mixture of the keto and enol form. This mixture was alkylated a second time using the conditions employed for 5,5-dialkylation of barbituric acid to deliver intermediates **3k-q**. Yields ranged from 5 to 61%, depending on the reactivity of the employed electrophiles.

Starting from intermediates **3**, a wide range of *N,N'*-dialkylated barbituric acid derivatives were prepared, employing a range of methods for *N*-alkylation depending on the availability of reactants



Scheme 1. Synthesis of core structures **3a-q**. **I:** Reaction conditions: i) Alkylating agent, NaHCO_3 , PEG-400, 45–100 °C, 5–92%. **II:** Reaction conditions: ii) 3,5-dibromobenzaldehyde, $\text{H}_2\text{O}/\text{EtOH}$ (3:1), 105 °C, 58%; iii) NaBH_4 , EtOH, 70 °C, 80%; iv) Alkyl bromide, NaHCO_3 , PEG-400, 50–100 °C, 5–61%.

(Scheme 2).

All compounds synthesized are summarized in Tables 1–5. Compounds denoted with capital **A** have an amine as a cationic group and those denoted with capital **G** have cationic guanidino groups, correspondingly. The compounds are grouped into five series (*series 1–5*) based on their structural variations.

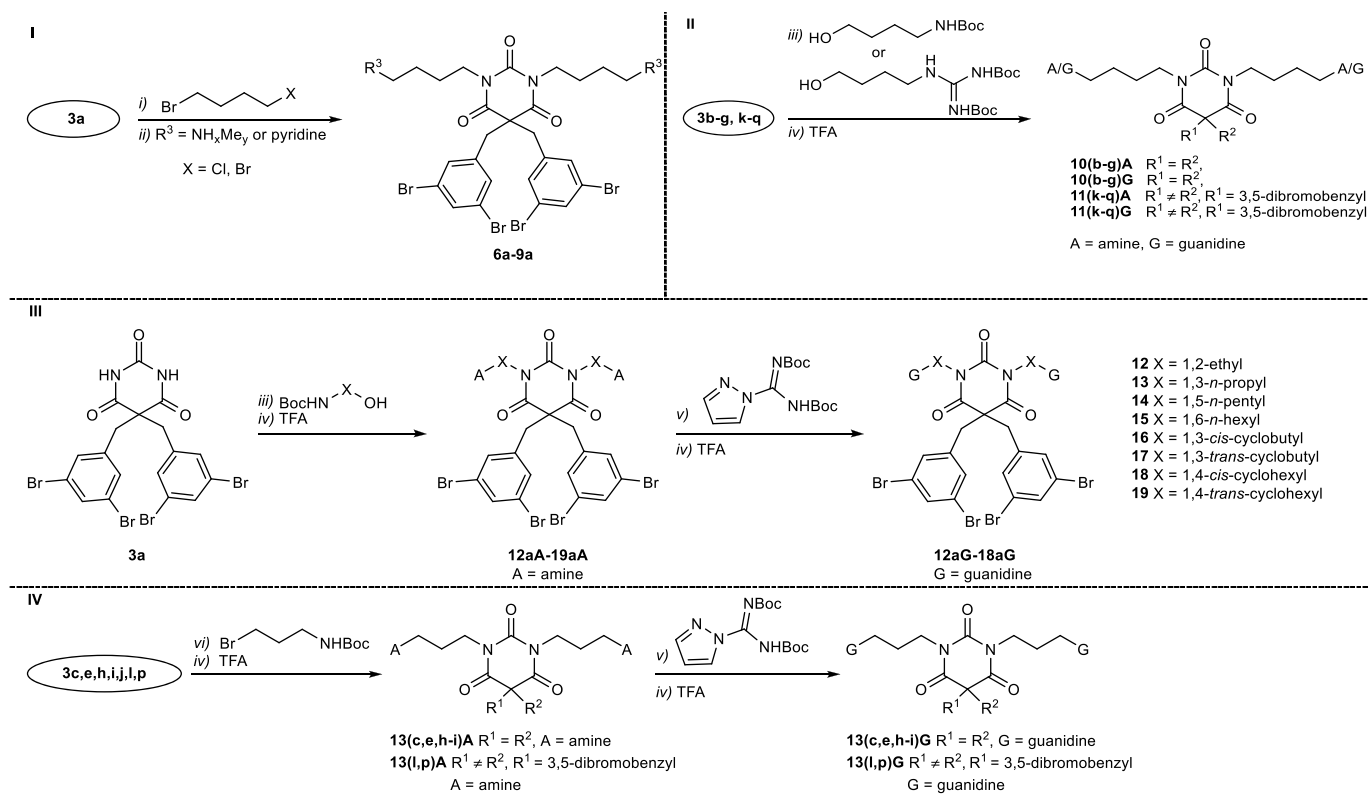
Series 1 (Table 1) encompasses compounds with varying cationic groups, while the C-5 substituents (3,5-dibromobenzyl) and hydrocarbon linker (*n*-butyl) were kept unchanged. To obtain the methylated amines and pyridinium containing compounds **6a-9a**, 5,5-bis(3,5-dibromobenzyl)barbituric acid **3a** was *N,N'*-dialkylated with either 1-bromo-4-chlorobutane or 1,4-dibromobutane and Cs_2CO_3 in acetone (Scheme 2-I). Subsequent $\text{S}_{\text{N}}2$ substitution of the terminal halo substituent with methylated ammonia or pyridine in acetonitrile at elevated temperature led to compounds **6a-9a** in 33–88% yield. Having a bromide as leaving group proved to be necessary for substitution with methylamine and dimethylamine. Substitutions were only successful with organic solutions of the amines, while hydrohalo salts of the amines could not be used. An optimized method for preparation of the previously reported 1° amine **1aA** and guanidine **1aG** [28] is described in the next paragraph.

Compound *series 2* (Scheme 2-II) contained identically 5,5-disubstituted barbiturates and *series 3* (Scheme 2-II) contained unsymmetrically 5,5-disubstituted barbiturates, while the hydrocarbon linker for both series was a *n*-butyl chain. As cationic groups, both amino (**A**) or guanidino (**G**) groups were explored. Compounds were synthesized from the barbituric acid derivatives **3b-g** or **3k-q** by *N,N'*-dialkylation with *N*-Boc protected 4-aminobutanol or *N,N'*-di-Boc protected 1-(4-hydroxybutyl)guanidine (Scheme 2-II). Due to the low pK_a value of the imidic hydrogens [42] a Mitsunobu protocol using diisopropylazodicarboxylate (DIAD) and PPh_3 could be employed. Removal of the Boc protection mediated by TFA:DCM and subsequent reversed phase (RP)

chromatography gave target *series 2* ($R^1 = R^2$) and *series 3* ($R^1 \neq R^2$) as di-TFA salts in 20–89% yield. In some cases the TFA salts were contaminated with reduced DIAD, which could largely be removed by trituration with Et_2O . Interestingly, employment of the more reactive coupling system 1,1'-(azodicarbonyl)dipiperidine ADDP/ $\text{P}(n\text{-Bu})_3$ and *N,N,N',N'*-tetramethyldicarboxamide TMAD/ $\text{P}(n\text{-Bu})_3$ [42] led to lower yields and mono-alkylation.

Series 4 (Table 4) contained compounds with varying linkers, such as aliphatic chains with 2–6 carbons length as well as cyclic hydrocarbons. The C-5 substituents were set to 3,5-dibromobenzyl and the cationic groups were either amino (**A**) or guanidino (**G**) groups. As the relevant linkers were commercially available as *N*-Boc-amino alcohols, we decided to explore the above Mitsunobu protocol in a stepwise synthetic approach (Scheme 2-III). The 5,5-bis(3,5-dibromobenzyl)barbituric acid **3a** was *N,N'*-dialkylated with the appropriate Boc-protected amino alcohol using the Mitsunobu conditions followed by TFA:DCM treatment to obtain compounds **12aA-19aA** in 23–73% over 2 steps. Treatment of the amines **12aA-19aA** with *N,N'*-Di-Boc-1*H*-pyrazole-1-carboxamide and DIPEA or DBU, followed by Boc removal with TFA in DCM delivered the guanidines **12aG-18aG** in 14–92% yield. Employing the well-known and cheaper alternative *N,N'*-bis(*tert*-butoxycarbonyl)-*S*-methylisothiourea [43,44] led to an inseparable mixture of Boc protected amine and Boc protected guanyl compounds.

Based on the bioactivities observed for *series 1–4*, a fifth collection of compounds (*series 5*, Table 5), exploring the effect of an *n*-propyl linker more broadly, was prepared. *Series 5* contained selected identically (*series 2*) or unsymmetrically (*series 3*) 5-substituted barbiturates with both 1-propyl-3-amino (**A**) or 1-propyl-3-guanidino groups (**G**) as *N,N'*-substituents. Starting from compounds **3c**, **e**, **h**, **i**, **j**, **l**, **p**, *N,N'*-alkylation with *N*-Boc *n*-propylbromide, followed by TFA mediated Boc removal and purification by RP chromatography gave identically **13(c,e,h,i,j)A**



Scheme 2. Synthetic approach to target series 1–5, where **A** denotes amine head groups and **G** the guanidine derivatives. All final compounds were obtained as di-TFA salts. I $R^3 = NH_2Me, NHMe_2, NMe_3, \text{pyridinyl}$; Reaction conditions: i) CS_2CO_3 , acetone, $55^\circ C$, 57–85%; ii) MeCN, $70\text{--}90^\circ C$, 33–88%. II Reaction conditions: iii) DIAD, PPh_3 , anhydrous DCM or THF, $0^\circ C$ to r.t., iv) TFA, DCM, r.t., 20–89% o2s. III Reaction conditions: iii) DIAD, PPh_3 , anhydrous DCM or THF, $0^\circ C$ to r.t., iv) TFA, DCM, r.t., 23–73% o2s, v) DIPEA or DBU, THF, $45^\circ C$, 14–92% o2s (after TFA deprotection). IV Reaction conditions: vi) base, TBAI, acetone, $50\text{--}70^\circ C$, then iv) TFA, DCM, r.t., 34–76% o2s (after TFA deprotection); v) DIPEA or DBU, THF, $45^\circ C$, then iv) TFA, DCM, r.t., 20–91% o2s (after TFA deprotection).

Table 1

Antimicrobial activity (MIC in $\mu g/mL$) against bacterial reference strains and haemolytic activity against human RBC (EC_{50} in $\mu g/mL$) for compounds in series 1.

Core structure	Comp. ID	R^3	CLogP ^a	Antimicrobial activity				EC_{50}^b
				S. a	B. s	E. c	P. a	
	1aG ^c		−2.39	2	2	2	8	62
	1aA ^d		−1.20	4	2	4	8	79
	6a		−0.66	8	4	8	16	73
	7a		−0.52	8	4	8	64	157
	8a		0.42	4	8	128	256	>539
9a		0.72	2	4	8	128	>559	
Ciprofloxacin				0.06	<0.03	<0.03	0.25	

Bacterial reference strains: S. a – *Staphylococcus aureus* ATCC 9144, B. s – *Bacillus subtilis* 168, E. c – *Escherichia coli* ATCC 25922, and P. a – *Pseudomonas aeruginosa* ATCC 27853. All compounds were tested as di-TFA salts.

^a CLogP values were calculated for the respective non protonated cationic group (calculated with ChemBioDraw Ultra v19.0.0.1.28).

^b Values given as greater than correspond to the highest concentration (500 μM) tested in the RBC assay.

^c We have reported this compound previously having the following MIC values: S. a: 1 $\mu g/mL$, B. s: 2 $\mu g/mL$, E. c: 2 $\mu g/mL$, P. a: 4 $\mu g/mL$ [28].

^d Values were taken from Ref. [28].

or unsymmetrically **13(l,p)A** substituted primary amines in 34–76% yield (Scheme 2-IV). The Mitsunobu protocol was evaluated but discarded due to difficulties with purification of some compounds. Treatment of the primary amines with *N,N'*-di-Boc-1*H*-pyrazole-1-carboxamide and DIPEA, followed by TFA facilitated Boc removal and RP flash chromatography purification yielded the respective guanidines

13(c,e,h,i,j,l,p)G in 20–91% yield.

2.3. SAR analysis

All compounds were screened for antimicrobial activity against antibiotic susceptible Gram-positive and Gram-negative reference

Table 2Antimicrobial activity (MIC in $\mu\text{g/mL}$) against bacterial reference strains and haemolytic activity against human RBC (EC_{50} in $\mu\text{g/mL}$) for compounds in series 2.

Core structure	Comp. ID	$R^1 = R^2$	A/G	CLogP ^a	Antimicrobial activity				EC_{50} ^b
					S. a	B. s	E. c	P. a	
	10bA			2.53	256	64	>256	>256	>390
	10bG			2.53	8	16	128	>256	>432
	10cA			3.39	16	4	256	256	>469
	10cG			3.39	2	4	16	128	461
	10dA			3.87	16	8	32	64	>333
	10dG			3.87	2	2	4	16	143
	10eA			4.68	2	2	4	4	27
	10eG			4.68	4	4	4	8	36
	10fA			5.03	4	4	8	8	27
	10fG			5.03	4	4	4	8	32
	10gA			5.03	2	2	4	4	30
	10gG			5.03	2	1	4	4	30

Bacterial reference strains: S. a – *Staphylococcus aureus* ATCC 9144, B. s – *Bacillus subtilis* 168, E. c – *Escherichia coli* ATCC 25922, and P. a – *Pseudomonas aeruginosa* ATCC 27853. All compounds were tested as di-TFA salts.

^a CLogP values were calculated for the respective lipophilic side chains (calculated with ChemBioDraw Ultra v19.0.0.1.28).

^b Values given as *greater than* correspond to the highest concentration (500 μM) tested in the RBC assay.

strains (Tables 1–5). Haemolytic activity against human red blood cells (RBCs), expressed by the EC_{50} value, was used as a measurement of cytotoxicity. We have earlier reported compounds **1aA** and **1aG** [28], which here are used as reference compounds together with the known antibiotic ciprofloxacin as a positive control. The descriptors for amine derivatives (A) and guanidine derivatives (G) are omitted for derivatives with other cationic groups.

2.3.1. Compound series 1: Exploring the cationic head group (R^3)

First, we set out to investigate the influence of the effective charge of the cationic groups (Table 1, R^3 group and Fig. 2, blue space holders). Upon *N*-methylation the electron density at the nitrogen increases, as does its basicity, but the polarity decreases. Successive introduction of one (**6a**), two (**7a**) or three (**8a**) methyl groups had no noteworthy influence on the activity against the Gram-positive strains (MIC: 4–8 $\mu\text{g/mL}$), but the activity against the Gram-negative strains dropped considerably for compound **8a** (MIC: 128–256 $\mu\text{g/mL}$). It is suggested that, among other factors, the electrostatic interaction between these compounds and bacterial membrane plays an important role in the compound's activity [45]. Successive introduction of methyl groups lowers the effective charge of the amine head groups, thus reducing their interaction with the lower charge per area membrane of Gram-negative bacteria compared to Gram-positive strains [46]. Additionally, quaternary ammonium compounds (quats or QACs) are known for their impaired ability to cross the outer membrane of Gram-negative *Pseudomonas aeruginosa* (*P. aeruginosa*) [47]. Recent studies showed generally impaired uptake of compounds containing methylated primary amines in *E. coli* [31]. Despite that presumably lower uptake, secondary (**6a**) and tertiary amines (**7a**) were still active against *E. coli* (MIC: 8 $\mu\text{g/mL}$). By replacing the quaternary trimethylated ammonium (**8a**) with a pyridinium group (**9a**), the activity against the Gram-positive

strains improved (MIC: 2–4 $\mu\text{g/mL}$) and the activity against *E. coli* was restored (MIC: 8 $\mu\text{g/mL}$), probably due to increased accumulation [32]. Tertiary (**7a**), EC_{50} : 157 $\mu\text{g/mL}$ and quaternary amines (**8a** and **9a**; both EC_{50} : >500 $\mu\text{g/mL}$) displayed lower haemolytic activity compared to the primary (**1aA**, EC_{50} : 79 $\mu\text{g/mL}$) and secondary (**6a**, EC_{50} : 73 $\mu\text{g/mL}$) amines.

The quaternary ammonium compound **8a** exhibited narrow-spectrum antimicrobial activity against Gram-positive strains and was non-haemolytic. Compared to the above investigated head groups, the recently reported amine (**1aA**) and guanidine derivatives (**1aG**) appeared to be the most effective against the Gram-negative strains, thus rendering them suitable for broad-spectrum applications. The consecutively developed compounds were therefore synthesized with either amino or guanidino groups.

2.3.2. Compound series 2: Exploring new lipophilic side chains ($R^1 = R^2$)

In series 2, the influence of heterocyclic, aliphatic and highly brominated lipophilic side chains (Table 2, R^1/R^2 groups and Fig. 2, red space holders) on the biological activity was examined. Both side chains employed were identical.

The antimicrobial activity for the amine barbiturates **10(b-g)A** ranged from MIC: 2–256 $\mu\text{g/mL}$ and for the guanidine barbiturates **10(b-g)G** from MIC: 1–16 $\mu\text{g/mL}$ against the Gram-positive strains *Staphylococcus aureus* (*S. aureus*) and *Bacillus subtilis* (*B. subtilis*). Against the Gram-negative strains *E. coli* and *P. aeruginosa* both, the amine and guanidine derivatives, showed MIC values of 4 – >256 $\mu\text{g/mL}$. We included quinoline and 6-bromoquinoline as heterocyclic alternatives. The amine derivative **10bA** (R^1/R^2 = quinolin-2-ylmethyl) was neither antibacterial (MIC: ≥ 64 $\mu\text{g/mL}$) nor haemolytic, whereas the guanidine derivative **10bG** exhibited some activity against the Gram-positive strains (MIC: 8–16 $\mu\text{g/mL}$).

Table 3

Antimicrobial activity (MIC in $\mu\text{g/mL}$) against bacterial reference strains and haemolytic activity against human RBC (EC_{50} in $\mu\text{g/mL}$) for compounds in series 3.

Core structure	Comp. ID	R^2	A/G	CLogP ^a	Antimicrobial activity				EC_{50} ^b
					S. a	B. s	E. c	P. a	
	11kA			3.45	32	8	128	256	>444
	11kG			3.45	2	4	32	32	450
	11IA			3.95	16	8	32	64	342
	11IG			3.95	2	4	2	16	161
	11mA			3.58	16	8	64	64	>407
	11nA			4.12	4	4	16	16	144
	11nG			4.12	2	4	4	8	58
	11oA			4.39	8	2	8	8	93
	11oG			4.39	2	2	2	4	36
	11pA			4.42	4	4	8	8	82
	11pG			4.42	2	2	2	4	39
	11qA			4.52	4	4	4	8	47
	11qG			4.52	1	4	4	8	58

Bacterial reference strains: S. a – *Staphylococcus aureus* ATCC 9144, B. s – *Bacillus subtilis* 168, E. c – *Escherichia coli* ATCC 25922, and P. a – *Pseudomonas aeruginosa* ATCC 27853. Guanidyl barbiturate **11mG** could not be obtained. All compounds were tested as di-TFA salts.

^a CLogP values were calculated for the respective lipophilic side chains and are presented as the average for the two substituents. (calculated with ChemBioDraw Ultra v19.0.0.1.28).

^b Values given as *greater than* correspond to the highest concentration (500 μM) tested in the RBC assay.

Upon inserting a bromine in the 6-position for **10cA** ($R^1/R^2 = (6\text{-bromoquinolin-2-yl)methyl}$) the CLogP rose considerably, and the amine derivative became active against the Gram-positive bacteria (MIC: 4–16 $\mu\text{g/mL}$). The respective guanidine **10cG** was found to be active against both the Gram-positive strains and *E. coli* (MIC: 2–16 $\mu\text{g/mL}$), while being nonhaemolytic. The bromine substituent seemed to be essential for good antimicrobial activity against Gram-positive strains and *E. coli*.

In the next step we replaced the aromatic side chains by alkyl chains as found in antimicrobial quats [48,49]. We decided to incorporate two hexyl chains, which mimic the single long alkyl chain commonly found in quats [50]. The amine derivative **10dA** ($R^1/R^2 = n\text{-hexyl}$) showed weak activity against all bacterial strains (MIC: 8–64 $\mu\text{g/mL}$), whereas the guanidine derivative **10dG** showed high antibacterial activity with MIC values of 2–4 $\mu\text{g/mL}$ against all strains except for *P. aeruginosa*. Haemolysis was still moderate, with EC_{50} : 143 $\mu\text{g/mL}$. Interestingly, the shorter hexyl chains perform just as good as the longer alkyl chains in quats [48], suggesting that the overall hydrophobic bulk is more important than the actual chain length.

Compounds **10e** ($R^1/R^2 = (4\text{-bromonaphthalen-1-yl)methyl}$) were prepared based on the previously reported (4-fluoronaphthalen-1-yl) methyl barbituric acid [28]. Introduction of electron withdrawing fluorine into molecules is known to hamper *in vivo* oxidation of aromatic side chains during Phase I metabolism [51,52]. Replacing the fluorine for a bromine increases the hydrophobic bulk, while having similar electronic effects [53]. Surprisingly, the amine derivative **10eA** was equally potent as the guanidine **10eG** with MIC values of 2–8 $\mu\text{g/mL}$ against all reference strains. However, both, **10eA** and **10eG**, were also highly haemolytic (EC_{50} : 27–36 $\mu\text{g/mL}$).

Previously, we have found bromo substituents on the phenyl ring having a positive effect on the biological activity, with 3,5-dibromophenyl providing the highest activity [26]. We therefore prepared derivatives **10fA** and **10fG** ($R^1/R^2 = 2,4,5\text{-tribromobenzyl}$) and **10gA** and **10gG** ($R^1/R^2 = 2,4,6\text{-tribromobenzyl}$) being at the far end of the hydrophobicity scale. They all displayed potent antibacterial activity, with MIC values ≤ 8 $\mu\text{g/mL}$ against all strains. However, haemolytic activity also increased for all these compounds (EC_{50} : 27–32 $\mu\text{g/mL}$). The positioning of the bromines on the phenyl ring had a minor influence on antibacterial activity, with **10gA** and **10gG** being most potent.

In summary, halogenated heterocycles are promising side chains for narrow-spectrum application. The hydrophobicity of the C-5 substituents had the greatest influence, while the structure being secondary. When exceeding CLogP ≈ 4.50 , the structures mostly became too haemolytic to be of interest for further studies.

2.3.3. Compound series 3: Exploring mixed lipophilic groups ($R^1 \neq R^2$)

A series of compounds containing two different side chains were prepared to tune lipophilicity and side chain structure with respect to antimicrobial activity and haemolytic activity. We intended to pair the potent 3,5-dibromobenzyl side chain (R^1) with side chains (R^2) of different varying lipophilicity (Table 3; R^2 group; Fig. 2, red space holders).

First, we chose to incorporate previously documented non potent side chains (see series 2 and previously reported [26,28]) in compounds **11k** ($R^2 = \text{quinolin-2-ylmethyl}$) and **11l** ($R^2 = 4\text{-(trifluoromethyl)benzyl}$). The amine derivatives **11kA** and **11IA** displayed weak activity, mainly against *B. subtilis* (MIC: 8 $\mu\text{g/mL}$) but can be considered non-haemolytic. The guanidine derivatives **11kG** and **11IG** were still

Table 4

Antimicrobial activity (MIC in $\mu\text{g/mL}$) against bacterial reference strains and haemolytic activity against human RBC (EC_{50} in $\mu\text{g/mL}$) for compounds in series 4.

Core structure	Comp. ID	X	A/G	CLogP ^a	Antimicrobial activity				EC ₅₀
					S. a	B. s	E. c	P. a	
	12aA			1.75	4	4	4	8	39
	12aG			1.75	2	2	4	16	164
	13aA			2.28	4	4	8	8	99
	13aG			2.28	2	2	4	8	187
	14aA			3.34	4	4	8	8	24
	14aG			3.34	4	4	4	8	29 ^b
	15aA			3.87	4	4	4	16	30
	15aG			3.87	4	4	4	32	57 ^b
	16aA			2.24	8	4	4	8	50
	16aG			2.24	2	2	4	8	75
	17aA			2.24	4	4	4	8	93
	17aG			2.24	2	4	4	8	62
	18aA			3.35	4	4	4	8	15
	18aG			3.35	2	1	4	4	30
	19aA			3.35	2	2	2	4	16

Bacterial reference strains: S. a – *Staphylococcus aureus* ATCC 9144, B. s – *Bacillus subtilis* 168, E. c – *Escherichia coli* ATCC 25922, and P. a – *Pseudomonas aeruginosa* ATCC 27853. All compounds were tested as di-TFA salts. Compound **19aG** was not obtained in satisfying purity.

^a CLogP values were calculated for the respective hydrocarbon linkers (calculated with ChemBioDraw Ultra v19.0.0.1.28).

^b Precipitation in the RBC assay observed.

almost non-haemolytic (EC_{50} : down to 161 $\mu\text{g/mL}$) and displayed potent activity against the Gram-positive strains (MIC: 2–4 $\mu\text{g/mL}$).

The derivative **11iG** showed additionally good activity against the Gram-negative *E. coli* (MIC: 4 $\mu\text{g/mL}$). The superior performance of **11iG** over **11kG** may be attributed to the higher average CLogP value of the lipophilic side chain of **11iG**. The polar nitrogen atom in the quinolinyl side chain (**11iG**) might also reduce the compounds' activity.

Next, we tested two hydrocarbon analogues **11m** (R^2 = cyclopentyl) and **11n** (R^2 = *n*-hexyl), with comparable average hydrophobicity to **11k** and **11l**, respectively. Compound **11mA** was potent against both Gram-positive strains and non-haemolytic. The amine derivative **11nA** was mainly acting against the Gram-positive strains (MIC: 4 $\mu\text{g/mL}$) but showed 3-fold higher haemolytic activity compared to **11IA**. The guanyl derivative **11nG** exhibited potent antibacterial activity, with MIC-values of 2–8 $\mu\text{g/mL}$ against all strains tested. Even though its average CLogP was only marginally higher than **11iG**, its haemolytic activity was pronouncedly higher (EC_{50} : 58 $\mu\text{g/mL}$). The compounds **11m** and **11n** indicated that a combination of an aromatic and a hydrocarbon lipophilic side chain leads to higher haemolytic activity, compared to two aromatic side chains.

To study the influence of the structure of the lipophilic side chains we prepared structurally different, but of similar lipophilicity, compounds **11o** (R^2 = 3,5-bis(trifluoromethyl)benzyl), **11p** (R^2 = 4-(*tert*-butyl)benzyl), and **11q** (R^2 = (4-bromonaphthalen-1-yl)methyl). All their amine derivatives displayed low MIC values of 2–8 $\mu\text{g/mL}$ against all reference strains and **11oA** was least haemolytic (EC_{50} : 93 $\mu\text{g/mL}$).

Upon guanylation, a further improvement in antimicrobial activity was achieved, but haemolytic activity was also increased. Thus, **11oG** and **11pG** became twice as potent and haemolytic (EC_{50} : 36–39 $\mu\text{g/mL}$), rendering them unfavorable for systemic *in vivo* treatment. The bromonaphthyl containing **11qG** became more potent against *S. aureus* (MIC: 1 $\mu\text{g/mL}$), yet haemolytic activity (EC_{50} : 58 $\mu\text{g/mL}$) was still unfavorably high. No clear trend for the antimicrobial activity could be deduced, based on the structure of the lipophilic side chains.

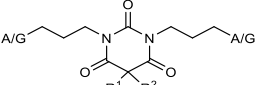
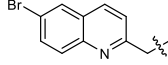
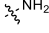
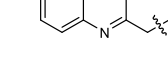
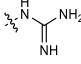

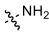
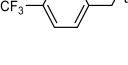
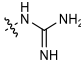
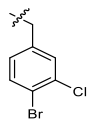
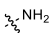
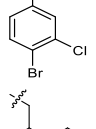
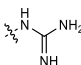
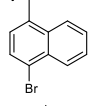
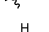
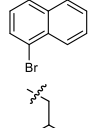
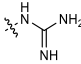
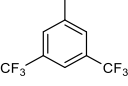
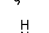
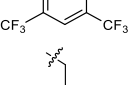
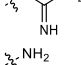
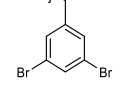
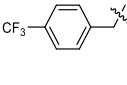
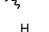
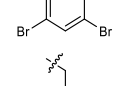
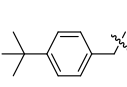
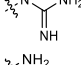
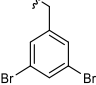
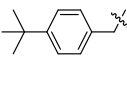
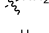
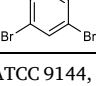
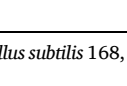
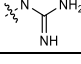
Taken all together, **11kG** displayed promising narrow-spectrum activity against Gram-positive strains and absence of haemolytic activity. Compounds **11oG** and **11pG** are highly potent derivatives but displayed high haemolytic activity.

2.3.4. Compound series 4: Exploring the hydrocarbon linker chain (X)

We incorporated various linear and cyclic hydrocarbon linkers (Tables 4 and X group; Fig. 2, green space holder) between the central scaffold and the cationic residue. 3,5-Dibromobenzyl was kept fixed as the lipophilic side chain and the previously reported compounds **1aA** and **1aG** (both X = *n*-butyl) served as reference substances for comparison. Shortening or elongating the alkyl chains to 2, 3, 5 or 6 methylene groups (**12aA–15aA**) led to no significant change in antibacterial activity (MIC: 4–16 $\mu\text{g/mL}$ against all strains). The haemolytic activity increased slightly compared to **1aA** (X = *n*-butyl), except for **13aA** (X = *n*-propyl), which became slightly less haemolytic. So far, guanidine derivatives tended to have a higher haemolytic activity (*vide supra*) compared to amine derivatives. In contrast, **13aG** (X = *n*-propyl) and

Table 5

Antimicrobial activity (MIC in $\mu\text{g/mL}$) against bacterial reference strains and haemolytic activity against human RBC (EC_{50} in $\mu\text{g/mL}$) for compounds in series 5.

Core structure	Comp ID	R ¹	R ²	A/G	CLogP ^a	Antimicrobial activity				EC ₅₀ ^b	
						S. a	B. s	E. c	P. a		
	13cA		R ² = R ¹		3.39	32	8	64	256	>455	
	13cG				3.39	8	4	64	>128	>497	
	13hA		R ² = R ¹		3.87	64	16	64	128	>393	
	13hG				3.87	8	4	128	256	>435	
	13iA		R ² = R ¹		4.08	8	4	8	16	323	
	13iG				4.08	2	2	8	32	348	
	13eA		R ² = R ¹		4.68	2	2	4	4	23	
	13eG				4.68	2	2	4	8	61	
	13jA		R ² = R ¹		5.03	8	4	8	8	176	
	13jG				5.03	4	2	8	16	445	
	13lA					3.95	32	8	16	32	>438
	13lG					3.95	4	4	16	64	>480
	13pA					4.42	4	2	8	8	47
	13pG					4.42	1	1	2	16	169

Bacterial reference strains: S. a – *Staphylococcus aureus* ATCC 9144, B. s – *Bacillus subtilis* 168, E. c – *Escherichia coli* ATCC 25922, and P. a – *Pseudomonas aeruginosa* ATCC 27853. All compounds were tested as di-TFA salts.

^a CLogP values were calculated for the respective lipophilic side chains. For non-identical side chains, the value stated is the average of both individual side chains. Values were calculated for substituted benzyl groups (calculated with ChemBioDraw Ultra v19.0.0.1.28).

^b Values given as *greater than* correspond to the highest concentration (500 μM) tested in the RBC assay.

12aG (X = ethyl) were observed to exhibit 2-fold and 4-fold decreased haemolytic activity, respectively, compared to their amine counterparts. The activity against the Gram-positive strains was slightly improved, whereas the potencies against the Gram-negative *P. aeruginosa* were retained or a little diminished. The derivatives **14aA** and **14aG** (X = *n*-pentyl) displayed virtually the same MIC and EC₅₀ values, whereas **15aG** (X = *n*-hexyl) was less potent against *P. aeruginosa* (MIC: 32 $\mu\text{g/mL}$) compared to **15aA** (X = *n*-hexyl) (MIC: 16 $\mu\text{g/mL}$). Both guanylated compounds were less potent than the previously investigated derivative **1aG** (X = *n*-butyl) and their haemolytic levels were comparably high (EC₅₀: 29–57 $\mu\text{g/mL}$). Compounds **14aG** (X = *n*-pentyl) and **15aG** (X = *n*-hexyl) led also to precipitation in the RBC assay upon sample preparation, possibly due to their higher overall hydrophobicity, demonstrating an unfavorable solubility profile.

To investigate if the conformational freedom of the linker influenced the compounds potency, 1,3-cyclobutyl and 1,4-cyclohexyl were used as surrogates for the *n*-propyl and *n*-butyl chains, taking advantage of their restricted spatial arrangement. Compounds **16aA** (X = *cis*-1,3-cyclobutyl) and **17aA** (X = *trans*-1,3-cyclobutyl) displayed the same MIC values (4–8 $\mu\text{g/mL}$) as **13aA** (X = *n*-propyl) against all strains, but **16aA** (*cis*) was almost twice as haemolytic as **13aA** (X = *n*-propyl) and **17aA** (*trans*). Their guanylated counterparts **16aG** (*cis*) and **17aG** (*trans*), were more potent against the Gram-positive strains, but no change in MIC was observed against the Gram-negative strains. Both derivatives exhibited considerably higher haemolytic activity compared to **13aG** (X = *n*-propyl).

While being equally haemolytic (EC₅₀: 15 $\mu\text{g/mL}$) and 5-times more haemolytic than **1aA** (X = *n*-butyl), **19aA** (X = *trans*-1,4-cyclohexyl) was twice as potent as **18aA** (X = *cis*-1,4-cyclohexyl). The guanidine derivative **18aG** (*cis*) was highly potent (MIC: 1–4 $\mu\text{g/mL}$) against all bacterial strains, but its haemolytic activity was also too high to be of therapeutic value for systemic application. Of note, the guanylated derivative (**18aG**) was nevertheless less haemolytic than the amine derivative (**18aA**).

In summary, compounds with rigid cyclic linkers showed similar or slightly higher potency compared to their linear analogues, but they tended to be more haemolytic. Furthermore, compounds with pentyl and hexyl linkers showed furthermore decreased water solubility. The amine derivatives having ethyl, *n*-propyl or *n*-butyl linkers displayed similar antibacterial bioactivity profiles, whereas the equivalent guanidine derivatives displayed descending antimicrobial activity as follows: *n*-butyl > *n*-propyl > ethyl. The best balance between high antimicrobial activity and low haemolytic activity was presented by compounds having *n*-propyl hydrocarbon linker chains.

2.3.5. Compound series 5: Investigating compounds with a *n*-propyl hydrocarbon linker

In series 5 (Table 5), we studied the effect of the *n*-propyl linker more closely due to the promising balance between high antimicrobial activity and low haemolytic activity seen in series 4. We selected the lipophilic side chains (R¹/R²) based on our previous findings. We reasoned that compounds **13c**, **13h** and **13l** would mainly act against

Gram-positive strains, whereas compounds **13e**, **13i**, **13j** and **13p** should provide a higher broad-spectrum activity. Amines **13cA** ($R^1/R^2 = (6\text{-bromoquinolin-2-yl)methyl}$) and **13hA** ($R^1/R^2 = 4\text{-}(trifluoromethyl)\text{benzyl}$) displayed generally low antibacterial activity against all strains (MIC: 8–256 $\mu\text{g/mL}$). However, the guanyl equivalents **13cG** and **13hG** exhibited fair activity and selectivity for Gram-positive strains (MIC: 4–8 $\mu\text{g/mL}$) and weak activity towards Gram-negative strain (MIC: ≥ 64 $\mu\text{g/mL}$). None of the four compounds was haemolytic.

Compound **13iA** ($R^1/R^2 = 4\text{-bromo-3-chlorobenzyl}$) displayed good activity against all strains (MIC: 4–8 $\mu\text{g/mL}$) except for the Gram-negative *P. aeruginosa* (MIC: 16 $\mu\text{g/mL}$). The guanyl derivative **13iG** displayed further improved activity against the Gram-positive strains (MIC: 2 $\mu\text{g/mL}$), but the activity against *P. aeruginosa* was lost. Noteworthy, the amine **13iA** and guanidine **13iG** derivatives were non-haemolytic (EC_{50} : >300 $\mu\text{g/mL}$), despite the relatively high CLogP values of their lipophilic side chains.

Derivatives **13eA** and **13eG** contained the bulky bromo-naphthyl ($R^1/R^2 = (4\text{-bromonaphthalen-1-yl)methyl}$) group. The amine derivative **13eA** was highly potent (MIC: 2–4 $\mu\text{g/mL}$) against all strains, but too haemolytic to be of practical use (EC_{50} : 23 $\mu\text{g/mL}$). Upon guanylation, **13eG** still had good activity against all strains (MIC: 2–8 $\mu\text{g/mL}$) and an almost three-fold decrease in haemolytic activity (EC_{50} : 61 $\mu\text{g/mL}$) was observed. The relatively high haemolytic activity was still unfavorable, but the positive effect of exchanging *n*-butyl linkers (**10eG**) for *n*-propyl linkers (**13eG**) was well demonstrated.

The amine derivative **13jA**, featuring 3,5-bis(trifluoromethyl)benzyl side chains, was potent against all strains (MIC: 4–8 $\mu\text{g/mL}$) and displayed low haemolytic activity (EC_{50} : 176 $\mu\text{g/mL}$). The guanyl analogue **13jG** was twice as potent against the Gram-positive strains, while the activity against *P. aeruginosa* was reduced (MIC: 16 $\mu\text{g/mL}$). Pleasingly, the guanylation rendered the compound non-haemolytic.

The unsymmetrically C-5 substituted amine **13lA** ($R^1 = 3,5\text{-dibromobenzyl}$, $R^2 = 4\text{-}(trifluoromethyl)\text{benzyl}$) displayed acceptable activity only against *B. subtilis* (MIC: 8 $\mu\text{g/mL}$). The guanyl derivative **13lG** exhibited good activity against both Gram-positive strains (MIC: 4 $\mu\text{g/mL}$), but its intermediate activity against Gram-negative *E. coli* (MIC: 16 $\mu\text{g/mL}$) limits its narrow-spectrum application against Gram-positive bacteria.

The unsymmetrically substituted amine **13pA** ($R^1 = 3,5\text{-dibromobenzyl}$, $R^2 = 4\text{-}(tert\text{-butyl})\text{benzyl}$) was potent against all strains tested (MIC: 2–8 $\mu\text{g/mL}$) but was quite haemolytic (EC_{50} : 47 $\mu\text{g/mL}$). The guanyl derivative **13pG** became more potent against all strains but *P. aeruginosa* (MIC: 16 $\mu\text{g/mL}$), accompanied by an almost 4-fold decrease in haemolytic activity (EC_{50} : 169 $\mu\text{g/mL}$), rendering it a very promising candidate for further studies.

Using *n*-propyl linkers clearly had a positive effect and led to development of the potent derivatives **13iA**, **13jA**, **13jG**, **13lG** and **13pG** with broad-spectrum activity. All five derivatives displayed low haemolytic activity, making them promising candidates for further evaluation.

2.3.6. Trends in haemolytic activity

When examining the haemolytic activity of our compounds we saw a pronounced difference between compounds having *n*-propyl and *n*-butyl linkers. The core findings are presented in the following paragraph and a more detailed section on how the structures were compared can be found in chapter 1 of the Supporting Information.

For our comparison, we selected 24 compounds and assorted them into four scaffold groups (Fig. S1) based on the combination of linkers and cationic head groups. Compounds with (i) *n*-propyl linkers and amine groups were placed in group 3CA, (ii) *n*-propyl linkers and guanidyl groups in group 3CG, (iii) *n*-butyl linkers and amine groups in group 4CA and (iv) *n*-butyl linkers and guanidyl groups in group 4CG. Each scaffold group contained compounds with the following side chain combinations: **a** (3,5-dibromobenzyl), **e** ((4-bromonaphthalen-1-yl)methyl), **i** (4-bromo-3-chlorobenzyl), **j** (3,5-bis(trifluoromethyl)benzyl),

l ($R^2 = 4\text{-}(trifluoromethyl)\text{benzyl}$) and **p** (4-(*tert*-butyl)benzyl). To represent the trends, we have looked at the difference in EC_{50} values between 3CG – 3CA and 4CG – 4CA (Fig. S2) as well as 3CA – 4CA and 4CG – 3CG (Fig. S3).

First, we compared guanidyl- and amine-containing compounds with the same linkers and lipophilic side chains. For compounds with *n*-butyl linkers (4CG – 4CA), all guanidyl containing compounds were more haemolytic than their amine counterparts except for when the (4-bromonaphthalen-1-yl)methyl (**e**) was present. Comparing *n*-propyl containing derivatives (3CG – 3CA), we observed the reversed trend. The guanidyl derivatives were equally to pronouncedly less haemolytic than their amine counterparts. The difference in EC_{50} values ranged from 0 $\mu\text{g/mL}$ for side chain combination **l** to 269 $\mu\text{g/mL}$ for side chain combination **j**.

Next, we compared the *n*-butyl with *n*-propyl linkers in the presence of amine groups (3CA – 4CA). For side chain combinations **a**, **e**, **j** and **p** the compounds were of comparable haemolytic activity regardless of the linker length. Only for side chain combinations **i** and **l** the derivatives with *n*-propyl linkers (3CA) were less haemolytic by 151 and 158 $\mu\text{g/mL}$, respectively, compared to their *n*-butyl counterparts (4CA). The difference between *n*-butyl and *n*-propyl linkers was most eminent in the presence of guanidyl groups (4CG – 3CG). All compounds having *n*-propyl linkers (3CG) were less haemolytic than compounds with *n*-butyl linkers (4CG). The difference ranged from 25 $\mu\text{g/mL}$ for side chain combination **e** to an impressive 347 $\mu\text{g/mL}$ for side chain combination **j**.

This comparison clearly shows that *n*-propyl linkers not only led to derivatives with good broad-spectrum activity, but also low haemolytic activity. Despite the often noteworthy difference in EC_{50} values for the two linkers, no obvious SAR could be delineated.

2.3.7. Summary of SAR analysis

The general trends of our SAR analysis are summarized in Fig. 3. When assessing the potency of the lipophilic side chains and the hydrocarbon linkers, amine and guanidine derivatives were not distinguished, as they generally follow the same trends.

We found that the antimicrobial activity decreased along the line of *n*-butyl > *n*-propyl > ethyl and haemolytic activity increased as follows: *n*-propyl < ethyl < *n*-butyl. The cyclic hydrocarbons, *n*-pentyl and *n*-hexyl displayed varying MIC values, but where all too haemolytic to be of any practical use and were therefore excluded from the list. Guanyl compounds with *n*-butyl linkers were more haemolytic than their amine counterparts. As mentioned before, for ethyl and *n*-propyl linkers this

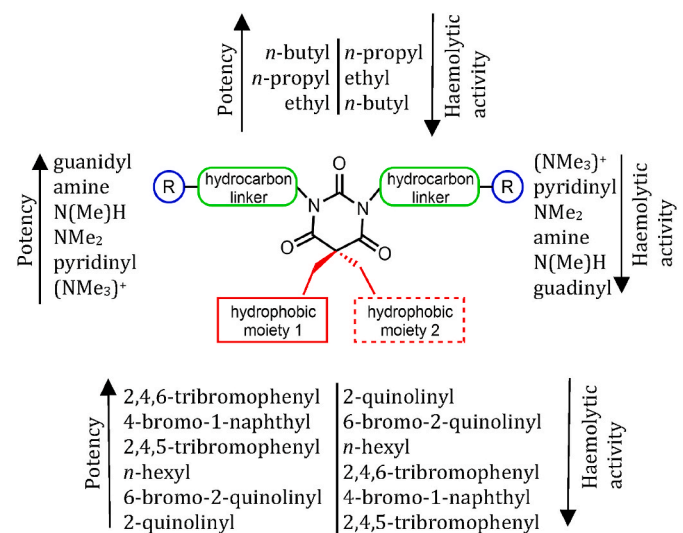


Fig. 3. Overview over the general trends observed during the SAR investigation. The trends for haemolytic activity were assessed for the average between the respective amines and guanidines.

trend was reversed. Based on this, *n*-propyl seemed to be the best compromise to achieve high antimicrobial activity and moderate haemolytic activity.

In line with our previous findings, the compounds potency and haemolytic activity increased with higher CLogP values of the lipophilic side chains for both, amines and guanidines. Bromines proved to be a good modulator of the hydrophobicity of aryl groups. The structure of the side chains seemed thereby to be secondary. The most potent compounds proved to be too haemolytic for future therapeutic considerations. By combining two lipophilic side chains of different structure and hydrophobicity (**11kG** and **11IG**), antimicrobial potency and haemolytic activity of the compounds could be fine-tuned.

To achieve good broad-spectrum activity, amine or guanidine groups proved to be necessary. Methylated primary amines showed reduced activity against Gram-negative *P. aeruginosa* alongside reduced haemolytic activity. The least haemolytic cationic groups were the quaternary ammonium compounds in **8a** and **9a**. Due to its lack of haemolytic activity and high activity against Gram-positive bacterial strains, **8a** could prove valuable for narrow-spectrum applications against Gram-positive bacteria.

2.4. Selectivity index

A common measurement for the efficiency of antimicrobial agents is the selectivity index (SI) given by the ratio EC₅₀/MIC values (for all SI values see Table S1). Our efforts led to promising candidates for narrow as well as broad-spectrum applications. We have grouped them into three groups (Table 6) based on their activity and SI against Gram-positive strains (entries 1–4), Gram-positive strains and *E. coli* (entries 5–7) and all strains tested (entries 8–11), respectively. Compounds were considered active if the MIC values were ≤16 µg/mL.

The first group, **8a**, **11kG**, **13cG** and **13hG** (Table 6, entries 1–4), comprised compounds that had a SI ≥ 54 for the Gram-positive strains, while showing no activity against Gram-negative strains and human red blood cells. These properties make them ideal candidates for narrow-spectrum application against Gram-positive bacteria.

Compounds in the second group had SI ≥ 40 (Table 6, entries 5–7) against the Gram-positive strains and the Gram-negative *E. coli* and a medium SI (<20) against Gram-negative *P. aeruginosa*. Of the three compounds **9**, **11IG** and **13pG**, only pyridinyl derivative **9** (entry 5) did not show measurable haemolytic activity. But despite having moderate EC₅₀ values (161 and 169 µg/mL), guanyl derivatives **11IG** and **13pG**

Table 6

Selectivity index (SI) of the most promising wide and narrow-spectrum antimicrobials. EC₅₀ values are given in [µg/mL].

Entry	Comp. ID	SI (EC ₅₀ /MIC) ^a				EC ₅₀ ^b
		S. a	B. s	E. c	P. a	
1	8a	>135	>67	–	–	>539
2	11kG	225	113	–	–	450
3	13cG	>62	>124	–	–	>497
4	13hG	>54	>109	–	–	>435
5	9a	>280	>140	>70	–	>559
6	11IG	81	40	81	10	161
7	13pG	169	169	85	11	169
8	13aG	93	93	47	23	187
9	13jA	23	46	23	23	176
10	13jG	111	222	56	28	445
11	13iA	40	81	40	20	323
12	1aA	20	40	20	10	79
13	1aG	31	31	31	8	62

Bacterial reference strains: S. a – *Staphylococcus aureus* ATCC 9144, B. s – *Bacillus subtilis* 168, E. c – *Escherichia coli* ATCC 25922, and P. a – *Pseudomonas aeruginosa* ATCC 27853.

^a No SI was calculated if the MIC was >16 µg/mL.

^b Values given as *greater than* correspond to the highest concentration (500 µM) tested in the RBC assay.

had a high SI.

The third group comprises molecules with a SI ≥ 20 (Table 6, entries 8–11) against all four strains. Compounds **13aG** and **13jA** (entries 8–9) displayed a good overall SI and had also good activity against the Gram-negative *P. aeruginosa* (MIC: 8 µg/mL). Compounds **13jG** and **13iA** (entries 10–11) were mildly potent against *P. aeruginosa* (MIC: 16 µg/mL), but due to their low haemolytic activity they still display promising SI values. Their absence of cytotoxicity makes them promising candidates, despite their mild activity against Gram-negative *P. aeruginosa*, keeping in mind that most naturally occurring AMPs display low activity against this Gram-negative strain as well [17]. Additionally, group 3 compounds generally matched or outperformed our reference compounds **1aA** and **1aG** (entries 12–13).

2.5. Effect of the counterion on solubility and activity

The counterion of acidic and basic drugs is known to greatly influence their overall physicochemical properties such as solubility, membrane permeability and stability [54,55]. From the long list of physiological anions for basic active pharmaceutical ingredients (APIs), hydrochloride salts are predominant [55] and known to improve water solubility [56].

We found that the water solubility of the TFA salts decreased noticeably when the CLogP values of the lipophilic side chains rose beyond 4. To study if we could counteract this trend, we converted selected compounds to HCl salts. Additionally, we wanted to investigate if the counterion affected the biological activity. Table 7 summarizes the re-evaluated MIC and EC₅₀ values of selected compounds as hydrochloride salts. Water solubility was assessed qualitatively by setting the threshold at 1 mg/mL. Entries 1–3 show that previously not soluble (–) TFA salts became soluble (+). Compound **13iG** (entry 4) and several others (data not shown) remained poorly soluble in water, especially if several bromine substituents were present in the lipophilic side chain.

Hydrochloride salts of the amine derivatives **13iA** and **13jA** exhibited no change in their MIC values and showed only slightly differing EC₅₀ values (entries 1–2). No clear trend could be observed whether hydrochloride salts tended to be more or less haemolytic than TFA salts. Surprisingly, the HCl salts of guanyl derivatives **13iG** and **13jG** displayed improved MIC values against *S. aureus* (Entries 3–4), while the activity against *E. coli* remained unchanged. Compound **13jG** was the only HCl salt being considerably more haemolytic than its TFA counterpart (Entry 3), for yet undetermined reasons. The deceptively higher haemolytic activity of derivatives **13iA** and **13iG** as HCl salts (Entry 2 and 4) can be attributed to the lower molecular weight of the HCl salts.

2.6. Mode of action studies

Luciferase-based biosensor assays (viability and membrane integrity)

Table 7

MIC and EC₅₀ values in µg/mL of selected di-TFA (first value) and dihydrochloride (HCl, second value) salts. Improved values are highlighted in green.

Entry	Code	MIC [µg/mL] ^a		EC ₅₀ [µg/mL]	Solubility ^b
		S. a	E. c		
1	13jA	8/8	8/8	176/224	–/+
2	13iA	8/8	8/8	323/271 ^c	–/+
3	13jG	4/2	8/8	445/118	–/+
4	13iG	2/0.5	8/8	348/291 ^d	–/–

^a Bacterial reference strains: S. a – *Staphylococcus aureus* ATCC 9144 and E. c – *Escherichia coli* ATCC 25922.

^b If solubility in pure water is equal or greater than 1 mg/mL it is denoted with (+), if lower (–).

^c EC₅₀ = 368/375 µM (TFA/HCl).

^d EC₅₀ = 362/362 µM (TFA/HCl).

were performed to explore the mode of action of promising compounds on *B. subtilis* 168 and *E. coli* K12 [57]. The biosensor-based viability assay measures bacterial viability as light production through recombinantly expressed bacterial luciferase originating from the *Photobacterium luminescens lux* operon. The addition of external substrates does not affect the production of light by the bacterial *lux* operon. The bacterium itself provides the pool of reduced flavin mononucleotide (FMNH₂) and long-chain aliphatic aldehydes, which are the substrates responsible for light production. Bacterial luciferase is an excellent real-time sensor for bacterial viability, as NADH, NADPH, and ATP are necessary to constantly top up the substrates' pool.

The biosensor-based membrane integrity assay depends on the luciferase (*lucGR* gene) originating from the luminous click beetle *Pyrophorus plagiophthalmus*. In contrast to bacterial luciferase, the light reaction of *lucGR* is stringently reliant on the substrate D-luciferin, which is added externally. D-luciferin is inadequately crossing intact biological membranes at neutral pH. After the addition of antimicrobial substances, the uptake is explored to determine if the membrane becomes permeable to the substrate D-luciferin. An increase in light production occurs when D-luciferin enters (increased influx) through a compromised membrane. Light production peaks rapidly if membrane integrity is compromised and, thereafter, usually decreases while the ATP from dying cells is consumed.

Based on structural modifications, MIC values, haemolytic activity, and selectivity index, 17 compounds were selected for mode of action studies against *B. subtilis* 168 (see Supporting Information, Table S2) as they were mainly potent against Gram-positive bacteria. Furthermore, based on their broad-spectrum activity, 14 additional compounds were tested against both, the Gram-positive *B. subtilis* 168 and the Gram-negative *E. coli* K12 biosensor strain (see the Supporting Information, Tables S2 and S3). In general, most of the compounds tested affected viability and showed strong membrane disrupting activity against both bacterial strains. However, some of the compounds showed a more pronounced effect on viability and a faster membranolytic effect against

B. subtilis compared to *E. coli*. For most compounds, both viability and membrane integrity were affected when the concentration of the compounds was higher than the MIC value. Additionally, increasing concentrations affected viability and membranolytic activity in increasing rates, indicating a concentration-dependent killing effect. We could not determine any relationship between structure/activity and the mode of action profiles.

We selected the broad-spectrum barbiturate **111G** to exemplify the results of the viability and membrane integrity assay in detail (Fig. 4 and Fig. 5). Barbiturate **111G** clearly affected the viability of *B. subtilis* (Fig. 4A, left). The membrane integrity assay was performed on the *B. subtilis* biosensor strain to confirm that the rapid decrease in bacterial viability was caused by membrane damage. Derivative **111G** showed a membrane-related mode of action as light emission decreased rapidly in a dose-dependent manner (Fig. 4B, left), similar to chlorhexidine (CHX) (Fig. 4B, right). The reference control CHX is a bactericidal agent recognized for its cell wall and membrane disruptive properties [58], with MIC values of 1.5 µg/mL against both, *B. subtilis* 168 and *E. coli* K12. The disruptive membrane effect of barbiturate **111G** on *B. subtilis* was shown at a concentration as low as 6.4 µg/mL, which is approximately 1.6 times higher than its MIC (4 µg/mL) (Fig. 4B, left). The lowest concentration (3.2 µg/mL), which is slightly lower than its MIC value, showed a limited membrane disruption effect and the peak emission did not decline during the assay period. The bacterial concentration for these experiments was approximately 100 times higher than the concentration used in the MIC assay, which could explain why slightly higher concentrations of barbiturate **111G** were needed to affect the viability and membrane integrity.

When it comes to the effects of barbiturate **111G** on the viability and membrane integrity in the Gram-negative *E. coli*, the picture is somewhat different from that of the Gram-positive *B. subtilis*. The broad-spectrum derivative **111G** affected the viability of the *E. coli* strain and showed a concentration-dependent killing effect like CHX (Fig. 5A). Although **111G** affected the viability, a much less prominent inner

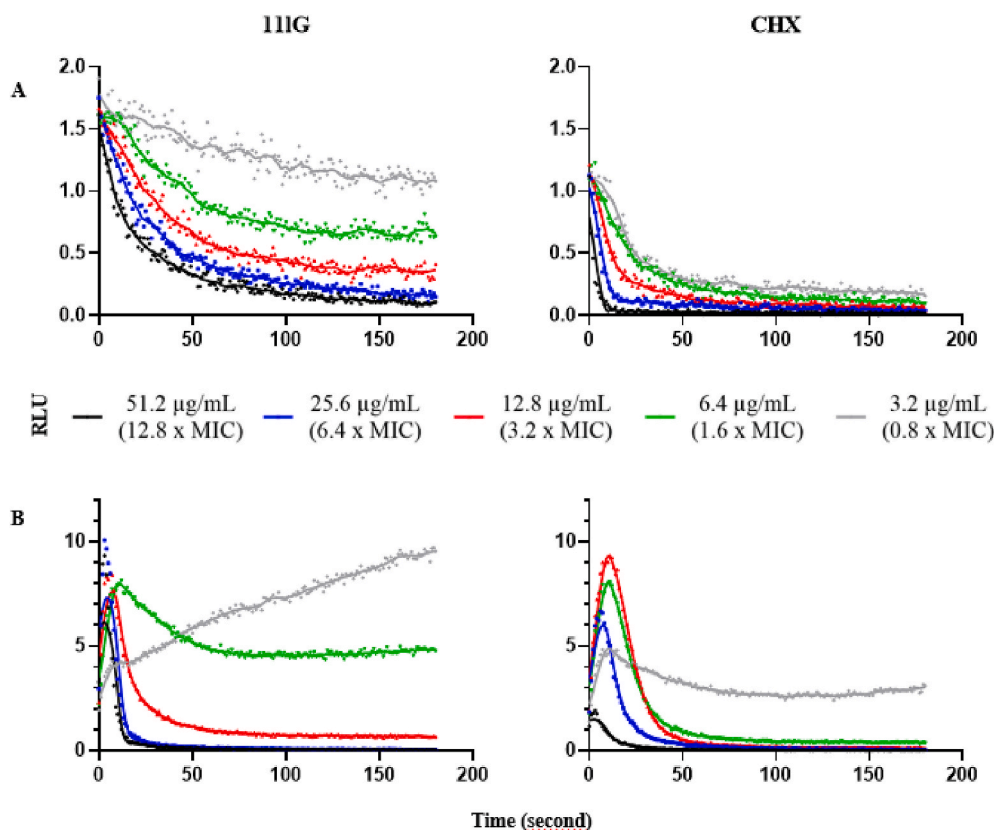


Fig. 4. The effects of **111G** (broad-spectrum) and CHX (positive control) on the kinetics of (A) viability and (B) membrane integrity in *B. subtilis* 168. Normalized light emission (normalized with a negative, untreated water control) is plotted as relative light units (RLU) over time (seconds). Light emission was measured each second for 180 s after adding the bacterial cell suspension (with 1 mM D-luciferin for the membrane integrity assay) to the analytes in separate wells. The multiples of the MIC values given in parentheses refers only to compound **111G**. The figure shows a representative data set from at least three independent experiments.

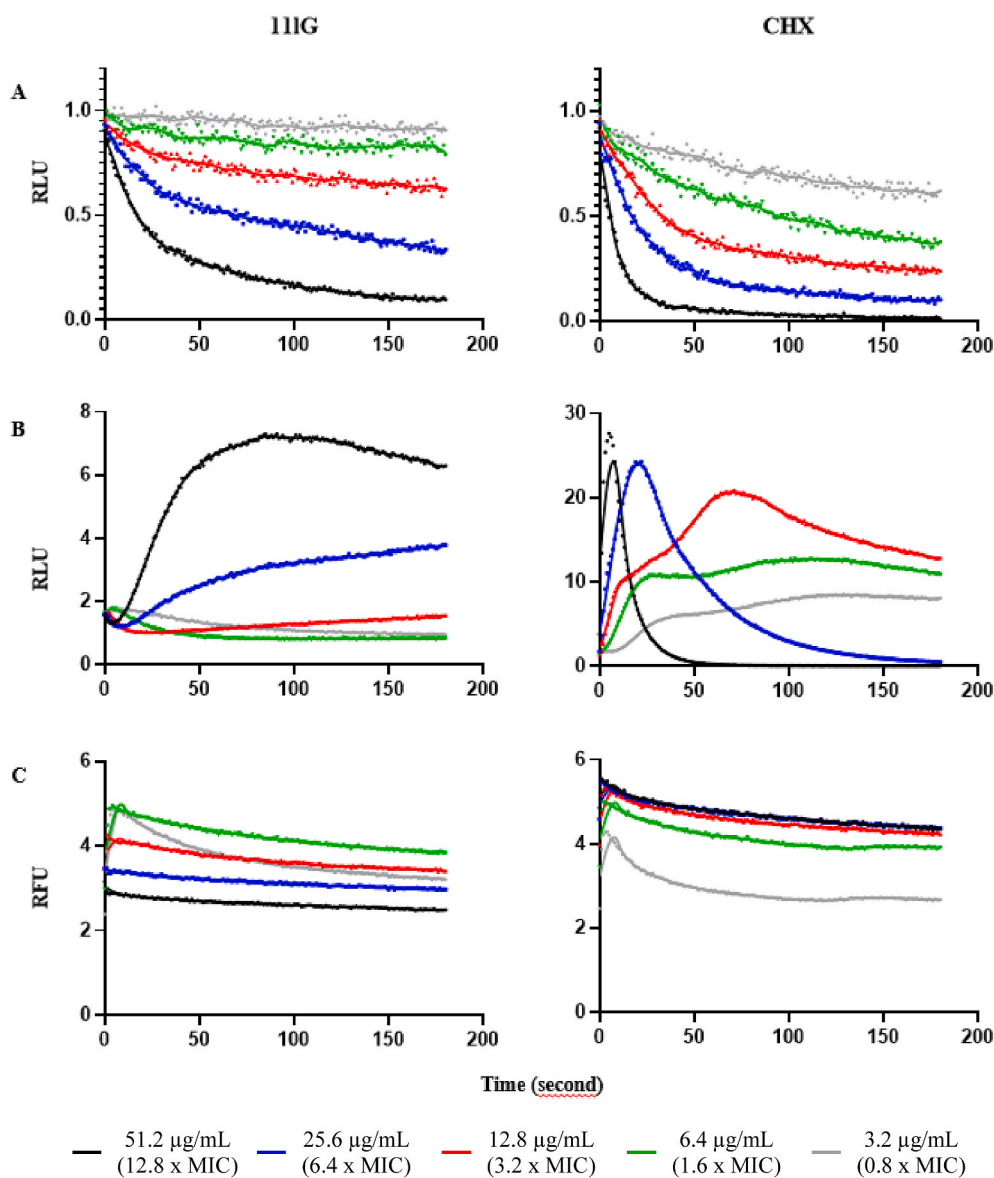


Fig. 5. The effects of **111G** (broad-spectrum) and a **CHX** (positive control) on the kinetics of (A) viability and (B) inner membrane integrity (C) outer membrane integrity in *E. coli* K12. Normalized light emission (normalized with a negative, untreated water control) is plotted as relative light units (RLU) over time (seconds) for A and B. For C, normalized fluorescence (normalized with a negative, untreated water control) is plotted as relative fluorescence units (RFU) over time (seconds). Light emission/fluorescence was measured each second for 180 s after adding the bacterial cell suspension (with 1 mM D-luciferin for the inner membrane integrity assay and 20 μ M 1-N-phenyl-naphthylamine for outer membrane integrity assay) to the analytes in separate wells. The multiples of the MIC values given in parentheses refers only to compound **111G**. The figure shows a representative data set from at least three independent experiments.

membrane disruptive effect was observed as only the two highest concentrations (6.4 – 12.8x MIC) gave a rise in light emission (and did not decline during the test period) (Fig. 5B, left). The delayed and reduced action of **111G** on the membrane integrity might be due to the outer membrane of *E. coli*, which probably acts as an additional barrier.

To confirm the assumption about the outer membrane barrier in *E. coli*, we used the 1-N-phenyl-naphthylamine (NPN) fluorescent probe to determine whether compound **111G** can affect the outer membrane to become more permeable. The small molecule NPN (219 Da) is weakly fluorescent in an aqueous solution, but when bound to phospholipids, it gives strong fluorescence [59]. The hydrophobic NPN cannot efficiently cross the outer membrane of intact *E. coli* cells, yielding low fluorescence, but if the outer membranes is compromised, NPN can reach the periplasmic space and bind phospholipids of the inner and outer membranes, thus producing increased fluorescence. In this assay, low concentrations (3.2 μ g/mL) of barbiturate **111G** led to higher fluorescence levels (Fig. 5C, left), but did not initially give any increase in luminescence in the inner membrane integrity assay (Fig. 5B, left). This phenomenon suggests that most of the cells are intact and viable without having significantly compromised integrity of the inner membrane but have increased permeability of the outer membrane. Upon increasing

the concentration of barbiturate **111G**, the fluorescence levels were lower (Fig. 5C, left) indicating either an intact outer membrane or rapid membrane disintegration before the start of the measurement. At the same time the viability of the bacterial cells was clearly reduced (Fig. 5A, left) and the inner membrane integrity was impaired (Fig. 5B, left).

When the 10 μ L sample of the NPN assay was spotted on an agar plate after the test period, the viability of the bacterial cells was clearly reduced for concentrations of 25.6–51.2 μ g/mL (6.4 – 12.8x MIC) (see Fig. S4), confirming the bactericidal effect of barbiturate **111G**. Those results strongly suggest that barbiturate **111G** disrupts both the outer and the inner membrane at the same rate when the concentration is high enough. However, it cannot be excluded that higher concentrations of **111G** induce a different mode of action, resulting in the compound crossing the outer membrane without disrupting it.

Our results indicate that the primary mode of action for most of the compounds, including the broad-spectrum barbiturate **111G**, against both the Gram-positive *B. subtilis* and the Gram-negative *E. coli*, is the disruption of the membrane integrity in a concentration-dependent manner. However, it is known that certain cationic AMPs exhibit a concentration-dependent dual mode of action [60]. For example, the

N-terminal 1–35 fragment of Bac7 (a proline-arginine-rich AMP) is known to affect the inner membrane at high concentrations and bind to and affect intracellular chaperone protein DnaK and 70S ribosomes at lower concentrations [61–63]. Therefore, there might also be other targets than the bacterial cytoplasmic membrane, and more work is required to conclude if there is any dual mode of action present or not.

3. Conclusion

In the present study, we have investigated the qualitative influence of the individual structural components of *N,N*-dialkylated-5,5-disubstituted amphipathic barbiturates on their bioactivity. We found that *n*-propyl linkers provide the best balance between antibacterial potency and haemolytic activity and *n*-butyl linkers provide the highest potency. Guanidyl head-groups led to the highest antimicrobial potency, whereas trimethylated amines proved to be attractive for narrow-spectrum application. By choosing the individual components carefully, we were able to prepare several compounds having SI values ≥ 20 and being active towards two (8a, 11kG, 13cG, 13hG), three (9a, 11iG, 13pG) or all four (13aG, 13iA, 13jA, 13jG) strains of our test panel. The best compounds (13aG, 13jG and 13jA) had an improved selectivity index compared to the initial starting point (1aG).

Studies on the integrity of the membranes and the viability of bacterial cells suggest that our compounds exert their bactericidal activity by disrupting the bacterial cell wall of Gram-positive *B. subtilis* in a concentration-dependent manner as exemplified by barbiturate 11iG. In Gram-negative *E. coli* both, the inner and outer membrane, were supposedly rapidly disrupted at higher compound concentration, but a second mechanism of action might be present in addition.

We believe that our detailed analysis can help to devise new amphipathic cationic mimics of antimicrobial peptides.

4. Experimental section

For a detailed description of all chemical and biological experimental procedures, chemical analysis, and supporting results, see the Supporting Information. Additional raw data is available through the DataverseNO repository, link: <https://doi.org/10.18710/GNTWOG>.

Author contributions

M.K.L., A.B. and M.B.S. designed the compound library; M.K.L. and F. Z. performed the compound synthesis and analysis; A.R., H.D., H.-M.B., T.H. and K.S. determined the biological assays; A.R., H.D., T.A. performed the biological assays and M.K.L., A.R., H.D., H.-M.B., T.H., K.S., A.B. and M.B.S. analysed and interpreted the data. The manuscript was written through contributions of all authors. All authors have given approval to the final version of the manuscript.

Declaration of competing interest

The authors declare that they have no known competing financial interests or personal relationships that could have appeared to influence the work reported in this paper.

Data availability

Additional raw data is available through the DataverseNO repository, link: <https://doi.org/10.18710/GNTWOG>.

Acknowledgements

MKL, AR and HD thank for a PhD fellowship provided by UiT as part of the AntifoMar and LeadScAMR grants.

Appendix A. Supplementary data

Supplementary data to this article can be found online at <https://doi.org/10.1016/j.ejmech.2022.114632>.

References

- [1] M.I. Hutchings, A.W. Truman, B. Wilkinson, Antibiotics: past, present and future, *Curr. Opin. Microbiol.* 51 (2019) 72–80.
- [2] Global Action Plan on Antimicrobial Resistance, World Health Organization, Geneva, 2015.
- [3] P.D. Tamma, S.E. Cosgrove, L.L. Maragakis, Combination therapy for treatment of infections with gram-negative bacteria, *Clin. Microbiol. Rev.* 25 (2012) 450–470.
- [4] M. Laws, A. Shaaban, K.M. Rahman, Antibiotic resistance breakers: current approaches and future directions, *FEMS Microbiol. Rev.* 43 (2019) 490–516.
- [5] S.M. Mandal, A. Roy, A.K. Ghosh, T.K. Hazra, A. Basak, O.L. Franco, Challenges and future prospects of antibiotic therapy: from peptides to phages utilization, *Front. Pharmacol.* 5 (2014) 1–12.
- [6] M.R. Hamblin, T. Hasan, Photodynamic therapy: a new antimicrobial approach to infectious disease? *Photochem. Photobiol. Sci.* 3 (2004) 436–450.
- [7] A. DiGiandomenico, B.R. Sellman, Antibacterial monoclonal antibodies: the next generation? *Curr. Opin. Microbiol.* 27 (2015) 78–85.
- [8] N. Beyth, Y. Hourri-Haddad, A. Domb, W. Khan, R. Hazan, Alternative antimicrobial approach: nano-antimicrobial materials, *Evid. base Compl. Alternative Med.* 2015 (2015), 246012.
- [9] M.S. Mulani, E.E. Kamble, S.N. Kumkar, M.S. Tawre, K.R. Pardesi, Emerging strategies to combat ESKAPE pathogens in the era of antimicrobial resistance: a review, *Front. Microbiol.* 10 (2019) 1–24.
- [10] R.E. Hancock, A. Patrzykat, Clinical development of cationic antimicrobial peptides: from natural to novel antibiotics, *Curr. Drug Targets: Infect. Disord.* 2 (2002) 79–83.
- [11] M. Mahlapuu, J. Håkansson, L. Ringstad, C. Björn, Antimicrobial peptides: an emerging category of therapeutic agents, *Front. Cell. Infect. Microbiol.* 6 (2016) 1–12.
- [12] R.E.W. Hancock, H.-G. Sahl, Antimicrobial and host-defense peptides as new anti-infective therapeutic strategies, *Nat. Biotechnol.* 24 (2006) 1551–1557.
- [13] M. Pasupuleti, A. Schmidtchen, M. Malmsten, Antimicrobial peptides: key components of the innate immune system, *Crit. Rev. Biotechnol.* 32 (2012) 143–171.
- [14] M.R. Yeaman, N.Y. Yount, Mechanisms of antimicrobial peptide action and resistance, *Pharmacol. Rev.* 55 (2003) 27–55.
- [15] R.E.W. Hancock, Peptide antibiotics, *Lancet* 349 (1997) 418–422.
- [16] K.L. Brown, R.E.W. Hancock, Cationic host defense (antimicrobial) peptides, *Curr. Opin. Immunol.* 18 (2006) 24–30.
- [17] A. Ebbensgaard, H. Mordhorst, M.T. Overgaard, C.G. Nielsen, F.M. Aarestrup, E. B. Hansen, Comparative evaluation of the antimicrobial activity of different antimicrobial peptides against a range of pathogenic bacteria, *PLoS One* 10 (2015), e0144611.
- [18] K. Fosgerau, T. Hoffmann, Peptide therapeutics: current status and future directions, *Drug Discov. Today* 20 (2015) 122–128.
- [19] Y. Yang, Z. Cai, Z. Huang, X. Tang, X. Zhang, Antimicrobial cationic polymers: from structural design to functional control, *Polym. J.* 50 (2018) 33–44.
- [20] A. Strassburg, F. Kracke, J. Wenners, A. Jemeljanova, J. Kuepper, H. Petersen, J. C. Tiller, Nontoxic, hydrophilic cationic polymers—identified as class of antimicrobial polymers, *Macromol. Biosci.* 15 (2015) 1710–1723.
- [21] D. Liu, W.F. DeGrado, De novo design, synthesis, and characterization of antimicrobial β -peptides, *J. Am. Chem. Soc.* 123 (2001) 7553–7559.
- [22] P. Sang, Y. Shi, P. Teng, A. Cao, H. Xu, Q. Li, J. Cai, Antimicrobial AApeptides, *Curr. Top. Med. Chem.* 17 (2017) 1266–1279.
- [23] T. Hansen, T. Alst, M. Havelkova, M.B. Ström, Antimicrobial activity of small β -peptidomimetics based on the pharmacophore model of short cationic antimicrobial peptides, *J. Med. Chem.* 53 (2010) 595–606.
- [24] P. Teng, A. Nimmagadda, M. Su, Y. Hong, N. Shen, C. Li, L.-Y. Tsai, J. Cao, Q. Li, J. Cai, Novel bis-cyclic guanidines as potent membrane-active antibacterial agents with therapeutic potential, *Chem. Commun.* 53 (2017) 11948–11951.
- [25] M.H. Paulsen, E.A. Karlens, D. Ausbacher, T. Anderssen, A. Bayer, P. Ochtrop, C. Hedberg, T. Haug, J.U. Ericson Sollid, M.B. Ström, An amphipathic cyclic tetrapeptide scaffold containing halogenated $\beta^{2,2}$ -amino acids with activity against multidrug-resistant bacteria, *J. Pept. Sci.* 24 (2018) e3117.
- [26] M.H. Paulsen, D. Ausbacher, A. Bayer, M. Engqvist, T. Hansen, T. Haug, T. Anderssen, J.H. Andersen, J.U.E. Sollid, M.B. Ström, Antimicrobial activity of amphipathic α,α -disubstituted β -amino amide derivatives against ESBL – CARBA producing multi-resistant bacteria; effect of halogenation, lipophilicity and cationic character, *Eur. J. Med. Chem.* 183 (2019), 111671.
- [27] M. Wang, X. Feng, R. Gao, P. Sang, X. Pan, L. Wei, C. Lu, C. Wu, J. Cai, Modular design of membrane-active antibiotics: from macromolecular antimicrobials to small scorpionlike peptidomimetics, *J. Med. Chem.* 64 (2021) 9894–9905.
- [28] M.H. Paulsen, M. Engqvist, D. Ausbacher, T. Anderssen, M.K. Langer, T. Haug, G. R. Morello, L.E. Liikanen, H.-M. Blencke, J. Isaksson, E. Juskevit, A. Bayer, M. B. Ström, Amphipathic barbiturates as mimics of antimicrobial peptides and the marine natural products eusynstyelamides with activity against multi-resistant clinical isolates, *J. Med. Chem.* 64 (2021) 11395–11417.
- [29] D.M. Tapiolas, B.F. Bowden, E. Abou-Mansour, R.H. Willis, J.R. Doyle, A. N. Muirhead, C. Liprot, L.E. Llewellyn, C.W. Wolff, A.D. Wright, C.A. Motti,

- B. Eusynstyelamides A, C. nNOS inhibitors, From the ascidian Eusynstyela latericius, *J. Nat. Prod.* 72 (2009) 1115–1120.
- [30] M. Tadesse, J.N. Tabudravu, M. Jaspars, M.B. Strom, E. Hansen, J.H. Andersen, P. E. Kristiansen, T. Haug, The antibacterial ent-eusynstyelamide B and eusynstyelamides D, E, and F from the Arctic bryozoan *Tegella cf. spitzbergensis*, *J. Nat. Prod.* 74 (2011) 837–841.
- [31] M.F. Richter, B.S. Drown, A.P. Riley, A. Garcia, T. Shirai, R.L. Svec, P. J. Hergenrother, Predictive compound accumulation rules yield a broad-spectrum antibiotic, *Nature* 545 (2017) 299–304.
- [32] S.J. Perlmutter, E.J. Geddes, B.S. Drown, S.E. Motika, M.R. Lee, P.J. Hergenrother, Compound uptake into *E. coli* can be facilitated by N-alkyl guanidiniums and pyridiniums, *ACS Infect. Dis.* 7 (2021) 162–173.
- [33] S. Zhang, Z. Shi, W. Cao, T. Gao, H. Deng, Synthesis of a series of perfluoroalkyl containing spiro cyclic barbituric acid derivatives, *J. Chem. Res.* 2009 (2009) 381–383.
- [34] S. Kotha, A.C. Deb, R.V. Kumar, Spiro-annulation of barbituric acid derivatives and its analogs by ring-closing metathesis reaction, *Bioorg. Med. Chem. Lett.* 15 (2005) 1039–1043.
- [35] K.T. Mahmudov, M.N. Kopylovich, A.M. Maharramov, M.M. Kurbanova, A. V. Gurbanov, A.J.L. Pombeiro, Barbituric acids as a useful tool for the construction of coordination and supramolecular compounds, *Coord. Chem. Rev.* 265 (2014) 1–37.
- [36] J.T. Bojarski, J.L. Mokrosz, H.J. Bartoń, M.H. Paluchowska, Recent progress in barbituric acid chemistry, in: A.R. Katritzky (Ed.), *Adv. Heterocycl. Chem.*, Academic Press, 1985, pp. 229–297.
- [37] J.V. Tate, W.N. Tinnerman II, V. Jurevics, H. Jeskey, E.R. Biehl, Preparation of 5-substituted benzylbarbituric acids and investigation of the effect of the benzyl and substituted benzyl groups on the acidity of barbituric acid, *J. Heterocycl. Chem.* 23 (1986) 9–11.
- [38] D.B. Ramachary, M. Kishor, Y.V. Reddy, Development of pharmaceutical drugs, drug intermediates and ingredients by using direct organo-click reactions, *Eur. J. Org. Chem.* 2008 (2008) 975–993.
- [39] S.J. Kalita, D.C. Deka, 2-Phenyl-2,3-dihydrobenzo[d]thiazole: a mild, efficient, and highly active in situ generated chemoselective reducing agent for the one-pot synthesis of 5-monoalkylbarbiturates in water, *Synlett* 29 (2018) 477–482.
- [40] J.D. Figueroa-Villar, E.R. Cruz, N. Lucia dos Santos, Synthesis of oxadiazaflavines from barbituric acid and aromatic aldehydes, *Synth. Commun.* 22 (1992) 1159–1164.
- [41] A.A. Vieira, B.G. Marinho, L.G. de Souza, P.D. Fernandes, J.D. Figueroa-Villar, Design, synthesis and in vivo evaluation of sodium 2-benzyl-chloromalonates as new central nervous system depressants, *MedChemComm* 6 (2015) 1427–1437.
- [42] S. Fletcher, The Mitsunobu reaction in the 21st century, *Org. Chem. Front.* 2 (2015) 739–752.
- [43] A.R. Katritzky, B.V. Rogovoy, Recent developments in guanylating agents, *Archive for Organic Chem.* 2005 (2005) 49–87.
- [44] T. Gers, D. Kunce, P. Markowski, J. Izdebski, Reagents for efficient conversion of amines to protected guanidines, *Synthesis* 2004 (2004) 37–42.
- [45] K. Midura-Nowaczek, A. Markowska, Antimicrobial peptides and their analogs: searching for new potential therapeutics, *Perspect. Med. Chem.* 6 (2014) 73–80.
- [46] J.S. Dickson, M. Koohmarai, Cell surface charge characteristics and their relationship to bacterial attachment to meat surfaces, *Appl. Environ. Microbiol.* 55 (1989) 832–836.
- [47] G.M. Bruinsma, M. Rustema-Abbing, H.C. van der Mei, C. Lakkis, H.J. Busscher, Resistance to a polyquaternium-1 lens care solution and isoelectric points of *Pseudomonas aeruginosa* strains, *J. Antimicrob. Chemother.* 57 (2006) 764–766.
- [48] A. Skrzypczak, B. Brycki, I. Mirska, J. Pernak, Synthesis and antimicrobial activities of new quats, *Eur. J. Med. Chem.* 32 (1997) 661–668.
- [49] F. Devínský, I. Lacko, F. Bittererová, D. Mlynářčík, Quaternary ammonium-salts. 18. Preparation and relationship between structure, IR spectral characteristics, and antimicrobial activity of some new bis-quaternary isomers of 1,5-pentanediammonium dibromides, *Chem. Pap.* 6 (1987) 803–814.
- [50] P. Gilbert, L.E. Moore, Cationic antiseptics: diversity of action under a common epithet, *J. Appl. Microbiol.* 99 (2005) 703–715.
- [51] T. Hansen, M.K. Moe, T. Anderssen, M.B. Strøm, Metabolism of small antimicrobial β 2,2-amino acid derivatives by murine liver microsomes, *Eur. J. Drug Metab. Pharmacokinet.* 37 (2012) 191–201.
- [52] E.P. Gillis, K.J. Eastman, M.D. Hill, D.J. Donnelly, N.A. Meanwell, Applications of fluorine in medicinal chemistry, *J. Med. Chem.* 58 (2015) 8315–8359.
- [53] D.H. McDaniel, H.C. Brown, An extended table of hammett substituents constants based on the ionization of substituted benzoic acids, *J. Org. Chem.* 23 (1958) 420–427.
- [54] D. Gupta, D. Bhatia, V. Dave, V. Sutariya, S. Varghese Gupta, Salts of therapeutic agents: chemical, physicochemical, and biological considerations, *Molecules* 23 (2018) 1719.
- [55] A.T.M. Serajuddin, Salt formation to improve drug solubility, *Adv. Drug Deliv. Rev.* 59 (2007) 603–616.
- [56] P.L. Gould, Salt selection for basic drugs, *Int. J. Pharm.* 33 (1986) 201–217.
- [57] M. Virta, K.E.O. Åkerman, P. Saviranta, C. Oker-Blom, M.T. Karp, Real-time measurement of cell permeabilization with low-molecular-weight membranolytic agents, *J. Antimicrob. Chemother.* 36 (1995) 303–315.
- [58] T. Kuyyakanond, L.B. Quesnel, The mechanism of action of chlorhexidine, *FEMS Microbiol. Lett.* 100 (1992) 211–215.
- [59] B. Loh, C. Grant, R.E. Hancock, Use of the fluorescent probe 1-N-phenyl-naphthylamine to study the interactions of aminoglycoside antibiotics with the outer membrane of *Pseudomonas aeruginosa*, *Antimicrob. Agents Chemother.* 26 (1984) 546–551.
- [60] M. Graf, M. Mardrossian, F. Nguyen, A.C. Seefeldt, G. Guichard, M. Scocchi, C. A. Innis, D.N. Wilson, Proline-rich antimicrobial peptides targeting protein synthesis, *Nat. Prod. Rep.* 34 (2017) 702–711.
- [61] E. Podda, M. Benincasa, S. Pacor, F. Micali, M. Mattiuzzo, R. Gennaro, M. Scocchi, Dual mode of action of Bac7, a proline-rich antibacterial peptide, *Biochim. Biophys. Acta* 1760 (2006) 1732–1740.
- [62] M.L. Scocchi, P. Decarli, G. Mignogna, P. Christen, R. Gennaro, The proline-rich antibacterial peptide Bac7 binds to and inhibits in vitro the molecular chaperone DnaK, *Int. J. Pept. Res. Therapeut.* 15 (2009) 147–155.
- [63] M. Mardrossian, R. Grzela, C. Giglione, T. Meinel, R. Gennaro, P. Mergaert, M. Scocchi, The host antimicrobial peptide Bac71-35 binds to bacterial ribosomal proteins and inhibits protein synthesis, *Chem. Biol.* 21 (2014) 1639–1647.

Supporting Information

for

A concise SAR-analysis of antimicrobial cationic amphipathic barbiturates for an improved activity-toxicity profile

Manuel K. Langer^{a#}, Ataur Rahman^{b#}, Hymonti Dey^b, Trude Anderssen^c, Francesco Zilioli^a, Tor Haug^b, Hans-Matti Blencke^b, Klara Stensvåg^b, Morten B. Strøm^{c*}, Annette Bayer^{a*}

^a Department of Chemistry, UiT – The Arctic University of Norway, NO-9037 Tromsø, NORWAY.

^b The Norwegian College of Fishery Science, Faculty of Biosciences, Fisheries and Economics, UiT – The Arctic University of Norway, NO-9037 Tromsø, NORWAY.

^c Department of Pharmacy, Faculty of Health Sciences, UiT – The Arctic University of Norway, NO-9037 Tromsø, NORWAY.

Authors contributed equally; * Corresponding authors.

Table of Contents

1	Trends in haemolytic activity	2
1.1	Comparison of amines vs. guanidines by linker length.....	2
1.2	Comparison of <i>n</i> -propyl vs. <i>n</i> -butyl linkers by cationic group.....	3
2	Experimental procedures	5
2.1	General methods.....	5
2.2	Synthesis of starting materials.....	5
2.3	General procedures.....	5
2.4	Synthesis of barbiturates with identical lipophilic side chains 3a-j	7
2.5	Synthesis of barbiturates with mixed hydrophobic residues 3k-q	10
2.6	Synthesis of <i>series 1</i>	12
2.7	Synthesis of <i>series 2</i>	13
2.8	Synthesis of <i>series 3</i>	17
2.9	Synthesis of <i>series 4</i>	22
2.10	Synthesis of <i>series 5</i>	27
3	¹ H and ¹³ C NMR spectra of final compounds	33
3.1	¹ H and ¹³ C NMR spectra of compounds in <i>series 1</i>	33
3.2	¹ H and ¹³ C NMR spectra of compounds in <i>series 2</i>	37
3.3	¹ H and ¹³ C NMR spectra of compounds in <i>series 3</i>	49
3.4	¹ H and ¹³ C NMR spectra of compounds in <i>series 4</i>	62
3.5	¹ H and ¹³ C NMR spectra of compounds in <i>series 5</i>	77
4	SFC analysis of final compounds	91
5	Full selectivity index table.....	99
6	Biological methods.....	100
6.1	Minimum inhibitory concentration (MIC) assay.....	100
6.2	Membrane integrity assays.....	100
6.3	Viability assay	101
6.4	Red Blood Cell Haemolysis Assay.....	101
7	Membrane integrity and viability assay	102
8	Literature	104

1 Trends in haemolytic activity

We have grouped selected compounds into four scaffold groups for this comparison (**Figure S1**). Each group consisted of compounds with six different hydrophobic side chain combinations **a**, **e**, **i**, **j**, **l** and **p** for a given scaffold: *n*-propyl linkers and amine head groups **3CA** (**13A**, **13eA**, **13iA**, **13jA**, **13lA**, **13pA**) *n*-propyl linkers and guanidine head groups **3CG** (**13G**, **13eG**, **13iG**, **13jG**, **13lG**, **13pG**), *n*-butyl linkers and amine head groups **4CA** (**1aA**, **10eA**, **11lA**, **11pA**) and *n*-butyl linkers and guanidine head groups **4CG** (**1aG**, **10eG**, **11lG**, **11pG**). Compounds having two 6-bromo-2-quinolylyl (**10cA**, **10cG**, **13cA** and **13cG**) or two 4-trifluoromethylbenzyl (**13hA** and **13hG**) side chains were excluded due to their lack of haemolytic activity. EC₅₀ values for compounds containing *n*-butyl linkers and hydrophobic moieties 4-bromo-3-chlorobenzyl (**i**) and 3,5-bis(trifluoromethyl)benzyl (**j**) were obtained in our previous study.[1]

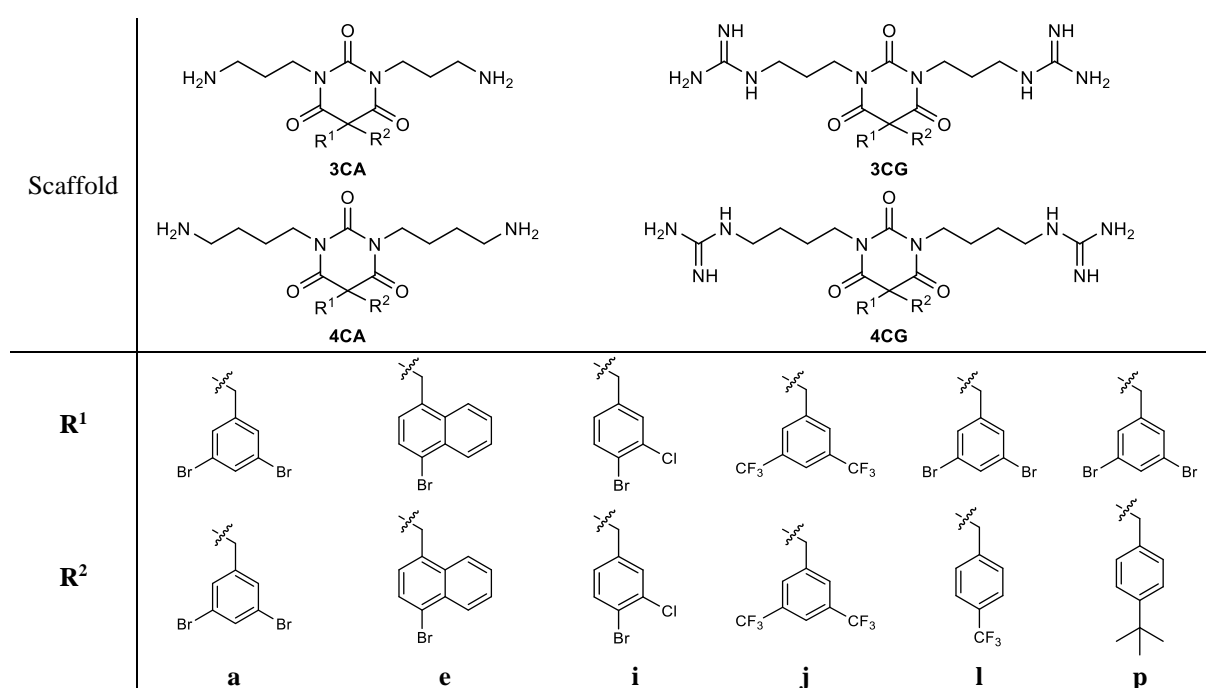


Figure S1. Overview of the scaffolds **3CA** (**13A**, **13eA**, **13iA**, **13jA**, **13lA**, **13pA**), **3CG** (**13G**, **13eG**, **13iG**, **13jG**, **13lG**, **13pG**), **4CA** (**1aA**, **10eA**, **11lA**, **11pA**) and **4CG** (**1aG**, **10eG**, **11lG**, **11pG**) and the linker combinations **a**, **e**, **i**, **j**, **l** and **p**.

1.1 Comparison of amines vs. guanidines by linker length

Figure S2 shows the comparison of haemolytic activity for amine and guanidine derivatives by linker length. For each compound series with a specific linker length (*n*-propyl **3C** or *n*-butyl **4C**) and hydrophobic side chain combination **a**, **e**, **i**, **j**, **l** and **p** we subtracted the EC₅₀ values, given in µg/mL, for the amine derivative (**A**) from the guanidyl derivative (**G**). For a negative value, the guanidine derivative was more and for a positive value less haemolytic than its amine counterpart.

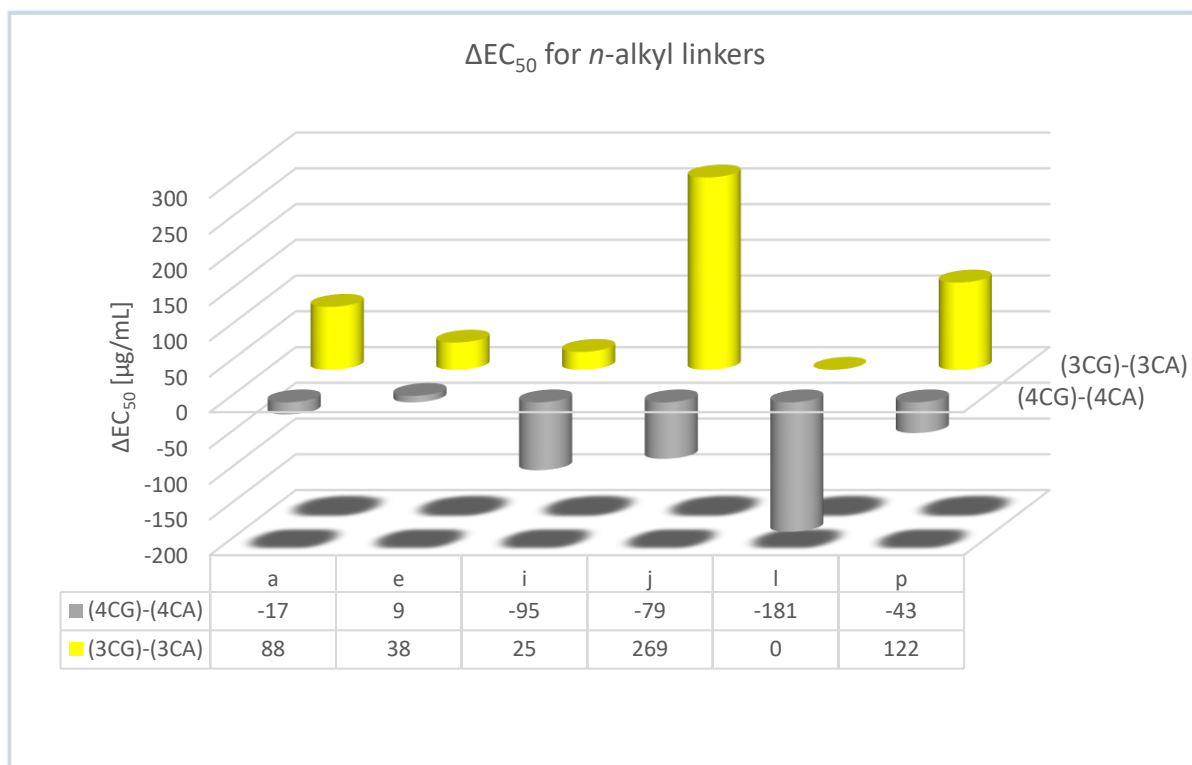


Figure S2. Comparison of the difference in haemolytic activity (EC_{50} values in $\mu\text{g/mL}$) between the amine and guanidine derivatives for two linker series. For a given hydrophobic side chain combination (**a**, **e**, **i**, **j**, **l** and **p**) and hydrophobic linker (*n*-propyl **3C** or *n*-butyl **4C**), the EC_{50} value of the amine derivative (**A**) was subtracted from the EC_{50} value of the guanidyl derivatives (**G**), stated as (**3CG**)-(**3CA**) and (**4CG**)-(**4CA**). For negative values the guanidine derivative was more haemolytic than the amine. For positive values the guanidine derivative was less haemolytic than the amine. X-axis: hydrophobic moieties **a**, **e**, **i**, **j**, **l** and **p**; Y-axis: ΔEC_{50} values in ($\mu\text{g/mL}$); Z-axis: linker series. Grey: Comparison of derivatives with a *n*-butyl linker. Yellow: Comparison of derivatives with a *n*-propyl.

1.2 Comparison of *n*-propyl vs. *n*-butyl linkers by cationic group

Using the same grouping (**Figure S1**) we looked at the difference of the haemolytic activity between amine derivatives (**A**) having either a *n*-butyl (**4CA**) or *n*-propyl linker (**3CA**). The same comparison was composed for the guanidine derivatives (**3CG** and **4CG**) (both **Figure S3**). For each compound series with a specific cationic group (**A** or **G**) and hydrophobic side chain combination **a**, **e**, **i**, **j**, **l** and **p**, we subtracted the EC_{50} values, given in $\mu\text{g/mL}$, for the *n*-butyl linker derivative (**4C**) from the *n*-propyl linker derivative (**3C**). For positive values the *n*-propyl derivatives were less and for negative values more haemolytic than their *n*-butyl containing counterparts.

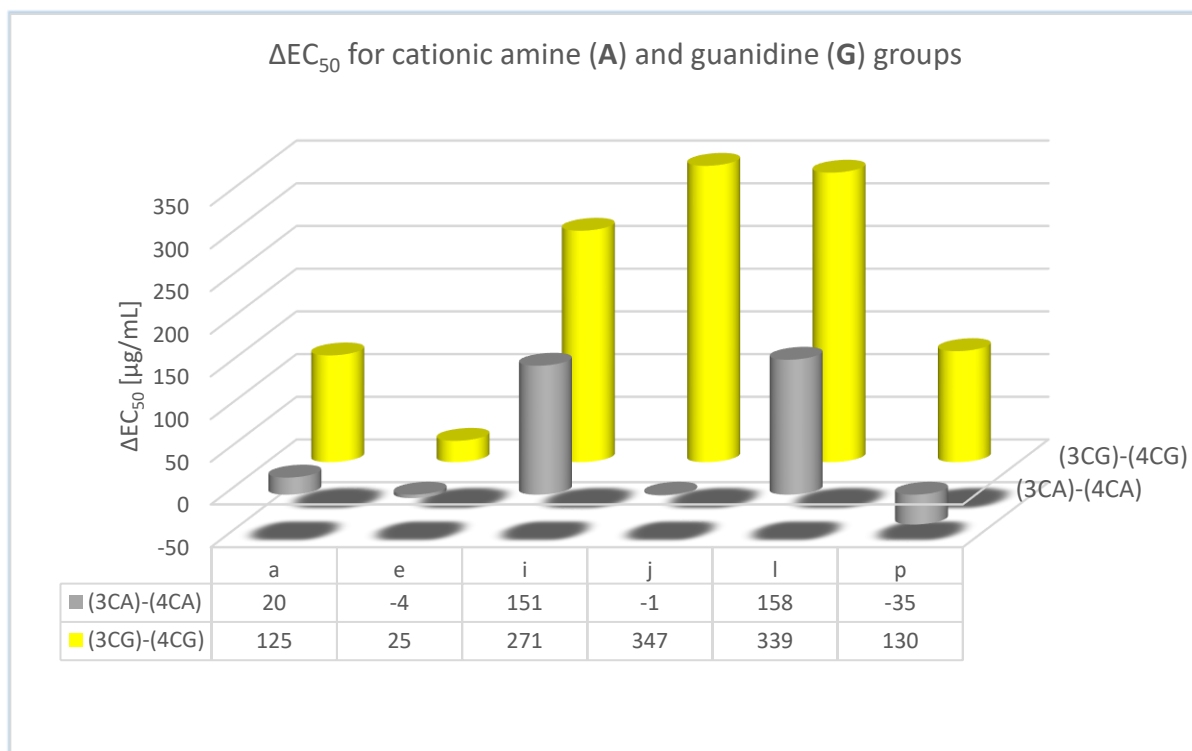


Figure S3. Comparison of the difference in haemolytic activity (EC_{50} values in $\mu\text{g/mL}$) between the *n*-propyl and *n*-butyl derivatives for the amine and guanidine series. For a given hydrophobic side chain (**a**, **e**, **i**, **j**, **l** and **p**) and cationic group (amine **A** or guanidine **G**), the EC_{50} value of the *n*-butyl (**4C**) was subtracted from the EC_{50} value of the *n*-propyl (**3C**) derivative, stated as (**3CG**)-(**4CG**) and (**3CA**)-(**4CA**). For a positive value the *n*-propyl (**3C**) containing derivatives were less and for a negative value they were more haemolytic than the *n*-butyl derivatives. X-axis: hydrophobic moieties **a**, **e**, **i**, **j**, **l** and **p**; Y-axis: ΔEC_{50} values in ($\mu\text{g/mL}$); Z-axis: cationic group series. Grey: Comparison of derivatives with an amine group (**A**). Yellow: Comparison of derivatives with a guanidine group (**G**).

2 Experimental procedures

2.1 General methods

Unless otherwise noted, purchased chemicals were used as received without further purification. Solvents were dried according to standard procedures over molecular sieves of appropriate size. Normal phase flash chromatography was carried out on silica gel 60 (230–400 mesh) or on an interchim® PuriFlash XS420 flash system with the sample preloaded on a Samplet® cartridge belonging to a Biotage SP-1 system. Purification by reversed phase (RP) C18 column chromatography (H₂O with 0.1 % TFA/MeCN with 0.1 % TFA) was performed on an interchim® PuriFlash XS420 flash system with the sample preloaded on a Samplet® cartridge. Thin layer chromatography was carried out using Merck TLC Silica gel 60 F254 and visualized by short-wavelength ultraviolet light or by treatment with an appropriate stain.

NMR spectra were obtained on a 400 MHz Bruker Advance III HD spectrometer equipped with a 5 mm SmartProbe BB/1H (BB = 19F, 31P-15N) at 20 °C. The chemical shifts are reported in ppm relative to the solvent residual peak (CDCl₃: δH 7.26 and δC 77.16; Methanol-d₄: δH 3.31 and δC 49.00; deuterium oxide: δH 4.79; DMSO-d₆ δH 2.51 and δC 39.52). ¹³C NMR spectra were obtained with ¹H decoupling. Data are represented as follows: chemical shift, multiplicity (s = singlet, d = doublet, t = triplet, q = quartet, p = pentet, h = heptet, dt = doublet of triplet, tt = triplet of triplet, m = multiplet), coupling constant (*J* in Hz) and integration. The raw data was analyzed with MestReNova (Version 14.0.0-23239).

High-resolution mass spectra (HRMS) were recorded from methanol solutions on an LTQ Orbitrap XL (Thermo Scientific) either in negative or in positive electrospray ionization (ESI) mode. The data was analyzed with Thermo Scientific Xcalibur software.

The purity of all tested compounds was determined to be ≥95%. The analyses were carried out on a Waters ACQUITY UPC² system equipped with a Torus™ DEA 130Å, 1.7 μm, 2.1 mm x 50 mm column or a Torus™ 2-PIC 130Å, 1.7 μm, 2.1 mm x 50 mm column. Compounds were detected on a Waters ACQUITY PDA detector spanning wavelengths from 190 to 650 nm, coupled to a Waters ACQUITY QDA detector for low resolution mass (LRMS) detection. The derivatives were eluted with a mobile phase consisting of supercritical CO₂ and MeOH containing 0.1 % NH₃ and a linear gradient of 2 – 40 % MeOH over 2 or 4 min followed by isocratic 0.5 min of 40% MeOH. The flow rate was 1.5 mL/min.

2.2 Synthesis of starting materials

1-bromo-4-(bromomethyl)naphthalene[2], 2-(bromomethyl)quinoline[2, 3], 6-bromo-2-(bromomethyl)quinoline[3], *tert*-butyl (2-bromoethyl)carbamate, *tert*-butyl (3-bromopropyl)carbamate [4], *tert*-butyl (2-hydroxyethyl)carbamate[5], *tert*-butyl (4-hydroxybutyl)carbamate[6], *N,N'*-di(*tert*-butoxycarbonyl)-guanidinybutanol[7] were prepared as described in literature. *tert*-butyl (5-hydroxypentyl)carbamate and *tert*-butyl (6-hydroxyhexyl)carbamate were purchased from commercial sources. Compounds **1eA** and **1eG** were synthesized as described in literature.[1]

Note: All final compounds were obtained as di-TFA salts. TFA is typically observed at δ 162.1 (q, J = 35.7 Hz) and δ 117.7 (q, J = 290.3 Hz) in ¹³C-NMR and is not reported for each compound individually.

2.3 General procedures

General procedure A: Synthesis of identically 5,5-disubstituted barbituric acids **3a-j**

Barbituric acid **2** was taken up in PEG-400 and sodium bicarbonate was added. The reaction mixture was stirred for 5 min before the respective benzyl bromide or alkyl halide was added in one portion. The suspension was stirred at elevated temperature until full conversion was achieved (TLC) and was then allowed to cool to ambient temperature. Upon addition of 10% NaHCO_{3(aq)} solution a white solid precipitated, which was filtered off and washed with 10% NaHCO_{3(aq)} solution, water, and heptane. The obtained solid was collected, mixed with water, and the suspension was heated to reflux for 15 min. After the suspension had cooled to ambient temperature, the solid was collected by filtration and lyophilized for 24 h. MeOH was added, and the resulting suspension was sonicated for 5 min. The suspension was filtered, and the residue was collected and dried to yield the 5,5-disubstituted barbituric acids.

If no precipitate was obtained upon addition of 10% NaHCO_{3(aq)} solution, the aqueous layer was extracted with a suitable solvent three times. The combined organics were dried over Na₂SO₄, filtered and the solvent was removed. The crude was purified by column chromatography on silica gel with EtOAc in heptane as eluent.

General procedure B: *N*-alkylation with alkyl halides and subsequent Boc deprotection

The 5,5-disubstituted barbituric acid **3c**, **e**, **h**, **i**, **j**, **l** or **p** was mixed with acetone and an inorganic base. The reaction mixture was stirred at ambient temperature for 10 min before *tert*-butyl-(3-bromopropyl)carbamate and TBAI were added. The suspension was heated until TLC indicated full conversion. The mixture was allowed to cool to ambient temperature and EtOAc and 10% NaHCO₃ (aq) solution were added. The layers were separated, and the organic layer was washed twice with 10 % NaHCO₃ (aq) solution. The organic layer was dried over MgSO₄, filtered and the solvent was removed under reduced pressure. The crude was purified on an automated flash system equipped with a silica column and EtOAc in heptane as eluent, to deliver the *N*-Boc-protected amines.

To the *N*-Boc-protected amine in DCM, was added TFA and the mixture was stirred at ambient temperature until HRMS indicated full conversion. The solvent was removed, and the crude product was purified on an automated flash system equipped with a C18 column and MeCN/H₂O containing 0.1% TFA as solvents. The product containing fractions were collected, the solvent was removed, and the product lyophilized for 48 h. The amines were obtained as di-TFA salts.

General procedure C: Guanidine formation

The di-TFA salts of the amines were mixed with THF and DIPEA and stirred at ambient temperature for 10 min. *N,N*-Di-Boc-1*H*-pyrazole-1-carboximidine was added and the solution was stirred at elevated temperatures until TLC indicated full conversion. The mixture was allowed to cool to ambient temperature and sat. NH₄Cl_(aq) solution and EtOAc were added. The layers were separated, and the aqueous layer was extracted twice with EtOAc. The combined organics were dried over Na₂SO₄, filtered and the solvent was removed. The crude products were purified on an automated flash system equipped with a silica column and EtOAc/heptane as eluent to yield the *N,N'*-di-Boc-protected guanidines.

The *N,N'*-di-Boc-protected guanidines were stirred with TFA in DCM at ambient temperature until HRMS indicated full conversion. In some cases, multiple additions of TFA were needed. The solvent was removed, and the crude product was purified on an automated flash system equipped with a C18 column and MeCN/H₂O containing 0.1% TFA as eluent. The product-containing fractions were collected, the solvent was removed, and the product was lyophilized for 48 h. The guanidines were obtained as di-TFA salts.

General Procedure D: *N*-alkylation via the Mitsunobu reaction

The respective 5,5-disubstituted barbituric acid **3b-g** and **3k-q**, the alcohol of choice and PPh₃ were mixed with anhydrous DCM in a heat dried vial under argon atmosphere. The mixture was cooled to 0 °C and upon dropwise addition of DIAD a clear yellow solution was obtained. The mixture was left stirring in the melting ice-water bath until TLC indicated full conversion. Then 10% NaHCO_{3(aq)} solution and EtOAc were added, and the layers were separated. The aqueous layer was extracted twice with EtOAc and the combined organics were dried over Na₂SO₄, filtered and the solvent was removed under reduced pressure. The crude product was purified by column chromatography on silica gel with EtOAc/heptane as eluent to yield the *N,N*-alkylated barbituric acids.

To the di-*N*-Boc amines or di-*N,N'*-di-Boc protected guanidines, dissolved in DCM, was added TFA and the mixture was stirred at ambient temperature until HRMS indicated full conversion. Sometimes multiple TFA additions were needed. The solvent was removed, and the crude product was purified on an automated flash system equipped with a C18 column and MeCN/H₂O containing 0.1% TFA as eluent. The product containing fractions were collected, the solvent was removed, and the product was lyophilized for 24 h. The obtained solids were triturated three times with Et₂O or heptane. The solids were dissolved in MeOH, and water was added. The mixture was lyophilized for 48 h to yield the desired amines or guanidines as di-TFA salts.

General Procedure E: Introduction of alkylated amines

1,3-bis(4-chlorobutyl)-5,5-bis(3,5-dibromobenzyl)pyrimidine-2,4,6(1*H*,3*H*,5*H*)-trione **S1** was mixed with MeCN and methylamine, dimethylamine or trimethylamine were added. The mixture was heated until HRMS indicated full conversion. It was allowed to cool to ambient temperature and the solvent was removed. The crude product was purified by automated RP chromatography with MeCN/H₂O containing 0.1% TFA as solvent. The product containing fractions were collected, the solvent was removed, and the product was lyophilized for 48 h. The amines were obtained as di-TFA salts.

General Procedure F: Synthesis of 5,5-disubstituted barbituric acids **3k-q** with mixed substituents

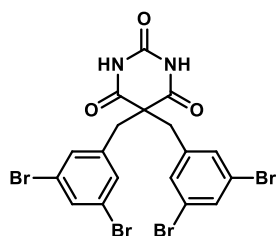
5-monoalkylated barbituric acid **5** was taken up in PEG-400, NaHCO₃ was added, and the suspension was stirred at ambient temperature. After 10 min the alkylating agent was added, and the mixture was stirred at elevated temperature until HRMS indicated full conversion. The mixture was allowed to cool to ambient temperature and Et₂O and 10% NaHCO_{3(aq)} solution were added. The layers were separated, and the aqueous layer was extracted once with Et₂O and EtOAc each. The combined organics were dried over Na₂SO₄, filtered and the solvent was removed under reduced pressure. The crude products were purified by column chromatography on silica with EtOAc/heptane as eluent to yield the desired barbituric acids **3k-q**.

General Procedure G: Preparation of di-hydrochloric (HCl) salts

The previously obtained di-TFA salts of the amines and guanidines were taken up in MeOH and HCl in MeOH (1.25 M, 10.0 eq) was added. The solution was stirred for 5 min, before removal of the solvent under a nitrogen stream. The resulting residue was lyophilized for 24 h. The procedure was repeated twice more to yield the respective di-HCl salts. The absence of fluorine was confirmed by ¹⁹F NMR (not included).

2.4 Synthesis of barbiturates with identical lipophilic side chains **3a-j**

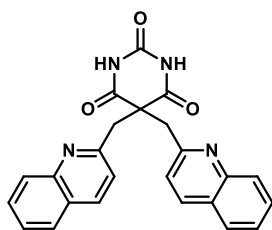
All compounds were synthesized according to General Procedure A



*5,5-bis(3,5-dibromobenzyl)pyrimidine-2,4,6(1*H*,3*H*,5*H*)-trione **3a**.*

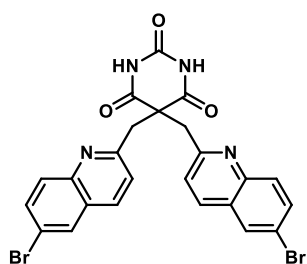
Barbituric acid (500 mg, 3.90 mmol, 1.0 eq), PEG-400 (15 mL), NaHCO₃ (656 mg, 7.81 mmol, 2.0 eq), 1,3-dibromo-5-(bromomethyl)benzene (2.05 g, 6.25 mmol, 1.6 eq). The mixture was stirred at 45 °C for 20 h. The title compound **3a** (1.62 g, 3.12 mmol, 83%) was obtained as a white solid. ¹H NMR (400 MHz, DMSO-*d*₆) δ 11.60 (s, 2H), 7.76 (t, *J* = 1.8 Hz, 2H), 7.22 (d, *J* = 1.8 Hz, 4H), 3.26 (s, 4H). ¹³C NMR (101 MHz, DMSO-*d*₆) δ 171.3 (2C), 148.9, 139.6 (2C), 132.6 (2C), 131.5 (4C), 122.4 (4C), 58.1, 41.7 (2C).

HRMS (ESI): calcd for C₁₈H₁₁Br₄N₂O₃⁻ [M-H]⁻ 618.7509, found 618.7514.



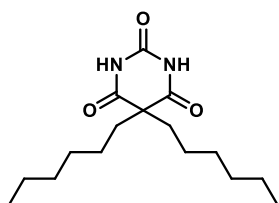
*5,5-bis(quinolin-2-ylmethyl)pyrimidine-2,4,6(1*H*,3*H*,5*H*)-trione **3b**.*

Barbituric acid (600 mg, 4.68 mmol, 1.0 eq), PEG-400 (30 mL), NaHCO₃ (786 mg, 9.36 mmol, 2.0 eq), 2-(bromomethyl)quinoline (1.71 g, 7.94 mmol, 1.70 eq). The mixture was stirred at 45 °C for 16 h and then at 60 °C for 24 h. The title compound **3b** (981 mg, 2.39 mmol, 56%) was obtained as a white solid. ¹H NMR (400 MHz, DMSO-*d*₆) δ 10.86 (s, 2H), 8.27 (d, *J* = 8.5 Hz, 2H), 7.93 (dd, *J* = 8.1, 1.3 Hz, 2H), 7.77 (dd, *J* = 8.5, 1.4 Hz, 2H), 7.72 (ddd, *J* = 8.3, 6.6, 1.4 Hz, 2H), 7.56 (ddd, *J* = 8.1, 6.6, 1.5 Hz, 2H), 7.40 (d, *J* = 8.5 Hz, 2H), 3.71 (s, 4H). ¹³C NMR (101 MHz, DMSO-*d*₆) δ 173.7 (2C), 156.8 (2C), 151.3, 146.4 (2C), 136.4 (2C), 129.6 (2C), 128.0 (2C), 127.8 (2C), 126.5 (2C), 126.3 (2C), 121.5 (2C), 52.2, 45.7 (2C). **HRMS** (ESI): calcd for C₂₄H₁₇N₄O₃⁻ [M-H]⁻ 409.1306, found 409.1304.



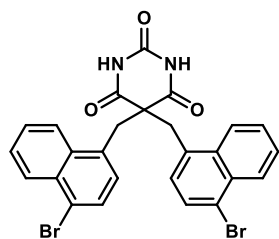
5,5-bis((6-bromoquinolin-2-yl)methyl)pyrimidine-2,4,6(1H,3H,5H)-trione **3c**.

Barbituric acid (90 mg, 0.70 mmol, 1.0 eq), PEG-400 (10 mL), NaHCO₃ (112 mg, 1.34 mmol, 1.90 eq), 6-bromo-2-(bromomethyl)quinoline (402 mg, 1.34 mmol, 1.90 eq). The mixture was stirred at 60 °C for 20 h and then at 60 °C for 24 h. The title compound **3c** (109 mg, 0.19 mmol, 27%) was obtained as an off-white solid. ¹H NMR (400 MHz, DMSO-*d*₆) δ 11.17 (s, 2H), 8.29 (d, *J* = 8.5 Hz, 2H), 8.26 (d, *J* = 2.2 Hz, 2H), 7.90 (dd, *J* = 8.9, 2.3 Hz, 2H), 7.66 (d, *J* = 8.9 Hz, 2H), 7.48 (d, *J* = 8.6 Hz, 2H), 3.75 (s, 4H). ¹³C NMR (101 MHz, DMSO-*d*₆) δ 173.5 (2C), 157.6 (2C), 151.2, 145.0 (2C), 135.3 (2C), 132.8 (2C), 130.1 (2C), 129.9 (2C), 127.8 (2C), 122.5 (2C), 119.1 (2C), 52.01, 45.6 (2C). HRMS (ESI): calcd for C₂₄H₁₅Br₂N₄O₃⁻ [M-H]⁻ 564.9516, found 564.9517.



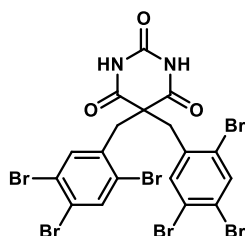
5,5-dihexylpyrimidine-2,4,6(1H,3H,5H)-trione **3d**.

Barbituric acid (445 mg, 3.47 mmol, 1.0 eq), PEG-400 (6 mL), NaHCO₃ (730 mg, 8.69 mmol, 2.50 eq), 1-iodohexane (1.33 g, 0.92 mL, 6.25 mmol, 1.80 eq). The mixture was stirred at 100 °C for 48 h and then allowed to cool to ambient temperature and 10% NaHCO_{3(aq)} was added. The aqueous layer was extracted with THF (2x) and MTBE (1x), the combined organics dried over Na₂SO₄, filtered and the solvent was removed under reduced pressure. The crude product was purified by column chromatography on silica with 25% EtOAc in heptane. The title compound **3d** (42 mg, 0.18 mmol, 5%) was obtained as a yellow solid. ¹H NMR (400 MHz, DMSO-*d*₆) δ 11.51 (s, 2H), 1.81 – 1.73 (m, 4H), 1.29 – 1.13 (m, 12H), 1.12 – 0.99 (m, 4H), 0.87 – 0.77 (m, 6H). ¹³C NMR (101 MHz, DMSO-*d*₆) δ 173.2 (2C), 149.8, 55.0, 38.3 (2C), 30.7 (2C), 28.5 (2C), 24.3 (2C), 21.8 (2C), 13.8 (2C). HRMS (ESI): calcd for C₁₆H₂₇N₂O₃⁻ [M-H]⁻ 295.2027, found 295.2024.



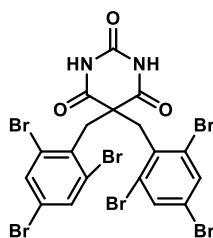
5,5-bis((4-bromonaphthalen-1-yl)methyl)pyrimidine-2,4,6(1H,3H,5H)-trione **3e**.

Barbituric acid (650 mg, 5.07 mmol, 1.0 eq), PEG-400 (15 mL), NaHCO₃ (853 mg, 10.15 mmol, 2.0 eq), 1-bromo-4-(bromomethyl)naphthalene (1.71 g, 8.65 mmol, 1.71 eq). The mixture was stirred at 45 °C for 24 h. The title compound **3e** (2.25 g, 3.98 mmol, 92%) was obtained as a white solid. ¹H NMR (400 MHz, DMSO-*d*₆) δ 10.44 (s, 2H), 7.57 – 7.46 (m, 2H), 7.38 – 7.30 (m, 2H), 7.00 (d, *J* = 7.8 Hz, 2H), 6.87 (dq, *J* = 12.8, 6.6 Hz, 4H), 6.30 (d, *J* = 7.8 Hz, 2H), 3.16 (s, 4H). ¹³C NMR (101 MHz, DMSO-*d*₆) δ 172.2 (2C), 149.1, 133.1 (2C), 132.5 (2C), 131.2 (2C), 129.5 (2C), 127.8 (2C), 127.5 (2C), 127.1 (2C), 126.9 (2C), 125.1 (2C), 121.6 (2C), 69.8, 57.5 (2C). HRMS (ESI): calcd for C₂₆H₁₇Br₂N₂O₃⁻ [M-H]⁻ 562.9611, found 562.9612.



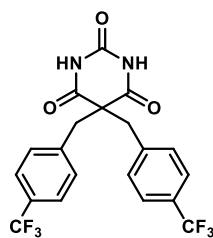
5,5-bis(2,4,5-tribromobenzyl)pyrimidine-2,4,6(1H,3H,5H)-trione **3f**.

Barbituric acid (350 mg, 2.73 mmol, 1.0 eq), PEG-400 (13 mL), NaHCO₃ (377 mg, 4.49 mmol, 1.65 eq), 1,2,4-tribromo-5-(bromomethyl)benzene (1.51 g, 3.71 mmol, 1.36 eq). The mixture was stirred at 45 °C for 4.5 d. Instead of sonicating the solids were boiled in MeOH for 30 min, cooled to ambient temperature and filtered. The title compound **3f** (1.07 g, 1.37 mmol, 74%) was obtained as a white solid. ¹H NMR (400 MHz, DMSO-*d*₆) δ 11.81 (s, 1H), 8.07 (s, 1H), 7.35 (s, 1H), 3.45 (s, 2H). ¹³C NMR (101 MHz, DMSO-*d*₆) δ 170.7 (2C), 149.1, 136.7 (2C), 136.4 (2C), 134.5 (2C), 124.7 (2C), 123.7 (2C), 123.1 (2C), 70.2, 55.3 (2C). HRMS (ESI): calcd for C₁₈H₉Br₆N₂O₃⁻ [M-H]⁻ 774.5719, found 774.5727.



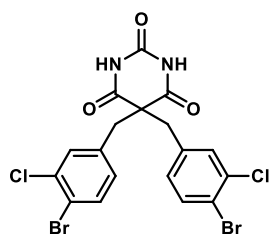
5,5-bis(2,4,6-tribromobenzyl)pyrimidine-2,4,6(1H,3H,5H)-trione 3g.

Barbituric acid (300 mg, 2.34 mmol, 1.0 eq), PEG-400 (20 mL), NaHCO₃ (374 mg, 4.45 mmol, 1.90 eq), 1,3,5-tribromo-2-(bromomethyl)benzene (1.51 g, 3.71 mmol, 1.59 eq). The mixture was stirred at 45 °C for 66 h. Instead of sonicating, the solids were boiled in MeOH for 30 min, cooled to ambient temperature and filtered. The title compound **3g** (1.13 g, 1.37 mmol, 78%) was obtained as a white solid. ¹H NMR (400 MHz, DMSO-*d*₆) δ 11.47 (s, 2H), 7.90 (s, 4H), 3.83 (s, 4H). ¹³C NMR (101 MHz, DMSO-*d*₆) δ 170.7 (2C), 149.7, 135.7 (2C), 134.4 (4C), 127.3 (4C), 121.4 (2C), 54.6, 43.0 (2C). HRMS (ESI): calcd for C₁₈H₉Br₆N₂O₃⁻ [M-H]⁻ 774.5719, found 774.5718.



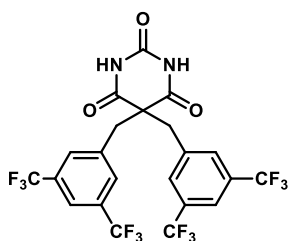
5,5-bis(4-(trifluoromethyl)benzyl)pyrimidine-2,4,6(1H,3H,5H)-trione 3h.

Barbituric acid (1.25 g, 9.76 mmol, 1.0 eq), PEG-400 (50 mL), NaHCO₃ (1.64 g, 19.52 mmol, 2.0 eq), 1-(bromomethyl)-4-(trifluoromethyl)benzene (4.20 g, 17.59 mmol, 1.8 eq). The mixture was stirred at 45 °C for 45 h. The title compound **3h** (1.62 g, 3.12 mmol, 84%) was obtained as a white solid. ¹H NMR (400 MHz, DMSO-*d*₆) δ 11.40 (s, 2H), 7.68 (d, *J* = 8.0 Hz, 4H), 7.27 (d, *J* = 8.0 Hz, 4H), 3.40 (s, 4H). ¹³C NMR (101 MHz, DMSO-*d*₆) δ 171.4 (2C), 148.8, 139.8 (2C), 130.3 (4C), 128.1 (q, *J* = 31.7 Hz, 2C), 125.5 – 125.3 (m, 4C), 124.15 (q, *J* = 272.1 Hz, 2C), 58.4, 43.0 (2C). HRMS (ESI): calcd for C₂₀H₁₃F₆N₂O₃⁻ [M-H]⁻ 443.0836, found 443.0831.



5,5-bis(4-bromo-3-chlorobenzyl)pyrimidine-2,4,6(1H,3H,5H)-trione 3i.

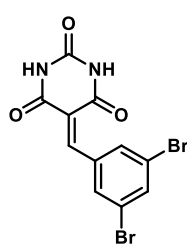
Barbituric acid (324 mg, 2.53 mmol, 1.0 eq), PEG-400 (30 mL), NaHCO₃ (489 mg, 5.82 mmol, 2.3 eq), 1-bromo-4-(bromomethyl)-2-chlorobenzene (1.37 g, 4.81 mmol, 1.9 eq). The mixture was stirred at 45 °C for 15 h and then at 65 °C for 22 h. The crude compound was purified by column chromatography on silica with 15% EtOAc/hepante containing 2.5% MeOH as eluent. The title compound **3i** (752 mg, 1.41 mmol, 56%) was obtained as a white solid. ¹H NMR (400 MHz, DMSO-*d*₆) δ 11.51 (s, 2H), 7.71 (d, *J* = 8.2 Hz, 2H), 7.24 (d, *J* = 2.1 Hz, 2H), 6.93 (dd, *J* = 8.3, 2.1 Hz, 2H), 3.26 (s, 4H). ¹³C NMR (101 MHz, DMSO-*d*₆) δ 171.4 (2C), 148.8, 136.7 (2C), 134.0 (2C), 133.0 (2C), 131.3 (2C), 129.8 (2C), 120.6 (2C), 58.2, 41.9 (2C). HRMS (ESI): calcd for C₁₈H₁₁Br₂Cl₂N₂O₃⁻ [M-H]⁻ 530.8519, found 530.8520.



5,5-bis(3,5-bis(trifluoromethyl)benzyl)pyrimidine-2,4,6(1H,3H,5H)-trione 3j.

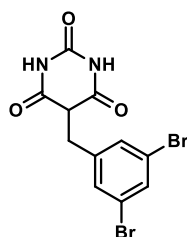
Barbituric acid (650 mg, 5.07 mmol, 1.0 eq), PEG-400 (35 mL), NaHCO₃ (853 mg, 10.15 mmol, 2.0 eq), 1-(bromomethyl)-3,5-bis(trifluoromethyl)benzene (2.73 g, 1.63 mL, 8.88 mmol, 1.75 eq). The mixture was stirred at 45 °C for 22 h. The title compound **3j** (2.33 g, 4.01 mmol, 79%) was obtained as a white solid. ¹H NMR (400 MHz, DMSO-*d*₆) δ 11.64 (s, 2H), 8.04 (s, 2H), 7.71 (d, *J* = 1.7 Hz, 4H), 3.53 (s, 4H). ¹³C NMR (101 MHz, DMSO-*d*₆) δ 171.2 (2C), 148.6, 138.3 (2C), 130.7 – 130.5 (m, 4C), 130.2 (q, *J* = 32.9 Hz, 4C), 123.2 (q, *J* = 274 Hz), 121.5 – 121.3 (m, 2C), 57.9, 41.3 (2C). HRMS (ESI): calcd for C₂₂H₁₁F₁₂N₂O₃⁻ [M-H]⁻ 579.0584, found 579.0566.

2.5 Synthesis of barbiturates with mixed hydrophobic residues 3k-q



5-(3,5-dibromobenzylidene)pyrimidine-2,4,6(1H,3H,5H)-trione **4**.

Barbituric acid (485 mg, 3.79 mmol, 1.0 eq) was taken up in water (15 mL) and heated to 105 °C until the compound dissolved. 3,5-dibromobenzaldehyde (1.00 g, 3.79 mmol, 1.0 eq) was dissolved in EtOH (5 mL) and added to the aqueous solution. A fine white precipitate formed which dissolved again after 1 min. After a few minutes a yellow precipitate formed. The mixture was stirred for a total of 25 min. After cooling to ambient temperature, it was filtered and the residue was washed with water and EtOAc. The solids were collected and dried to yield pure **4** (817 mg, 2.19 mmol, 58%) as a yellow solid. **¹H NMR** (400 MHz, DMSO-*d*₆) δ 11.46 (s, 1H), 11.30 (s, 1H), 8.17 (s, 1H), 8.12 (d, *J* = 1.8 Hz, 2H), 7.94 (t, *J* = 2.0 Hz, 1H). **¹³C NMR** (101 MHz, DMSO-*d*₆) δ 162.7, 161.3, 150.4, 150.2, 137.1, 135.3, 133.0 (2C), 121.9, 121.7 (2C). **HRMS** (ESI): calcd for C₁₁H₅Br₂N₂O₃⁻ [M-H]⁻ 370.8672, found 370.8672.



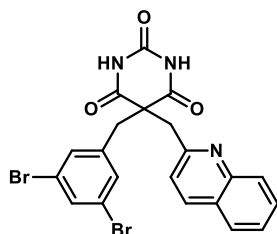
5-(3,5-dibromobenzyl)pyrimidine-2,4,6(1H,3H,5H)-trione **5**.

Compound **4** (1.00 g, 2.67 mmol, 1.0 eq) was taken up in EtOH (22 mL) and NaBH₄ (202 mg, 5.35 mmol, 2.0 eq) was added in one portion. After stirring at 70 °C for 5 min the yellow solid turned white. The mixture was allowed to cool to ambient temperature and the mixture was acidified to pH = 1 with 1 N HCl. The solid was collected by filtration to yield **5** (805 mg, 2.14 mmol, 80%) as a white solid. A 2:1 mixture of the Keto and Enol-form was obtained. The mixture was used without further purification.

Keto-9: **¹H NMR** (400 MHz, DMSO-*d*₆) δ 11.25 (s, 2H), 7.67 (s, 1H), 7.36 (d, *J* = 1.8 Hz, 2H), 4.08 (t, *J* = 5.3 Hz, 1H), 3.22 (d, *J* = 5.3 Hz, 1H). **¹³C NMR** (101 MHz, DMSO-*d*₆) δ 169.6, 150.7, 143.3, 131.6, 131.0 (2C), 122.2 (2C), 49.2, 31.5.

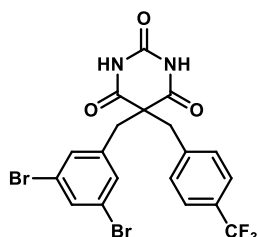
Enol-9: **¹H NMR** (400 MHz, DMSO-*d*₆) δ 10.72 (s, 2H), 7.60 (t, *J* = 1.8 Hz, 1H), 7.36 (d, *J* = 1.8 Hz, 2H), 3.55 (s, 1H). **¹³C NMR** (101 MHz, DMSO-*d*₆) δ 150.4, 146.7, 131.1, 130.4 (2C), 122.6 (2C), 88.2, 27.1. **HRMS** (ESI): calcd for C₁₁H₇Br₂N₂O₃⁻ [M-H]⁻ 372.8829, found. 372.8828.

The following compounds were synthesized according to *General Procedure F*:



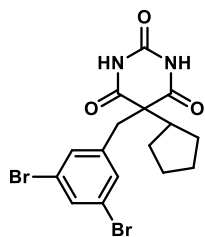
5-(3,5-dibromobenzyl)-5-(quinolin-2-ylmethyl)pyrimidine-2,4,6(1H,3H,5H)-trione **3k**.

Compound **5** (200 mg, 532 μmol, 1.0 eq), 2-(bromomethyl)quinoline (118 mg, 532 μmol, 1.0 eq), NaHCO₃ (67 mg, 798 μmol, 1.50 eq) and PEG-400 (3 mL) were stirred at 60 °C for 41 h. The crude was purified with 20-35% EtOAc in heptane to yield **3k** (110 mg, 213 μmol, 40%) as a white solid. **¹H NMR** (400 MHz, Methanol-*d*₄) δ 8.15 (d, *J* = 8.1 Hz, 1H), 7.81 (dd, *J* = 7.6, 1.2 Hz, 1H), 7.70 – 7.64 (m, 2H), 7.61 (ddd, *J* = 8.4, 6.7, 1.5 Hz, 1H), 7.48 (ddd, *J* = 8.1, 5.4, 1.4 Hz, 1H), 7.36 (d, *J* = 8.7 Hz, 1H), 7.33 (d, *J* = 1.7 Hz, 2H), 3.92 (s, 2H), 3.28 (s, 2H). **¹³C NMR** (101 MHz, Methanol-*d*₄) δ 175.1, 158.2, 152.2, 148.0, 140.1, 137.8, 134.4, 132.8, 130.6, 129.1, 128.8, 128.2, 127.4, 123.9, 121.7, 56.4, 45.3, 45.0. **HRMS** (ESI): calcd for C₂₁H₁₄Br₂N₃O₃⁻ [M-H]⁻ 513.9407, found.: 513.9406.



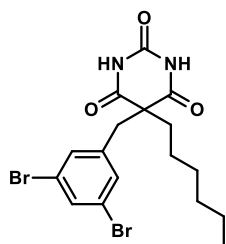
5-(3,5-dibromobenzyl)-5-(4-(trifluoromethyl)benzyl)pyrimidine-2,4,6(1H,3H,5H)-trione **3l**.

Compound **5** (200 mg, 532 μmol, 1.0 eq), 1-(bromomethyl)-4-(trifluoromethyl)benzene (82 μL, 532 μmol, 1.0 eq), NaHCO₃ (67 mg, 798 μmol, 1.50 eq) and PEG-400 (3 mL) were stirred at 50 °C for 18h. The crude was purified with 15% EtOAc in heptane to yield **3l** (83 mg, 155 μmol, 29%) as a white solid. **¹H NMR** (400 MHz, Methanol-*d*₄) δ 16.82 (t, *J* = 1.8 Hz, 1H), 6.76 (d, *J* = 8.1 Hz, 2H), 6.52 (d, *J* = 8.1 Hz, 2H), 6.49 (d, *J* = 1.7 Hz, 2H), 2.63 (s, 2H), 2.56 (s, 2H). **¹³C NMR** (101 MHz, Methanol-*d*₄) δ 163.6, 140.6, 131.3 (2C), 124.9, 123.3, 122.0, 121.5 (q, *J* = 32.4 Hz), 117.0 (t, *J* = 3.9 Hz), 116.1 (q, *J* = 273.0 Hz), 114.5, 51.2, 35.4, 34.4. **HRMS** (ESI): calcd for C₂₂H₁₄Br₂N₃O₃⁻ [M-H]⁻ 590.8560, found.: 590.8565.



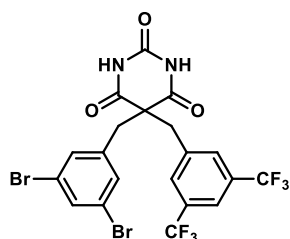
5-(3,5-dibromobenzyl)pyrimidine-2,4,6(1H,3H,5H)-trione 3m.

Compound **5** (158 mg, 420 μmol , 1.0 eq), bromocyclopentane (43 μL , 399 μmol , 0.95 eq), NaHCO_3 (34 mg, 399 μmol , 0.95 eq), TBAI (23 mg, 63 μmol , 0.15 eq) and PEG-400 (2 mL) were stirred at 100 $^\circ\text{C}$ for 48 h and then at 140 $^\circ\text{C}$ for 72 h. The crude was purified with 15% EtOAc in heptane to yield impure **3m** (9 mg, 20 μmol , 5%) as a yellow solid. **NMR** no suitable data was obtained. **HRMS** (ESI): calcd for $\text{C}_{16}\text{H}_{15}\text{Br}_2\text{N}_2\text{O}_3^-$ $[\text{M}-\text{H}]^-$ 440.9455, found: 440.9464.



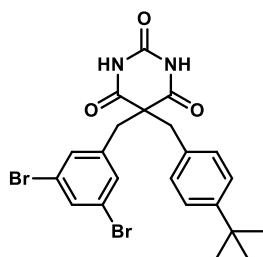
5-(3,5-dibromobenzyl)-5-hexylpyrimidine-2,4,6(1H,3H,5H)-trione 3n.

Compound **5** (200 mg, 532 μmol , 1.0 eq), 1-iodohexane (75 μL , 506 μmol , 0.95 eq), NaHCO_3 (45 mg, 532 μmol , 1.00 eq) and PEG-400 (2 mL) were stirred at 100 $^\circ\text{C}$ for 5 d. The crude was purified with 0-45% EtOAc in heptane to yield **3n** (129 mg, 280 μmol , 53%) as a colorless foam. $^1\text{H NMR}$ (400 MHz, Methanol-*d*₄) δ 7.61 (t, $J = 1.8$ Hz, 1H), 7.24 (d, $J = 1.8$ Hz, 2H), 3.16 (s, 2H), 2.09 – 2.00 (m, 2H), 1.38 – 1.16 (m, 8H), 0.94 – 0.84 (m, 3H). $^{13}\text{C NMR}$ (101 MHz, Methanol-*d*₄) δ 174.0, 150.7, 141.1, 134.2, 132.6, 123.9, 59.0, 44.2, 40.1, 32.4, 30.2, 25.9, 23.5, 14.3. **HRMS** (ESI): calcd for $\text{C}_{17}\text{H}_{19}\text{Br}_2\text{N}_2\text{O}_3^-$ $[\text{M}-\text{H}]^-$ 456.9768, found.: 456.9767.



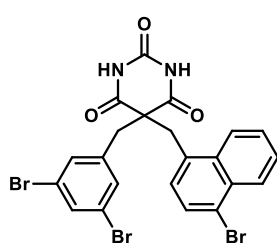
5-(3,5-bis(trifluoromethyl)benzyl)-5-(3,5-dibromobenzyl)pyrimidine-2,4,6(1H,3H,5H)-trione 3o.

Compound **5** (294 mg, 782 μmol , 1.0 eq), 1-(bromomethyl)-3,5-bis(trifluoromethyl)benzene (143 μL , 798 μmol , 1.00 eq), NaHCO_3 (99 mg, 1.17 mmol, 1.50 eq), and PEG-400 (20 mL) were stirred at 50 $^\circ\text{C}$ for 7 d. 10% NaHCO_3 (aq) solution was added, the aqueous layer was extracted with DCM (3x) and the combined organic layers dried over MgSO_4 . The crude was purified with 30% EtOAc in heptane to yield **3o** (471 mg, 327 μmol , 42%) as a white solid. $^1\text{H NMR}$ (400 MHz, DMSO-*d*₆) δ 11.63 (s, 2H), 8.05 (s, 1H), 7.77 (d, $J = 1.8$ Hz, 1H), 7.70 (s, 2H), 7.23 (d, $J = 1.8$ Hz, 2H), 3.50 (s, 2H), 3.30 (s, 2H). $^{13}\text{C NMR}$ (101 MHz, DMSO-*d*₆) δ 171.3 (2C), 148.7, 139.5, 138.4, 132.6, 131.6 (2C), 130.6 – 130.4 (m, 2C), 130.2 (q, $J = 32.8$ Hz, 2C), 123.2 (q, $J = 273.9$ Hz, 2C), 122.4 (2C), 121.6 – 121.4 (m, 1C) 58.1, 41.6, 41.5. **HRMS** (ESI): calcd for $\text{C}_{20}\text{H}_{11}\text{Br}_2\text{F}_6\text{N}_2\text{O}_3^-$ $[\text{M}-\text{H}]^-$ 598.9046, found: 598.9040.



5-(4-(tert-butyl)benzyl)-5-(3,5-dibromobenzyl)pyrimidine-2,4,6(1H,3H,5H)-trione 3p.

Compound **5** (200 mg, 532 μmol , 1.0 eq), 1-(bromomethyl)-4-(tert-butyl)benzene (147 μL , 798 μmol , 1.50 eq), NaHCO_3 (67 mg, 798 μmol , 1.50 eq), and PEG-400 (6 mL) were stirred at 100 $^\circ\text{C}$ for 21 h. The crude was purified with 10-15% EtOAc in heptane to yield **3p** (169 mg, 324 μmol , 61%) as a white solid. $^1\text{H NMR}$ (400 MHz, DMSO-*d*₆) δ 11.40 (s, 2H), 7.75 (t, $J = 1.8$ Hz, 1H), 7.33 – 7.25 (m, 2H), 7.22 (d, $J = 1.8$ Hz, 2H), 7.00 – 6.93 (m, 2H), 3.28 (s, 2H), 3.21 (s, 2H), 1.22 (s, 9H). $^{13}\text{C NMR}$ (101 MHz, DMSO-*d*₆) δ 171.6, 149.7, 148.8, 134.0, 132.5, 131.7, 131.4, 129.0, 125.2, 122.4, 58.5, 43.3, 42.0, 34.2, 31.0. **HRMS** (ESI): calcd for $\text{C}_{22}\text{H}_{21}\text{Br}_2\text{N}_2\text{O}_3^-$ $[\text{M}-\text{H}]^-$ 518.9924, found: 518.9924.

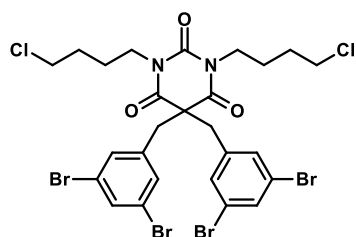


5-((4-bromonaphthalen-1-yl)methyl)-5-(3,5-dibromobenzyl)pyrimidine-2,4,6(1H,3H,5H)-trione 3q.

Compound **5** (75 mg, 200 μmol , 1.0 eq), 1-bromo-4-(bromomethyl)naphthalene (60 mg, 200 μmol , 1.0 eq), NaHCO_3 (25 mg, 300 μmol , 1.50 eq) and PEG-400 (1 mL) were stirred at 50 $^\circ\text{C}$ for 14h. The crude was purified with 20% EtOAc in heptane to yield **3q** (66 mg, 111 μmol , 56%) as a white solid. $^1\text{H NMR}$ (400 MHz, DMSO-*d*₆) δ 1.40 (s, 2H), 8.22 (d, $J = 7.8$ Hz, 1H), 8.16 (dd, $J = 8.4, 1.4$ Hz, 1H), 7.84 (d, $J = 7.8$ Hz, 1H), 7.75 (t, $J = 1.8$ Hz, 1H), 7.70 (ddd, $J = 8.3, 6.8, 1.2$ Hz, 1H), 7.64 (ddd, $J = 8.3, 6.8, 1.5$ Hz, 1H), 7.27 (d, $J = 1.8$ Hz, 2H), 7.13

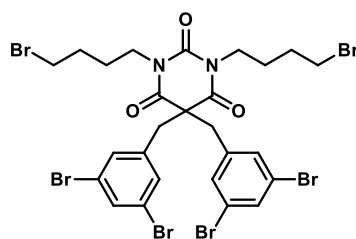
(d, $J = 7.8$ Hz, 1H), 3.81 (s, 2H), 3.45 (s, 2H). ^{13}C NMR (101 MHz, DMSO- d_6) δ 171.6, 148.7, 140.0, 132.9, 132.5, 132.0, 131.6, 131.2, 129.4, 128.0, 127.8, 127.1, 126.9, 125.0, 122.3, 121.8, 57.9, 41.5. HRMS (ESI): calcd for $\text{C}_{22}\text{H}_{14}\text{Br}_3\text{N}_2\text{O}_3^-$ $[\text{M}-\text{H}]^-$ 590.8560, found.: 590.8565.

2.6 Synthesis of series 1



1,3-bis(4-chlorobutyl)-5,5-bis(3,5-dibromobenzyl)pyrimidine-2,4,6(1H,3H,5H)-trione S1.

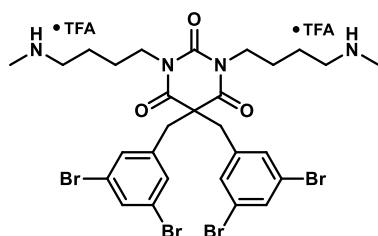
5,5-bis(3,5-dibromobenzyl)pyrimidine-2,4,6(1H,3H,5H)-trione 3a (250 mg, 400 μmol , 1.0 eq) and Cs_2CO_3 (326 mg, 1.00 mmol, 2.50 eq) were stirred in acetone (5 mL) at ambient temperature for 10 min. 1-bromo-4-chlorobutane (208 μL , 1.80 mmol, 4.50 eq) was added and the mixture was heated to 55 $^\circ\text{C}$ for 72 h. EtOAc and 10% $\text{NaHCO}_3(\text{aq})$ solution were added, the layers were separated and the organic layer was washed with 10% $\text{NaHCO}_3(\text{aq})$ solution twice. The organic layer was dried over Na_2SO_4 , filtered and the solvent was removed. The crude product was purified on an automated flash system equipped with a silica column and gradient 0-30 % EtOAc/heptane. **S1** (273 mg, 339 μmol , 85%) was obtained as a colorless oil. ^1H NMR (400 MHz, Chloroform- d) δ 7.53 (dq, $J = 3.2, 1.8$ Hz, 2H), 7.13 (q, $J = 2.2$ Hz, 4H), 3.65 (td, $J = 7.1, 2.5$ Hz, 4H), 3.51 (td, $J = 6.4, 2.8$ Hz, 4H), 3.36 – 3.25 (m, 4H), 1.62 – 1.53 (m, 4H), 1.53 – 1.43 (m, 4H). ^{13}C NMR (101 MHz, Chloroform- d) δ 169.9 (2C), 149.1, 138.4 (2C), 133.8 (2C), 131.3 (4C), 123.3 (4C), 59.9, 44.2 (2C), 41.4 (2C), 29.8 (2C), 25.4 (2C). HRMS (ESI): not found.



1,3-bis(4-bromobutyl)-5,5-bis(3,5-dibromobenzyl)pyrimidine-2,4,6(1H,3H,5H)-trione S2.

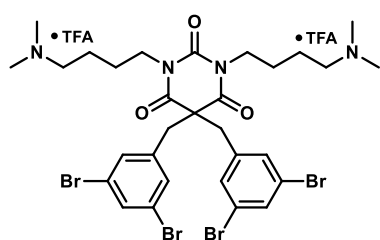
5,5-bis(3,5-dibromobenzyl)pyrimidine-2,4,6(1H,3H,5H)-trione 3a (112 mg, 180 μmol , 1.0 eq) and Cs_2CO_3 (146 mg, 1.00 mmol, 2.50 eq) were stirred in acetone (5 mL) at ambient temperature for 10 min. 1,4-dibromobutane (156 μL , 1.08 mmol, 6.0 eq) was added and the mixture was heated to 55 $^\circ\text{C}$ for 72 h. EtOAc and 10% $\text{NaHCO}_3(\text{aq})$ solution were added, the layers were separated and the organic layer was washed with 10% $\text{NaHCO}_3(\text{aq})$ solution twice. The organic layer was dried over Na_2SO_4 , filtered and the solvent was removed. The crude product was purified on an automated flash system equipped with a silica column and gradient 10-55 % EtOAc/heptane. **S2** (91 mg, 102 μmol , 57%) was obtained as a colorless oil. ^1H NMR (400 MHz, Chloroform- d) δ 7.54 (t, $J = 1.7$ Hz, 2H), 7.14 (d, $J = 1.7$ Hz, 4H), 3.69 – 3.62 (m, 4H), 3.38 (t, $J = 6.7$ Hz, 4H), 3.33 (s, 4H), 1.67 (p, $J = 6.8$ Hz, 4H), 1.49 (p, $J = 7.5$ Hz, 4H). ^{13}C NMR (101 MHz, Chloroform- d) δ 169.9 (2C), 149.1, 138.4 (2C), 133.8 (2C), 131.3 (4C), 123.3 (4C), 59.9, 44.2 (2C), 41.3 (2C), 29.9 (2C), 26.6 (2C). HRMS (ESI): calcd for $\text{C}_{26}\text{H}_{26}\text{Br}_6\text{N}_2\text{O}_3\text{Na}^+$ $[\text{M}+\text{Na}]^+$ 910.6936, found: 910.6938.

The following compounds were synthesized according to General Procedure E



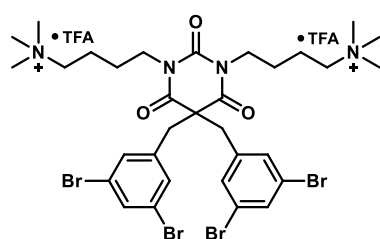
5,5-bis(3,5-dibromobenzyl)-1,3-bis(4-(methylamino)butyl)pyrimidine-2,4,6(1H,3H,5H)-trione 6a.

S2 (40 mg, 45 μmol , 1.0 eq), methylamine (2M in THF, 179 μL , 358 μmol , 8.0 eq) and MeCN (1 mL) were stirred at 70 $^\circ\text{C}$ for 40 h. The crude was purified by automated RP column chromatography with gradient 15-53% MeCN/ H_2O + 0.1% TFA to yield the di-TFA salt of **6a** (15 mg, 15 μmol , 33%) as a slightly yellow solid. ^1H NMR (400 MHz, Methanol- d_4) δ 7.65 (t, $J = 1.6$ Hz, 2H), 7.22 (d, $J = 1.8$ Hz, 4H), 3.68 (t, $J = 7.6$ Hz, 4H), 3.42 (s, 4H), 3.11 – 2.96 (m, 4H), 2.69 (s, 6H), 1.58 (p, $J = 7.7$ Hz, 4H), 1.41 (p, $J = 7.8$ Hz, 4H). ^{13}C NMR (101 MHz, Methanol- d_4) δ 171.2 (2C), 150.5, 140.5 (2C), 134.5 (2C), 132.7 (4C), 124.1 (4C), 61.2, 49.7 (2C), 44.8 (2C), 42.2 (2C), 33.5 (2C), 26.3 (2C), 24.3 (2C). HRMS (ESI): calcd for $\text{C}_{28}\text{H}_{35}\text{Br}_4\text{N}_4\text{O}_3^+$ $[\text{M}+\text{H}]^+$ 790.9437, found 790.9436. SFC: 98.0%.



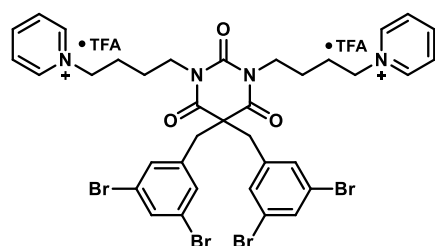
5,5-bis(3,5-dibromobenzyl)-1,3-bis(4-(dimethylamino)butyl)pyrimidine-2,4,6(1*H*,3*H*,5*H*)-trione **7a**.

S2 (40 mg, 45 μ mol, 1.0 eq), dimethylamine (2M in THF, 179 μ L, 358 μ mol, 8.0 eq) and MeCN (1 mL) were stirred at 70 °C for 24 h. The crude was purified by automated RP column chromatography with gradient 15-53% MeCN/H₂O + 0.1% TFA to yield the di-TFA salt of **7a** (35 mg, 33 μ mol, 75%) as a slightly yellow solid. ¹H NMR (400 MHz, Methanol-*d*₄) δ 7.66 (t, *J* = 1.6 Hz, 2H), 7.22 (d, *J* = 1.8 Hz, 4H), 3.69 (t, *J* = 7.7 Hz, 4H), 3.42 (s, 4H), 3.20 – 3.09 (m, 4H), 2.88 (d, *J* = 1.6 Hz, 12H), 1.70 – 1.55 (m, 4H), 1.40 (p, *J* = 7.7 Hz, 4H). ¹³C NMR (101 MHz, Methanol-*d*₄) δ 171.2 (2C), 150.5, 140.5 (2C), 134.5 (2C), 132.6 (4C), 124.1 (4C), 61.2, 58.4 (2C), 44.8 (2C), 43.4 (4C), 42.1 (2C), 26.2 (2C), 22.8 (2C). HRMS (ESI): calcd for C₃₀H₃₉Br₄N₄O₃⁺ [M+H]⁺ 818.9750, found 818.9744. SFC: 96.4%.



4,4'-(5,5-bis(3,5-dibromobenzyl)-2,4,6-trioxodihydropyrimidine-1,3(2*H*,4*H*)-diyl)bis(*N,N,N*-trimethylbutan-1-aminium) **8a**.

S1 (45 mg, 56 μ mol, 1.0 eq), trimethylamine (1M in THF, 783 μ L, 783 μ mol, 14.0 eq), NaI (15 mg, 100 μ mol, 1.8 eq) and MeCN (1 mL) were stirred at 70 °C for 96 h. The crude was purified by automated RP column chromatography with gradient 15-55% MeCN/H₂O + 0.1% TFA to yield the di-TFA salt of **8a** (53 mg, 49 μ mol, 88%) as a slightly yellow solid. ¹H NMR (400 MHz, Methanol-*d*₄) δ 7.66 (t, *J* = 1.8 Hz, 2H), 7.22 (d, *J* = 1.8 Hz, 4H), 3.78 – 3.66 (m, 4H), 3.43 (s, 4H), 3.41 – 3.34 (m, 4H), 3.13 (s, 18H), 1.82 – 1.68 (m, 4H), 1.39 (tt, *J* = 10.6, 6.4 Hz, 4H). ¹³C NMR (101 MHz, Methanol-*d*₄) δ 171.2 (2C), 150.4, 139.8 (2C), 134.5 (2C), 132.6 (4C), 124.2 (4C), 67.1 (t, *J* = 3.0 Hz, 2C), 61.1, 53.6 (t, *J* = 4.0 Hz 6C), 44.8 (2C), 42.2 (2C), 26.0 (2C), 21.3 (2C). HRMS (ESI): calcd for C₃₂H₄₄Br₄N₄O₃²⁺ [M]²⁺ 424.0068, found 424.0068. SFC: 97.7%.

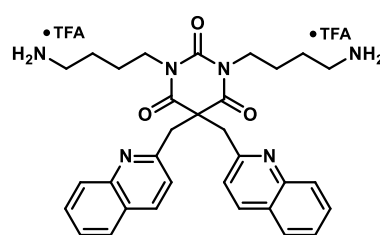


1,1'-((5,5-bis(3,5-dibromobenzyl)-2,4,6-trioxodihydropyrimidine-1,3(2*H*,4*H*)-diyl)bis(butane-4,1-diyl))bis(pyridin-1-ium) **9a**.

S1 (28 mg, 35 μ mol, 1.0 eq), pyridine (500 μ L), NaI (2.6 mg, 17 μ mol, 0.5 eq) and MeCN (0.5 mL) were stirred at 90 °C for 64 h. The crude was purified by automated RP column chromatography with gradient 10-70% MeCN/H₂O + 0.1% TFA to yield the di-TFA salt of **9a** (21 mg, 19 μ mol, 54%) as a slightly yellow solid. ¹H NMR (400 MHz, Methanol-*d*₄) δ 9.10 – 8.99 (m, 4H), 8.64 (tt, *J* = 7.8, 1.3 Hz, 2H), 8.23 – 8.12 (m, 4H), 7.62 (t, *J* = 1.8 Hz, 2H), 7.20 (d, *J* = 1.8 Hz, 4H), 4.75 – 4.65 (m, 4H), 3.80 – 3.68 (m, 4H), 3.44 (s, 4H), 1.95 (p, *J* = 7.5 Hz, 4H), 1.45 (tt, *J* = 9.7, 6.6 Hz, 4H). ¹³C NMR (101 MHz, Methanol-*d*₄) δ 171.3 (2C), 150.5, 147.2 (2C), 146.0 (4C), 140.5 (2C), 134.5 (2C), 132.6 (4C), 129.7 (4C), 124.1 (4C), 62.1 (2C), 61.2, 44.8 (2C), 42.0 (2C), 29.4 (2C), 25.6 (2C). HRMS (ESI): calcd for C₃₆H₃₆Br₄N₄O₃²⁺ [M]²⁺ 443.9755, found. 443.9757 SFC: >99.5%.

2.7 Synthesis of series 2

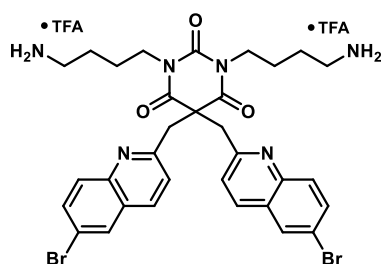
The compounds were prepared according to General Procedure D.



1,3-bis(4-aminobutyl)-5,5-bis(quinolin-2-ylmethyl)pyrimidine-2,4,6(1*H*,3*H*,5*H*)-trione **10bA**.

Barbiturate **3b** (145 mg, 350 μ mol, 1.0 eq), *tert*-butyl (4-hydroxybutyl)carbamate (166 mg, 875 μ mol, 2.5 eq), PPh₃ (273 mg, 1.05 mmol, 3.0 eq) and DIAD (206 μ L, 1.05 mmol, 3.0 eq) were stirred in DCM (2.0 mL) for 25 h. The crude was purified with 0-70% EtOAc in heptane to yield boc-**10bA** (84 mg, 112 μ mol, 32%) as a slightly yellow solid.

TFA (130 μ L, 1.70 mmol, 15.5 eq) and DCM (1.5 mL) were added, and the mixture was stirred at ambient temperature for 18 h. The crude was purified by automated RP column chromatography with a gradient of 0-70% MeCN/H₂O + 0.1% TFA to yield the di-TFA salt of **10bA** (61 mg, 78 μ mol, 22% o2s) as a white solid, m.p. 85-95 °C. ¹H NMR (400 MHz, Methanol-*d*₄) δ 8.31 (d, *J* = 8.5 Hz, 2H), 7.93 (d, *J* = 8.2 Hz, 2H), 7.76 (d, *J* = 3.5 Hz, 4H), 7.59 (dt, *J* = 8.1, 4.0 Hz, 2H), 7.45 (d, *J* = 8.6 Hz, 2H), 3.98 (s, 4H), 3.82 (t, *J* = 6.9 Hz, 4H), 2.60 (t, *J* = 7.4 Hz, 4H), 1.51 – 1.30 (m, 8H). ¹³C NMR (101 MHz, Methanol-*d*₄) δ 174.1 (2C), 158.2 (2C), 153.4, 148.2 (2C), 138.2 (2C), 131.0 (2C), 129.2 (2C), 129.1 (2C), 128.5 (2C), 127.7 (2C), 122.6 (2C), 54.8, 42.0 (2C), 39.9 (2C), 25.9 (2C), 25.7 (2C). One carbon signal was not observed. HRMS (ESI): calcd for C₃₂H₃₇N₆O₃⁺ [M+H]⁺ 553.2922, found 553, 2920. SFC: >99.5%.

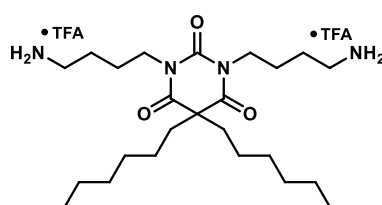


1,3-bis(4-aminobutyl)-5,5-bis((6-bromoquinolin-2-yl)methyl)pyrimidine-2,4,6(1H,3H,5H)-trione 10cA.

Barbiturate **3c** (39 mg, 69 μ mol, 1.0 eq), *tert*-butyl (4-hydroxybutyl)carbamate (32 mg, 172 μ mol, 2.5 eq), PPh₃ (54 mg, 206 μ mol, 3.0 eq) and DIAD (43 μ L, 206 μ mol, 3.0 eq) were stirred in DCM (1.0 mL) for 20 h. The crude was purified with 20-62% EtOAc in heptane to yield boc-**10cA** (40 mg, 44 μ mol, 64%) as a white solid.

TFA (79 μ L, 1.03 mmol, 15.0 eq) and DCM (0.7 mL) were added, and the mixture was stirred at ambient temperature for 17 h. The

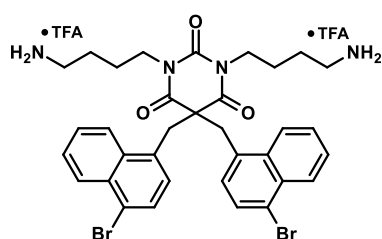
crude was purified by automated RP column chromatography with a gradient of 10-60% MeCN/H₂O + 0.1% TFA to yield the di-TFA salt of **10cA** (40 mg, 43 μ mol, 62% o2s) as a white solid. ¹H NMR (400 MHz, Methanol-*d*₄) δ 8.22 – 8.15 (m, 2H), 8.10 (d, *J* = 2.2 Hz, 2H), 7.81 (dd, *J* = 8.9, 2.2 Hz, 2H), 7.61 (d, *J* = 9.0 Hz, 2H), 7.41 (d, *J* = 8.5 Hz, 2H), 3.93 (s, 4H), 3.79 (t, *J* = 6.8 Hz, 4H), 2.66 (t, *J* = 7.2 Hz, 4H), 1.49 – 1.34 (m, 8H). ¹³C NMR (101 MHz, Methanol-*d*₄) δ 173.8 (2C), 158.9 (2C), 153.3, 146.7 (2C), 137.2 (2C), 134.3 (2C), 131.3 (2C), 131.0 (2C), 129.6 (2C), 123.6 (2C), 121.2 (2C), 54.5, 48.2 (2C), 42.0 (2C), 39.9 (2C), 25.9 (2C), 25.7 (2C). HRMS (ESI): calcd for C₃₂H₃₅Br₂N₆O₃⁺ [M+H]⁺ 709.1132, found 709.1129. SFC: 99.2%.



1,3-bis(4-aminobutyl)-5,5-dihexylpyrimidine-2,4,6(1H,3H,5H)-trione 10dA.

Barbiturate **3d** (37 mg, 125 μ mol, 1.0 eq), *tert*-butyl (4-hydroxybutyl)carbamate (59 mg, 312 μ mol, 2.5 eq), PPh₃ (98 mg, 375 μ mol, 3.0 eq) and DIAD (78 μ L, 374 μ mol, 3.0 eq) were stirred in DCM (1.0 mL) for 20 h. The crude was purified with 10-40% EtOAc in heptane to yield boc-**10dA** (66 mg, 103 μ mol, 83%) as a white solid.

TFA (96 μ L, 1.25 mmol, 10.0 eq) and DCM (1.0 mL) were added, and the mixture was stirred at ambient temperature for 22 h. The crude was purified by automated RP column chromatography with a gradient of 10-60% MeCN/H₂O + 0.1% TFA to yield the di-TFA salt of **10dA** (58 mg, 87 μ mol, 70% o2s) as a white powder. ¹H NMR (400 MHz, Methanol-*d*₄) δ 4.00 – 3.86 (m, 4H), 3.06 – 2.93 (m, 4H), 1.99 – 1.89 (m, 4H), 1.70 (h, *J* = 3.8 Hz, 8H), 1.32 – 1.18 (m, 12H), 1.09 (dt, *J* = 9.5, 4.6 Hz, 4H), 0.87 (t, *J* = 6.8 Hz, 6H). ¹³C NMR (101 MHz, Methanol-*d*₄) δ 173.2 (2C), 151.9, 57.8, 42.2 (2C), 41.0 (2C), 40.2 (2C), 32.3 (2C), 30.2 (2C), 26.0 (2C), 25.9 (4C), 23.5 (2C), 14.3 (2C). HRMS (ESI): calcd for C₂₄H₄₇N₄O₃⁺ [M+H]⁺ 439.3643, found 439.3642. SFC: 96.5%.

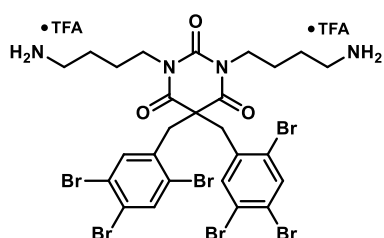


1,3-bis(4-aminobutyl)-5,5-bis((4-bromonaphthalen-1-yl)methyl)pyrimidine-2,4,6(1H,3H,5H)-trione 10eA.

Barbiturate **3e** (201 mg, 350 μ mol, 1.0 eq), *tert*-butyl (4-hydroxybutyl)carbamate (166 mg, 880 μ mol, 2.5 eq), PPh₃ (277 mg, 1.06 mmol, 3.0 eq) and DIAD (205 μ L, 1.04 mmol, 3.0 eq) were stirred in DCM (2.0 mL) for 24 h. The crude was purified with 0-70% EtOAc in heptane to yield boc-**10eA** (315 mg, 346 μ mol, 99%) as a white solid.

TFA (0.42 mL, 5.48 mmol, 15.8 eq) and DCM (2.0 mL) were added, and the mixture was stirred at ambient temperature for 18 h. The crude was purified by automated RP column chromatography with a

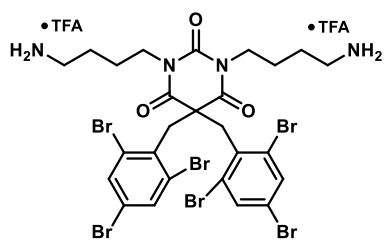
gradient of 0-70% MeCN/H₂O + 0.1% TFA to yield the di-TFA salt of **10eA** (153 mg, 163 μmol, 47% o2s) as a white solid, m.p. 105-110°C. ¹H NMR (400 MHz, Methanol-*d*₄) δ 8.35 – 8.27 (m, 2H), 8.25 – 8.18 (m, 2H), 7.75 – 7.57 (m, 6H), 7.13 (d, *J* = 7.8 Hz, 2H), 4.10 (s, 4H), 3.35 (t, 4H), 2.60 (t, *J* = 7.7 Hz, 4H), 1.06 (p, 4H), 0.78 (p, *J* = 15.0, 7.6 Hz, 4H). ¹³C NMR (101 MHz, Methanol-*d*₄) δ 172.0 (2C), 150.7, 134.4 (2C), 133.5 (2C), 133.4 (2C), 130.5 (2C), 129.3 (2C), 128.7 (2C), 128.5 (2C), 128.1 (2C), 126.6 (2C), 123.8 (2C), 60.4, 41.7 (2C), 41.5 (2C), 40.0 (2C), 25.2 (2C), 25.1 (2C). HRMS (ESI): calcd for C₃₄H₃₇Br₂N₄O₃⁺ [M+H]⁺ 707.1227, found 707.1230. SFC: 95.3%.



1,3-bis(4-aminobutyl)-5,5-bis(2,4,5-tribromobenzyl)pyrimidine-2,4,6(1H,3H,5H)-trione 10fA.

Barbiturate **10f** (80 mg, 102 μmol, 1.0 eq), *tert*-butyl (4-hydroxybutyl)carbamate (58 mg, 307 μmol, 3.0 eq), PPh₃ (81 mg, 307 μmol, 3.0 eq) and DIAD (64 μL, 307 μmol, 3.0 eq) were stirred in DCM (0.5 mL) for 12 h. The crude was purified with 0-40% EtOAc in heptane to yield boc-**10fA** (97 mg, 86 μmol, 84%) as a slightly yellow oil.

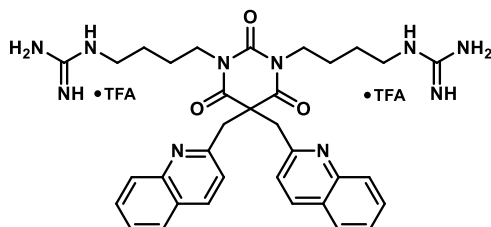
TFA (66 μL, 0.86 mmol, 10.0 eq) and DCM (1.0 mL) were added, and the mixture was stirred at ambient temperature for 18 h. The crude was purified by automated RP column chromatography with a gradient of 20-45% MeCN/H₂O + 0.1% TFA to yield the di-TFA salt of **10fA** (57 mg, 50 μmol, 49% o2s) as a white powder. ¹H NMR (400 MHz, Methanol-*d*₄) δ 7.95 (s, 2H), 7.34 (s, 2H), 3.81 (t, *J* = 7.0 Hz, 4H), 3.64 (s, 4H), 2.92 (t, *J* = 7.4 Hz, 4H), 1.61 – 1.44 (m, 8H). ¹³C NMR (101 MHz, Methanol-*d*₄) δ 170.6 (2C), 150.9, 138.6 (2C), 137.6 (2C), 136.0 (2C), 125.7 (2C), 125.5 (2C), 124.6 (2C), 58.1, 43.5 (2C), 42.7 (2C), 40.2 (2C), 26.0 (2C), 25.8 (2C). HRMS (ESI): calcd for C₂₆H₂₉Br₆N₄O₃⁺ [M+H]⁺ 918.7334, found: 918.7343. SFC: 98.8%.



1,3-bis(4-aminobutyl)-5,5-bis(2,4,6-tribromobenzyl)pyrimidine-2,4,6(1H,3H,5H)-trione 10gA.

Barbiturate **3g** (70 mg, 90 μmol, 1.0 eq), *tert*-butyl (4-hydroxybutyl)carbamate (42 mg, 224 μmol, 2.5 eq), PPh₃ (70 mg, 269 μmol, 3.0 eq) and DIAD (56 μL, 269 μmol, 3.0 eq) were stirred in anhydrous DMPU:dimethylcarbonate (1:1, 4.0 mL) for 24 h. The crude was purified with 10-40% EtOAc in heptane to yield impure boc-**10gA** (101 mg, 90 μmol, 100%) as a colorless viscous oil.

TFA (69 μL, 0.90 mmol, 10.0 eq) and DCM (1.0 mL) were added, and the mixture was stirred at ambient temperature for 18 h. The crude was purified by automated RP column chromatography with a gradient of 15-50% MeCN/H₂O + 0.1% TFA to yield the di-TFA salt of **10gA** (26 mg, 23 μmol, 25% o2s) as a white powder. ¹H NMR (400 MHz, Methanol-*d*₄) δ 7.81 (s, 2H), 4.03 (s, 2H), 3.77 (t, *J* = 7.3 Hz, 2H), 2.94 – 2.83 (m, 2H), 1.55 (p, *J* = 7.7 Hz, 2H), 1.43 – 1.32 (m, 2H). ¹³C NMR (101 MHz, Methanol-*d*₄) δ 170.6 (2C), 151.7, 137.0 (2C), 136.1 (4C), 128.6 (4C), 123.0 (2C), 57.3, 45.7 (2C), 42.6 (2C), 40.2 (2C), 25.9 (2C), 25.6 (2C). TFA signals were observed but are not reported. HRMS (ESI): calcd for C₂₆H₂₉Br₆N₄O₃⁺ [M+H]⁺ 918.7334, found: 918.7332. SFC: 96.5%.



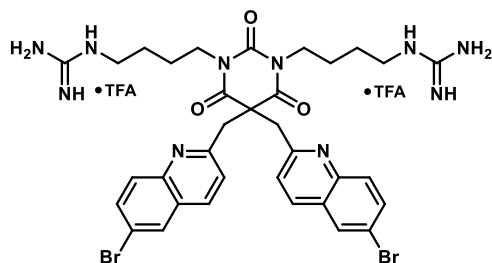
1,1'-((2,4,6-trioxo-5,5-bis(quinolin-2-ylmethyl)dihydropyrimidine-1,3(2H,4H)-diyl)bis(butane-4,1-diyl))diguanidine 10bG.

Barbiturate **3b** (49 mg, 120 μmol, 1.0 eq), *N,N'*-di(*tert*-butoxycarbonyl)-guanidinybutanol (80 mg, 240 μmol, 2.5 eq), PPh₃ (273 mg, 1.05 mmol, 3.0 eq) and DIAD (75 μL, 360 μmol, 3.0 eq) were stirred in DCM (1.0 mL)

for 16 h. The crude was purified with 10-70% EtOAc in heptane to yield boc-**10bG** (85 mg, 82 μmol, 68%) as a slightly yellow highly viscous oil.

TFA (138 μL, 1.80 mmol, 15.0 eq) and DCM (1.0 mL) were added, and the mixture was stirred at ambient temperature for 17 h. The crude was purified by automated RP column chromatography with a gradient of 0-70% MeCN/H₂O + 0.1% TFA to yield the di-TFA salt of **10bG** (39 mg, 45 μmol, 38% o2s) as a slightly brown solid. ¹H NMR (400 MHz, Methanol-*d*₄) δ 8.22 (d, *J* = 8.5 Hz, 2H), 7.93 – 7.82

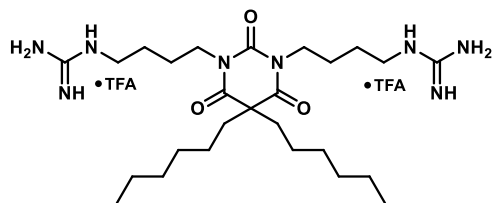
(m, 2H), 7.75 – 7.66 (m, 4H), 7.55 (dq, $J = 8.1, 4.5, 4.0$ Hz, 2H), 7.37 (d, $J = 8.5$ Hz, 2H), 3.94 (s, 4H), 3.81 (t, $J = 7.0$ Hz, 4H), 2.82 (t, $J = 7.4$ Hz, 4H), 1.40 (p, $J = 7.1$ Hz, 4H), 1.22 – 1.11 (m, 4H). ^{13}C NMR (101 MHz, Methanol- d_4) δ 172.9 (2C), 156.9 (2C), 156.7 (2C), 152.1, 146.8 (2C), 136.7 (2C), 129.6 (2C), 127.7 (4C), 127.1 (2C), 126.3 (2C), 121.1 (2C), 53.5, 47.0 (2C), 40.9 (2C), 40.4 (2C), 25.5 (2C), 24.8 (2C). HRMS (ESI): calcd for $\text{C}_{34}\text{H}_{41}\text{N}_{10}\text{O}_3^+$ $[\text{M}+\text{H}]^+$ 637.3358, found 637.3353. SFC: 99.3%.



1,1'-((5,5-bis((6-bromoquinolin-2-yl)methyl)-2,4,6-trioxodihydropyrimidine-1,3(2H,4H)-diyl)bis(butane-4,1-diyl)diguanidine 10cG.

Barbiturate **3c** (35 mg, 62 μmol , 1.0 eq), *N,N'*-di(*tert*-butoxycarbonyl)-guanidinybutanol (51 mg, 154 μmol , 2.5 eq), PPh_3 (48 mg, 185 μmol , 3.0 eq) and DIAD (39 μL , 185 μmol , 3.0 eq) were stirred in DCM (1.0 mL) for 20 h. The crude was purified with 30-70% EtOAc in heptane to yield boc-**10cG** (72 mg, 60 μmol , 98%) as a yellow highly viscous oil.

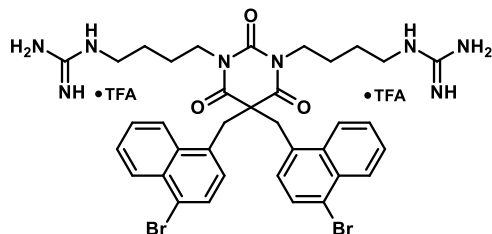
TFA (71 μL , 0.92 mmol, 15.0 eq) and DCM (1.0 mL) were added, and the mixture was stirred at ambient temperature for 22 h. The crude was purified by automated RP column chromatography with a gradient of 10-60% MeCN/ H_2O + 0.1% TFA to yield the di-TFA salt of **10cG** (41 mg, 40 μmol , 65% o2s) as a white powder. ^1H NMR (400 MHz, Methanol- d_4) δ 8.17 (d, $J = 8.5$ Hz, 2H), 8.09 (d, $J = 2.2$ Hz, 2H), 7.80 (dd, $J = 9.0, 2.2$ Hz, 2H), 7.60 (d, $J = 9.0$ Hz, 2H), 7.41 (d, $J = 8.5$ Hz, 2H), 3.92 (s, 4H), 3.82 (t, $J = 7.0$ Hz, 4H), 2.85 (t, $J = 7.4$ Hz, 4H), 1.41 (p, $J = 7.1$ Hz, 4H), 1.19 (qd, $J = 7.1, 5.9, 3.9$ Hz, 4H). ^{13}C NMR (101 MHz, Methanol- d_4) δ 174.0 (2C), 158.9 (2C), 158.3 (2C), 153.4, 146.7 (2C), 137.3 (2C), 134.3 (2C), 131.3 (2C), 131.0 (2C), 129.6 (2C), 123.5 (2C), 121.2 (2C), 54.5, 48.3 (2C), 42.3 (2C), 41.8 (2C), 26.8 (2C), 26.2 (2C). HRMS (ESI): calcd for $\text{C}_{34}\text{H}_{39}\text{Br}_2\text{N}_{10}\text{O}_3^+$ $[\text{M}+\text{H}]^+$ 793.1568, found 793.1575. SFC: >99.5%.



1,1'-((5,5-dihexyl-2,4,6-trioxodihydropyrimidine-1,3(2H,4H)-diyl)bis(butane-4,1-diyl)diguanidine 10dG.

Barbiturate **3d** (22 mg, 74 μmol , 1.0 eq), *N,N'*-di(*tert*-butoxycarbonyl)-guanidinybutanol (62 mg, 186 μmol , 2.5 eq), PPh_3 (58 mg, 223 μmol , 3.0 eq) and DIAD (48 μL , 223 μmol , 3.0 eq) were stirred in DCM (1.0 mL) for 20 h. The crude was purified with 10-40% EtOAc in heptane to yield boc-**10dG** (66 mg, 72 μmol , 96%) as a yellow oil.

TFA (85 μL , 1.11 mmol, 15.0 eq) and DCM (1.0 mL) were added, and the mixture was stirred at ambient temperature for 22 h. The crude was purified by automated RP column chromatography with a gradient of 10-60% MeCN/ H_2O + 0.1% TFA to yield the di-TFA salt of **10dG** (48 mg, 64 μmol , 86% o2s) as a white powder. ^1H NMR (400 MHz, Methanol- d_4) δ 3.94 (t, $J = 6.9$ Hz, 4H), 3.23 (t, $J = 6.8$ Hz, 4H), 2.00 – 1.91 (m, 4H), 1.74 – 1.57 (m, 8H), 1.33 – 1.17 (m, 12H), 1.08 (dd, $J = 10.4, 6.4$ Hz, 4H), 0.87 (t, $J = 6.9$ Hz, 6H). ^{13}C NMR (101 MHz, Methanol- d_4) δ 173.3 (2C), 158.9 (2C), 152.0, 57.8, 42.4 (2C), 42.0 (2C), 41.1 (2C), 32.4 (2C), 30.1 (2C), 27.2 (2C), 26.2 (2C), 26.0 (2C), 23.5 (2C), 14.3 (2C). HRMS (ESI): calcd for $\text{C}_{26}\text{H}_{51}\text{N}_8\text{O}_3^+$ $[\text{M}+\text{H}]^+$ 523.4079, found 523.4078. SFC: >99.5%.

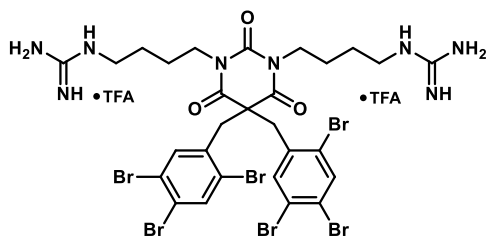


1,1'-((5,5-bis((4-bromonaphthalen-1-yl)methyl)-2,4,6-trioxodihydropyrimidine-1,3(2H,4H)-diyl)bis(butane-4,1-diyl)diguanidine 10eG.

Barbiturate **3e** (71 mg, 125 μmol , 1.0 eq), *N,N'*-di(*tert*-butoxycarbonyl)-guanidinybutanol (83 mg, 250 μmol , 2.0 eq), PPh_3 (98 mg, 375 μmol , 3.0 eq) and DIAD (79 μL , 275 μmol , 3.0 eq) were stirred in DCM (1.5 mL) for 16 h. The crude was purified with 10-60% EtOAc in heptane to yield boc-**10eG** (124 mg, 104 μmol , 83%) as a colorless oil.

TFA (287 μL , 3.76 mmol, 30.0 eq) and DCM (1.5 mL) were added, and the mixture was stirred at ambient temperature for 36 h. The crude was purified by automated RP column chromatography with a gradient of 0-70% MeCN/ H_2O + 0.1% TFA to yield the di-TFA salt of **10eG** (85 mg, 83 μmol , 67%

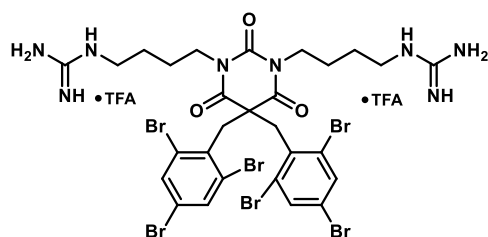
o2s) as a white solid. **¹H NMR** (400 MHz, Methanol-*d*₄) δ 8.38 – 8.29 (m, 2H), 8.22 (dt, *J* = 7.8, 2.7 Hz, 2H), 7.68 (d, *J* = 7.8 Hz, 2H), 7.66 – 7.61 (m, 4H), 7.15 (d, *J* = 7.8 Hz, 2H), 4.13 (s, 4H), 3.36 (t, *J* = 7.2 Hz, 4H), 2.87 (t, *J* = 7.1 Hz, 4H), 0.97 (ddd, *J* = 14.3, 7.5, 4.0 Hz, 4H), 0.84 (tt, *J* = 8.4, 6.2 Hz, 4H). **¹³C NMR** (101 MHz, Methanol-*d*₄) δ 172.0 (2C), 158.5 (2C), 150.9, 134.4 (2C), 133.5 (2C), 133.4 (2C), 130.4 (2C), 129.4 (2C), 128.7 (2C), 128.5 (2C), 128.1 (2C), 126.2 (2C), 123.8 (2C), 60.4, 42.1 (2C), 41.8 (2C), 41.6 (2C), 26.5 (2C), 25.4 (2C). **HRMS** (ESI): calcd for C₃₆H₄₁Br₂N₈O₃⁺ [M+H]⁺ 791.1663, found 791.1665. **SFC**: >99.5%.



1,1'-((2,4,6-trioxo-5,5-bis(2,4,5-tribromobenzyl)dihydropyrimidine-1,3(2H,4H)-diyl)bis(butane-4,1-diyl))diguanidine 10fG.

3f (80 mg, 102 μmol, 1.0 eq), *N,N'*-di(*tert*-butoxycarbonyl)-guanidinybutanol (58 mg, 307 μmol, 3.0 eq), PPh₃ (81 mg, 307 μmol, 3.0 eq) and DIAD (64 μL, 307 μmol, 3.0 eq) were stirred in DCM (0.5 mL) for 12 h. The crude was purified with 0-40% EtOAc in heptane to yield boc-**10fG** (98 mg, 70 μmol, 68%) as a slightly yellow oil.

TFA (80 μL, 1.04 mmol, 15.0 eq) and DCM (1.0 mL) were added, and the mixture was stirred at ambient temperature for 18 h. The crude was purified by automated RP column chromatography with a gradient of 20-45% MeCN/H₂O + 0.1% TFA to yield the di-TFA salt of **10fG** (43 mg, 35 μmol, 34% o2s) as a white powder. **¹H NMR** (400 MHz, Methanol-*d*₄) δ 7.95 (s, 2H), 7.31 (s, 2H), 3.81 (t, *J* = 6.9 Hz, 4H), 3.64 (s, 4H), 3.16 (t, *J* = 6.6 Hz, 4H), 1.57 – 1.41 (m, 8H). **¹³C NMR** (101 MHz, Methanol-*d*₄) δ 170.7 (2C), 158.6 (2C), 150.9, 138.6 (2C), 137.6 (2C), 135.8 (2C), 125.7 (2C), 125.5 (2C), 124.7 (2C), 58.0, 43.5 (2C), 43.0 (2C), 42.0 (2C), 27.0 (2C), 26.2 (2C). **HRMS** (ESI): calcd for C₂₈H₃₃Br₆N₈O₃⁺ [M+H]⁺ 1002.7770, found: 1002.7768. **SFC**: 98.5%.



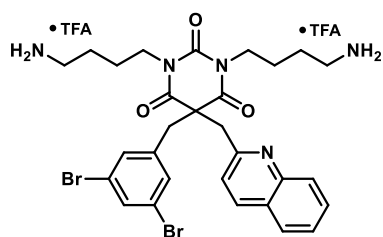
1,1'-((2,4,6-trioxo-5,5-bis(2,4,6-tribromobenzyl)dihydropyrimidine-1,3(2H,4H)-diyl)bis(butane-4,1-diyl))diguanidine 10gG.

Barbiturate **3g** (70 mg, 90 μmol, 1.0 eq), *N,N'*-di(*tert*-butoxycarbonyl)-guanidinybutanol (74 mg, 224 μmol, 2.5 eq), PPh₃ (70 mg, 269 μmol, 3.0 eq) and DIAD (56 μL, 269 μmol, 3.0 eq) were stirred in anhydrous DMPU:dimethylcarbonate (1:1, 4.0 mL) for 24 h. The crude was purified with 10-40% EtOAc in heptane to yield boc-**10gG** (79 mg, 56 μmol, 63%) as a colorless oil.

TFA (206 μL, 2.68 mmol, 30.0 eq) and DCM (1.0 mL) were added, and the mixture was stirred at ambient temperature for 43 h. The crude was purified by automated RP column chromatography with a gradient of 20-55% MeCN/H₂O + 0.1% TFA to yield the di-TFA salt of **10gG** (37 mg, 30 μmol, 33% o2s) as a white powder. **¹H NMR** (400 MHz, Methanol-*d*₄) δ 7.80 (s, 4H), 4.02 (s, 4H), 3.77 (t, *J* = 7.1 Hz, 4H), 3.13 (t, *J* = 7.0 Hz, 4H), 1.52 – 1.31 (m, 8H). **¹³C NMR** (101 MHz, Methanol-*d*₄) δ 170.6 (2C), 158.7 (2C), 151.7, 137.0 (2C), 136.1 (4C), 128.5 (4C), 123.0 (2C), 57.3, 45.8 (2C), 42.9 (2C), 42.0 (2C), 27.2 (2C), 25.8 (2C). **HRMS** (ESI): calcd for C₂₈H₃₄Br₆N₈O₃ for [M+2H]²⁺ 501.8922, found: 501.8917. **SFC**: 98.1%.

2.8 Synthesis of series 3

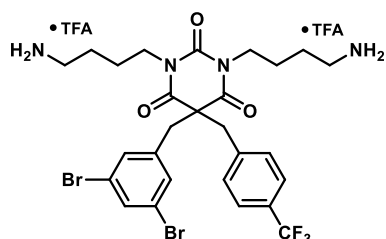
The following products were synthesized according to General Procedure D:



1,3-bis(4-aminobutyl)-5-(3,5-dibromobenzyl)-5-(quinolin-2-ylmethyl)pyrimidine-2,4,6(1H,3H,5H)-trione 11kA.

Barbiturate **3k** (55 mg, 107 μmol, 1.0 eq), *tert*-butyl (4-hydroxybutyl)carbamate (50 mg, 266 μmol, 2.5 eq), PPh₃ (84 mg, 319 μmol, 3.0 eq) and DIAD (67 μL, 319 μmol, 3.0 eq) were stirred in DCM (0.5 mL) for 16 h. The crude was purified with 10-50% EtOAc in heptane to yield impure boc-**11kA** (145 mg, 169 μmol, 159%) as a colorless oil.

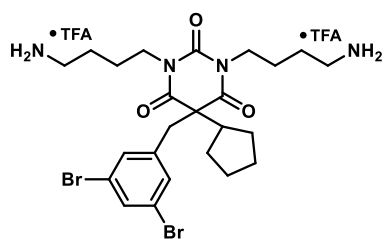
TFA (81 μ L, 1.06 mmol, 10.00 eq) and DCM (0.7 mL) were added, and the mixture was stirred at ambient temperature for 21 h. The crude was purified by automated RP column chromatography with a gradient of 15-53% MeCN/H₂O + 0.1% TFA to yield the di-TFA salt of **11kA** (70 mg, 81 μ mol, 76% o2s) as a white solid. ¹H NMR (400 MHz, Methanol-*d*₄) δ 8.21 (d, *J* = 8.5 Hz, 1H), 7.86 (dd, *J* = 8.1, 1.5 Hz, 1H), 7.72 (t, *J* = 1.7 Hz, 1H), 7.65 (ddd, *J* = 8.4, 6.9, 1.5 Hz, 1H), 7.51 (ddd, *J* = 8.2, 6.9, 1.2 Hz, 1H), 7.48 – 7.44 (m, 1H), 7.41 (d, *J* = 8.5 Hz, 1H), 7.25 (d, *J* = 1.8 Hz, 2H), 4.03 (s, 2H), 3.87 – 3.69 (m, 4H), 3.36 (s, 2H), 2.87 – 2.71 (m, 4H), 1.67 – 1.38 (m, 8H). ¹³C NMR (101 MHz, Methanol-*d*₄) δ 173.2 (2C), 158.6, 152.4, 147.8, 140.1, 138.11, 134.6, 132.7 (2C), 130.9, 129.2, 128.6, 128.4, 127.5, 124.0 (2C), 122.0, 56.8, 46.4, 45.9, 42.2 (2C), 40.1 (2C), 26.3 (2C), 25.9 (2C). HRMS (ESI): calcd for C₂₉H₃₄Br₂N₅O₃⁺ [M+H]⁺ 658.1023, found 658.1027. SFC: >99.5%.



1,3-bis(4-aminobutyl)-5-(3,5-dibromobenzyl)-5-(4-(trifluoromethyl)benzyl)pyrimidine-2,4,6(1H,3H,5H)-trione 11IA.

Barbiturate **3l** (36 mg, 67 μ mol, 1.0 eq), *tert*-butyl (4-hydroxybutyl)carbamate (32 mg, 169 μ mol, 2.5 eq), PPh₃ (53 mg, 202 μ mol, 3.0 eq) and DIAD (42 μ L, 202 μ mol, 3.0 eq) were stirred in DCM (0.5 mL) for 16 h. The crude was purified with 10-40% EtOAc in heptane to yield boc-**11IA** (55 mg, 63 μ mol, 93%) as a colorless oil. TFA (41 μ L, 539 μ mol, 8.00 eq) and DCM (0.7 mL) were added, and the mixture was stirred at ambient temperature for 17 h. The crude

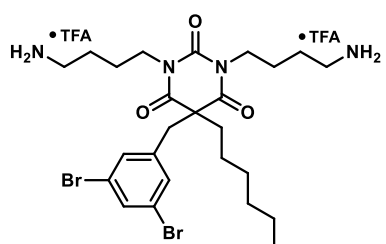
was purified by automated RP column chromatography with a gradient of 15-60% MeCN/H₂O + 0.1% TFA to yield the di-TFA salt of **11IA** (41 mg, 47 μ mol, 69% o2s) as a white powder. ¹H NMR (400 MHz, Methanol-*d*₄) δ 7.66 (t, *J* = 1.8 Hz, 1H), 7.57 (d, *J* = 8.1 Hz, 2H), 7.27 (d, *J* = 8.1 Hz, 2H), 7.24 (d, *J* = 1.8 Hz, 2H), 3.70 (ddd, *J* = 13.0, 9.3, 5.7 Hz, 2H), 3.59 (ddd, *J* = 13.0, 9.0, 5.9 Hz, 2H), 3.53 (s, 2H), 3.46 (s, 2H), 2.97 – 2.86 (m, 4H), 1.56 – 1.45 (m, 4H), 1.45 – 1.24 (m, 4H). ¹³C NMR (101 MHz, Methanol-*d*₄) δ 171.3 (2C), 150.6, 140.8 – 140.7 (m, 2C), 140.7, 134.5, 132.8 (2C), 131.4 (2C), 131.08 (q, *J* = 32.4 Hz), 126.7 (q, *J* = 3.5 Hz, 2C), 124.1 (2C), 61.1, 45.6, 45.1, 42.1 (2C), 40.2 (2C), 26.0 (2C), 25.7 (2C). CF₃ carbon was not observed, due to too low intensity. HRMS (ESI): calcd for C₂₇H₃₂Br₂F₃N₄O₃⁺ [M+H]⁺ 675.0788, found 675.0793. SFC: 95.3%.



1,3-bis(4-aminobutyl)-5-cyclopentyl-5-(3,5-dibromobenzyl)pyrimidine-2,4,6(1H,3H,5H)-trione 11mA.

Barbiturate **3m** (45 mg, 101 μ mol, 1.0 eq), *tert*-butyl (4-hydroxybutyl)carbamate (48 mg, 253 μ mol, 2.5 eq), PPh₃ (81 mg, 304 μ mol, 3.0 eq) and DIAD (64 μ L, 304 μ mol, 3.0 eq) were stirred in DCM (1.0 mL) for 16 h. The crude was purified with 10-50% EtOAc in heptane to yield boc-**11mA** (63 mg, 80 μ mol, 79%) as a yellow oil.

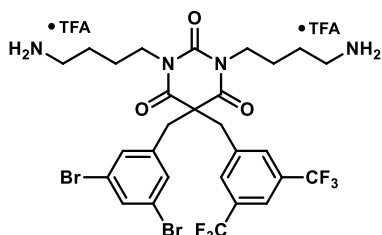
TFA (116 μ L, 1.52 mmol, 15.00 eq) and DCM (1.0 mL) were added, and the mixture was stirred at ambient temperature for 17 h. The crude was purified by automated RP column chromatography with a gradient of 15-60% MeCN/H₂O + 0.1% TFA to yield the di-TFA salt of **11mA** (21 mg, 26 μ mol, 25% o2s) as a white powder. ¹H NMR (400 MHz, Methanol-*d*₄) δ 7.61 (t, *J* = 1.8 Hz, 1H), 7.23 (d, *J* = 1.8 Hz, 2H), 3.83 (t, *J* = 7.3 Hz, 4H), 3.37 (s, 2H), 3.03 – 2.90 (m, 4H), 2.60 (h, *J* = 8.1 Hz, 1H), 1.78 (d, *J* = 8.9 Hz, 2H), 1.69 – 1.45 (m, 14H). ¹³C NMR (101 MHz, Methanol-*d*₄) δ 171.6 (2C), 151.4, 141.9, 134.0, 133.1 (2C), 123.8 (2C), 61.3, 51.8, 42.2 (2C), 42.0, 40.3 (2C), 28.4, 26.2 (2C), 25.9, 25.5 (2C). HRMS (ESI): calcd for C₂₄H₃₅Br₂N₄O₃⁺ [M+H]⁺ 585.1070, found 585.1068. SFC: >99.5%.



1,3-bis(4-aminobutyl)-5-(3,5-dibromobenzyl)-5-hexylpyrimidine-2,4,6(1H,3H,5H)-trione 11nA.

Barbiturate **3n** (52 mg, 113 μ mol, 1.0 eq), *tert*-butyl (4-hydroxybutyl)carbamate (54 mg, 283 μ mol, 2.5 eq), PPh₃ (89 mg, 339 μ mol, 3.0 eq) and DIAD (71 μ L, 339 μ mol, 3.0 eq) were stirred in DCM (1.0 mL) for 20 h. The crude was purified with 10-50% EtOAc in heptane to yield boc-**11nA** (86 mg, 107 μ mol, 95%) as a colorless oil.

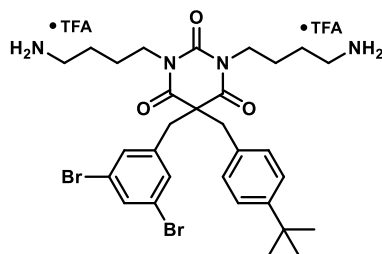
TFA (87 μL , 1.13 mmol, 10.0 eq) and DCM (1.0 mL) were added, and the mixture was stirred at ambient temperature for 22 h. The crude was purified by automated RP column chromatography with a gradient of 15–60% MeCN/H₂O + 0.1% TFA to yield the di-TFA salt of **11nA** (68 mg, 82 μmol , 73% o2s) as a white powder. ¹H NMR (400 MHz, Methanol-*d*₄) δ 7.64 (t, *J* = 1.8 Hz, 1H), 7.17 (d, *J* = 1.8 Hz, 2H), 3.80 (tdd, *J* = 13.0, 8.8, 7.3 Hz, 4H), 3.23 (s, 2H), 2.97 (td, *J* = 7.2, 3.0 Hz, 4H), 2.17 – 2.08 (m, 2H), 1.70 – 1.54 (m, 6H), 1.47 (qt, *J* = 10.6, 3.3 Hz, 2H), 1.34 – 1.20 (m, 6H), 1.11 (tt, *J* = 11.7, 6.6 Hz, 2H), 0.93 – 0.84 (m, 3H). ¹³C NMR (101 MHz, Methanol-*d*₄) δ 172.1 (2C), 151.1, 140.9, 134.3, 132.6 (2C), 124.0 (2C), 59.4, 45.7, 42.3 (2C), 40.7, 40.3 (2C), 32.3, 30.1, 26.2 (2C), 25.9, 25.8 (2C), 23.5, 14.23. HRMS (ESI): calcd for C₂₅H₃₉Br₂N₄O₃⁺ [M+H]⁺ 601.1383, found 601.1384. SFC: 95.2%.



1,3-bis(4-aminobutyl)-5-(3,5-bis(trifluoromethyl)benzyl)-5-(3,5-dibromobenzyl)pyrimidine-2,4,6(1H,3H,5H)-trione 11oA.

Barbiturate **3o** (90 mg, 150 μmol , 1.0 eq), *tert*-butyl (4-hydroxybutyl)carbamate (85 mg, 449 μmol , 3.0 eq), PPh₃ (118 mg, 449 μmol , 3.0 eq) and DIAD (94 μL , 449 μmol , 3.0 eq) were stirred in anhydrous THF (1.0 mL) for 12 h. The crude was purified with 0–40% EtOAc in heptane to yield boc-**11oA** (110 mg, 117 μmol , 78%) as a pale-yellow oil.

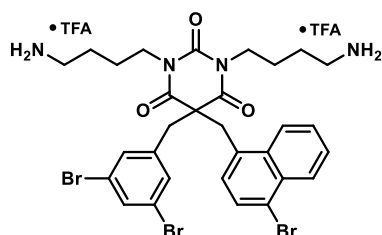
TFA (90 μL , 1.17 mmol, 10.0 eq) and DCM (1.0 mL) were added, and the mixture was stirred at ambient temperature for 18 h. The crude was purified by automated RP column chromatography with a gradient of 20–45% MeCN/H₂O + 0.1% TFA to yield the di-TFA salt of **11oA** (82 mg, 84 μmol , 56% o2s) as a white foam. ¹H NMR (400 MHz, Methanol-*d*₄) δ 7.90 (s, 1H), 7.68 – 7.64 (m, 3H), 7.24 (d, *J* = 1.7 Hz, 2H), 3.71 – 3.53 (m, 4H), 3.65 (s, 2H), 3.47 (s, 2H), 2.90 (dd, *J* = 9.1, 6.6 Hz, 4H), 1.59 – 1.48 (m, 4H), 1.46 – 1.26 (m, 4H). ¹³C NMR (101 MHz, Methanol-*d*₄) δ 171.1 (2C), 150.3, 140.3, 139.6, 134.7, 133.0 (q, *J* = 33.3 Hz, 2C) 132.7 (2C), 131.4 (q, *J* = 2.7 Hz, 2C), 124.6 (q, *J* = 272.2 Hz, 2C), 124.2 (2C), 122.9 – 122.7 (m, 1C), 61.2, 45.3, 44.4, 42.2 (2C), 40.1 (2C), 26.1 (2C), 25.7 (2C). HRMS (ESI): calcd for C₂₈H₃₁Br₂F₆N₄O₃⁺ [M+H]⁺ 743.0662, found 743.0670. SFC: 97.4%.



1,3-bis(4-aminobutyl)-5-(4-(tert-butyl)benzyl)-5-(3,5-dibromobenzyl)pyrimidine-2,4,6(1H,3H,5H)-trione 11pA.

Barbiturate **3p** (56 mg, 107 μmol , 1.0 eq), *tert*-butyl (4-hydroxybutyl)carbamate (51 mg, 268 μmol , 2.5 eq), PPh₃ (85 mg, 322 μmol , 3.0 eq) and DIAD (67 μL , 322 μmol , 3.0 eq) were stirred in DCM (1.0 mL) for 6 h. The crude was purified with 0–45% EtOAc in heptane to yield impure boc-**11pA** (101 mg, 117 μmol , 109%) as a yellow solid.

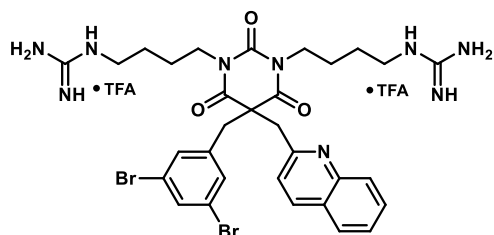
TFA (82 μL , 1.07 mmol, 10.00 eq) and DCM (1.0 mL) were added, and the mixture was stirred at ambient temperature for 17 h. The crude was purified by automated RP column chromatography with a gradient of 10–65% MeCN/H₂O + 0.1% TFA to yield the di-TFA salt of **11pA** (85 mg, 95 μmol , 89% o2s) as a white powder. ¹H NMR (400 MHz, Methanol-*d*₄) δ 7.63 (t, *J* = 1.8 Hz, 1H), 7.30 – 7.25 (m, 2H), 7.24 (d, *J* = 1.7 Hz, 2H), 7.00 – 6.93 (m, 2H), 3.68 (ddd, *J* = 13.0, 8.8, 6.0 Hz, 2H), 3.56 (ddd, *J* = 13.0, 8.7, 6.2 Hz, 2H), 3.44 (s, 2H), 3.38 (s, 2H), 2.91 (td, *J* = 7.2, 1.9 Hz, 4H), 1.57 – 1.44 (m, 4H), 1.44 – 1.30 (m, 4H), 1.25 (s, 9H). ¹³C NMR (101 MHz, Methanol-*d*₄) δ 171.7 (2C), 152.2, 150.70, 141.21, 134.2, 132.8 (2C), 130.2 (2C), 126.6 (2C), 124.0 (2C), 61.6, 46.5, 44.2, 41.9 (2C), 40.17 (2C), 35.3, 31.7 (3C), 26.0 (2C), 25.7 (2C). HRMS (ESI): calcd for C₃₀H₄₁Br₂N₄O₃⁺ [M+H]⁺ 663.1540, found 663.1545. SFC: 98.8%.



1,3-bis(4-aminobutyl)-5-((4-bromonaphthalen-1-yl)methyl)-5-(3,5-dibromobenzyl)pyrimidine-2,4,6(1H,3H,5H)-trione 11qA.

Barbiturate **3q** (55 mg, 92 μmol , 1.0 eq), *tert*-butyl (4-hydroxybutyl)carbamate (44 mg, 231 μmol , 2.5 eq), PPh₃ (73 mg, 277 μmol , 3.0 eq) and DIAD (58 μL , 277 μmol , 3.0 eq) were stirred in DCM (0.5 mL) for 16 h. The crude was purified with 10–65% EtOAc in heptane to yield boc-**11qA** (85 mg, 91 μmol , 98%) as a colorless oil.

TFA (57 μ L, 740 μ mol, 8.00 eq) and DCM (0.7 mL) were added, and the mixture was stirred at ambient temperature for 17 h. The crude was purified by automated RP column chromatography with a gradient of 15-60% MeCN/H₂O + 0.1% TFA to yield the di-TFA salt of **11qA** (62 mg, 66 μ mol, 71% o2s) as a white powder. ¹H NMR (400 MHz, Methanol-*d*4) δ 8.30 – 8.22 (m, 1H), 8.17 (dt, *J* = 7.9, 2.6 Hz, 1H), 7.72 (d, *J* = 7.7 Hz, 1H), 7.68 – 7.60 (m, 3H), 7.28 (d, *J* = 1.8 Hz, 2H), 7.15 (d, *J* = 7.8 Hz, 1H), 3.96 (s, 2H), 3.62 (s, 2H), 3.50 (ddd, *J* = 13.1, 8.9, 6.0 Hz, 2H), 3.39 (ddd, *J* = 13.1, 8.9, 5.9 Hz, 2H), 2.88 – 2.73 (m, 4H), 1.31 (h, *J* = 7.4 Hz, 4H), 1.21 – 0.99 (m, 4H). ¹³C NMR (101 MHz, Methanol-*d*4) δ 171.5 (2C), 150.5, 141.2, 134.3, 134.2, 133.4, 133.1 (2C), 132.8, 130.6, 128.8, 128.7, 128.3, 126.2, 124.0, 123.9 (2C), 61.1, 44.0, 42.4, 42.0 (2C), 40.2 (2C), 25.7 (2C), 25.6 (2C). HRMS (ESI): calcd for C₃₀H₃₄Br₃N₄O₃⁺ [M+H]⁺ 735.0176, found 735.0181. SFC: 96.1%.

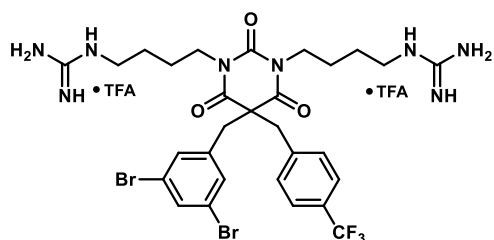


1,1'-((5-(3,5-dibromobenzyl)-2,4,6-trioxo-5-(quinolin-2-ylmethyl)dihydropyrimidine-1,3(2H,4H)-diyl)bis(butane-4,1-diyl))diguanidine 11kG.

Barbiturate **3k** (42 mg, 81 μ mol, 1.0 eq), *N,N'*-di(*tert*-butoxycarbonyl)-guanidinybutanol (67 mg, 203 μ mol, 2.5 eq), PPh₃ (64 mg, 244 μ mol, 3.0 eq) and DIAD (51 μ L, 245 μ mol, 3.0 eq) were stirred in DCM (1.0 mL) for 20 h. The crude was purified with 10-45% EtOAc in heptane to

yield impure boc-**11kG** (149 mg, 130 μ mol, 160%) as a white solid.

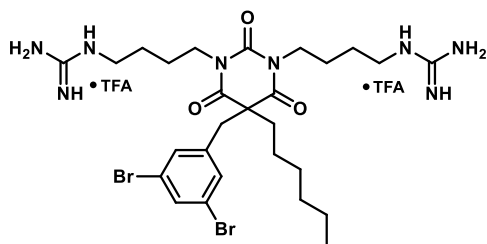
TFA (187 μ L, 2.44 mmol, 30.00 eq) and DCM (0.7 mL) were added, and the mixture was stirred at ambient temperature for 48 h. The crude was purified by automated RP column chromatography with a gradient of 15-53% MeCN/H₂O + 0.1% TFA to yield the di-TFA salt of **11kG** (32 mg, 33 μ mol, 41% o2s) as a white powder. ¹H NMR (400 MHz, Methanol-*d*4) δ 8.20 (d, *J* = 8.5 Hz, 1H), 7.89 – 7.82 (m, 1H), 7.70 (t, *J* = 1.8 Hz, 1H), 7.64 (ddd, *J* = 8.4, 7.0, 1.4 Hz, 1H), 7.50 (ddd, *J* = 8.1, 7.0, 1.2 Hz, 1H), 7.47 (d, *J* = 8.4 Hz, 1H), 7.41 (d, *J* = 8.5 Hz, 1H), 7.24 (d, *J* = 1.7 Hz, 2H), 4.02 (s, 2H), 3.88 – 3.68 (m, 4H), 3.35 (d, *J* = 2.0 Hz, 2H), 3.11 – 2.91 (m, 5H), 1.67 – 1.33 (m, 8H). ¹³C NMR (101 MHz, Methanol-*d*4) δ 173.2 (2C), 158.6 (2C), 158.4, 152.4, 147.8, 140.1, 138.1, 134.5, 132.6 (2C), 130.9, 129.2, 128.6, 128.3, 127.5, 124.0 (2C), 122.0, 56.8, 46.4, 45.9, 42.5 (2C), 42.0 (2C), 27.0 (2C), 26.4 (2C). HRMS (ESI): calcd for C₂₇H₄₃Br₂N₈O₃⁺ [M+H]⁺ 742.1459, found 742.1456. SFC: >99.5%.



(4-(5-(3,5-dibromobenzyl)-3-(4-guanidinobutyl)-2,4,6-trioxo-5-(4-(trifluoromethyl)benzyl)tetrahydropyrimidin-1(2H)-yl)butyl)-12-azanecarboximidamide 11IG.

Barbiturate **3l** (43 mg, 81 μ mol, 1.0 eq), *N,N'*-di(*tert*-butoxycarbonyl)-guanidinybutanol (67 mg, 201 μ mol, 2.5 eq), PPh₃ (63 mg, 242 μ mol, 3.0 eq) and DIAD (51 μ L, 242 μ mol, 3.0 eq) were stirred in DCM (1.0 mL) for 20 h. The crude was purified with 10-35% EtOAc in heptane to yield boc-**11IG** (82 mg, 71 μ mol, 88%) as a white solid.

TFA (185 μ L, 2.42 mmol, 30.00 eq) and DCM (0.7 mL) were added, and the mixture was stirred at ambient temperature for 48 h. The crude was purified by automated RP column chromatography with a gradient of 15-60% MeCN/H₂O + 0.1% TFA to yield the di-TFA salt of **11IG** (55 mg, 56 μ mol, 69% o2s) as a white powder. ¹H NMR (400 MHz, Methanol-*d*4) δ 7.64 (t, *J* = 1.8 Hz, 1H), 7.59 – 7.53 (m, 2H), 7.26 (d, *J* = 8.7 Hz, 2H), 7.23 (d, *J* = 1.8 Hz, 2H), 3.75 – 3.64 (m, 2H), 3.64 – 3.55 (m, 2H), 3.52 (s, 2H), 3.45 (s, 2H), 3.16 (t, *J* = 6.6 Hz, 4H), 1.48 – 1.28 (m, 8H). ¹³C NMR (101 MHz, Methanol-*d*4) δ 171.4 (2C), 158.7 (2C), 150.6, 140.7 (2C), 134.4, 132.9 (2C), 131.4 (2C), 131.1 (q, *J* = 32.4 Hz), 126.6 (q, *J* = 3.8 Hz, 2C), 125.4 (q, *J* = 272.7 Hz), 124.1 (2C), 61.1, 45.7, 45.0, 42.4 (2), 41.9 (2C), 26.9 (2C), 26.1 (2C). HRMS (ESI): calcd for C₂₉H₃₆Br₂F₃N₈O₃⁺ [M+H]⁺ 759.1224, found 759.1221. SFC: 98.5%.

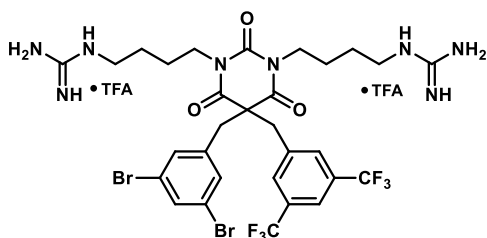


1,1'-((5-(3,5-dibromobenzyl)-5-hexyl-2,4,6-trioxodihydropyrimidine-1,3(2H,4H)-diyl)bis(butane-4,1-diyl)diguani-dine **11nG**.

Barbiturate **3n** (32 mg, 70 μ mol, 1.0 eq), *N,N'*-di(*tert*-butoxycarbonyl)-guanidinybutanol (58 mg, 174 μ mol, 2.5 eq), PPh_3 (55 mg, 209 μ mol, 3.0 eq) and DIAD (44 μ L, 209 μ mol, 3.0 eq) were stirred in DCM (1.0 mL) for 20 h. The crude was purified with 10-42% EtOAc in heptane to

yield impure boc-**11nG** (81 mg, 75 μ mol, 107%) as a white solid.

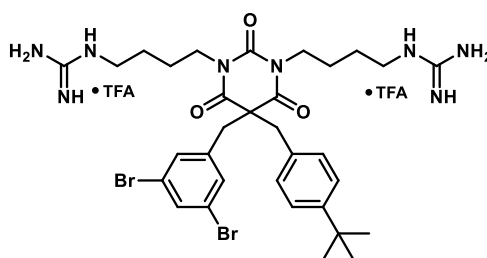
TFA (80 μ L, 1.04 mmol, 15.00 eq) and DCM (1.0 mL) were added, and the mixture was stirred at ambient temperature for 22 h. The crude was purified by automated RP column chromatography with a gradient of 10-55% MeCN/ H_2O + 0.1% TFA to yield the di-TFA salt of **11nG** (54 mg, 59 μ mol, 85% o2s) as a white powder. $^1\text{H NMR}$ (400 MHz, Methanol-*d*4) δ 7.63 (t, J = 1.8 Hz, 1H), 7.17 (d, J = 1.7 Hz, 2H), 3.88 – 3.73 (m, 4H), 3.28 – 3.17 (m, 6H), 2.17 – 2.08 (m, 2H), 1.66 – 1.39 (m, 8H), 1.34 – 1.19 (m, 7H), 1.11 (dd, J = 10.6, 5.9 Hz, 2H), 0.93 – 0.85 (m, 3H). $^{13}\text{C NMR}$ (101 MHz, Methanol-*d*4) δ 172.2 (2C), 158.7, 151.2, 140.9, 134.3, 132.5 (2C), 124.1 (2C), 59.4, 45.6, 42.5 (2C), 42.0 (2C), 40.9, 32.3, 30.1, 27.1 (2C), 26.4 (2C), 26.0, 23.5, 14.3. **HRMS** (ESI): calcd for $\text{C}_{27}\text{H}_{43}\text{Br}_2\text{N}_8\text{O}_3^+$ [$\text{M}+\text{H}$] $^+$ 685.1819, found 685.1821. **SFC**: 99.1%.



1,1'-((5-(3,5-bis(trifluoromethyl)benzyl)-5-(3,5-dibromo-benzyl)-2,4,6-trioxodihydropyrimidine-1,3(2H,4H)-diyl)bis(butane-4,1-diyl)diguani-dine **11oG**.

Barbiturate **3o** (90 mg, 150 μ mol, 1.0 eq), *N,N'*-di(*tert*-butoxycarbonyl)-guanidinybutanol (149 mg, 449 μ mol, 3.0 eq), PPh_3 (118 mg, 449 μ mol, 3.0 eq) and DIAD (94 μ L, 449 μ mol, 3.0 eq) were stirred in anhydrous THF (1.0 mL) for 12 h. The crude was purified with 0-40% EtOAc in heptane to yield boc-**11oG** (64 mg, 52 μ mol, 35%) as a pale-yellow oil.

TFA (60 μ L, 781 μ mol, 15.0 eq) and DCM (1.0 mL) were added, and the mixture was stirred at ambient temperature for 18 h. The crude was purified by automated RP column chromatography with a gradient of 20-45% MeCN/ H_2O + 0.1% TFA to yield the di-TFA salt of **11oG** (31 mg, 29 μ mol, 20% o2s) as a white foam. $^1\text{H NMR}$ (400 MHz, Methanol-*d*4) δ 7.90 (d, J = 1.8 Hz, 1H), 7.65 (t, J = 1.8 Hz, 1H), 7.64 (d, J = 1.5 Hz, 2H), 7.23 (d, J = 1.7 Hz, 2H), 3.65 (s, 2H), 3.71 – 3.53 (m, 4H), 3.47 (s, 2H), 3.15 (t, J = 6.8 Hz, 4H), 1.50 – 1.26 (m, 8H). $^{13}\text{C NMR}$ (101 MHz, Methanol-*d*4) δ 171.1 (2C), 158.7 (2C), 150.3, 140.3, 139.6, 134.7, 133.0 (q, J = 33.4 Hz, 2C), 132.7 (2C), 131.3 (q, J = 2.5 Hz, 2C), 124.5 (q, J = 272.1 Hz, 2C), 124.2 (2C), 122.8 – 122.6 (m, 1C), 61.2, 45.2, 44.6, 42.5 (2C), 41.9 (2C), 26.9 (2C), 26.2 (2C). **HRMS** (ESI): calcd for $\text{C}_{30}\text{H}_{35}\text{Br}_2\text{F}_6\text{N}_8\text{O}_3^+$ [$\text{M}+\text{H}$] $^+$ 827.1098, found: 827.1106. **SFC**: 98.0%.

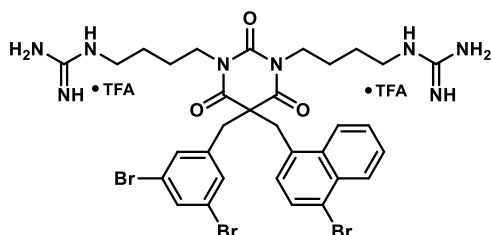


(4-(5-(4-(*tert*-butyl)benzyl)-5-(3,5-dibromobenzyl)-3-(4-guanidinobutyl)-2,4,6-trioxotetrahydropyrimidin-1(2H)-yl)butyl)-12-azanecarboximidamide **11pG**.

Barbiturate **3p** (58 mg, 111 μ mol, 1.0 eq), *N,N'*-di(*tert*-butoxycarbonyl)-guanidinybutanol (92 mg, 278 μ mol, 2.5 eq), PPh_3 (88 mg, 333 μ mol, 3.0 eq) and DIAD (70 μ L, 333 μ mol, 3.0 eq) were stirred in DCM (1.0 mL) for 48 h. The crude was purified with 0-40% EtOAc in heptane to yield boc-**11pG** (110 mg, 96 μ mol, 86%) as a yellow oil.

TFA (128 μ L, 166 μ mol, 15.0 eq) and DCM (1.0 mL) were added, and the mixture was stirred at ambient temperature for 17 h. The crude was purified by automated RP column chromatography with a gradient of 10-65% MeCN/ H_2O + 0.1% TFA to yield the di-TFA salt of **11pG** (82 mg, 84 μ mol, 76% o2s) as a white powder. $^1\text{H NMR}$ (400 MHz, Methanol-*d*4) δ 7.61 (t, J = 1.8 Hz, 1H), 7.29 – 7.24 (m, 2H), 7.24 (d, J = 1.8 Hz, 2H), 7.01 – 6.90 (m, 2H), 3.73 – 3.62 (m, 1H), 3.56 (ddd, J = 12.9, 8.0, 5.2 Hz, 2H), 3.43 (s, 2H), 3.37 (s, 2H), 3.16 (t, J = 6.6 Hz, 4H), 1.48 – 1.31 (m, 8H), 1.24 (s, 9H). $^{13}\text{C NMR}$ (101 MHz, Methanol-*d*4) δ 171.8 (2C), 158.7 (2C), 152.2, 150.8, 141.2, 134.2, 132.8, 132.7 (2C), 130.2 (2C), 126.6

(2C), 124.0 (2C), 61.6, 46.6, 44.3, 42.3 (2C), 42.0 (2C), 35.3, 31.7 (3C), 26.9 (2C), 26.1 (2C). **HRMS** (ESI): calcd for $C_{32}H_{45}Br_2N_8O_3^+$ $[M+H]^+$ 747.1976, found: 747.1981. **SFC**: 95.4%.



*1,1'-((5-((4-bromonaphthalen-1-yl)methyl)-5-(3,5-dibromobenzyl)-2,4,6-trioxodihydropyrimidine-1,3(2H,4H)-diyl)bis(butane-4,1-diyl))diguanidine **11qG**.*

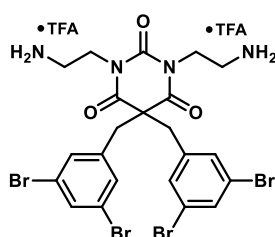
Barbiturate **3q** (103 mg, 173 μ mol, 1.0 eq), *N,N'*-di(*tert*-butoxycarbonyl)-guanidinybutanol (143 mg, 434 μ mol, 2.5 eq), PPh_3 (136 mg, 519 μ mol, 3.0 eq) and DIAD (109 μ L, 519 μ mol, 3.0 eq) were stirred in DCM (1.0 mL) for 20 h. The crude was purified with 10-38% EtOAc in heptane

to yield impure boc-**11qG** (216 mg, 177 μ mol, 102%) as a white solid.

TFA (398 μ L, 5.20 mmol, 30.00 eq) and DCM (0.7 mL) were added, and the mixture was stirred at ambient temperature for 48 h. The crude was purified by automated RP column chromatography with a gradient of 10-65% MeCN/H₂O + 0.1% TFA to yield the di-TFA salt of **11qG** (133 mg, 128 μ mol, 74% o2s) as a white powder. **¹H NMR** (400 MHz, Methanol-*d*₄) δ 8.28 – 8.20 (m, 1H), 8.20 – 8.13 (m, 1H), 7.71 (d, *J* = 7.7 Hz, 1H), 7.68 – 7.62 (m, 2H), 7.61 (t, *J* = 1.8 Hz, 1H), 7.28 (d, *J* = 1.7 Hz, 2H), 7.15 (d, *J* = 7.8 Hz, 1H), 3.95 (s, 2H), 3.62 (s, 2H), 3.50 (ddd, *J* = 12.9, 8.6, 6.0 Hz, 2H), 3.38 (ddd, *J* = 13.3, 8.4, 5.8 Hz, 2H), 3.04 (t, *J* = 7.0 Hz, 4H), 1.35 – 1.00 (m, 8H). **¹³C NMR** (101 MHz, Methanol-*d*₄) δ 171.6 (2C), 158.6 (2C), 150.6, 141.2, 134.2, 133.4, 133.0 (2C), 132.8, 130.5, 129.7, 128.8, 128.7, 128.3, 126.2, 124.1, 124.0 (2C), 61.1, 44.0, 42.5, 42.3 (2C), 42.0 (2C), 26.7 (2C), 25.9 (2C). **HRMS** (ESI): calcd for $C_{32}H_{38}Br_3N_8O_3^+$ $[M+H]^+$ 819.0612, found 819.0610. **SFC**: 96.3%.

2.9 Synthesis of series 4

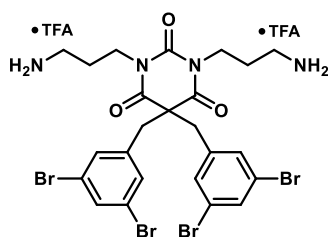
2.9.1 Amine derivatives



*1,3-bis(2-aminoethyl)-5,5-bis(3,5-dibromobenzyl)pyrimidine-2,4,6(1H,3H,5H)-trione **12aA**.*

The compound was synthesized according to General Procedure D. Barbiturate **3a** (80 mg, 128 μ mol, 1.0 eq), *tert*-butyl (2-hydroxyethyl)carbamate (52 mg, 321 μ mol, 2.5 eq), PPh_3 (101 mg, 385 μ mol, 3.0 eq) and DIAD (81 μ L, 385 μ mol, 3.0 eq) were stirred in DCM (1.0 mL) for 20 h. The crude was purified with 10-50% EtOAc in heptane to yield boc-**12aA** (97 mg, 107 μ mol, 83%) as a colorless oil. TFA (98 μ L, 1.28 mmol, 10.0 eq) and DCM

(1.0 mL) were added, and the mixture was stirred at ambient temperature for 22 h. The crude was purified by automated RP column chromatography with a gradient of 10-60% MeCN/H₂O + 0.1% TFA to yield the di-TFA salt of **12aA** (83 mg, 89 μ mol, 69% o2s) as a white powder. **¹H NMR** (400 MHz, Methanol-*d*₄) δ 7.64 (t, *J* = 1.8 Hz, 2H), 7.29 (d, *J* = 1.8 Hz, 4H), 4.00 (t, *J* = 6.6 Hz, 4H), 3.39 (s, 4H), 3.02 (t, *J* = 6.6 Hz, 4H). **¹³C NMR** (101 MHz, Methanol-*d*₄) δ 171.3 (2C), 151.1, 140.3 (2C), 134.6 (2C), 133.0 (4C), 124.0 (4C), 60.7, 44.0 (2C), 40.4 (2C), 38.6 (2C). **HRMS** (ESI): calcd for $C_{22}H_{23}Br_4N_4O_3^+$ $[M+H]^+$ 706.8498, found 706.8502. **SFC**: 96.7%.



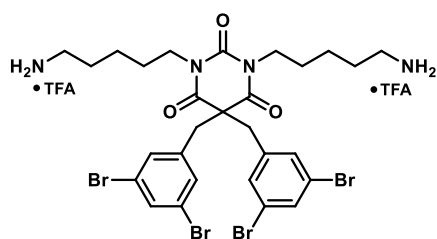
*1,3-bis(3-aminopropyl)-5,5-bis(3,5-dibromobenzyl)pyrimidine-2,4,6(1H,3H,5H)-trione **13aA**.*

The compound was synthesized according to General Procedure B. Barbiturate **3a** (468 mg, 0.75 mmol, 1.0 eq), *tert*-butyl (3-bromopropyl)carbamate (366 mg, 1.53 mmol, 2.05 eq), K_2CO_3 (311 mg, 2.25 mmol, 3.0 eq), TBAI (28 mg, 75 μ mol, 0.1 eq) and acetone (7 mL) were stirred at 50 °C for 20 h. Boc-**13aA** (600 mg, 0.64 mmol, 85%) was obtained as a yellow solid. TFA (0.75 mL, 9.78 mmol, 15.0 eq) and DCM (2.5 mL)

were added, and the mixture was stirred at ambient temperature for 17 h. The crude was purified by automated RP column chromatography with a gradient of 0-70% MeCN/H₂O + 0.1% TFA to yield the di-TFA salt of **13aA** (495 mg, 0.42 mmol, 56% o2s) as a white powder, m.p. 208-212 °C. **¹H NMR** (400 MHz, Methanol-*d*₄) δ 7.67 (s, 2H), 7.25 (d, *J* = 1.8 Hz, 4H), 3.78 (t, 4H), 3.45 (s, 4H), 2.85 (t, *J* = 7.1 Hz, 4H), 1.77 (p, *J* = 7.1 Hz, 4H). **¹³C NMR** (101 MHz, Methanol-*d*₄) δ 171.3 (2C), 150.8, 140.4 (2C),

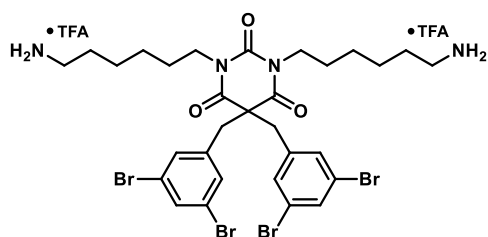
134.7 (2C), 132.6 (4C), 124.2 (4C), 61.4, 44.8 (2C), 40.2 (2C), 38.2 (2C), 27.3 (2C). **HRMS** (ESI): calcd for $C_{24}H_{27}Br_4N_4O_3^+$ $[M+H]^+$ 734.8811, found 734.8806. **SFC**: >99.5%.

The following compounds were synthesized according to General Procedure D.



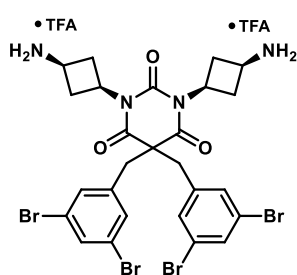
1,3-bis(5-aminopentyl)-5,5-bis(3,5-dibromobenzyl)pyrimidine-2,4,6(1H,3H,5H)-trione 14aA.

Barbiturate **3a** (82 mg, 131 μ mol, 1.0 eq), *tert*-butyl (5-hydroxypentyl)carbamate (67 mg, 329 μ mol, 2.5 eq), PPh_3 (103 mg, 394 μ mol, 3.0 eq) and DIAD (83 μ L, 394 μ mol, 3.0 eq) were stirred in DCM (1.0 mL) for 20 h. The crude was purified with 10-50% EtOAc in heptane to yield boc-**14aA** (104 mg, 105 μ mol, 80%) as a slightly yellow solid. TFA (101 μ L, 1.31 mmol, 10.0 eq) and DCM (1.0 mL) were added, and the mixture was stirred at ambient temperature for 22 h. The crude was purified by automated RP column chromatography with a gradient of 10-60% MeCN/H₂O + 0.1% TFA to yield the di-TFA salt of **14aA** (92 mg, 69 μ mol, 69% o2s) as a white powder. **¹H NMR** (400 MHz, Methanol-*d*₄) δ 7.63 (t, J = 1.8 Hz, 2H), 7.20 (d, J = 1.7 Hz, 4H), 3.71 – 3.58 (m, 4H), 3.40 (s, 4H), 2.97 – 2.86 (m, 4H), 1.75 – 1.63 (m, 4H), 1.42 – 1.31 (m, 4H), 1.31 – 1.21 (m, 4H). **¹³C NMR** (101 MHz, Methanol-*d*₄) δ 171.1 (2C), 150.3, 140.5 (2C), 134.4 (2C), 132.6 (4C), 124.1 (4C), 61.1, 44.8 (2C), 42.6 (2C), 40.5 (2C), 28.6 (2C), 28.2 (2C), 24.6 (2C). **HRMS** (ESI): calcd for $C_{28}H_{35}Br_4N_4O_3^+$ $[M+H]^+$ 790.9437, found 790.9443. **SFC**: >99.5%.



1,3-bis(6-aminohexyl)-5,5-bis(3,5-dibromobenzyl)pyrimidine-2,4,6(1H,3H,5H)-trione 15aA.

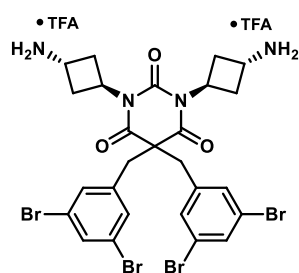
Barbiturate **3a** (80 mg, 128 μ mol, 1.0 eq), *tert*-butyl (6-hydroxyhexyl)carbamate (70 mg, 321 μ mol, 2.5 eq), PPh_3 (101 mg, 385 μ mol, 3.0 eq) and DIAD (81 μ L, 385 μ mol, 3.0 eq) were stirred in DCM (1.0 mL) for 20 h. The crude was purified with 10-40% EtOAc in heptane to yield boc-**15aA** (105 mg, 103 μ mol, 80%) as a colorless oil. TFA (98 μ L, 1.28 mmol, 10.0 eq) and DCM (1.0 mL) were added, and the mixture was stirred at ambient temperature for 22 h. The crude was purified by automated RP column chromatography with a gradient of 10-60% MeCN/H₂O + 0.1% TFA to yield the di-TFA salt of **15aA** (98 mg, 93 μ mol, 73% o2s) as a white powder. **¹H NMR** (400 MHz, Methanol-*d*₄) δ 7.63 (t, J = 1.7 Hz, 2H), 7.20 (d, J = 1.8 Hz, 4H), 3.72 – 3.56 (m, 4H), 3.39 (s, 4H), 2.97 – 2.86 (m, 4H), 1.71 – 1.57 (m, 4H), 1.38 (dp, J = 22.6, 8.1, 7.7 Hz, 8H), 1.25 – 1.13 (m, 4H). **¹³C NMR** (101 MHz, Methanol-*d*₄) δ 171.1 (2C), 150.4, 140.5 (2C), 134.4 (2C), 132.6 (4C), 124.1 (4C), 61.0, 44.9 (2C), 42.8 (2C), 40.6 (2C), 28.9 (2C), 28.5 (2C), 27.2 (2C), 27.0 (2C). **HRMS** (ESI): calcd for $C_{30}H_{39}Br_4N_4O_3^+$ $[M+H]^+$ 818.9750, found 818.9756. **SFC**: 98.5%.



1,3-bis((1S,3S)-3-aminocyclobutyl)-5,5-bis(3,5-dibromobenzyl)pyrimidine-2,4,6(1H,3H,5H)-trione 16aA.

Barbiturate **3a** (300 mg, 481 μ mol, 1.0 eq), *tert*-butyl trans-(3-hydroxycyclobutyl)carbamate (225 mg, 1.20 mmol, 2.5 eq), PPh_3 (378 mg, 1.44 mmol, 3.0 eq) and DIAD (302 μ L, 1.44 mmol, 3.0 eq) were stirred in anhydrous DCM (1.5 mL) at ambient temperature for 24 h. The crude was purified with 0-40% EtOAc in heptane to yield boc-**16aA** (404 mg, 420 μ mol, 87%) as a colorless oil. Boc-**16aA** (404 mg, 420 μ mol, 1.0 eq), TFA (161 μ L, 2.10 mmol, 5.0 eq) and DCM (3.0 mL) were combined, and the mixture was stirred at ambient temperature until HRMS indicated full conversion. The crude was purified by automated RP column chromatography with a gradient of 15-45% MeCN/H₂O + 0.1% TFA to yield the di-TFA salt of **16aA** (306 mg, 309 μ mol, 64% o2s) as a white solid. **¹H NMR** (400 MHz, Methanol-*d*₄) δ 7.64 (t, J = 1.8 Hz, 2H), 7.25 (d, J = 1.8 Hz, 4H), 4.89 (p, J = 8.8 Hz, 2H), 3.56 (p, J = 7.8 Hz, 2H), 3.43 (s, 4H), 2.82 (tdd, J = 10.5, 9.4, 5.7, 1.8 Hz, 4H), 2.70 – 2.60 (m, 4H). *Partial overlap of a methylene signals with residual water.* **¹³C NMR** (101 MHz, Methanol-*d*₄) δ 171.5 (2C), 150.4, 140.4 (2C), 134.6

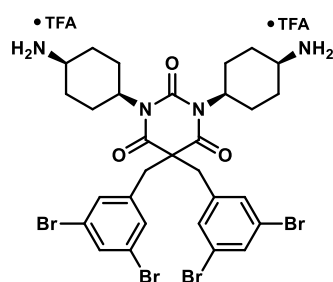
(2C), 132.7 (4C), 124.2 (4C), 61.6, 44.7 (2C), 43.5 (2C), 40.7 (2C), 33.8 (4C). **HRMS** (ESI): calcd for $C_{26}H_{27}Br_4N_4O_3^+$ $[M+H]^+$ 758.8811, found: 758.8810. **SFC**: >99.5%



1,3-bis((1r,3R)-3-aminocyclobutyl)-5,5-bis(3,5-dibromobenzyl)pyrimidine-2,4,6(1H,3H,5H)-trione 17aA.

Barbiturate **3a** (300 mg, 481 μ mol, 1.0 eq), *tert*-butyl *trans*-(3-hydroxycyclobutyl)carbamate (225 mg, 1.20 mmol, 2.5 eq), PPh_3 (378 mg, 1.44 mmol, 3.0 eq) and DIAD (302 μ L, 1.44 mmol, 3.0 eq) were stirred in anhydrous THF (2.5 mL) at ambient temperature for 24 h. The crude was purified with 0-40% EtOAc in heptane to yield *boc*-**17aA** (262 mg, 272 μ mol, 67%) as a colorless oil.

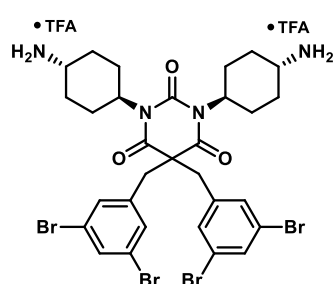
Boc-**17aA** (262 mg, 272 μ mol, 1.0 eq), TFA (125 μ L, 1.63 mmol, 6.0 eq) and DCM (2.0 mL) were combined, and the mixture was stirred at ambient temperature for 38 h. The crude was purified by automated RP column chromatography with a gradient of 15-45% MeCN/H₂O + 0.1% TFA to yield the di-TFA salt of **17aA** (125 mg, 126 μ mol, 26% o2s) as a white solid. **¹H NMR** (400 MHz, Methanol-*d*₄) δ 7.66 (t, J = 1.8 Hz, 2H), 7.24 (d, J = 1.8 Hz, 4H), 5.41 (ttd, J = 10.1, 7.2, 1.0 Hz, 2H), 4.07 (tdd, J = 9.1, 4.4, 3.4 Hz, 2H), 3.44 (s, 4H), 2.90 – 2.74 (m, 4H), 2.54 – 2.41 (m, 4H). **¹³C NMR** (101 MHz, Methanol-*d*₄) δ 171.3 (2C), 150.0, 140.5 (2C), 134.5 (2C), 132.6 (4C), 124.2 (4C), 61.5 (2C), 45.3 (2C), 44.8 (2C), 43.5 (2C), 32.7 (4C). **HRMS** (ESI): calcd for $C_{26}H_{27}Br_4N_4O_3^+$ $[M+H]^+$ 758.8811, found: 758.8813. **SFC**: >99.5%



1,3-bis((1s,4S)-4-aminocyclohexyl)-5,5-bis(3,5-dibromobenzyl)pyrimidine-2,4,6(1H,3H,5H)-trione 18aA.

Barbiturate **3a** (200 mg, 321 μ mol, 1.0 eq), *tert*-butyl (*trans*-4-hydroxycyclohexyl)carbamate (173 mg, 801 μ mol, 2.5 eq), PPh_3 (252 mg, 962 μ mol, 3.0 eq) and DIAD (201 μ L, 962 μ mol, 3.0 eq) were stirred in DCM (1.0 mL) for 18 h. The crude was purified with 0-40% EtOAc in heptane to yield *boc*-**18aA** (179 mg, 176 μ mol, 55%) as a colorless oil.

Boc-**18aA** (160 mg, 157 μ mol, 1.0 eq), TFA (98 μ L, 1.28 mmol, 10.0 eq) and DCM (1.0 mL) were combined, and the mixture was stirred at ambient temperature for 22 h. The crude was purified by automated RP column chromatography with a gradient of 15-50% MeCN/H₂O + 0.1% TFA to yield the di-TFA salt of **18aA** (138 mg, 132 μ mol, 46% o2s) as a white powder. **¹H NMR** (400 MHz, Methanol-*d*₄) δ 7.66 (t, J = 1.8 Hz, 2H), 7.24 (d, J = 1.8 Hz, 4H), 4.61 – 4.41 (m, 2H), 3.54 – 3.47 (m, 2H), 3.43 (s, 4H), 2.54 – 2.21 (m, 4H), 2.06 – 1.94 (m, 4H), 1.94 – 1.78 (m, 4H), 1.29 – 1.17 (m, 4H). **¹³C NMR** (101 MHz, Methanol-*d*₄) δ 171.6 (2C), 149.9, 140.5 (2C), 134.5 (2C), 132.7 (4C), 124.3 (4C), 61.3, 55.2 (2C), 46.8 (2C), 45.0 (2C), 29.2 (4C), 24.1 (4C). **HRMS** (ESI): calcd for $C_{30}H_{35}Br_4N_4O_3^+$ $[M+H]^+$ 814.9437, found 814.9444. **SFC**: >99.5%



1,3-bis((1r,4R)-4-aminocyclohexyl)-5,5-bis(3,5-dibromobenzyl)pyrimidine-2,4,6(1H,3H,5H)-trione 19aA.

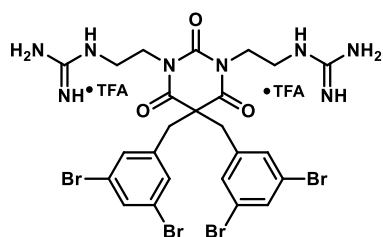
Barbiturate **3a** (300 mg, 481 μ mol, 1.0 eq), *tert*-butyl (*cis*-4-hydroxycyclohexyl)carbamate (259 mg, 1.20 mmol, 2.5 eq), PPh_3 (378 mg, 1.44 mmol, 3.0 eq) and DIAD (302 μ L, 1.44 mmol, 3.0 eq) were stirred in anhydrous THF (2.5 mL) at 45 $^{\circ}$ C for 72 h. The crude was purified with 0-40% EtOAc in heptane to yield *boc*-**19aA** (169 mg, 166 μ mol, 35%) as a colorless oil.

Boc-**19aA** (169 mg, 166 μ mol, 1.0 eq), TFA (127 μ L, 1.66 mmol, 10.0 eq) and DCM (2.0 mL) were combined, and the mixture was stirred at ambient temperature until HRMS indicated full conversion. The crude was purified by automated RP column chromatography with a gradient of 15-45% MeCN/H₂O + 0.1% TFA to yield the di-TFA salt of **19aA** (116 mg, 111 μ mol, 23% o2s) as a white solid. **¹H NMR** (400 MHz, Dimethylsulfoxide-*d*₆) δ 7.94 (s, 6H), 7.80 (t, J = 1.7 Hz, 2H), 7.13 (d, J = 1.8 Hz, 4H), 4.36 – 4.17 (m, 2H), 3.08 – 2.92 (m, 2H), 2.21 – 2.04 (m, 4H), 2.03 – 1.91 (m, 4H), 1.47 – 1.29 (m, 4H), 1.28 – 1.13 (m, 4H). **¹³C NMR** (101 MHz, Dimethylsulfoxide-*d*₆) δ 169.7 (2C), 148.4, 139.0 (2C), 132.8 (2C), 131.3 (4C), 122.8 (4C), 59.5, 53.6 (2C), 48.0 (2C), 43.2 (2C), 29.6

(4C), 26.2 (4C). **HRMS** (ESI): calcd for $C_{30}H_{35}Br_4N_4O_3^+$ $[M+H]^+$ 814.9437, found: 814.9441. **SFC**: 91.0%

2.9.2 Guanidine derivatives

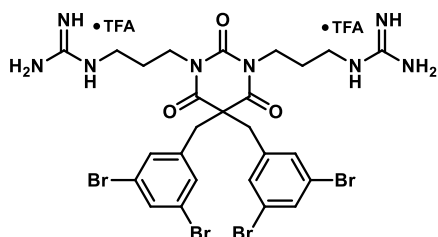
The compounds were synthesized according to General Procedure C.



1,1'-((5,5-bis(3,5-dibromobenzyl)-2,4,6-trioxodihydropyrimidine-1,3(2H,4H)-diyl)bis(ethane-2,1-diyl))diguanidine 12aG.

Barbiturate **12aA** (18 mg, 19 μ mol, 1.0 eq), *N,N'*-di-Boc-1*H*-pyrazole-1-carboxamidine (18 mg, 58 μ mol, 3.0 eq), DIPEA (10 μ L, 57 μ mol, 3.00 eq) and THF (1 mL) were stirred at 45 °C for 3.0 h. The crude was purified with 10-45% EtOAc in heptane to yield impure boc-**12aG** (30 mg, 25 μ mol, 131%) as a colorless oil.

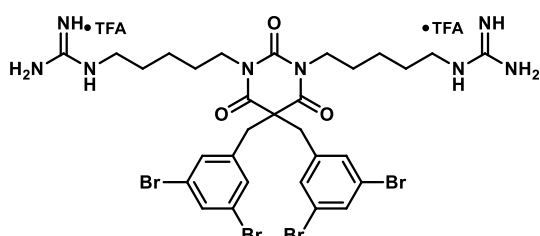
TFA (22 μ L, 287 μ mol, 15.0 eq) and DCM (1 mL) were added, and the mixture was stirred at ambient temperature for 40 h. The crude was purified by automated RP column chromatography with a gradient of 25-65% MeCN/H₂O + 0.1% TFA to yield the di-TFA salt of **12aG** (18 mg, 18 μ mol, 92% o2s) as a white solid. **¹H NMR** (400 MHz, Methanol-*d*₄) δ 7.67 (t, *J* = 1.6 Hz, 2H), 7.29 (d, *J* = 1.8 Hz, 4H), 3.88 (t, *J* = 6.5 Hz, 4H), 3.43 (s, 4H), 3.25 (t, *J* = 6.6 Hz, 4H). **¹³C NMR** (101 MHz, Methanol-*d*₄) δ 171.4 (2C), 158.9 (2C), 151.1 (2C), 140.3 (2C), 134.7 (2C), 132.9 (4C), 124.1 (4C), 61.1, 44.4 (2C), 41.6 (2C), 40.5 (2C). **HRMS** (ESI): calcd for $C_{24}H_{28}Br_4N_8O_3^{2+}$ $[M+2H]^{2+}$ 395.9503, found 395.9511. **SFC**: 98.2%.



1,1'-((5,5-bis(3,5-dibromobenzyl)-2,4,6-trioxodihydropyrimidine-1,3(2H,4H)-diyl)bis(propane-3,1-diyl))diguanidine 13aG.

Barbiturate **13aA** (70 mg, 73 μ mol, 1.0 eq), *N,N'*-di-Boc-1*H*-pyrazole-1-carboxamidine (56 mg, 181 μ mol, 2.50 eq), DIPEA (51 μ L, 290 μ mol, 4.00 eq) and THF (1 mL) were stirred at 45 °C for 2.5 h. The crude was purified with 20% EtOAc in heptane to yield boc-**13aG** (54 mg, 44 μ mol, 61%) as a white foam.

TFA (83 μ L, 1.09 mmol, 15.0 eq) and DCM (1 mL) were added, and the mixture was stirred at ambient temperature for 40 h. The crude was purified by automated RP column chromatography with a gradient of 10-60% MeCN/H₂O + 0.1% TFA to yield the di-TFA salt of **13aG** (43 mg, 41 μ mol, 57% o2s) as a white powder. **¹H NMR** (400 MHz, Methanol-*d*₄) δ 7.65 (t, *J* = 1.8 Hz, 2H), 7.23 (d, *J* = 1.8 Hz, 4H), 3.77 – 3.67 (m, 4H), 3.44 (s, 4H), 3.08 (t, *J* = 7.0 Hz, 4H), 1.62 (dq, *J* = 9.2, 7.1 Hz, 4H). **¹³C NMR** (101 MHz, Methanol-*d*₄) δ 171.3 (2C), 158.7 (2C), 150.5, 140.5 (2C), 134.58 (2C), 132.6 (4C), 124.2 (4C), 61.4, 44.8 (2C), 40.4 (2C), 39.6 (2C), 28.9 (2C). **HRMS** (ESI): calcd for $C_{26}H_{31}Br_4N_8O_3^+$ $[M+H]^+$ 818.9247, found 818.9250. **SFC**: >99.5%.



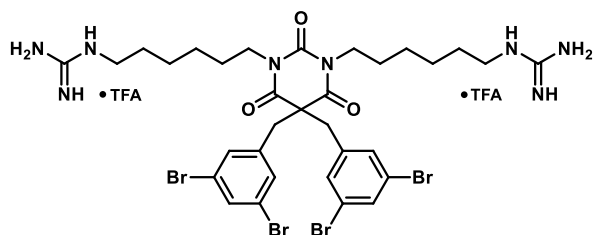
1,1'-((5,5-bis(3,5-dibromobenzyl)-2,4,6-trioxodihydropyrimidine-1,3(2H,4H)-diyl)bis(pentane-5,1-diyl))diguanidine 14aG.

Barbiturate **14aA** (13 mg, 13 μ mol, 1.0 eq), *N,N'*-di-Boc-1*H*-pyrazole-1-carboxamidine (12 mg, 38 μ mol, 3.0 eq), DIPEA (7 μ L, 38 μ mol, 3.00 eq) and THF (1 mL) were stirred at 45 °C for 3.0 h. The crude was purified with 10-45% EtOAc in heptane to yield boc-

14aG (15 mg, 12 μ mol, 92%) as a yellow oil.

TFA (15 μ L, 191 μ mol, 15.0 eq) and DCM (1 mL) were added, and the mixture was stirred at ambient temperature for 20 h. The crude was purified by automated RP column chromatography with a gradient of 25-65% MeCN/H₂O + 0.1% TFA to yield the di-TFA salt of **14aG** (12 mg, 11 μ mol, 85% o2s) as a white solid. **¹H NMR** (400 MHz, Methanol-*d*₄) δ 7.64 (t, *J* = 1.6 Hz, 2H), 7.21 (d, *J* = 1.7 Hz, 4H), 3.63 (t, *J* = 7.6 Hz, 4H), 3.41 (s, 4H), 3.16 (t, *J* = 7.2 Hz, 4H), 1.62 (p, *J* = 7.3 Hz, 4H), 1.42 – 1.30 (m, 4H), 1.25 (p, *J* = 7.6 Hz, 4H). **¹³C NMR** (101 MHz, Methanol-*d*₄) δ 171.2 (2C), 158.7 (2C), 150.4, 140.6

(2C), 134.4 (2C), 132.6 (4C), 124.1 (4C), 61.1, 44.9 (2C), 42.8 (2C), 42.3 (2C), 29.5 (2C), 28.8 (2C), 24.8 (2C). **HRMS** (ESI): calcd for $C_{30}H_{40}Br_4N_8O_3^{2+}$ $[M+2H]^{2+}$ 437.9973, found 437.9978. **SFC**: 98.4%.



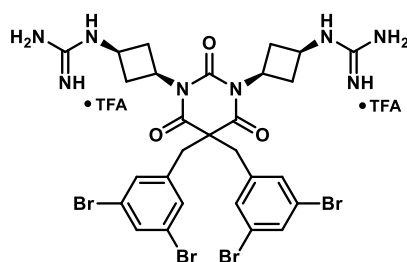
1,1'-((5,5-bis(3,5-dibromobenzyl)-2,4,6-trioxodihydropyrimidine-1,3(2H,4H)-diyl)bis(hexane-6,1-diyl))diguanidine 15aG.

Barbiturate **15aA** (38 mg, 36 μ mol, 1.0 eq), *N,N'*-di-Boc-1*H*-pyrazole-1-carboxamide (34 mg, 109 μ mol, 3.0 eq), DBU (22 μ L, 148 μ mol, 4.00 eq) and THF (1 mL) were stirred at 45 °C for 3.5 h.

The organic layer was washed with 10% citric

acid_(aq) solution instead of 10% NaHCO_{3(aq)} solution. Partial cleavage of the Boc groups was observed. Boc-**15aG** was used without further purification.

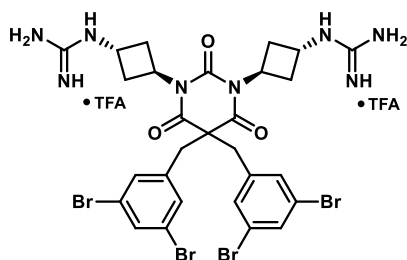
4M HCl in Dioxane (452 μ L, 1.81 mmol, 50.0 eq) was added and the mixture was stirred at ambient temperature for 24 h. The crude was purified by RP chromatography with a gradient of 10-70% MeCN/H₂O + 0.1% TFA to yield the di-TFA salt of **15aG** (30 mg, 26 μ mol, 73% o2s) as a white solid. **¹H NMR** (400 MHz, Methanol-*d*₄) δ 7.63 (t, *J* = 1.8 Hz, 2H), 7.20 (d, *J* = 1.7 Hz, 4H), 3.68 – 3.57 (m, 4H), 3.40 (s, 4H), 3.17 (t, *J* = 7.1 Hz, 4H), 1.57 (p, *J* = 7.3 Hz, 4H), 1.47 – 1.27 (m, 8H), 1.20 (p, *J* = 7.7 Hz, 4H). **¹³C NMR** (101 MHz, Methanol-*d*₄) δ 171.2 (2C), 158.6 (2C), 150.5, 140.6 (2C), 134.4 (2C), 132.6 (4C), 124.1 (4C), 61.1, 44.9 (2C), 42.9 (2C), 42.4 (2C), 29.8 (2C), 29.0 (2C), 27.3 (2C), 27.3 (2C). **HRMS** (ESI): calcd for $C_{32}H_{44}Br_4N_8O_3^{2+}$ $[M+2H]^{2+}$ 452.0129, found 452.0137. **SFC**: 98.1%.



1,1'-((1S,1'S,3s,3's)-(5,5-bis(3,5-dibromobenzyl)-2,4,6-trioxodihydropyrimidine-1,3(2H,4H)-diyl)bis(cyclobutane-3,1-diyl))diguanidine 16aG.

Barbiturate **16aA** (200 mg, 202 μ mol, 1.0 eq), *N,N'*-di-Boc-1*H*-pyrazole-1-carboxamide (157 mg, 505 μ mol, 2.5 eq), DIPEA (140 μ L, 808 μ mol, 4.0 eq) and THF (4.0 mL) were stirred at 45 °C for 3 h. The crude was purified with 10-45% EtOAc in heptane to yield boc-**16aG** (134 mg, 108 μ mol, 53%) as a colorless oil.

TFA (124 μ L, 1.61 mmol, 15.0 eq) and DCM (0.5 mL) were added, and the mixture was stirred at ambient temperature until HRMS indicated full conversion. The crude was purified by automated RP column chromatography with a gradient of 18-45% MeCN/H₂O + 0.1% TFA to yield the di-TFA salt of **16aG** (52 mg, 48 μ mol, 24% o2s) as a white solid. **¹H NMR** (400 MHz, Methanol-*d*₄) δ 7.65 (t, *J* = 1.8 Hz, 2H), 7.23 (d, *J* = 1.8 Hz, 4H), 4.67 (tt, *J* = 9.3, 8.1 Hz, 2H), 3.80 – 3.69 (m, 2H), 2.79 – 2.67 (m, 4H), 2.63 – 2.51 (m, 4H). **¹³C NMR** (101 MHz, Methanol-*d*₄) δ 171.6 (2C), 157.7 (2C), 150.3, 140.4 (2C), 134.5 (2C), 132.6 (4C), 124.2 (4C), 61.5, 44.8 (2C), 43.8 (2C), 41.4 (2C), 36.3 (4C). **HRMS** (ESI): calcd for $C_{28}H_{31}Br_4N_8O_3^+$ $[M+H]^+$ 842.9247, found 842.9238. **SFC**: 98.6%.



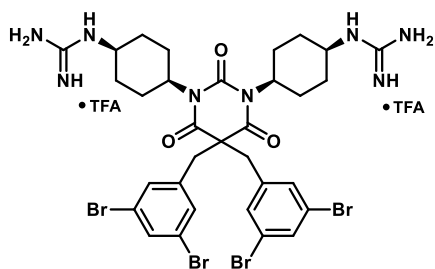
1,1'-((1R,1'R,3r,3'r)-(5,5-bis(3,5-dibromobenzyl)-2,4,6-trioxodihydropyrimidine-1,3(2H,4H)-diyl)bis(cyclobutane-3,1-diyl))diguanidine 17aG.

Barbiturate **17aA** (87 mg, 88 μ mol, 1.0 eq), *N,N'*-di-Boc-1*H*-pyrazole-1-carboxamide (68 mg, 220 μ mol, 2.5 eq), DIPEA (61 μ L, 351 μ mol, 4.0 eq) and THF (4.0 mL) were stirred at 45 °C for 3 h. The crude was purified with 10-45% EtOAc in heptane to yield impure boc-**17aG** (116 mg, 93 μ mol, 106%) as a colorless oil.

TFA (107 μ L, 1.39 mmol, 15.0 eq) and DCM (0.5 mL) were added,

and the mixture was stirred at ambient temperature until HRMS indicated full conversion. The crude was purified by automated RP column chromatography with a gradient of 15-45% MeCN/H₂O + 0.1% TFA to yield the di-TFA salt of **17aG** (31 mg, 29 μ mol, 32% o2s) as a white solid. **¹H NMR** (400 MHz, Methanol-*d*₄) δ 7.64 (t, *J* = 1.7 Hz, 2H), 7.23 (d, *J* = 1.7 Hz, 4H), 5.32 – 5.20 (m, 2H), 4.26 – 4.17 (m, 2H), 3.42 (s, 4H), 2.97 – 2.85 (m, 4H), 2.36 – 2.25 (m, 4H). **¹³C NMR** (101 MHz, Methanol-*d*₄) δ 171.4 (2C), 158.3 (2C), 150.0, 140.5 (2C), 134.5 (2C), 132.6 (4C), 124.2 (4C), 61.5, 46.5 (2C), 44.8 (2C), 43.9

(2C), 35.2 (4C). **HRMS** (ESI): calcd for $C_{28}H_{31}Br_4N_8O_3^+$ $[M+H]^+$ 842.9247, found 842.9254. **SFC**: 92.1%.



1,1'-((1S,1'S,4s,4's)-(5,5-bis(3,5-dibromobenzyl)-2,4,6-trioxodihydropyrimidine-1,3(2H,4H)-diyl)bis(cyclohexane-4,1-diyl))diguanidine 18gG.

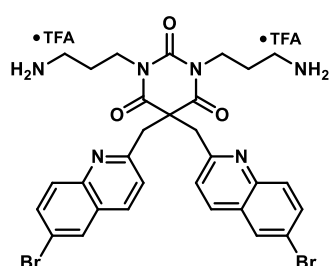
Barbiturate **18aA** (125 mg, 120 μ mol, 1.0 eq), *N,N'*-di-Boc-1*H*-pyrazole-1-carboxamidine (93 mg, 299 μ mol, 2.5 eq), DIPEA (83 μ L, 478 μ mol, 4.0 eq) and THF (0.5 mL) were stirred at 45 °C for 17 h. The crude was purified with 45% EtOAc in heptane to yield boc-**18gG** (106 mg, 81 μ mol, 68%) as a colorless oil.

TFA (94 μ L, 1.22 mmol, 15.0 eq) and DCM (0.5 mL) were added, and the mixture was stirred at ambient temperature until HRMS indicated full conversion. The crude was purified by automated RP column chromatography with a gradient of 15-45% MeCN/H₂O + 0.1% TFA to yield the di-TFA salt of **18gG** (19 mg, 17 μ mol, 14% o2s) as a white solid. **¹H NMR** (400 MHz, Methanol-*d*₄) δ 7.64 (t, *J* = 1.8 Hz, 2H), 7.22 (d, *J* = 1.7 Hz, 4H), 4.60 – 4.32 (m, 2H), 3.80 – 3.70 (m, 2H), 3.40 (s, 4H), 2.55 – 2.18 (m, 4H), 1.93 (d, *J* = 14.0 Hz, 4H), 1.78 – 1.62 (m, 4H), 1.25 – 1.11 (m, 4H). **¹³C NMR** (101 MHz, Methanol-*d*₄) δ 171.6 (2C), 158.0 (2C), 150.0, 140.6 (2C), 134.4 (2C), 132.7 (4C), 124.3 (4C), 61.2, 55.6 (2C), 46.6 (2C), 45.0 (2C), 30.6 (4C), 24.5 (4C). **HRMS** (ESI): calcd for $C_{32}H_{39}Br_4N_8O_3^+$ $[M+H]^+$ 898.9873, found 898.9880. **SFC**: 97.2%.

2.10 Synthesis of series 5

2.10.1 Amine derivatives

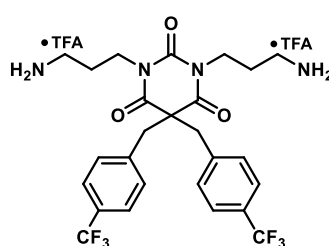
All compounds were synthesized according to General procedure B:



1,3-bis(3-aminopropyl)-5,5-bis((6-bromoquinolin-2-yl)methyl)pyrimidine-2,4,6(1H,3H,5H)-trione 13cA.

Barbiturate **3c** (54 mg, 95 μ mol, 1.0 eq), *tert*-butyl (3-bromopropyl)carbamate (57 mg, 0.24 mmol, 2.50 eq), Cs₂CO₃ (77 mg, 0.24 mmol, 2.50 eq), TBAI (7 mg, 19 μ mol, 0.2 eq) and acetone (1.5 mL) were stirred at 60 °C for 40 h. The crude was purified with 10-70% EtOAc in heptane to yield boc-**13cA** (29 mg, 33 μ mol, 35%) as a colorless oil.

TFA (73 μ L, 0.95 mmol, 10.0 eq) and DCM (0.7 mL) were added, and the mixture was stirred at ambient temperature for 22 h. The crude was purified by automated RP column chromatography with a gradient of 10-60% MeCN/H₂O + 0.1% TFA to yield the di-TFA salt of **13cA** (29 mg, 32 μ mol, 34% o2s) as a white powder. **¹H NMR** (400 MHz, Methanol-*d*₄) δ 8.25 – 8.18 (m, 2H), 8.13 (d, *J* = 2.2 Hz, 2H), 7.83 (dd, *J* = 8.9, 2.2 Hz, 2H), 7.61 (d, *J* = 9.0 Hz, 2H), 7.44 (d, *J* = 8.5 Hz, 2H), 3.97 (s, 4H), 3.89 (t, *J* = 6.9 Hz, 4H), 2.62 (t, *J* = 7.0 Hz, 4H), 1.82 (p, *J* = 7.0 Hz, 4H). **¹³C NMR** (101 MHz, Methanol-*d*₄) δ 174.3 (2C), 158.9 (2C), 153.2, 146.7 (2C), 137.5 (2C), 134.7 (2C), 131.4 (2C), 130.7 (2C), 129.6 (2C), 123.5 (2C), 121.3 (2C), 54.5, 48.2 (2C), 39.9 (2C), 38.1 (2C), 27.0 (2C). **HRMS** (ESI): calcd for $C_{30}H_{31}Br_2N_6O_3^+$ $[M+H]^+$ 681.0819, found 681.0823. **SFC**: >99.5%.

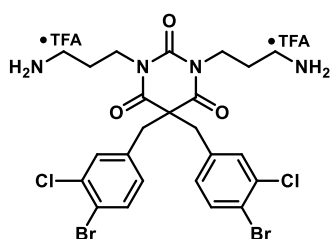


1,3-bis(3-aminopropyl)-5,5-bis(4-(trifluoromethyl)benzyl)pyrimidine-2,4,6(1H,3H,5H)-trione 13hA.

Barbiturate **3h** (332 mg, 0.75 mmol, 1.0 eq), *tert*-butyl (3-bromopropyl)carbamate (368 mg, 1.55 mmol, 2.07 eq), K₂CO₃ (315 mg, 2.28 mmol, 3.0 eq), TBAI (28 mg, 75 μ mol, 0.1 eq) and acetone (8 mL) were stirred at 50 °C for 21 h. Boc-**13hA** (469 mg, 0.62 mmol, 83%) was obtained as a yellow solid and used without further purification.

TFA (0.72 mL, 9.38 mmol, 15.1 eq) and DCM (2.5 mL) were added, and the mixture was stirred at ambient temperature for 17 h. The crude was purified by automated RP column chromatography with a gradient of 0-70% MeCN/H₂O + 0.1% TFA to yield the di-TFA salt of **13hA**

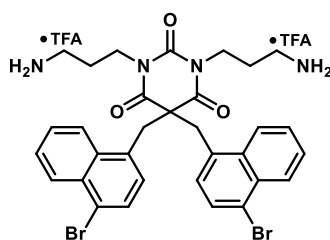
(448 mg, 0.57 mmol, 76% o2s) as a white powder, m.p. 180-184 °C. $^1\text{H NMR}$ (400 MHz, Methanol-*d*₄) δ 7.60 (d, *J* = 8.1 Hz, 4H), 7.30 (d, *J* = 8.0 Hz, 4H), 3.70 (t, 4H), 3.58 (s, 4H), 2.72 (t, *J* = 7.3 Hz, 4H), 1.69 (p, *J* = 7.3 Hz, 4H). $^{13}\text{C NMR}$ (101 MHz, Methanol-*d*₄) δ 171.5 (2C), 150.9, 140.6 (2C), 131.4 (4C), 131.2 (q, *J* = 32.4 Hz, 2C), 126.7 (q, *J* = 3.7 Hz, 4C), 125.4 (q, *J* = 271.0 Hz, 2C), 61.3, 45.7 (2C), 40.0 (2C), 38.0 (2C), 26.7 (2C). **HRMS** (ESI): calcd for C₂₆H₂₉F₆N₄O₃⁺ [M+H]⁺ 559.2138, found 559.2145. **SFC**: 95.6%.



1,3-bis(3-aminopropyl)-5,5-bis(4-bromo-3-chlorobenzyl)pyrimidine-2,4,6(1H,3H,5H)-trione 13iA.

Barbiturate **3i** (401 mg, 0.75 mmol, 1.0 eq), *tert*-butyl (3-bromopropyl)carbamate (366 mg, 1.54 mmol, 2.05 eq), K₂CO₃ (314 mg, 2.27 mmol, 3.0 eq), TBAI (28 mg, 75 μ mol, 0.1 eq) and acetone (7 mL) were stirred at 50 °C for 21 h. Boc-**13iA** (564 mg, 0.68 mmol, 91%) was obtained as a beige highly viscous oil and used without further purification.

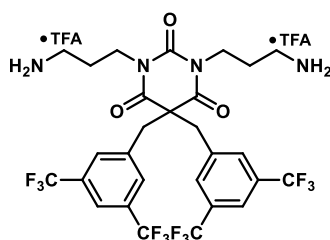
TFA (0.78 mL, 10.2 mmol, 15.0 eq) and DCM (2.5 mL) were added, and the mixture was stirred at ambient temperature for 18 h. The crude was purified by automated RP column chromatography with a gradient of 0-70% MeCN/H₂O + 0.1% TFA to yield the di-TFA salt of **13iA** (365 mg, 0.42 mmol, 55% o2s) as a white powder, m.p. 213-216 °C. $^1\text{H NMR}$ (400 MHz, Methanol-*d*₄) δ 7.61 (d, *J* = 8.2 Hz, 2H), 7.24 (d, *J* = 2.1 Hz, 2H), 6.94 (dd, *J* = 8.3, 2.1 Hz, 2H), 3.74 (t, 4H), 3.44 (s, 4H), 2.80 (t, *J* = 7.2 Hz, 4H), 1.74 (p, *J* = 7.2 Hz, 4H). $^{13}\text{C NMR}$ (101 MHz, Methanol-*d*₄) δ 171.5 (2C), 150.9, 137.6 (2C), 135.6 (2C), 135.4 (2C), 132.5 (2C), 130.7 (2C), 122.8 (2C), 61.2, 44.8 (2C), 40.1 (2C), 38.1 (2C), 27.0 (2C). **HRMS** (ESI): calcd for C₂₄H₂₇Br₂Cl₂N₄O₃⁺ [M+H]⁺ 646.9821, found 646.9832. **SFC**: 95.2%.



1,3-bis(3-aminopropyl)-5,5-bis(4-bromonaphthalen-1-yl)methylpyrimidine-2,4,6(1H,3H,5H)-trione 13eA.

Barbiturate **3e** (428 mg, 0.75 mmol, 1.0 eq), *tert*-butyl (3-bromopropyl)carbamate (369 mg, 1.55 mmol, 2.07 eq), K₂CO₃ (313 mg, 2.26 mmol, 3.0 eq), TBAI (28 mg, 75 μ mol, 0.1 eq) and acetone (7 mL) were stirred at 50 °C for 21 h. The crude was purified with 15-60% EtOAc in heptane to yield boc-**13eA** (379 mg, 0.43 mmol, 57%) as a white solid. TFA (0.49 mL, 6.40 mmol, 15.0 eq) and DCM (2.0 mL) were added, and

the mixture was stirred at ambient temperature for 18 h. The crude was purified by automated RP column chromatography with a gradient of 0-70% MeCN/H₂O + 0.1% TFA to yield the di-TFA salt of **13eA** (355 mg, 0.39 mmol, 52% o2s) as a white powder. m.p.: 204-207 °C. $^1\text{H NMR}$ (400 MHz, Methanol-*d*₄) δ 8.40 – 8.11 (m, 4H), 7.73 (dd, *J* = 7.8, 2.3 Hz, 2H), 7.70 – 7.59 (m, 4H), 7.26 – 7.03 (m, 2H), 4.15 (s, 4H), 3.41 (t, *J* = 7.0 Hz, 4H), 2.44 (t, *J* = 6.5, 5.4 Hz, 4H), 1.38 (p, *J* = 7.1 Hz, 4H). $^{13}\text{C NMR}$ (101 MHz, Methanol-*d*₄) δ 172.2 (2C), 151.2, 134.4 (2C), 133.4 (2C), 133.3 (2C), 130.5 (2C), 129.1 (2C), 128.8 (2C), 128.7 (2C), 128.4 (2C), 126.3 (2C), 124.0 (2C), 60.2, 41.7 (2C), 39.9 (2C), 37.8 (2C), 26.6 (2C). **HRMS** (ESI): calcd for C₃₂H₃₃Br₂N₄O₃⁺ [M+H]⁺ 679.0914, found 679.0903. **SFC**: 96.5%.

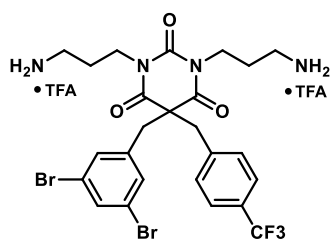


1,3-bis(3-aminopropyl)-5,5-bis(3,5-bis(trifluoromethyl)benzyl)pyrimidine-2,4,6(1H,3H,5H)-trione 13jA.

Barbiturate **3j** (261 mg, 0.45 mmol, 1.0 eq), *tert*-butyl (3-bromopropyl)carbamate (214 mg, 0.90 mmol, 2.00 eq), Cs₂CO₃ (323 mg, 0.99 mmol, 2.2 eq), TBAI (17 mg, 45 μ mol, 0.1 eq) and acetone (2.5 mL) were stirred at 70 °C for 3.5 d. The crude was purified with 0-70% EtOAc in heptane to yield boc-**13jA** (265 mg, 0.30 mmol, 66%) as a white solid. TFA (0.28 mL, 3.60 mmol, 8.0 eq) and DCM (2.0 mL) were added, and

the mixture was stirred at ambient temperature for 12 h. The crude was purified by automated RP column chromatography with a gradient of 0-70% MeCN/H₂O + 0.1% TFA to yield the di-TFA salt of **13jA** (251 mg, 0.27 mmol, 61% o2s) as a white powder. $^1\text{H NMR}$ (400 MHz, Methanol-*d*₄) δ 7.93 (s, 2H), 7.73 – 7.68 (m, 4H), 3.76 – 3.68 (m, 8H), 2.80 (t, *J* = 7.1 Hz, 4H), 1.67 (dq, *J* = 9.0, 7.2 Hz, 4H). $^{13}\text{C NMR}$ (101 MHz, Methanol-*d*₄) δ 171.1 (2C), 150.6, 139.3 (2C), 133.1 (q, *J* = 33.4 Hz, 4C), 131.6 –

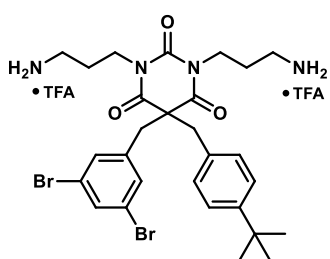
131.4 (m, 4C), 124.6 (q, $J = 272$ Hz, 4C), 123.1 – 122.8 (m, 2C), 61.0, 44.6 (2C), 40.3 (2C), 38.0 (2C), 26.9 (2C). **HRMS** (ESI): calcd for $C_{28}H_{27}F_{12}N_4O_3^+$ $[M+H]^+$ 695.1886, found 695.1884. **SFC**: 95.2%.



1,3-bis(3-aminopropyl)-5-(3,5-dibromobenzyl)-5-(4-(trifluoromethyl)benzyl)pyrimidine-2,4,6(1H,3H,5H)-trione 13IA.

Barbiturate **3l** (479 mg, 0.90 mmol, 1.0 eq), *tert*-butyl (3-bromopropyl)carbamate (470 mg, 1.97 mmol, 2.2 eq), K_2CO_3 (372 mg, 2.69 mmol, 3.0 eq), TBAI (33 mg, 90 μ mol, 0.1 eq) and acetone (15 mL) were stirred at 50 °C for 18 h. The crude was purified by column chromatography on silica gel with EtOAc in heptane to yield boc-**13IA** (340 mg, 0.40 mmol, 45%) as a pale-yellow oil.

TFA (0.30 mL, 3.88 mmol, 10.0 eq) and DCM (3.0 mL) were added, and the mixture was stirred at ambient temperature for 17 h. The crude was purified by automated RP column chromatography with a gradient of 15-50% MeCN/H₂O + 0.1% TFA to yield the di-TFA salt of **13IA** (334 mg, 0.39 mmol, 44% o2s) as a white powder. **¹H NMR** (400 MHz, Methanol-*d*₄) δ 7.67 (t, $J = 1.8$ Hz, 1H), 7.60 (d, $J = 8.0$ Hz, 2H), 7.29 (d, $J = 8.0$ Hz, 2H), 7.26 (d, $J = 1.8$ Hz, 2H), 3.81 – 3.67 (m, 4H), 3.56 (s, 2H), 3.48 (s, 2H), 2.89 – 2.71 (m, 4H), 1.82 – 1.62 (m, 4H). **¹³C NMR** (101 MHz, Methanol-*d*₄) δ 171.4 (2C), 150.9, 140.7 – 140.6 (m, 1C), 140.5, 134.6, 132.6 (2C), 131.5, 131.2 (q, $J = 32.5$ Hz, 1C) 126.8 (q, $J = 3.9$ Hz, 2C), 125.4 (q, $J = 271.9$ Hz, 1C), 124.2 (2C), 61.4, 45.4, 45.0, 40.1 (2C), 38.1 (2C), 27.0 (2C). **HRMS** (ESI): calcd for $C_{25}H_{28}Br_2F_3N_4O_3^+$ $[M+H]^+$ 647.0475, found 647.0473. **SFC**: 97.3%.



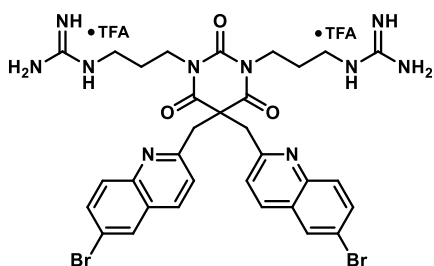
1,3-bis(3-aminopropyl)-5-(4-(tert-butyl)benzyl)-5-(3,5-dibromobenzyl)pyrimidine-2,4,6(1H,3H,5H)-trione 13pA.

Barbiturate **3p** (100 mg, 192 μ mol, 1.0 eq), *tert*-butyl (3-hydroxypropyl)carbamate (84 mg, 479 μ mol, 2.5 eq), PPh_3 (151 mg, 575 μ mol, 3.0 eq) and DIAD (120 μ L, 574 μ mol, 3.0 eq) were stirred in anhydrous DCM (0.5 mL) for 16 h. The crude was purified with 0-40% EtOAc in heptane to yield impure boc-**13pA** (161 mg, 192 μ mol, 101%) as a colorless oil.

TFA (129 μ L, 1.67 mmol, 10.0 eq) and DCM (1.0 mL) were added, and the mixture was stirred at ambient temperature for 18 h. The crude was purified by automated RP column chromatography with a gradient of 15-50% MeCN/H₂O + 0.1% TFA to yield the di-TFA salt of **13pA** (118 mg, 137 μ mol, 71% o2s) as a white powder. **¹H NMR** (400 MHz, Methanol-*d*₄) δ 7.64 (t, $J = 1.7$ Hz, 1H), 7.31 (d, $J = 8.3$ Hz, 2H), 7.26 (d, $J = 1.7$ Hz, 2H), 6.99 (d, $J = 8.3$ Hz, 2H), 3.79 – 3.64 (m, 4H), 3.46 (s, 2H), 3.41 (s, 2H), 2.76 (oct, $J = 7.1$ Hz, 4H), 1.83 – 1.62 (m, 4H). **¹³C NMR** (101 MHz, Methanol-*d*₄) δ 171.9 (2C), 152.5, 151.1, 141.1, 134.4, 132.7, 132.6 (2C), 130.2 (2C), 126.7 (2C), 124.1 (2C), 61.9, 46.5, 44.2, 40.0 (2C), 38.2 (2C), 35.4, 31.7 (3C), 27.0 (2C). **HRMS** (ESI): calcd for $C_{28}H_{37}Br_2N_4O_3^+$ $[M+H]^+$ 635.1227, found: 635.1232. **SFC**: 97.0%.

2.10.2 Guanidine derivatives

All compounds were synthesized according to General Procedure C:

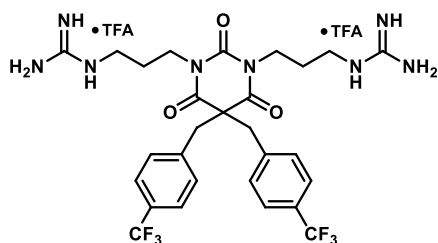


1,1'-((5,5-bis((6-bromoquinolin-2-yl)methyl)-2,4,6-trioxodihydropyrimidine-1,3(2H,4H)-diyl)bis(propane-3,1-diyl))diguanidine 13cG.

Barbiturate **13aA** (11 mg, 12.1 μ mol, 1.0 eq), *N,N'*-di-Boc-1H-pyrazole-1-carboxamide (9.4 mg, 30.2 μ mol, 2.50 eq), DIPEA (5.3 μ L, 30.2 μ mol, 2.50 eq) and THF (0.5 mL) were stirred at 45 °C for 2.5 h. The crude was purified with 20-60% EtOAc in heptane to yield boc-**13cG** (13 mg, 11.1 μ mol, 92%) as a white foam.

TFA (28 μ L, 181 μ mol, 30.0 eq) and DCM (0.5 mL) were added, and the mixture was stirred at ambient temperature for 24 h. The crude was purified by automated RP column chromatography with a gradient of 20-60% MeCN/H₂O + 0.1% TFA to yield the di-TFA salt of **13cG** (11 mg, 11 μ mol, 91% o2s) as a

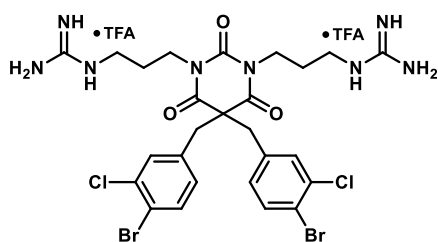
white powder. $^1\text{H NMR}$ (400 MHz, Methanol- d_4) δ 8.20 (d, J = 8.5 Hz, 2H), 8.11 (d, J = 2.2 Hz, 2H), 7.81 (dd, J = 8.9, 2.2 Hz, 2H), 7.58 (d, J = 9.0 Hz, 2H), 7.44 (d, J = 8.6 Hz, 2H), 3.97 (s, 4H), 3.86 (t, J = 6.8 Hz, 4H), 2.80 (t, J = 6.9 Hz, 4H), 1.64 (p, J = 6.9 Hz, 4H). $^{13}\text{C NMR}$ (101 MHz, Methanol- d_4) δ 174.2 (2C), 159.0 (2C), 158.4, 153.4 (2C), 146.7 (2C), 137.4 (2C), 134.5 (2C), 131.4 (2C), 130.8 (2C), 129.6 (2C), 123.5 (2C), 121.3 (2C), 54.5, 48.3 (2C), 40.2 (2C), 39.7 (2C), 28.5 (2C). **HRMS** (ESI): calcd for $\text{C}_{32}\text{H}_{35}\text{Br}_2\text{N}_{10}\text{O}_3^+$ $[\text{M}+\text{H}]^+$ 765.1255, found 765.1259. **SFC**: 97.4%



1,1'-((2,4,6-triisopropoxy-5,5-bis(4-(trifluoromethyl)benzyl)dihydropyrimidine-1,3(2H,4H)-diyl)bis(propane-3,1-diyl))diguanidine **13hG**.

Barbiturate **13hA** (70 mg, 89 μmol , 1.0 eq), *N,N'*-di-Boc-1*H*-pyrazole-1-carboxamidine (69 mg, 223 μmol , 2.50 eq), DIPEA (62 μL , 356 μmol , 4.00 eq) and THF (1 mL) were stirred at 45 $^\circ\text{C}$ for 2.5 h. The crude was purified with 15% EtOAc in heptane to yield boc-**13hG** (73 mg, 70 μmol , 79%) as a white foam.

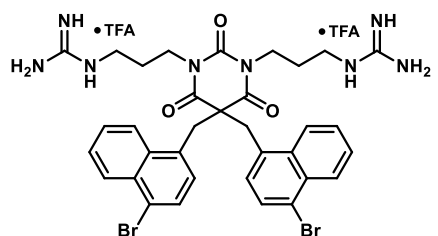
TFA (102 μL , 1.33 mmol, 15.0 eq) and DCM (1 mL) were added, and the mixture was stirred at ambient temperature for 40 h. The crude was purified by automated RP column chromatography with a gradient of 10-60% MeCN/ H_2O + 0.1% TFA to yield the di-TFA salt of **13hG** (61 mg, 70 μmol , 79% o2s) as a white powder. $^1\text{H NMR}$ (400 MHz, Methanol- d_4) δ 7.57 (d, J = 8.0 Hz, 4H), 7.29 (d, J = 8.0 Hz, 4H), 3.72 – 3.63 (m, 4H), 3.58 (s, 4H), 2.93 (t, J = 6.8 Hz, 4H), 1.53 (dq, J = 8.8, 7.0 Hz, 4H). $^{13}\text{C NMR}$ (101 MHz, Methanol- d_4) δ 171.5 (2C), 158.7 (2C), 150.8, 140.8 (2C), 131.5 (4C), 131.2 (q, J = 32.5 Hz, 2C), 126.7 (q, J = 3.7 Hz, 4C), 125.4 (d, J = 271 Hz, 4C), 61.2, 45.8 (2C), 40.3 (2C), 39.6 (2C), 28.2 (2C). **HRMS** (ESI): calcd for $\text{C}_{28}\text{H}_{33}\text{F}_6\text{N}_8\text{O}_3^+$ $[\text{M}+\text{H}]^+$ 643.2574, found 643.2579. **SFC**: 98.6%.



1,1'-((5,5-bis(4-bromo-3-chlorobenzyl)-2,4,6-trioxodihydropyrimidine-1,3(2H,4H)-diyl)bis(propane-3,1-diyl))diguanidine **13iG**.

Barbiturate **13iA** (70 mg, 80 μmol , 1.0 eq), *N,N'*-di-Boc-1*H*-pyrazole-1-carboxamidine (62 mg, 200 μmol , 2.50 eq), DIPEA (56 μL , 319 μmol , 4.00 eq) and THF (1 mL) were stirred at 45 $^\circ\text{C}$ for 2.5 h. The crude was purified with 20% EtOAc in heptane to yield boc-**13iG** (81 mg, 71 μmol , 90%) as a clear solid.

TFA (92 μL , 1.20 mmol, 15.0 eq) and DCM (1 mL) were added, and the mixture was stirred at ambient temperature for 40 h. The crude was purified by automated RP column chromatography with a gradient of 10-60% MeCN/ H_2O + 0.1% TFA to yield the di-TFA salt of **13iG** (61 mg, 64 μmol , 80% o2s) as a white powder. $^1\text{H NMR}$ (400 MHz, Methanol- d_4) δ 7.57 (d, J = 8.3 Hz, 2H), 7.22 (d, J = 2.1 Hz, 2H), 6.91 (dd, J = 8.3, 2.1 Hz, 2H), 3.75 – 3.67 (m, 4H), 3.42 (s, 4H), 3.00 (t, J = 6.9 Hz, 4H), 1.64 – 1.52 (m, 4H). $^{13}\text{C NMR}$ (101 MHz, Methanol- d_4) δ 171.4 (2C), 158.7 (2C), 150.7, 137.6 (2C), 135.6 (2C), 135.3 (2C), 132.5 (2C), 130.6 (2C), 122.7 (2C), 61.1, 44.9 (2C), 40.3 (2C), 39.6 (2C), 28.5 (2C). **HRMS** (ESI): calcd for $\text{C}_{26}\text{H}_{31}\text{Br}_2\text{Cl}_2\text{N}_8\text{O}_3^+$ $[\text{M}+\text{H}]^+$ 731.0257, found 731.0263. **SFC**: >99.5%.

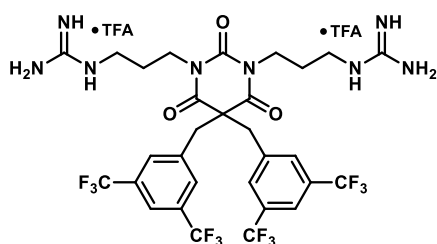


1,1'-((5,5-bis((4-bromonaphthalen-1-yl)methyl)-2,4,6-trioxodihydropyrimidine-1,3(2H,4H)-diyl)bis(propane-3,1-diyl))diguanidine **13eG**.

Barbiturate **13eA** (70 mg, 77 μmol , 1.0 eq), *N,N'*-di-Boc-1*H*-pyrazole-1-carboxamidine (60 mg, 193 μmol , 2.50 eq), DIPEA (54 μL , 308 μmol , 4.00 eq) and THF (1 mL) were stirred at 45 $^\circ\text{C}$ for 2.5 h. The crude was purified with 15% EtOAc in heptane to yield boc-**13eG** (83 mg, 71 μmol , 93%) as a white foam.

TFA (89 μL , 1.16 mmol, 15.0 eq) and DCM (1 mL) were added, and the mixture was stirred at ambient temperature for 40 h. The crude was purified by automated RP column chromatography with a gradient of 10-60% MeCN/ H_2O + 0.1% TFA to yield the di-TFA salt of **13eG** (67 mg, 68 μmol , 88% o2s) as a white powder. $^1\text{H NMR}$ (400 MHz, Methanol- d_4) δ 8.39 – 8.30 (m, 2H), 8.29 – 8.19 (m, 2H), 7.70 (d, J = 7.8 Hz, 2H), 7.65 (td, J = 7.0, 6.6, 3.6 Hz, 4H), 7.16 (d, J = 7.8 Hz, 2H), 4.17 (s, 4H), 3.45 – 3.35 (m, 4H), 2.57 (t, J = 6.9 Hz, 4H), 1.09 (p, J = 7.0 Hz, 4H). $^{13}\text{C NMR}$ (101 MHz, Methanol- d_4) δ 172.2

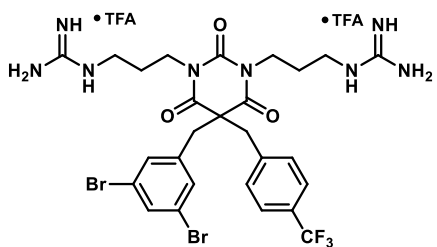
(2C), 158.4 (2C), 150.9, 134.4 (2C), 133.4 (2C), 130.4 (2C), 129.3 (2C), 128.8 (2C), 128.6 (2C), 128.2 (2C), 126.5 (2C), 123.9 (2C), 60.6, 41.5 (2C), 40.1 (2C), 39.2 (2C), 27.8 (2C). **HRMS** (ESI): calcd for $C_{34}H_{37}Br_2N_8O_3^+$ $[M+H]^+$ 763.1350, found 763.1356. **SFC**: >99.5%.



*1,1'-((5,5-bis(3,5-bis(trifluoromethyl)benzyl)-2,4,6-trioxodihydropyrimidine-1,3(2H,4H)-diyl)bis(propane-3,1-diyl))diguanidine **13jG**.*

Barbiturate **13jA** (50 mg, 54 μ mol, 1.0 eq), *N,N'*-di-Boc-1*H*-pyrazole-1-carboxamidine (42 mg, 136 μ mol, 2.50 eq), DIPEA (38 μ L, 217 μ mol, 4.00 eq) and THF (1 mL) were stirred at 45 °C for 2.5 h. The crude was purified with 15% EtOAc in heptane to yield boc-**13jG** (49 mg, 42 μ mol, 77%) as a white foam.

TFA (62 μ L, 0.81 mmol, 15.0 eq) and DCM (1 mL) were added, and the mixture was stirred at ambient temperature for 40 h. The crude was purified by automated RP column chromatography with a gradient of 10–60% MeCN/H₂O + 0.1% TFA to yield the di-TFA salt of **13jG** (42 mg, 42 μ mol, 77% o2s) as a white powder. **¹H NMR** (400 MHz, Methanol-*d*₄) δ 7.93 (s, 2H), 7.69 (d, *J* = 1.6 Hz, 4H), 3.72 (s, 4H), 3.69 – 3.60 (m, 4H), 3.03 (t, *J* = 6.9 Hz, 4H), 1.49 (dq, *J* = 9.4, 7.0 Hz, 4H). **¹³C NMR** (101 MHz, Methanol-*d*₄) δ 171.1 (2C), 158.7 (2C), 150.2, 139.4 (2C), 133.10 (q, *J* = 33.4 Hz, 4C), 131.5 – 131.3 (m, 4C), 124.5 (q, *J* = 272 Hz, 4C) 123.1 – 122.8 (m, 2C), 61.2, 44.8 (2C), 40.5 (2C), 39.5 (2C), 28.5 (2C). **HRMS** (ESI): calcd for $C_{30}H_{31}F_{12}N_8O_3^+$ $[M+H]^+$ 779.2322, found 779.2324. **SFC**: >99.5%.

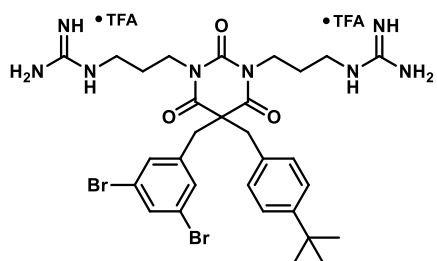


*1,1'-((5-(3,5-dibromobenzyl)-2,4,6-trioxo-5-(4-(trifluoromethyl)benzyl)dihydropyrimidine-1,3(2H,4H)-diyl)bis(propane-3,1-diyl))diguanidine **13iG**.*

Barbiturate **13iA** (150 mg, 171 μ mol, 1.0 eq), *N,N'*-di-Boc-1*H*-pyrazole-1-carboxamidine (90 mg, 291 μ mol, 1.7 eq), DIPEA (119 μ L, 685 μ mol, 4.0 eq) and THF (0.5 mL) were stirred at 45 °C for 2.5 h. The crude was purified with 10–45% EtOAc in heptane to yield boc-**13iG** (121 mg, 107 μ mol, 62%) as a white

foam.

TFA (246 μ L, 3.20 mmol, 30.0 eq) and DCM (1.5 mL) were added, and the mixture was stirred at ambient temperature for 36 h. The crude was purified by automated RP column chromatography with a gradient of 15–45% MeCN/H₂O + 0.1% TFA to yield the di-TFA salt of **13iG** (11 mg, 11 μ mol, 20% o2s) as a white powder. **¹H NMR** (400 MHz, Methanol-*d*₄) δ 7.64 (t, *J* = 1.8 Hz, 1H), 7.57 (d, *J* = 8.0 Hz, 2H), 7.27 (d, *J* = 8.0 Hz, 2H), 7.24 (d, *J* = 1.7 Hz, 2H), 3.74 (ddd, *J* = 13.3, 8.6, 6.2 Hz, 2H), 3.65 (ddd, *J* = 13.2, 8.6, 6.0 Hz, 2H), 3.54 (s, 2H), 3.47 (s, 2H), 1.58 (dddd, *J* = 22.8, 13.3, 6.9, 2.0 Hz, 4H). **¹³C NMR** (101 MHz, Methanol-*d*₄) δ 171.4 (2C), 158.7 (2C), 150.7, 140.6 (2C), 134.5, 132.7 (2C), 131.4, 131.2 (q, *J* = 32.6 Hz, 1C), 126.7 (q, *J* = 3.8 Hz, 2C), 125.4 (q, *J* = 271.1 Hz, 1C) 124.2 (2C), 61.3, 45.7, 44.9, 40.3 (2C), 39.6 (2C), 28.6 (2C). **HRMS** (ESI): calcd for $C_{27}H_{32}Br_2F_3N_8O_3^+$ $[M+H]^+$ 731.0911, found: 731.0919 **SFC**: 97.8%.



*1,1'-((5-(4-(tert-butyl)benzyl)-5-(3,5-dibromobenzyl)-2,4,6-trioxodihydropyrimidine-1,3(2H,4H)-diyl)bis(propane-3,1-diyl))diguanidine **13pG**.*

Barbiturate **13pA** (60 mg, 69 μ mol, 1.0 eq), *N,N'*-di-Boc-1*H*-pyrazole-1-carboxamidine (54 mg, 174 μ mol, 2.5 eq), DIPEA (30 μ L, 174 μ mol, 2.5 eq) and THF (1.5 mL) were stirred at 50 °C for 2.5 h. The crude was purified with 10–50% EtOAc in heptane to yield impure boc-**13pG** (86 mg, 77 μ mol, 111%) as a white solid.

TFA (80 μ L, 1.04 mmol, 15.0 eq) and DCM (1.5 mL) were added, and the mixture was stirred at ambient temperature for 24 h. The crude was purified by automated RP column chromatography with a gradient of 10–45% MeCN/H₂O + 0.1% TFA to yield the di-TFA salt of **13pG** (39 mg, 41 μ mol, 59% o2s) as a white powder. **¹H NMR** (400 MHz, Methanol-*d*₄) δ 7.62 (t, *J* = 1.8 Hz, 1H), 7.30 – 7.26 (m, 2H), 7.25 (d, *J* = 1.8 Hz, 2H), 7.00 – 6.94 (m, 2H), 3.72 (ddd, *J* = 13.2, 8.1, 6.7 Hz, 2H), 3.63 (ddd, *J* = 13.5, 8.0,

6.2 Hz, 2H), 3.45 (s, 2H), 3.39 (s, 2H), 2.98 (td, $J = 6.9, 5.1$ Hz, 4H), 1.65 – 1.49 (m, 4H), 1.25 (s, 9H). ^{13}C NMR (101 MHz, Methanol- d_4) δ 171.9 (2C), 158.7 (2C), 152.4, 150.9, 141.2, 134.3, 132.7, 130.2 (2C), 126.7 (2C), 124.1 (2C), 61.8, 46.7, 44.1, 40.2 (2C), 39.6 (2C), 35.3, 31.6 (3C), 28.5 (2C). **HRMS** (ESI): calcd for $\text{C}_{30}\text{H}_{41}\text{Br}_2\text{N}_8\text{O}_3^+$ $[\text{M}+\text{H}]^+$ 719.1663, found: 719.1664. **SFC**: 98.6%

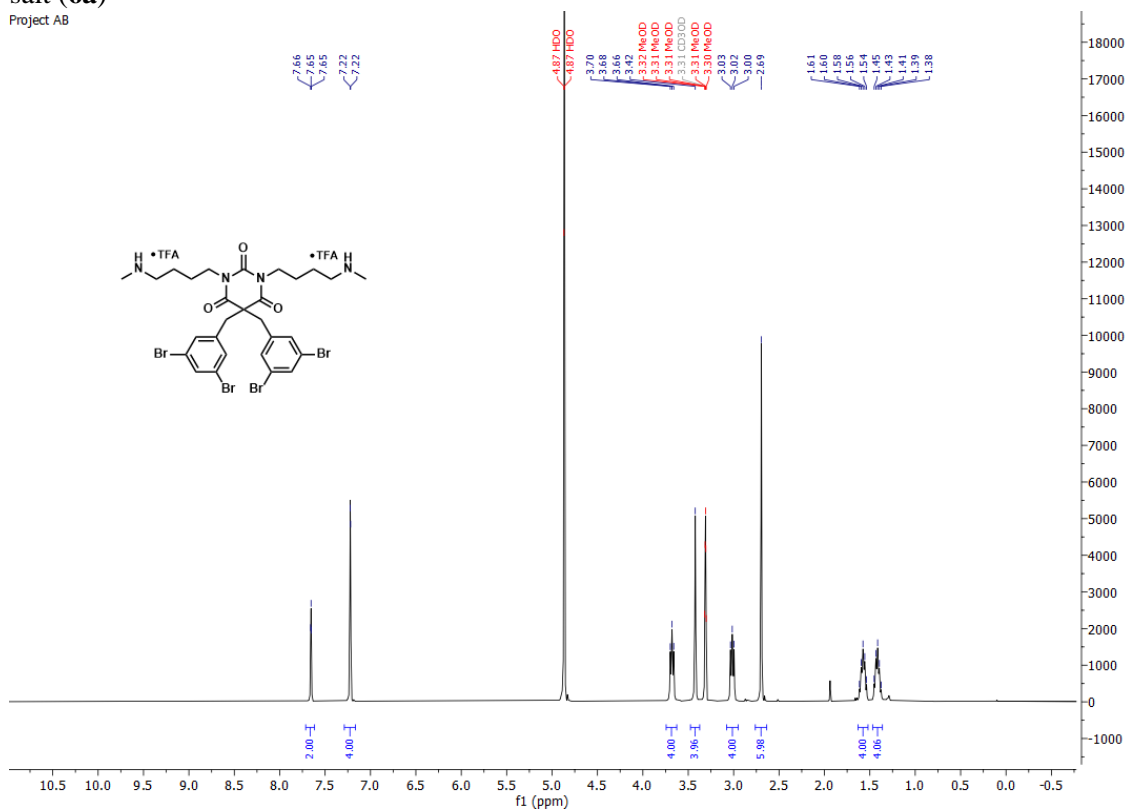
3 ^1H and ^{13}C NMR spectra of final compounds

NMR raw data of all intermediates can be found here: <https://doi.org/10.18710/GNTWOG>.

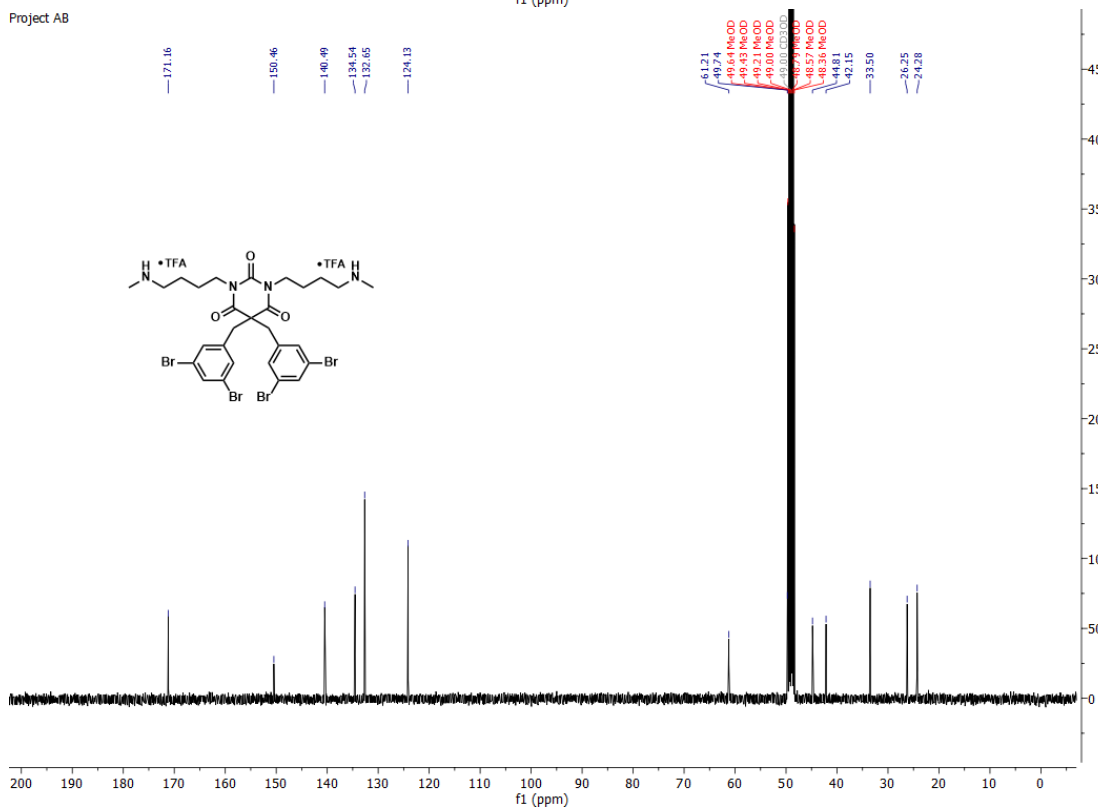
3.1 ^1H and ^{13}C NMR spectra of compounds in series 1

5,5-bis(3,5-dibromobenzyl)-1,3-bis(4-(methylamino)butyl)pyrimidine-2,4,6(1*H*,3*H*,5*H*)-trione di-TFA salt (**6a**)

Project AB

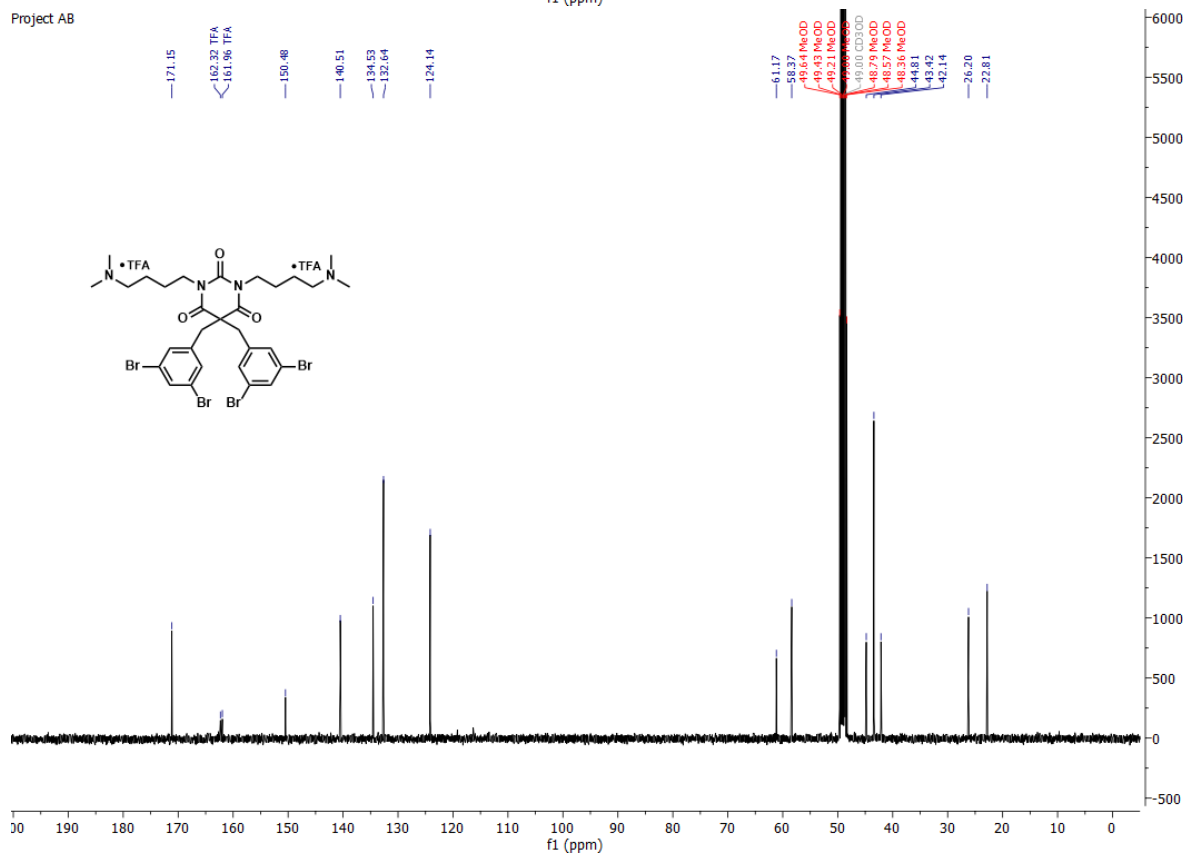
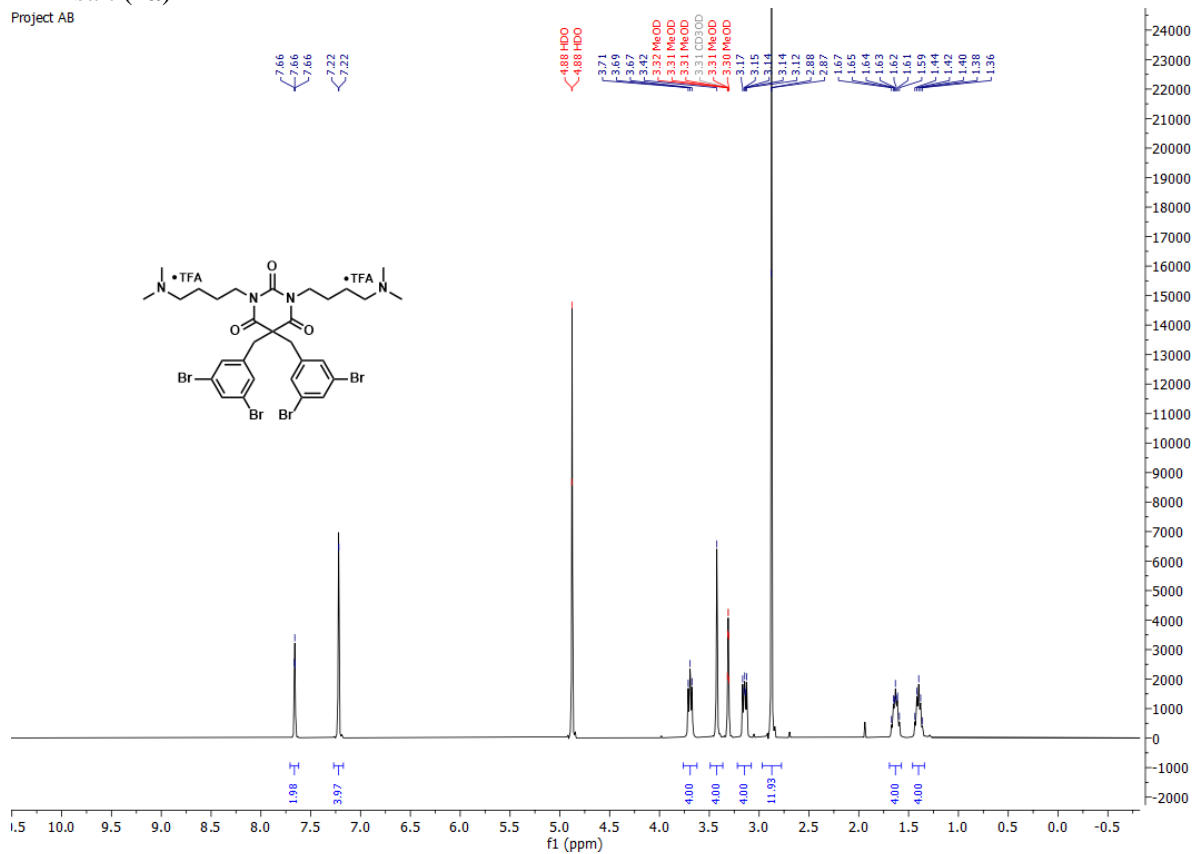


Project AB



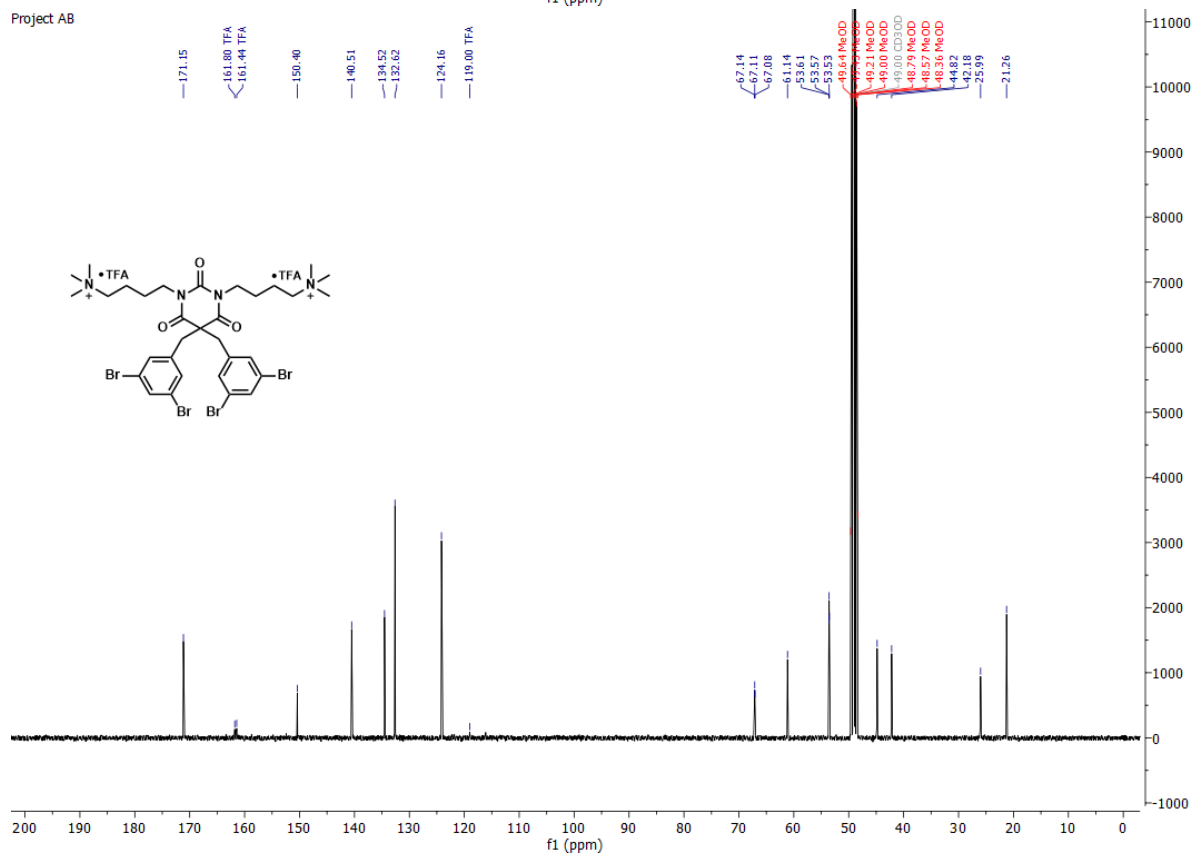
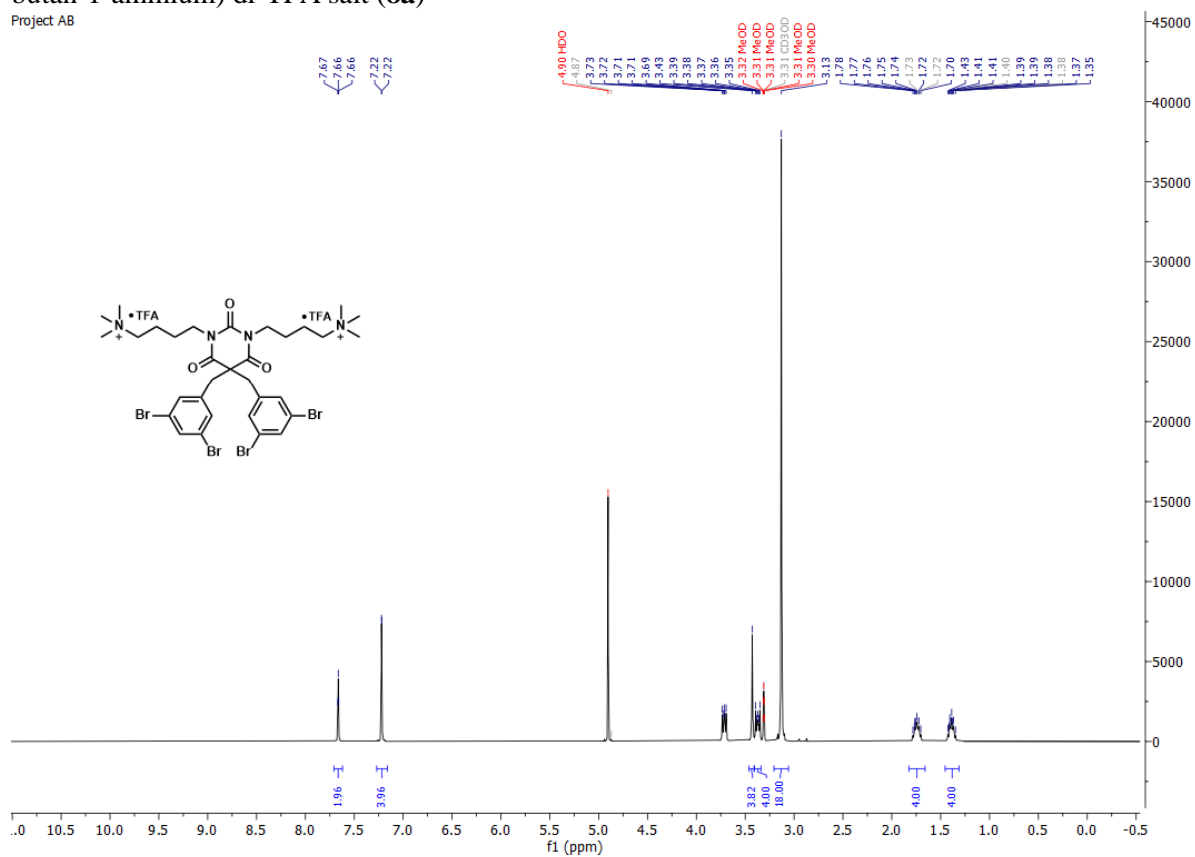
5,5-bis(3,5-dibromobenzyl)-1,3-bis(4-(dimethylamino)butyl)pyrimidine-2,4,6(1*H*,3*H*,5*H*)-trione di-TFA salt (**7a**)

Project AB



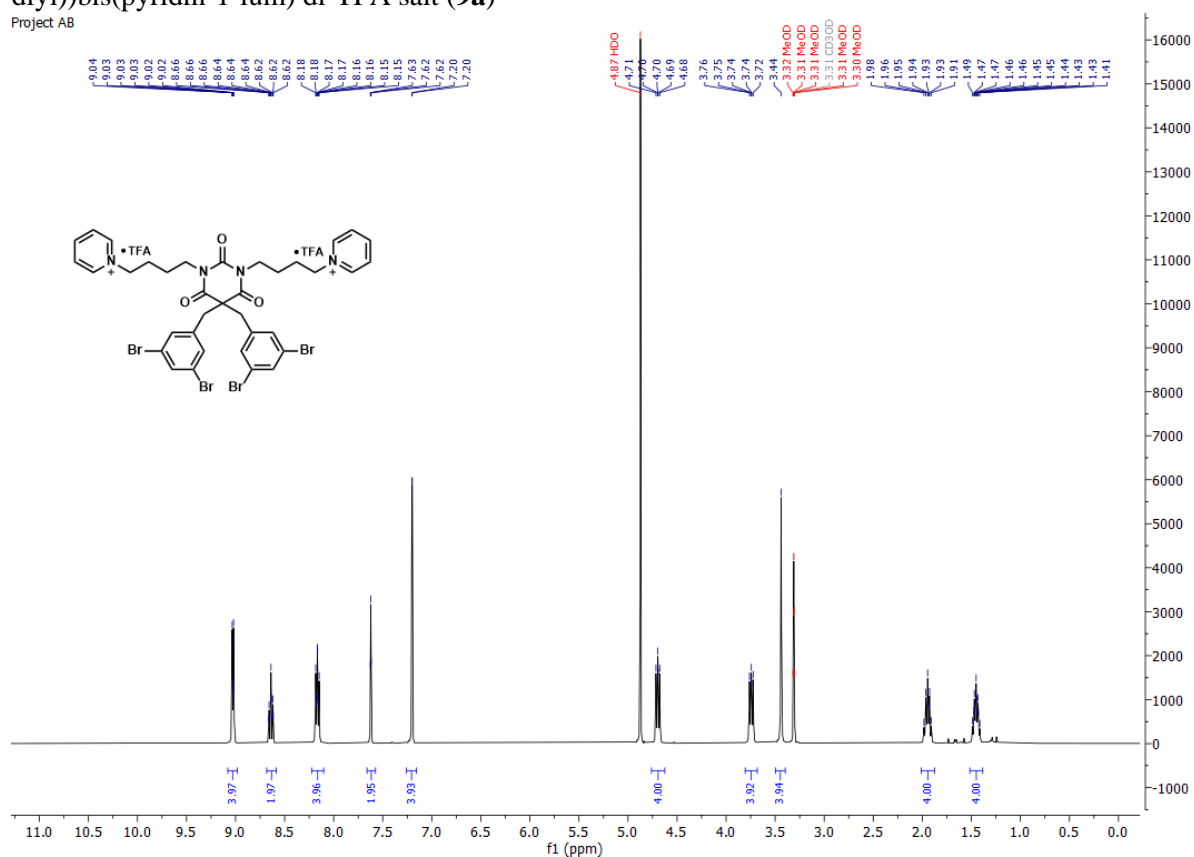
4,4'-(5,5-bis(3,5-dibromobenzyl)-2,4,6-trioxodihydropyrimidine-1,3(2*H*,4*H*)-diyl)bis(*N,N,N*-trimethylbutan-1-aminium) di-TFA salt (**8a**)

Project AB

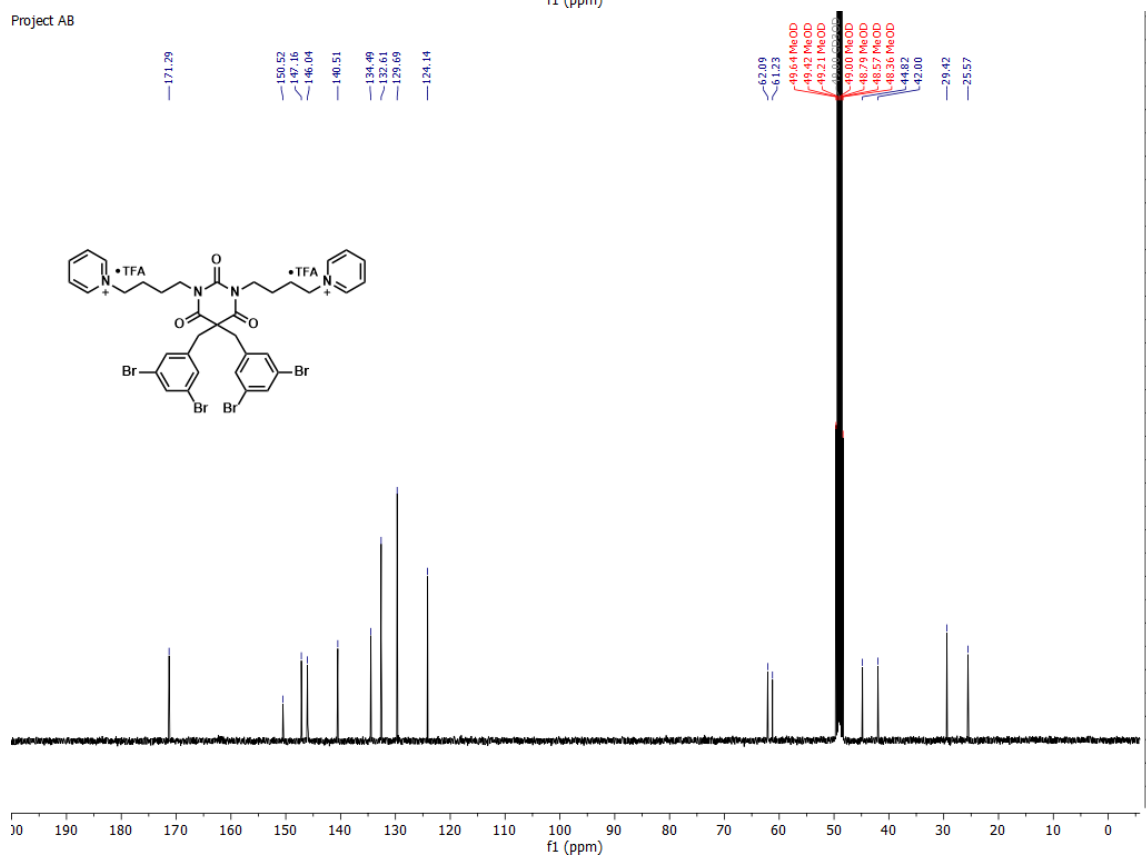


1,1'-((5,5-bis(3,5-dibromobenzyl)-2,4,6-trioxodihydropyrimidine-1,3(2*H*,4*H*)-diyl)bis(butane-4,1-diyl))bis(pyridin-1-ium) di-TFA salt (**9a**)

Project AB



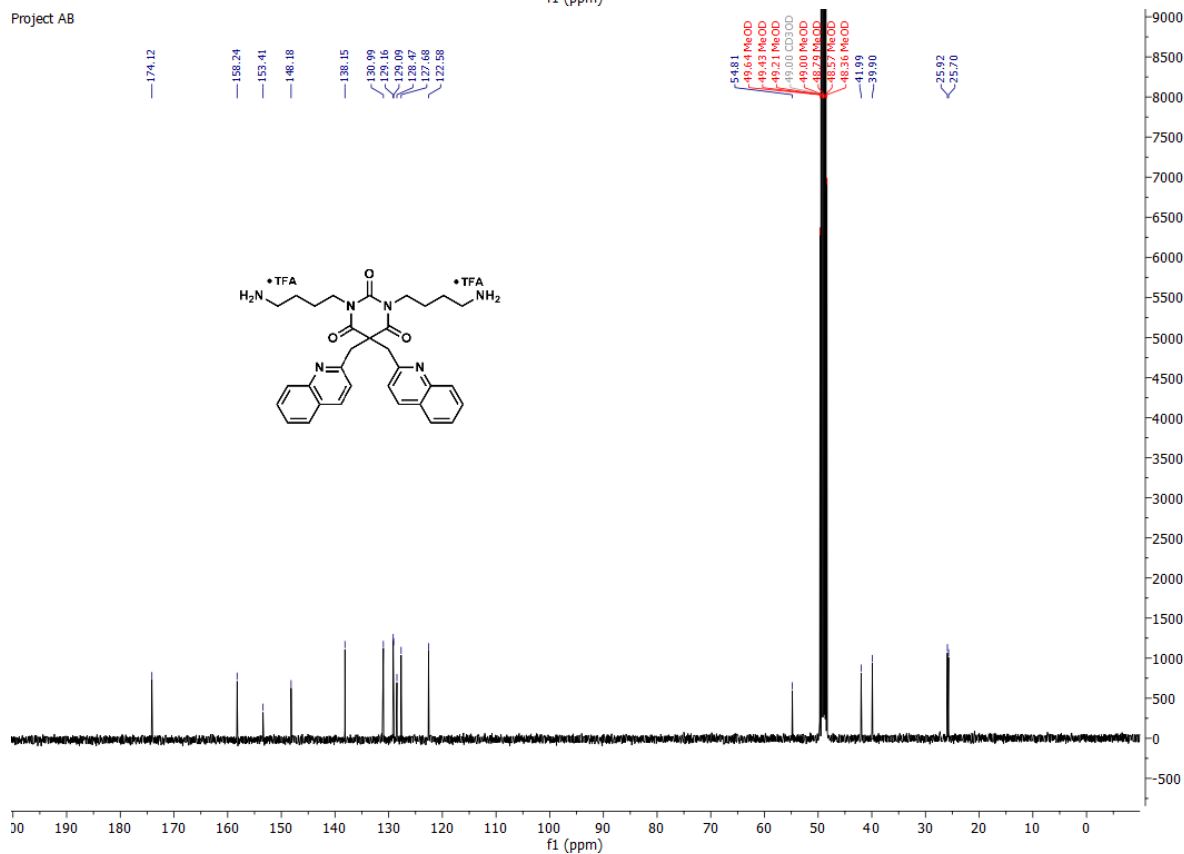
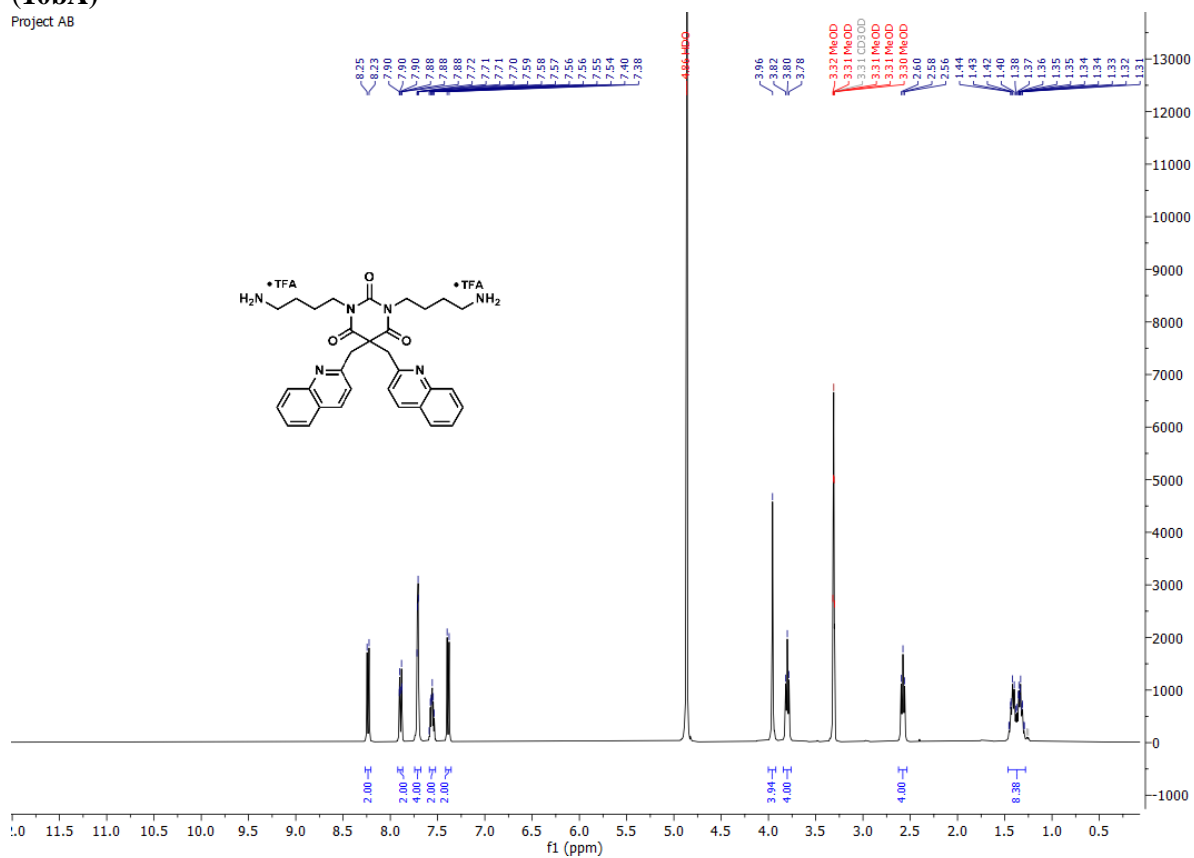
Project AB



3.2 ^1H and ^{13}C NMR spectra of compounds in series 2

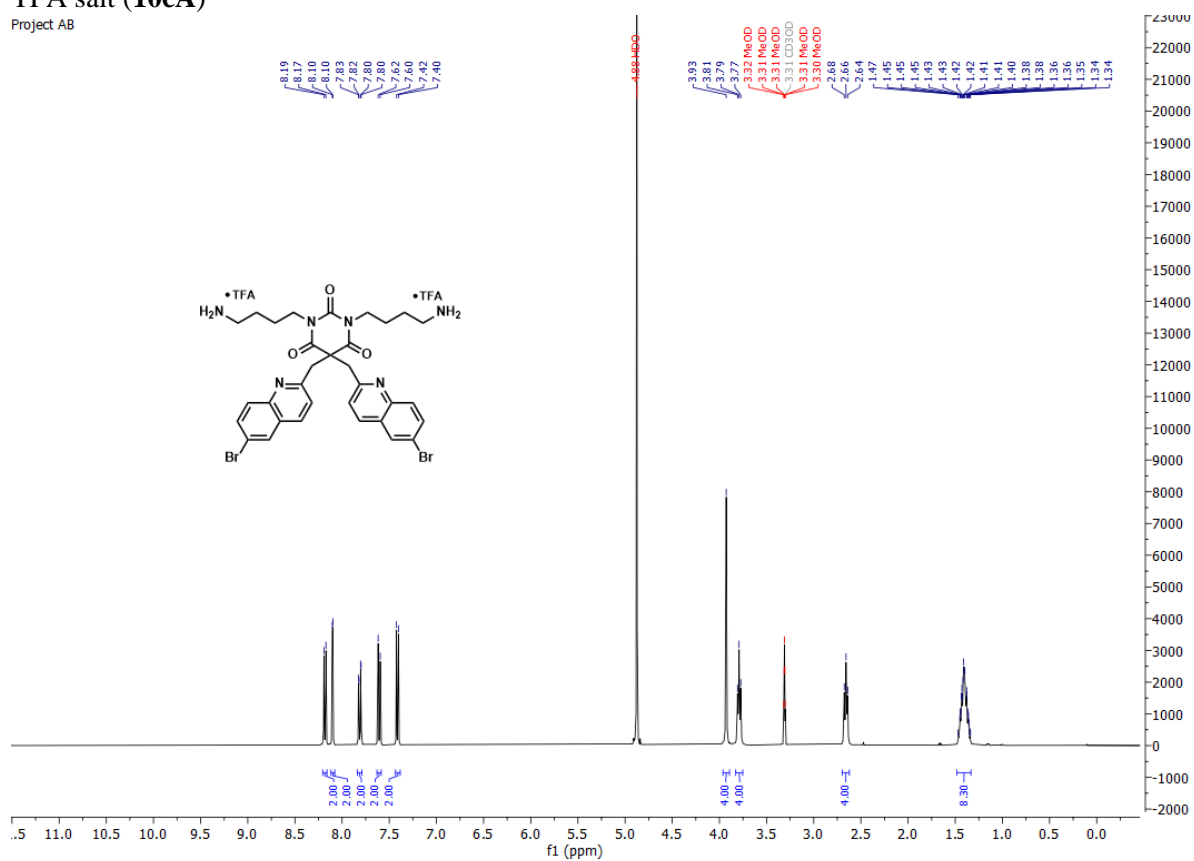
1,3-bis(4-aminobutyl)-5,5-bis(quinolin-2-ylmethyl)pyrimidine-2,4,6(1*H*,3*H*,5*H*)-trione di-TFA salt (**10bA**)

Project AB

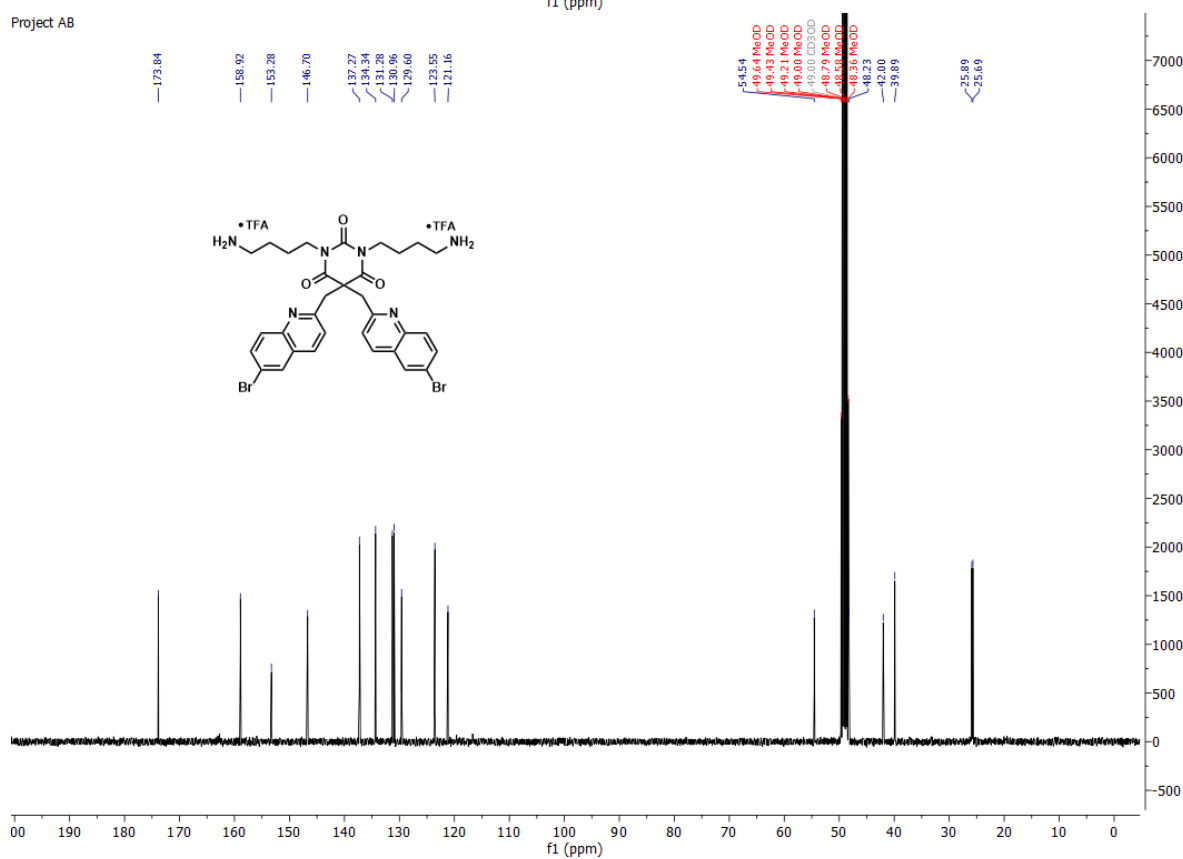


1,3-bis(4-aminobutyl)-5,5-bis((6-bromoquinolin-2-yl)methyl)pyrimidine-2,4,6(1*H*,3*H*,5*H*)-trione di-TFA salt (**10cA**)

Project AB

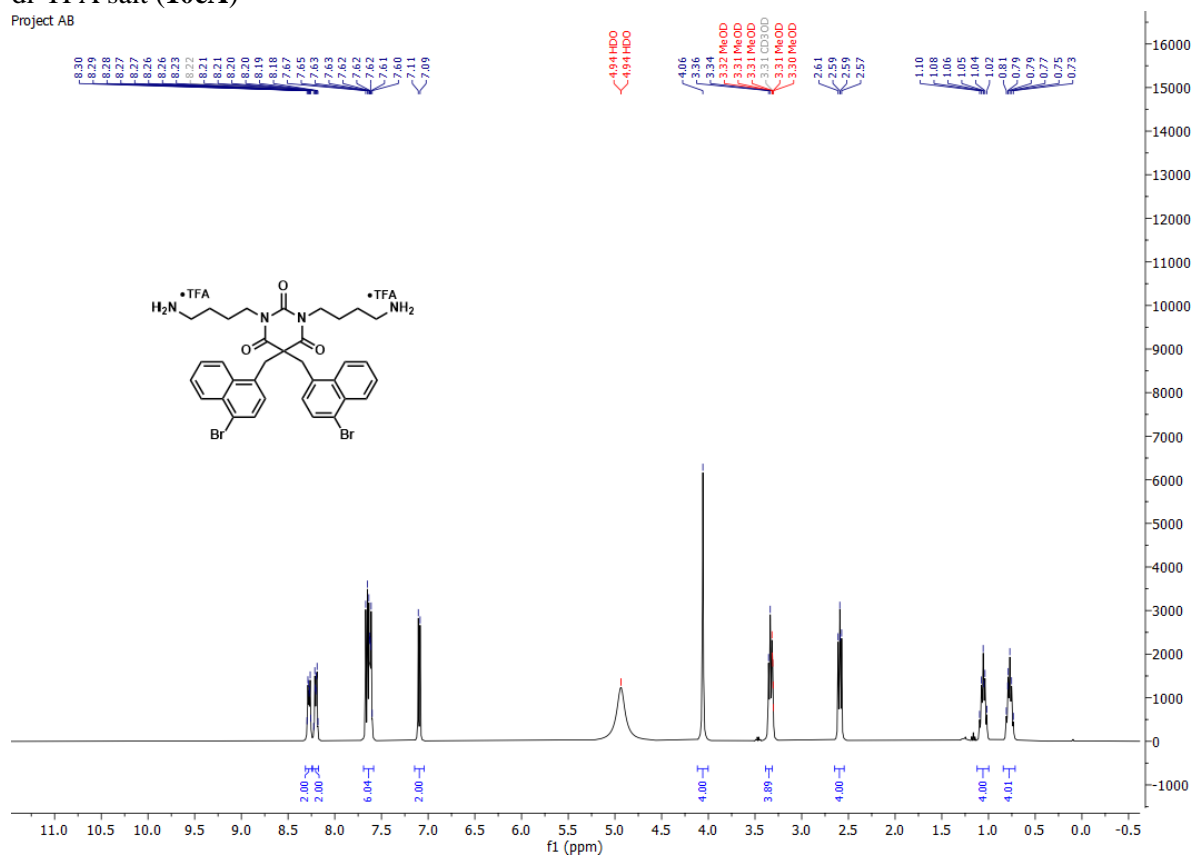


Project AB

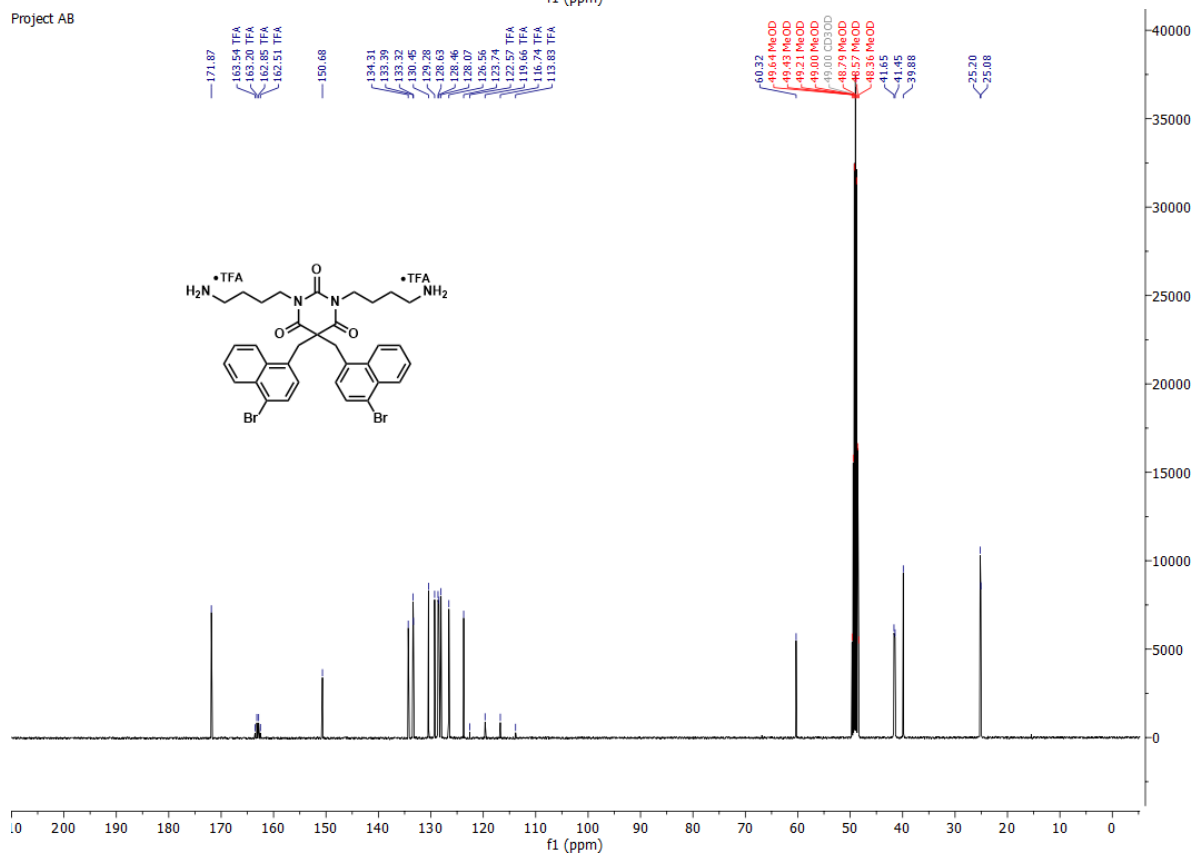


1,3-bis(4-aminobutyl)-5,5-bis((4-bromonaphthalen-1-yl)methyl)pyrimidine-2,4,6(1H,3H,5H)-trione di-TFA salt (**10eA**)

Project AB

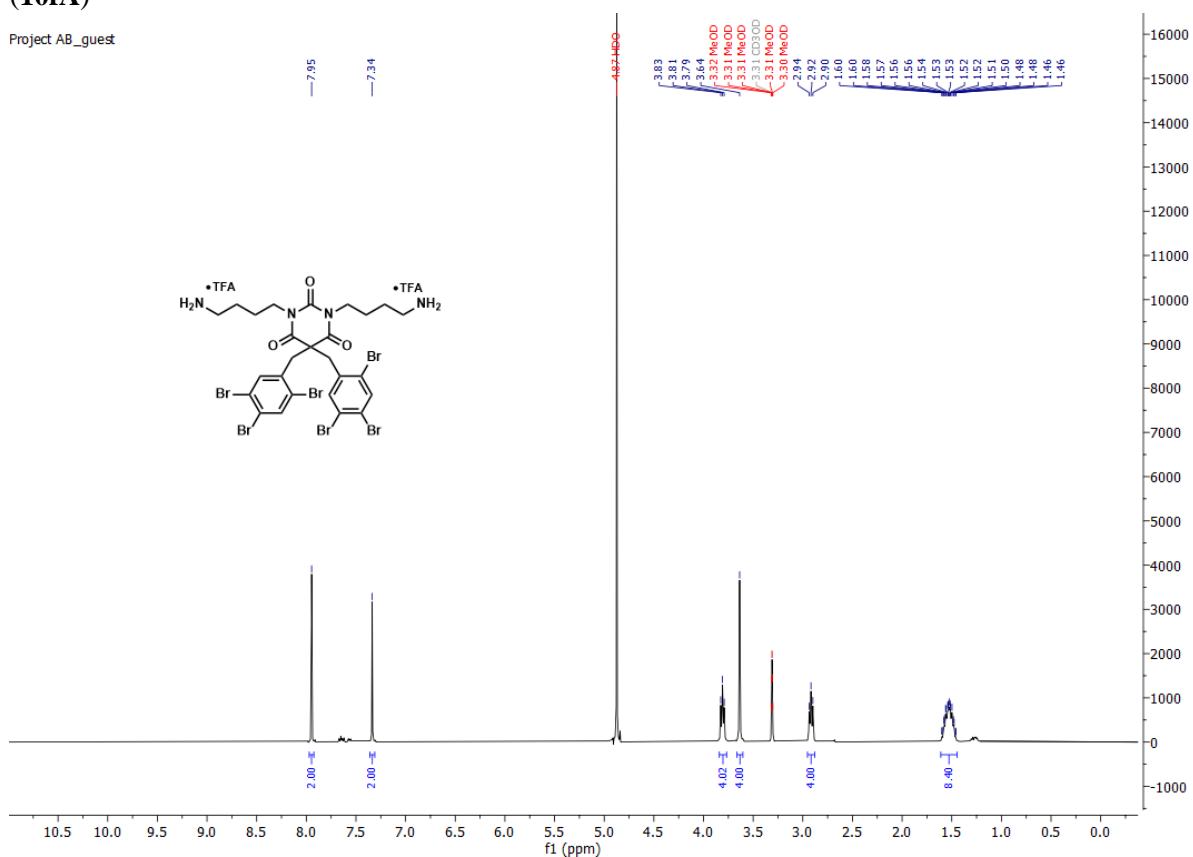


Project AB

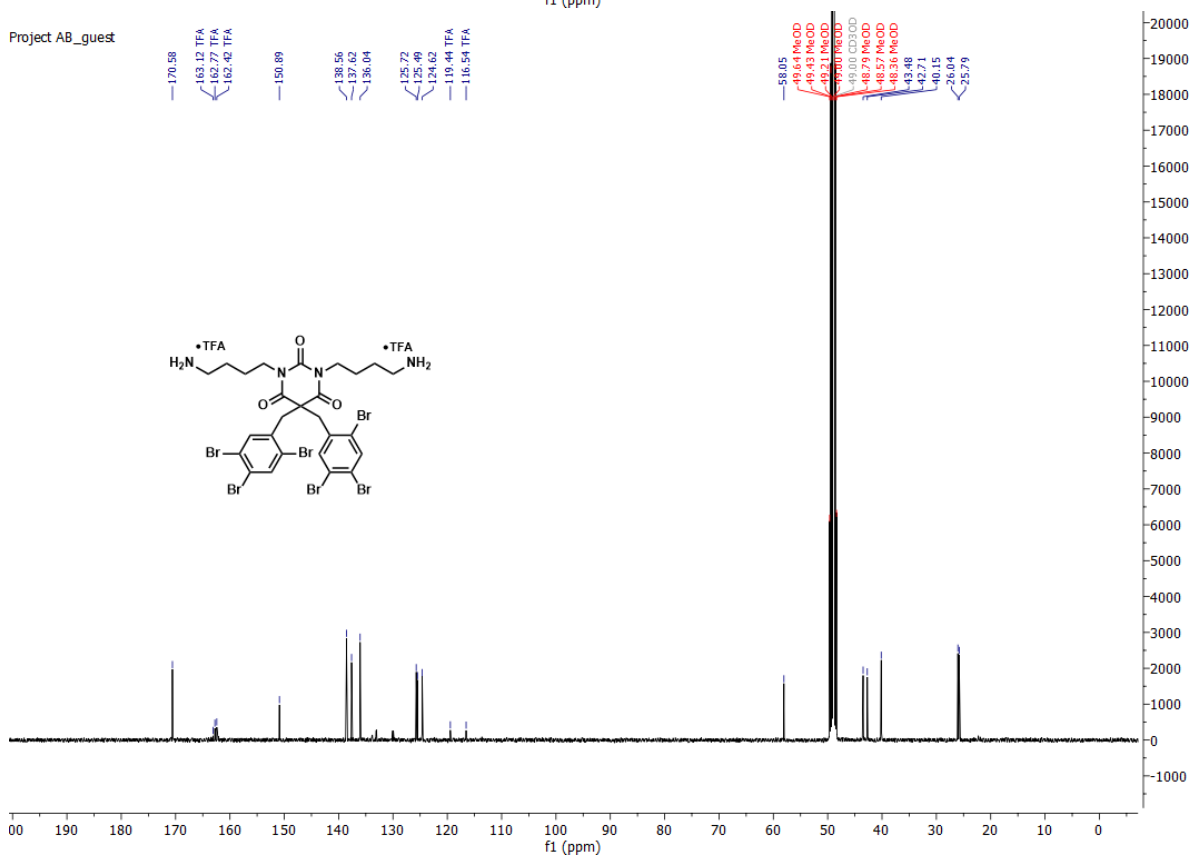


1,3-bis(4-aminobutyl)-5,5-bis(2,4,5-tribromobenzyl)pyrimidine-2,4,6(1*H*,3*H*,5*H*)-trione di-TFA salt (**10fA**)

Project AB_guest

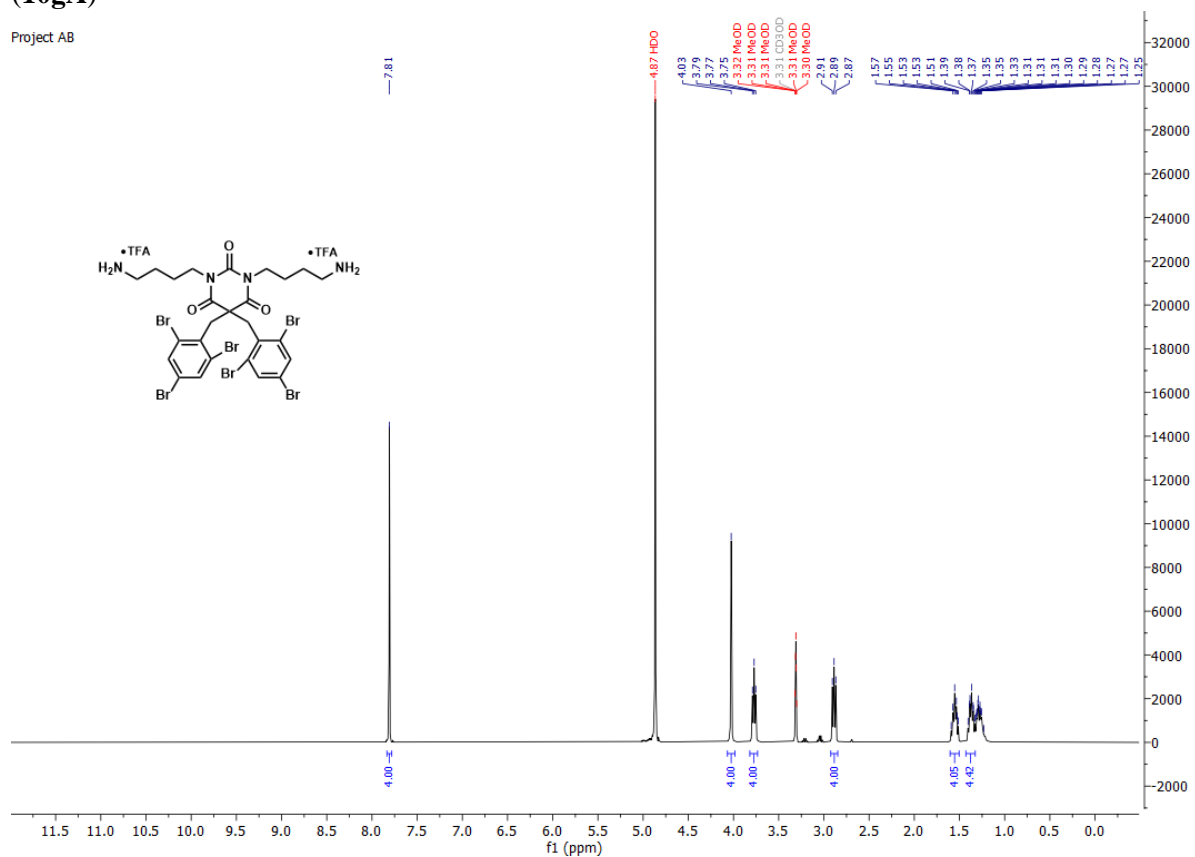


Project AB_guest

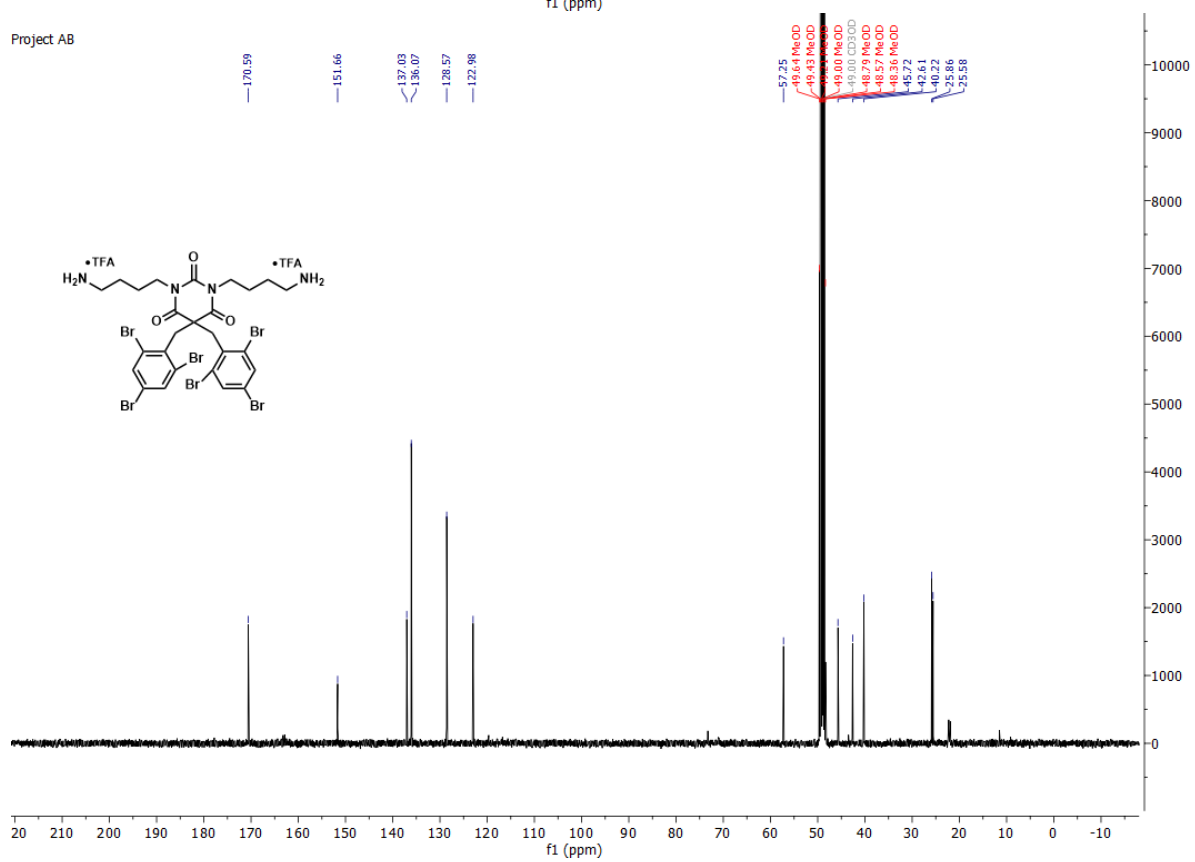


1,3-bis(4-aminobutyl)-5,5-bis(2,4,6-tribromobenzyl)pyrimidine-2,4,6(1*H*,3*H*,5*H*)-trione di-TFA salt (**10gA**)

Project AB

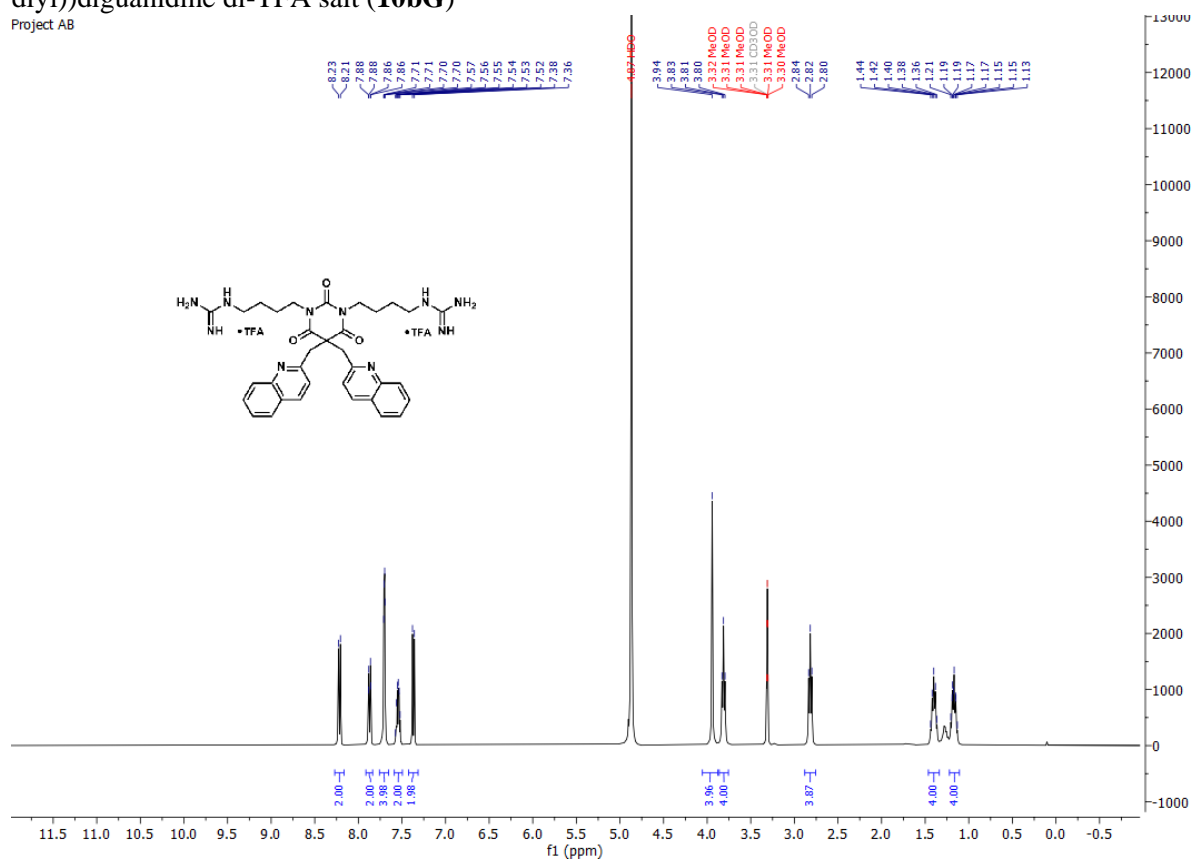


Project AB

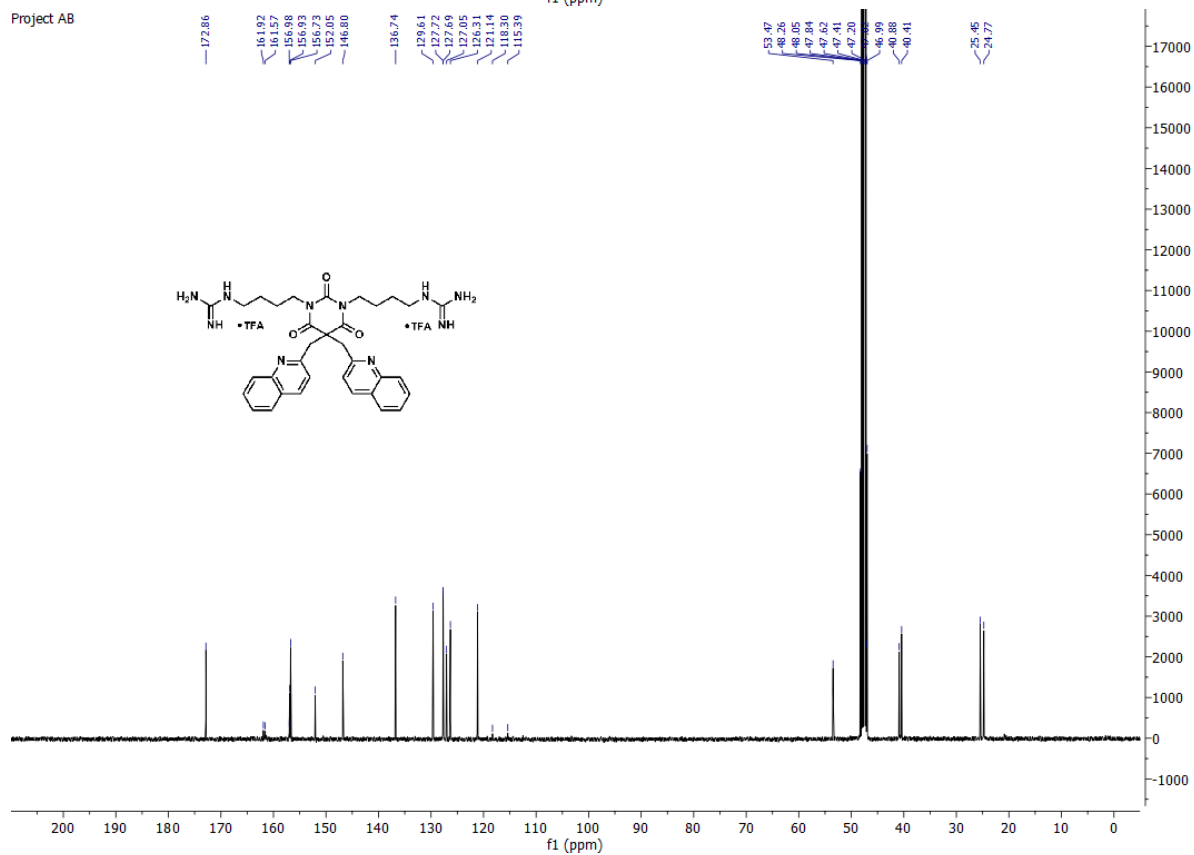


1,1'-((2,4,6-trioxo-5,5-bis(quinolin-2-ylmethyl)dihydropyrimidine-1,3(2*H*,4*H*)-diyl)bis(butane-4,1-diyl))diguanidine di-TFA salt (**10bG**)

Project AB

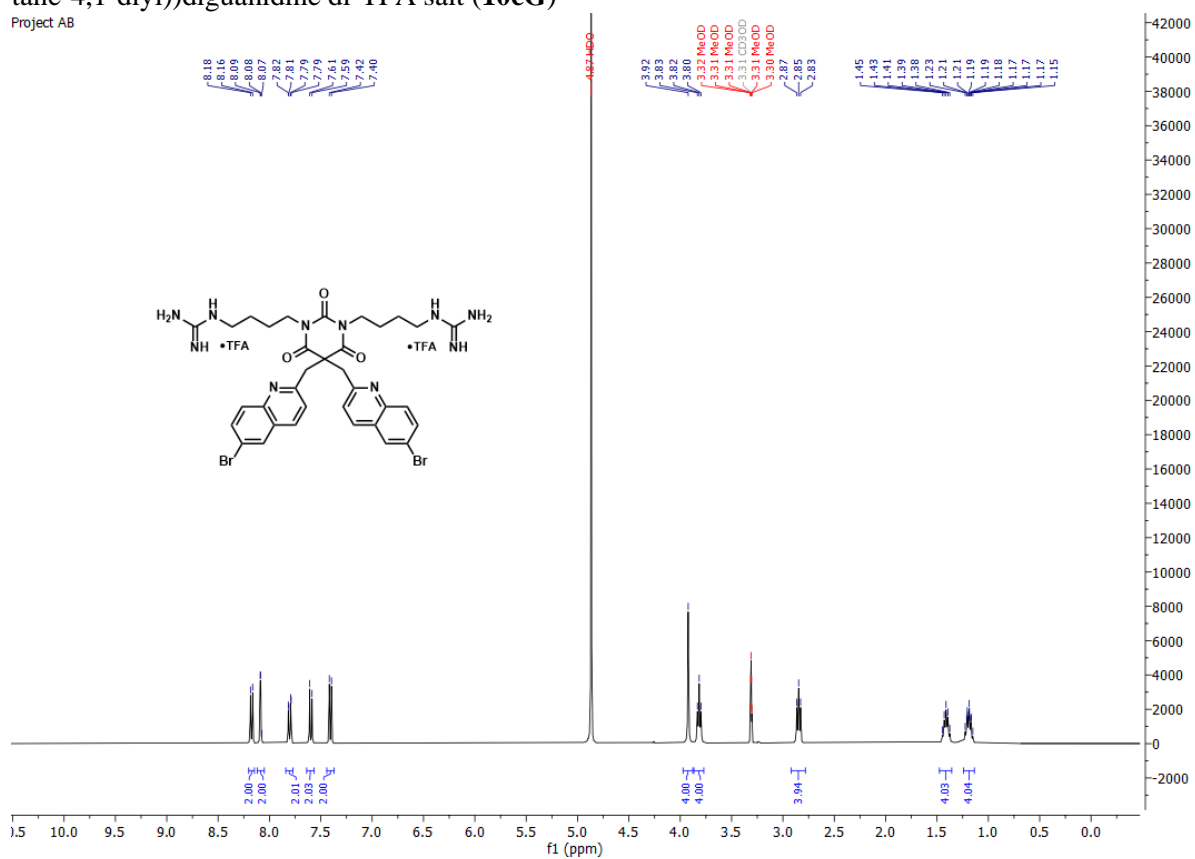


Project AB

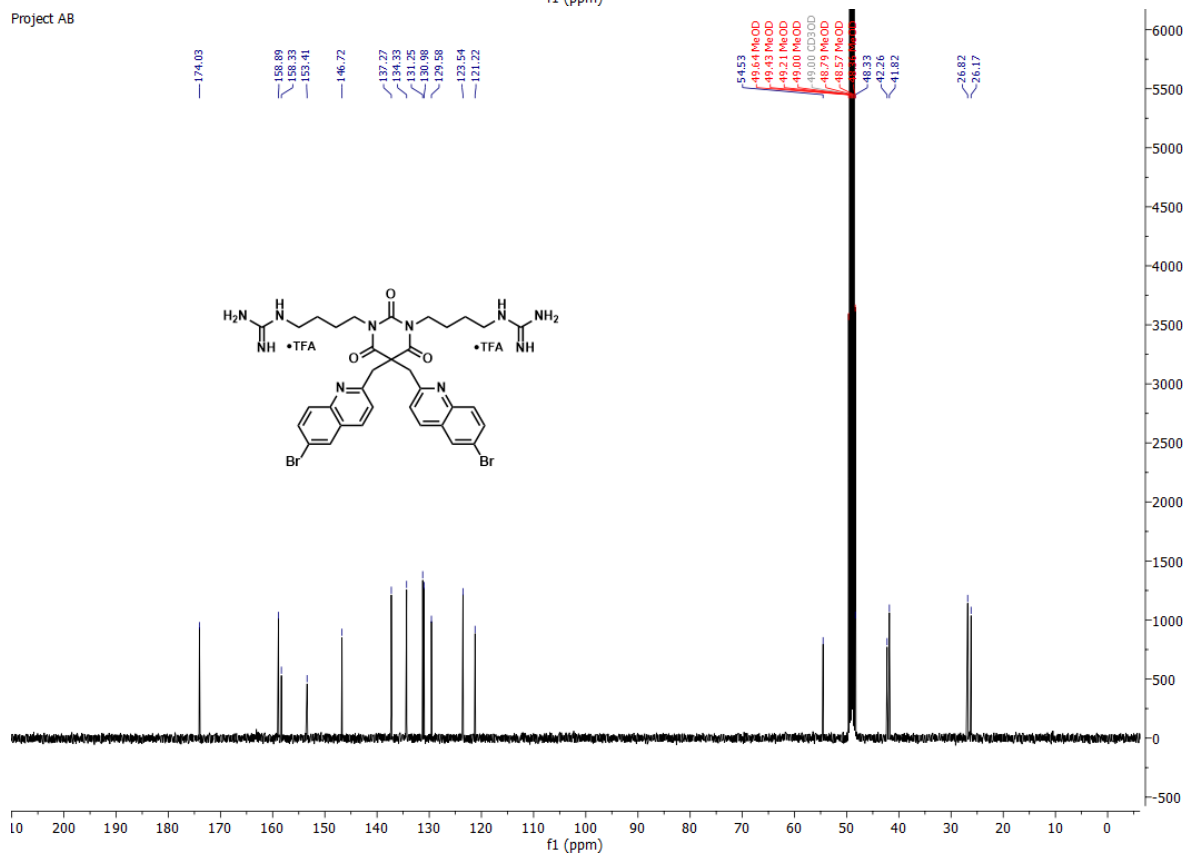


1,1'-((5,5-bis((6-bromoquinolin-2-yl)methyl)-2,4,6-trioxodihydropyrimidine-1,3(2*H*,4*H*)-diyl)bis(butane-4,1-diyl))diguandine di-TFA salt (**10cG**)

Project AB

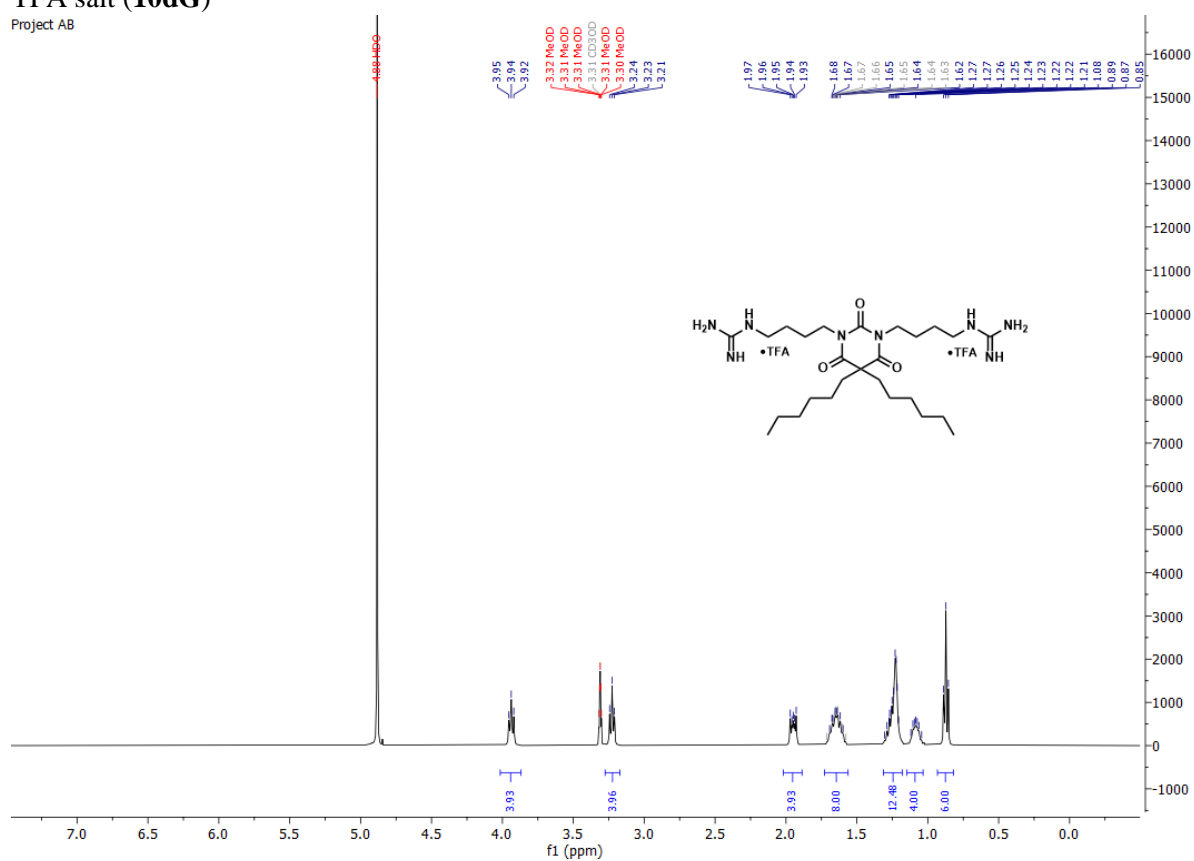


Project AB

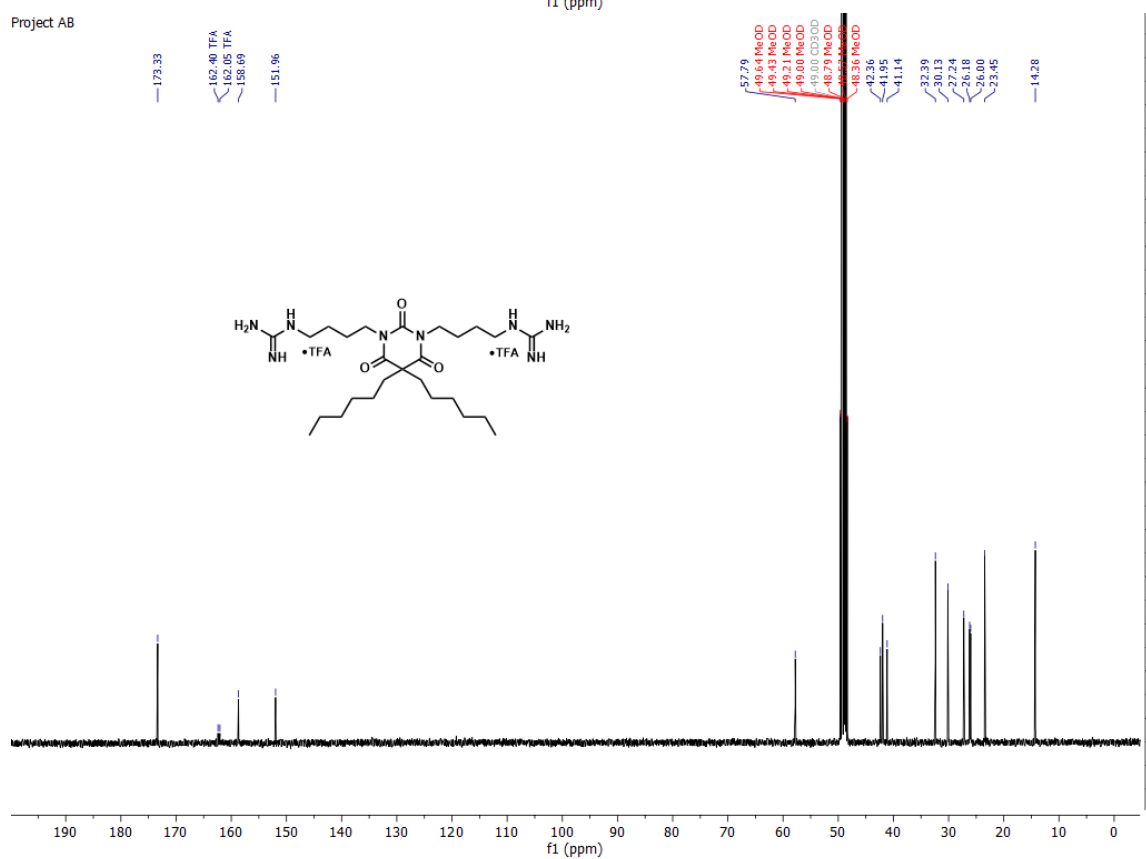


1,1'-((5,5-dihexyl-2,4,6-trioxodihydropyrimidine-1,3(2*H*,4*H*)-diyl)bis(butane-4,1-diyl)diguanidine di-TFA salt (**10dG**)

Project AB

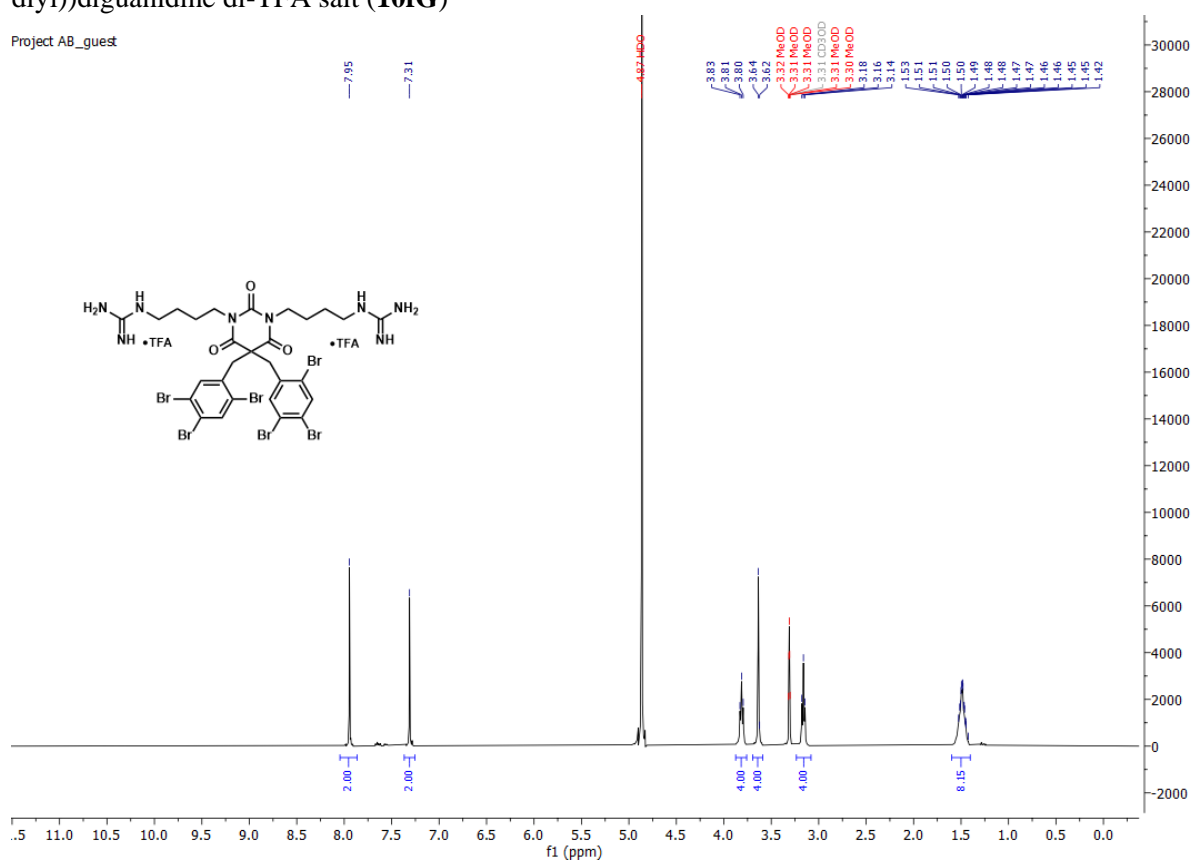


Project AB

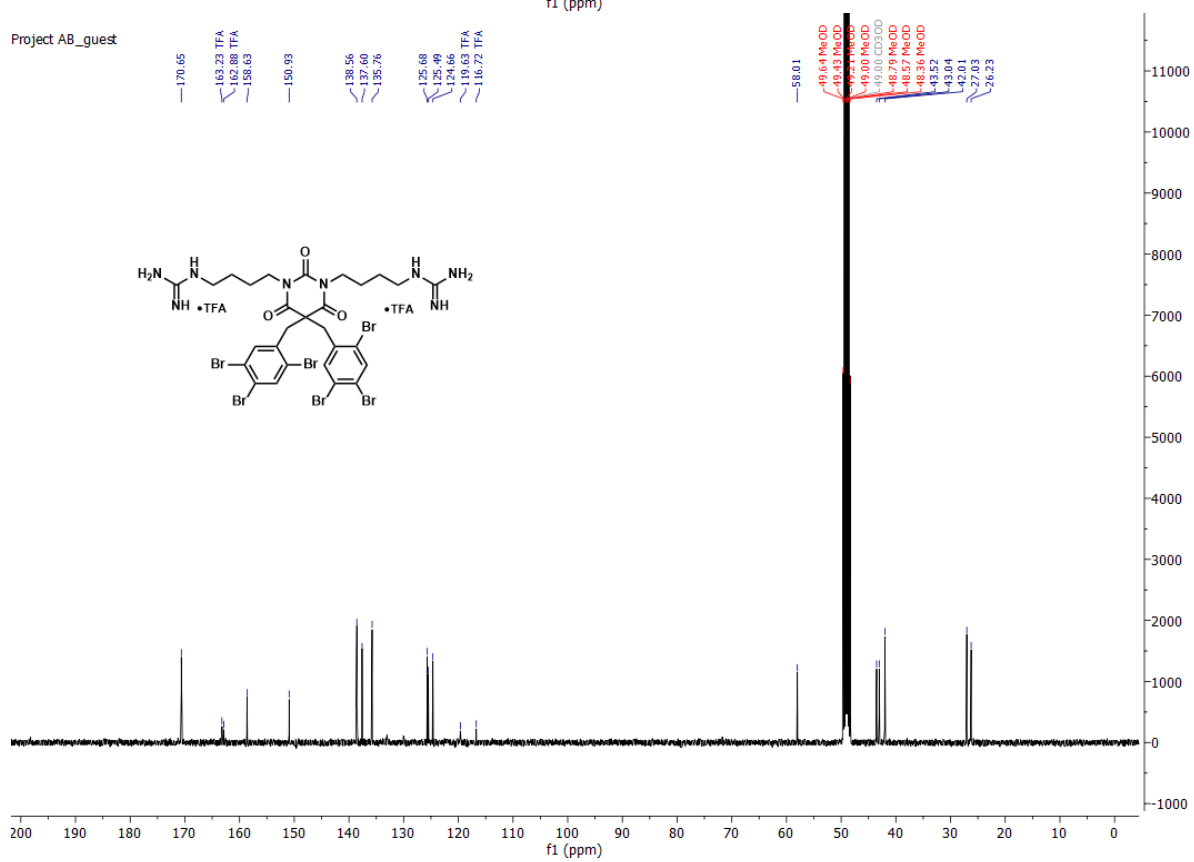


1,1'-((2,4,6-trioxo-5,5-bis(2,4,5-tribromobenzyl)dihydropyrimidine-1,3(2*H*,4*H*)-diyl)bis(butane-4,1-diyl))diguanidine di-TFA salt (**10fG**)

Project AB_guest

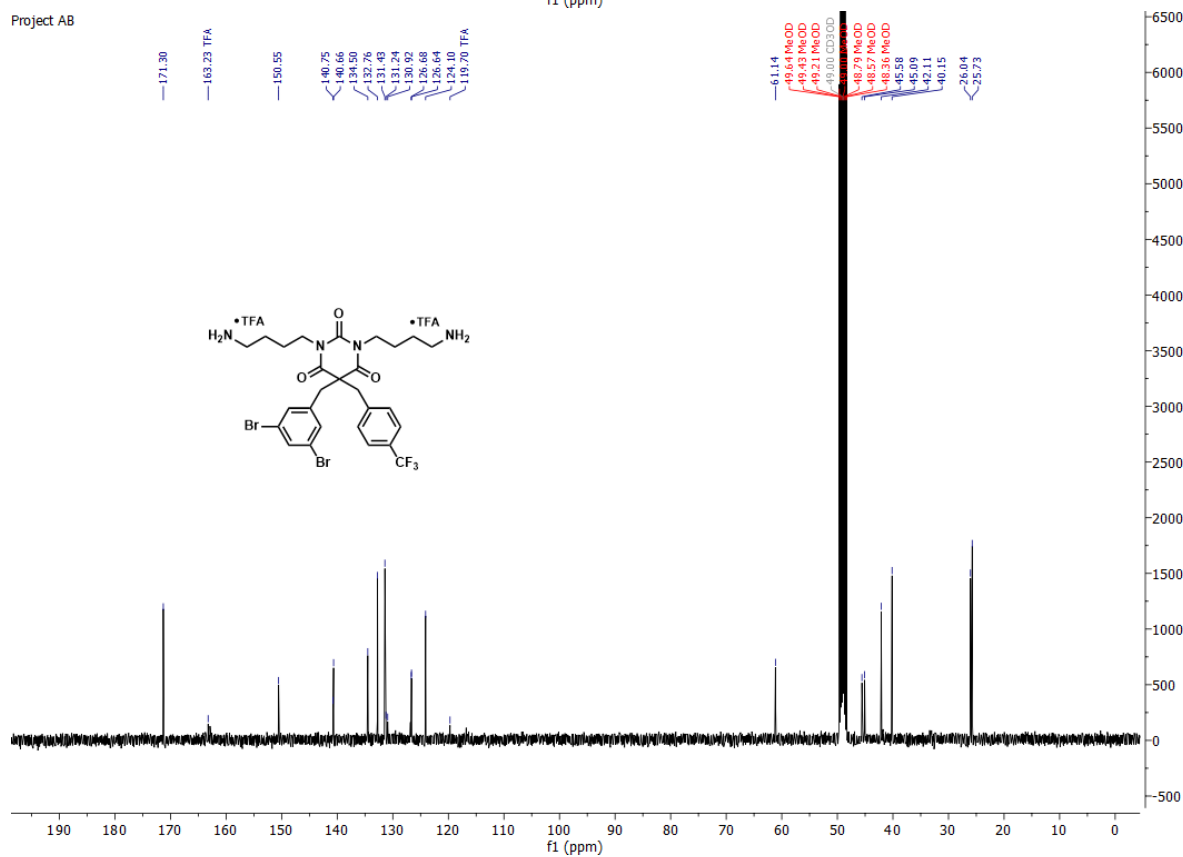
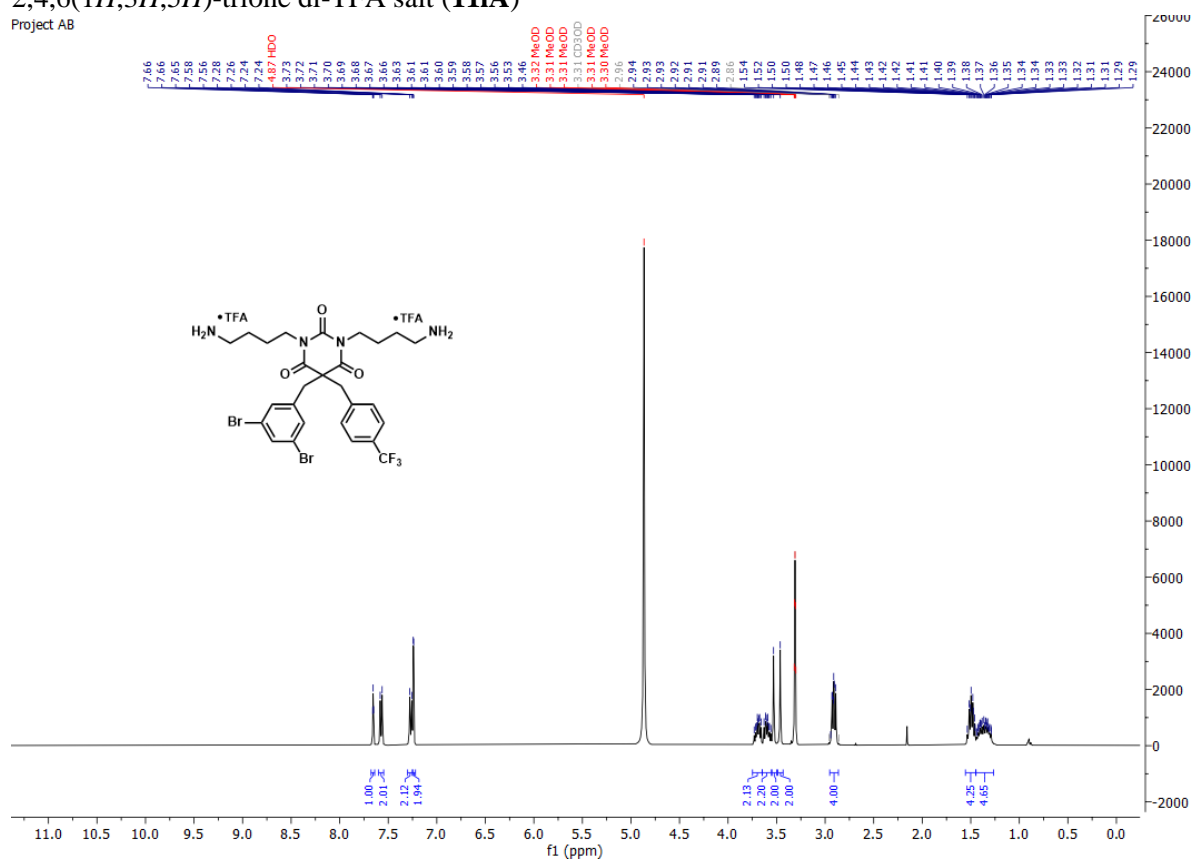


Project AB_guest



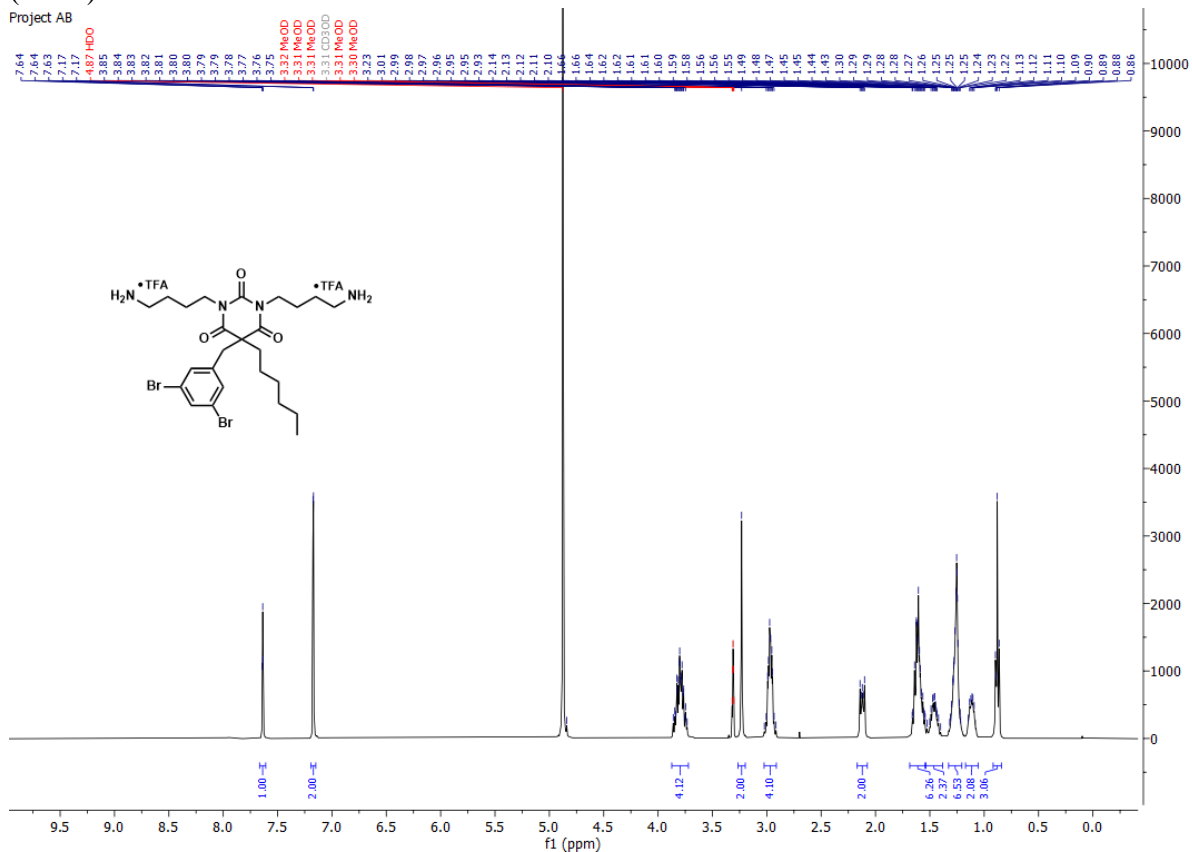
1,3-bis(4-aminobutyl)-5-(3,5-dibromobenzyl)-5-(4-(trifluoromethyl)benzyl)pyrimidine-2,4,6(1H,3H,5H)-trione di-TFA salt (**111A**)

Project AB

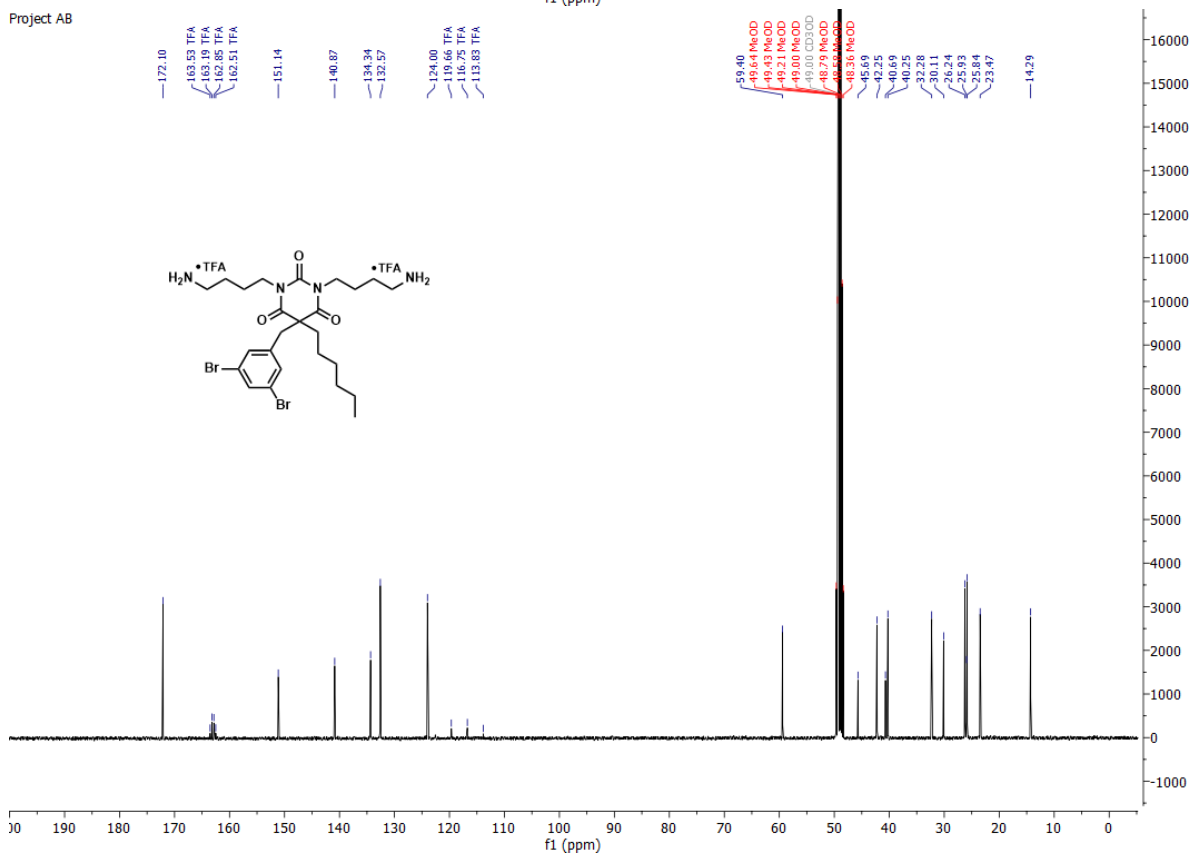


1,3-bis(4-aminobutyl)-5-(3,5-dibromobenzyl)-5-hexylpyrimidine-2,4,6(1*H*,3*H*,5*H*)-trione di-TFA salt (**11nA**)

Project AB

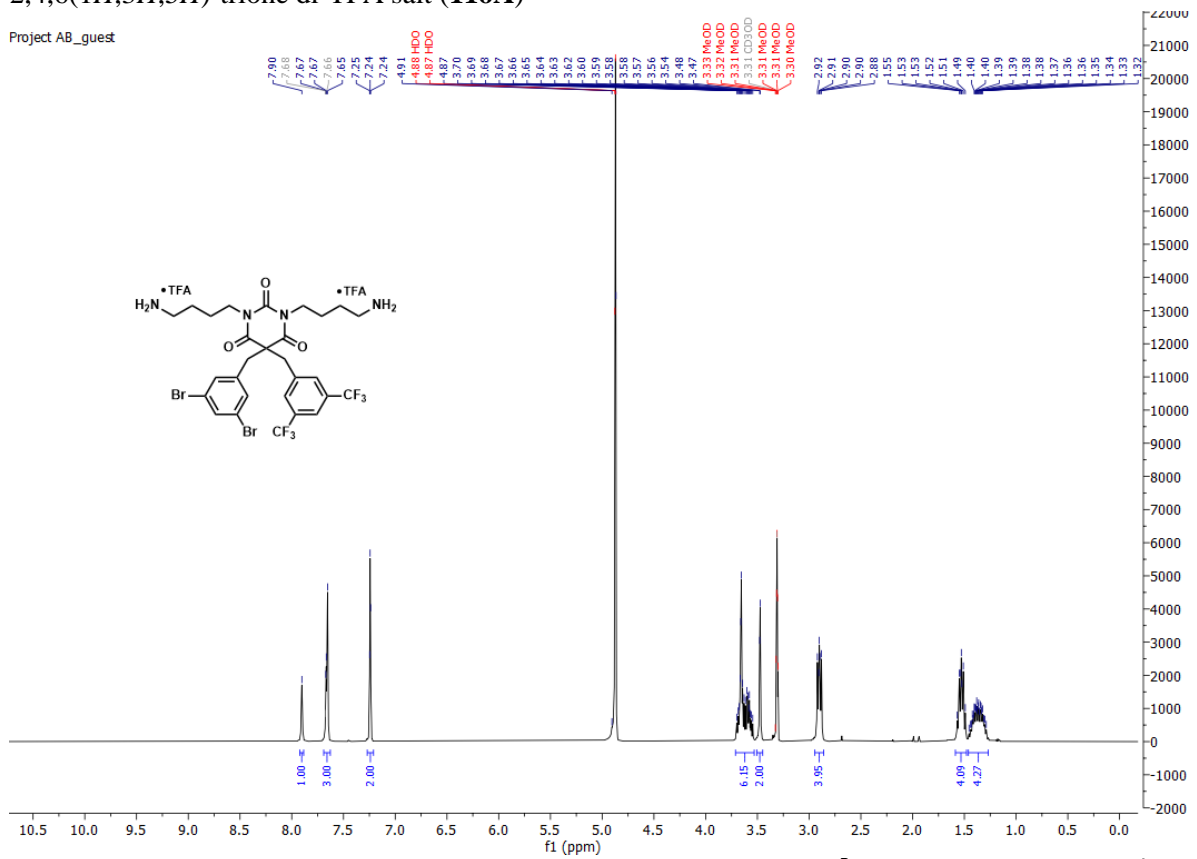


Project AB

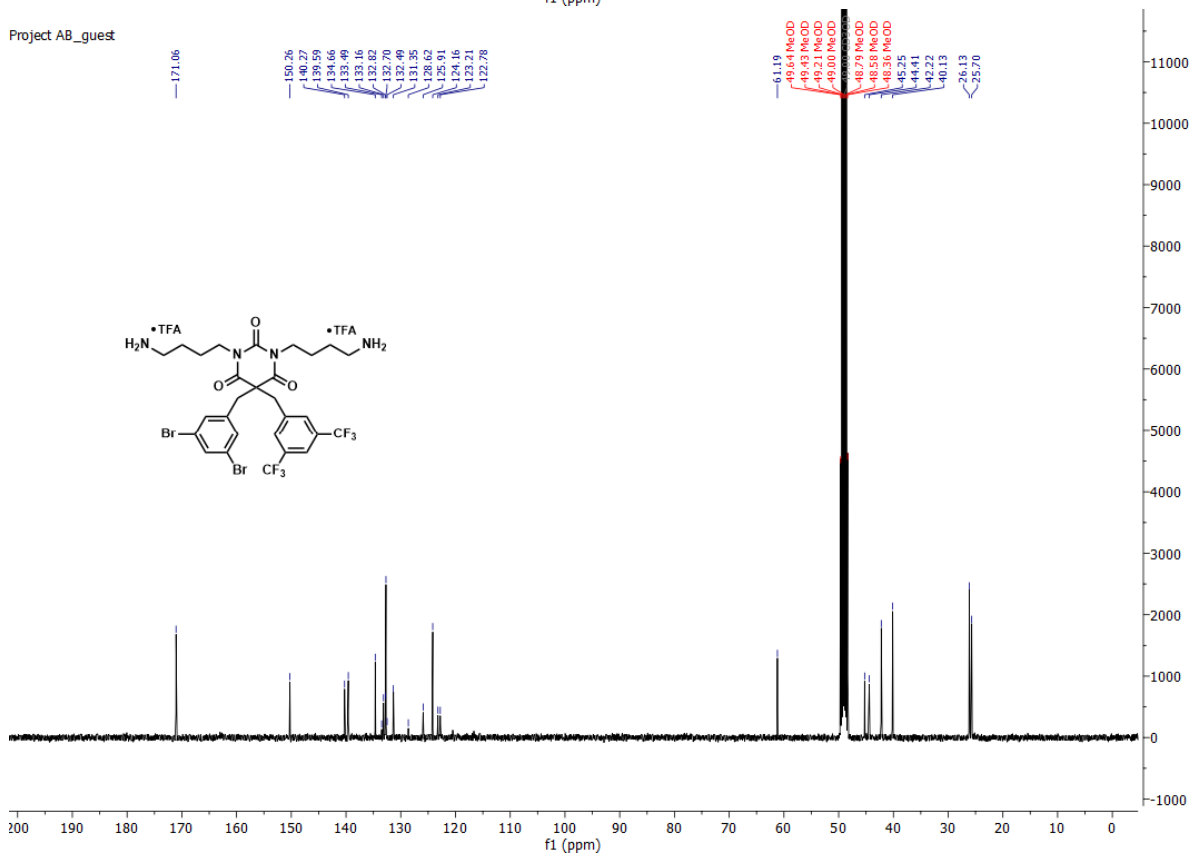


1,3-bis(4-aminobutyl)-5-(3,5-bis(trifluoromethyl)benzyl)-5-(3,5-dibromobenzyl)pyrimidine-2,4,6(1*H*,3*H*,5*H*)-trione di-TFA salt (**11oA**)

Project AB_guest

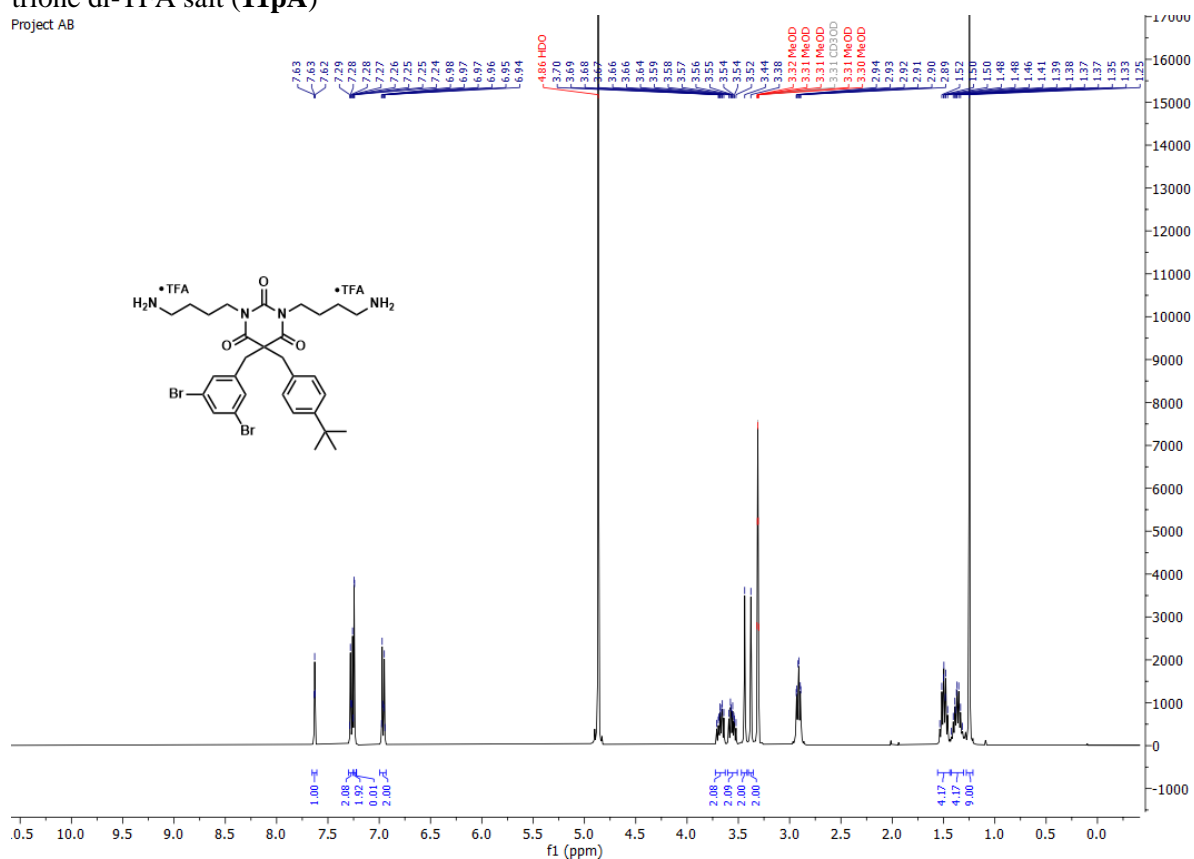


Project AB_guest

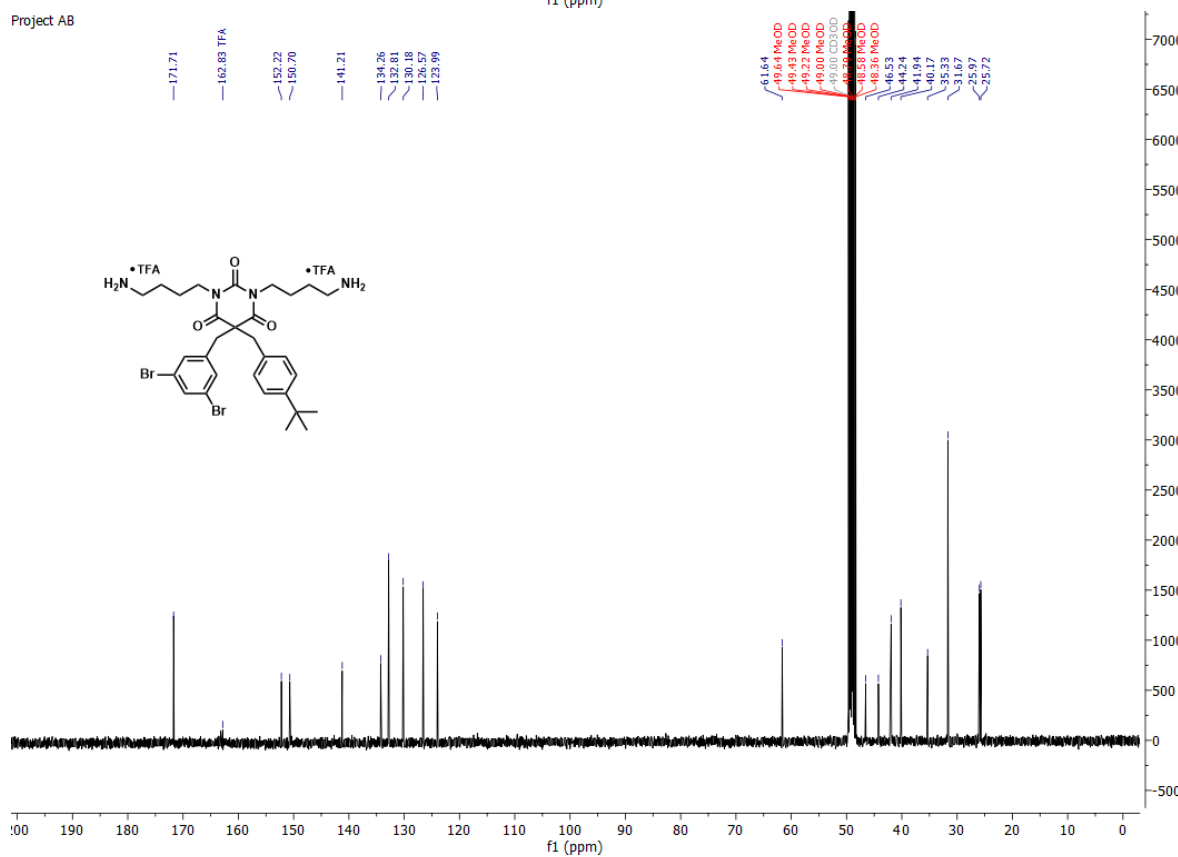


1,3-bis(4-aminobutyl)-5-(4-(*tert*-butyl)benzyl)-5-(3,5-dibromobenzyl)pyrimidine-2,4,6(1*H*,3*H*,5*H*)-trione di-TFA salt (**11pA**)

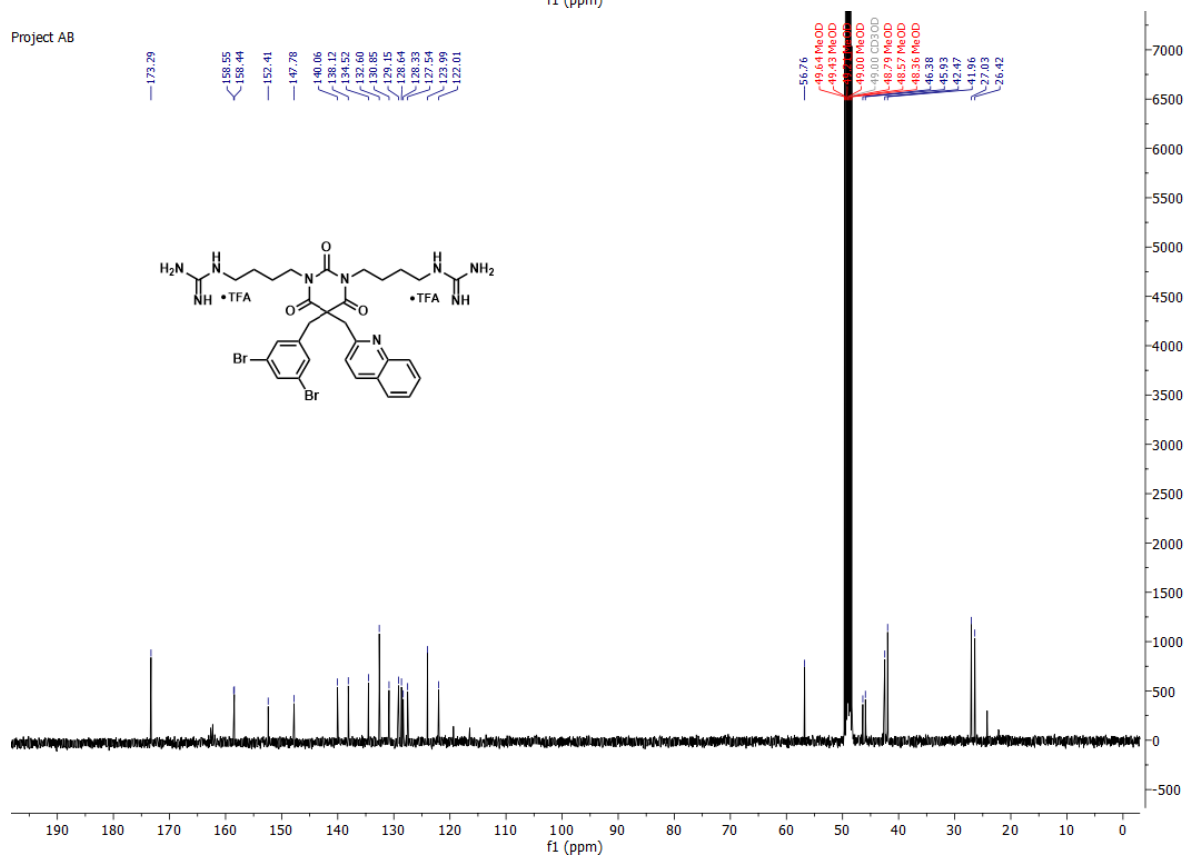
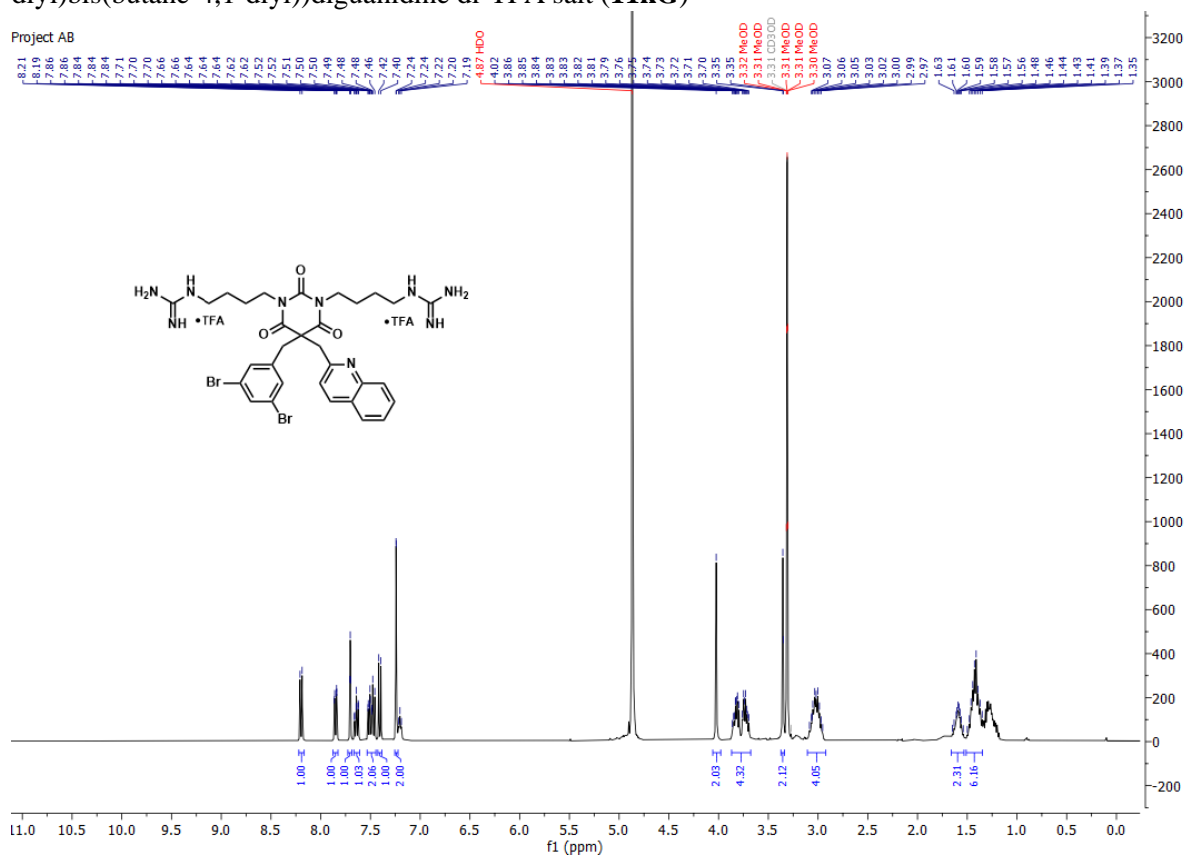
Project AB



Project AB

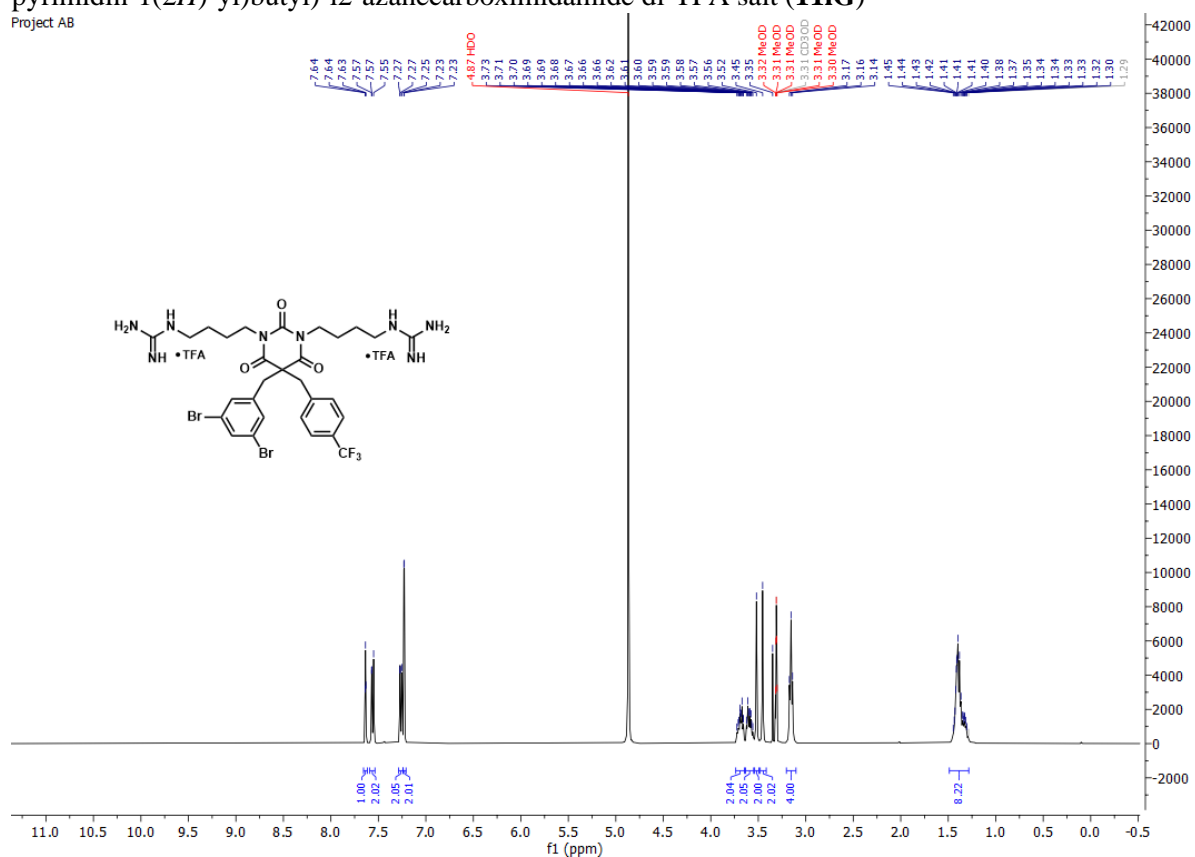


1,1'-((5-(3,5-dibromobenzyl)-2,4,6-trioxo-5-(quinolin-2-ylmethyl) dihydropyrimidine-1,3(2H,4H)-diyl)bis(butane-4,1-diyl)diguandine di-TFA salt (**11kG**)

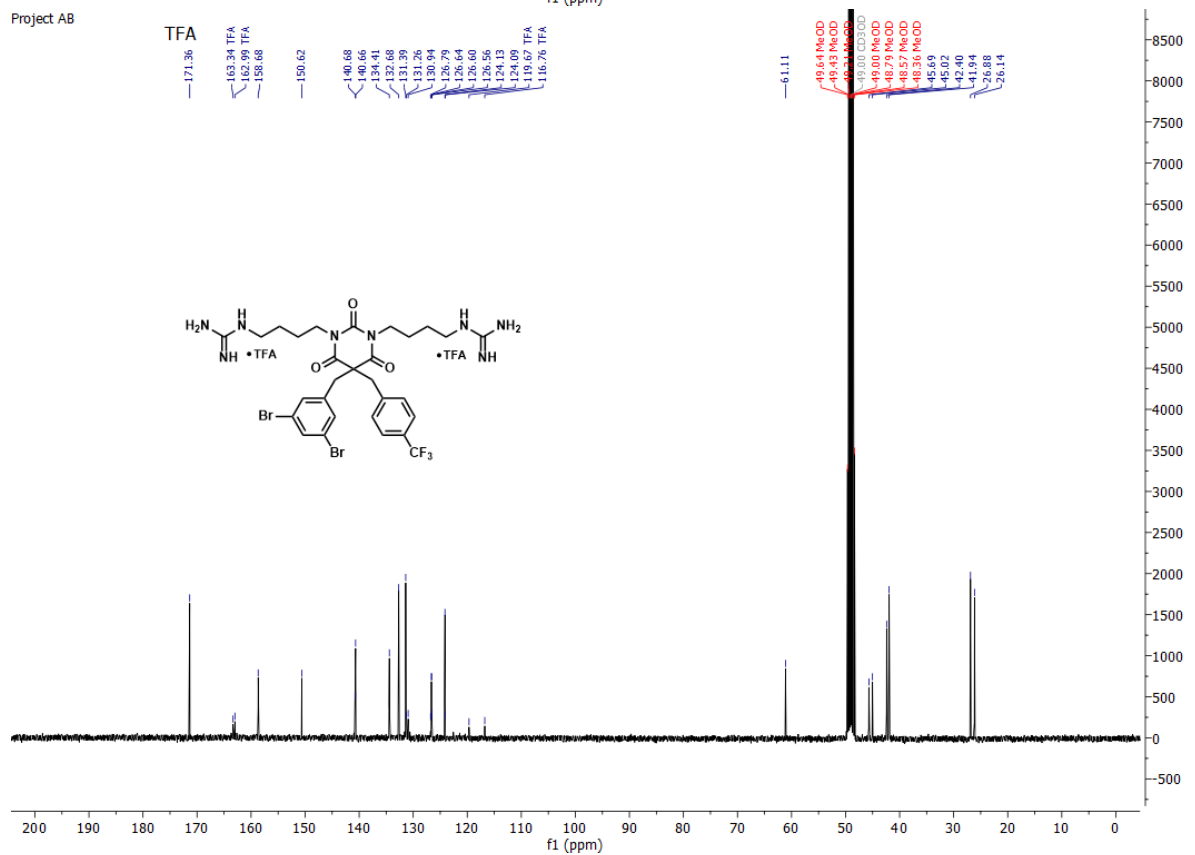


(4-(5-(3,5-dibromobenzyl)-3-(4-guanidinobutyl)-2,4,6-trioxo-5-(4-(trifluoromethyl)benzyl)tetrahydro-pyrimidin-1(2H)-yl)butyl)-1,2-azancarboximidamide di-TFA salt (**111G**)

Project AB

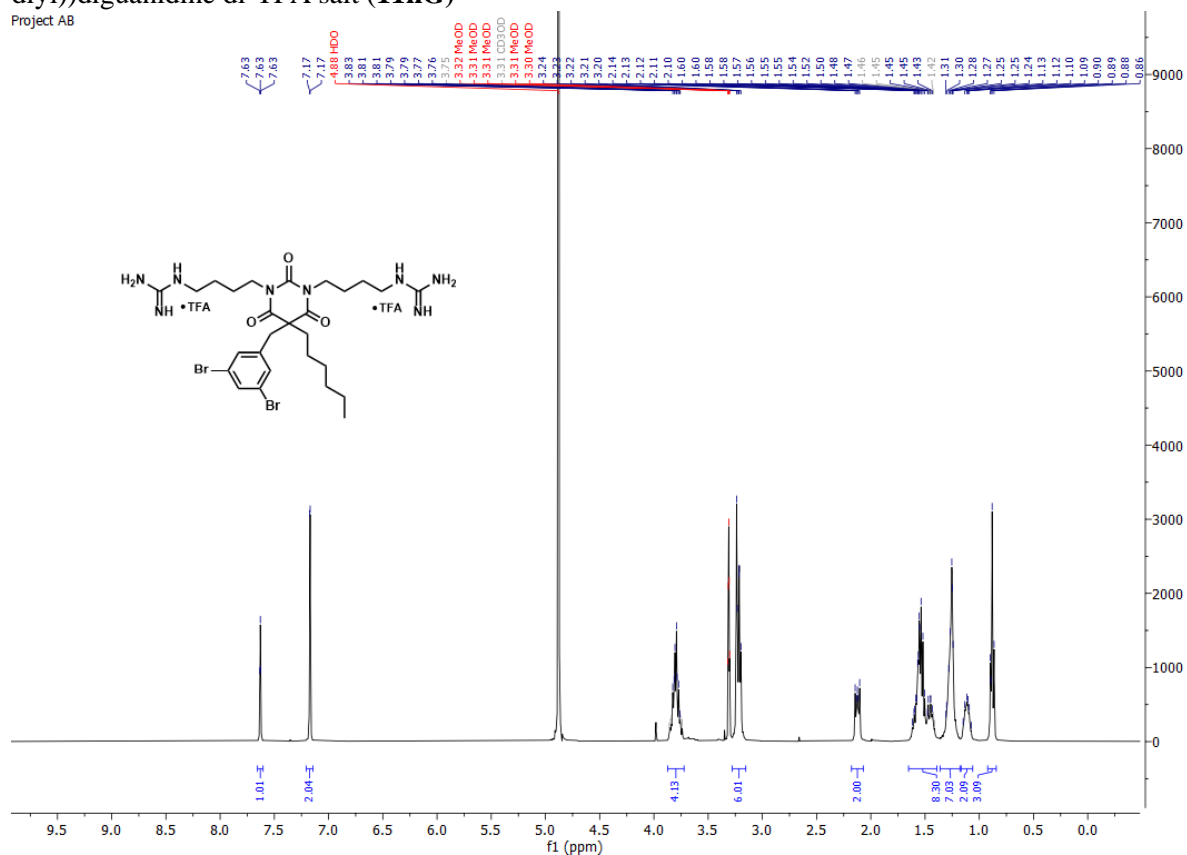


Project AB

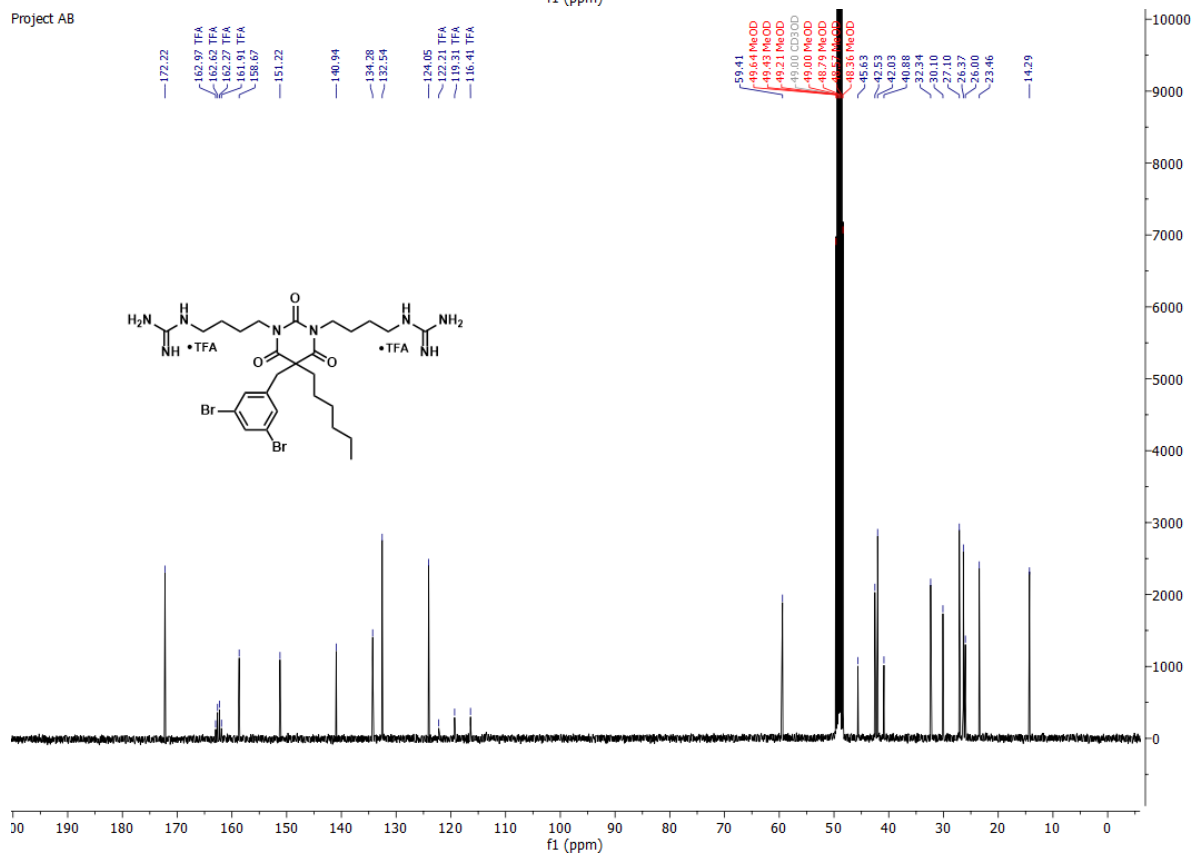


1,1'-((5-(3,5-dibromobenzyl)-5-hexyl-2,4,6-trioxodihydropyrimidine-1,3(2*H*,4*H*)-diyl)bis(butane-4,1-diyl))diguanidine di-TFA salt (**11nG**)

Project AB

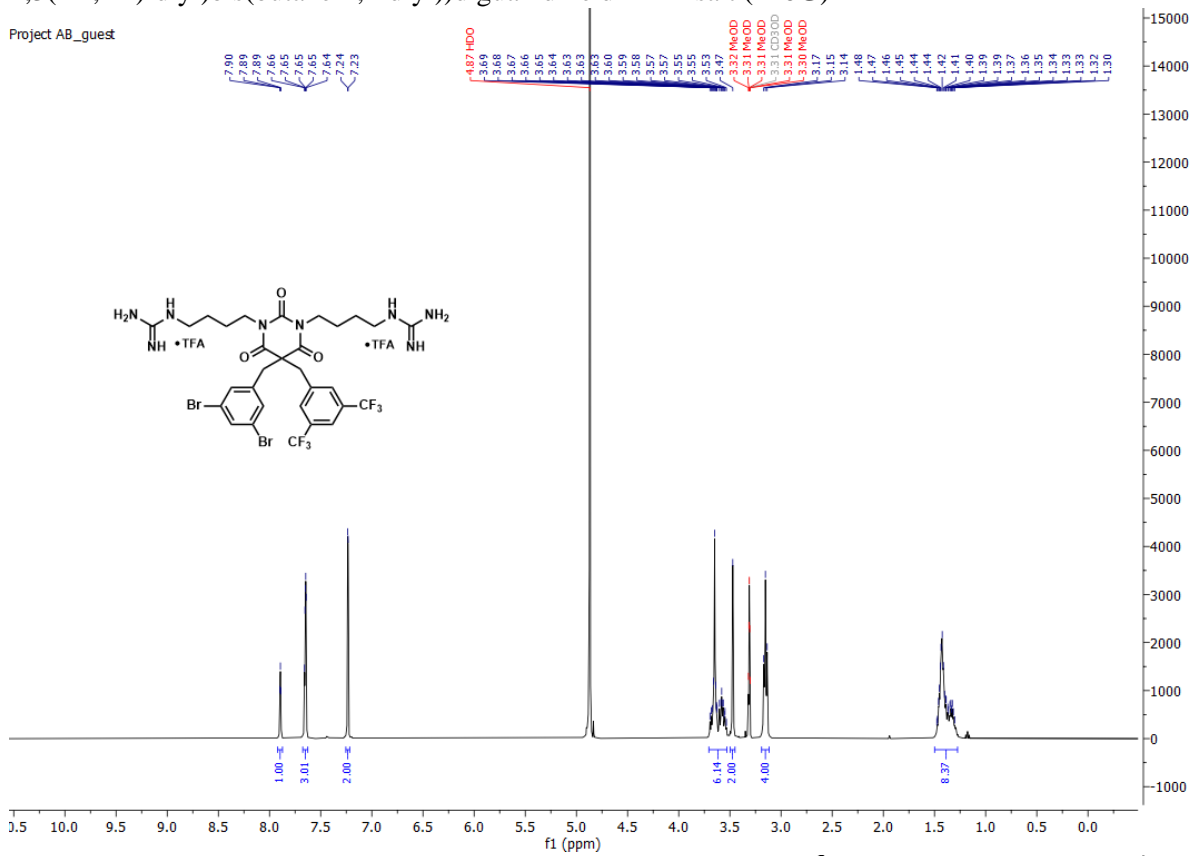


Project AB

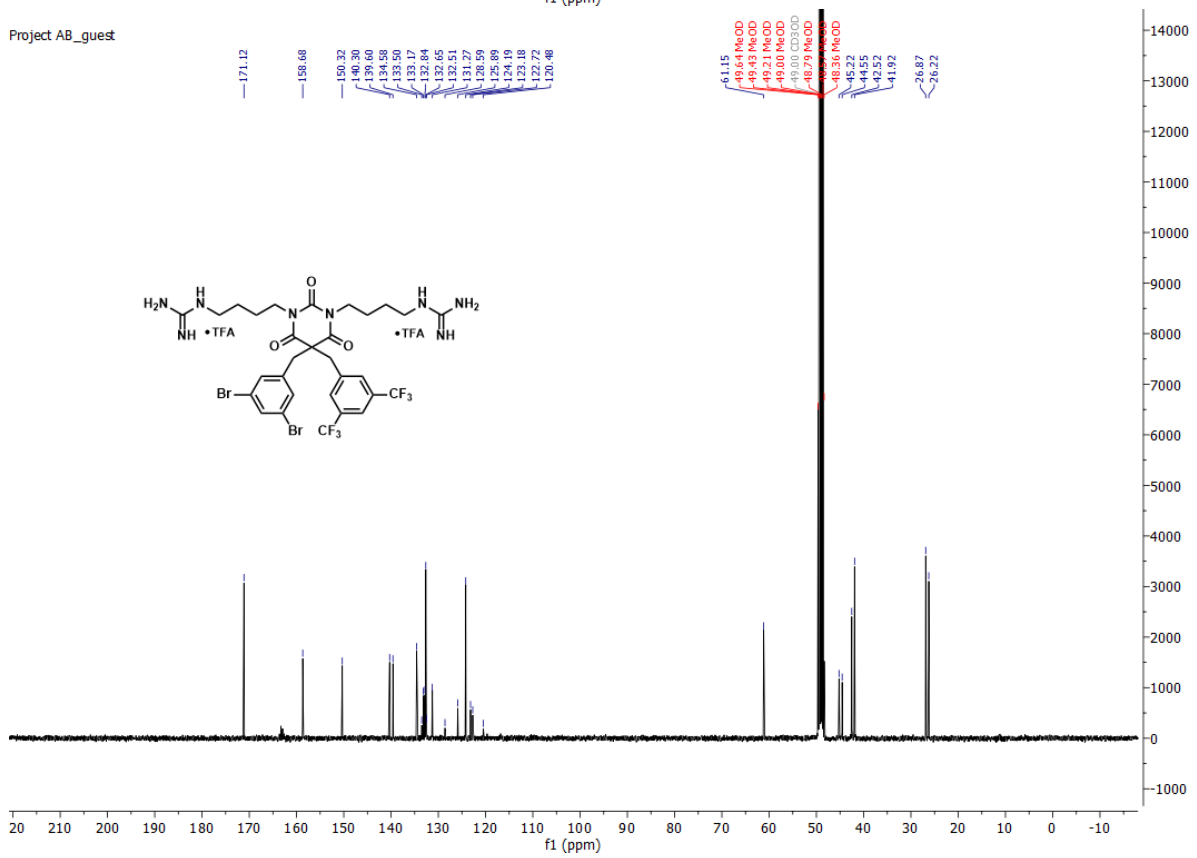


1,1'-((5-(3,5-bis(trifluoromethyl)benzyl)-5-(3,5-dibromobenzyl)-2,4,6-trioxodihydropyrimidine-1,3(2*H*,4*H*)-diyl)bis(butane-4,1-diyl)diguandine di-TFA salt (**11oG**)

Project AB_guest

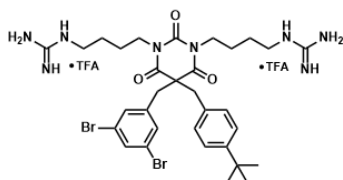
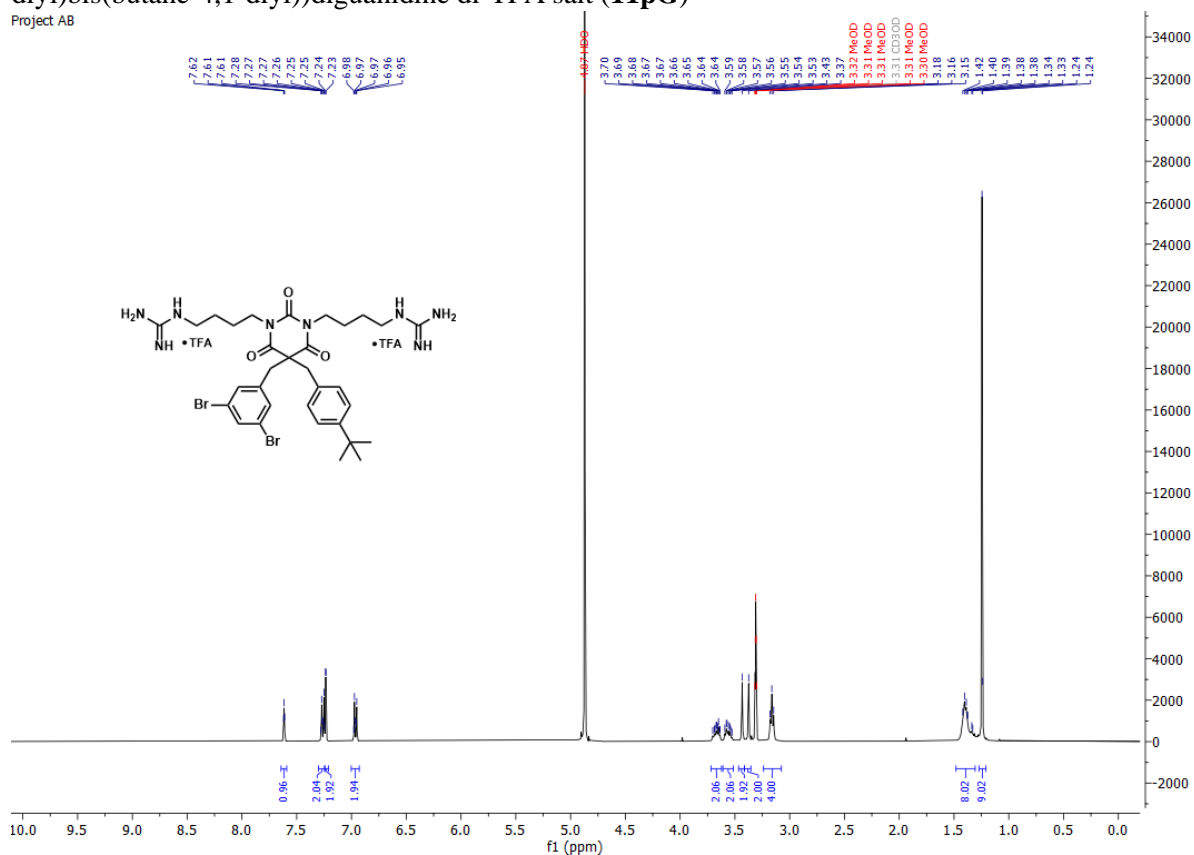


Project AB_guest

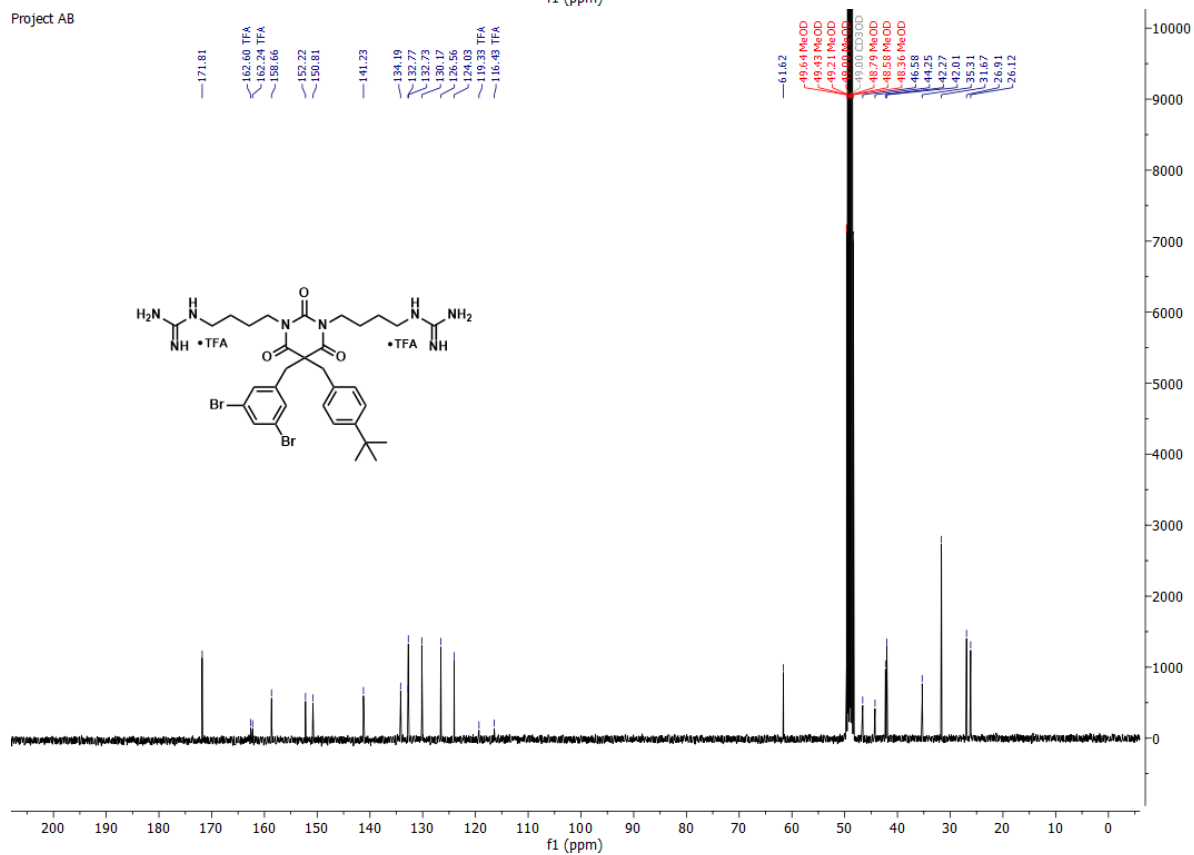


1,1'-((5-(4-(*tert*-butyl)benzyl)-5-(3,5-dibromobenzyl)-2,4,6-trioxodihydropyrimidine-1,3(2*H*,4*H*)-diyl)bis(butane-4,1-diyl)diguandine di-TFA salt (**11pG**)

Project AB

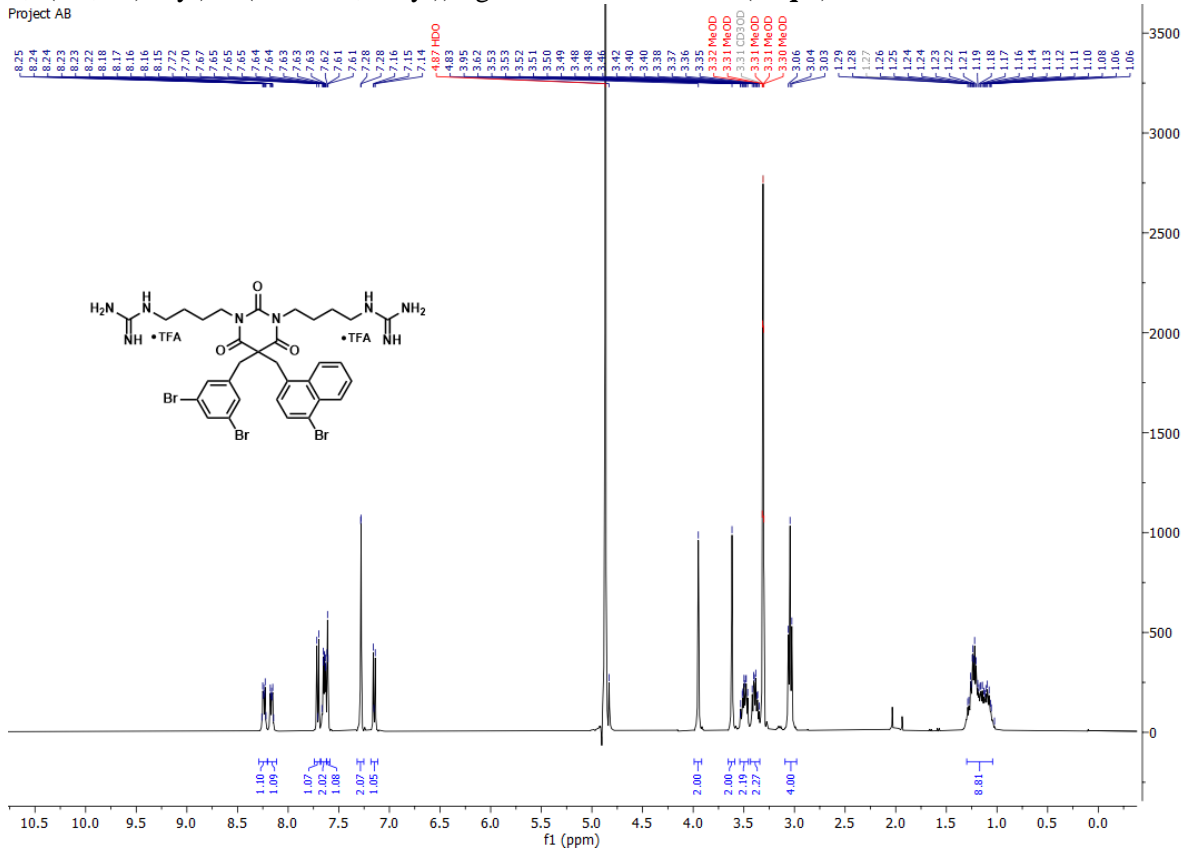


Project AB



1,1'-((5-((4-bromonaphthalen-1-yl)methyl)-5-(3,5-dibromobenzyl)-2,4,6-trioxodihydropyrimidine-1,3(2*H*,4*H*)-diyl)bis(butane-4,1-diyl)diguandine di-TFA salt (**11qG**)

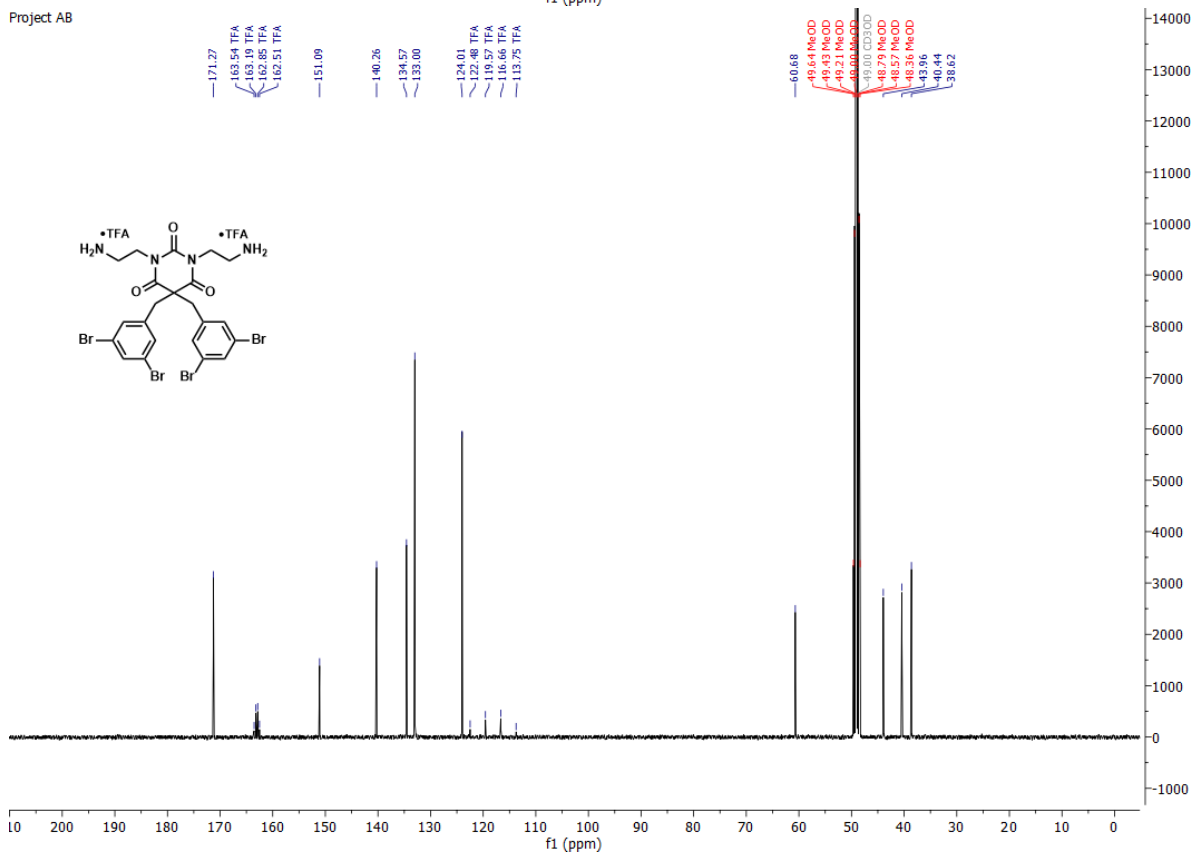
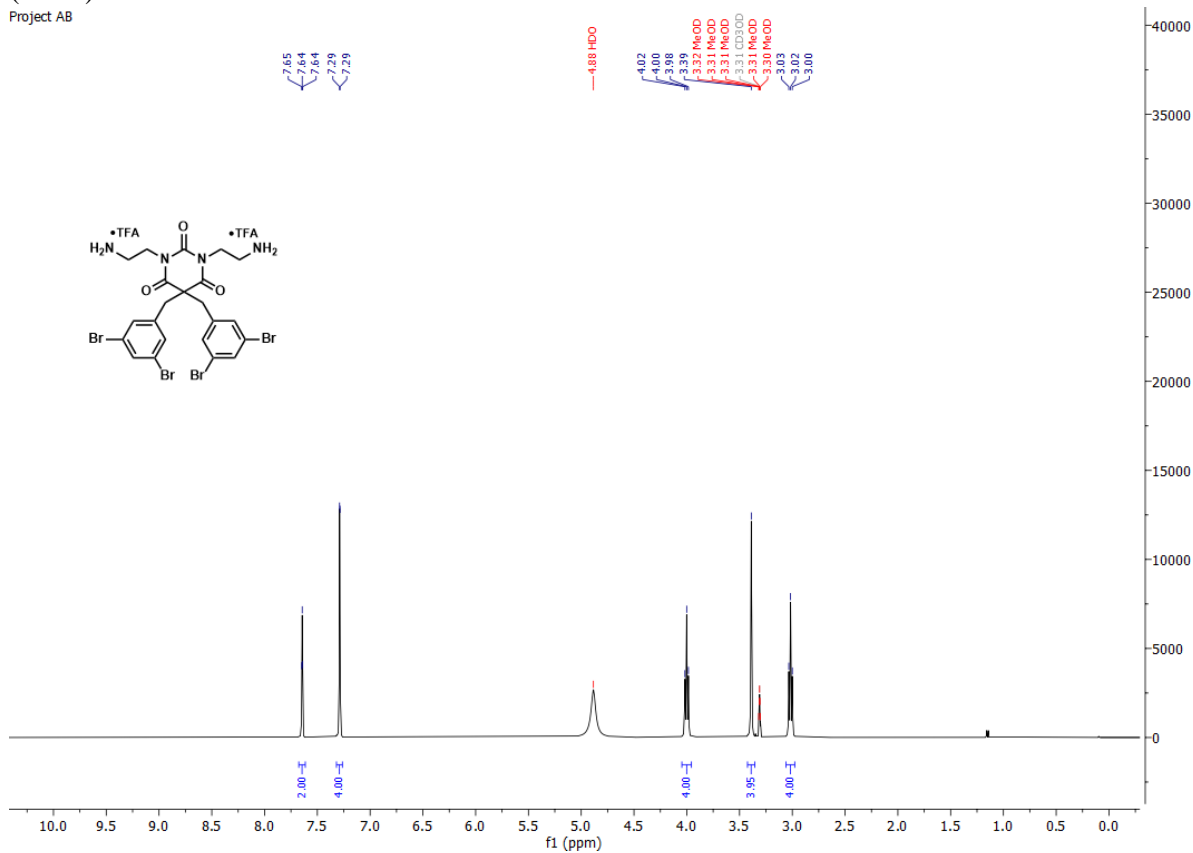
Project AB



3.4 ^1H and ^{13}C NMR spectra of compounds in series 4

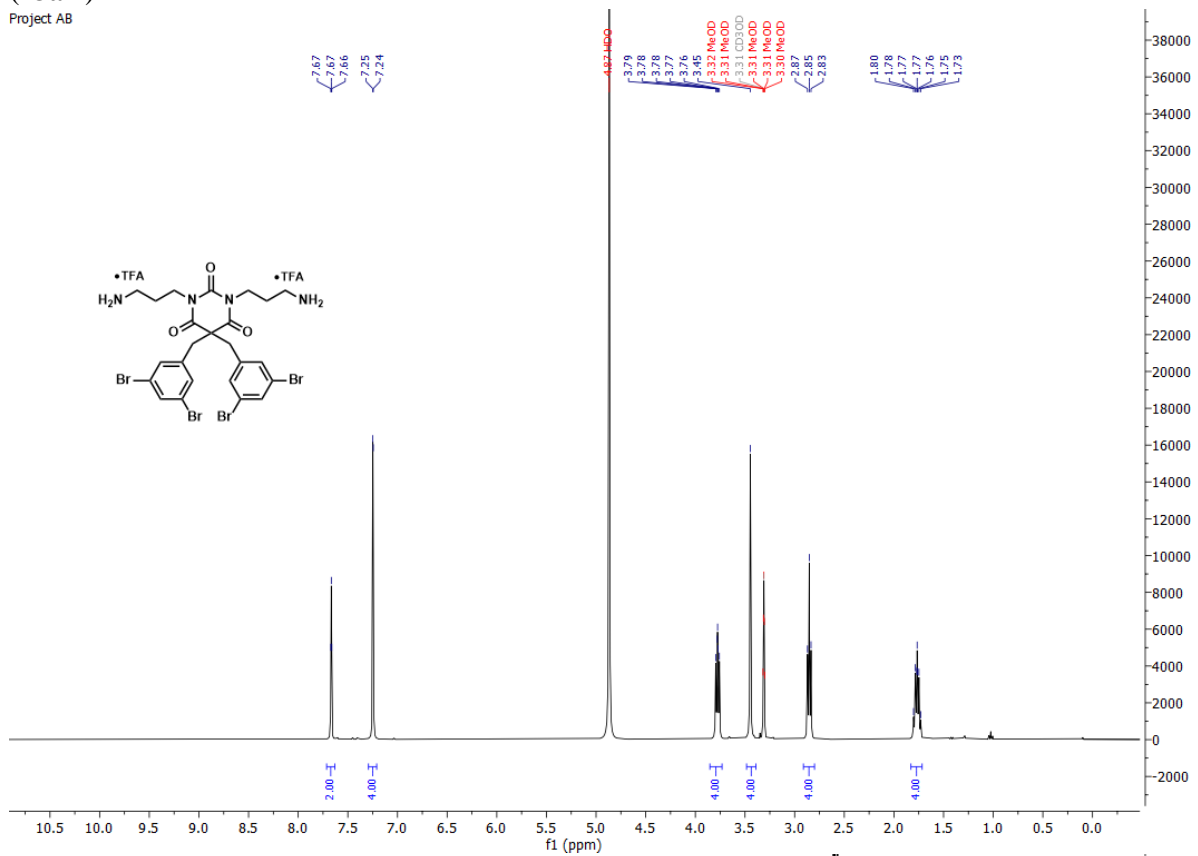
1,3-bis(2-aminoethyl)-5,5-bis(3,5-dibromobenzyl)pyrimidine-2,4,6(1*H*,3*H*,5*H*)-trione di-TFA salt (**12aA**)

Project AB

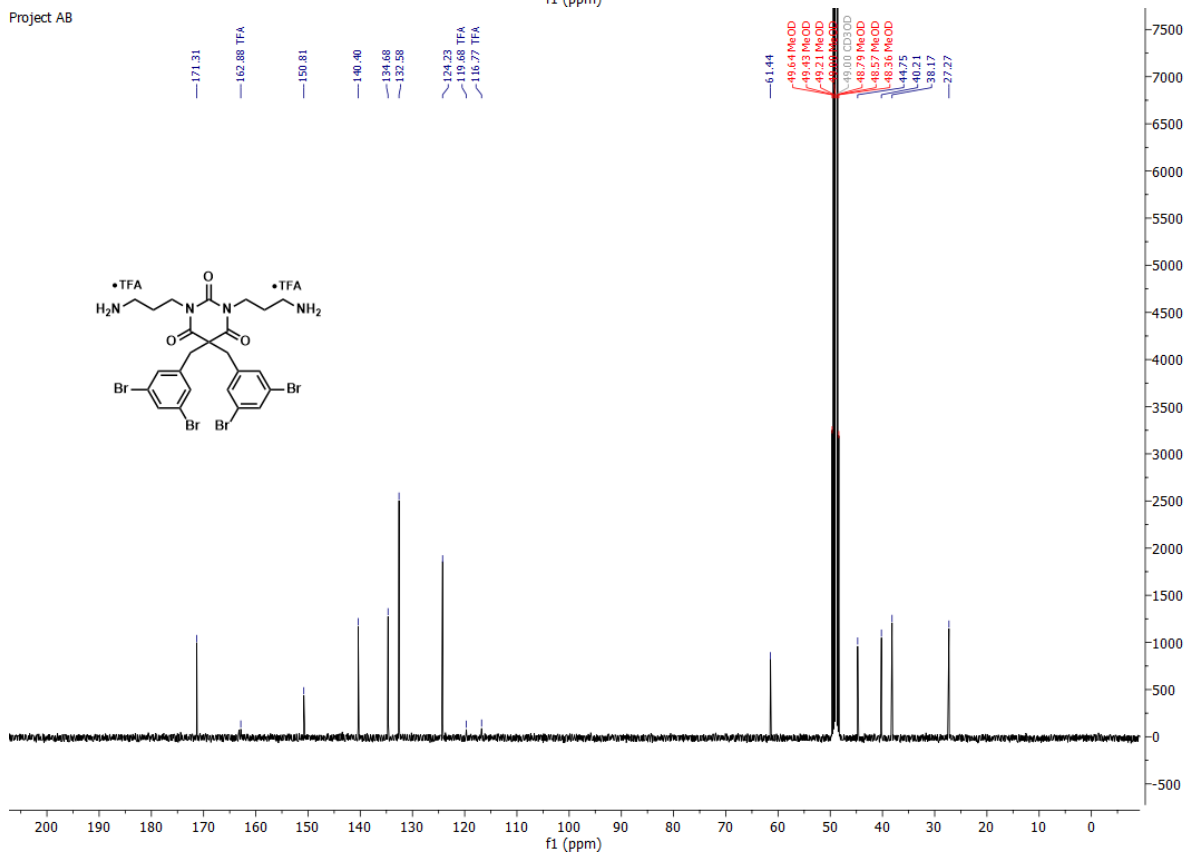


1,3-bis(3-aminopropyl)-5,5-bis(3,5-dibromobenzyl)pyrimidine-2,4,6(1*H*,3*H*,5*H*)-trione di-TFA salt
(13aA)

Project AB

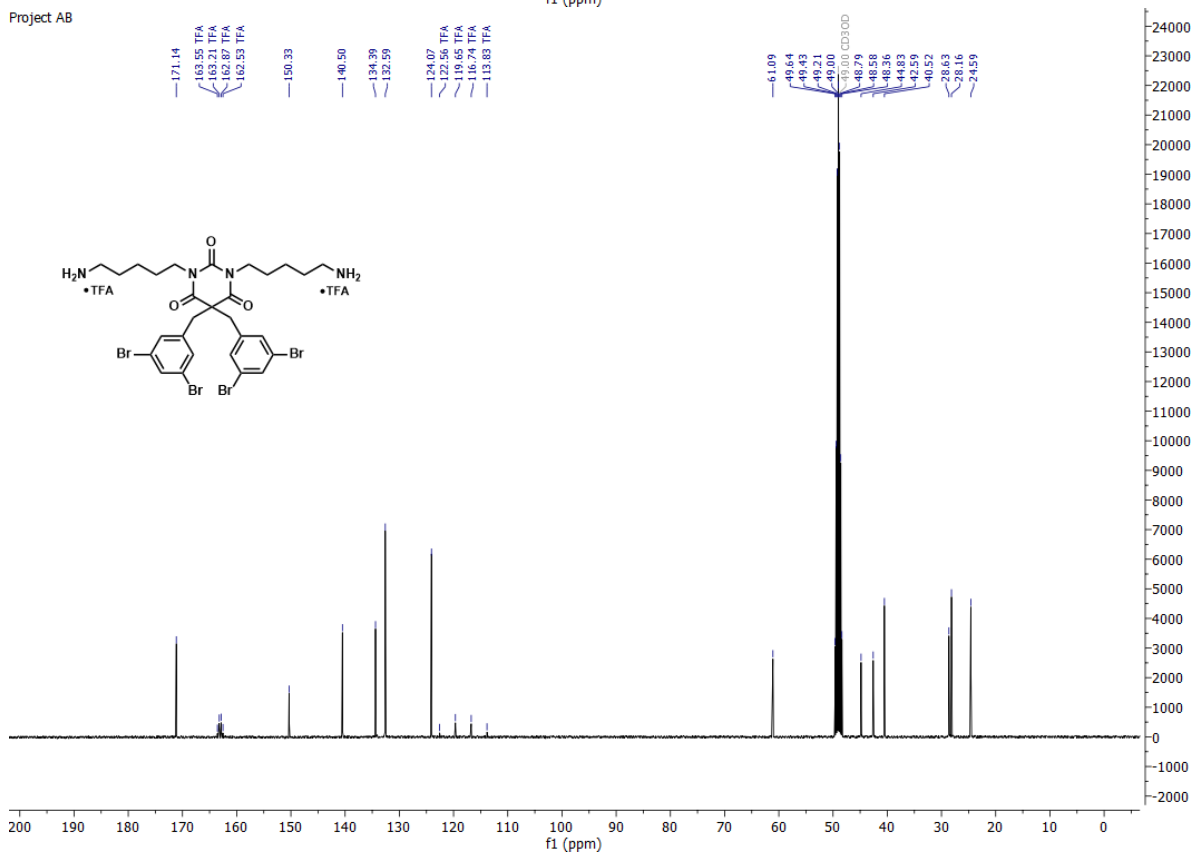
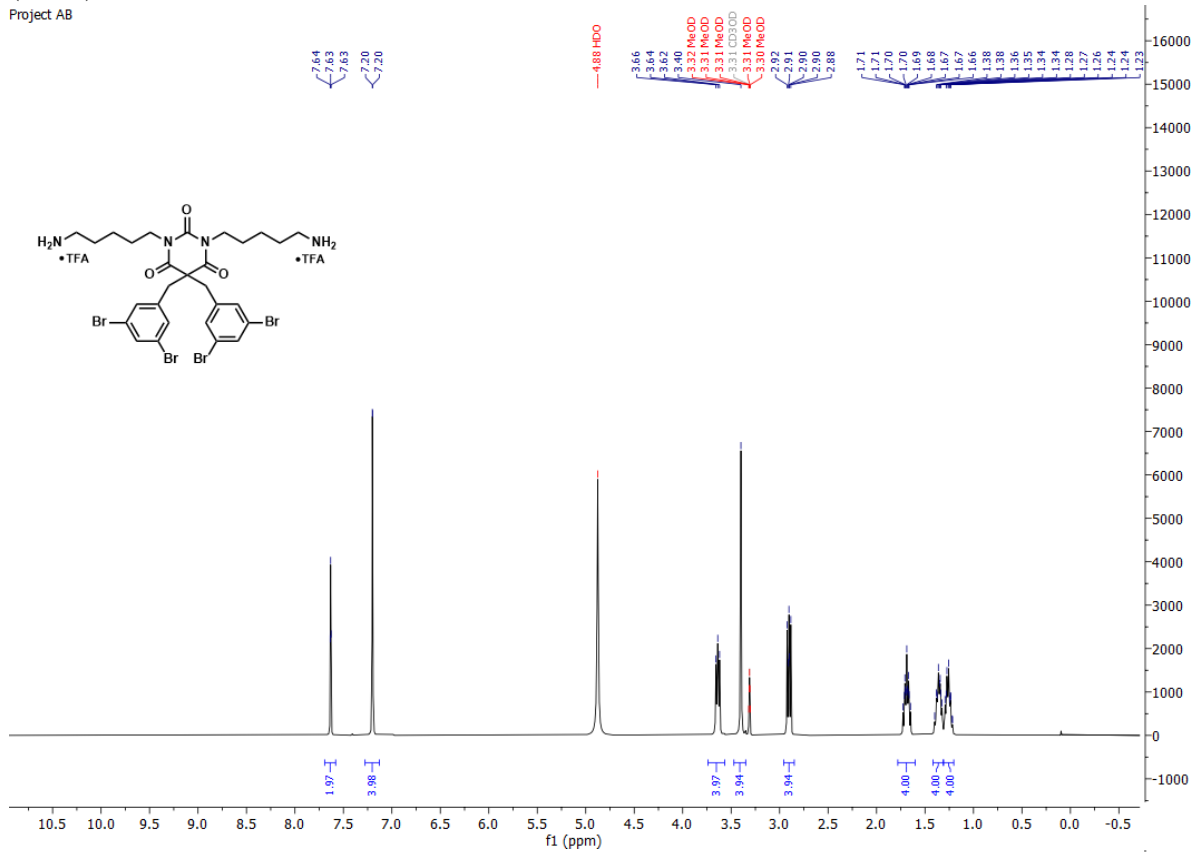


Project AB



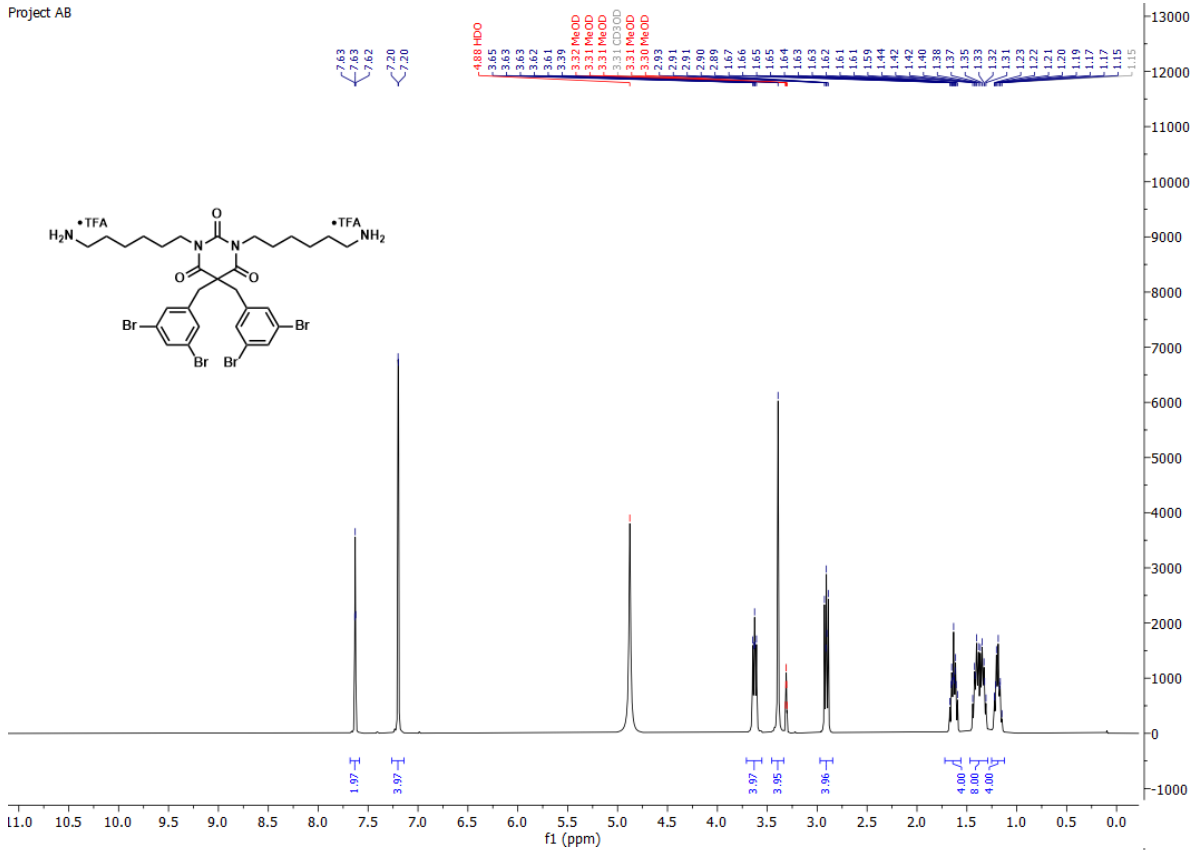
1,3-bis(5-aminopentyl)-5,5-bis(3,5-dibromobenzyl)pyrimidine-2,4,6(1*H*,3*H*,5*H*)-trione di-TFA salt (**14aA**)

Project AB

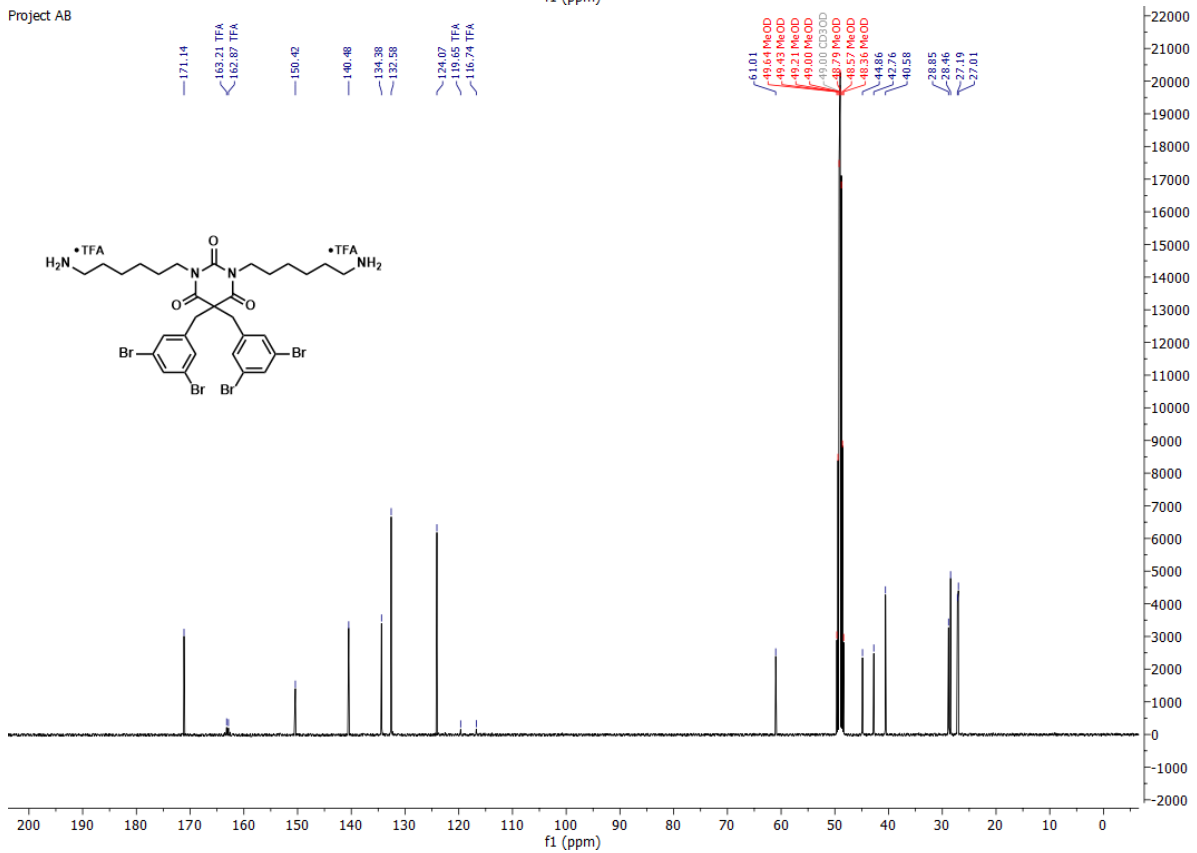


1,3-bis(6-aminohexyl)-5,5-bis(3,5-dibromobenzyl)pyrimidine-2,4,6(1H,3H,5H)-trione di-TFA salt (15aA)

Project AB

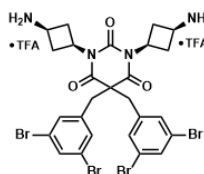
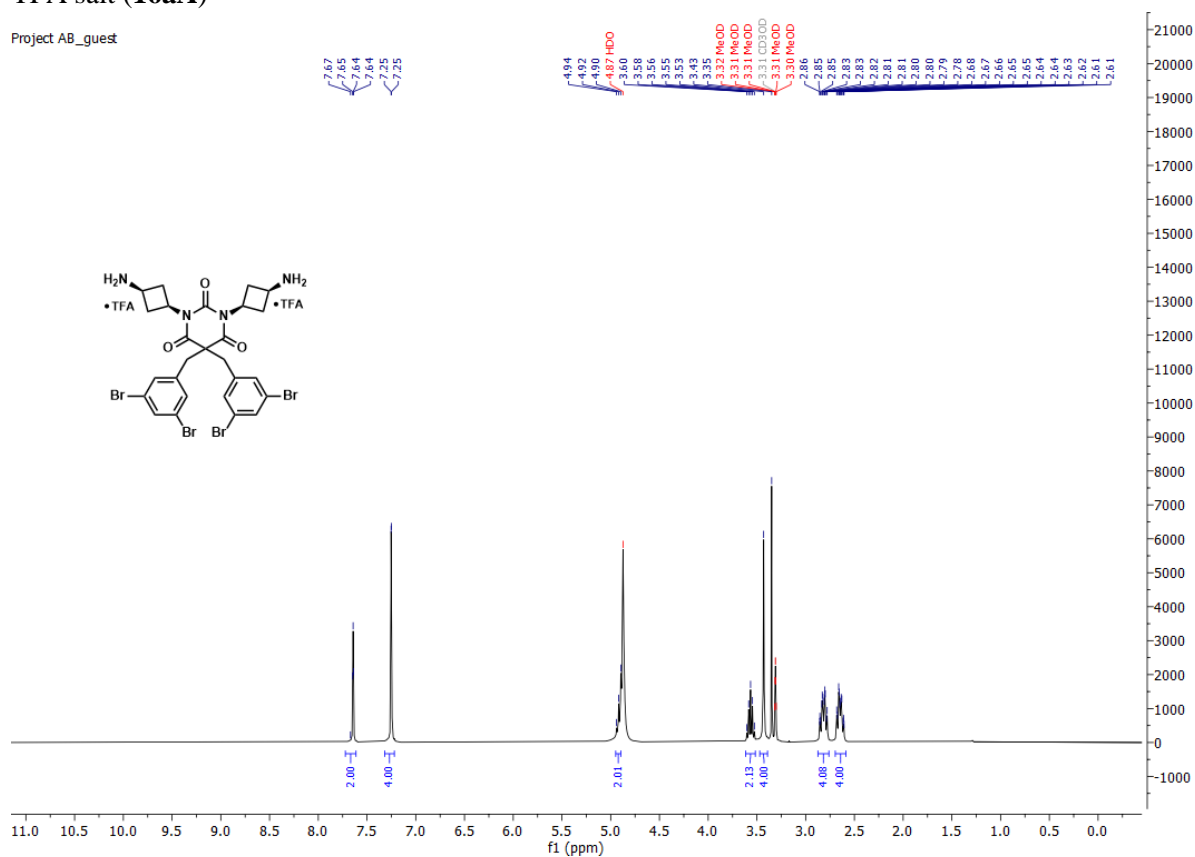


Project AB

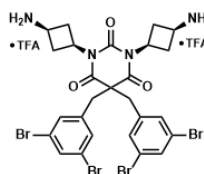
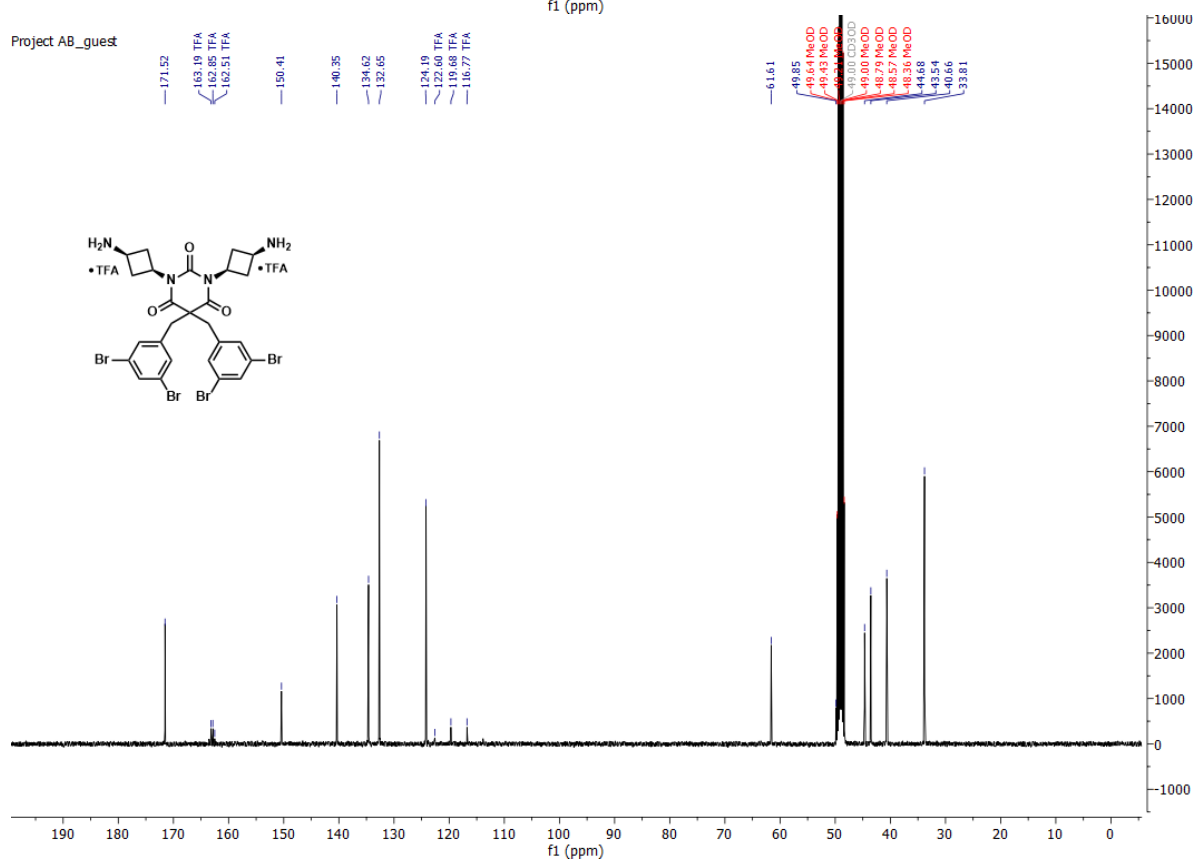


1,3-bis((1*s*,3*S*)-3-aminocyclobutyl)-5,5-bis(3,5-dibromobenzyl)pyrimidine-2,4,6(1*H*,3*H*,5*H*)-trione di-TFA salt (**16aA**)

Project AB_guest

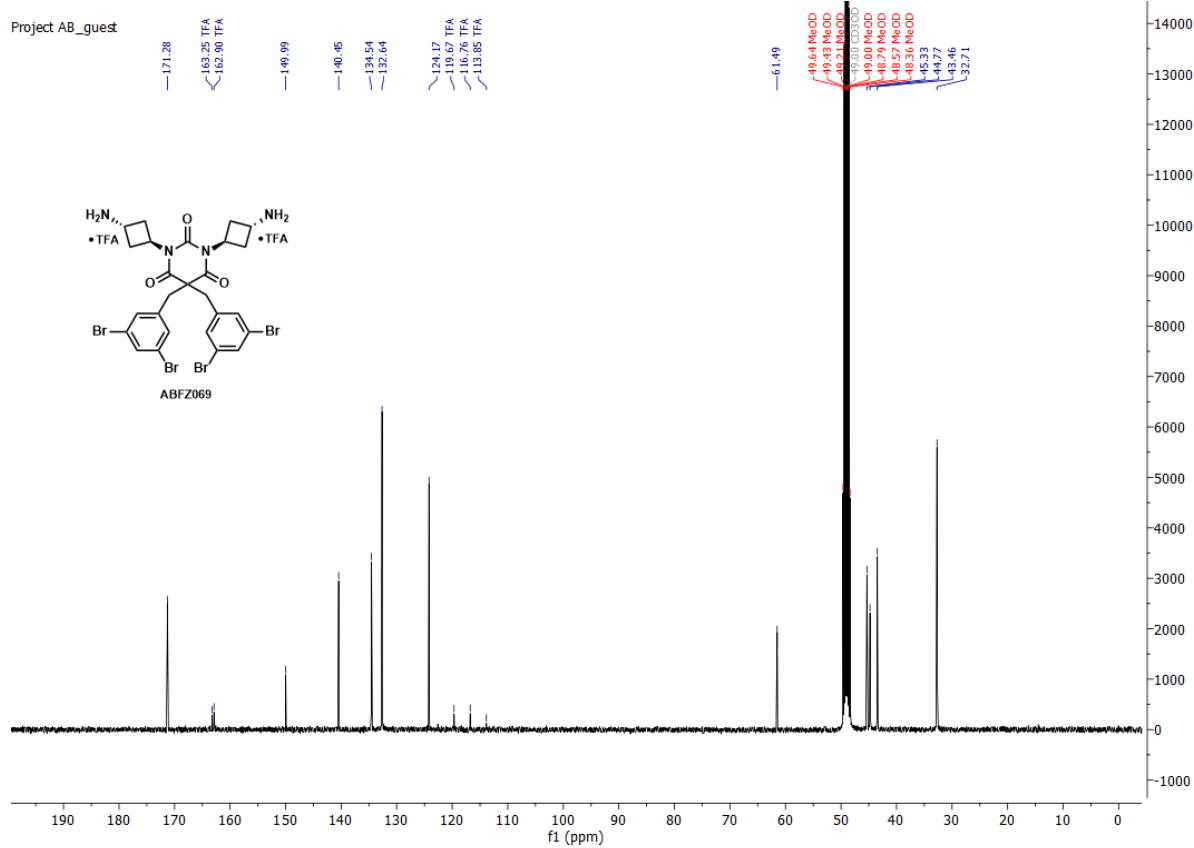
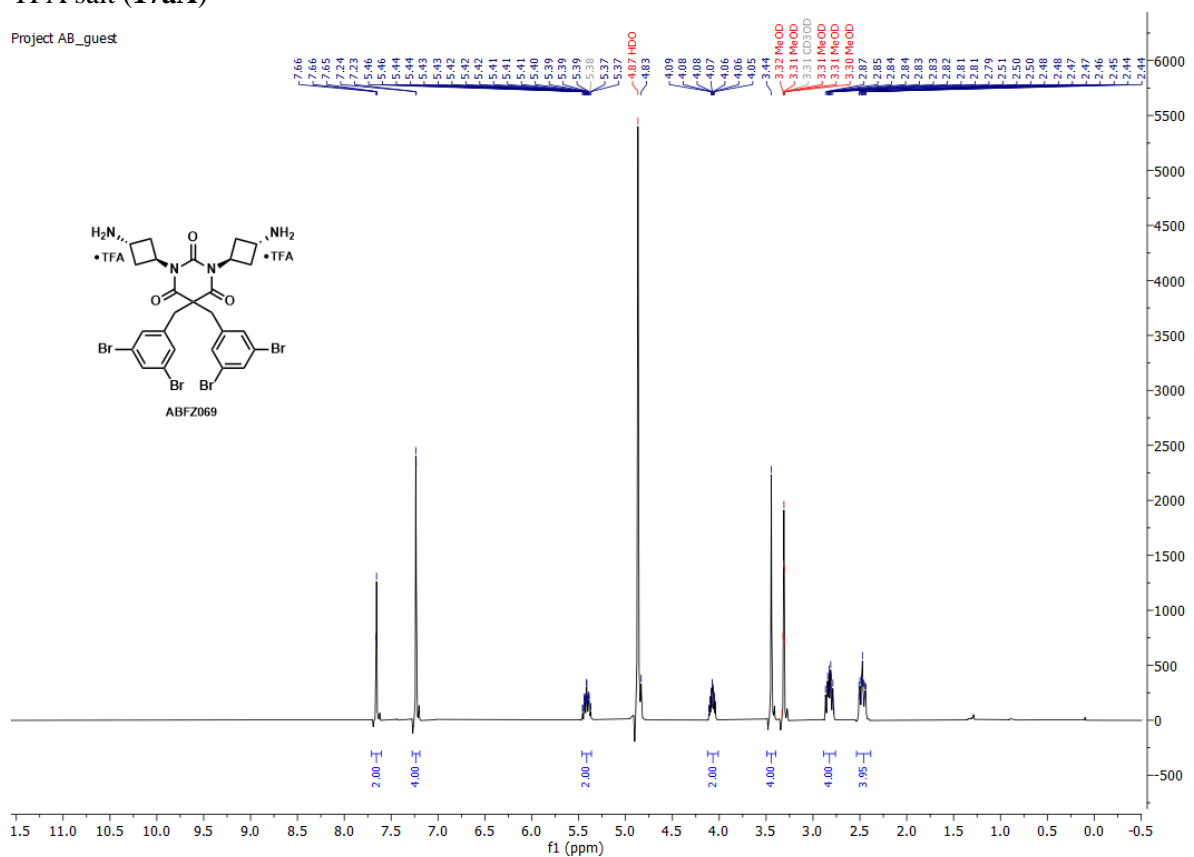


Project AB_guest



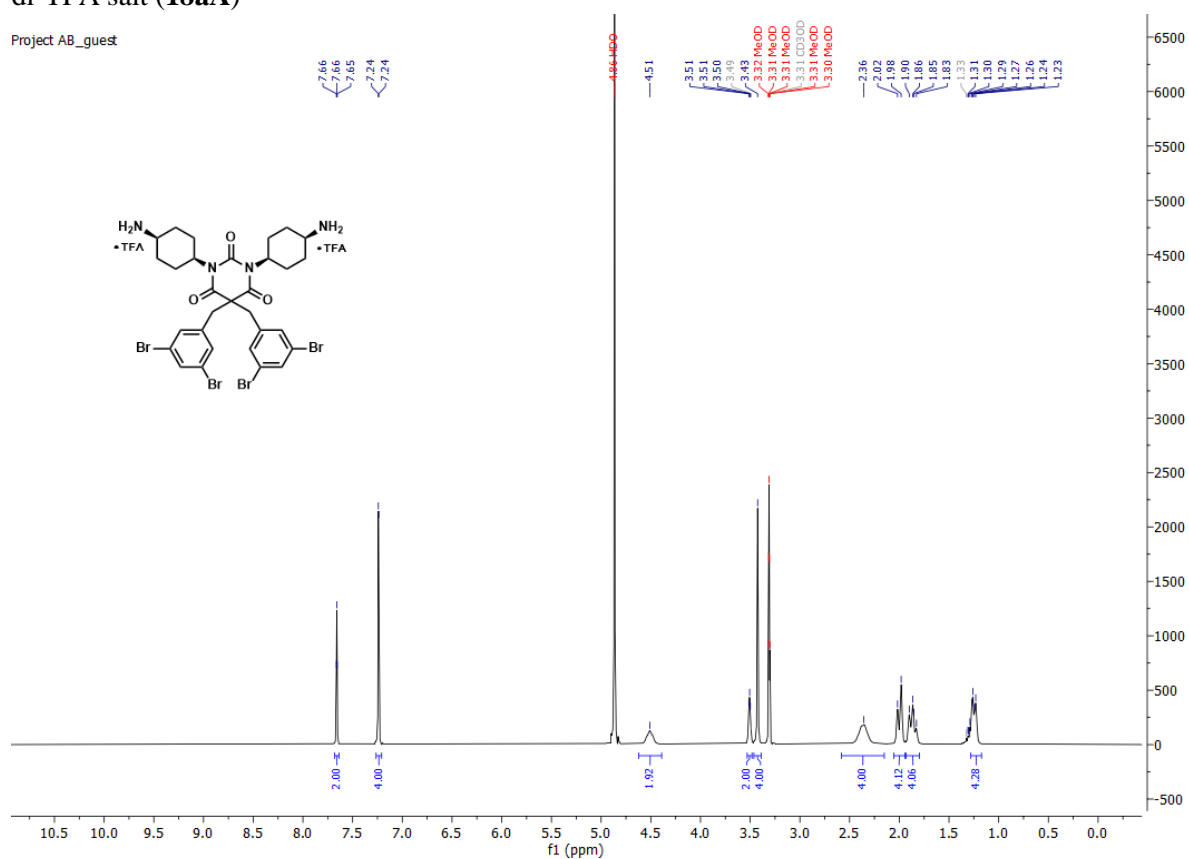
1,3-bis((1*r*,3*R*)-3-aminocyclobutyl)-5,5-bis(3,5-dibromobenzyl)pyrimidine-2,4,6(1*H*,3*H*,5*H*)-trione di-TFA salt (**17aA**)

Project AB_guest

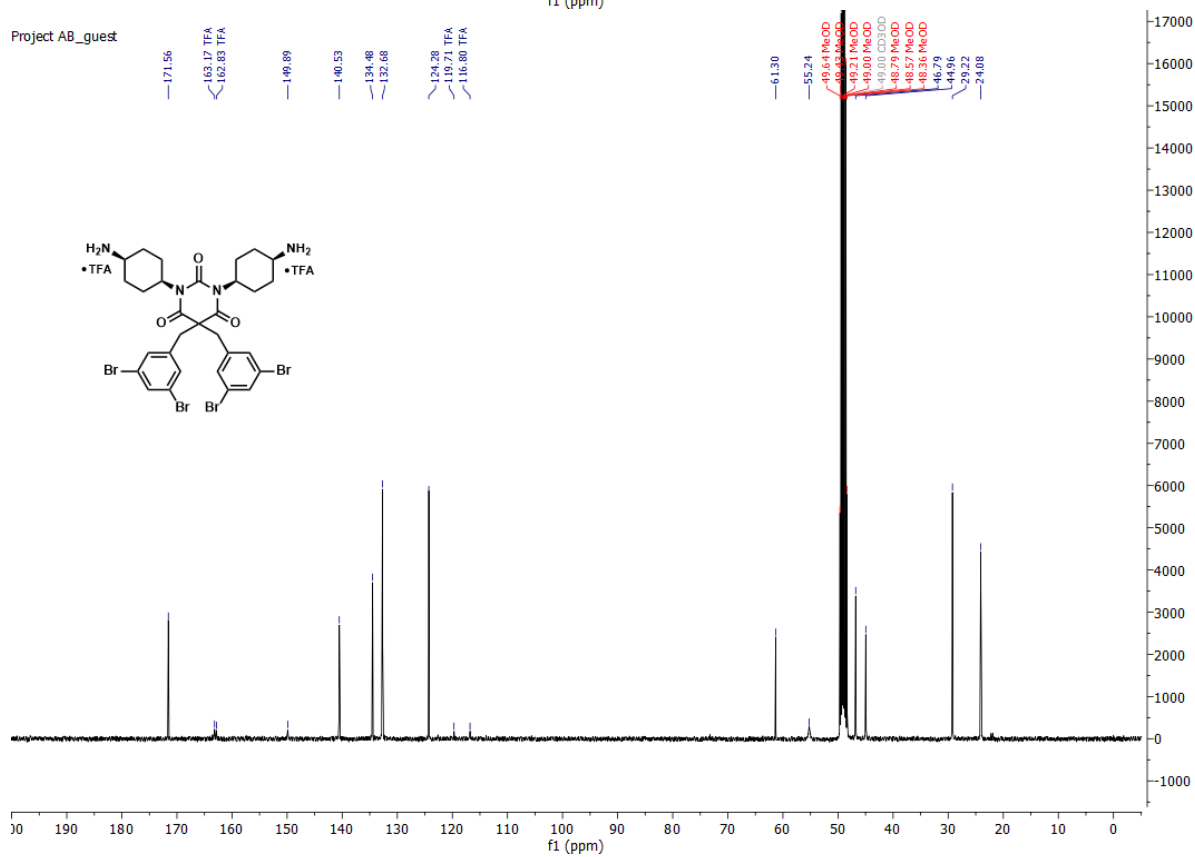


1,3-bis((1*s*,4*S*)-4-aminocyclohexyl)-5,5-bis(3,5-dibromobenzyl)pyrimidine-2,4,6(1*H*,3*H*,5*H*)-trione di-TFA salt (**18aA**)

Project AB_guest

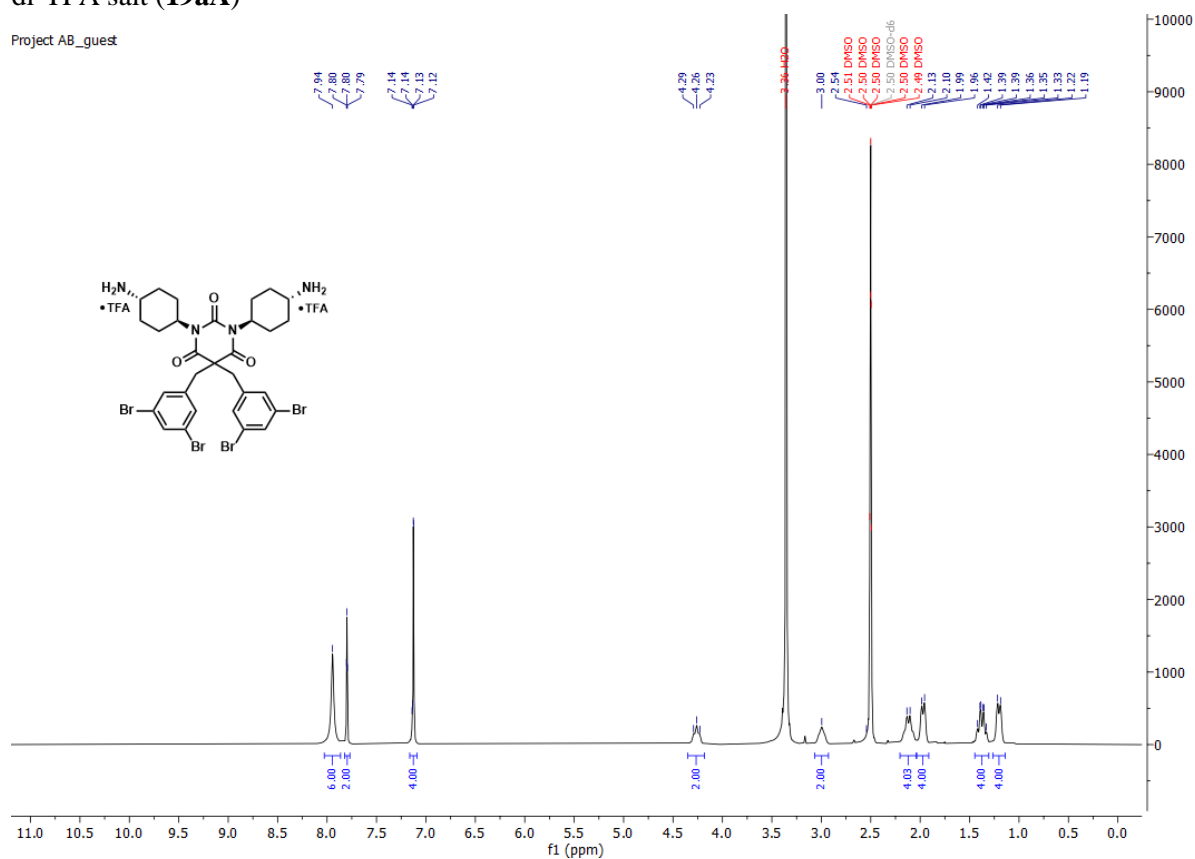


Project AB_guest

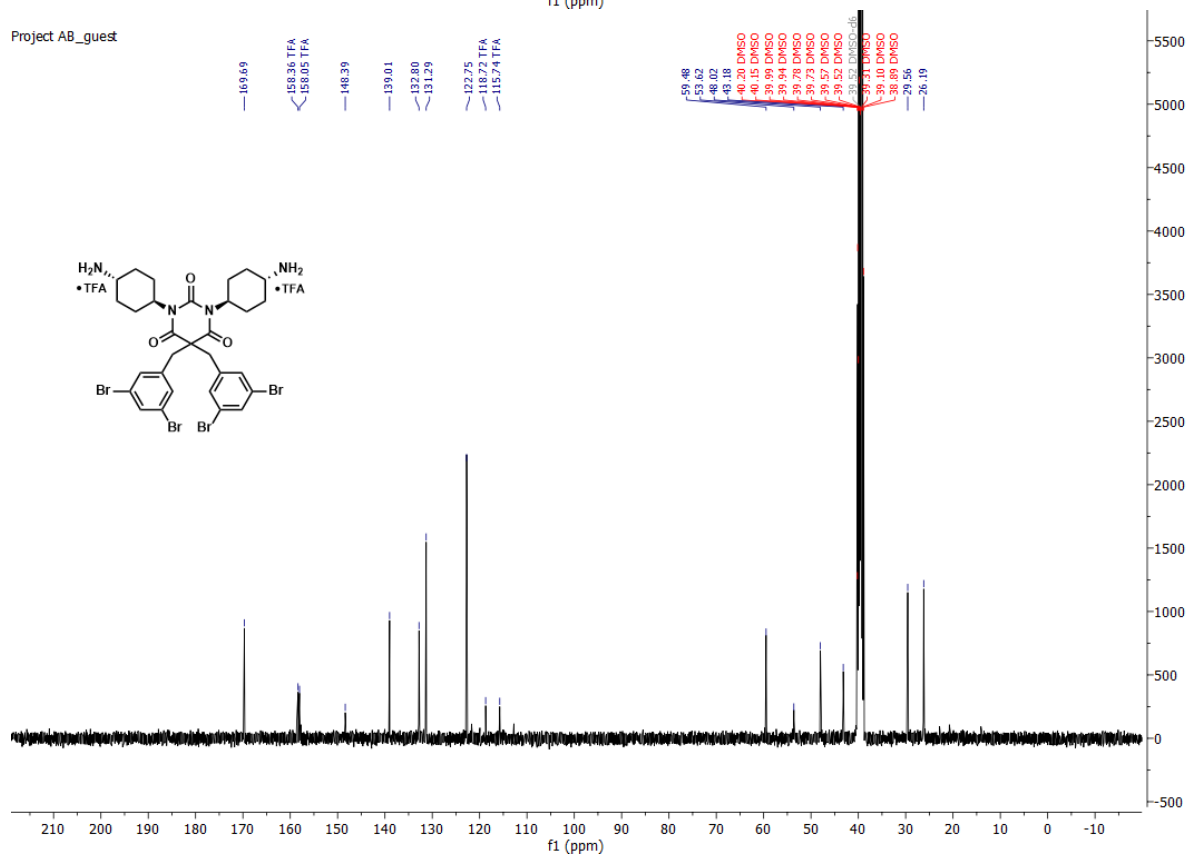


1,3-bis((1*r*,4*R*)-4-aminocyclohexyl)-5,5-bis(3,5-dibromobenzyl)pyrimidine-2,4,6(1*H*,3*H*,5*H*)-trione di-TFA salt (**19aA**)

Project AB_guest

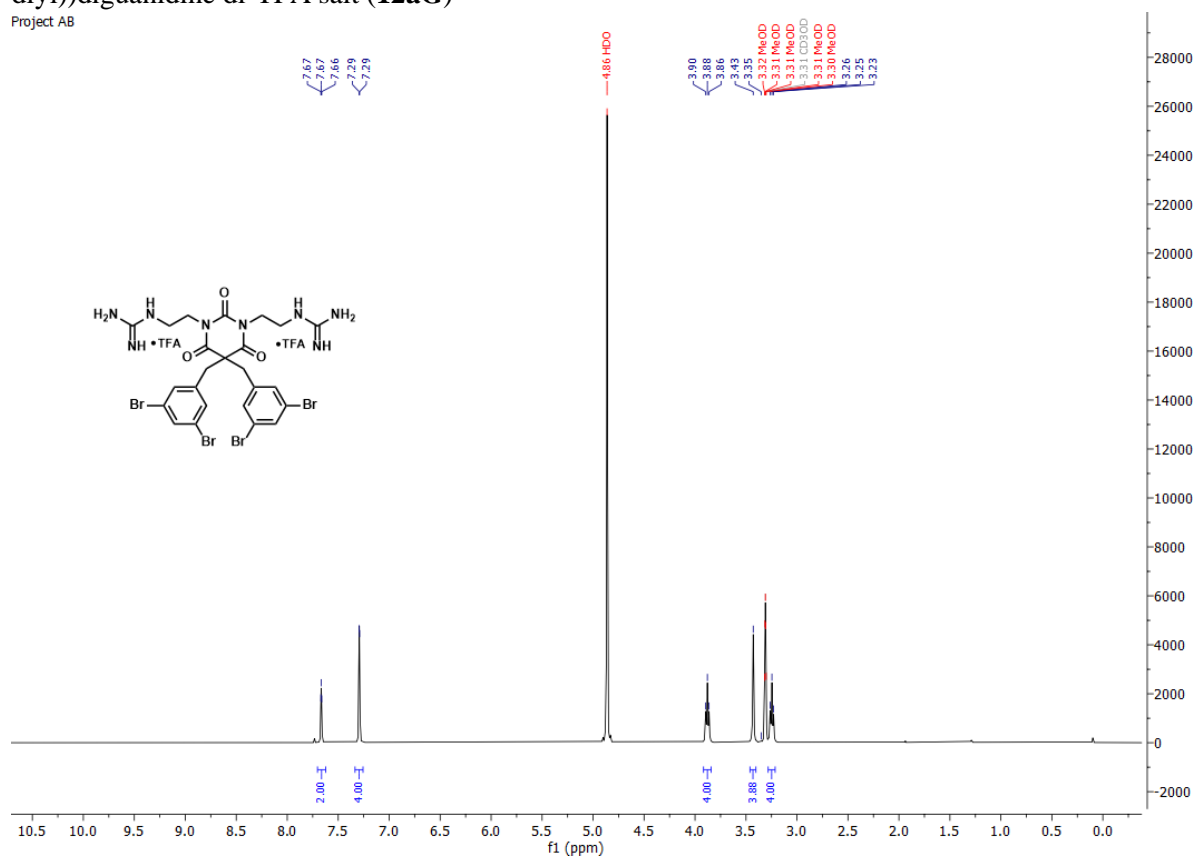


Project AB_guest

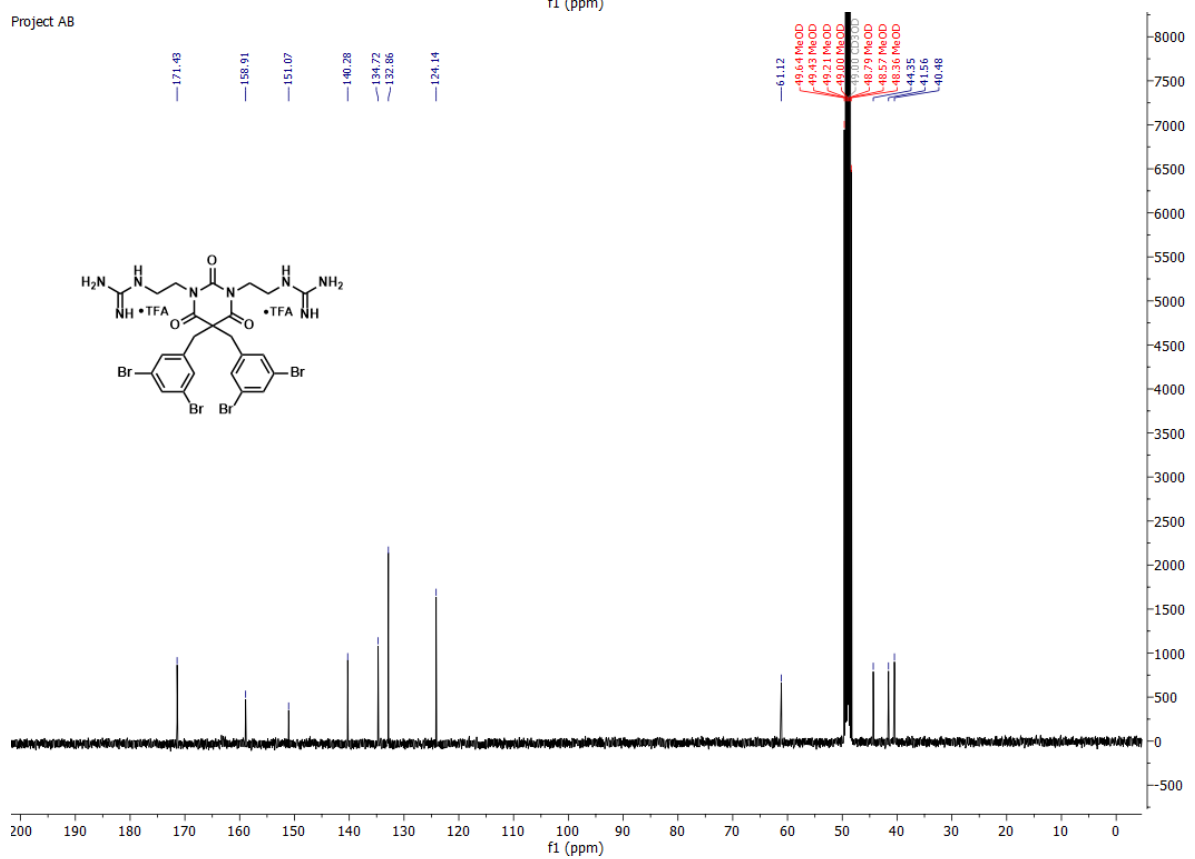


1,1'-((5,5-bis(3,5-dibromobenzyl)-2,4,6-trioxodihydropyrimidine-1,3(2*H*,4*H*)-diyl)bis(ethane-2,1-diyl))diguanidine di-TFA salt (**12aG**)

Project AB

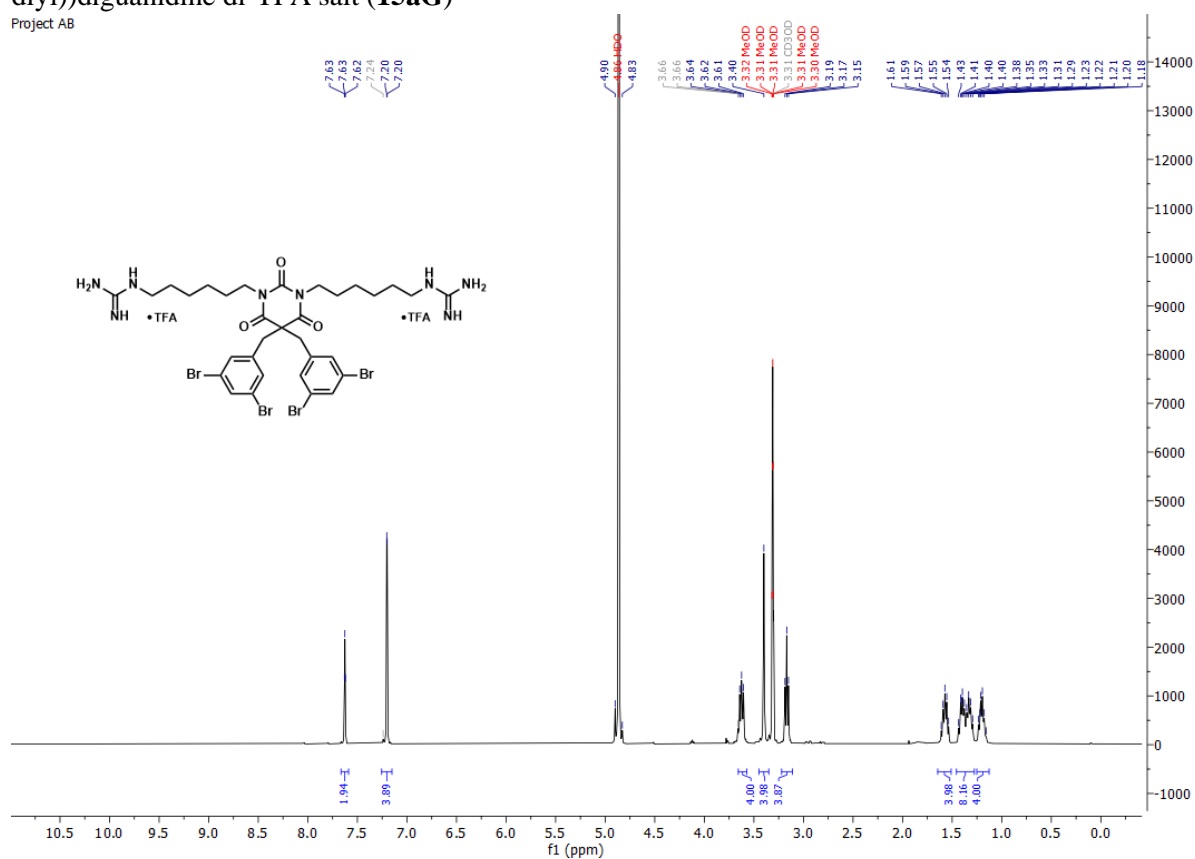


Project AB

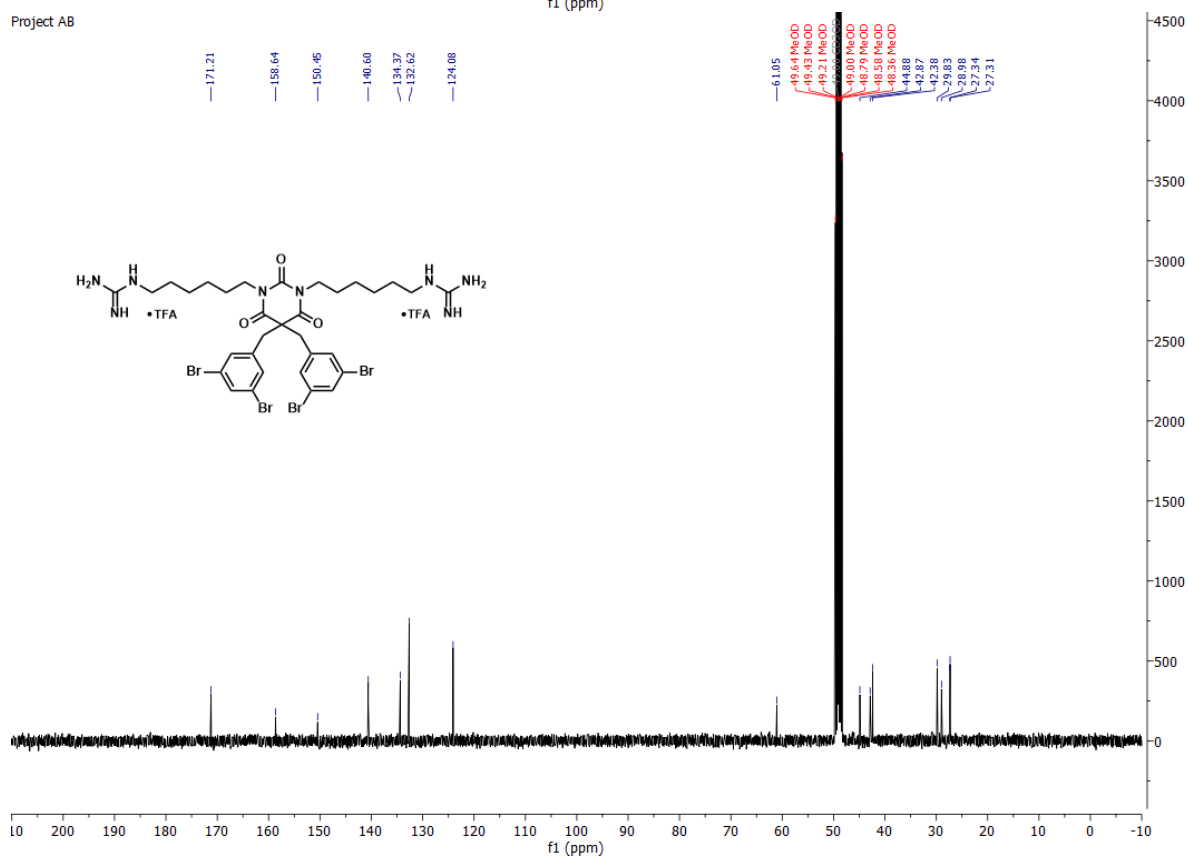


1,1'-((5,5-bis(3,5-dibromobenzyl)-2,4,6-trioxodihydropyrimidine-1,3(2H,4H)-diyl)bis(hexane-6,1-diy))diguanidine di-TFA salt (**15aG**)

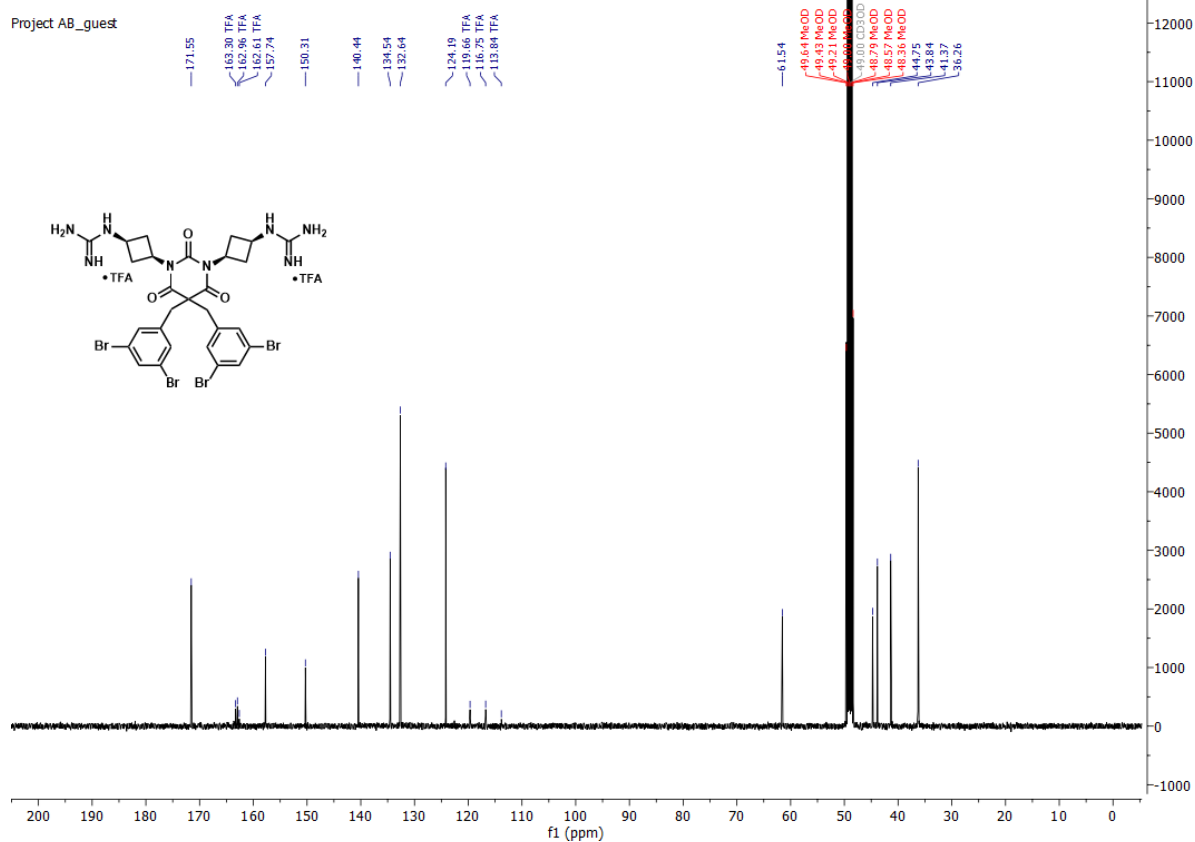
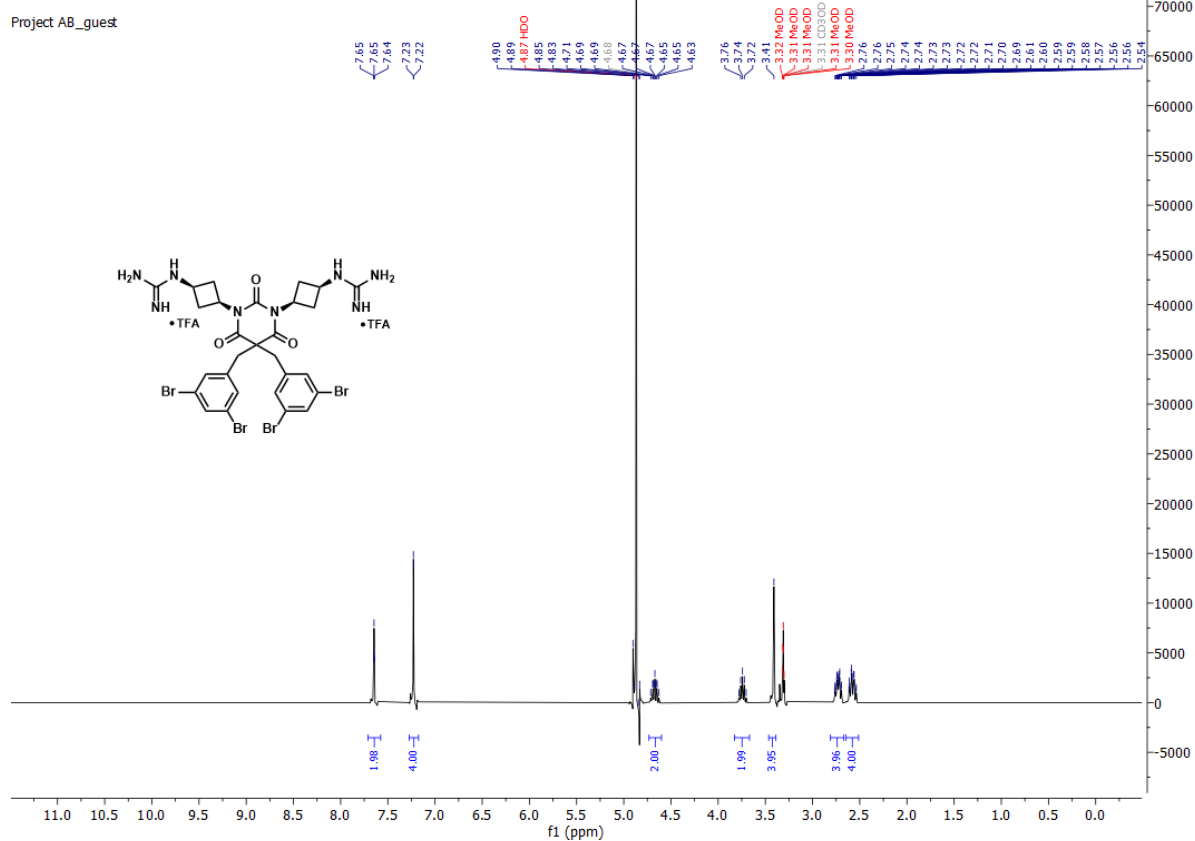
Project AB



Project AB

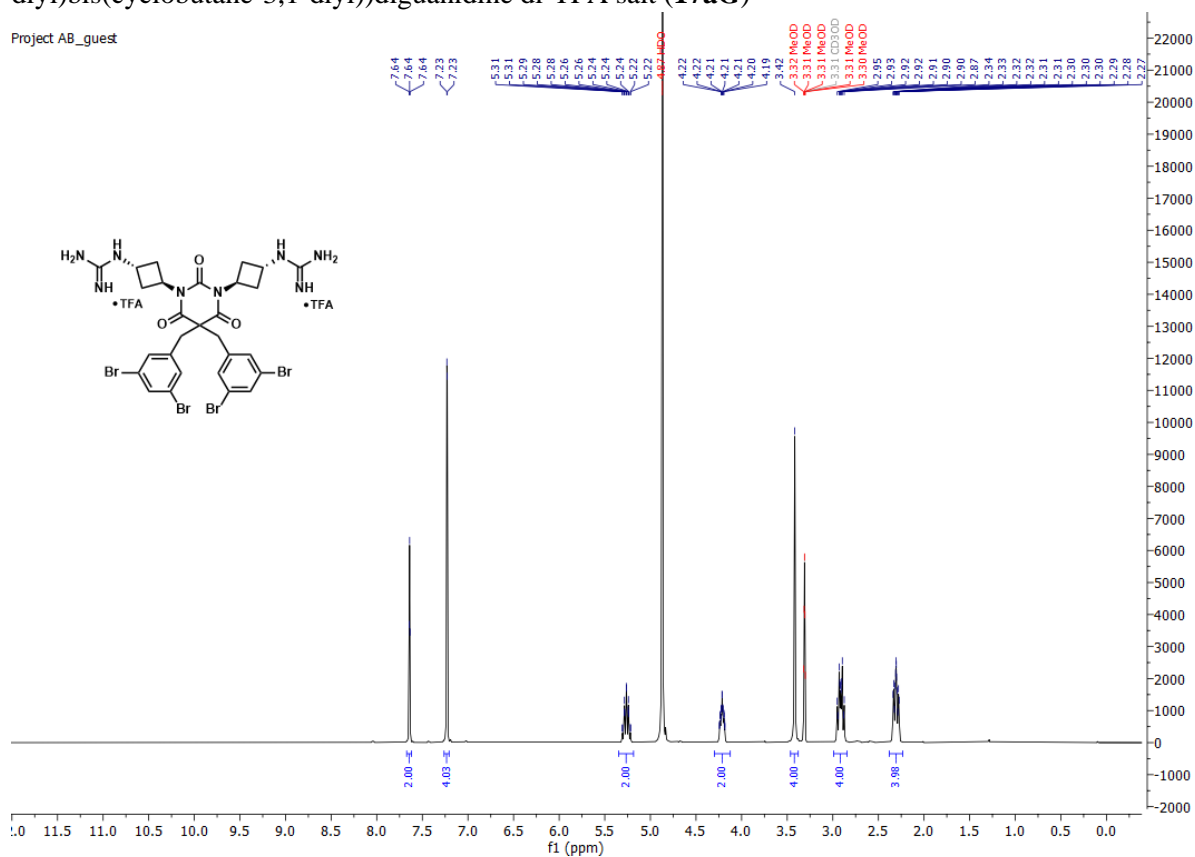


1,1'-((1*S*,1'*S*,3*s*,3'*s*)-(5,5-bis(3,5-dibromobenzyl)-2,4,6-trioxodihydropyrimidine-1,3(2*H*,4*H*)-diyl)bis(cyclobutane-3,1-diyl))diguanidine di-TFA salt (**16aG**)

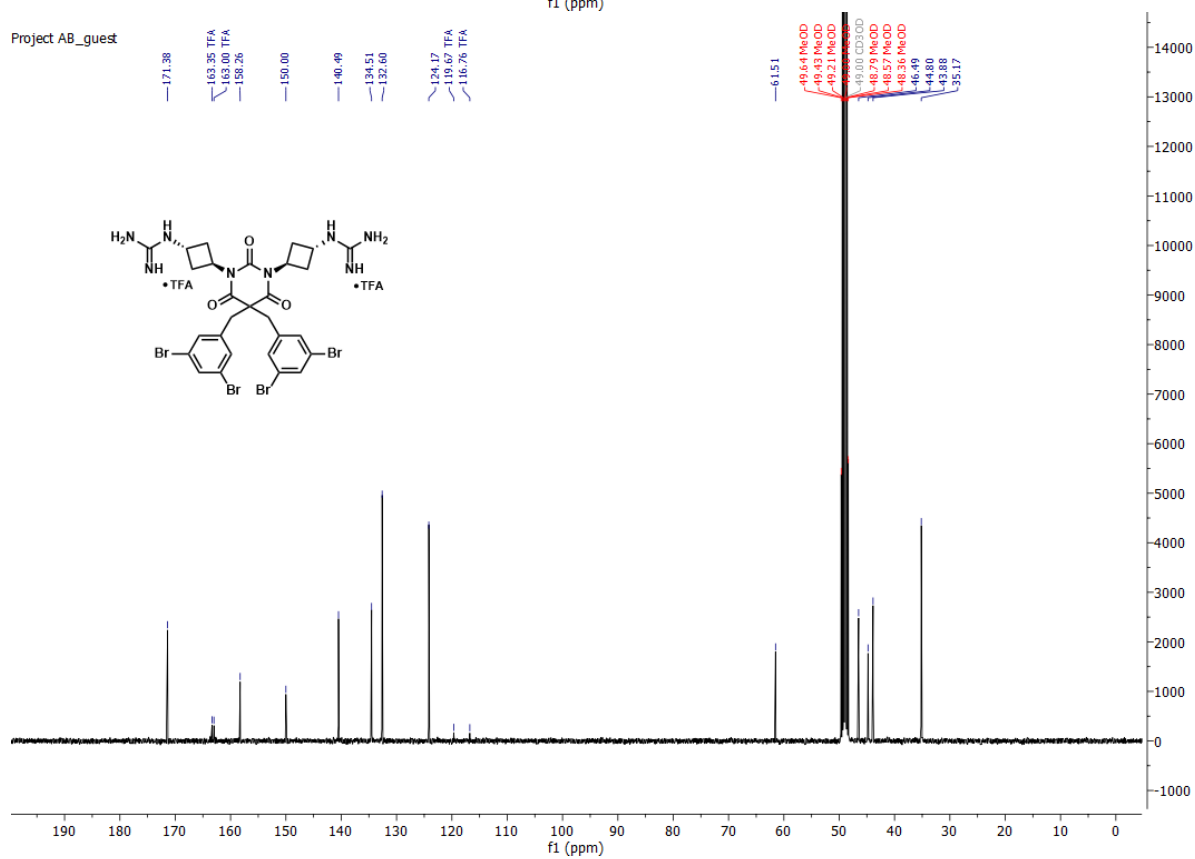


1,1'-((1*R*,1'*R*,3*r*,3'*r*)-(5,5-bis(3,5-dibromobenzyl)-2,4,6-trioxodihydropyrimidine-1,3(2*H*,4*H*)-diyl)bis(cyclobutane-3,1-diyl))diguanidine di-TFA salt (**17aG**)

Project AB_guest

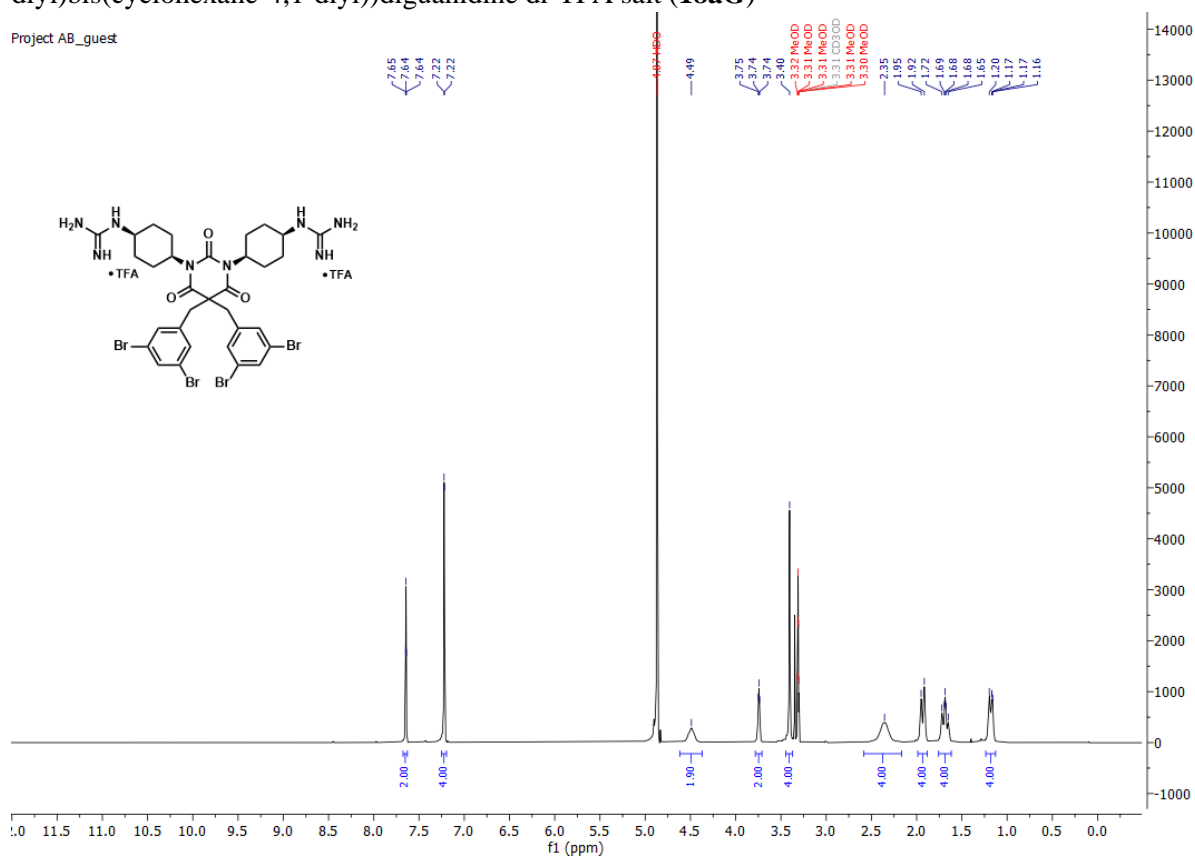


Project AB_guest

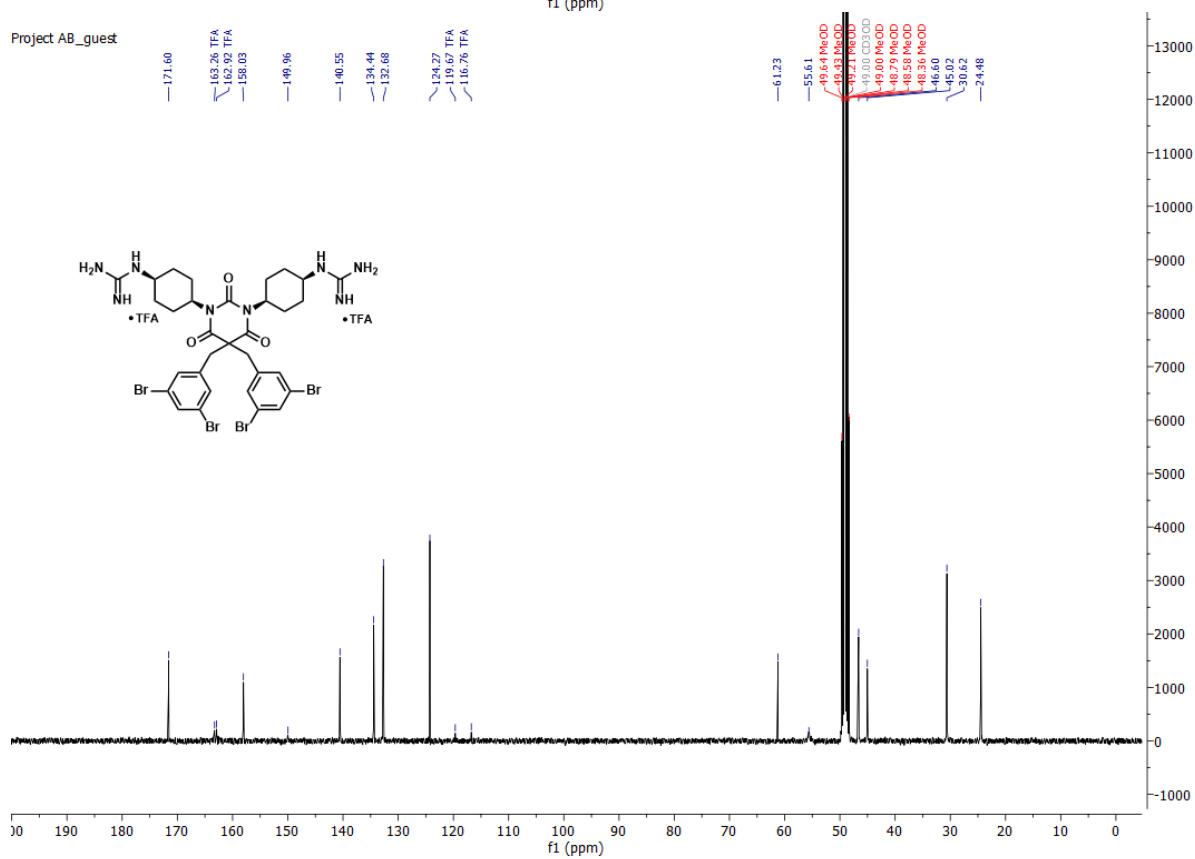


1,1'-((1*S*,1'*S*,4*s*,4'*s*)-(5,5-bis(3,5-dibromobenzyl)-2,4,6-trioxodihydropyrimidine-1,3(2*H*,4*H*)-diyl)bis(cyclohexane-4,1-diyl))diguanidine di-TFA salt (**18aG**)

Project AB_guest



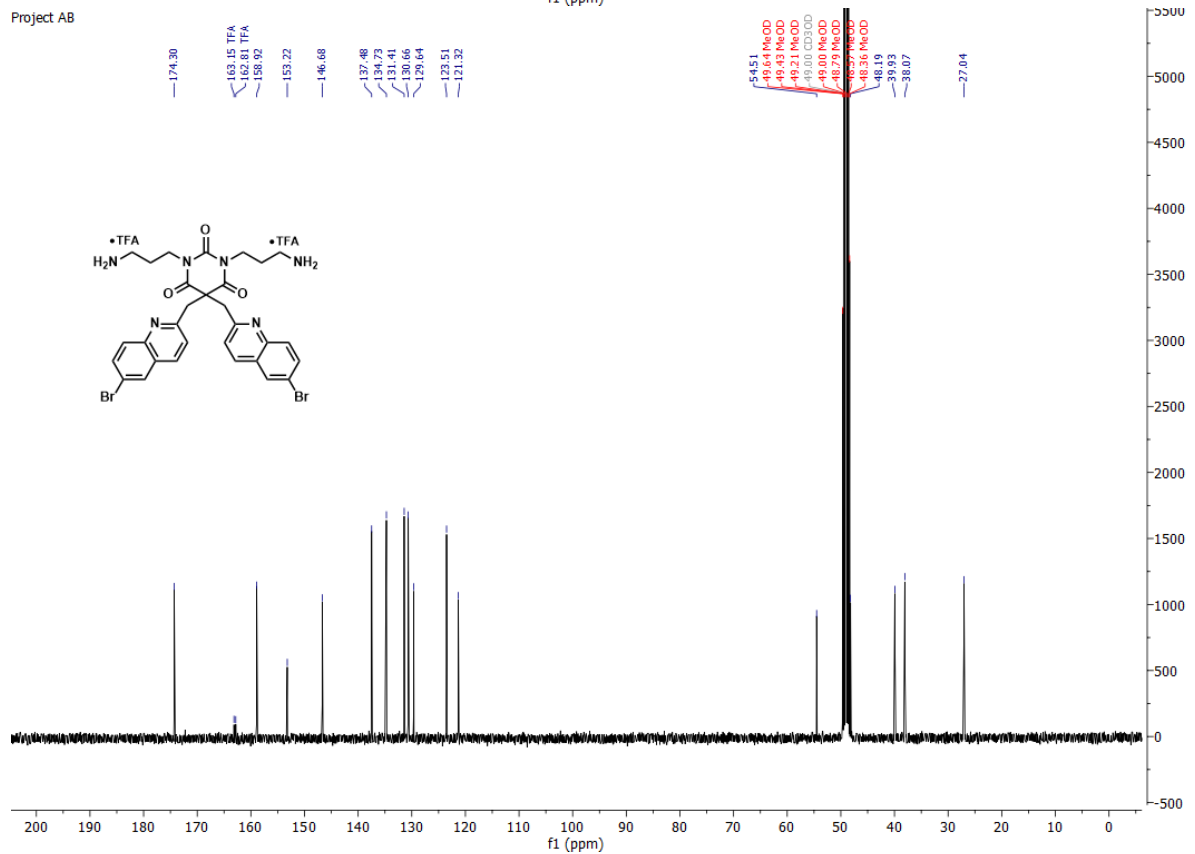
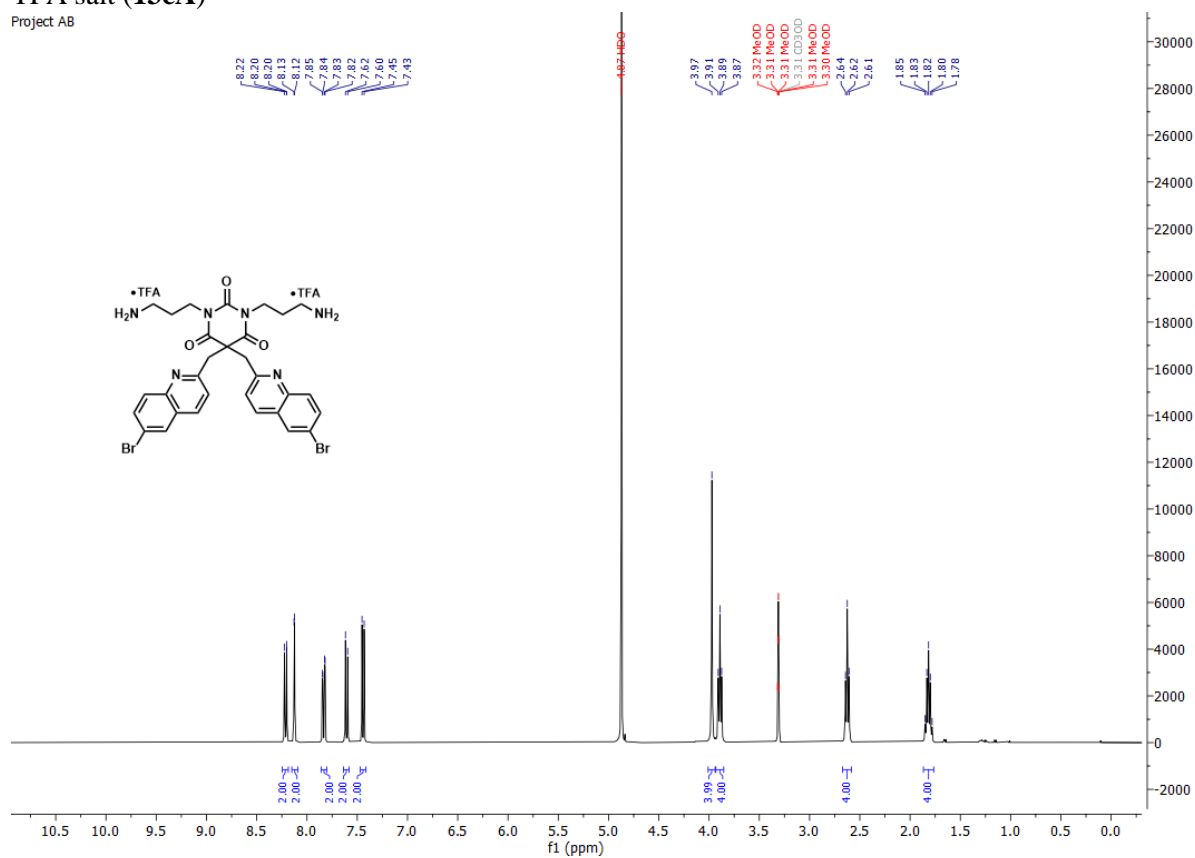
Project AB_guest



3.5 ^1H and ^{13}C NMR spectra of compounds in series 5

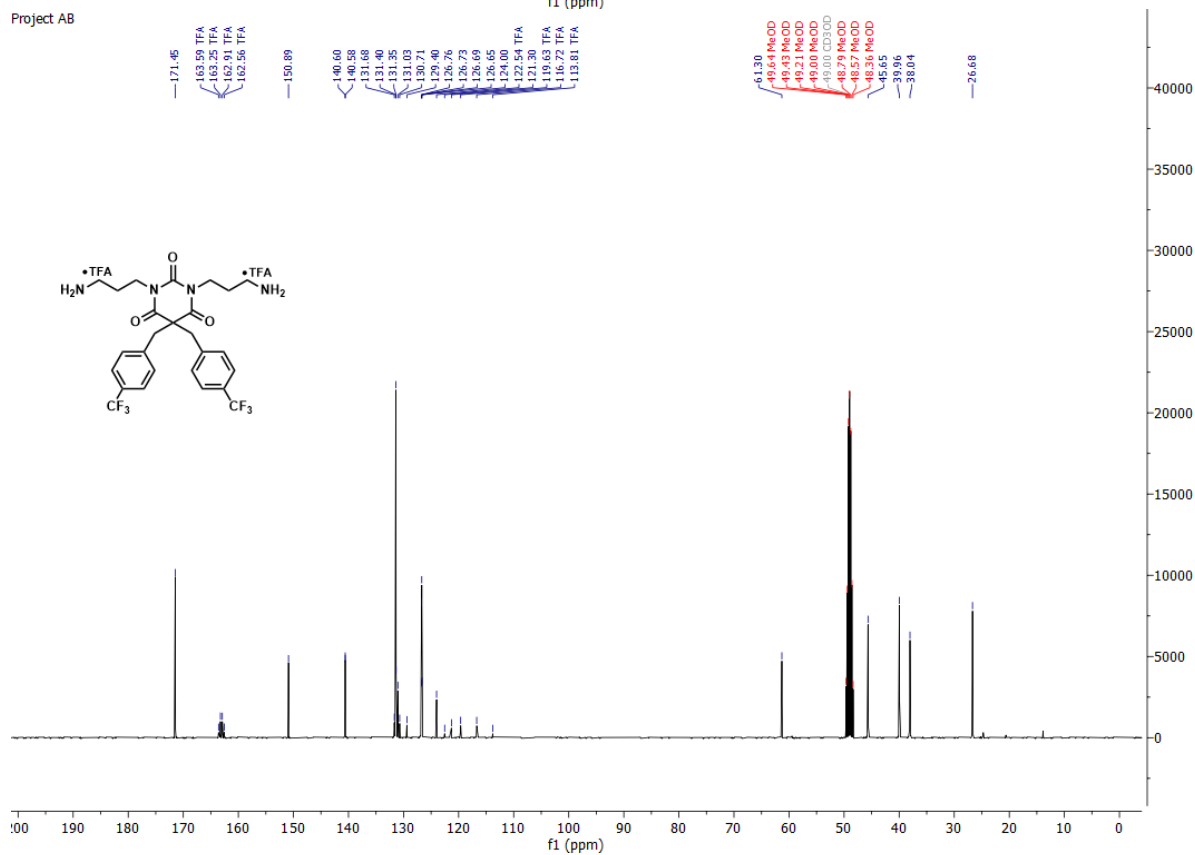
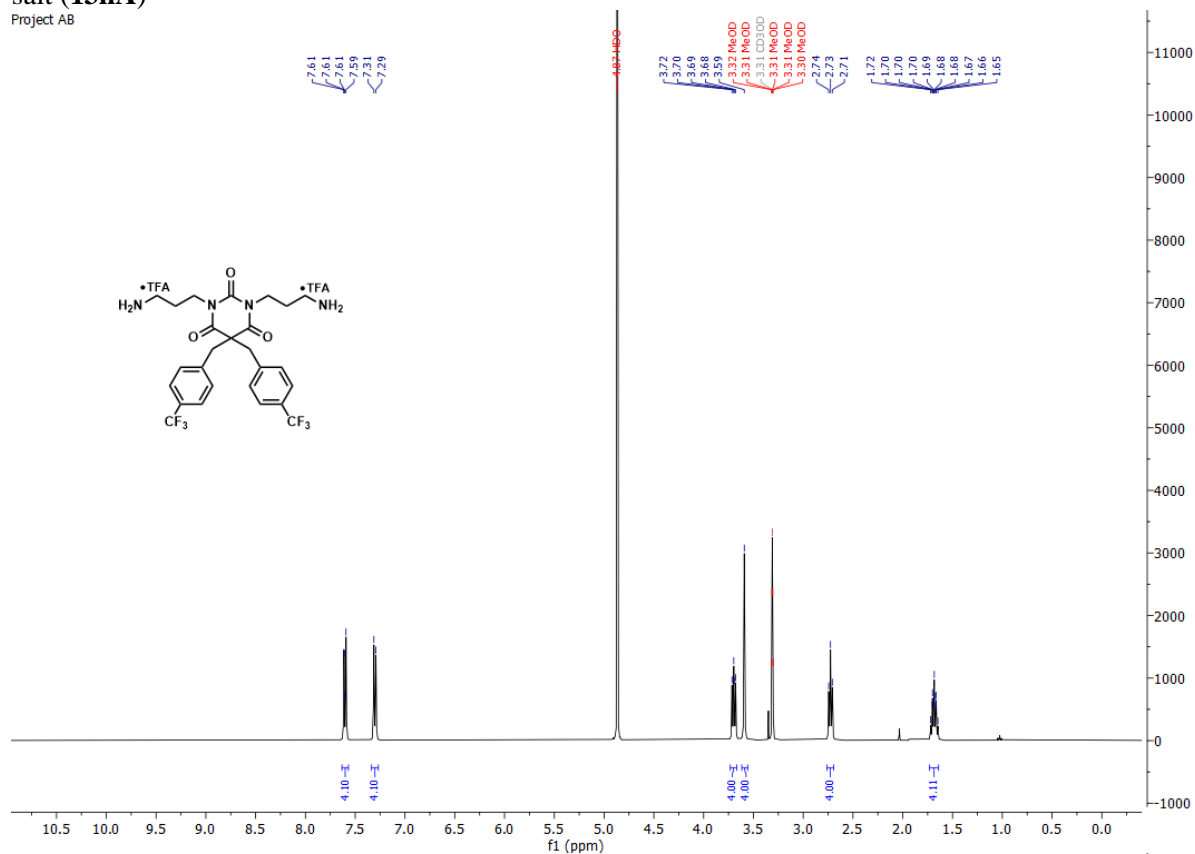
1,3-bis(3-aminopropyl)-5,5-bis((6-bromoquinolin-2-yl)methyl)pyrimidine-2,4,6(1*H*,3*H*,5*H*)-trione di-TFA salt (**13cA**)

Project AB



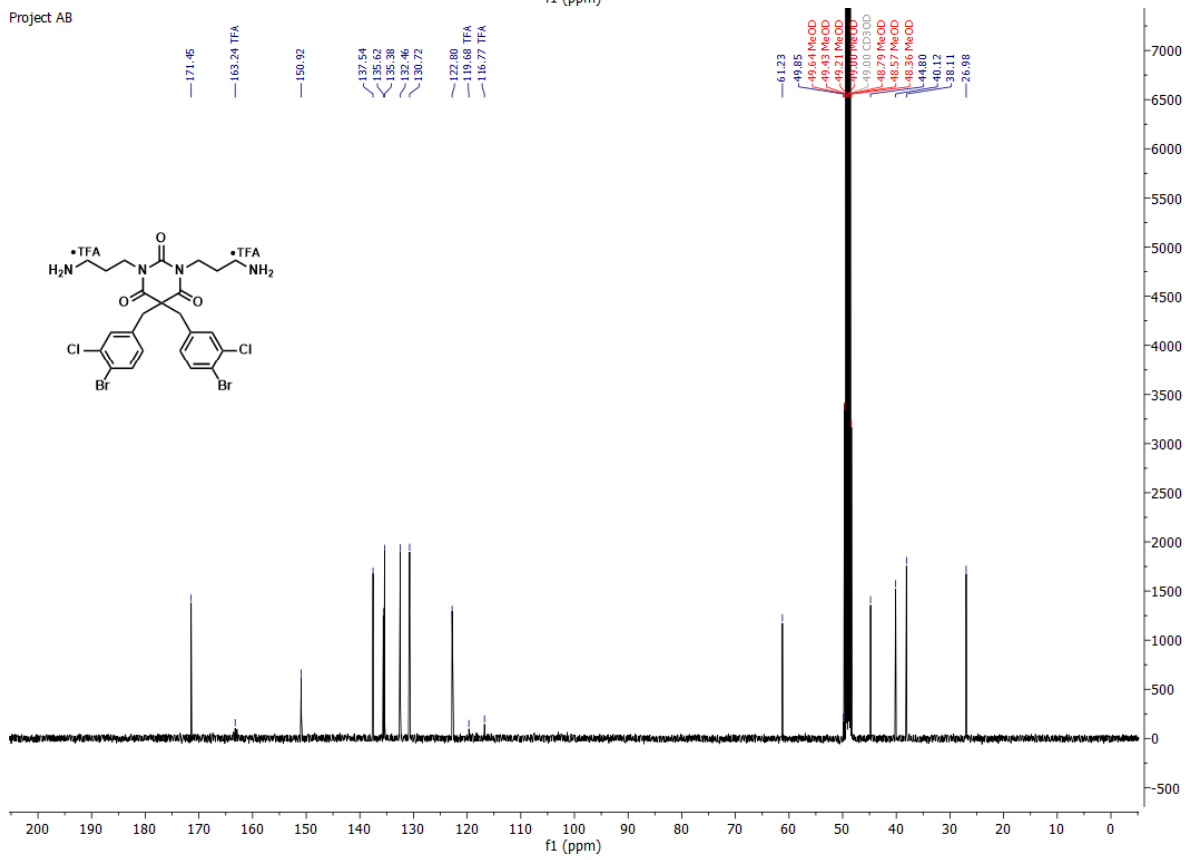
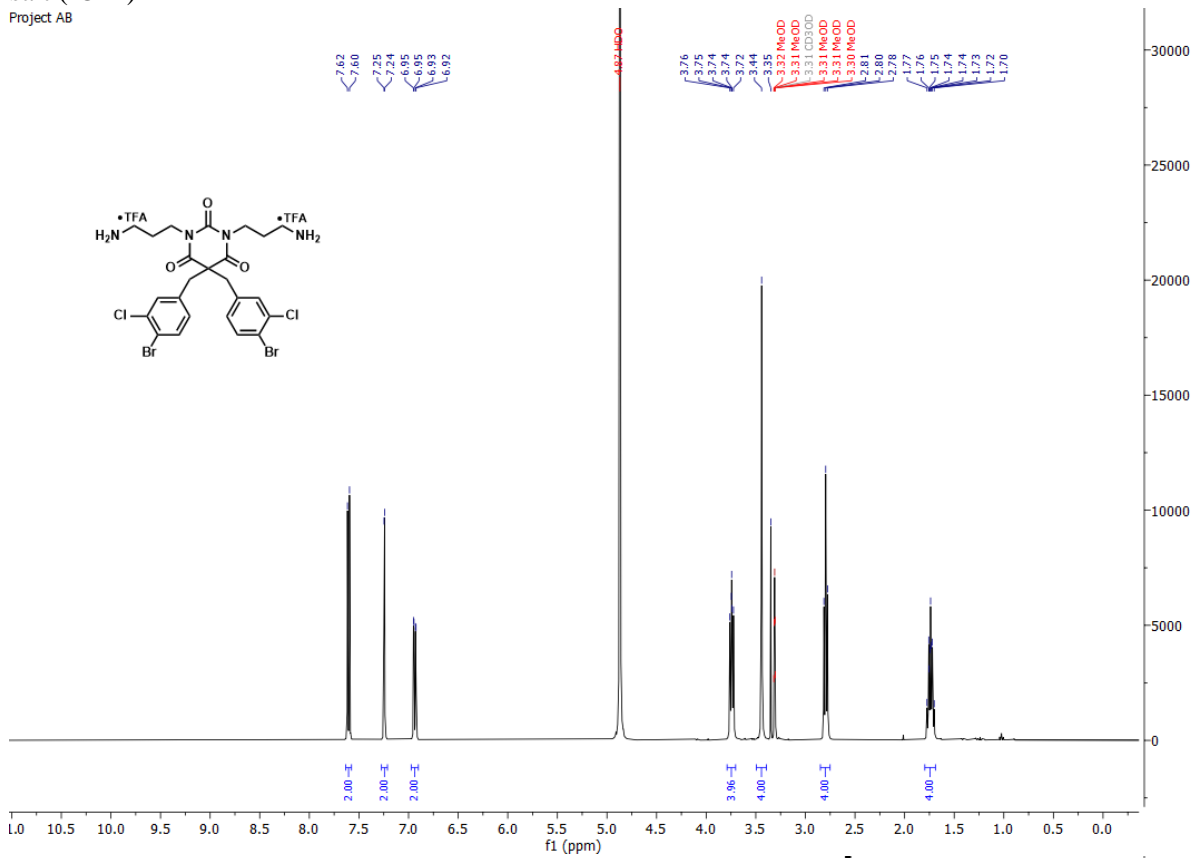
1,3-bis(3-aminopropyl)-5,5-bis(4-(trifluoromethyl)benzyl)pyrimidine-2,4,6(1*H*,3*H*,5*H*)-trione di-TFA salt (**13hA**)

Project AB



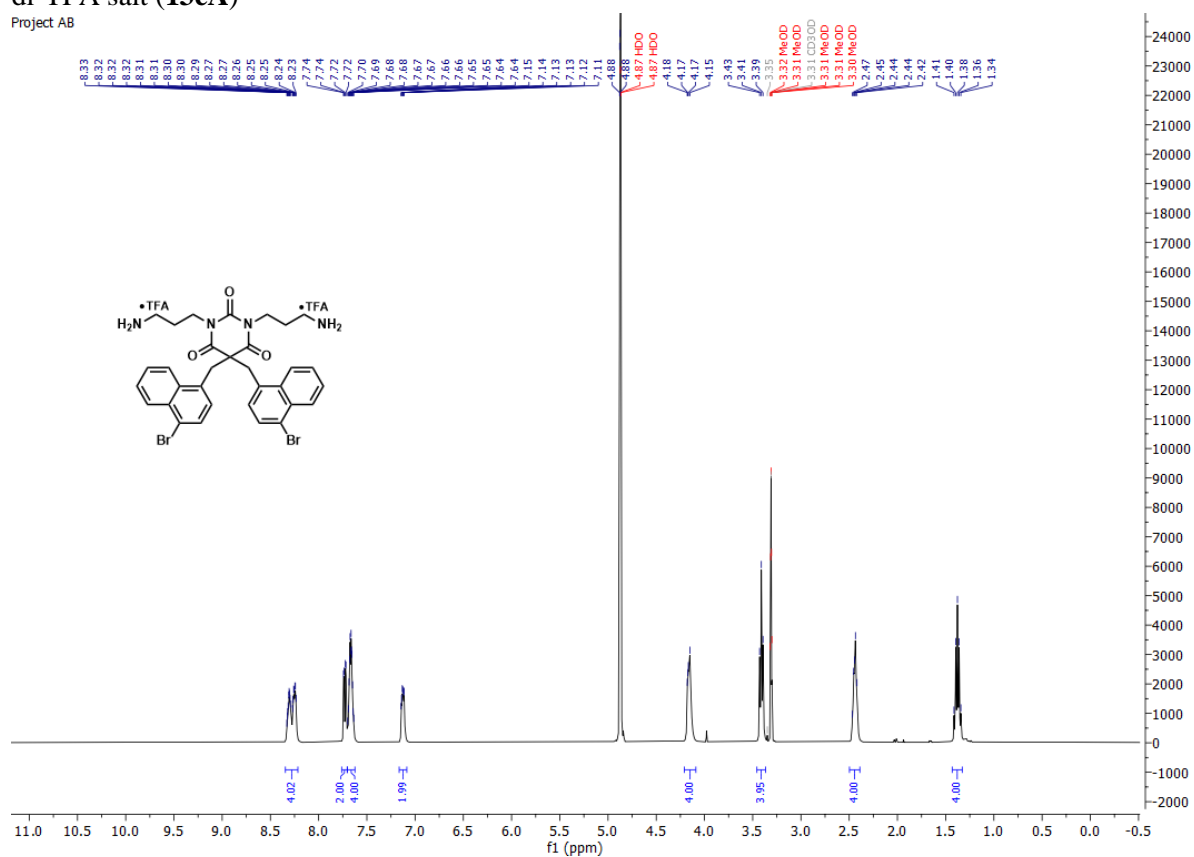
1,3-bis(3-aminopropyl)-5,5-bis(4-bromo-3-chlorobenzyl)pyrimidine-2,4,6(1*H*,3*H*,5*H*)-trione di-TFA salt (**13iA**)

Project AB

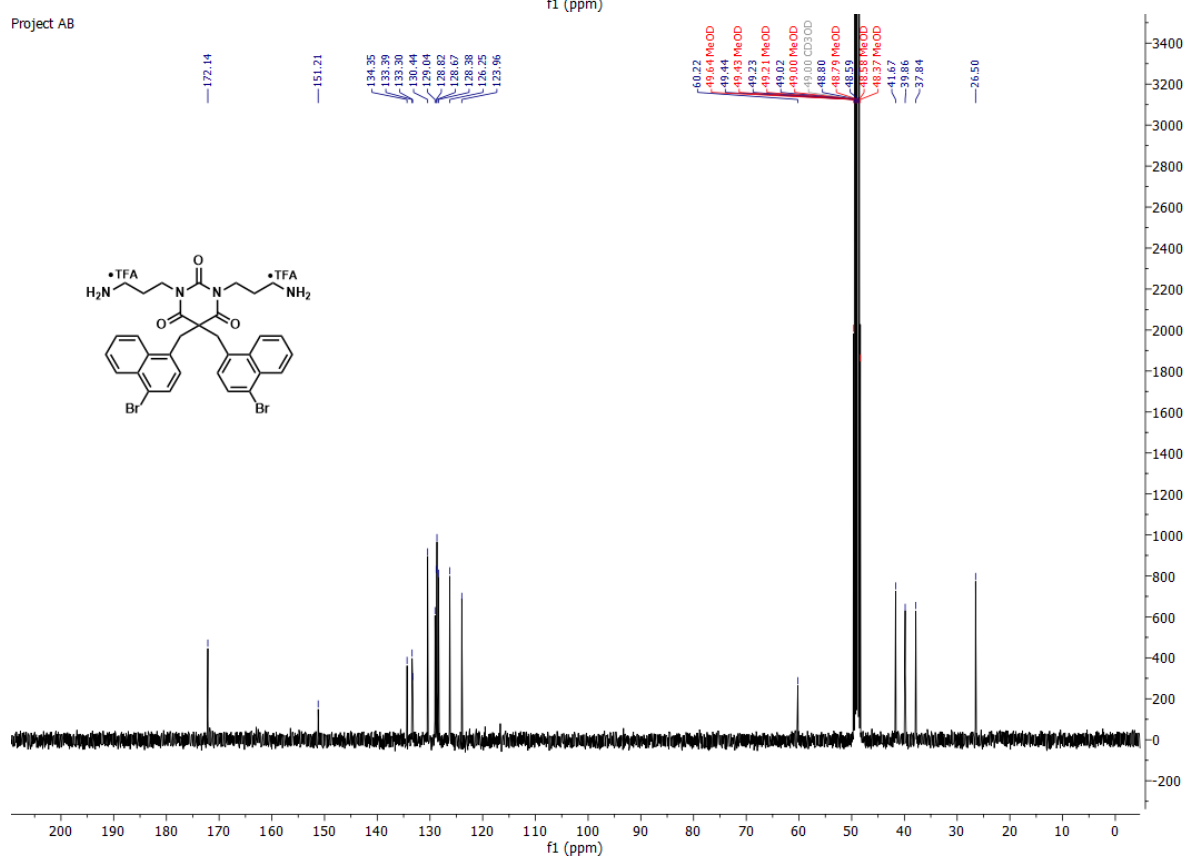


1,3-bis(3-aminopropyl)-5,5-bis((4-bromonaphthalen-1-yl)methyl)pyrimidine-2,4,6(1*H*,3*H*,5*H*)-trione di-TFA salt (**13eA**)

Project AB

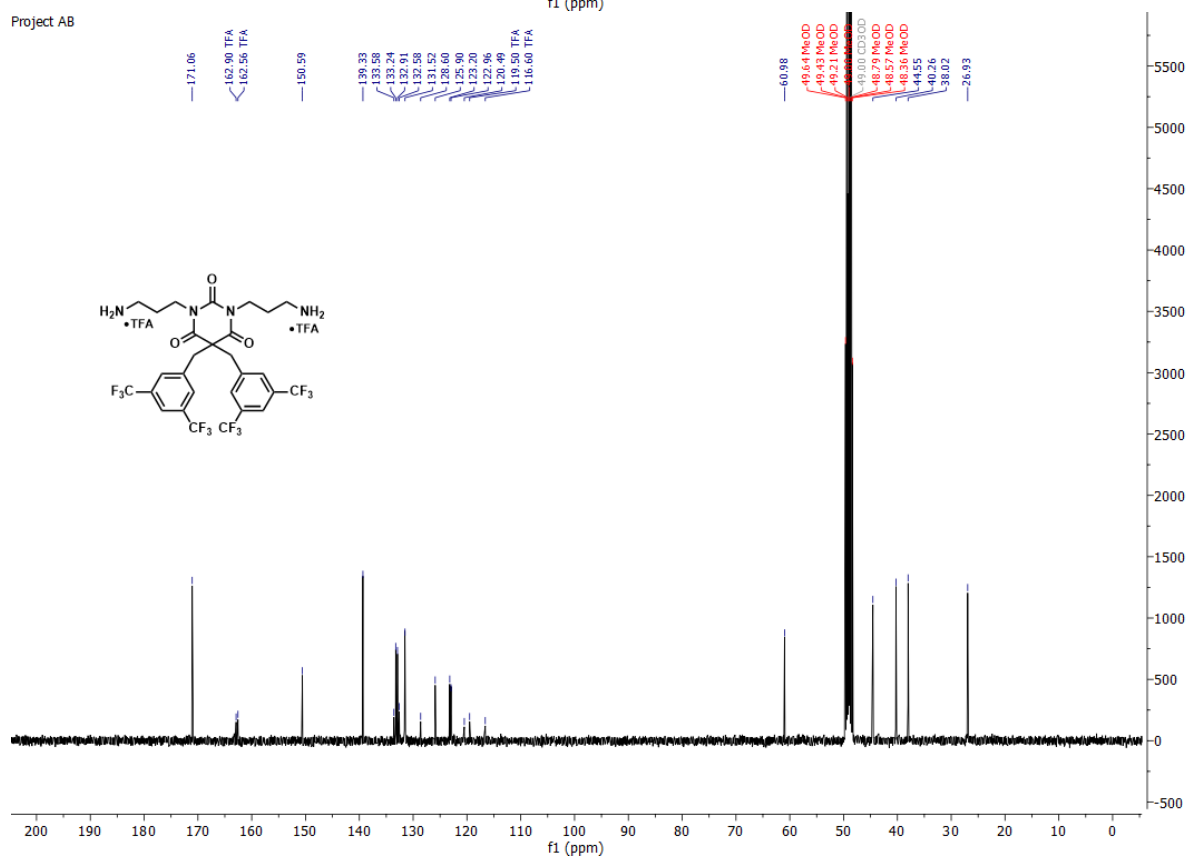
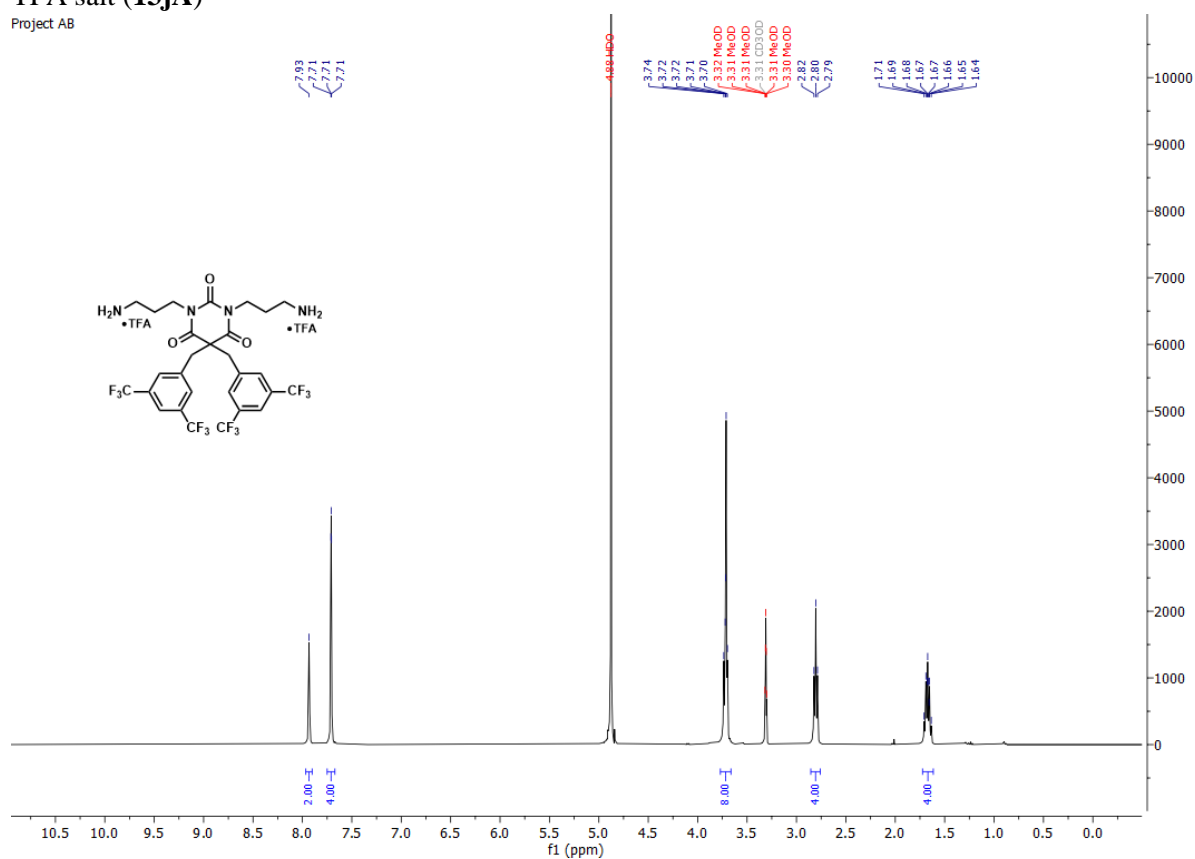


Project AB



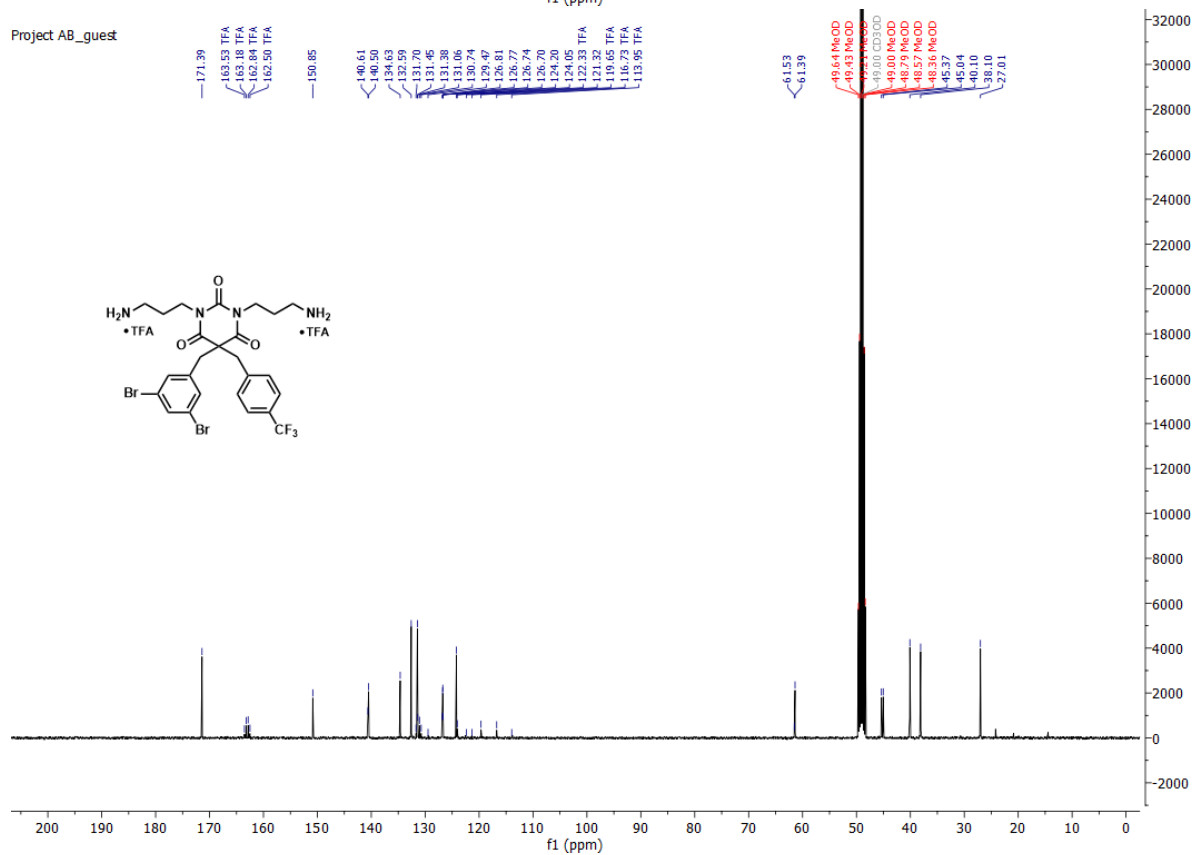
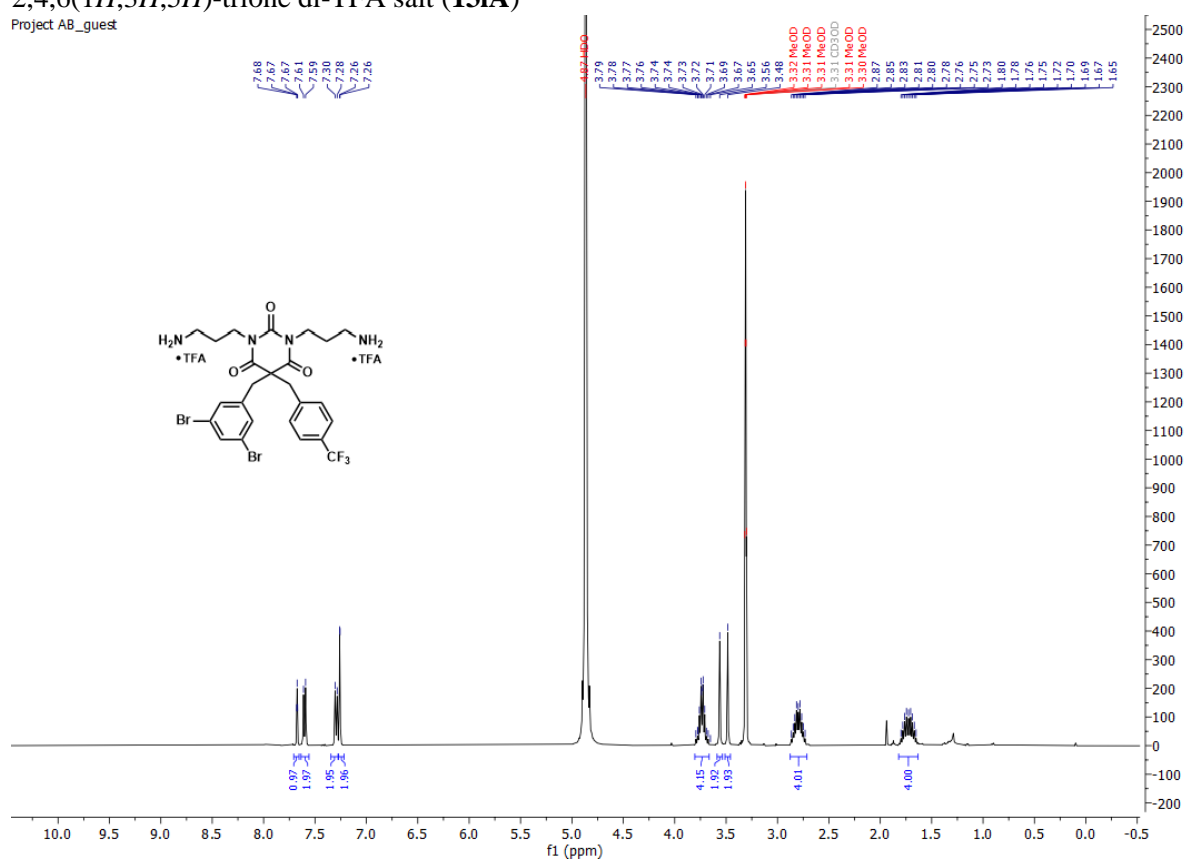
1,3-bis(3-aminopropyl)-5,5-bis(3,5-bis(trifluoromethyl)benzyl)pyrimidine-2,4,6(1*H*,3*H*,5*H*)-trione di-TFA salt (**13jA**)

Project AB



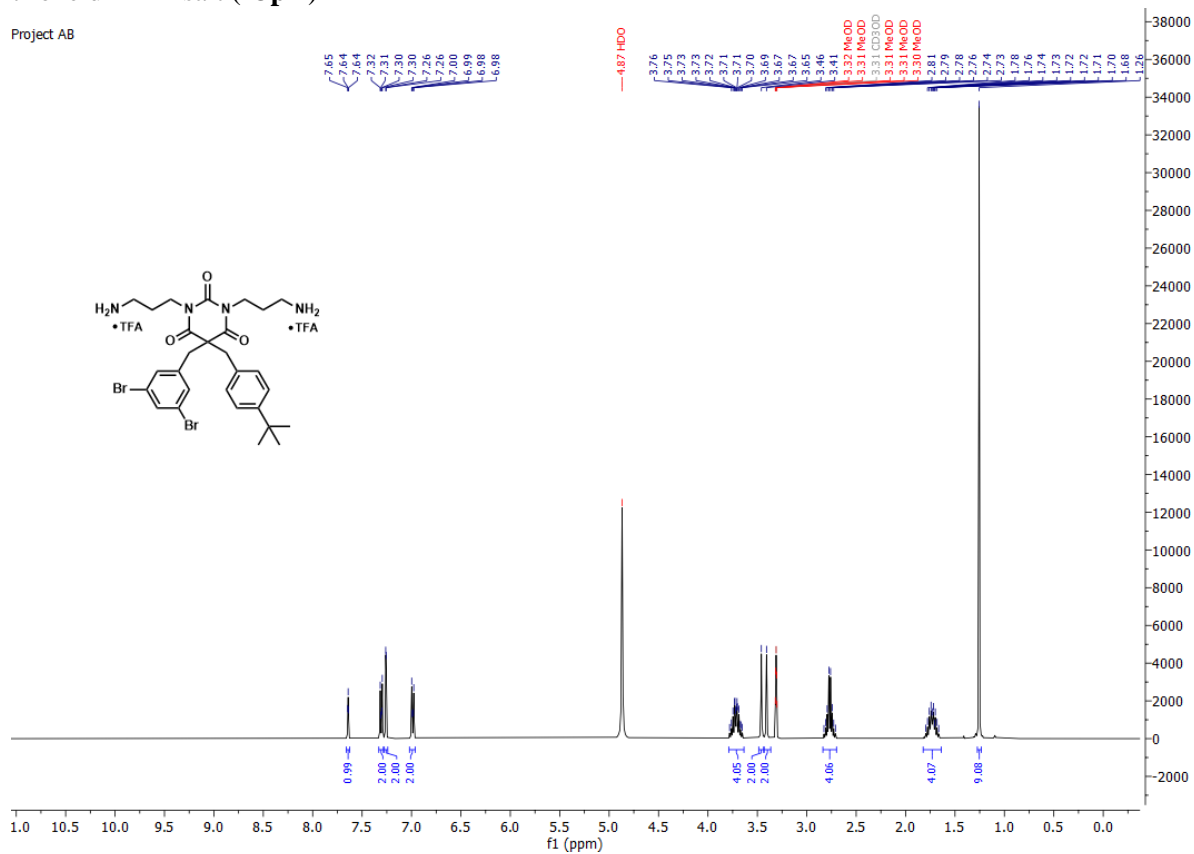
1,3-bis(3-aminopropyl)-5-(3,5-dibromobenzyl)-5-(4-(trifluoromethyl)benzyl)pyrimidine-2,4,6(1*H*,3*H*,5*H*)-trione di-TFA salt (**13IA**)

Project AB_guest

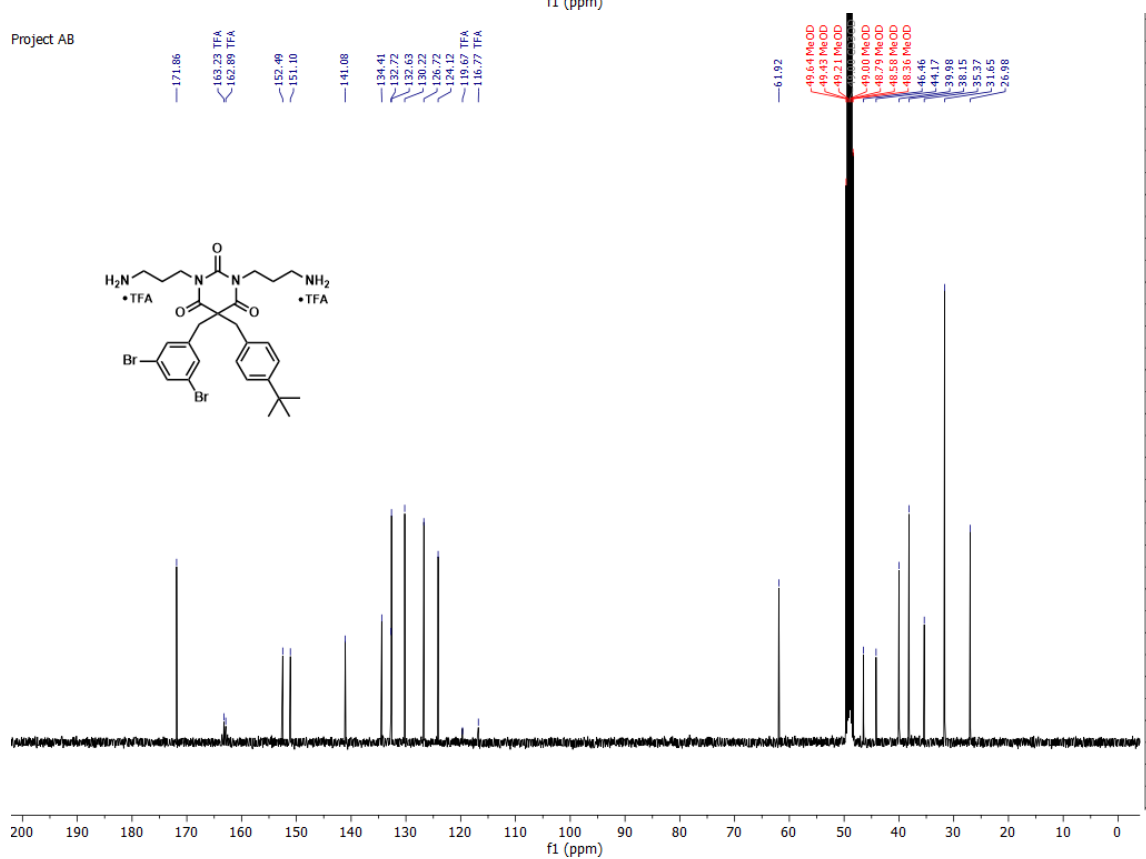


1,3-bis(3-aminopropyl)-5-(4-(*tert*-butyl)benzyl)-5-(3,5-dibromobenzyl)pyrimidine-2,4,6(1*H*,3*H*,5*H*)-trione di-TFA salt (**13pA**)

Project AB

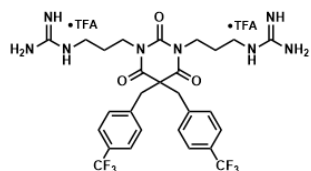
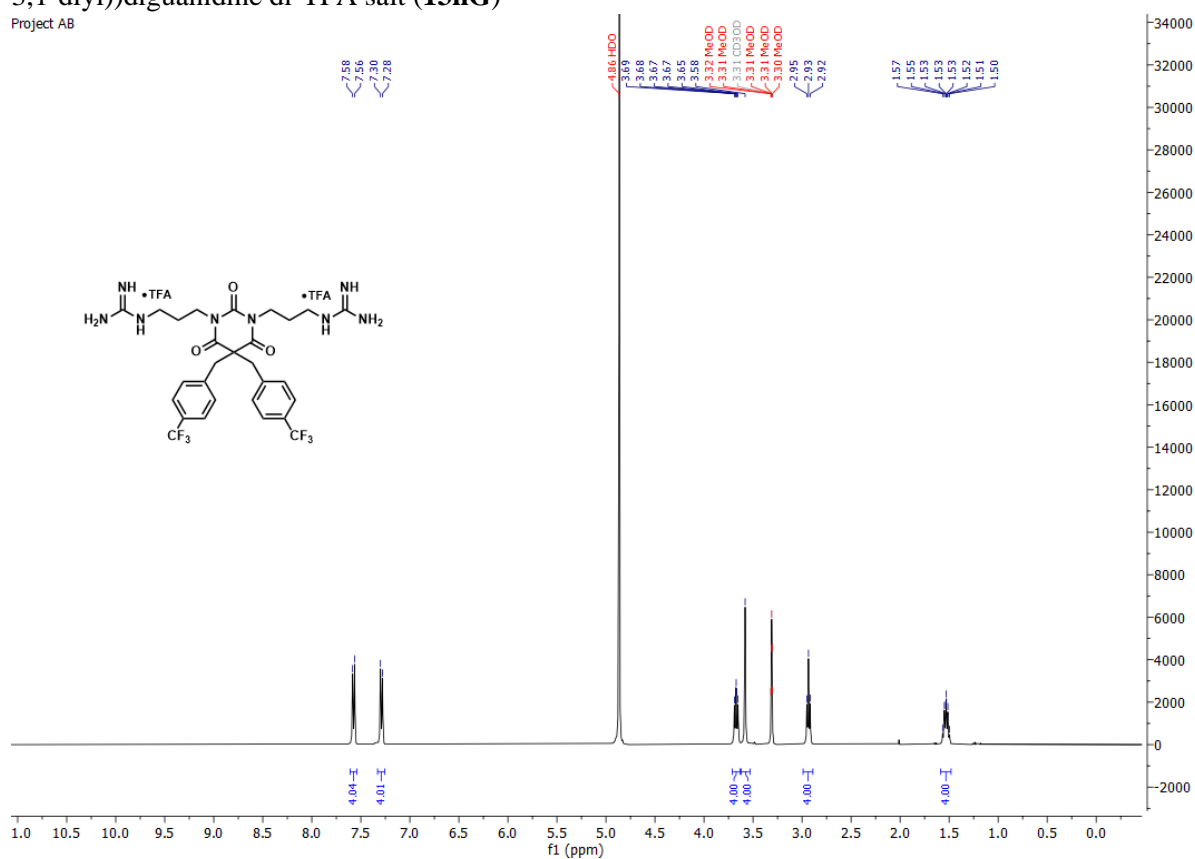


Project AB

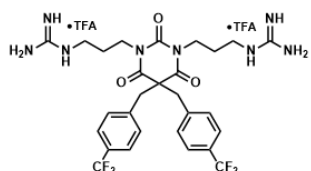
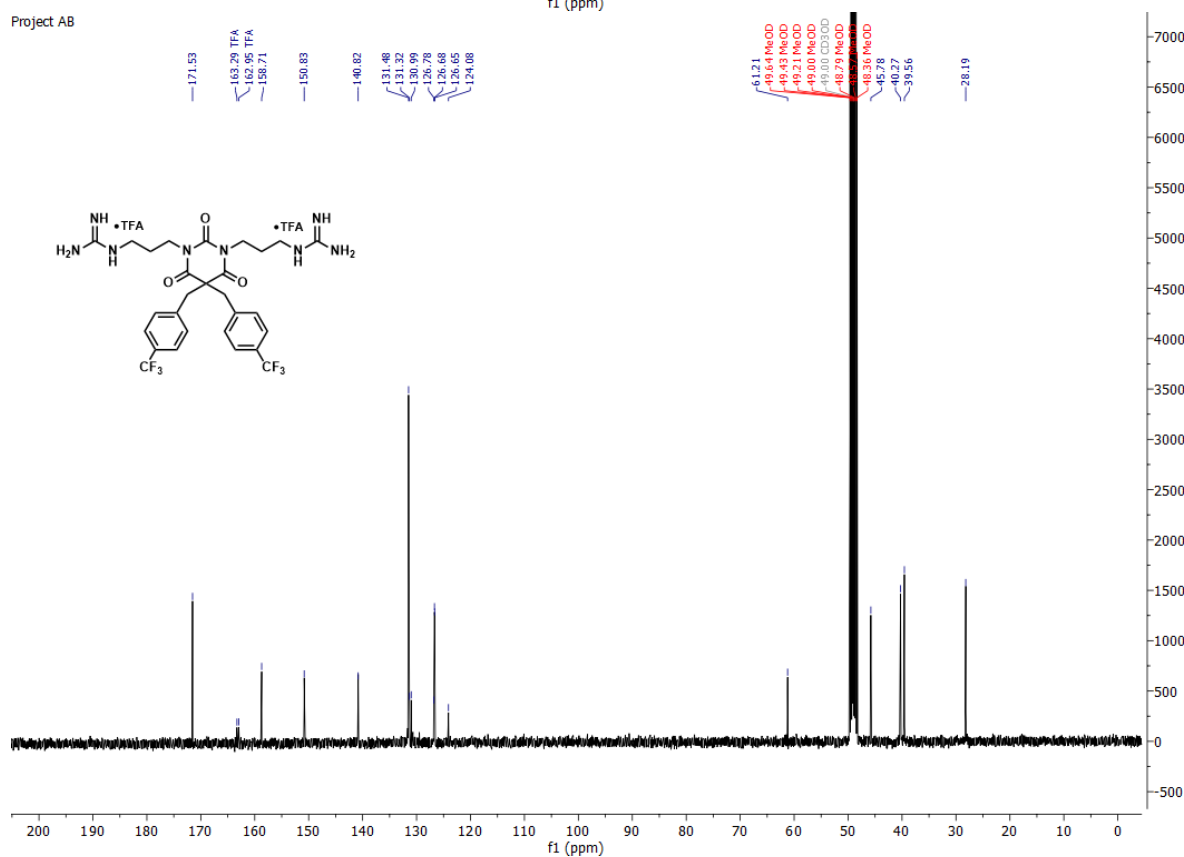


1,1'-((2,4,6-trioxo-5,5-bis(4-(trifluoromethyl)benzyl)dihydropyrimidine-1,3(2H,4H)-diyl)bis(propane-3,1-diyl))diguanidine di-TFA salt (**13hG**)

Project AB

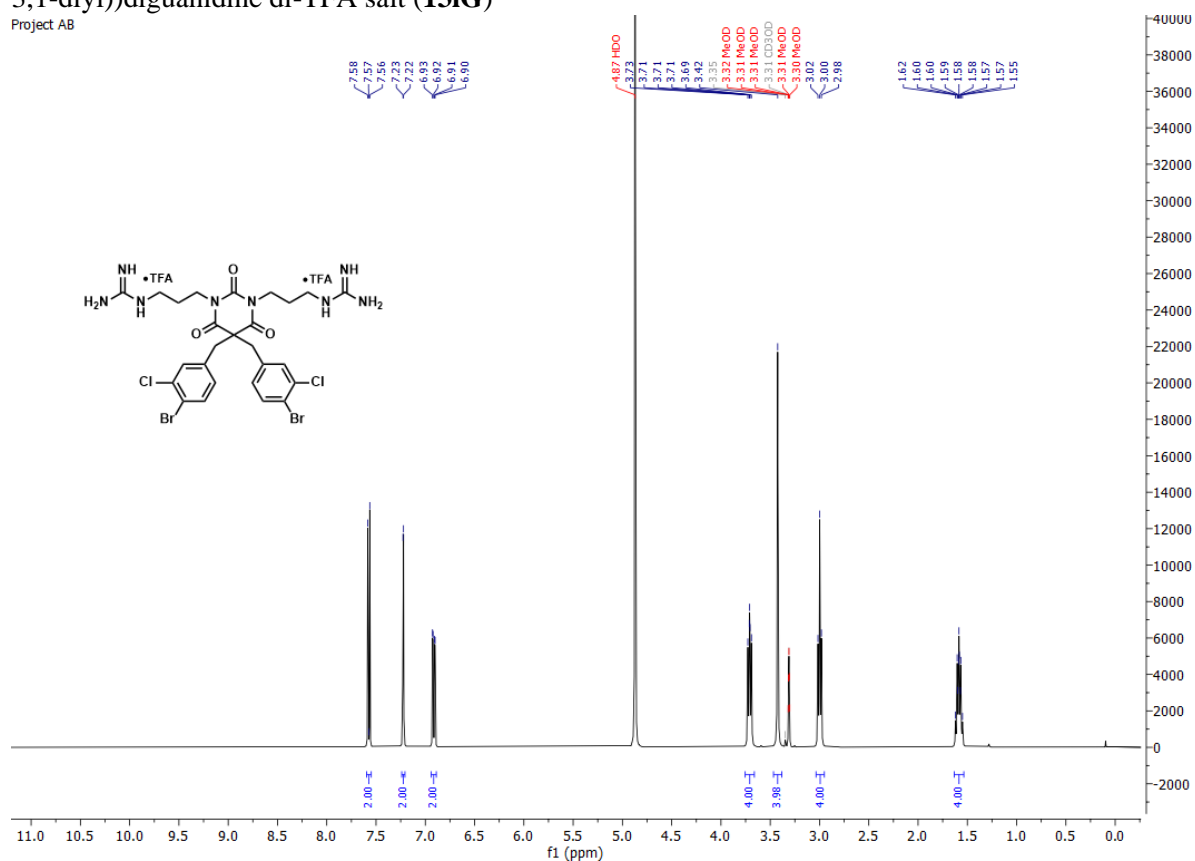


Project AB

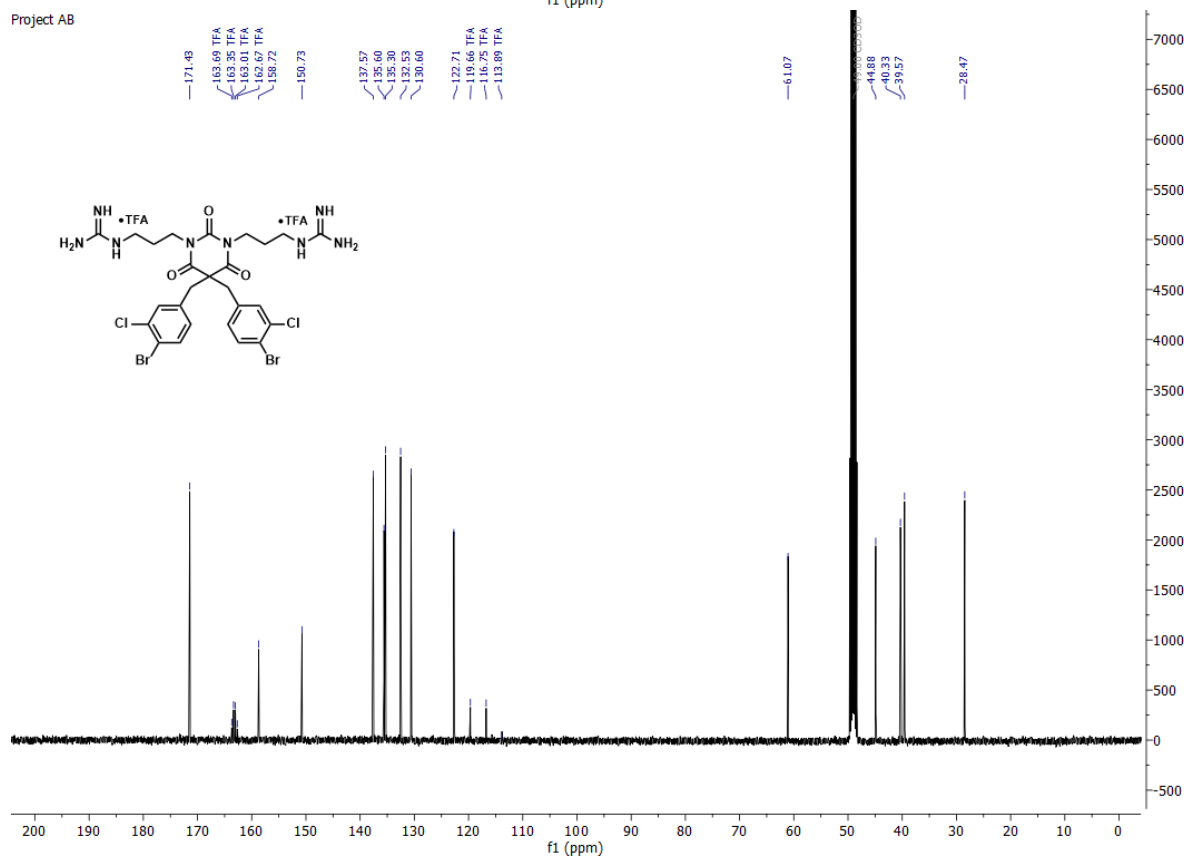


1,1'-((5,5-bis(4-bromo-3-chlorobenzyl)-2,4,6-trioxodihydropyrimidine-1,3(2*H*,4*H*)-diyl)bis(propane-3,1-diyl))diguanidine di-TFA salt (**13iG**)

Project AB

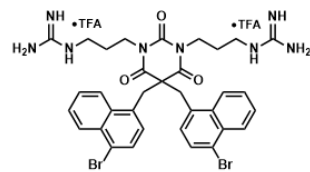
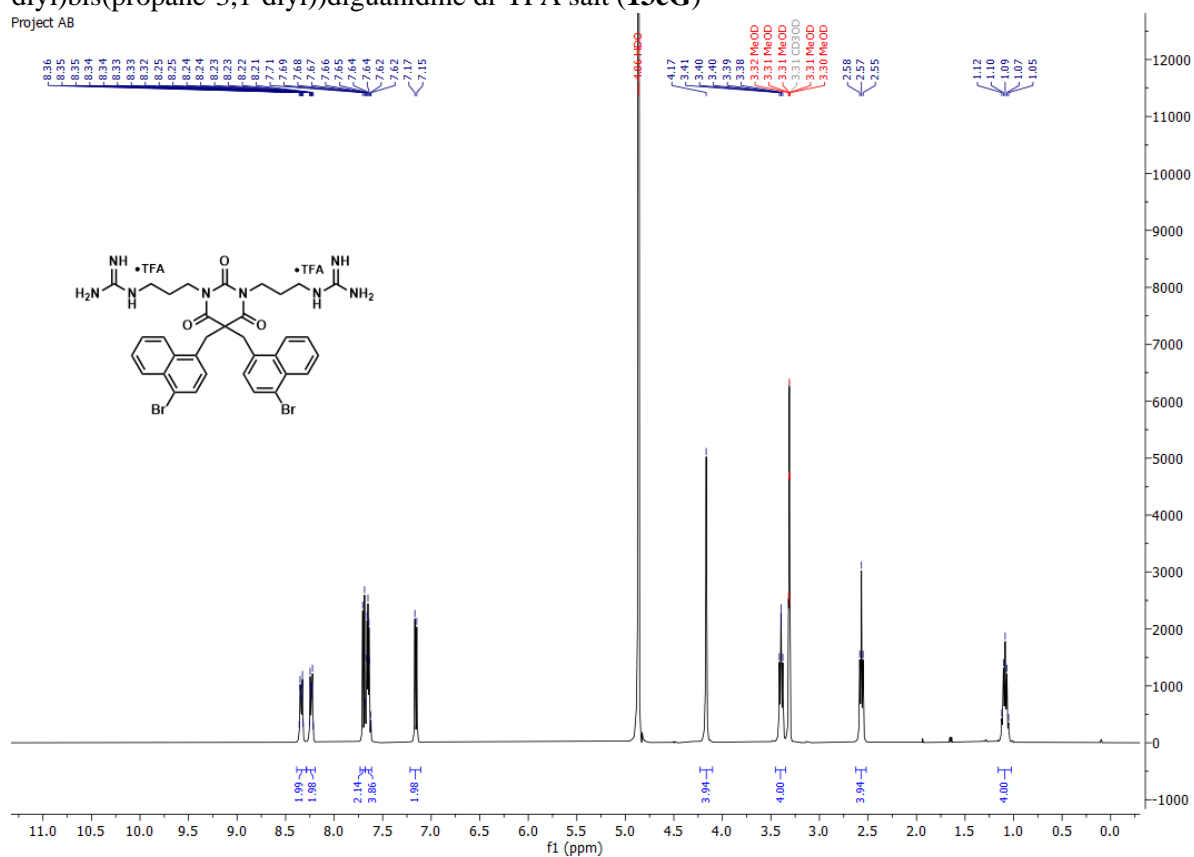


Project AB

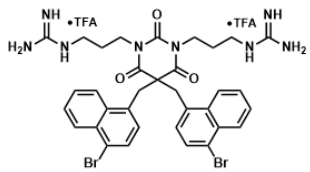
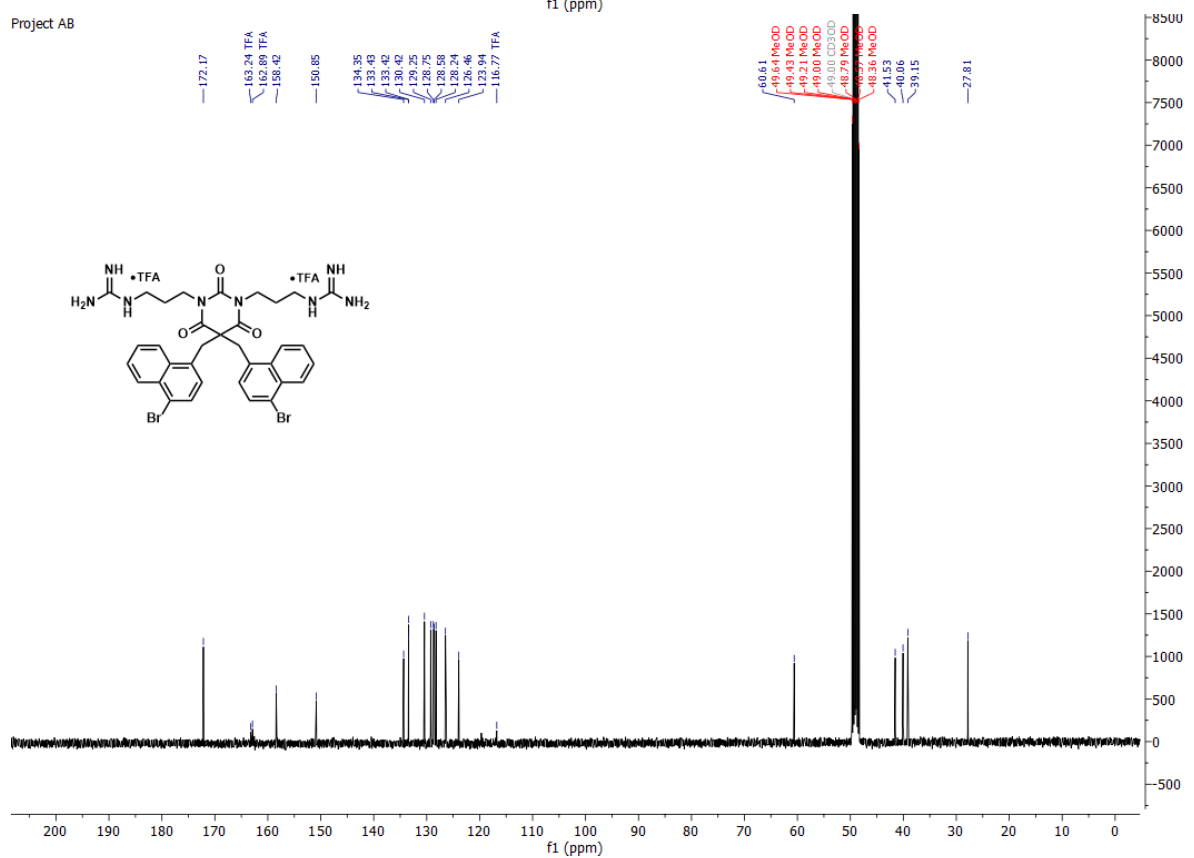


1,1'-((5,5-bis((4-bromonaphthalen-1-yl)methyl)-2,4,6-trioxodihydropyrimidine-1,3(2*H*,4*H*)-diyl)bis(propane-3,1-diyl)diguandine di-TFA salt (**13eG**)

Project AB

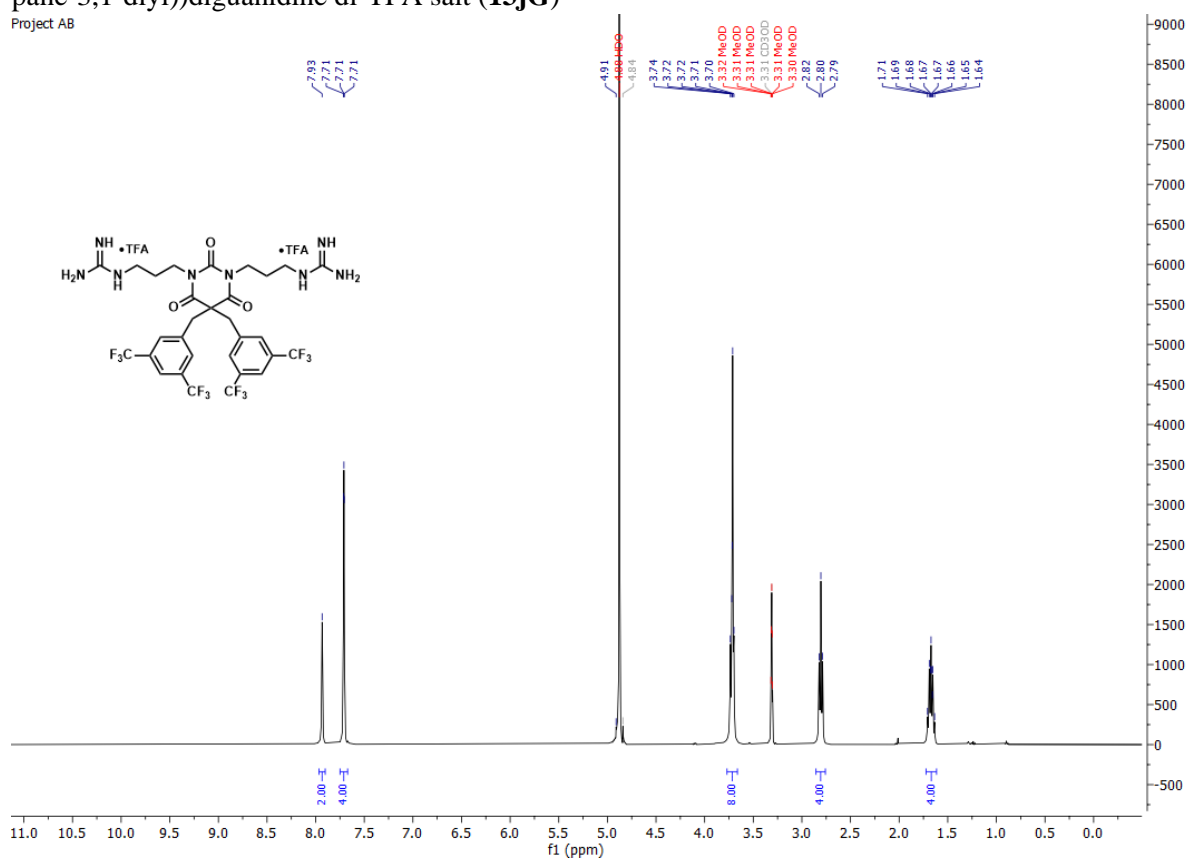


Project AB

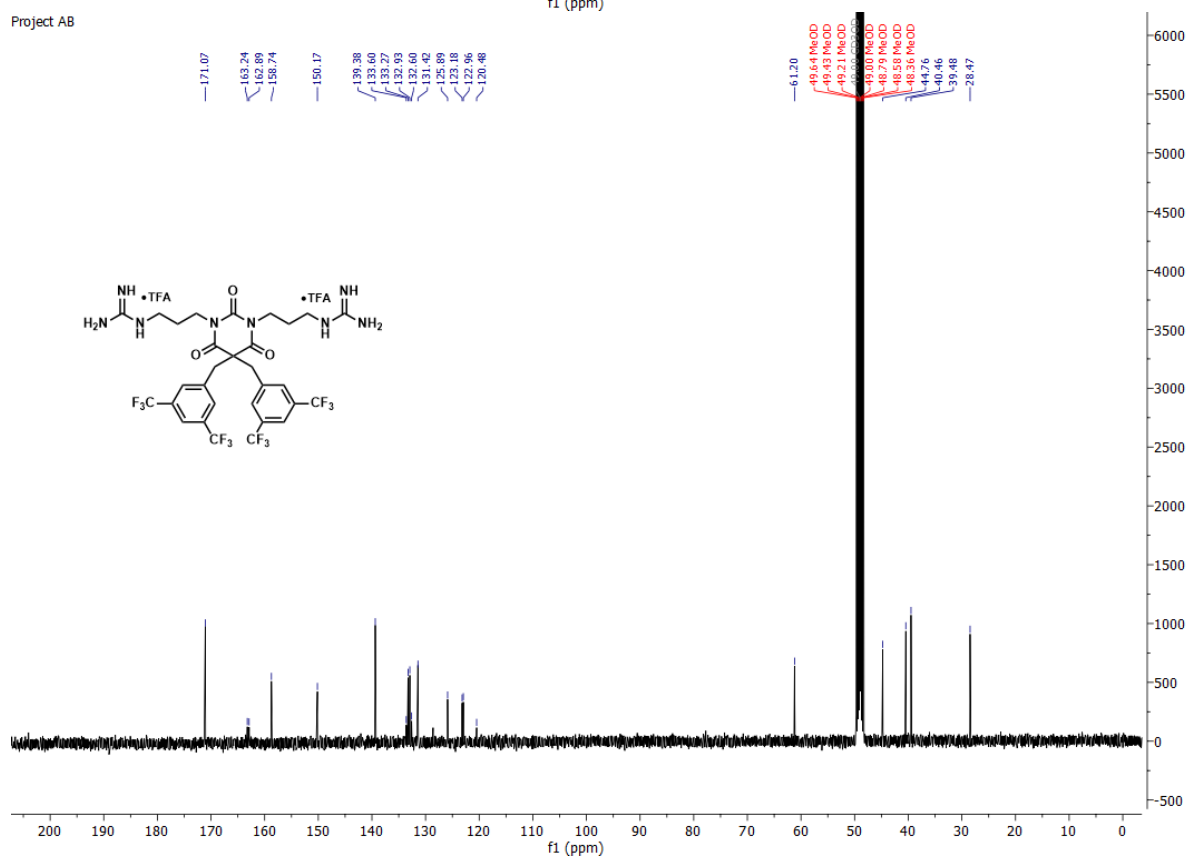


1,1'-((5,5-bis(3,5-bis(trifluoromethyl)benzyl)-2,4,6-trioxodihydropyrimidine-1,3(2H,4H)-diyl)bis(propane-3,1-diyl))diguanidine di-TFA salt (**13jG**)

Project AB

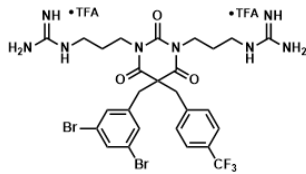
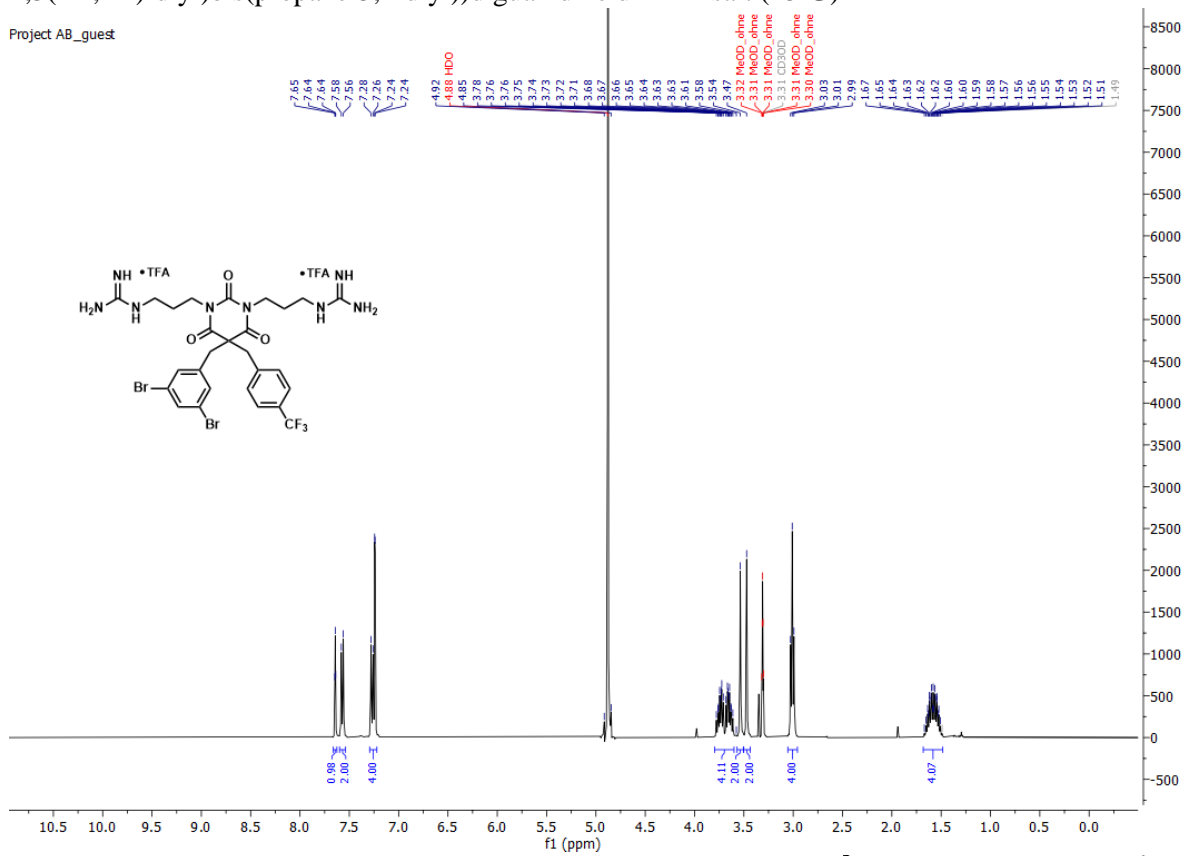


Project AB

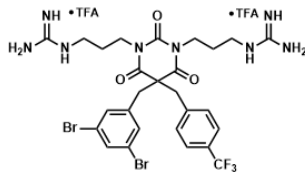
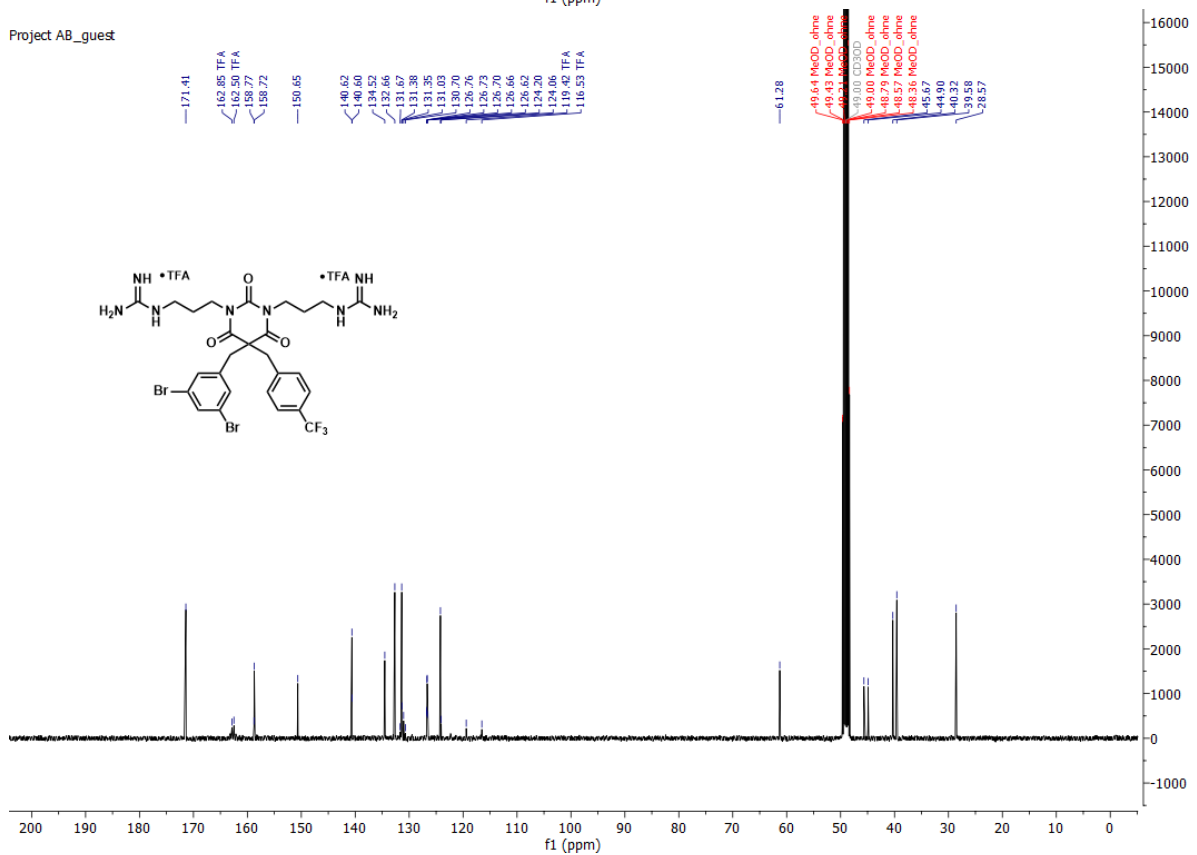


1,1'-((5-(3,5-dibromobenzyl)-2,4,6-trioxo-5-(4-(trifluoromethyl)benzyl)dihydropyrimidine-1,3(2*H*,4*H*)-diyl)bis(propane-3,1-diyl))diguandine di-TFA salt (**131G**)

Project AB_guest

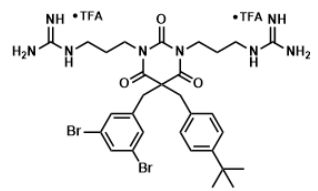
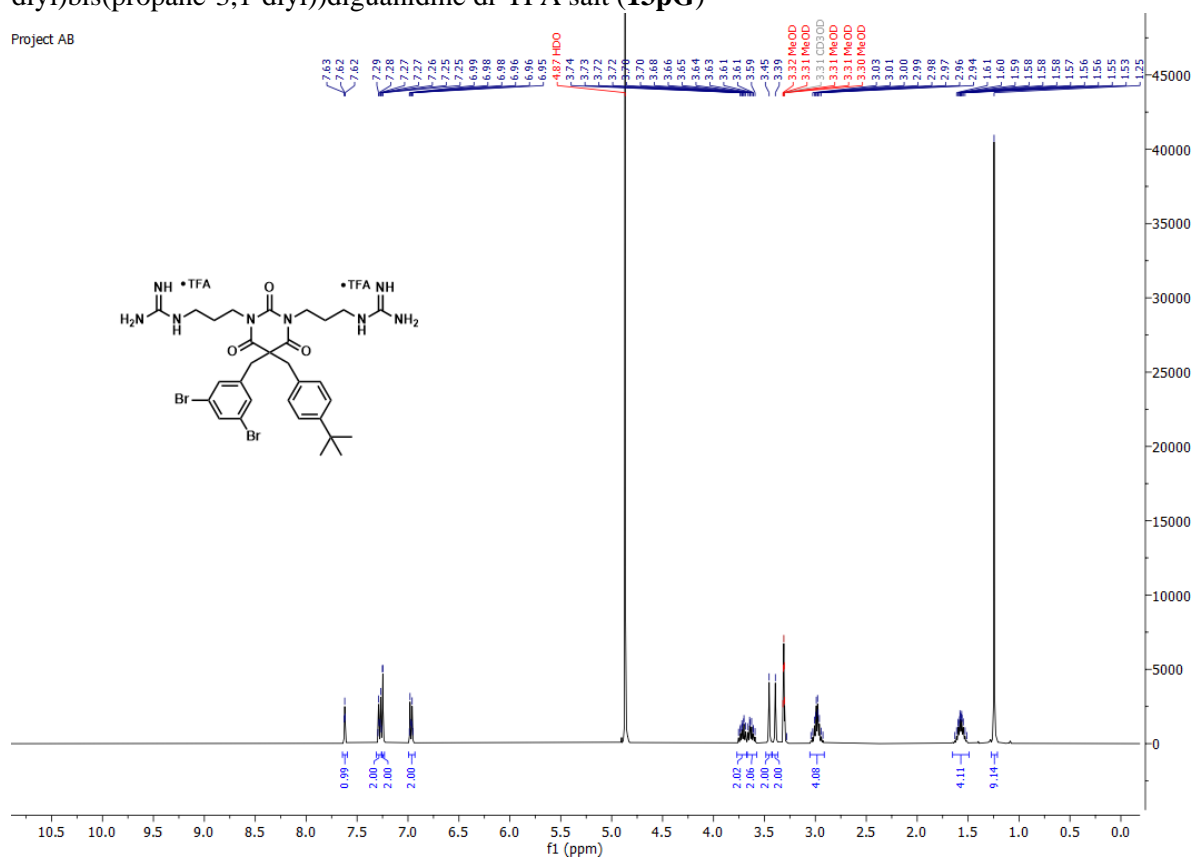


Project AB_guest

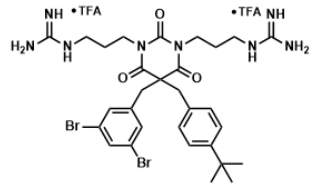
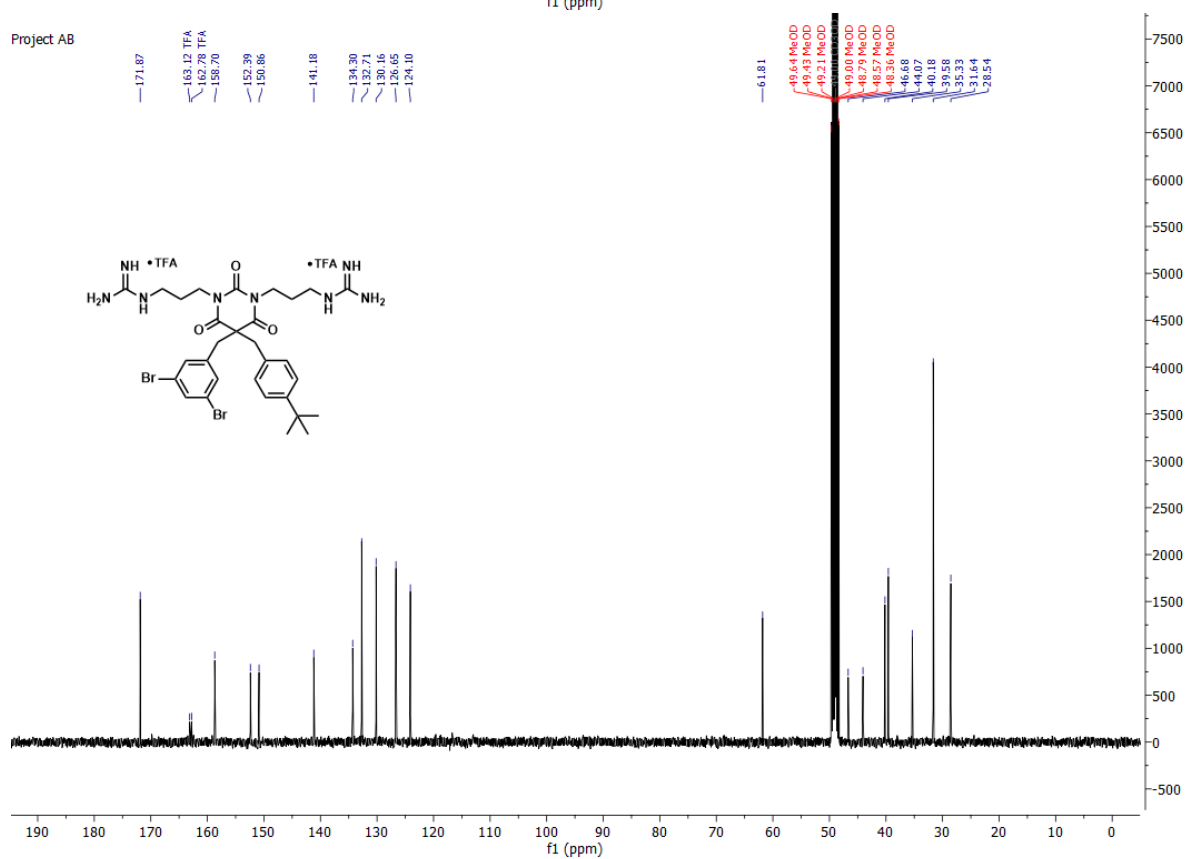


1,1'-((5-(4-(*tert*-butyl)benzyl)-5-(3,5-dibromobenzyl)-2,4,6-trioxodihydropyrimidine-1,3(2*H*,4*H*)-diyl)bis(propane-3,1-diyl)diguanidine di-TFA salt (**13pG**)

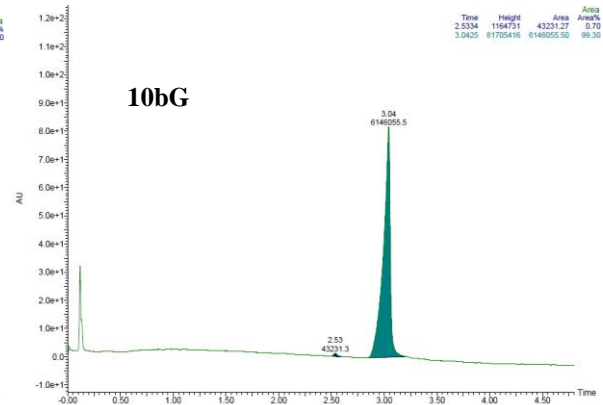
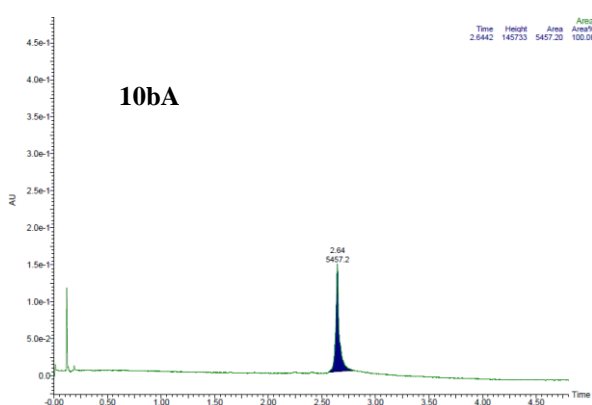
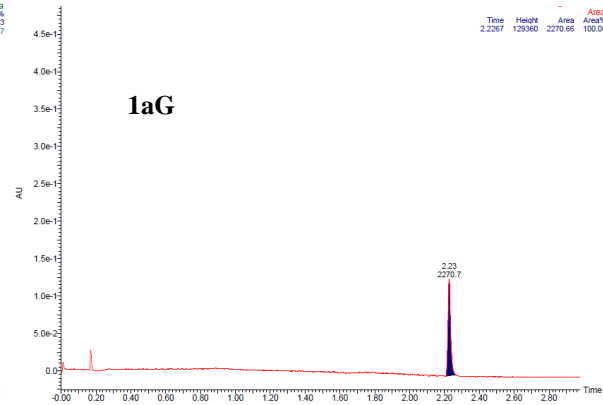
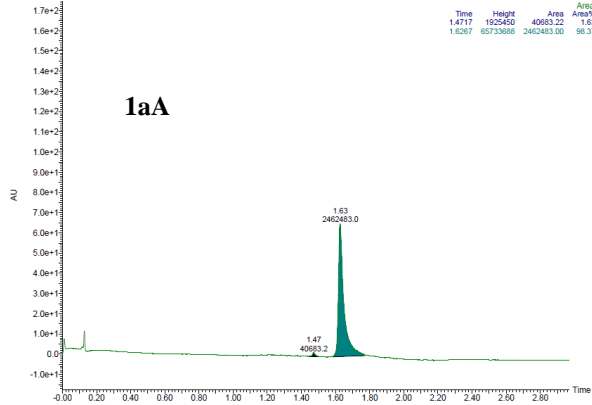
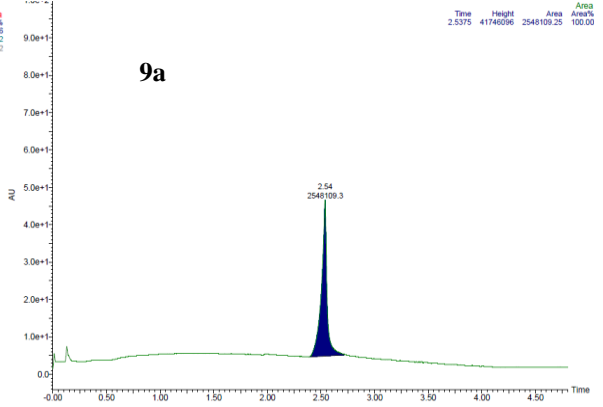
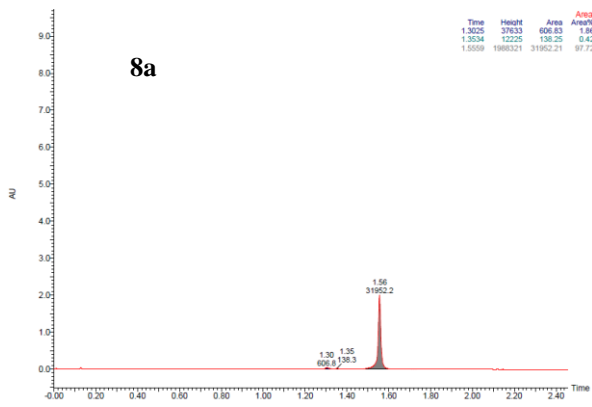
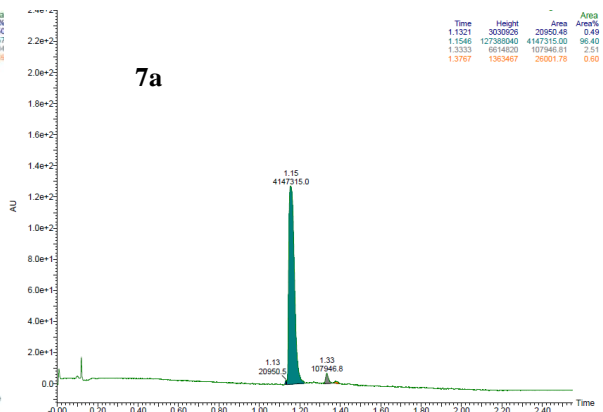
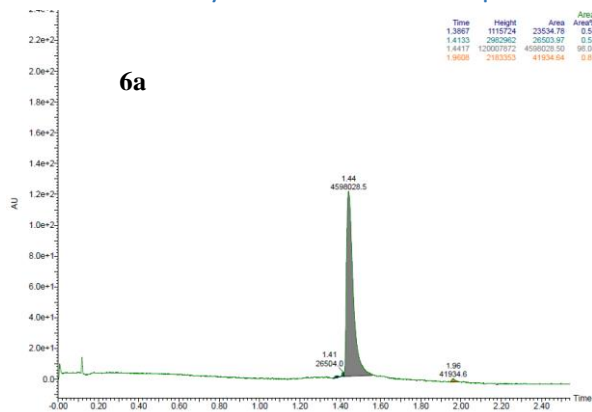
Project AB

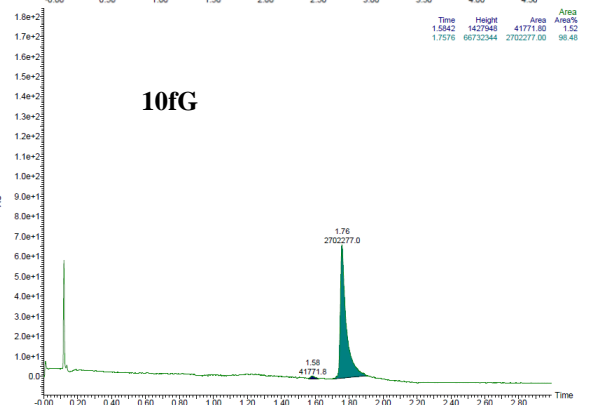
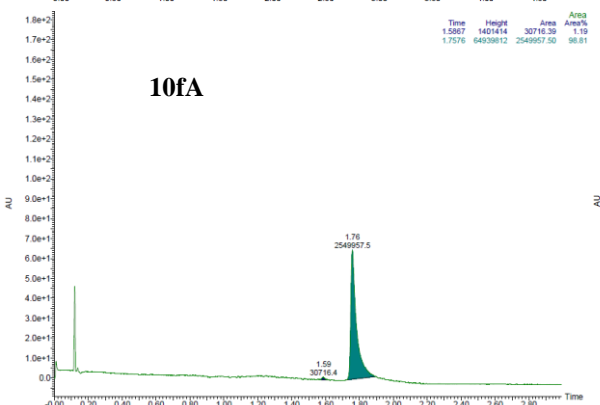
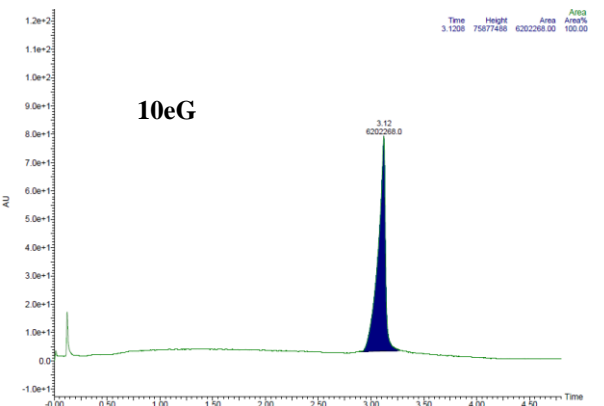
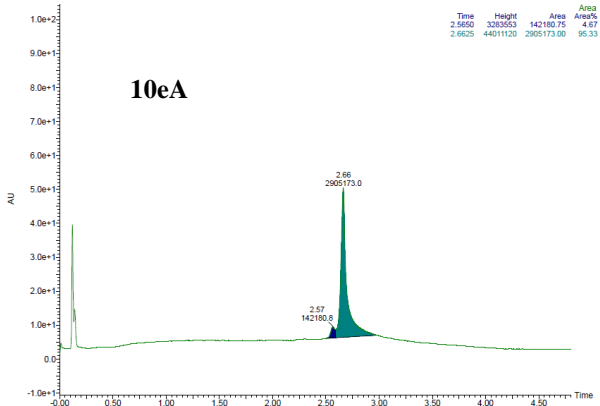
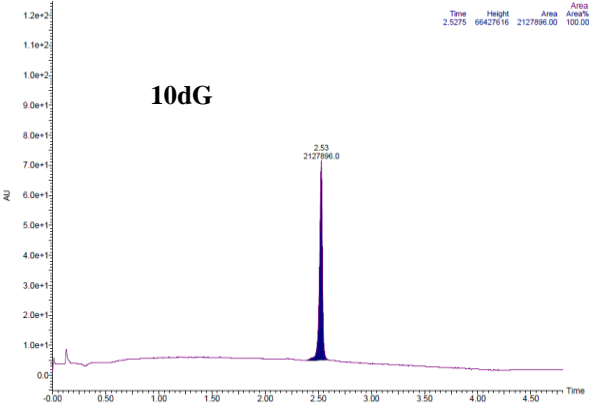
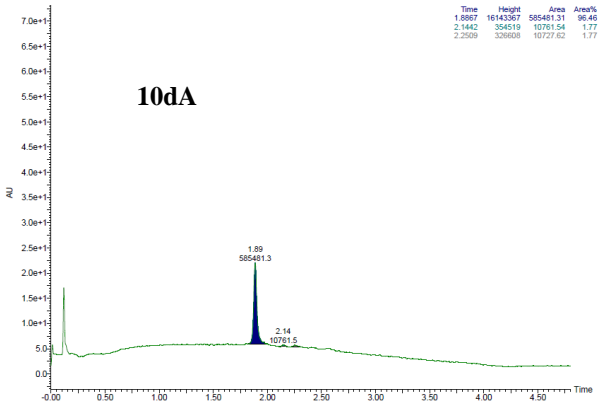
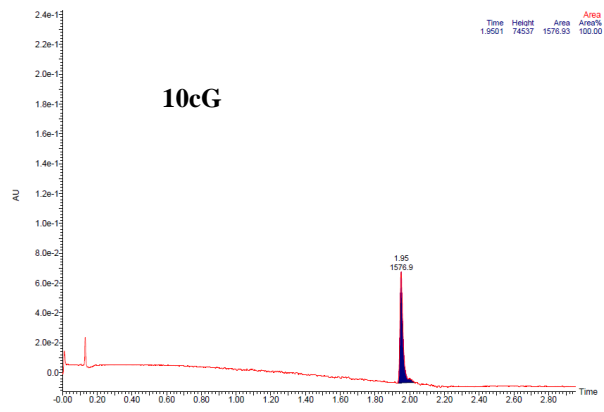
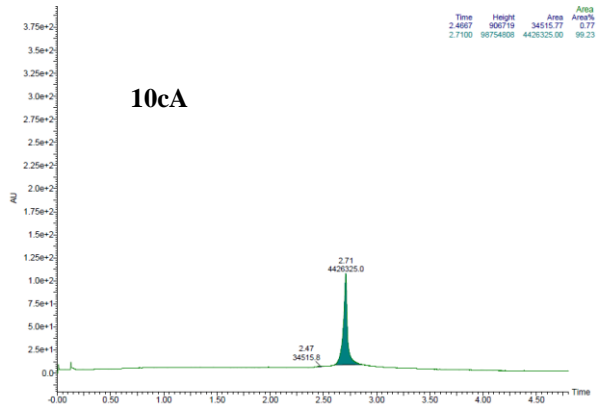


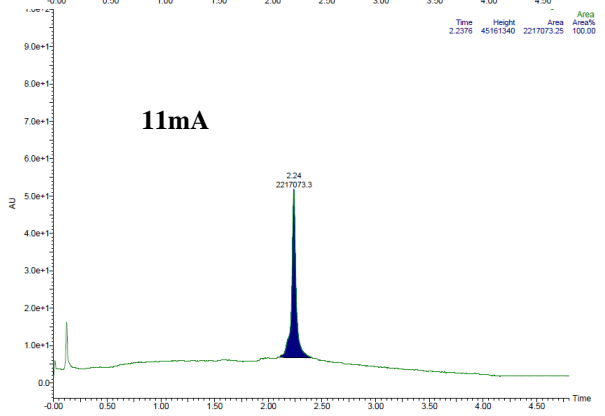
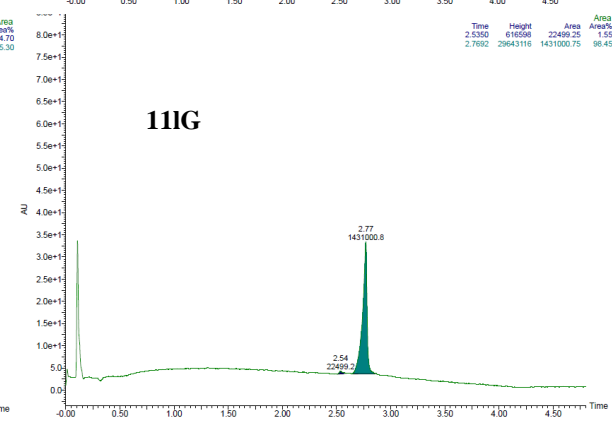
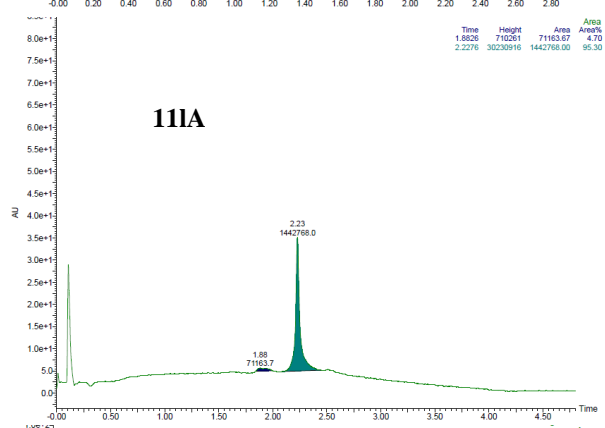
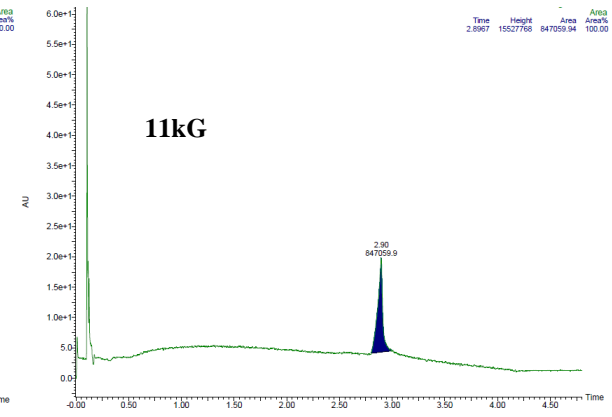
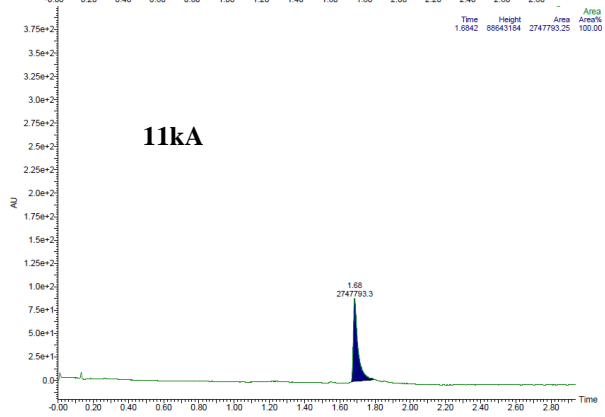
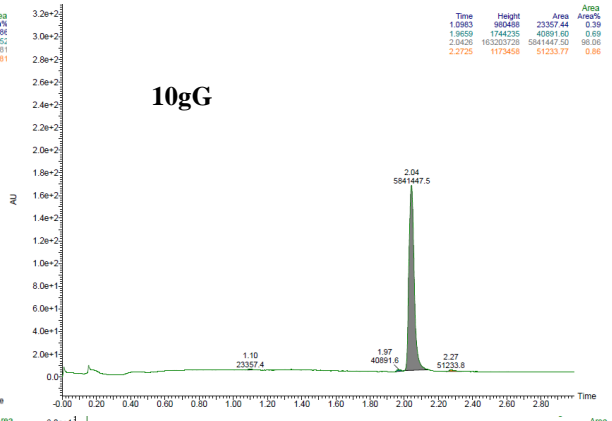
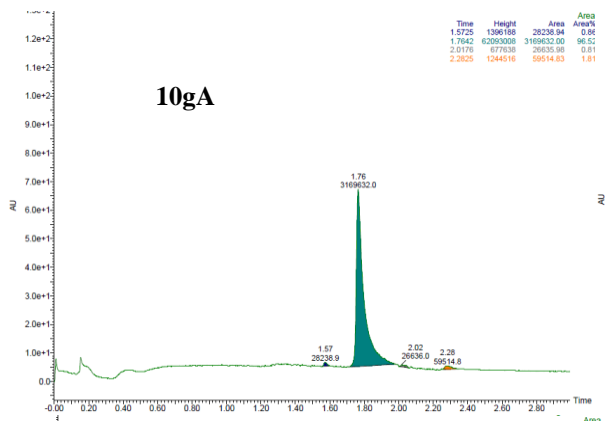
Project AB

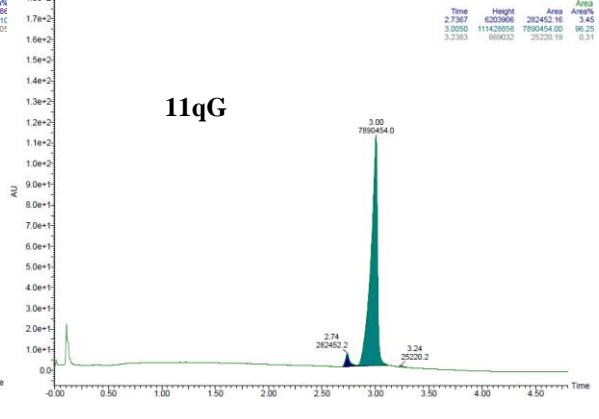
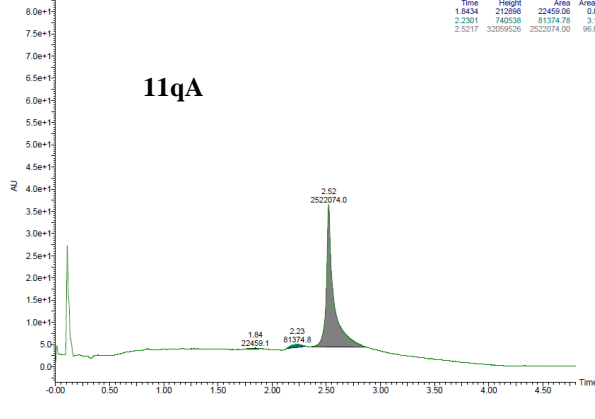
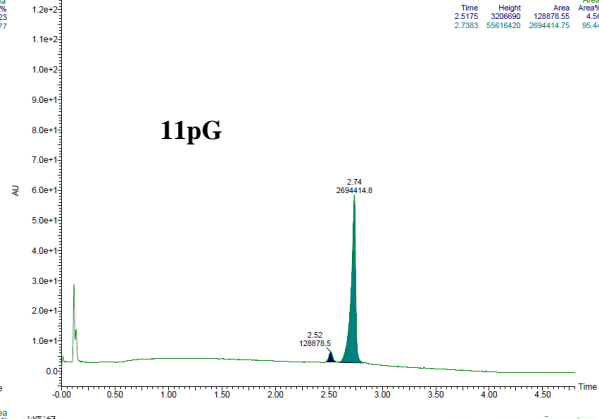
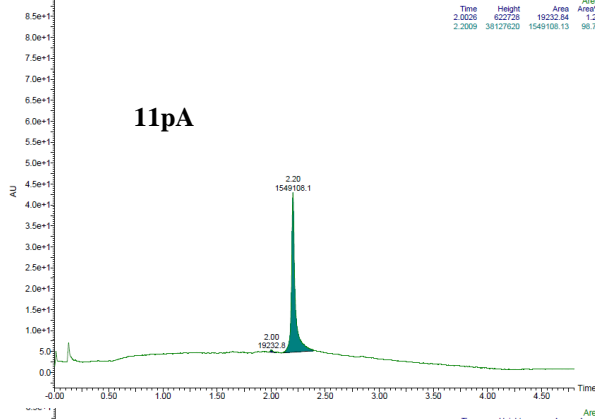
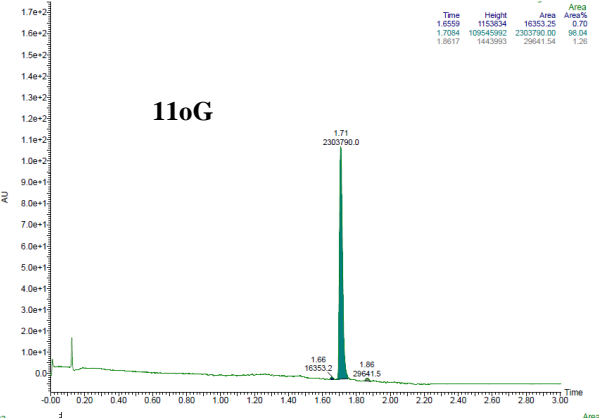
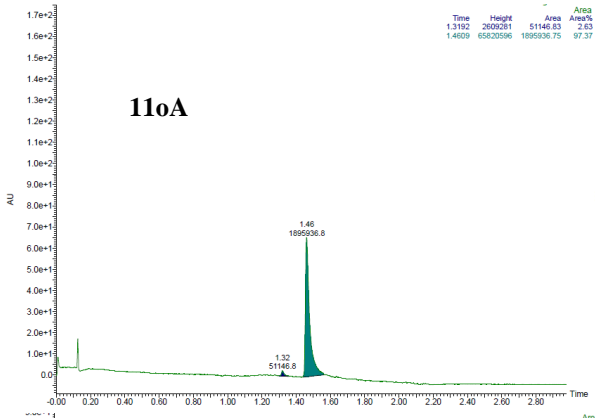
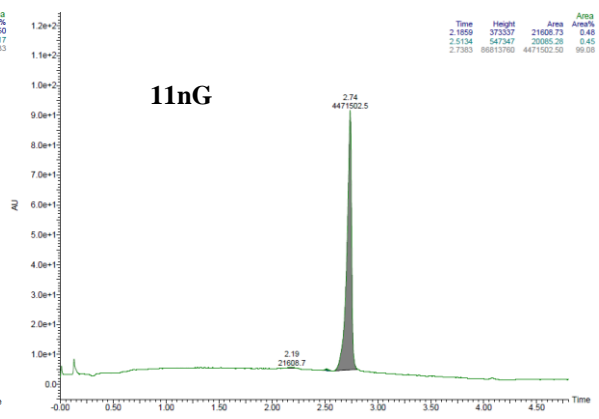
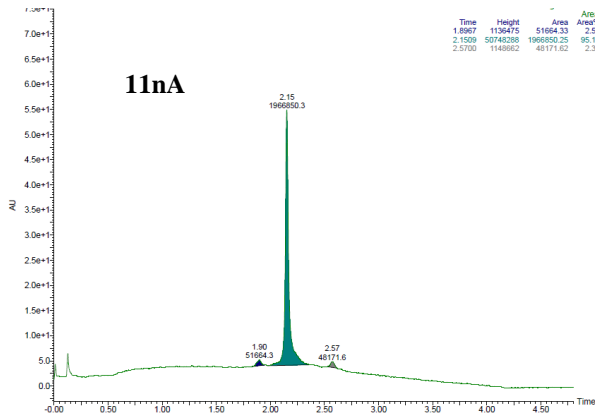


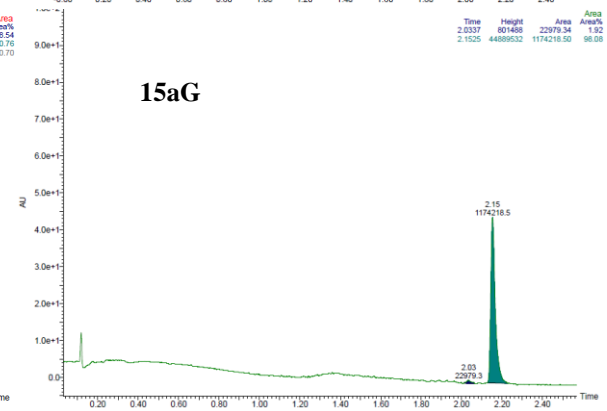
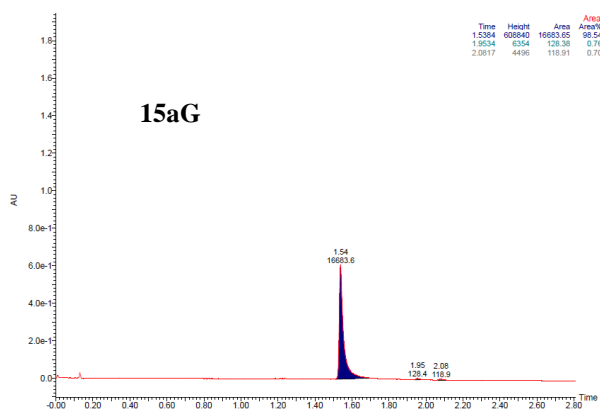
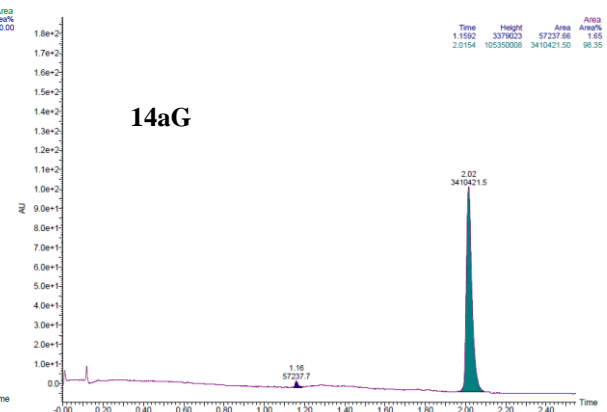
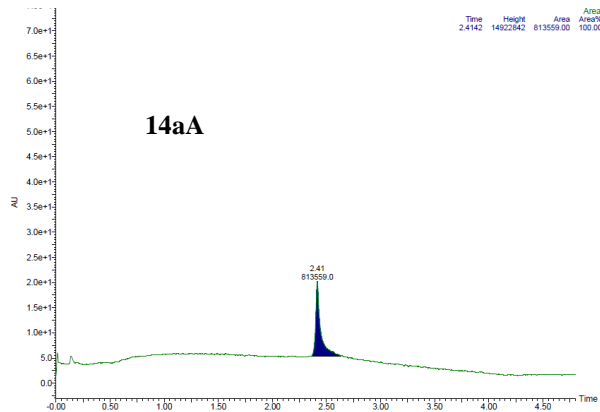
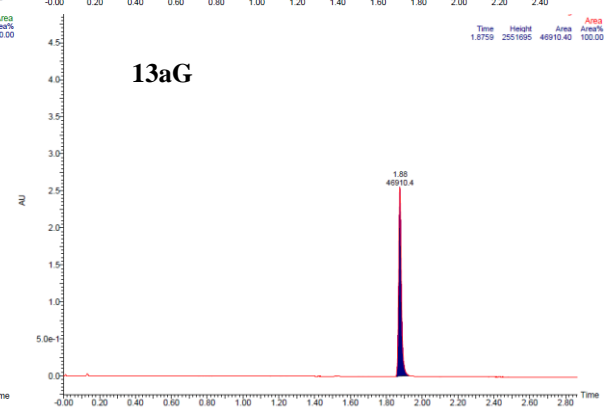
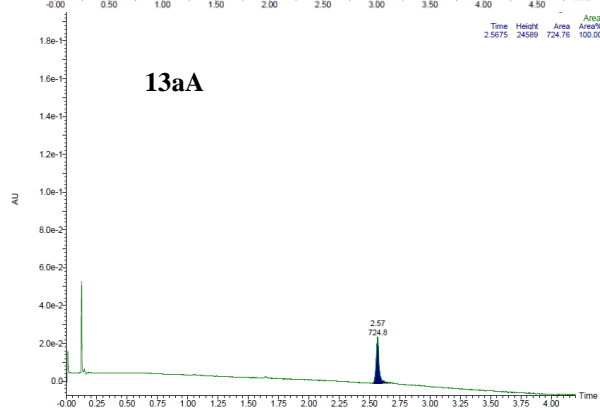
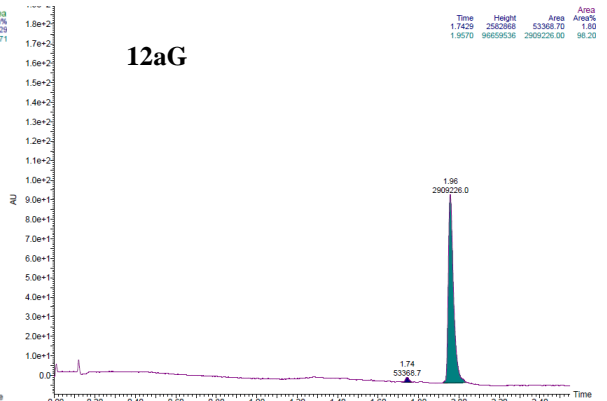
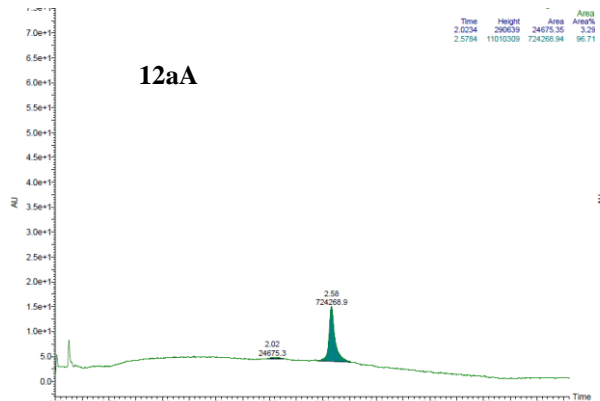
4 SFC analysis of final compounds

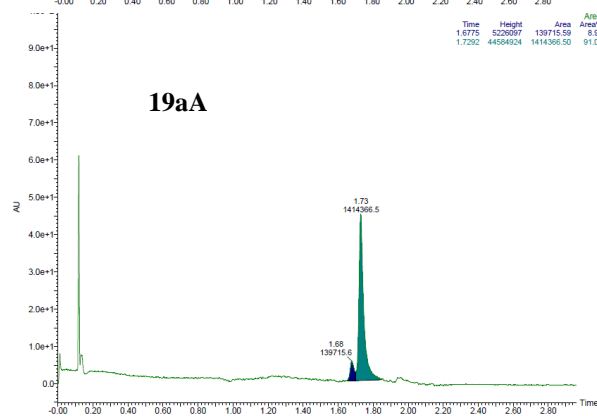
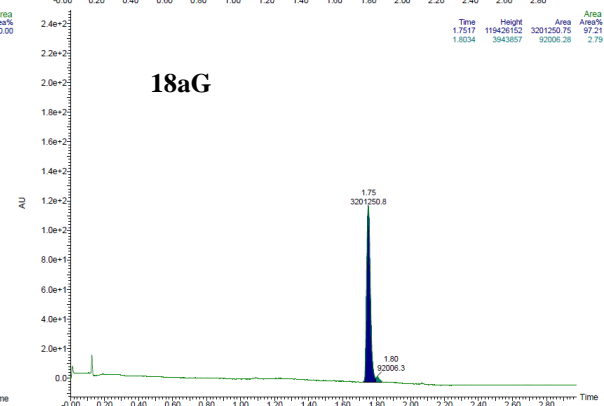
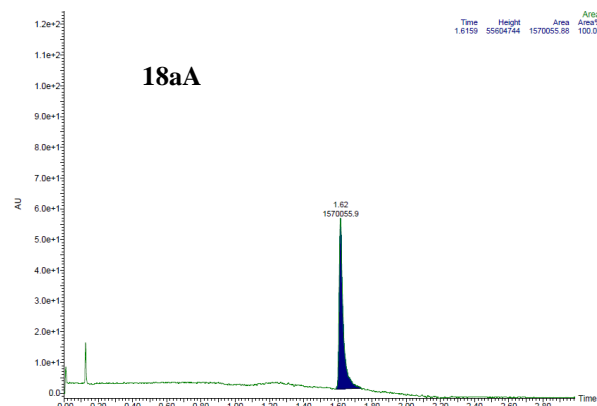
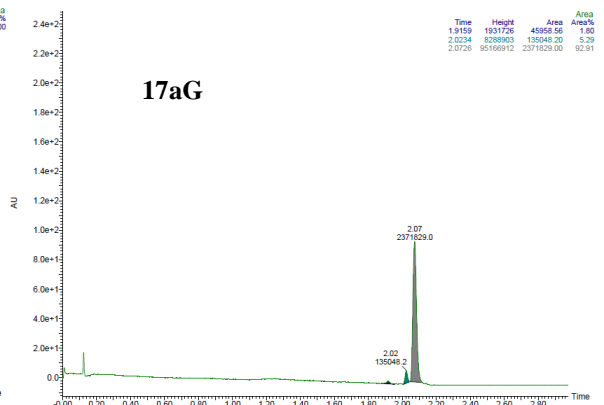
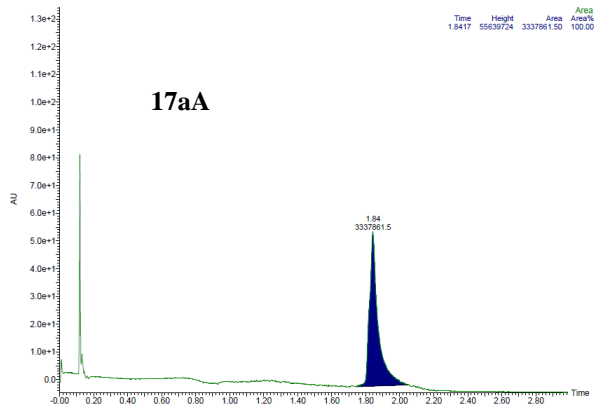
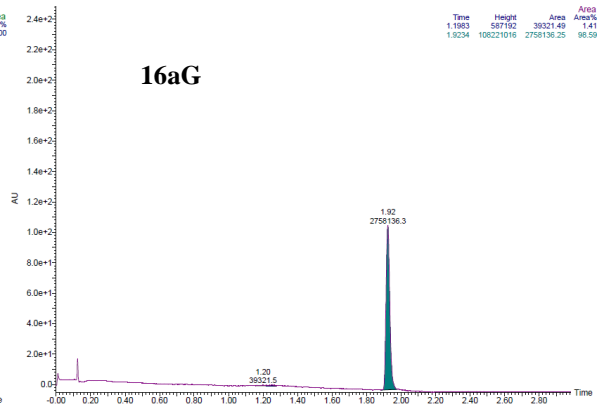
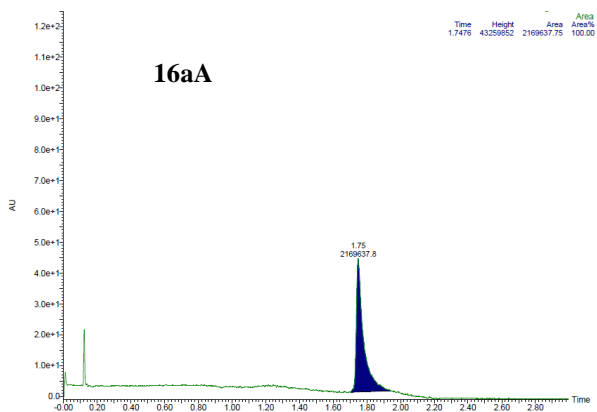


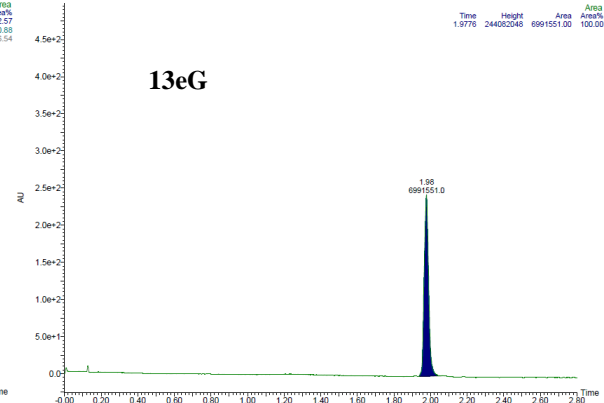
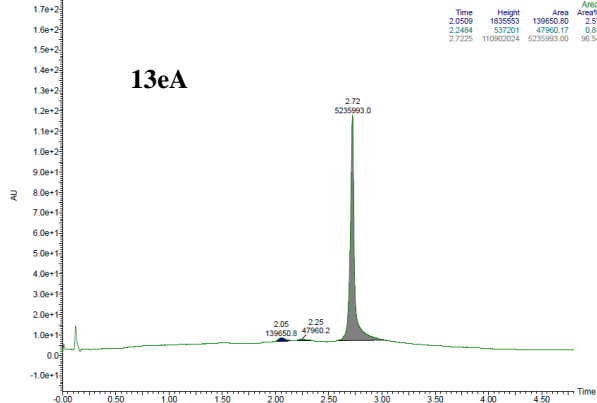
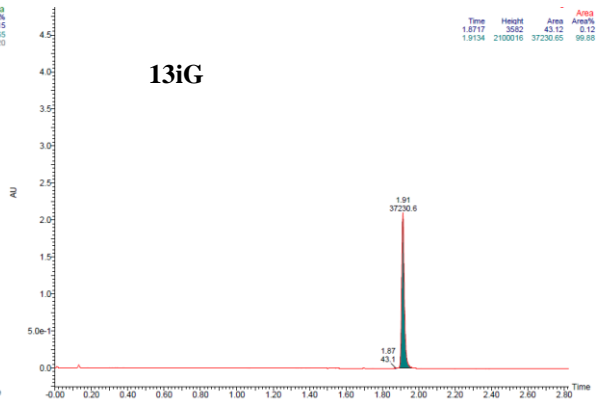
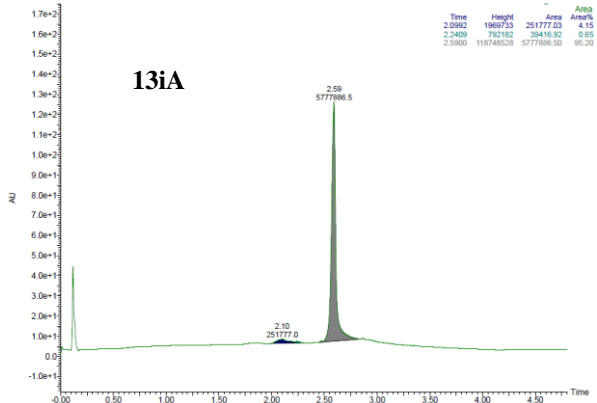
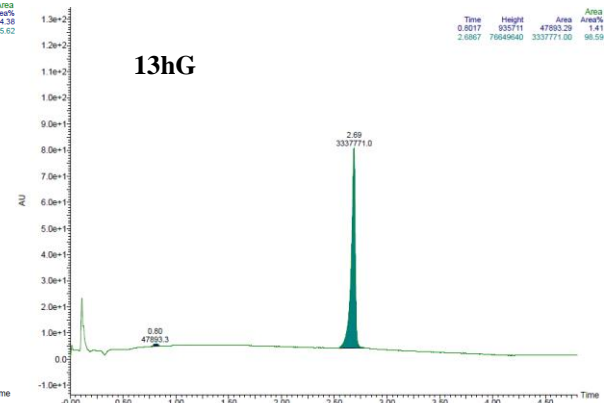
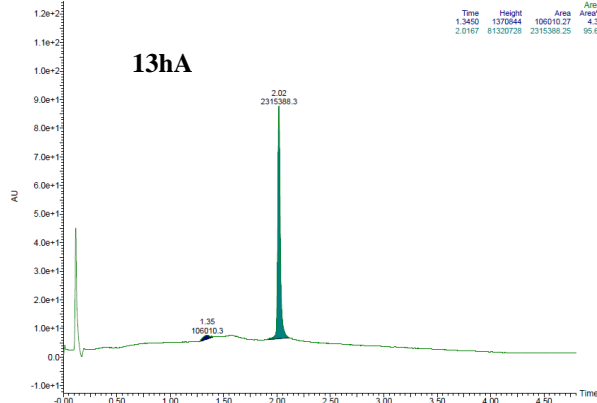
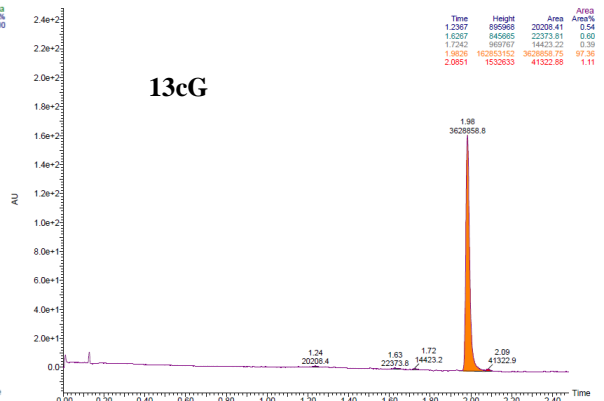
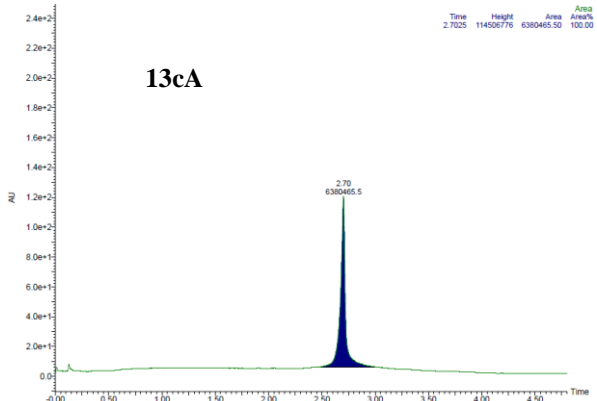


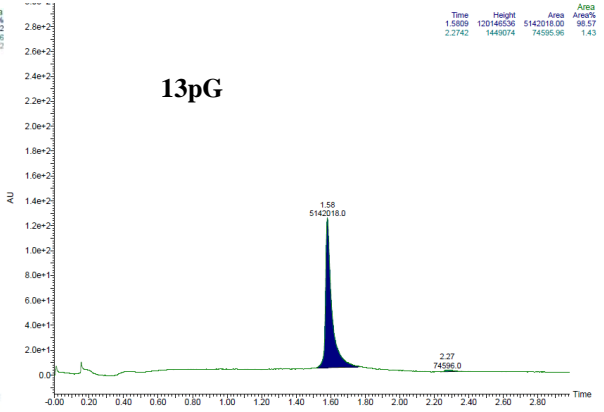
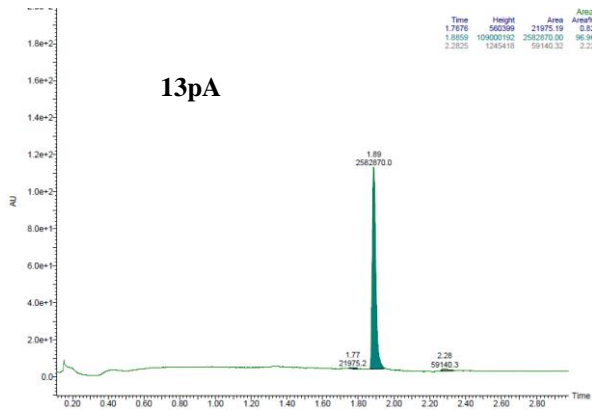
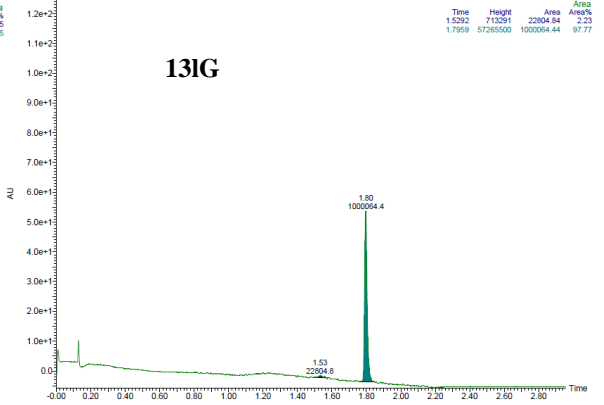
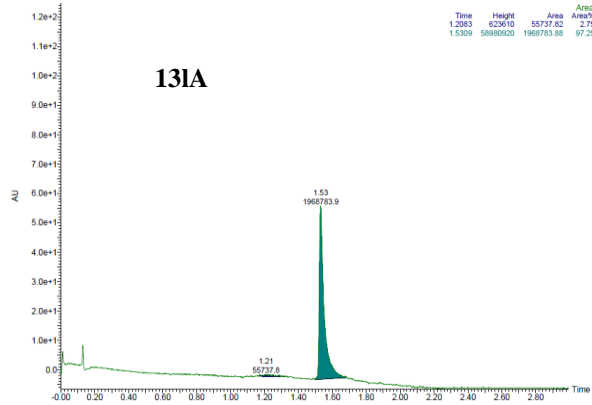
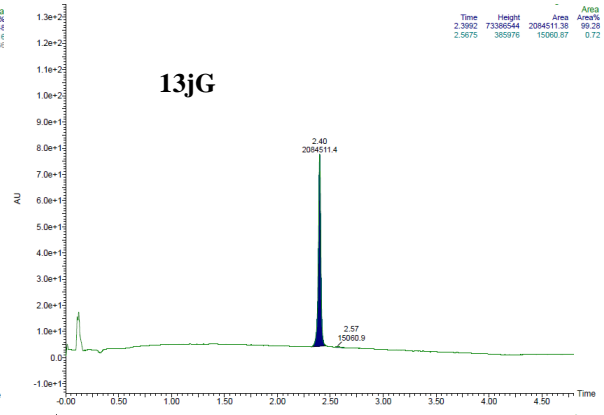
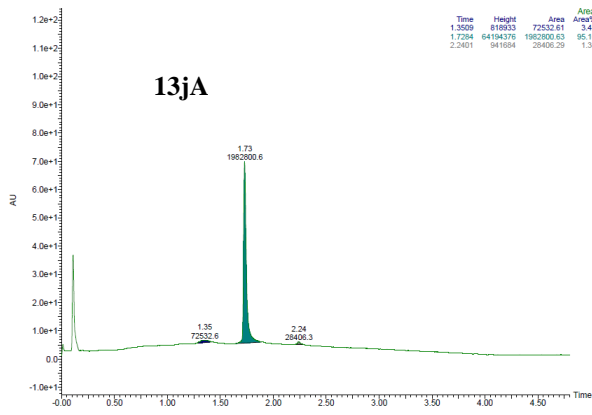












5 Full selectivity index table

Table S1 Selectivity index (SI) of all compounds towards all bacterial strains tested. EC₅₀ values are given in [μg/mL].

Code	Basic group	X	SI (MIC/EC ₅₀) ^a				
			S. a	B. s	E. c	P. a	EC ₅₀
6a	(N(Me)H)	<i>n</i> -butyl	9	18	9	5	73
7a	(NMe ₂)	<i>n</i> -butyl	20	39	20	–	157
8a	(NMe ₃)	<i>n</i> -butyl	>135	>67	–	–	>539
9a	(pyridinyl)	<i>n</i> -butyl	>280	>140	>70	–	>559
1aA	NH ₂	<i>n</i> -butyl	20	40	20	10	79
1aG	guanidyl	<i>n</i> -butyl	31	31	31	8	62

Code	R ¹	X	SI (MIC/EC ₅₀) ^a					Code	SI (MIC/EC ₅₀) ^a				
			S. a	B. s	E. c	P. a	EC ₅₀		S. a	B. s	E. c	P. a	EC ₅₀
10bA	(2-methylquinoline)	<i>n</i> -butyl	–	–	–	–	>390	10bG	>54	>27	–	–	>432
10cA	(6-Br-2-methylquinoline)	<i>n</i> -butyl	>29	>117	–	–	>469	10cG	230	115	29	–	461
10dA	(<i>n</i> -hexyl)	<i>n</i> -butyl	>21	>42	–	–	>333	10dG	72	72	36	9	143
10eA	(4-Br-1-Me-Nal)	<i>n</i> -butyl	14	14	7	7	27	10eG	9	9	9	5	36
10fA	(2,4,5-tri-BrBn)	<i>n</i> -butyl	7	7	3	3	27	10fG	8	8	8	4	32
10gA	(2,4,6-tri-BrBn)	<i>n</i> -butyl	15	15	8	8	30	10gG	15	15	8	8	30

Code	Basic group	X	SI (MIC/EC ₅₀) ^a					Code	SI (MIC/EC ₅₀) ^a				
			S. a	B. s	E. c	P. a	EC ₅₀		S. a	B. s	E. c	P. a	EC ₅₀
11kA	(2-methylquinoline)	<i>n</i> -butyl	–	>56	–	–	>444	11kG	225	113	–	–	450
11lA	(4-CF ₃ Bn)	<i>n</i> -butyl	21	43	–	–	342	11lG	81	40	81	10	161
11mA	(cyclopentyl)	<i>n</i> -butyl	25	51	–	–	>407						
11nA	(<i>n</i> -hexyl)	<i>n</i> -butyl	36	36	9	9	144	11nG	29	15	15	7	58
11oA	(3,5-di-CF ₃ Bn)	<i>n</i> -butyl	12	46	12	12	93	11oG	18	18	18	9	36
11pA	(4- <i>tert</i> -butylBn)	<i>n</i> -butyl	12	12	12	6	47	11pG	20	20	20	10	39
11qA	(4-Br-1-Me-Nal)	<i>n</i> -butyl	21	21	10	10	82	11qG	15	15	15	7	58

Code	R ¹	X	SI (MIC/EC ₅₀) ^a					Code	SI (MIC/EC ₅₀) ^a				
			S. a	B. s	E. c	P. a	EC ₅₀		S. a	B. s	E. c	P. a	EC ₅₀
12aA	(3,5-di-BrBn)	(1,2-C ₂ H ₄)	10	10	10	5	39	12aG	82	82	41	10	164
13aA	(3,5-di-BrBn)	(1,3-C ₃ H ₆)	25	25	12	12	99	13aG	93	93	47	23	187
14aA	(3,5-di-BrBn)	(1,5-C ₅ H ₁₀)	6	6	3	3	24	14aG	5	5	5	4	29 ^b
15aA	(3,5-di-BrBn)	(1,6-C ₆ H ₁₂)	8	8	8	2	30	15aG	14	14	14	2	57 ^b
16aA	(3,5-di-BrBn)	(1,3- <i>cis</i> -cyclobutane)	6	13	13	6	50	16aG	37	37	19	9	75
17aA	(3,5-di-BrBn)	(1,3- <i>trans</i> -cyclobutane)	23	23	23	12	93	17aG	31	16	16	8	62
18aA	(3,5-di-BrBn)	(1,4- <i>cis</i> -cyclohexyl)	4	4	4	2	15	18aG	15	>30	8	8	30
19aA	(3,5-di-BrBn)	(1,4- <i>trans</i> -cyclohexyl)	8	8	8	4	16						

Code	R ¹	X	SI (MIC/EC ₅₀) ^a					Code	SI (MIC/EC ₅₀) ^a				
			S. a	B. s	E. c	P. a	EC ₅₀		S. a	B. s	E. c	P. a	EC ₅₀
13cA	(6-Br-2-methylquinoline)	<i>n</i> -propyl	–	>57	–	–	>455	13cG	>62	>124	–	–	>497
13hA	(4-CF ₃ Bn)	<i>n</i> -propyl	–	>25	–	–	>393	13hG	>54	>109	–	–	>435
13iA	(3-Cl, 4-BrBn)	<i>n</i> -propyl	40	81	40	20	323	13iG	174	174	44	–	348
13eA	(4-Br-1-Nal)	<i>n</i> -propyl	11	11	6	6	23	13eG	31	31	15	8	61
13jA	(3,5-di-CF ₃ Bn)	<i>n</i> -propyl	23	46	23	23	176	13jG	111	222	56	28	445
13IA^c	R ² = (4-CF ₃ Bn)	<i>n</i> -propyl	–	>55	>27	–	>438	13IG	>120	>120	>30	–	>480
13pA^c	R ² = (4- <i>tert</i> -butylBn)	<i>n</i> -propyl	11	11	6	6	23	13pG	169	169	85	11	169

Bacterial reference strains: S. a – *Staphylococcus aureus* ATCC 9144, B. s – *Bacillus subtilis* 168, E. c – *Escherichia coli* ATCC 25922, and P. a – *Pseudomonas aeruginosa* ATCC 27853; ^aNo SI was calculated if MIC > 16 μg/mL; –: not calculated. ^bPrecipitation in the RBC assay. ^cMixed lipophilic side chain, 3,5-dibromobenzyl and R₂.

6 Biological methods

6.1 Minimum inhibitory concentration (MIC) assay

Stock solutions of the water-soluble compounds were prepared by dissolving them in ultrapure water (Milli-Q H₂O, Millipore, MA, USA). The less water-soluble compounds were first dissolved in 25 - 50 μ L 100% DMSO before further dilution with ultrapure water. The DMSO concentration was always less than 1% in the working concentration of each compound. A modified broth microdilution susceptibility test[8], based on the CLSI M07-A9 protocol,[9] was used to determine minimal inhibitory concentrations (MIC). Briefly, the test compounds were two-fold diluted with ultrapure water in polystyrene 96-well flat-bottom microplates (NUNC, Roskilde, Denmark). The bacterial inoculum was diluted to $2.5 - 3 \times 10^4$ cells/mL in Mueller-Hinton broth (MHB, Difco Laboratories, USA) and added to the different diluted compounds in a ratio of 1:1. Positive control (ciprofloxacin, Sigma-Aldrich, USA), negative control (bacteria + water), and media control (media + water) were included in each experiment. The microplates were incubated for 48 h at 35 °C in an EnVision microplate reader (Perkin-Elmer, Turku, Finland). The lowest concentration of compounds that caused no bacterial growth, as determined by optical density (OD₆₀₀) measurements, was defined as the MIC value. All compounds were tested in 3 technical replicates.

6.2 Membrane integrity assays

6.2.1 Inner membrane

The inner membrane integrity assay was performed in a real-time manner using *Bacillus subtilis* 168 (ATCC 23857) and *Escherichia coli* K12 (ATCC MC1061) as test strains, both transformed with the reporter plasmid pCSS962 containing the gene encoding eukaryotic luciferase (*lucGR* gene).[10] Externally added D-luciferin was used as a substrate for the luciferase to detect light emission. *B. subtilis* and *E. coli* colonies were suspended in MH media supplemented with 5 μ g/mL chloramphenicol (Merck KGaA, Darmstadt, Germany) and a mixture of 20 μ g/mL chloramphenicol and 100 μ g/mL ampicillin (Sigma-Aldrich, USA), respectively, and grown overnight at RT. Overnight cultures were further diluted and grown at RT for 2-3 hrs until they reached OD₆₀₀ = 0.1. D-luciferin potassium salt (Synchem Inc., Elk Grove Village, IL, USA) was added to the bacterial cultures at a final concentration of 1 mM, and the background luminescence was measured before the actual assay. Black round-bottom 96-well microtiter plates (Nunc, Roskilde, Denmark) were prepared with two-fold dilution series of the compounds (10 μ L per well) at final concentrations ranging from 50 to 1.56 μ g/mL. Chlorhexidine acetate (Frese-nius Kabi, Halden, Norway) and MQ-H₂O were used as positive and negative control, respectively. A Synergy H1 Hybrid Reader (BioTek, Winooski, VT, USA) was primed with bacterial suspension before the assay plate was loaded into the plate reader. Aliquots of 90 μ L bacterial inoculum with D-luciferin were successively (well by well) injected into the test wells by an automated injector. The light (luminescence) emission, as a result of bacterial membrane disruption, was monitored every second for 3 minutes. Each study was performed at least three times independently, and the figures show a representative dataset.

6.2.2 Outer membrane

The outer membrane integrity assay was performed in a real-time manner using *E. coli*, the same strain as used in the inner membrane integrity assay. Externally added 1-*N*-phenyl-naphthylamine (NPN) was used as a substrate for the fluorescence to detect light emission. *E. coli* colonies were suspended in MH media and grown overnight at RT. Overnight cultures were further diluted and grown at RT for 2-3 hrs until they reached OD₆₀₀ = 0.1. NPN (Sigma-Aldrich, USA) was added to the bacterial cultures at a final concentration of 20 μ M in glucose hepes buffer (5mM), and the background fluorescence was measured before the actual assay. Black round-bottom 96-well microtiter plates were prepared with two-fold dilution series of the compounds (10 μ L per well) at final concentrations ranging from 50 to 1.56 μ g/mL. Chlorhexidine acetate and MQ-H₂O were used as positive and negative control. A Synergy H1 Hybrid Reader was primed with bacterial suspension before the assay plate was loaded into the plate reader. Aliquots of 90 μ L bacterial inoculum with NPN were successively (well by well) injected into the test

wells by an automated injector. The light (fluorescence) emission, as a result of bacterial outer membrane disruption, was monitored every second for 3 minutes. Each study was performed at least three times independently, and the figures show a representative dataset.

6.3 Viability assay

The real-time measurement of bacterial viability was performed by using *B. subtilis* 168 and *E. coli* K12, the same strains as used in the inner membrane integrity assay. However, in this assay *B. subtilis* 168 is carrying a constitutively expressed lux operon as a chromosomal integration in the *sacA* locus (Pli_AG) and *E. coli* K12 was transformed with the reporter plasmid pCGLS-1.[11, 12] *B. subtilis* and *E. coli* cultures were prepared the same way as the membrane integrity assay in MH media supplemented with 5 µg/mL chloramphenicol and a mixture of 20 µg/mL chloramphenicol and 100 µg/mL ampicillin, respectively. The continuous light production by these biosensors was monitored in the Synergy H1 Hybrid Reader, and the respective injector was primed with bacterial suspension. Black round-bottom 96-well microtiter plates were prepared with 10 µL of each compound at the final concentration ranging from 50 to 1.56 µg/mL (two-fold dilutions), including Chlorhexidine as a positive control and MQ-H₂O as a negative control. An aliquot of 90 µL bacterial suspension was subsequently added by the automated injector. As a result of changes in bacterial viability, the decrease in light emission was monitored every second for 3 minutes. Each study was performed at least three times independently, and the figures show a representative dataset.

6.4 Red Blood Cell Haemolysis Assay

The protocol was adapted from Paulsen *et al.*[1] Haemolysis was determined using a heparinized fraction (10 IU/mL) of freshly drawn blood. The blood collected in ethylenediaminetetraacetic acid-containing test tubes (Vacutest, KIMA, Arzergrande, Italy) was used for the determination of the hematocrit (hct). The heparinized blood was washed 3× with pre-warmed phosphate-buffered saline (PBS) and adjusted to a final hct of 4%. Derivatives in DMSO (50 mM) were added to a 96-well polypropylene V-bottom plate (NUNC, Fisher Scientific, Oslo, Norway) and serially diluted. The test concentration range was 500–4 µM with DMSO contents ≤1%. A solution of 1% triton X-100 was used as a positive control for 100% haemolysis. As a negative control, a solution of 1% DMSO in PBS was included. No signs of DMSO toxicity were detected. RBCs (1% v/v final concentration) were added to the well plate and incubated at 37 °C and 800 rpm for 1 h. After centrifugation (5 min, 3000g), 100 µL of each well was transferred to a 96-well flat-bottomed microtiter plate, and absorbance was measured at 545 nm with a microplate reader (VersaMax™, Molecular Devices, Sunnyvale, CA, USA). The percentage of haemolysis was calculated as the ratio of the absorbance in the derivative-treated and surfactant-treated samples, corrected for the PBS background. Three independent experiments were performed, and EC₅₀ values are presented as averages.

7 Membrane integrity and viability assay

Table S2 Summary of the membrane integrity and viability assay against *B. subtilis* 168.

Code	MIC ¹ (μg/ml, 24h)	MIA (activity and speed) ²	VA (effects) ³
B. s			
7	4	+++	+
8	8	–	–
9	4	+	+
10cA	4	++	+
10cG	4	++	++
10dG	2	++++	++
11kG	4	+++	++
11lA	8	+++	+
11lG	4	++++	++
11nA	4	+++	+
11nG	4	++++	++
11oA	2	++++	++
11oG	2	++++	+++
11pA	4	++++	++
11pG	2	++++	+++
12aA	4	+++	++
12aG	2	++++	+++
13aA	4	+++	+++
13aG	2	++++	+++
16aG	2	++	+++
17aA	4	++	++
13cG	4	++	+
13hG	4	–	+
13iA	4	++	+
13iG	2	++++	++
13eG	2	+++	+++
13jA	4	+++	+
13jG	2	+++	+
13lG	4	++++	++
13pA	2	+++	++
13pG	1	++++	+++

B. s: *Bacillus subtilis* 168.

¹MIC assay was also performed in biosensor assay, and the value was similar.

²For membrane integrity assay: High active, fast speed (++++) Medium active, Intermediate speed (+++), Medium active, Slow speed (++) Low active, Slow speed (+) and Not active (–).

³For viability assay: High effect (+++), Medium effect (++) Low effect (+) and No effect (–). The highest concentration (51.2 μg/mL) was used to compare and evaluate the membrane integrity and viability assay results.

Table S3 Summary of the membrane integrity and viability assay against *E. coli* K12.

Code	MIC ¹ (µg/mL, 24h)	MIA (activity and speed) ²	VA (effects) ³
E. c			
10dG	4	+++	++
11IG	4	++	++
11nG	4	+++	++
11oA	8	++	++
11oG	2	++	++
11pG	2	++	++
12aA	4	++++	++
13aA	8	++	+
13aG	4	+++	++
16aG	4	+	++
17aA	4	++	++
13eG	4	+	++
13jA	8	++	++
13jG	8	+++	++

E. c: *Escherichia coli* K12.

¹MIC assay was also performed in biosensor assay, and the value was similar.

²For membrane integrity assay: High active, fast speed (++++) Medium active, Intermediate speed (+++), Medium active, Slow speed (++), Low active, Slow speed (+) and Not active (-).

³For viability assay: High effect (+++), Medium effect (++) , Low effect (+) and No effect (-). The highest concentration (51.2 µg/mL) was used to compare and evaluate the membrane integrity and viability assay results.

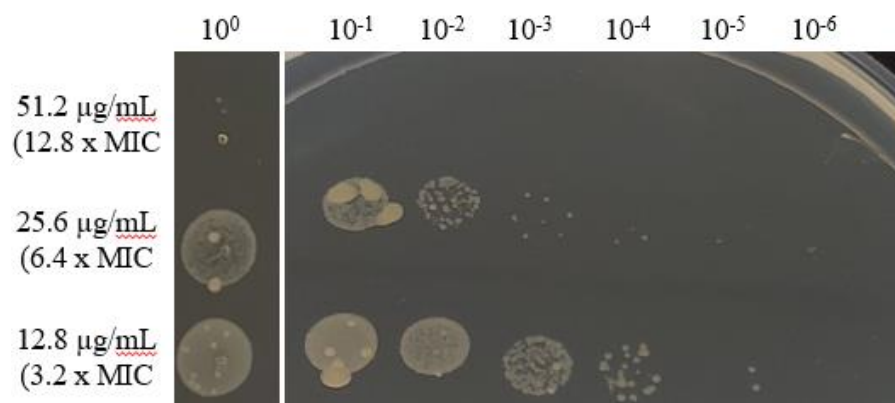


Figure S4. Bactericidal effect of barbiturate **11IG** against *E. coli* K12 after the outer membrane study with NPN. Horizontal: Dilution of the bacterial load.

8 Literature

- [1] M.H. Paulsen, M. Engqvist, D. Ausbacher, T. Anderssen, M.K. Langer, T. Haug, G.R. Morello, L.E. Liikanen, H.-M. Blencke, J. Isaksson, E. Juskewitz, A. Bayer, M.B. Strøm, Amphipathic Barbiturates as Mimics of Antimicrobial Peptides and the Marine Natural Products Eusynstyelamides with Activity against Multi-resistant Clinical Isolates, *J. Med. Chem.*, 64 (2021) 11395-11417.
- [2] C. Huixiong, L. Jean-Philippe, G. Nohad, G. Christiane, An Efficient and Enantioselective Synthesis of Suitably Protected β -[1-(4-Malonyl)naphthyl]-L-alanine and β -[1-(4-Malonylmethyl)naphthyl]-L-alanine: Novel Fluorescent and Non-Hydrolysable Phosphotyrosine Mimetics, *Eur. J. Org. Chem.*, 2006 (2006) 2329-2335.
- [3] W.Z. Bi, C. Qu, X.L. Chen, S.K. Wei, L.B. Qu, S.Y. Liu, K. Sun, Y.F. Zhao, Copper(II) catalyzed heterobenzylic C(sp³)-H activation: Two efficient halogenation methodologies towards heterobenzylic halides, *Tetrahedron*, 74 (2018) 1908-1917.
- [4] M. Donnier-Maréchal, P. Carato, P.-E. Larchanché, S. Ravez, R. Boulahjar, A. Barczyk, B. Oxombre, P. Vermersch, P. Melnyk, Synthesis and pharmacological evaluation of benzamide derivatives as potent and selective sigma-1 protein ligands, *Eur. J. Med. Chem.*, 138 (2017) 964-978.
- [5] M. Delor, J. Dai, T.D. Roberts, J.R. Rogers, S.M. Hamed, J.B. Neaton, P.L. Geissler, M.B. Francis, N.S. Ginsberg, Exploiting Chromophore-Protein Interactions through Linker Engineering To Tune Photoinduced Dynamics in a Biomimetic Light-Harvesting Platform, *J. Am. Chem. Soc.*, 140 (2018) 6278-6287.
- [6] P.H. Huy, J.C. Westphal, A.M.P. Koskinen, Concise, stereodivergent and highly stereoselective synthesis of cis- and trans-2-substituted 3-hydroxypiperidines – development of a phosphite-driven cyclodehydration, *Beilstein J. Org. Chem.*, 10 (2014) 369-383.
- [7] M. Botta, F. Corelli, G. Maga, F. Manetti, M. Renzulli, S. Spadari, Research on anti-HIV-1 agents. Part 2: Solid-phase synthesis, biological evaluation and molecular modeling studies of 2,5,6-trisubstituted-4(3H)-pyrimidinones targeting HIV-1 reverse transcriptase, *Tetrahedron*, 57 (2001) 8357-8367.
- [8] E.M. Igumnova, E. Mishchenko, T. Haug, H.-M. Blencke, J.U.E. Sollid, E.G.A. Fredheim, S. Lauksund, K. Stensvåg, M.B. Strøm, Synthesis and antimicrobial activity of small cationic amphipathic aminobenzamide marine natural product mimics and evaluation of relevance against clinical isolates including ESBL-CARBA producing multi-resistant bacteria, *Biorg. Med. Chem.*, 24 (2016) 5884-5894.
- [9] F.R. Cockerill, Methods for Dilution Antimicrobial Susceptibility Tests for Bacteria That Grow Aerobically. Approved Standard. M07-A9 in: C.a.L.S. Institut (Ed.), Wayne, Pa : Clinical and Laboratory Standards Institut, 2012.
- [10] M. Virta, K.E.O. Åkerman, P. Saviranta, C. Oker-Blom, M.T. Karp, Real-time measurement of cell permeabilization with low-molecular-weight membranolytic agents, *J. Antimicrob. Chemother.*, 36 (1995) 303-315.
- [11] J. Radeck, K. Kraft, J. Bartels, T. Cikovic, F. Dürr, J. Emenegger, S. Kelterborn, C. Sauer, G. Fritz, S. Gebhard, T. Mascher, The *Bacillus* BioBrick Box: generation and evaluation of essential genetic building blocks for standardized work with *Bacillus subtilis*, *J. Biol. Eng.*, 7 (2013) 29.
- [12] S. Frackman, M. Anhalt, K.H. Nealson, Cloning, organization, and expression of the bioluminescence genes of *Xenorhabdus luminescens*, *J. Bacteriol.*, 172 (1990) 5767-5773.

Paper II



Research paper

Investigation of tetrasubstituted heterocycles reveals hydantoins as a promising scaffold for development of novel antimicrobials with membranolytic properties

Manuel K. Langer^a, Aatur Rahman^b, Hymonti Dey^b, Trude Anderssen^c, Hans-Matti Blencke^b, Tor Haug^b, Klara Stensvåg^b, Morten B. Strøm^{c,*}, Annette Bayer^{a,*}

^a Department of Chemistry, UiT – The Arctic University of Norway, NO-9037, Tromsø, Norway

^b The Norwegian College of Fishery Science, Faculty of Biosciences, Fisheries and Economics, UiT – The Arctic University of Norway, NO-9037, Tromsø, Norway

^c Department of Pharmacy, Faculty of Health Sciences, UiT – The Arctic University of Norway, NO-9037, Tromsø, Norway



ARTICLE INFO

Keywords:

Antimicrobial peptides (AMP)
Synthetic mimics of antimicrobial peptides (SMAMPs)
Peptidomimetics
Hydantoin
Membranolytic

ABSTRACT

Mimics of antimicrobial peptides (AMPs) have been proposed as a promising class of antimicrobial agents. We report the analysis of five tetrasubstituted, cationic, amphipathic heterocycles as potential AMP mimics. The analysis showed that the heterocyclic scaffold had a strong influence on the haemolytic activity of the compounds, and the hydantoin scaffold was identified as a promising template for drug lead development. Subsequently, a total of 20 hydantoin derivatives were studied for their antimicrobial potency and haemolytic activity. We found 19 of these derivatives to have very low haemolytic toxicity and identified three lead structures, **2dA**, **6cG**, and **6dG** with very promising broad-spectrum antimicrobial activity. Lead structure **6dG** displayed minimum inhibitory concentration (MIC) values as low as 1 µg/mL against Gram-positive bacteria and 4–16 µg/mL against Gram-negative bacteria. Initial mode of action (MoA) studies performed on the amine derivative **6cG**, utilizing a luciferase-based biosensor assay, suggested a strong membrane disrupting effect on the outer and inner membrane of *Escherichia coli*. Our findings show that the physical properties and structural arrangement induced by the heterocyclic scaffolds are important factors in the design of AMP mimics.

1. Introduction

Antimicrobial resistance is now considered to have a similar impact on humans as global climate change [1]. Despite that, only around 30–40 new antimicrobial agents are currently in clinical trials and they are mainly derivatives of already marketed compound classes [2]. To combat the rising resistance, new and underdeveloped classes of compounds have to be utilized.

One promising group of antibiotic agents are the naturally occurring cationic antimicrobial peptides (AMPs), found in practically all higher forms of life [3]. Their amphipathic nature allows them to associate with the negatively charged bacterial outer membrane simultaneously as the lipophilic residues can insert and disrupt the membrane [3]. It is believed that due to the lack of a specific target, AMPs are less likely to induce antibiotic resistance development [4]. However, proteolytic instability [5], sometimes tedious synthetic procedures [6] and moderate activity [4] are among the drawbacks AMPs have been facing, thus

retarding their development. To address these issues a range of synthetic AMP analogues have been reported including peptoids [7,8], oligoureas [9], γ-AApeptides [10,11] and other small synthetic mimics of antimicrobial peptides (SMAMPs) [6,12,13].

In recent years, we have focussed on the development of synthetic analogues of AMPs that fulfil and operate at the limit of the pharmacophore model for AMPs. That is, the presence of two cationic groups and two lipophilic groups of sufficient bulk to exert broad-spectrum activity [14]. Among these were β-amino amides [15,16], cyclic tetrapeptides [16], barbiturates [17] and others [18,19]. The barbituric acid framework **1** has proven to be a valuable scaffold for the preparation of highly active antimicrobials [17,20], and we were curious if our previous results would translate to other scaffold structures.

In this work we initially investigated five heterocyclic scaffolds **2–5** and **15** (Fig. 1), that would allow for the same substitution pattern of two lipophilic side chains and two cationic chains as demonstrated for barbituric acid **1** [17,20]. To achieve segregation of the cationic and

* Corresponding authors.

E-mail addresses: morten.strom@uit.no (M.B. Strøm), annette.bayer@uit.no (A. Bayer).

<https://doi.org/10.1016/j.ejmech.2023.115147>

Received 13 November 2022; Received in revised form 19 December 2022; Accepted 21 January 2023

Available online 24 January 2023

0223-5234/© 2023 The Authors. Published by Elsevier Masson SAS. This is an open access article under the CC BY license (<http://creativecommons.org/licenses/by/4.0/>).

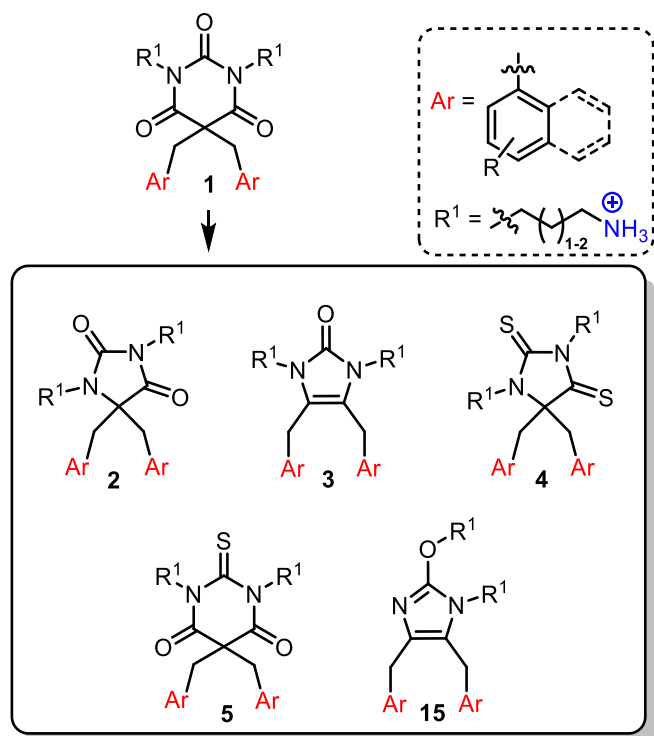


Fig. 1. Previously utilized barbituric acid **1** and core structures **2–5** and **15** used in this study. Ar = lipophilic side chain, R¹ = *n*-alkyl linker with a cationic head group. Red: lipophilic part, blue: cationic part.

lipophilic part we intended to attach the lipophilic side chains (Ar) at the bottom side of the heterocycles, bound to carbon atoms (Fig. 1). The *n*-alkyl linkers bearing the cationic head group (R¹) were incorporated onto the top side, bound to the nitrogen atoms (Fig. 1).

We then constructed a small library based on the most promising scaffold, the hydantoin **2**, and evaluated the effect of different lipophilic and cationic side chains. For the most potent analogues, their membranolytic behaviour was studied.

2. Results and discussion

2.1. Design of the study

We planned three sets of compounds. In the first set all core structures (**2–5** and **15**) shown in Fig. 1 were synthesized with a combination of substituents (Fig. 2, left) that we had evaluated in previous studies of amphipathic, antimicrobial barbituric acid derivatives [17,20].

Lipophilic 3,5-dibromobenzyl (3,5-di-Br) side chains were found earlier to be beneficial for the antimicrobial potency [16,17]. Aliphatic *n*-propyl linkers exhibited a good balance between antimicrobial potency and haemolytic activity [20] and amine groups were most accessible. It should be noted that we did not aim for the 2-(hydroxy)-1*H*-imidazole **15A** in the initial plan, but **15A** was obtained as a side product during synthesis. The second set was comprised of tetrasubstituted hydantoins **2** (Fig. 2, right) with different lipophilic side chains, *n*-propyl linkers, and amines and guanidines as cationic head groups. The lipophilic side chains and cationic groups were chosen based on their performance in previous studies [16,17,20,21]. For the third set we used promising lipophilic side chains from the second set and incorporated *n*-butyl linkers to deliver hydantoins **6** (Fig. 2, right). The *n*-butyl linkers have previously demonstrated to result in more potent derivatives [17,20].

Imidazolidine-2,4-dione **2**, commonly known as hydantoin, is a privileged scaffold in medicinal chemistry, found in drugs against

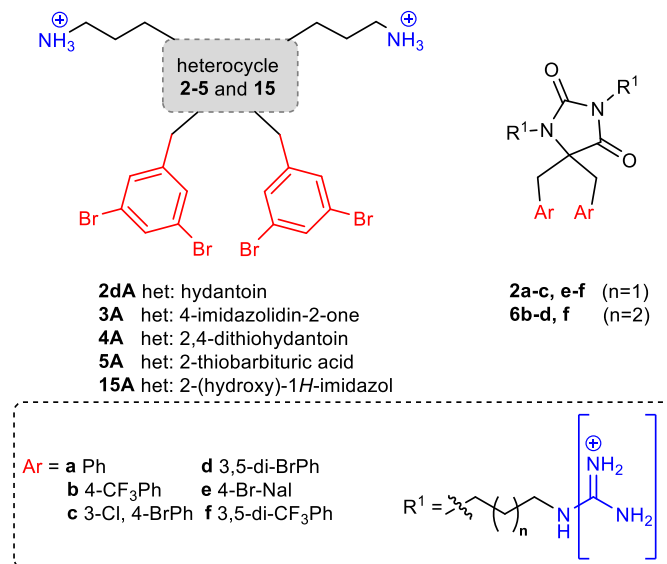


Fig. 2. Illustration of the three sets of compounds investigated. Brackets imply variations between cationic amine and guanidine groups.

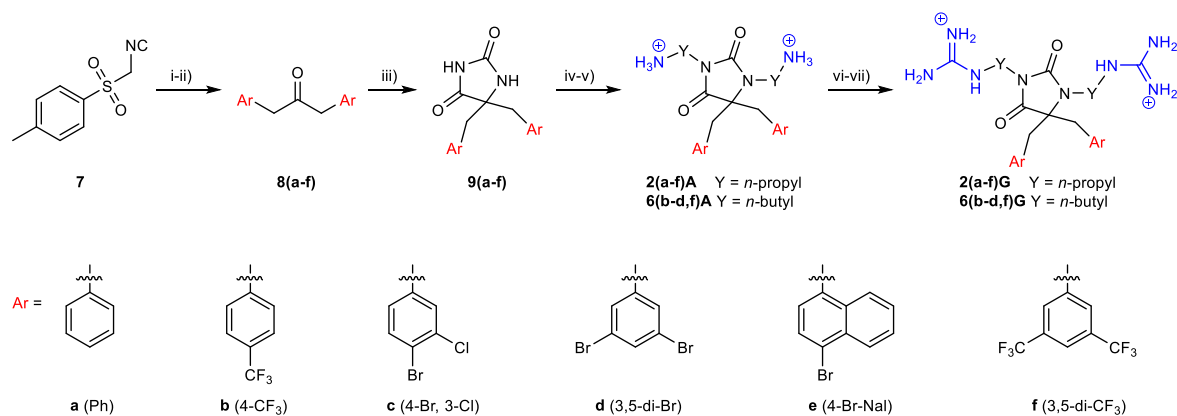
various conditions [22–27]. However, it is only rarely seen in antimicrobial agents [6,28–30]. Of particular interest to this work, is a study by Cai and co-workers who demonstrated that suitably substituted hydantoins can effectively target bacterial membranes [6]. In the related 4-imidazolidin-2-one **3**, the lipophilic side chains were attached to two vicinal sp² hybridized carbons, providing more spatial separation and altered dihedral angle between the side chains. Additionally, removal of the amidic oxygen from hydantoin **2** led to a slight change in polarity. The changes in structure and physical properties may affect the compounds' ability to interact with the bacterial membrane. Lastly, we wanted to investigate the effect of sulphur on the biological activity. Thioamides are often utilized in peptide synthesis [31] and are known to hamper enzymatic degradation of peptides [32]. Sulphur is also found in a variety of different drugs [33,34], including some antimicrobial thio-peptides [35,36] and β -lactam antibiotics such as penicillins and cephalosporins [37]. In most of these structures the sulphur atom is part of a heterocyclic ring or a (di)sulfide, but not a thioamide or a related motif. Therefore, we were interested in joining those two areas by replacing some oxygens for sulphur atoms in the hydantoin and barbituric acid [17] core structures. The resulting structures were **2**, 4-dithiohydantoin **4** and 2-thiobarbituric acid **5**.

2.2. Synthesis

2.2.1. Hydantoins **2** and **6**

The hydantoin structure can be accessed from a range of different reactions [38–41], including the Read [42], Bucherer-Bergs [43] and Biltz [44] syntheses. To achieve higher substitution patterns and to facilitate the access of compound libraries, modern strategies have been developed such as multicomponent reactions [45,46].

Based on the required substitution pattern and the nature of substituents, we decided to utilize the Bucherer-Bergs reaction as the key step in our synthetic strategy towards hydantoins **2A** and **6A** (Scheme 1). To that end, we prepared symmetric ketones **6** from *p*-toluenesulfonylmethyl isocyanate (TosMIC) **7** [47]. TosMIC was α,α -dialkylated using phase-transfer catalysis (PTC) in DCM and an aqueous NaOH solution with the benzyl bromide of choice. The crude products were hydrolysed by treatment with concentrated HCl [47] to give symmetric ketones **8(a–f)** in 53–69% yield over two steps (o2s). The Bucherer-Bergs reaction is commonly performed in a mixture of EtOH/H₂O [43], with precipitation of the resulting hydantoins as the main driving force. Unfortunately, only the unsubstituted



Scheme 1. Synthetic strategy towards target hydantoin 2 and 6. Reaction conditions: i) ArCH₂Br, TBAB or TBAI, DCM, NaOH_(aq) (20–35 wt%), r.t.; ii) HCl_(conc), DCM/THF, r.t., 53–69% o2s; iii) KCN, NH₄CO₃, KOAc, DMSO or KCN, NH₄CO₃, EtOH/H₂O, 60–75 °C, 45–85%; iv) *N*-Boc-3-bromopropylamine or *N*-Boc-4-bromobutylamine, Cs₂CO₃, TBAI, acetone, 65 °C then v) TFA, DCM, r.t., 45–85% o2s; vi) *N,N'*-Di-Boc-1*H*-pyrazole-1-carboxamide, DIPEA, THF, 45 °C then vii) TFA, DCM, r.t., 33–91% o2s.

diphenylpropan-2-one (Ar = Ph) could be prepared following this protocol. The other derivatives proved to be insoluble and the solvent needed to be changed to DMSO. Interestingly, an additional base, potassium acetate, was needed to obtain the hydantoin 9(a–f) in moderate to high yields of 45–85%. For *N,N'*-dialkylation, the hydantoin 9(a–f) were treated with *N*-Boc-3-bromopropylamine or *N*-Boc-4-bromobutylamine, caesium carbonate (Cs₂CO₃) and tetrabutylammonium iodide (TBAI) in acetone at elevated temperature.

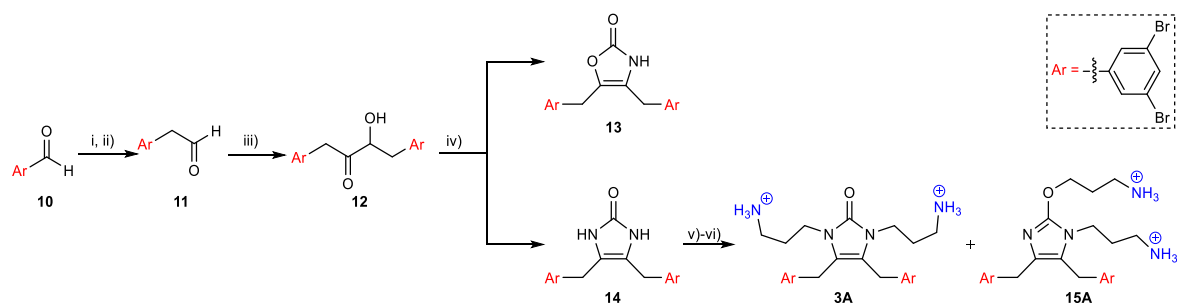
Subsequent TFA/DCM induced Boc removal delivered the target hydantoin 2A and 6A in 45–85% over two steps. Conversion of the amine-modified hydantoin 2A and 6A to their guanidyl counterparts was achieved with *N,N'*-di-Boc-1*H*-pyrazole-1-carboxamide and *N,N*-diisopropylethylamine (DIPEA) in THF. Ensuing Boc removal with TFA/DCM delivered guanidyl hydantoin 2G and 6G in 33–91% yield o2s.

2.2.2. 4-Imidazolidin-2-one 3A and 2-(hydroxy)-1*H*-imidazole 15A

We first set out to obtain the 4-imidazolidin-2-one derivative 3A by a two-step process from the Boc protected hydantoin 2dA (Ar = 3,5-di-BrPh) (see Supporting Information, Scheme S1 and Table S1). Even though the transformation was feasible, 3A could not be purified satisfyingly. Therefore, we changed the synthetic strategy as shown in Scheme 2. Starting from 3,5-dibromobenzaldehyde 10, we employed a Wittig reaction with Ph₃PCH₂(OMe)Cl to generate the corresponding vinyl ether in 91% yield as a 1.5:1.0 mixture of the *E*- and *Z*-isomer as by ¹H NMR. Treatment of the vinyl ether with hydrochloric acid in THF and formic acid or TFA in DCM resulted in complex mixtures. Using *in-situ* generated HCl by combining oxalyl chloride, EtOH and H₂O [48] led to quick and full conversion to the desired aldehyde, but the results were

not always reproducible. The most reliable results were finally achieved by using trimethylsilyl chloride (TMS-Cl) and sodium iodide in dry MeCN with high dilution [49]. The homologated aldehyde 11 was obtained in 60% yield. Aldehyde 11 was subsequently converted in a benzoin-type condensation to the α-hydroxy ketone 12 by treatment with Et₃N and catalytic amounts of 3-benzyl-5-(2-hydroxyethyl)-4-methylthiazolium chloride in dry PEG-400 [50]. We used PEG-400 instead of the more commonly employed EtOH [50], due to the low solubility of aldehyde 11. Based on literature [51], we condensed the α-hydroxy ketone 12 with urea in the presence of glacial acetic acid in anhydrous PEG-400. We obtained 4-imidazolin-2-one 14 in 39% yield as the major product and found unexpectedly 4-oxazolin-2-one 13 in 18% yield. In previous reports, the side product was only observed when the benzoin reagent had electron donating substituents (4,4'-dimethoxybenzoin) or heterocyclic nitrogen (2,2'-pyridoin) [51]. The authors were reasoning that the electron donating *para*-methoxy substituents would render the hydroxyl group of the intermediate more nucleophilic as does the basic pyridinyl nitrogen by intramolecular hydrogen bonding. One possible explanation could be the bromine atom acting as a Lewis base, forming a hydrogen bond to the hydroxyl hydrogen. This interaction would be comparable to the basic pyridinyl hydrogen and would facilitate an intramolecular attack of the urea oxygen, leading to compound 13.

We then alkylated 4-oxazolin-2-one 13 and 4-imidazolidin-2-one 14, respectively, with *N*-Boc-3-bromopropylamine using (*n*-hexadecyl)tri-*n*-butylphosphonium bromide as phase transfer catalyst and potassium carbonate as a base in a biphasic mixture of water and toluene under μ-wave irradiation. Subsequently, the di-alkylated products were



Scheme 2. Synthetic strategy towards tetrasubstituted 4-imidazolidin-2-one 3A and its constitutional isomer 15A. Ar = 3,5-dibromophenyl. Reaction conditions: i) Ph₃PCH₂(OMe)Cl, NaHMDS, THF (dry), –78 °C to r.t., 91%; *E/Z* = 1.5/1.0; ii) TMS-Cl, NaI, MeCN (dry), r.t., 60%; iii) 3-benzyl-5-(2-hydroxyethyl)-4-methylthiazolium chloride, Et₃N, PEG-400 (dry), 80 °C, 39%; iv) urea, AcOH, PEG-400 (dry), 130 °C, 18% for 13 and 39% for 14; v) *N*-Boc-3-bromopropylamine, K₂CO₃, (*n*-hexadecyl)tri-*n*-butylphosphonium bromide, toluene:water, μ-wave, 130–150 °C then vi) TFA, DCM, r.t., 17–19% o2s.

deprotected with TFA/DCM. Synthesis of the derivative from 4-oxazol-2-one **13** delivered a di-alkylated compound with an unresolved structure and was not further investigated.

Compound **14** delivered the desired *N,N'*-dialkylated 4-imidazolin-2-one **3A** in low yields (19% o2s). Surprisingly, *N,O*-dialkylated 2-(hydroxy)-1*H*-imidazole **15A** (17% o2s) was obtained from the same reaction mixture. The mono alkylated derivatives of structures **3A** and **15A** were obtained as well, partially explaining the low yields.

2.2.3. 2,4-Dithiohydantoin **4A**

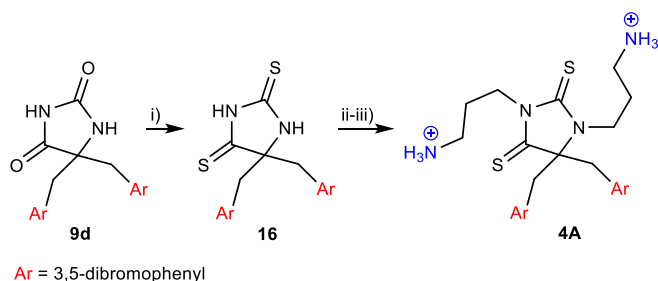
By employing *in situ* generated NH_4CN and CS_2 [52] we intended to obtain 2,4-thiohydantoin **4A** from ketone **8d** (Ar = 3,5-di-BrPh), but no conversion was observed. Instead hydantoin **9d** (3,5-di-Br) was treated with the Lawesson's reagent at elevated temperature [53] to deliver 2,4-thiohydantoin **16** (3,5-di-Br) in 82% yield (Scheme 3). *N,N'*-Dialkylation of **16** with *N*-Boc-3-bromopropylamine afforded 2,4-dithiohydantoin **4A** in 56% yield.

2.2.4. 2-Thiobarbituric acid **5A**

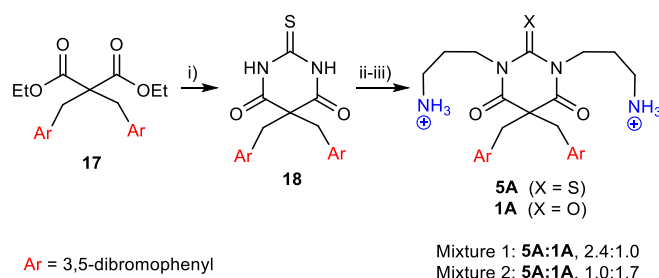
In a first approach we tried to thiolate 5,5-bis(3,5-dibromobenzyl) barbituric acid with the Lawesson's reagent under the same conditions as used to obtain 2,4-dithiohydantoin (vide supra). Unfortunately, we obtained an inseparable mixture of the mono-, di- and tri-thiolated barbituric acid. Therefore, we decided to adapt our previously reported procedure [17] by replacing urea with thiourea. Treatment of di-benzylated diethyl malonate **17** and thiourea with NaH in a mixture of anhydrous THF and DMF gave the 5,5-dibenzylated-2-thiobarbituric acid **18** in low yields (Scheme 4). *N*-alkylation with *N*-Boc-3-bromopropylamine, Cs_2CO_3 and TBAI in acetone at elevated temperature, followed by TFA/DCM mediated Boc removal delivered the tetrasubstituted barbiturates **5A** and **1A** in very low yields (9%). Partial desulfurization had taken place, resulting in two mixtures of tetrasubstituted 2-thiobarbituric acid **5A** (X = S) and barbituric acid **1A** (X = O). Mixture 1 constituted a ratio of 2.4:1.0 (**5A:1A**) and mixture 2 constituted a ratio of 1.0:1.7 (**5A:1A**). The mixtures were inseparable but stable in solid state and were tested as such. Only when the mixtures were in solution, we could see slow desulfurization take place, potentially by low amounts of peroxide formation from atmospheric oxygen under light exposure [54,55].

2.3. SAR analysis

All compounds were screened for their antimicrobial activity against antibiotic susceptible Gram-positive and Gram-negative bacterial reference strains. Antimicrobial potency of each compound was expressed by their minimum inhibitory concentration (MIC) values. Haemolytic activity against human red blood cells (RBC), expressed by the EC_{50} value, was used as a measurement of cytotoxicity. The ideal compound should display high bacterial activity (low MIC values) and low or no toxicity towards human cells (high EC_{50} values) i.e. acting



Scheme 3. Synthetic strategy towards 2,4-dithiohydantoin **4A**. Ar = 3,5-dibromophenyl. Reaction conditions: i) Lawesson's reagent, 1,4-dioxane, 115 °C, 82%; ii) *N*-Boc-3-bromopropylamine, Cs_2CO_3 , TBAI, acetone, 55 °C then iii) TFA, DCM, r.t., 56%.



Scheme 4. Synthetic strategy towards 2-thiobarbituric acid **5A**. Mixtures of 2-thiobarbituric acid **5A** (X = S) and barbituric acid **1A** (X = O) were obtained. Ar = 3,5-dibromophenyl. Reaction conditions: i) Thiourea, NaH, anhydrous THF:DMF, 65 °C, 24%; ii) *tert*-butyl (3-bromopropyl)carbamate, Cs_2CO_3 , TBAI, acetone, 70 °C, then iii) TFA, DCM, r.t., 9% o2s.

selectively against bacteria. As a reference compound we used the already reported barbiturate **1A** [20] (Table 1, entry 7). The commercially available antibiotic ciprofloxacin served as a positive control (entry 8). Capital A in the compound codes denotes cationic amine derivatives and capital G denotes cationic guanidine derivatives. For Series 2 and 3 the substituents on the phenyl groups are given in brackets for each compound to aid the discussion. The hydrophilicity of each core structure, bearing four substituents, was calculated using the ChemBioDraw Ultra software (PerkinElmer, v19.0.0.1.28).

2.3.1. Exploring new scaffolds

We started our investigation by comparing the different scaffolds **2dA**, **3A**, **4A**, **5A** and **15A** to identify the most promising candidate in terms of antimicrobial and haemolytic activity (Table 1). All scaffolds were decorated with the same lipophilic (Ar = 3,5-dibromophenyl) and cationic group ($\text{R}^1 = 3\text{-aminoprop-1-yl}$). The five membered hydantoin **2dA** (entry 1) was marginally less potent (MIC: 4–16 $\mu\text{g}/\text{mL}$) than the

Table 1

Antimicrobial activity (MIC in $\mu\text{g}/\text{mL}$) against bacterial reference strains and haemolytic activity against human RBC (EC_{50} in $\mu\text{g}/\text{mL}$) for compounds with different scaffold structures.

Entry	Comp. ID	CLogP ^a	Antimicrobial activity				EC ₅₀
			S. a	B. s	E. c	P. a	
1	2dA	-1.69	8	4	16	8	344
2	3A	-0.47	2	1	4	8	52
3	15A	0.26	2	2	4	4	44
4	4A	-1.22	8	8	16	32	385
5	Mixture 1 ^b	n.d.	8	4	8	16	305
6	Mixture 2 ^c	n.d.	8	4	8	8	182
7 [20]	1A	-1.44	4	4	8	8	99
8	Ciprofloxacin		0.06	<0.03	<0.03	0.25	

Bacterial reference strains: S. a – *Staphylococcus aureus* ATCC 9144, B. s – *Bacillus subtilis* 168, E. c – *Escherichia coli* ATCC 25922, and P. a – *Pseudomonas aeruginosa* ATCC 27853.

^a ClogP values were calculated for the respective tetrasubstituted core structures (calculated with ChemBioDraw Ultra). n.d.: not determined.

^b Mixture of 2.4:1.0 (**5A:1A**).

^c Mixture of 1.0:1.7 (**5A:1A**).

barbituric acid **1A** (entry 7), although it was estimated to be slightly more hydrophilic. Interestingly, hydantoin **2dA** was almost 3.5 times less haemolytic (EC_{50} : 344 $\mu\text{g/mL}$) than **1A** (EC_{50} : 99 $\mu\text{g/mL}$). The 4-imidazolidin-2-one core **3A** (entry 2) was one order of magnitude more lipophilic than the hydantoin core. **3A** demonstrated a 4-fold increase in antimicrobial potency (MIC: 1–4 $\mu\text{g/mL}$) against all strains except for the Gram-negative bacterium *Pseudomonas aeruginosa*, but also a 7–8-fold increase in haemolytic activity (EC_{50} : 52 $\mu\text{g/mL}$). The constitutional isomer 4-oxazolin-2-one **15A** (entry 3) gave a similar result (MIC: 2–4 $\mu\text{g/mL}$, EC_{50} : 44 $\mu\text{g/mL}$). Despite being very potent, the systemic application of these compounds is limited by their high haemolytic activity.

It did not become clear why these core structures were so distinctively more haemolytic than hydantoin **2dA**. The 2,4-dithiohydantoin **4A** (entry 4) displayed a 4-fold decrease in activity against *P. aeruginosa* (MIC: 32 $\mu\text{g/mL}$) compared to its dioxo counterpart **2dA**. The dithio-derivative **4A** was only marginally less haemolytic (EC_{50} : 385 $\mu\text{g/mL}$) than **2dA** (EC_{50} : 344 $\mu\text{g/mL}$).

Mixture 1 (entry 5), being enriched with 2-thiobarbituric acid **5A** (ClogP = -0.52), exhibited reduced potency against the Gram-negative *P. aeruginosa* (MIC: 16 $\mu\text{g/mL}$) and the haemolytic activity (EC_{50} : 305 $\mu\text{g/mL}$) was decreased by a factor of three compared to **1A** (EC_{50} = 99 $\mu\text{g/mL}$). By reduction of the amount of **5A** in mixture 2 (entry 6), antimicrobial activity (MIC: 4–8 $\mu\text{g/mL}$) and more pronouncedly the haemolytic activity (EC_{50} : 182 $\mu\text{g/mL}$) approached the values found for **1A** (entry 7). In conclusion, the sulphur containing derivatives were less

haemolytic and less potent against the Gram-negative *P. aeruginosa*. No major change in activity was observed against the other bacterial test strains. Combined with the synthetic challenges and the chemical instability, thionylated derivatives were not worthwhile to investigate further. Clearly the hydantoin scaffold was the most promising core structure for further development.

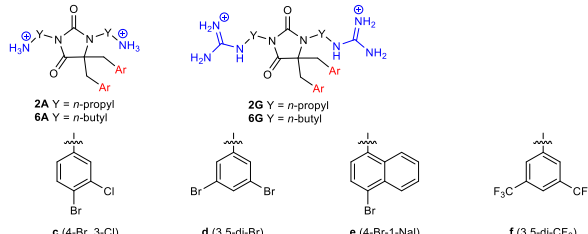
2.3.2. Hydantoins with *n*-propyl linkers (2)

A series of hydantoins **2** (Table 2) with *n*-propyl linkers connecting the cationic amino (**A**) or guanidino (**G**) groups to the core were constructed to screen additional lipophilic side chains (**a-c** and **e-f**) for their impact on the compounds' potency and haemolytic toxicity. We have chosen (pseudo)halogenated benzyl groups as lipophilic side chains based on their potential influence on the antimicrobial potency and haemolytic activity described in previous studies [16,17,20]. The trends observed in this study were similar to previous studies and will not be repeated in detail here. The compounds are ranged according to increasing lipophilicity.

Generally, the compounds in amine series **2(a-f)A** (Table 2, entry 1–6) exhibited improved antibacterial potency and increased haemolytic activity with higher CLogP values of the lipophilic side chains, except for hydantoin **2fA** (3,5-di- CF_3). Derivatives **2aA** (Ph) and **2bA** (4- CF_3) were practically inactive against all strains (MIC: 16–>256 $\mu\text{g/mL}$). Amine hydantoin **2cA** (4-Br, 3-Cl) was only active against the Gram-positive strains, *Bacillus subtilis* and *Staphylococcus aureus* (MIC: 4–8 $\mu\text{g/mL}$), whereas the amine hydantoins **2(d-f)A** (entries 4–6) were

Table 2

Antimicrobial activity (MIC in $\mu\text{g/mL}$) against bacterial reference strains and haemolytic activity against human RBC (EC_{50} in $\mu\text{g/mL}$) for tetrasubstituted hydantoins **2** and **6**.



Entry	Comp. ID	Ar	Y	CLogP ^a	Antimicrobial activity				EC_{50} ^b
					S. a	B. s	E. c	P. a	
1	2aA	(Ph)	<i>n</i> -propyl	2.64	>256	256	>256	>256	>311
2	2bA	(4- CF_3)	<i>n</i> -propyl	3.52	64	16	256	>256	>379
3	2cA	(4-Br, 3-Cl)	<i>n</i> -propyl	4.08	8	4	32	32	368
4	2dA	(3,5-di-Br)	<i>n</i> -propyl	4.38	8	4	16	8	344
5	2eA	(4-Br-1-Nal)	<i>n</i> -propyl	4.68	4	4	8	8	69
6	2fA	(3,5-di- CF_3)	<i>n</i> -propyl	5.03	16	8	16	16	399
7	2aG	(Ph)	<i>n</i> -propyl	2.64	64	128	>256	>256	>353
8	2bG	(4- CF_3)	<i>n</i> -propyl	3.52	16	8	128	>256	>421
9	2cG	(4-Br, 3-Cl)	<i>n</i> -propyl	4.08	2	2	32	64	>467
10	2dG	(3,5-di-Br)	<i>n</i> -propyl	4.38	2	4	16	32	486
11	2eG	(4-Br-1-Nal)	<i>n</i> -propyl	4.68	2	2	8	32	206
12	2fG	(3,5-di- CF_3)	<i>n</i> -propyl	5.03	4	2	32	32	>489
13	6bA	(4- CF_3)	<i>n</i> -butyl	3.52	64	16	>128	>128	>393
14	6cA	(4-Br, 3-Cl)	<i>n</i> -butyl	4.08	8	4	64	64	>439
15	6dA	(3,5-di-Br)	<i>n</i> -butyl	4.38	8	2	32	32	364
16	6fA	(3,5-di- CF_3)	<i>n</i> -butyl	5.03	16	4	64	64	>461
17	6bG	(4- CF_3)	<i>n</i> -butyl	3.52	4	4	64	>128	>503
18	6cG	(4-Br, 3-Cl)	<i>n</i> -butyl	4.08	1	1	8	32	347
19	6dG	(3,5-di-Br)	<i>n</i> -butyl	4.38	1	1	4	16	206
20	6fG	(3,5-di- CF_3)	<i>n</i> -butyl	5.03	2	2	8	32	384
21	Ciprofloxacin				0.06	<0.03	<0.03	0.25	

Bacterial reference strains: S. a – *Staphylococcus aureus* ATCC 9144, B. s – *Bacillus subtilis* 168, E. c – *Escherichia coli* ATCC 25922, and P. a – *Pseudomonas aeruginosa* ATCC 27853.

^a ClogP values were calculated for substituted benzyl groups (calculated with ChemBioDraw Ultra).

^b Values given as *greater than* correspond to the highest concentration (500 μM) tested in the RBC assay.

potent against all strains tested (MIC: 4–16 µg/mL). The most potent amine derivative was **2eA** (4-Br-1-Nal), showing good broad-spectrum potency (MIC: 4–8 µg/mL). Interestingly, it was at least 5-times more haemolytic (EC₅₀: 69 µg/mL) than any of the other amine derivatives (**2A**). Hydantoin **2fA** (3,5-di-CF₃) was more lipophilic than **2eA** (4-Br-1-Nal) but less potent (MIC: 8–16 µg/mL) than the latter by a factor of two to four. The electron withdrawing trifluoromethyl groups may lead to a slight polarisation of the aromatic ring, thus reducing its ability to interact with the lipid membrane. The most promising amine derivative was **2dA** (3,5-di-Br), having broad-spectrum activity (MIC: 4–16 µg/mL) and negligible haemolytic activity (EC₅₀: 344 µg/mL). Surprisingly, it demonstrated slightly higher activity against *P. aeruginosa* than *Escherichia coli*

The guanidyl series **2(a-f)G** (Table 2, entry 7–12) exhibited the same general trend for antimicrobial potency and haemolytic activity as in the amine series, except for derivative **2fG** (3,5-di-CF₃). The guanidyl derivatives were generally more potent against the Gram-positive strains than their amine counterparts by a factor of two to four. Guanidyl hydantoins **2(b-f)G** (entries 8–12) exhibited good to very good potency (MIC: 2–16 µg/mL) against the Gram-positive strains. The potency against the Gram-negative *E. coli* was virtually unchanged compared to their amine correlates. However, the activity against the Gram-negative *P. aeruginosa* decreased two-fold for **2cG** (4-Br, 3-Cl) and **2fG** (3,5-di-CF₃), and four-fold for **2dG** (3,5-di-Br) and **2eG** (4-Br-1-Nal), correspondingly. All guanidyl derivatives were pronouncedly less haemolytic than their amine equivalents. The most promising guanidine derivative was **2eG** (4-Br-1-Nal), which demonstrated good potency against all bacterial strains (MIC: 2–8 µg/mL) except for *P. aeruginosa* and had low haemolytic toxicity (EC₅₀: 206 µg/mL). The combination of *n*-propyl linkers and guanidyl head groups having improved potency against Gram-positive strains and reduced potency against the Gram-negative *P. aeruginosa*, as well as reduced haemolytic activity, has also been observed for amphipathic barbiturates [20].

In summary, guanidyl derivatives **2(c-f)G** showed good potency against both Gram-positive test strains (MIC: 2–4 µg/mL), but none of the guanidyl derivatives **2G** were potent against *P. aeruginosa*. Amines **2dA** (3,5-di-Br) and **2eA** (4-Br-1-Nal) were the most potent derivatives of hydantoins **2**, with **2dA** (3,5-di-Br) being non haemolytic.

2.3.3. Hydantoins with *n*-butyl linkers (**6**)

In our previous study on tetrasubstituted barbiturates, a combination of guanidyl head groups and *n*-butyl linkers achieved the highest broad-spectrum activity. Due to the structural similarity, we reasoned that *n*-butyl linkers would boost the hydantoins' potency. We chose the most promising side chains **b** (4-CF₃), **c** (4-Br, 3-Cl), **d** (3,5-di-Br) and **f** (3,5-di-CF₃) from hydantoin derivatives **2**.

Amine hydantoins **6A** displayed the same potency against the Gram-positive strains as derivatives **2A** but had reduced activity against the Gram-negative strains by a factor of two to four (Table 2). None of the derivatives were haemolytic (EC₅₀: ≥364 µg/mL).

Upon guanylation, all compounds of **6G** became highly potent against the Gram-positive strains (MIC: 1–4 µg/mL). Guanidino hydantoin **6cG** (4-Br, 3-Cl) demonstrated good activity against all strains (MIC: 1–8 µg/mL), except for *P. aeruginosa*, with no noteworthy haemolytic activity (EC₅₀: 347 µg/mL). Hydantoin **6dG** (3,5-di-Br) had excellent activity against the Gram-positive strains (MIC: 1 µg/mL) and good to moderate activity against the Gram-negative strains (MIC: 4–16 µg/mL).

In summary, we did observe increased potency and haemolytic activity for the guanidyl compounds **6G** compared to their amine counterparts **6A** (*vide supra*). While being non-haemolytic, the potency of the amine derivatives was rather unsatisfying. The guanidyl compounds **6cG** (4-Br, 3-Cl) and **6dG** (3,5-di-Br), however, displayed promising antimicrobial potency and low to no haemolytic activity.

2.4. Selectivity index and counterion effect

The selectivity index (SI) is a simple descriptor given by the ratio of EC₅₀/MIC for the efficiency of antimicrobial agents. We have summarized the most promising compounds with their SI values in Table 3. Compounds were only considered active if the MIC value was ≤16 µg/mL. SI values for all other compounds can be found in the Supporting Information, Table S3.

Compounds **2cG** (4-Br, 3-Cl), **2fG** (3,5-di-CF₃), **6cA** (4-Br, 3-Cl) **2dG** (3,5-di-Br), **2eG** (4-Br-1-Nal), **6cG** (4-Br, 3-Cl) and **6fG** (3,5-di-CF₃) demonstrated excellent selectivity for the Gram-positive strains (entries 1–7). Hydantoins **2dG**, **2eG**, **6cG** and **6fG** (entries 4–7) had additionally good selectivity (SI: >20) for *E. coli*. All seven derivatives showed low to no haemolytic toxicity. Derivatives **2dA** (3,5-di-Br), **2fA** (3,5-di-CF₃) and **6dG** (3,5-di-Br) had good SI values for all strains tested (entries 8–10). The hydantoins **2dA** (3,5-di-Br) and **2fA** (3,5-di-CF₃) had SI values >20 against the Gram-negative bacterium *P. aeruginosa*, while **6dG** (3,5-di-Br) had SI: 13 for *P. aeruginosa*. All these can be considered very promising compounds.

All compounds tested were obtained as di-trifluoroacetate (di-TFA) salts, which are non-physiological. Therefore, we converted **2cA**, **2cG**, **2dA** and **2dG** to physiological di-hydrochloride (di-HCl) salts, to assess if the biological behaviour would be altered (see Supporting Information, Table S2). We did not observe any major changes in the MIC or EC₅₀ values for any of these four derivatives. Minor improvements in antimicrobial activity could be observed for the di-HCl salts of **2cA** (4-Br, 3-Cl) and **2cG** (4-Br, 3-Cl), but no clear trend was apparent. Also, the haemolytic activity was only influenced to a small extent and could often be correlated to the lower molecular weight of the di-HCl salts compared to the di-TFA salts.

2.5. Mode of action (MoA) studies

We have examined the effects of the compounds on the viability of bacterial cells and the membrane integrity of bacterial cells. Seven compounds were selected (based on structural alterations, MIC values, haemolytic activity, and SI) for MoA studies against *B. subtilis* 168 (see Supporting Information, Table S4), as they were primarily potent against Gram-positive bacteria. Six additional compounds with broad-spectrum activity were selected for MoA studies against both, *B. subtilis* 168 and *E. coli* K12 (see Supporting Information, Tables S4 and S5) [56]. These two well-known strains of *B. subtilis* and *E. coli*, in combination with the respective sensor plasmids that carry the reporter constructs, serve as models to study the modes of action in

Table 3

Selectivity index (SI) of the most promising narrow- and broad-spectrum antimicrobials. EC₅₀ values are given in [µg/mL].

Entry	Comp. ID	SI (EC ₅₀ /MIC) ^a				EC ₅₀ ^b
		S. a	B. s	E. c	P. a	
1	2cG	>234	>234	–	–	>467
2	2fG	>122	>245	–	–	>489
3	6cA	>55	>110	–	–	>439
4	2dG	243	122	30	–	486
5	2eG	103	103	26	–	206
6	6cG	347	347	43	–	347
7	6fG	192	192	48	–	384
8	2dA	43	86	22	43	344
9	2fA	25	50	25	25	399
10	6dG	206	206	52	13	206

Bacterial reference strains: S. a – *Staphylococcus aureus* ATCC 9144, B. s – *Bacillus subtilis* 168, E. c – *Escherichia coli* ATCC 25922, and P. a – *Pseudomonas aeruginosa* ATCC 27853.

^a –: No SI was calculated if MIC was >16 µg/mL.

^b Values given as *greater than* correspond to the highest concentration (500 µM) tested in the RBC assay.

representatives of Gram-positive and Gram-negative bacteria, respectively.

To explore the MoA of promising compounds in *B. subtilis* 168 and *E. coli* K12, we conducted two luciferase-based biosensor tests – examining the effects on bacterial viability and membrane integrity. The biosensor-based viability test measures the viability of bacterial cells as light production by recombinantly expressed bacterial luciferase derived from the *Photobacterium luminescens lux* operon [57,58]. External substrates do not affect light production by bacterial lux operons. Bacteria themselves provide a reduced flavin mononucleotide (FMN₂) and a long-chain aldehyde pool, which is the substrate for light production. Bacterial luciferase is a very efficient real-time sensor of bacterial viability because NADH, NADPH, and ATP are required to constantly fill the substrate pool.

The biosensor-based membrane integrity test is based on the *lucGR* gene (luciferase) of *Pyrophorus plagiophthalmus*, which is a luminous click beetle [59]. Unlike bacterial luciferase, the light reaction is closely dependent on externally added D-luciferin as a substrate. D-luciferin cannot cross the intact biological membrane properly at neutral pH. The uptake of D-luciferin is explored after the addition of antimicrobial substances to determine whether the membrane has been affected and becomes permeable for D-luciferin or not. If D-luciferin enters through damaged membranes, light production increases. Light production peaks quickly if the integrity of the membrane is compromised and then usually decreases during the consumption of the dying cells' ATP.

In general, most of the compounds tested influenced survival (viability) and showed strong membrane disrupting activity against *B. subtilis*, and some of them were active against both bacterial species. However, some compounds had more prominent effects on survival and faster membranolytic effects on *B. subtilis* than *E. coli*. When the concentration of the compounds exceeded the MIC value against the respective bacterium, both the viability and the integrity of the membrane were affected for most compounds. Furthermore, increasing concentrations affected both viability and membranolytic activity at an increasing rate, indicating a concentration-dependent killing effect.

However, we were unable to determine the relationship between the structure/activity and the mode of action profiles. Compound **6cG** (4-Br, 3-Cl) was chosen as a broad-spectrum hydantoin to illustrate the results with regard to viability and membrane integrity (Figs. 3 and 4). During the 3 min test period, hydantoin **6cG** showed a substantial influence on the survival (viability) of *B. subtilis* (Fig. 3A, left). The derivative **6cG** showed a membrane-related action because the light emittance increased rapidly and dose-dependently (Fig. 3B, left), and the effect was prominent compared to chlorhexidine (CHX) (Fig. 3B, right). The CHX reference control is a bactericidal agent that affects the cell walls and membranes of both *B. subtilis* 168 [60] and *E. coli* K12 [61]. In the present study, the MIC value for CHX was determined to be 1.5 µg/mL against both *B. subtilis* 168 and *E. coli* K12. The disruptive membrane effect of hydantoin **6cG** on *B. subtilis* was shown to occur at a concentration of 25.6 and 51.2 µg/mL (blue and black line, Fig. 3B, left), which were 25.6 and 51.2 times higher than its MIC (1 µg/mL). Concentrations below 25.6 µg/mL showed a limited membrane disruption effect, with peak emissions not decreasing during the measurement period. The bacterial concentration in these experiments was approximately 100 times higher than that used in the MIC test, and this could explain why a higher concentration of **6cG** hydantoin was required to affect the viability and integrity of the membrane.

The effect of hydantoin **6cG** on the viability and membrane integrity of the Gram-negative *E. coli* showed somewhat incomparable effects as observed towards the Gram-positive *B. subtilis*. Being a broad-spectrum derivative, **6cG** could not influence the viability of *E. coli* as fast as the strong membranolytic agent CHX (Fig. 4A). Although a concentration-dependent declining trend of light emission was seen in the viability assay, only the highest concentration (51.2 µg/mL which is 6.4 x MIC) resulted in increased light emission in the inner membrane assay and it was not followed by a decline during the test period (indicating a less notable disruptive effect of the inner membrane) (Fig. 4B, left). The delay and reduction in the effect of **6cG** on membrane integrity could be caused by the outer membrane of *E. coli*, which may act as an additional barrier.

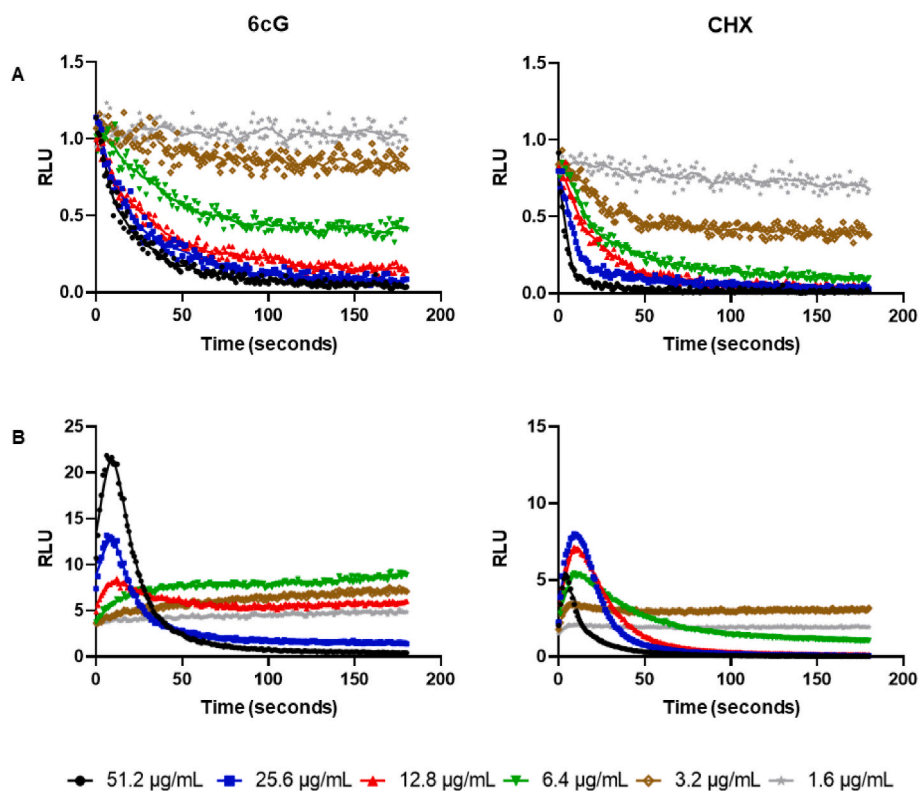


Fig. 3. The effects of **6cG** (broad spectrum) and chlorhexidine (CHX, positive control) on the kinetics of (A) viability and (B) membrane integrity in *B. subtilis* 168. Normalized light emission (normalized with a negative, untreated water control) is plotted as relative light units (RLU) over time (seconds). Light emission was measured each second for 180 s after adding the bacterial cell suspension (with 1 mM D-luciferin for the membrane integrity assay) to the analytes in separate wells. The figure shows a representative data set from at least three independent experiments.

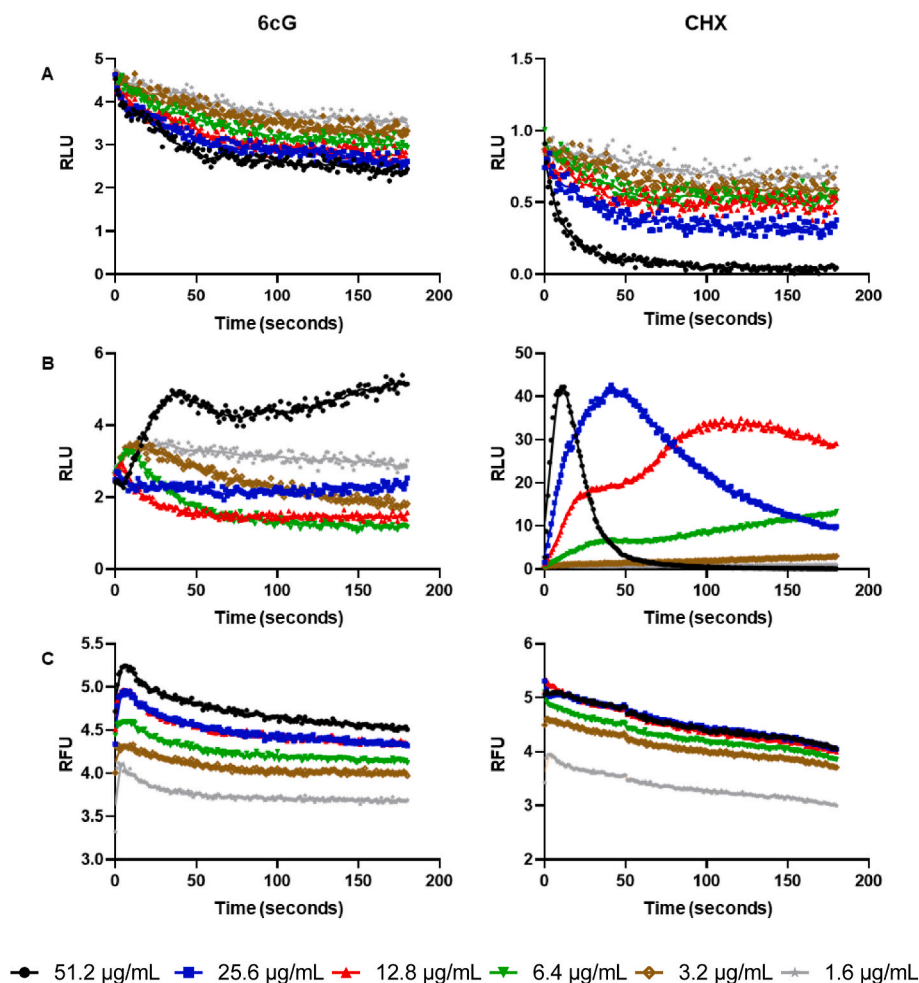


Fig. 4. The effects of **6cG** (broad spectrum) and chlorhexidine (**CHX**, positive control) on the kinetics of (A) viability, (B) inner membrane integrity, and (C) outer membrane integrity in *E. coli* K12. Normalized light emission (normalized with a negative, untreated water control) over time (seconds) for A and B. For C, normalized fluorescence (normalized with a negative, untreated water control) is plotted as relative fluorescence units (RFU) over time (seconds). Light emission/fluorescence was measured each second for 180 s after adding the bacterial cell suspension (with 1 mM D-luciferin for the inner membrane integrity assay and 20 μM 1-*N*-phenylnaphthylamine for outer membrane integrity assay) to the analytes in separate wells. The figure shows a representative data set from at least three independent experiments.

We used the 1-*N*-phenylnaphthylamine (NPN) fluorescent probe to determine whether **6cG** affected the outer membrane permeability of *E. coli*. The small NPN molecules (219 Da) have low fluorescence in water solutions, but if bound to phospholipids, they produce high fluorescence. Hydrophobic NPN cannot effectively pass through the outer membrane of intact *E. coli* cells, resulting in low fluorescence; however, if the outer membrane is damaged, NPN can reach the periplasmic space, bind to the phospholipids of the inner and outer membrane, and produce enhanced fluorescence [62]. In this test, high concentrations of hydantoin **6cG** produced high fluorescence levels (Fig. 4C, left), while no significant increase in luminescence was observed in the inner membrane integrity test, except in one concentration which is 51.2 μg/mL (Fig. 4B, left). This observation indicates that the presence of the outer membrane may be a rate-limiting step for this compound to act on the inner membrane. However, when the concentration of **6cG** increased, the fluorescence level was higher (Fig. 4C, left), indicating a rapid change in outer membrane permeability that was followed by membrane disruption as compared to **CHX** (Fig. 4C, right). At the same time, bacterial cell survival was reduced (Fig. 4A, left) and the integrity of the inner membrane was altered (Fig. 4B, left).

The viability of the bacterial cells was markedly reduced for a concentration of 51.2 μg/mL (6.4 × MIC) (see Fig. S1), and when samples from the NPN assay were spotted on an agar plate after the test period, a bactericidal effect of **6cG** was demonstrated. These results strongly suggest that when concentrations are high enough, hydantoin **6cG** disrupts the outer and inner membranes at the same speed. However, it cannot be excluded that higher concentrations of **6cG** cause a different

MoA, leading the compound to cross the outer membrane without affecting the latter.

Our results indicate that the main MoA of most of the synthesized compounds is to interrupt the integrity of the bacterial membranes in a concentration-dependent manner – as demonstrated for the broad-spectrum hydantoin **6cG**, against both the Gram-positive *B. subtilis* and the Gram-negative *E. coli*. However, some cationic AMPs have a concentration-dependent dual mode of action [63]. For example, it is known that the N-terminal fragment 1–35 of Bac7 (a proline-arginine rich AMP) has an effect on the internal membrane at high concentrations and binds to the intracellular chaperone protein DnaK and 70S ribosomes, and affect these target molecules at low concentrations [64–66]. Hence, other targets may exist in addition to the bacterial cytoplasmic membranes. Further studies are needed to determine whether there are other additional modes of action for these compounds.

3. Conclusion

We investigated five scaffolds for their suitability to develop novel tetrasubstituted, amphipathic SMAMP antimicrobials, revealing the hydantoin structure as a promising template for antibacterial drug lead development. By screening different combinations of lipophilic side chains, *n*-alkyl linkers and cationic groups we identified the tetrahalogenated compounds **2dA** (3,5-di-Br), **6cG** (4-Br, 3-Cl) and **6dG** (3,5-di-Br) as very promising lead structures. The results obtained from the viability and membrane integrity assays, suggested a rapid membranolytic effect, as demonstrated for hydantoin **6cG** in *B. subtilis* and *E. coli*. Interestingly, both the inner and the outer membrane in *E. coli*

seemed to be disrupted at a similar speed. We believe that our findings on the qualitative contribution of the scaffold structures can help the development of novel small molecule analogues of AMPs or SMAMPs.

4. Experimental section

For a detailed description of all chemical and biological experimental procedures, chemical analysis and further discussions see the Supporting Information. Additional raw data is available through the DataverseNO repository, link: <https://doi.org/10.18710/A6AJN4>.

Author contributions

M.K.L., A.B. and M.B.S. designed the compound library; M.K.L. carried out all chemical experiments and analysis; A.R., H.D., H.-M.B., T.H. and K.S. determined the biological assays; A.R., H.D., T.A. performed the biological assays and M.K.L., A.R., H.D., H.-M.B., T.H., K.S., A.B. and M.B.S. analysed and interpreted the data. The manuscript was written through contributions of all authors. All authors have given approval to the final version of the manuscript.

Declaration of competing interest

The authors declare the following financial interests/personal relationships which may be considered as potential competing interests: Morten B Strøm and Annette Bayer have patent #Barbituric acid derivatives comprising cationic and lipophilic groups. WO2018178198A1. Issued to UiT.

Data availability

NMR data files are available at DataverseNO: <https://doi.org/10.18710/A6AJN4>.

Acknowledgements

MKL, AR and HD thank for a PhD fellowship provided by UiT as part of the AntifoMar (2560700) and LeadScAMR (2017/6770) grants. We thank Senior Engineer Jostein Johansen for help with the HRMS and Prof. Máté Erdélyi for sharing his knowledge.

Appendix A. Supplementary data

Supplementary data to this article can be found online at <https://doi.org/10.1016/j.ejmech.2023.115147>.

References

- O. Nolte, Antimicrobial resistance in the 21st century: a multifaceted challenge, *Protein Pept. Lett.* 21 (2014) 330–335.
- M. Miethke, M. Pieroni, T. Weber, M. Brønstrup, P. Hammann, L. Halby, P. B. Arimondo, P. Glaser, B. Aigle, H.B. Bode, R. Moreira, Y. Li, A. Luzhetskyy, M. H. Medema, J.-L. Pernodet, M. Stadler, J.R. Tormo, O. Genilloud, A.W. Truman, K. J. Weissman, E. Takano, S. Sabatini, E. Stegmann, H. Brötz-Oesterhelt, W. Wohlleben, M. Seemann, M. Empting, A.K.H. Hirsch, B. Loretz, C.-M. Lehr, A. Titz, J. Herrmann, T. Jaeger, S. Alt, T. Hestekamp, M. Winterhalter, A. Schiefer, K. Pfarr, A. Hoerauf, H. Graz, M. Graz, M. Lindvall, S. Ramurthy, A. Karlén, M. van Dongen, H. Petkovic, A. Keller, F. Peyrane, S. Donadio, L. Fraisse, L.J.V. Piddock, I. H. Gilbert, H.E. Moser, R. Müller, Towards the sustainable discovery and development of new antibiotics, *Nat. Rev. Chem.* 5 (2021) 726–749.
- M. Pasupuleti, A. Schmidtchen, M. Malmsten, Antimicrobial peptides: key components of the innate immune system, *Crit. Rev. Biotechnol.* 32 (2012) 143–171.
- C.D. Fjell, J.A. Hiss, R.E. Hancock, G. Schneider, Designing antimicrobial peptides: form follows function, *Nat. Rev. Drug Discov.* 11 (2011) 37–51.
- G. Carmona, A. Rodriguez, D. Juarez, G. Corzo, E. Villegas, Improved protease stability of the antimicrobial peptide Pin2 substituted with D-amino acids, *Protein J.* 32 (2013) 456–466.
- M. Su, D. Xia, P. Teng, A. Nimmagadda, C. Zhang, T. Odom, A. Cao, Y. Hu, J. Cai, Membrane-active hydantoin derivatives as antibiotic agents, *J. Med. Chem.* 60 (2017) 8456–8465.
- R. Kapoor, P.R. Eimerman, J.W. Hardy, J.D. Cirillo, C.H. Contag, A.E. Barron, Efficacy of antimicrobial peptoids against *Mycobacterium tuberculosis*, *Antimicrob. Agents Chemother.* 55 (2011) 3058–3062.
- C. Ghosh, G.B. Manjunath, P. Akkapaddi, V. Yarlagadda, J. Hoque, D.S. Uppu, M. M. Konai, J. Haldar, Small molecular antibacterial peptoid mimics: the simpler the better, *J. Med. Chem.* 57 (2014) 1428–1436.
- A. Violette, S. Fournel, K. Lamour, O. Chaloin, B. Frisch, J.P. Briand, H. Monteil, G. Guichard, Mimicking helical antibacterial peptides with nonpeptidic folding oligomers, *Chem. Biol.* 13 (2006) 531–538.
- P. Teng, Y. Shi, P. Sang, J. Cai, γ -AApeptides as a new class of peptidomimetics, *Chem. Eur J.* 22 (2016) 5458–5466.
- Y. Shi, P. Teng, P. Sang, F. She, L. Wei, J. Cai, γ -AApeptides: design, structure, and applications, *Acc. Chem. Res.* 49 (2016) 428–441.
- P. Teng, A. Nimmagadda, M. Su, Y. Hong, N. Shen, C. Li, L.-Y. Tsai, J. Cao, Q. Li, J. Cai, Novel bis-cyclic guanidines as potent membrane-active antibacterial agents with therapeutic potential, *Chem. Commun.* 53 (2017) 11948–11951.
- M. Wang, R. Gao, M. Zheng, P. Sang, C. Li, E. Zhang, Q. Li, J. Cai, Development of bis-cyclic imidazolidine-4-one derivatives as potent antibacterial agents, *J. Med. Chem.* 63 (2020) 15591–15602.
- M.B. Strøm, B.E. Haug, M.L. Skar, W. Stensen, T. Stiberg, J.S. Svendsen, The pharmacophore of short cationic antibacterial peptides, *J. Med. Chem.* 46 (2003) 1567–1570.
- T. Hansen, T. Alst, M. Havelkova, M.B. Strøm, Antimicrobial activity of small β -peptidomimetics based on the pharmacophore model of short cationic antimicrobial peptides, *J. Med. Chem.* 53 (2010) 595–606.
- M.H. Paulsen, D. Ausbacher, A. Bayer, M. Engqvist, T. Hansen, T. Haug, T. Anderssen, J.H. Andersen, J.U.E. Sollid, M.B. Strøm, Antimicrobial activity of amphipathic α,α -disubstituted β -amino amide derivatives against ESBL – CARBA producing multi-resistant bacteria; effect of halogenation, lipophilicity and cationic character, *Eur. J. Med. Chem.* 183 (2019), 111671.
- M.H. Paulsen, M. Engqvist, D. Ausbacher, T. Anderssen, M.K. Langer, T. Haug, G. R. Morello, L.E. Liikainen, H.-M. Blencke, J. Isaksson, E. Juskevicius, A. Bayer, M. B. Strøm, Amphipathic barbiturates as mimics of antimicrobial peptides and the marine natural products eusynstetamides with activity against multi-resistant clinical isolates, *J. Med. Chem.* 64 (2021) 11395–11417.
- E.M. Igumnova, E. Mishchenko, T. Haug, H.-M. Blencke, J.U.E. Sollid, E.G. A. Fredheim, S. Lauksund, K. Stensvåg, M.B. Strøm, Synthesis and antimicrobial activity of small cationic amphipathic aminobenzamide marine natural product mimics and evaluation of relevance against clinical isolates including ESBL–CARBA producing multi-resistant bacteria, *Biorg. Med. Chem.* 24 (2016) 5884–5894.
- T.A. Bakka, M.B. Strøm, J.H. Andersen, O.R. Gautun, Synthesis and antimicrobial evaluation of cationic low molecular weight amphipathic 1,2,3-triazoles, *Biorg. Med. Chem. Lett.* 27 (2017) 1119–1123.
- M.K. Langer, A. Rahman, H. Dey, T. Anderssen, F. Zilioli, T. Haug, H.-M. Blencke, K. Stensvåg, M.B. Strøm, A. Bayer, A concise SAR-analysis of antimicrobial cationic amphipathic barbiturates for an improved activity-toxicity profile, *Eur. J. Med. Chem.* 241 (2022), 114632.
- M.H. Paulsen, E.A. Karlsen, D. Ausbacher, T. Anderssen, A. Bayer, P. Ochtrup, C. Hedberg, T. Haug, J.U. Ericson Sollid, M.B. Strøm, An amphipathic cyclic tetrapeptide scaffold containing halogenated β^{2-2} -amino acids with activity against multiresistant bacteria, *J. Pept. Sci.* 24 (2018) e3117.
- K. Kieć-Kononowicz, K. Stadnicka, A. Mitka, E. Pękala, B. Filipek, J. Sapa, M. Zygmunt, Synthesis, structure and antiarrhythmic properties evaluation of new basic derivatives of 5,5-diphenylhydantoin, *Eur. J. Med. Chem.* 38 (2003) 555–566.
- J. Handzlik, A.J. Bojarski, G. Satała, M. Kubacka, B. Sadek, A. Ashoor, A. Siwek, M. Więcek, K. Kucwaj, B. Filipek, K. Kieć-Kononowicz, SAR-studies on the importance of aromatic ring topologies in search for selective 5-HT7 receptor ligands among phenylpiperazine hydantoin derivatives, *Eur. J. Med. Chem.* 78 (2014) 324–339.
- T.R. Rodgers, M.P. LaMontagne, A. Markovac, A.B. Ash, Hydantoins as antitumor agents, *J. Med. Chem.* 20 (1977) 591–594.
- A.A. El-Barbary, A.I. Khodair, E.B. Pedersen, C. Nielsen, S-Glucosylated hydantoins as new antiviral agents, *J. Med. Chem.* 37 (1994) 73–77.
- S. Cortes, Z.-K. Liao, D. Watson, H. Kohn, Effect of structural modification of the hydantoin ring on anticonvulsant activity, *J. Med. Chem.* 28 (1985) 601–606.
- R. Sarges, R.C. Schnur, J.L. Belletire, M.J. Peterson, Spiro hydantoin aldose reductase inhibitors, *J. Med. Chem.* 31 (1988) 230–243.
- E. Szymańska, K. Kieć-Kononowicz, Antimicrobial activity of 5-arylidene aromatic derivatives of hydantoin, *Il Farmaco* 57 (2002) 355–362.
- E. Szymańska, K. Kieć-Kononowicz, A. Bialecka, A. Kasprovicz, Antimicrobial activity of 5-arylidene aromatic derivatives of hydantoin. Part 2, *Il Farmaco* 57 (2002) 39–44.
- J. Handzlik, E. Szymańska, J. Chevalier, E. Otrębska, K. Kieć-Kononowicz, J.-M. Pagès, S. Alibert, Amine-alkyl derivatives of hydantoin: new tool to combat resistant bacteria, *Eur. J. Med. Chem.* 46 (2011) 5807–5816.
- C.J. White, A.K. Yudin, Contemporary strategies for peptide macrocyclization, *Nat. Chem.* 3 (2011) 509–524.
- X. Chen, E.G. Mietlicki-Baase, T.M. Barrett, L.E. McGrath, K. Koch-Laskowski, J. J. Ferrie, M.R. Hayes, E.J. Petersson, Thioamide substitution selectively modulates proteolysis and receptor activity of therapeutic peptide hormones, *J. Am. Chem. Soc.* 139 (2017) 16688–16695.
- M. Feng, B. Tang, S.H. Liang, X. Jiang, Sulfur containing scaffolds in drugs: synthesis and application in medicinal chemistry, *Curr. Top. Med. Chem.* 16 (2016) 1200–1216.

- [34] S. Pathania, R.K. Narang, R.K. Rawal, Role of sulphur-heterocycles in medicinal chemistry: an update, *Eur. J. Med. Chem.* 180 (2019) 486–508.
- [35] M.C. Bagley, J.W. Dale, E.A. Merritt, X. Xiong, Thiopeptide antibiotics, *Chem. Rev.* 105 (2005) 685–714.
- [36] X. Just-Baringo, F. Albericio, M. Álvarez, Thiopeptide antibiotics: retrospective and recent advances, *Mar. Drugs* 12 (2014) 317–351.
- [37] H.C. Neu, β -Lactam Antibiotics: structural relationships affecting *in vitro* activity and pharmacologic properties, *Rev. Infect. Dis.* 8 (1986) 237–259.
- [38] E. Ware, The chemistry of the hydantoins, *Chem. Rev.* 46 (1950) 403–470.
- [39] M. Meusel, M. Gütschow, Recent developments in hydantoin chemistry, *A review, Org. Prep. Proced. Int.* 36 (2004) 391–443.
- [40] C.A. López, G.G. Trigo, The chemistry of hydantoins, in: A.R. Katritzky (Ed.), *Adv. Heterocycl. Chem.*, Academic Press, 1985, pp. 177–228.
- [41] L. Konnert, F. Lamaty, J. Martinez, E. Colacino, Recent advances in the synthesis of hydantoins: the state of the art of a valuable scaffold, *Chem. Rev.* 117 (2017) 13757–13809.
- [42] W.T. Read, Researches on hydantoins. Synthesis of the soporific, 4,4-phenylethyl-hydantoin (Nirvanol), *J. Am. Chem. Soc.* 44 (1922) 1746–1755.
- [43] H.T.L. Bucher V A, Syntheses of hydantoins. II. Formation of substituted hydantoins from aldehydes and ketones, *J. Prakt. Chem.* 141 (1934) 5–43.
- [44] H. Biltz, Constitution of the products of the interaction of substituted carbamides on benzil and certain new methods for the preparation of 5,5-diphenylhydantoin, *Ber. Dtsch. Chem. Ges.* 41 (1908) 1379–1393.
- [45] C. Hulme, L. Ma, J.J. Romano, G. Morton, S.-Y. Tang, M.-P. Cherrier, S. Choi, J. Salvino, R. Labaudiniere, Novel applications of carbon dioxide/MeOH for the synthesis of hydantoins and cyclic ureas via the Ugi reaction, *Tetrahedron Lett.* 41 (2000) 1889–1893.
- [46] C. Hulme, H. Bienaymé, T. Nixey, B. Chenera, W. Jones, P. Tempest, A.L. Smith, Library generation via postcondensation modifications of isocyanide-based multicomponent reactions, in: *Methods Enzymol.*, Academic Press, 2003, pp. 469–496.
- [47] D.V. Leusen, A.M.V. Leusen, Synthetic uses of tosylmethyl isocyanide (TosMIC), in: *Organic Reactions*, 2004, pp. 417–666.
- [48] R. Sakata, T. Soeta, Y. Ukaji, One-Carbon homologation of pyrrole carboxaldehyde via Wittig reaction and mild hydrolysis of vinyl ether - toward the synthesis of a sterically locked phytochrome chromophore, *Heterocycles* 91 (2015) 593–603.
- [49] Z. Kosarych, T. Cohen, Rapid, high-yield cleavage of enol and dienol methyl ethers under mild conditions using chlorotrimethylsilane/sodium iodide, *Tetrahedron Lett.* 21 (1980) 3959–3962.
- [50] H. Stetter, R.Y. Rämisch, Über die präparative Nutzung der 1,3-thiazoliumsalzkatalysierten Acyloin- und Benzoin-Bildung; IV1, Herstellung von Acyloinen mit funktionellen Gruppen, 1981, pp. 477–478. *Synthesis*, 1981.
- [51] Y.B. Kim, C.S. Kim, C.K. Lee, Condensation reactions of aryl acyloins with ureas in ethylene glycol, *J. Heterocycl. Chem.* 31 (1994) 1653–1656.
- [52] H.C. Carrington, Thiohydantoins. Part I. Preparation of 5 : 5-disubstituted 2 : 4-dithiohydantoins from the corresponding ketones, *J. Chem. Soc.* (1947) 681–683, 131.
- [53] M. Marinov, S. Minchev, N. Stoyanov, G. Ivanova, M. Spassova, V. Enchev, Synthesis, spectroscopic characterization and *ab initio* investigation of thioanalogues of spirohydantoins, *Croat. Chem. Acta* 78 (2005) 9–16.
- [54] G. Wenska, S. Paszyc, Photolysis of thiopurines in the presence of oxygen, *Z. Naturforsch. B Chem. Sci.* 36 (1981) 1628–1631.
- [55] M. Terada, R. Watanabe, II.3.6 barbiturates, in: *Drugs and Poisons in Humans*, Springer Berlin, Heidelberg, 2005, pp. 301–313.
- [56] M. Virta, K.E.O. Åkerman, P. Saviranta, C. Oker-Blom, M.T. Karp, Real-time measurement of cell permeabilization with low-molecular-weight membranolytic agents, *J. Antimicrob. Chemother.* 36 (1995) 303–315.
- [57] J. Chatterjee, E.A. Meighen, Biotechnological applications of bacterial bioluminescence (lux) genes, *Photochem. Photobiol.* 62 (1995) 641–650.
- [58] J. Lehtinen, M. Virta, E.-M. Lilius, Fluoro-luminometric real-time measurement of bacterial viability and killing, *J. Microbiol. Methods* 55 (2003) 173–186.
- [59] M. Virta, K.E. Åkerman, P. Saviranta, C. Oker-Blom, M.T. Karp, Real-time measurement of cell permeabilization with low-molecular-weight membranolytic agents, *J. Antimicrob. Chemother.* 36 (1995) 303–315.
- [60] E. Juskevicius, E. Mishchenko, V.K. Dubey, M. Jenssen, M. Jakubec, P. Rainsford, J. Isaksson, J.H. Andersen, J.U. Ericson, Lulworthinone: *In vitro* mode of action investigation of an antibacterial dimeric naphthopyrone isolated from a marine fungus, *Mar. Drugs* 20 (2022) 277.
- [61] T. Kuyyakanond, L.B. Quesnel, The mechanism of action of chlorhexidine, *FEMS Microbiol. Lett.* 100 (1992) 211–215.
- [62] B. Loh, C. Grant, R.E. Hancock, Use of the fluorescent probe 1-N-phenyl-naphthylamine to study the interactions of aminoglycoside antibiotics with the outer membrane of *Pseudomonas aeruginosa*, *Antimicrob. Agents Chemother.* 26 (1984) 546–551.
- [63] M. Graf, M. Mardirossian, F. Nguyen, A.C. Seefeldt, G. Guichard, M. Scocchi, C. A. Innis, D.N. Wilson, Proline-rich antimicrobial peptides targeting protein synthesis, *Nat. Prod. Rep.* 34 (2017) 702–711.
- [64] E. Podda, M. Benincasa, S. Pacor, F. Micali, M. Mattiuzzo, R. Gennaro, M. Scocchi, Dual mode of action of Bac7, a proline-rich antibacterial peptide, *Biochim. Biophys. Acta* 1760 (2006) 1732–1740.
- [65] M.L. Scocchi C, P. Decarli, G. Mignogna, P. Christen, R. Gennaro, The proline-rich antibacterial peptide Bac7 binds to and inhibits *in vitro* the molecular chaperone DnaK, *Int. J. Pept. Res. Therapeut.* 15 (2009) 147–155.
- [66] M. Mardirossian, R. Grzela, C. Giglione, T. Meinnel, R. Gennaro, P. Mergaert, M. Scocchi, The host antimicrobial peptide Bac71-35 binds to bacterial ribosomal proteins and inhibits protein synthesis, *Chem. Biol.* 21 (2014) 1639–1647.

Supporting Information

for

Investigation of Tetrasubstituted Heterocycles Reveals Hydantoins as a Promising Scaffold for Development of Novel Antimicrobials with Membranolytic Properties

Manuel K. Langer^a, Ataur Rahman^b, Hymonti Dey^b, Trude Anderssen^c, Hans-Matti Blencke^b, Tor Haug^b, Klara Stensvåg^b, Morten B. Strøm^{a*}, Annette Bayer^{b*}

^a Department of Chemistry, UiT – The Arctic University of Norway, NO-9037 Tromsø, NORWAY.

^b The Norwegian College of Fishery Science, Faculty of Biosciences, Fisheries and Economics, UiT – The Arctic University of Norway, NO-9037 Tromsø, NORWAY.

^c Department of Pharmacy, Faculty of Health Sciences, UiT – The Arctic University of Norway, NO-9037 Tromsø, NORWAY.

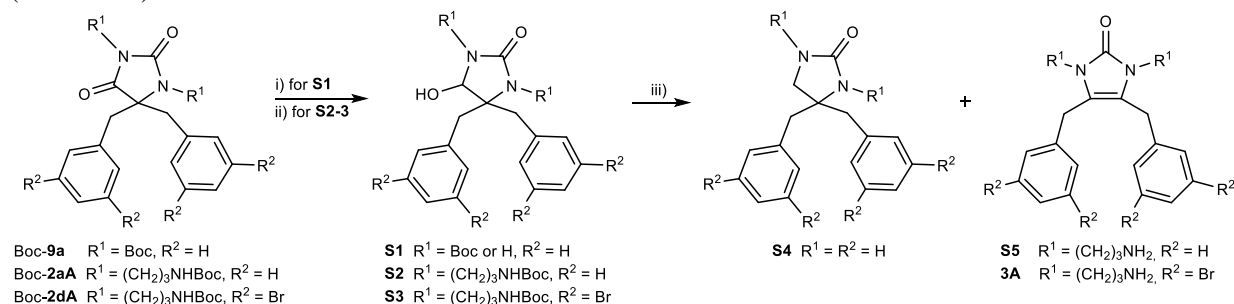
* Shared senior authorship and corresponding authors.

Table of Contents

1. 4-imidazolidin-2-ones <i>via</i> <i>N</i> -acyliminium ion rearrangement.....	2
2. Counterion effect.....	3
3. Experimental Details	4
4. NMR spectra	20
5. SFC traces	68
6. Full selectivity index table.....	71
7. Biological Methods	72
8. Membrane integrity and viability assay	74
9. Literature	76

1. 4-imidazolidin-2-ones via *N*-acyliminium ion rearrangement

Based on the pioneering work of Speckamp and co-workers^[1] *N*-acyliminium intermediates have been used in a variety of cationic cyclisations.^[2] Far less explored are the *N*-acyliminium ion triggered rearrangements, predominantly Cope-type, which are mostly reported as the underlying mechanism for certain cyclisations.^[3] But when Kohn et al. studied the preparation of annulated imidazolidinones from 4-hydroxy-5,5-dimethylimidazolidin-2-one, they also observed a 1,2-methylshift to the corresponding 4-imidazolin-2-one.^[4] As the 4-hydroxy-imidazolidinones can be accessed by reducing the corresponding hydantoin, we envisioned a similar sequence, starting from the di-Boc protected hydantoin Boc-**9a** and the previously prepared hydantoin Boc-**2aA** and Boc-**2dA** (Scheme S1).



Scheme S1. Synthetic strategy towards **3A** via a cationic rearrangement from an *in situ* generated *N*-acyliminium ion. Reaction conditions: i) NaBH₄, EtOH, r.t., 16 h, no yield determined; ii) DIBAL, DCM (dry), -78 to 0 °C, 3 h, 56-70%; iii) see **Table S1**.

Using Boc-**9a** was appealing, because a later introduction of the alkyl linkers would be advantageous for building libraries. NaBH₄ mediated reduction of the amidic carbonyl of Boc-**9a** delivered intermediate **S1**. Upon sequential treatment of the latter one with catalytic amounts of *para*-toluenesulfonic acid (*p*-TsOH) at 120 °C followed by TFA in DCM (Table S1, Entry 1) deoxygenated imidazolidine **S4** was obtained. Consequently, we decided to employ **2aA** and **2dA** instead. Both tetrasubstituted hydantoin could be reduced by DIBAL in DCM to yield 4-hydroxy-imidazolidinones **S2** and **S3** in 56% and 70%, respectively. Refluxing intermediate **S2** with a catalytic amount of *p*-TsOH in anhydrous toluene^[4] (Table S1, Entry 2) led to quantitative conversion. During this process we observed partial degradation of the Boc groups and decided to treat the crude with TFA in DCM and obtained fully deprotected 4-imidazolidin-2-one **S5** in a yield of 74%. Both TFA alone and with additional trifluoro acetic acid anhydride (TFAA) (Entry 3 and 4) effectively promoted the rearrangement. Using formic acid (Entry 4) led to a mixture of the desired product alongside unreacted starting material with zero to two Boc-groups being intact. When treating halo-aryl containing derivative **S3** with TFA (Entry 5), we observed only partial rearrangement to **3A**. Presumably, partial Boc removal takes place prior to the *N*-acyliminium ion formation, leading to a positively net charged compound and thus raising the barrier for the dehydration and subsequent introduction of another positive charge. Even though we could demonstrate the practical value of this strategy towards 4-imidazolidin-2-ones, the final products **S5** and **3A** were difficult to purify, supposedly due to partial fragmentation of the intermediate *N*-acyliminium ion. We decided therefore to abolish this strategy.

Table S1. Reaction conditions for the cationic rearrangement and subsequent Boc-deprotection

Entry	Reactant	Acid (eq)	Solvent ^a	Temperature [°C]	Time [h]	Product (Yield [%])
1	S1	1. <i>p</i> -TsOH (0.20) 2. TFA (20.0 eq)	1. Toluene 2. DCM	1. 120 2. 25	1. 24 2. 18	S4 (34)
2 ^b	S2	1. <i>p</i> -TsOH (0.20) 2. TFA (20.0)	1. Toluene 2. DCM	1. 120 2. 25	1. 5.5 2. 18	S5 (74)
3	S2	TFA (20.0 eq)	DCM	25	18	S5 (82)
4	S2	TFAA (1.30)	TFA:DCM (2:1)	50	18	S5 (83)
5	S2	Formic acid (1.05)	DCM	50	4	n.d. ^c
6	S3	TFA (15.0)	DCM	25	22	S17A (43%)

^a Anhydrous solvents were used. ^b Upon completion of the rearrangement toluene was removed and replaced by DCM. ^c A mixture of reactant, Boc-deprotected reactant and the rearranged product was obtained.

2. Counterion effect

Physicochemical properties like adsorption, solubility and membrane permeability of basic and acidic drugs can be greatly influenced by their counterions.^[5] We converted the di-trifluoroacetate (di-TFA) salts of hydantoins **2c** (3-Cl, 4-Br) and **2d** (3,5-di-Br) into their di-hydrochloride (di-HCl) salts to improve their water solubility^[6] and to evaluate the impact of counterions on their biological activity (**Table S2**).

Table S2. MIC and EC₅₀ values in [µg/mL] of selected di-trifluoroacetate (TFA) and di-hydrochloride (HCl) salts. Improved values are shown in green.

Comp. ID	Side chain	MIC (TFA)				EC ₅₀ (TFA)	MIC (HCl)				EC ₅₀ (HCl)	Solubility ^a
		S. a	B. s	E. c	P. a		S. a	B. s	E. c	P. a		
2cA	(3-Cl, 4-Br)	8	4	32	32	368	8	2	16	32	>400	+/+
2dA	(3,5-di-Br)	8	4	16	8	344	8	2	16	4	289	+/+
2cG	(3-Cl, 4-Br)	2	2	32	8	>467	<1	2	16	64	342	-/-
2dG	(3,5-di-Br)	2	1	16	16	486	2	2	16	32	303	-/-

S. a – *Staphylococcus aureus* ATCC 9144, B.s – *Bacillus subtilis* 168, E. c – *Escherichia coli* ATCC 25922, and P. a – *Pseudomonas aeruginosa* ATCC 27853. ^a If solubility in pure water is equal or greater than 1 mg/mL it is denoted with (+), if lower (–).

Water solubility was assessed qualitatively, by setting the threshold at 1 mg/mL. Di-TFA and di-HCl salts of the amine derivatives **2A** were water soluble, but neither of the salt forms of **2G** were water soluble according to the established criteria. The amine derivatives **2A** demonstrated a minor increase in antimicrobial potency against individual strains by a factor of two. The guanidyl derivatives **2G** did not follow a clear trend, except for Gram-negative *P. aeruginosa*. The di-HCl salts of both guanidyl hydantoins were less potent against *P. aeruginosa*, especially **2cG** showed an 8-fold decrease in potency for undetermined reasons. The haemolytic activity of the amine derivatives **2A** was comparable for both salt forms, but the di-HCl salts of the guanidyl analogues seemed to be more haemolytic than the di-TFA salts. The effect was less pronounced when EC₅₀ values given in µM were compared, but it was still observable. In summary, the di-HCl salts of the amine derivatives **2A** showed slightly improved biological properties, whereas for the guanidyl derivatives **2G** no clear conclusion could be drawn.

3. Experimental Details

3.1 General methods

Unless otherwise noted, purchased chemicals were used as received without further purification. Solvents were dried according to standard procedures over molecular sieves of appropriate size.

Normal phase flash chromatography was carried out on silica gel 60 (230–400 mesh) or on an interchim® PuriFlash XS420 flash system with the sample preloaded on a Samplet® cartridge belonging to a Biotage SP-1 system. Purification by reversed phase (RP) C18 column chromatography (H₂O with 0.1 % TFA/MeCN with 0.1 % TFA) was performed on an interchim® PuriFlash XS420 flash system with the sample preloaded on a Samplet® cartridge.

Thin layer chromatography was carried out using Merck TLC Silica gel 60 F254 and visualized by short-wavelength ultraviolet light or by treatment with an appropriate stain.

NMR spectra were obtained on a 400 MHz Bruker Advance III HD spectrometer equipped with a 5 mm SmartProbe BB/1H (BB = 19F, 31P-15N) at 20 °C. The chemical shifts are reported in ppm relative to the solvent residual peak (CDCl₃: δH 7.26 and δC 77.16; Methanol-d₄: δH 3.31 and δC 49.00; deuterium oxide: δH 4.79; DMSO-d₆ δH 2.51 and δC 39.52). ¹³C NMR spectra were obtained with ¹H decoupling. Data are represented as follows: chemical shift, multiplicity (s = singlet, d = doublet, t = triplet, q = quartet, qn = quintet, dt = doublet of triplet, m = multiplet), coupling constant (*J* in Hz) and integration. The raw data was analyzed with MestReNova (Version 14.0.0-23239).

High-resolution mass spectra (HRMS) were recorded from methanol solutions on an LTQ Orbitrap XL (Thermo Scientific) either in negative or in positive electrospray ionization (ESI) mode. The data was analyzed with Thermo Scientific Xcalibur software.

All final products were lyophilized for 48 h to yield their di-TFA salts.

The purity of all tested compounds was determined to be ≥95%. The analyses were carried out on a Waters ACQUITY UPC² system equipped with a Torus™ DEA 130Å, 1.7 μm, 2.1 mm x 50 mm column. Compounds were detected on a Waters ACQUITY PDA detector spanning wavelengths from 205 to 650 nm, coupled to a Waters ACQUITY QDA detector for low resolution mass (LRMS) detection. The derivatives were eluted with a mobile phase consisting of supercritical CO₂ and MeOH containing 0.1 % NH₃ and a linear gradient of 2 – 40 % MeOH over 2 or 4 min followed by isocratic 0.5 min of 40% MeOH. The flow rate was 1.5 mL/min.

3.2 Synthesis of building blocks

1-bromo-4-(bromomethyl)naphthalene **S6**^[7], *tert*-butyl (3-bromopropyl)carbamate **S7**^[8], and *tert*-butyl (4-bromobutyl)carbamate **S8**^[9] were prepared as described in literature.

Note: All compounds were obtained as di-TFA salts. TFA is typically observed at 162.1 (q, J = 35.7 Hz) and 117.7 (q, J = 290.3 Hz) in ¹³C-NMR and is not reported for each compound individually.

3.3 General procedures

General Procedure A: Synthesis of symmetrical ketones 8

Substituted benzyl bromide, TosMiC and TBAB or TBAI were mixed with DCM and a NaOH_(aq) solution was added. The mixture was stirred vigorously until TLC indicated full conversion. The layers were separated, and the organic layer was washed with water twice. The organic layer was dried over Na₂SO₄, filtered and the solvent was removed under reduced pressure. The disubstituted TosMiC derivative was obtained as a viscous oil.

The crude oil was taken up in a suitable solvent and HCl_(conc.) was added. The solution was stirred at room temperature until TLC indicated full conversion. Water was added and the pH was adjusted to 8–9 with a 2 N NaOH_(aq) solution. The aqueous layer was extracted with DCM (3x) and the combined organics were washed with a 10% NaHCO_{3(aq)} solution (2x), dried over Na₂SO₄, filtered and the solvent was removed under reduced pressure. The crude product was purified by column chromatography on silica gel with EtOAc/heptane as eluent. Some of the ketones were not obtained pure but used for the next synthetic step.

General Procedure B: Synthesis of Hydantoins 9 by the Bucherer-Bergs reaction

The symmetrical ketone **8** was taken up in DMSO and NH_4CO_3 , KOAc and KCN were added. The solution was stirred at 60 °C until all starting material had been consumed. Water was added and the pH was adjusted to 1-2 by dropwise addition of 1 N $\text{HCl}_{(\text{aq})}$, upon which a white solid precipitated. The mixture was stirred for 30 min at ambient temperature and then filtered. The residue was washed with water and chloroform extensively. The solids were collected and lyophilized for 24 h to yield the desired hydantoins.

General Procedure C: *N,N'*-dialkylation and subsequent Boc-removal

Hydantoin **9**, *tert*-butyl (3-bromopropyl)carbamate **S7** or *tert*-butyl (4-bromobutyl)carbamate **S8**, Cs_2CO_3 and TBAI were mixed with acetone and stirred at 65–75 °C until no more starting material and mono-alkylated compound could be observed (HRMS). The reaction mixture was allowed to cool to ambient temperature before water and EtOAc were added. The layers were separated and the aqueous layer was extracted twice more with EtOAc. The combined organics were dried over MgSO_4 , filtered and the solvent was removed under reduced pressure. The crude products were purified by automated column chromatography on silica gel with EtOAc in heptane as eluent to deliver the Boc protected *N,N'*-dialkylated intermediates Boc-**2A** and Boc-**6A**.

The Boc protected *N,N'*-dialkylated intermediates were dissolved in DCM and TFA was added. The resulting mixture was stirred at ambient temperature until HRMS indicated the cleavage of all Boc groups. The solvent was removed and the crude products were purified by automated RP column chromatography with a gradient of MeCN in H_2O (both containing 0.1% TFA). Fractions containing the target compound were collected, most of the solvent was removed under reduced pressure and the residual solution lyophilized for 48 h. The desired hydantoins **2A** and **6A** were obtained as di-TFA salts.

General procedure D: Guanidine formation

The d-TFA salts of **2A** or **6A** were mixed with THF and DIPEA and stirred at ambient temperature for 10 min. *N,N'*-Di-Boc-1*H*-pyrazole-1-carboximidine was added and the solution was stirred at elevated temperatures until TLC indicated full conversion. The mixture was allowed to cool to ambient temperature and sat. $\text{NH}_4\text{Cl}_{(\text{aq})}$ solution and EtOAc were added. The layers were separated and the aqueous layer was extracted twice more with EtOAc. The combined organics were dried over Na_2SO_4 , filtered and the solvent was removed. The crude products were purified by automated flash column chromatography on silica gel and EtOAc in heptane as eluent to yield the Boc-protected guanidine containing hydantoins Boc-**2G** or Boc-**6G**.

The Boc-protected guanidines were stirred with TFA in DCM at ambient temperature until HRMS indicated full conversion. The solvent was removed and the crude products were purified by automated RP column chromatography with a gradient of MeCN in H_2O (both containing 0.1% TFA). Fractions containing the product were collected, most of the solvent was removed and the residual solution was lyophilized for 48 h. The desired guanylated hydantoins **2G** and **6G** were obtained as di-TFA salts.

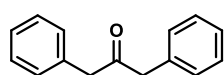
General Procedure E: Preparation of hydrochloric (HCl) salts

The previously obtained TFA salts were taken up in MeOH and HCl in MeOH (1.25 M, 10.0 eq) was added. The solvent was removed and the residue was lyophilized for 24 h. The procedure was repeated twice more to yield the respective HCl salts in $\geq 95\%$ purity. The absence of fluorine was confirmed by ^{19}F NMR (not included).

3.4 Experimental procedures for the synthesis of hydantoins

3.4.1 Synthesis of symmetric ketones **8**

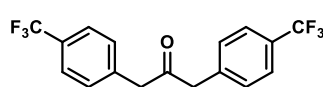
The following compounds were synthesized according to General Procedure A:



1,3-diphenylpropan-2-one **8a**.

Bromomethyl benzene (1.75 g, 10.24 mmol, 2.0 eq), TosMIC (1.00 g, 5.12 mmol, 1.0 eq), TBAB (661 mg, 2.05 mmol, 0.4 eq), NaOH (35 wt%, 35 mL) and DCM (70 mL) were stirred for 14 h. The addition product was obtained as a brown oil.

The addition product, HCl (37%, 2.0 mL), DCM (30 mL) and THF (7 mL) were stirred at ambient temperature for 17 h. Purification by column chromatography on silica gel with 5 % EtOAc in heptane as eluent delivered **8a** (857 mg, 1.78 mmol, 53% o/s) as a colorless liquid. ^1H NMR (400 MHz, Chloroform-*d*) δ 7.45 – 7.33 (m, 6H), 7.29 – 7.22 (m, 4H), 3.80 (s, 4H). ^{13}C NMR (101 MHz, Chloroform-*d*) δ 205.4, 134.0 (2C), 129.4 (4C), 128.6 (4C), 126.9 (2C), 48.9 (2C). HRMS (ESI): calcd for $\text{C}_{15}\text{H}_{14}\text{ONa}^+$ $[\text{M}+\text{Na}]^+$ 233.0937, found: 233.0938.

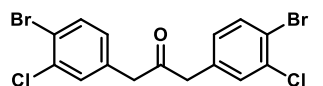


1,3-bis(4-(trifluoromethyl)phenyl)propan-2-one **8b**.

4-(trifluoromethyl)benzyl bromide (4.90 g, 20.50 mmol, 2.0 eq), TosMIC (2.00 g, 10.24 mmol, 1.0 eq), TBAB (1.65 g, 5.12 mmol, 0.5 eq), NaOH (20 wt%, 50 mL)

and DCM (100 mL) were stirred for 24 h. The addition product was obtained as a brown oil.

The addition product, HCl (37%, 8 mL), DCM (33 mL) and THF (7 mL) were stirred at ambient temperature for 17 h. Purification by column chromatography on silica gel with 15% EtOAc in heptane as eluent delivered impure **8b** (2.43 g, 7.02 mmol, 69% o2s) as an off-white solid. ¹H NMR (400 MHz, Methanol-*d*₄) δ 7.59 (d, *J* = 8.1 Hz, 4H), 7.36 (d, *J* = 8.0 Hz, 4H), 3.98 (s, 4H). ¹³C NMR (101 MHz, Methanol-*d*₄) δ 206.1, 140.2 (2C), 131.5 (4C), 130.2 (q, *J* = 32 Hz, 2C), 126.28 (q, *J* = 3.9, 4C), 125.8 (q, *J* = 271.0 Hz, 2C), 49.5 (2C). HRMS (ESI): calcd for C₁₇H₁₁F₆O⁻ [M-H]⁻ 345.0720, found: 345.0717.

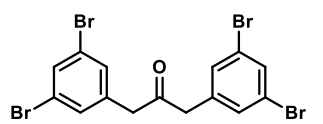


1,3-bis(4-bromo-3-chlorophenyl)propan-2-one **8c**.

1-bromo-4-(bromomethyl)-2-chlorobenzene (1.75 g, 6.15 mmol, 2.0 eq), TosMIC (600 mg, 3.07 mmol, 1.0 eq), TBAB (396 mg, 1.23 mmol, 0.4 eq), NaOH (20 wt%, 12 mL) and DCM (25 mL) were stirred for 24 h. The addition product was obtained

as a brown oil.

The addition product, HCl (37%, 1.5 mL), DCM (20 mL) and THF (5 mL) were stirred at ambient temperature for 6.5 h. Purification by column chromatography on silica gel with 12% EtOAc in heptane as eluent delivered impure **8c** (0.96 g, 3.97 mmol, 59% o2s) as an off-white solid. ¹H NMR (400 MHz, Chloroform-*d*) δ 7.56 (d, *J* = 8.2 Hz, 2H), 7.24 (d, *J* = 2.1 Hz, 2H), 6.90 (dd, *J* = 8.2, 2.1 Hz, 2H), 3.69 (s, 4H). ¹³C NMR (101 MHz, Chloroform-*d*) δ 203.0, 134.9, 134.3, 134.1, 131.9, 129.2, 122.2, 48.3 (2C). HRMS (ESI): calcd for C₁₅H₉Br₂Cl₂O⁻ [M-H]⁻ 432.8403, found: 432.8404.

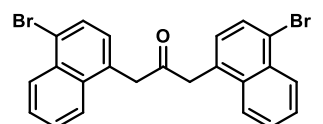


1,3-bis(3,5-dibromophenyl)propan-2-one **8d**.^[10]

1,3-dibromo-5-(bromomethyl)benzene (4.04 g, 12.30 mmol, 2.0 eq), TosMIC (1.20 g, 6.15 mmol, 1.0 eq), TBAB (793 mg, 2.55 mmol, 0.4 eq), NaOH (20 wt%, 60 mL) and DCM (125 mL) were stirred for 14 h. The addition product was obtained

as a brown oil.

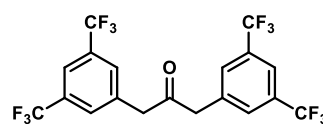
The addition product, HCl (37%, 5 mL), DCM (40 mL) and THF (7 mL) were stirred at ambient temperature for 5 h. The title compound was precipitated from DCM by addition of EtOH. The solids were collected and washed with H₂O and EtOH to yield pure **8d** (1.94 g, 3.68 mmol, 60% o2s) as a white solid. ¹H NMR (400 MHz, DMSO-*d*₆) δ 7.71 (t, *J* = 1.8 Hz, 2H), 7.44 (d, *J* = 1.8 Hz, 4H), 3.94 (s, 4H). ¹³C NMR (101 MHz, DMSO-*d*₆) δ 203.7, 139.8 (2C), 132.0 (4C), 131.5 (4C), 122.6 (2C), 47.2 (2C). HRMS (ESI): calcd for C₁₅H₉Br₄O⁻ [M-H]⁻ 520.7392, found: 520.7393.



1,3-bis(4-bromonaphthalen-1-yl)propan-2-one **8e**.

1-bromo-4-(bromomethyl)naphthalene **S6** (1.84 g, 6.15 mmol, 2.0 eq), TosMIC (600 mg, 3.07 mmol, 1.0 eq), TBAB (396 mg, 1.23 mmol, 0.4 eq), NaOH (20 wt%, 30 mL) and DCM (65 mL) were stirred for 14 h. The addition product was obtained as a brown oil.

The addition product, HCl (37%, 6.0 mL), DCM (30 mL) and THF (7 mL) were stirred at ambient temperature for 17 h. Upon addition of water and EtOH a white solid precipitated. The solids were collected and washed with water to deliver **8e** (820 mg, 3.07 mmol, 57% o2s) as a white solid. ¹H NMR (400 MHz, Chloroform-*d*) δ 8.31 – 8.24 (m, 2H), 7.70 (d, *J* = 7.6 Hz, 2H), 7.63 (dt, *J* = 8.5, 0.8 Hz, 2H), 7.58 (ddd, *J* = 8.2, 6.9, 1.2 Hz, 2H), 7.43 (ddd, *J* = 8.3, 6.8, 1.3 Hz, 2H), 7.10 (d, *J* = 7.6 Hz, 2H), 4.10 (s, 4H). ¹³C NMR (101 MHz, Chloroform-*d*) δ 205.4, 133.4, 132.3, 130.8, 129.7, 128.9, 128.2, 127.5, 127.4, 124.4, 123.0, 47.2. HRMS (ESI): calcd for C₂₃H₁₆Br₂O⁻Na⁺ [M+Na]⁺ 488.9460, found: 488.9458.



1,3-bis(3,5-bis(trifluoromethyl)phenyl)propan-2-one **8f**.

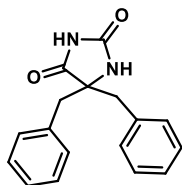
3,5-bis(trifluoromethyl)benzyl bromide (2.25 g, 7.32 mmol, 2.2 eq), TosMIC (650 mg, 3.33 mmol, 1.0 eq), TBAI (246 mg, 0.67 mmol, 0.2 eq), NaOH (30 wt%, 12 mL) and DCM (12 mL) were stirred for 24 h. The addition product was obtained as a brown oil.

The addition product, HCl (37%, 4.2 mL), DCM (20 mL) and THF (4 mL) were stirred at ambient temperature for 17 h. Purification by column chromatography on silica gel with 10% EtOAc in heptane as eluent delivered **8f** (857 mg, 1.78 mmol, 53% o2s) as an off-white solid. ¹H NMR (400 MHz, Methanol-*d*₄) δ 7.84 (s, 2H), 7.82 (s, 4H), 4.18 (s, 4H). ¹³C NMR (101 MHz, Methanol-*d*₄) δ 203.2, 137.4, 131.2 (q, *J* = 32.9 Hz, 2C), 130.3 – 130.1

(m, 2C), 123.5 (q, $J = 272.0$ Hz, 2C), 120.3 – 120.1 (m, 1C). Methylene-carbons were not observed, due to overlap with the deuterated solvent. **HRMS** (ESI): calcd for $C_{19}H_9F_{12}O$ $[M-H]^-$ 481.0467, found: 481.0461.

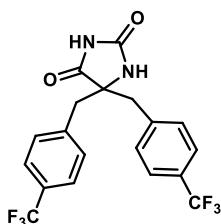
3.4.2 Synthesis of hydantoins 9

The following compounds were prepared according to general procedure B:



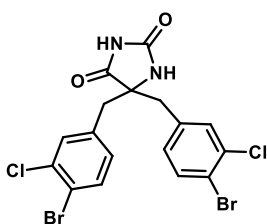
5,5-dibenzylimidazolidine-2,4-dione **9a**.

8a (36 mg, 0.17 mmol, 1.0 eq), KCN (22 mg, 0.34 mmol, 2.0 eq), NH_4CO_3 (82 mg, 0.86 mmol, 5.0 eq), water (0.5 mL) and EtOH (0.5 mL) were stirred at 75 °C for 24 h. Pure **9a** (35 mg, 125 μ mol, 73%) was obtained as a white solid. **1H NMR** (400 MHz, DMSO- d_6) δ 9.97 (s, 1H), 8.00 (s, 1H), 7.33 – 7.12 (m, 10H), 3.10 (d, $J = 13.4$ Hz, 2H), 2.86 (d, $J = 13.4$ Hz, 2H). **^{13}C NMR** (101 MHz, Methanol- d_4) δ 179.1, 158.6, 136.1 (2C), 131.4 (4C), 129.2 (4C), 128.2 (2C), 70.3, 43.9 (2C). **HRMS** (ESI): calcd for $C_{17}H_{16}N_2O_2^-$ $[M-H]^-$ 279.1139, found: 279.1137.



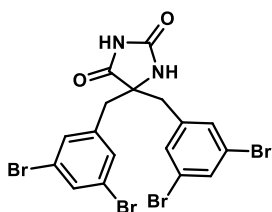
5,5-bis(4-(trifluoromethyl)benzyl)imidazolidine-2,4-dione **9b**.

8b (1.76 g, 5.07 mmol, 1.0 eq), KCN (826 mg, 12.69 mmol, 2.5 eq), NH_4CO_3 (1.95 g, 20.30 mmol, 4.0 eq), KOAc (996 mg, 10.15 mmol, 2.0 eq) and DMSO (15 mL) were stirred at 60 °C for 21 h. Pure **9b** (1.76 g, 4.23 mmol, 83%) was obtained as a slightly brown solid. **1H NMR** (400 MHz, DMSO- d_6) δ 10.01 (s, 1H), 8.16 (s, 1H), 7.67 (d, $J = 8.0$ Hz, 4H), 7.40 (d, $J = 7.9$ Hz, 4H), 3.23 (d, $J = 13.3$ Hz, 2H), 3.00 (d, $J = 13.3$ Hz, 2H). **^{13}C NMR** (101 MHz, DMSO- d_6) δ 174.7, 155.6, 139.9 (2C), 131.0 (4C), 127.6 (q, $J = 31.6$ Hz, 4C), 124.9 (q, $J = 3.8$ Hz, 4C), 124.3 (q, $J = 274$ Hz, 2C), 66.0, 41.8 (2C). **HRMS** (ESI): calcd for $C_{19}H_{13}F_6N_2O_2^-$ $[M-H]^-$ 415.0887, found: 415.0882.



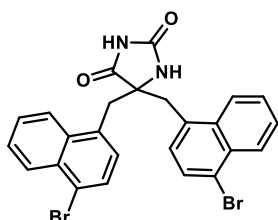
5,5-bis(4-bromo-3-chlorobenzyl)imidazolidine-2,4-dione **9c**.

8c (737 mg, 1.69 mmol, 1.0 eq), KCN (275 mg, 4.22 mmol, 2.5 eq), NH_4CO_3 (648 mg, 6.75 mmol, 4.0 eq), KOAc (331 mg, 3.37 mmol, 2.0 eq) and DMSO (7 mL) were stirred at 60 °C for 16 h. Pure **9c** (387 mg, 0.76 mmol, 45%) was obtained as an off-white solid. **1H NMR** (400 MHz, DMSO- d_6) δ 10.30 (s, 1H), 8.14 (s, 1H), 7.70 (d, $J = 8.2$ Hz, 2H), 7.39 (d, $J = 2.0$ Hz, 2H), 7.06 (dd, $J = 8.2, 2.0$ Hz, 2H), 3.09 (d, $J = 13.4$ Hz, 2H), 2.85 (d, $J = 13.5$ Hz, 2H). **^{13}C NMR** (101 MHz, DMSO- d_6) δ 175.7, 156.4, 136.7, 133.4, 132.5, 132.0, 130.7, 120.0, 66.6, 40.8 (2C). **HRMS** (ESI): calcd for $C_{17}H_{11}Br_2Cl_2N_2O_2^-$ $[M-H]^-$ 502.8570, found: 502.8570.



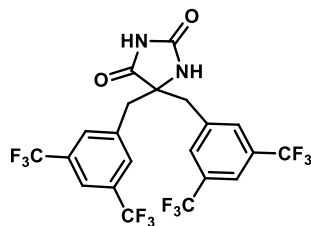
5,5-bis(3,5-dibromobenzyl)imidazolidine-2,4-dione **9d**.

8d (1.21 g, 2.30 mmol, 1.0 eq), KCN (374 mg, 5.75 mmol, 2.5 eq), NH_4CO_3 (884 mg, 9.20 mmol, 4.0 eq), KOAc (451 mg, 4.60 mmol, 2.0 eq) and DMSO (9 mL) were stirred at 60 °C for 16 h. Pure **9d** (1.17 g, 1.96 mmol, 85%) was obtained as a grey solid. **1H NMR** (400 MHz, DMSO- d_6) δ 10.42 (s, 1H), 8.22 (s, 1H), 7.73 (t, $J = 1.8$ Hz, 2H), 7.37 (d, $J = 1.9$ Hz, 4H), 3.09 (d, $J = 13.4$ Hz, 2H), 2.84 (d, $J = 13.4$ Hz, 2H). **^{13}C NMR** (101 MHz, DMSO- d_6) δ 175.7, 154.7, 139.6 (2C), 132.8 (4C), 132.0 (4C), 122.0 (2C), 67.0, 40.77 (2C). **HRMS** (ESI): calcd for $C_{17}H_{11}Br_4N_2O_2^-$ $[M-H]^-$ 590.7560, found: 590.7562.



5,5-bis((4-bromonaphthalen-1-yl)methyl)imidazolidine-2,4-dione **9e**.

8e (842 mg, 1.80 mmol, 1.0 eq), KCN (410 mg, 6.29 mmol, 3.5 eq), NH_4CO_3 (1.21 g, 12.59 mmol, 7.0 eq), KOAc (410 mg, 4.18 mmol, 2.0 eq) and DMSO (7 mL) were stirred at 75 °C for 90 h. Pure **9e** (627 mg, 1.16 mmol, 65%) was obtained as a red solid. **1H NMR** (400 MHz, DMSO- d_6) δ 9.91 (s, 1H), 8.41 (dt, $J = 8.0, 2.8$ Hz, 2H), 8.21 – 8.11 (m, 2H), 8.06 (d, $J = 1.7$ Hz, 1H), 7.83 (d, $J = 7.8$ Hz, 2H), 7.73 – 7.63 (m, 4H), 7.42 (d, $J = 7.8$ Hz, 2H), 3.86 (d, $J = 14.2$ Hz, 2H), 3.54 (d, $J = 14.2$ Hz, 2H). **^{13}C NMR** (101 MHz, DMSO- d_6) δ 176.8, 155.6, 133.6, 132.4, 131.1, 129.5, 129.3, 127.4, 126.7, 126.6, 126.0, 121.4, 68.0, 37.7. **HRMS** (ESI): calcd for $C_{25}H_{17}Br_2N_2O_2^-$ $[M-H]^-$ 534.9662, found: 534.9660.

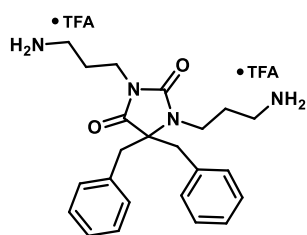


5,5-bis(3,5-bis(trifluoromethyl)benzyl)imidazolidine-2,4-dione **9f**.

8f (806 mg, 1.67 mmol, 1.0 eq), KCN (272 mg, 4.18 mmol, 2.5 eq), NH_4CO_3 (642 mg, 6.69 mmol, 4.0 eq), KOAc (410 mg, 4.18 mmol, 2.50eq) and DMSO (15 mL) were stirred at 60 °C for 20 h. Pure **9f** (470 mg, 0.85 mmol, 51%) was obtained as a white solid. $^1\text{H NMR}$ (400 MHz, DMSO-*d*₆) δ 10.38 (s, 1H), 8.34 (s, 1H), 8.02 (s, 2H), 7.84 (s, 4H), 3.40 (d, J = 13.3 Hz, 2H), 3.12 (d, J = 13.4 Hz, 2H). $^{13}\text{C NMR}$ (101 MHz, DMSO-*d*₆) δ 175.6, 155.5, 138.2 (2C), 131.0 – 130.8 (m, 4C), 129.9 (q, J = 32.7 Hz, 4C), 123.3 (q, J = 272.8 Hz, 4C), 121.1 – 120.8 (m, 2C), 68.1, 40.9 (2C). **HRMS** (ESI): calcd for $\text{C}_{21}\text{H}_{11}\text{F}_{12}\text{N}_2\text{O}_2^-$ [M-H]⁻ 551.0634, found: 551.0628

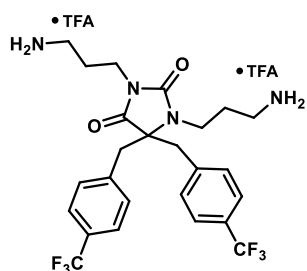
3.4.3 Synthesis of *N,N'*-dialkylated hydantoin 2A

The following compound were prepared according to General Procedure C:



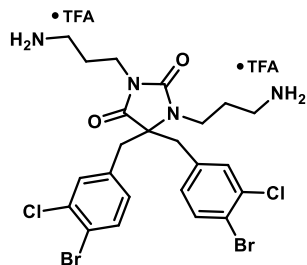
1,3-bis(3-aminopropyl)-5,5-dibenzylimidazolidine-2,4-dione **2aA**.

9a (168 mg, 0.60 mmol, 1.0 eq), *tert*-butyl (3-bromopropyl)carbamate **S7** (429 mg, 1.8 mmol, 3.0 eq), Cs_2CO_3 (586 mg, 1.8 mmol, 3.0 eq), TBAI (44 mg, 120 μmol , 0.2 eq) and acetone (8.0 mL) were stirred at 65 °C for 72 h. Purification by column chromatography on silica gel with a gradient of 0-70% EtOAc in heptane delivered the intermediate Boc-**2aA** (302 mg, 508 μmol , 85%) as a white solid. TFA (460 μL , 6.00 mmol, 10.0 eq) and DCM (3.0 mL) were added and the solution was stirred at ambient temperature for 3.5 h. The crude was purified by RP chromatography with a gradient of 0-70% MeCN/ H_2O + 0.1% TFA to yield the di-TFA salt of **2aA** (272 mg, 437 μmol , 73% o2s) as a white solid. $^1\text{H NMR}$ (400 MHz, Methanol-*d*₄) δ 7.33 – 7.22 (m, 6H), 7.21 – 7.15 (m, 4H), 3.65 – 3.58 (m, 2H), 3.35 (d, J = 14.5 Hz, 2H), 3.26 (d, J = 14.5 Hz, 2H), 3.25 (t, J = 6.7 Hz, 2H), 2.86 (t, J = 7.3 Hz, 2H), 2.27 (t, J = 7.3 Hz, 2H), 2.02 (qn, J = 7.4 Hz, 2H), 1.47 (qn, J = 7.4 Hz, 2H). $^{13}\text{C NMR}$ (101 MHz, Methanol-*d*₄) δ 175.9, 158.6, 135.9 (2C), 131.0 (4C), 129.7 (4C), 128.7 (2C), 73.6, 41.7 (2C), 39.5, 38.4, 37.7, 35.9, 28.2, 26.8. **HRMS** (ESI): calcd for $\text{C}_{23}\text{H}_{31}\text{N}_4\text{O}_2^+$ [M+H]⁺ 395.2442, found 395.2445. **SFC**: 93.2%.



1,3-bis(3-aminopropyl)-5,5-bis(4-(trifluoromethyl)benzyl)imidazolidine-2,4-dione **2bA**.

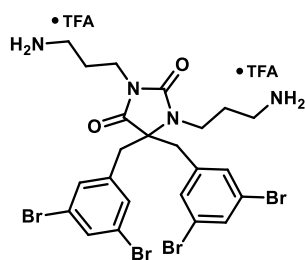
9b (250 mg, 0.60 mmol, 1.0 eq), *tert*-butyl (3-bromopropyl)carbamate **S7** (429 mg, 1.80 mmol, 3.0 eq), Cs_2CO_3 (586 mg, 1.8 mmol, 3.0 eq), TBAI (44 mg, 120 μmol , 0.2 eq) and acetone (8 mL) were stirred at 65 °C for 72 h. Purification by column chromatography on silica gel with a gradient of 0-70% EtOAc in heptane delivered the intermediate Boc-**2bA** (434 mg, 594 μmol , 99%) as a white solid. TFA (551 μL , 7.20 mmol, 12.0 eq) and DCM (2.5 mL) were added and the solution was stirred at ambient temperature for 16 h. The crude was purified by RP chromatography with a gradient of 0-70% MeCN/ H_2O + 0.1% TFA to yield the di-TFA salt of **2bA** (388 mg, 512 μmol , 85% o2s) as a white solid. $^1\text{H NMR}$ (400 MHz, Methanol-*d*₄) δ 7.60 (d, J = 8.1 Hz, 4H), 7.40 (d, J = 8.0 Hz, 4H), 3.69 – 3.62 (m, 2H), 3.41 (s, 4H), 3.27 (t, J = 6.9 Hz, 2H), 2.99 (t, J = 7.3 Hz, 2H), 2.44 (t, J = 7.0 Hz, 2H), 2.08 (qn, J = 7.4 Hz, 2H), 1.50 (qn, J = 6.9 Hz, 2H). $^{13}\text{C NMR}$ (101 MHz, Methanol-*d*₄) δ 175.2, 158.2, 140.3 (2C), 131.9 (4C), 130.9 (q, J = 32.5 Hz, 2C), 126.4 (q, J = 3.8 Hz, 4C), 125.5 (q, J = 271.3 Hz, 4C), 72.9, 41.2 (2C), 39.5, 38.4, 37.7, 35.9, 28.3, 26.8. **HRMS** (ESI): calcd for $\text{C}_{25}\text{H}_{29}\text{F}_6\text{N}_4\text{O}_2^+$ [M+H]⁺ 531.2189, found 531.2186. **SFC**: >99.0%.



1,3-bis(3-aminopropyl)-5,5-bis(4-bromo-3-chlorobenzyl)imidazolidine-2,4-dione **2cA**.

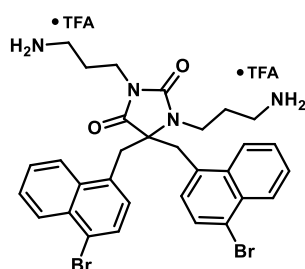
9c (127 mg, 0.25 mmol, 1.0 eq), *tert*-butyl (3-bromopropyl)carbamate **S7** (179 mg, 0.75 mmol, 3.0 eq), Cs_2CO_3 (244 mg, 0.75 mmol, 3.0 eq), TBAI (18 mg, 50 μmol , 0.2 eq) and acetone (1.5 mL) were stirred at 65 °C for 70 h. Purification by column chromatography on silica gel with a gradient of 0-55% EtOAc in heptane delivered the slightly impure intermediate Boc-**2cA** (201 mg, 245 μmol , 98%) as a white foam. TFA (230 μL , 3.00 mmol, 12.0 eq) and DCM (1.5 mL) were added and the solution was stirred at ambient temperature for 16 h. The crude was purified by RP chromatography with a gradient of 0-70% MeCN/ H_2O + 0.1% TFA to yield the di-TFA salt of **2cA** (170 mg, 203 μmol , 81% o2s) as a white solid. $^1\text{H NMR}$ (400 MHz, Methanol-*d*₄) δ 7.62 (d, J = 8.3 Hz, 2H), 7.34 (d, J = 2.1 Hz, 2H), 7.05 (dd, J = 8.3, 2.1 Hz, 2H), 3.64 – 3.55 (m, 2H), 3.36 – 3.31 (m, 2H), 3.29 – 3.25 (m, 4H), 3.00 (t, J = 7.3 Hz, 2H), 2.58 (t, J = 6.9 Hz, 2H), 2.06 (qn, J = 7.4 Hz, 2H), 1.58 (qn, J = 7.0 Hz, 2H). $^{13}\text{C NMR}$ (101 MHz, Methanol-*d*₄) δ 175.1, 158.1, 137.1

(2C), 135.3 (2C), 135.0 (2C), 132.9 (2C), 131.2 (2C), 122.4 (2C), 72.6, 40.4 (2C), 39.4, 38.4, 37.8, 36.0, 28.4, 27.1. **HRMS** (ESI): calcd for $C_{23}H_{27}Br_2Cl_2N_4O_2^+$ $[M+H]^+$ 618.9872, found 618.9878. **SFC**: 96.7%.



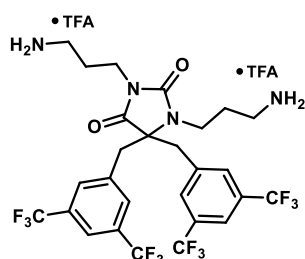
1,3-bis(3-aminopropyl)-5,5-bis(3,5-dibromobenzyl)imidazolidine-2,4-dione 2dA.

9d (149 mg, 0.25 mmol, 1.0 eq), *tert*-butyl (3-bromopropyl)carbamate **S7** (179 mg, 0.75 mmol, 3.0 eq), Cs_2CO_3 (244 mg, 0.75 mmol, 3.0 eq), TBAI (18 mg, 50 μ mol, 0.2 eq) and acetone (1.5 mL) were stirred at 65 °C for 70 h. Purification by column chromatography on silica gel with a gradient of 15-70% EtOAc in heptane delivered the impure intermediate Boc-**2dA** (169 mg, 159 μ mol, 74%) as a white foam. TFA (191 μ L, 2.50 mmol, 10.0 eq) and DCM (2.0 mL) were added and the solution was stirred at ambient temperature for 4 h. The crude was purified by RP chromatography with a gradient of 0-70% MeCN/H₂O + 0.1% TFA to yield the di-TFA salt of **2dA** (153 mg, 163 μ mol, 65% o2s) as a white solid. **¹H NMR** (400 MHz, Methanol-*d*4) δ 7.67 (t, *J* = 1.7 Hz, 2H), 7.36 (d, *J* = 1.7 Hz, 4H), 3.59 (dd, *J* = 8.5, 6.6 Hz, 2H), 3.41 – 3.33 (m, 2H), 3.27 (s, 4H), 3.00 (t, *J* = 7.2 Hz, 2H), 2.67 (t, *J* = 7.0 Hz, 2H), 2.06 (qn, *J* = 7.3 Hz, 2H), 1.63 (qn, *J* = 7.0 Hz, 2H). **¹³C NMR** (101 MHz, Methanol-*d*4) δ 174.9, 158.1, 140.0 (2C), 134.3 (2C), 133.0 (4C), 123.9 (4C), 72.5, 40.3 (2C), 39.3, 38.4, 37.9, 36.2, 28.5, 27.3. **HRMS** (ESI): calcd for $C_{23}H_{27}Br_4N_4O_2^+$ $[M+H]^+$ 706.8862, found 706.8856. **SFC**: >99.0%.



1,3-bis(3-aminopropyl)-5,5-bis((4-bromonaphthalen-1-yl)methyl)imidazolidine-2,4-dione 2eA.

9e (135 mg, 0.25 mmol, 1.0 eq), *tert*-butyl (3-bromopropyl)carbamate **S7** (179 mg, 0.75 mmol, 3.0 eq), Cs_2CO_3 (244 mg, 0.75 mmol, 3.0 eq), TBAI (18 mg, 50 μ mol, 0.2 eq) and acetone (1.5 mL) were stirred at 65 °C for 70 h. Purification by column chromatography on silica gel with a gradient of 10-25% EtOAc in heptane delivered the slightly impure intermediate Boc-**2eA** (208 mg, 244 μ mol, 98%) as a yellow solid. TFA (191 μ L, 2.50 mmol, 10.0 eq) and DCM (1.5 mL) were added and the solution was stirred at ambient temperature for 3.5 h. The crude was purified by RP chromatography with a gradient of 0-70% MeCN/H₂O + 0.1% TFA to yield the di-TFA salt of **2eA** (132 mg, 150 μ mol, 60% o2s) as a yellow solid. **¹H NMR** (400 MHz, Methanol-*d*4) δ 8.33 – 8.22 (m, 4H), 7.77 (d, *J* = 7.8 Hz, 2H), 7.71 – 7.62 (m, 4H), 7.18 (d, *J* = 7.8 Hz, 2H), 4.05 (d, *J* = 15.3 Hz, 2H), 3.86 (d, *J* = 15.3 Hz, 2H), 3.79 – 3.69 (m, 2H), 3.10 (t, *J* = 6.8 Hz, 2H), 2.83 (t, *J* = 7.4 Hz, 2H), 2.14 (t, *J* = 6.8 Hz, 2H), 1.70 (qn, *J* = 7.5 Hz, 2H), 1.01 (qn, *J* = 6.8 Hz, 2H). **¹³C NMR** (101 MHz, Methanol-*d*4) δ 175.3, 158.2, 134.9 (2C), 133.4 (2C), 132.7 (2C), 130.4 (2C), 129.1 (2C), 128.8 (2C), 128.7 (2C), 128.3 (2C), 126.1 (2C), 123.7 (2C), 71.7, 39.7, 38.3, 37.4, 37.1 (2C), 35.7, 28.2, 26.7. **HRMS** (ESI): calcd for $C_{31}H_{33}Br_2N_4O_2^+$ $[M+H]^+$ 651.0965, found 651.0965. **SFC**: >99.0%.

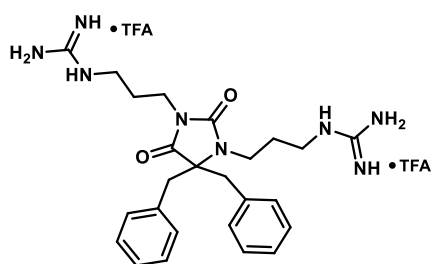


1,3-bis(3-aminopropyl)-5,5-bis(3,5-bis(trifluoromethyl)benzyl)imidazolidine-2,4-dione 2fA.

9f (200 mg, 0.36 mmol, 1.0 eq), *tert*-butyl (3-bromopropyl)carbamate **S7** (259 mg, 1.09 mmol, 3.0 eq), Cs_2CO_3 (354 mg, 1.09 mmol, 3.0 eq), TBAI (27 mg, 72 μ mol, 0.2 eq) and acetone (5.0 mL) were stirred at 65 °C for 72 h. Purification by column chromatography on silica gel with a gradient of 10-25% EtOAc in heptane delivered the slightly impure intermediate Boc-**2fA** (225 mg, 260 μ mol, 72%) as a white solid. TFA (277 μ L, 3.63 mmol, 10.0 eq) and DCM (2.0 mL) were added and the solution was stirred at ambient temperature for 17 h. The crude was purified by RP chromatography with a gradient of 10-65% MeCN/H₂O + 0.1% TFA to yield the di-TFA salt of **2fA** (144 mg, 161 μ mol, 45% o2s) as a white solid. **¹H NMR** (400 MHz, Methanol-*d*4) δ 7.92 (s, 2H), 7.80 (d, *J* = 1.7 Hz, 4H), 3.72 (dd, *J* = 8.5, 6.5 Hz, 2H), 3.56 (d, *J* = 14.2 Hz, 2H), 3.45 (d, *J* = 14.3 Hz, 2H), 3.26 (dd, *J* = 7.9, 6.5 Hz, 2H), 3.06 (t, *J* = 7.3 Hz, 2H), 2.63 (t, *J* = 7.0 Hz, 2H), 2.14 (q, *J* = 7.3 Hz, 2H), 1.48 (qn, *J* = 7.1 Hz, 2H). **¹³C NMR** (101 MHz, Methanol-*d*4) δ 174.5, 157.6, 138.8 (2C), 132.8 (q, *J* = 33.3 Hz, 4C), 132.1 – 131.8 (m, 4C), 124.7 (q, *J* = 272.1 Hz, 4C), 122.8 – 122.4 (m, 2C), 71.7, 40.3 (2C), 39.3, 38.4, 37.8, 36.2, 28.9, 27.0. **HRMS** (ESI): calcd for $C_{27}H_{27}F_{12}N_4O_2^+$ $[M+H]^+$ 667.1937, found 667.1940. **SFC**: 96.8%.

3.4.4 Synthesis of *N,N'*-dialkylated hydantoin 2G

The following compounds were prepared according to General Procedure D:

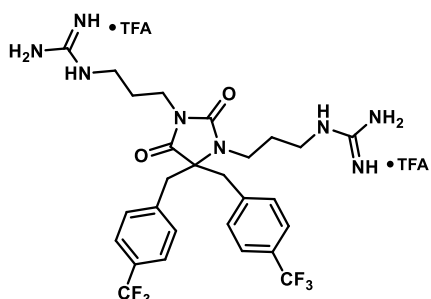


1,1'-((4,4-dibenzyl-2,5-dioxoimidazolidine-1,3-diyl)bis(propane-3,1-diyl))diguanidine **2aG**.

2aA (120 mg, 193 μmol , 1.0 eq), *N,N'*-Di-Boc-1*H*-pyrazole-1-carboxamidine (150 mg, 482 μmol , 2.50 eq), DIPEA (134 μL , 771 μmol , 4.00 eq) and THF (1 mL) were stirred at 45 °C for 2.0 h. The crude was purified with a gradient of 10-45% EtOAc in heptane to yield Boc-**2aG** (126 mg, 143 μmol , 74%) as a white foam.

TFA (221 μL , 2.89 mmol, 15.0 eq) and DCM (2 mL) were added and the solution was stirred at ambient temperature for 24 h. The crude was

purified by RP chromatography with a gradient of 10-55% MeCN/H₂O + 0.1% TFA to yield the di-TFA salt of **2aG** (86 mg, 122 μmol , 63% o2s) as a white powder. ¹H NMR (400 MHz, Methanol-*d*4) δ 7.31 – 7.21 (m, 6H), 7.16 (dd, *J* = 7.6, 1.9 Hz, 4H), 3.57 – 3.49 (m, 2H), 3.34 (d, *J* = 14.6 Hz, 2H), 3.25 (d, *J* = 14.5 Hz, 2H), 3.17 (dt, *J* = 11.1, 6.8 Hz, 4H), 2.58 (t, *J* = 6.9 Hz, 2H), 1.94 – 1.84 (m, 2H), 1.31 (qn, *J* = 6.8 Hz, 2H). ¹³C NMR (101 MHz, Methanol-*d*4) δ 176.1, 158.7, 158.6, 158.4, 135.9 (2C), 130.9 (4C), 129.6 (4C), 128.6 (2C), 73.4, 41.8 (2C), 40.2, 40.0, 39.4, 36.2, 29.4, 28.3. HRMS (ESI): calcd for C₂₅H₃₅N₈O₂⁺ [M+H]⁺ 479.2877, found 479.2868. SFC: >99.0%.

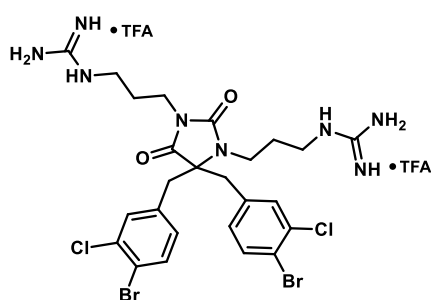


1,1'-((2,5-dioxo-4,4-bis(4-(trifluoromethyl)benzyl)imidazolidine-1,3-diyl)bis(propane-3,1-diyl))diguanidine **2bG**.

2bA (103 mg, 136 μmol , 1.0 eq), *N,N'*-Di-Boc-1*H*-pyrazole-1-carboxamidine (105 mg, 340 μmol , 2.50 eq), DIPEA (95 μL , 543 μmol , 4.00 eq) and THF (1 mL) were stirred at 45 °C for 2.0 h. The crude was purified with a gradient of 10-52% EtOAc in heptane to yield Boc-**2bG** (120 mg, 118 μmol , 87%) as a white foam.

TFA (156 μL , 2.04 mmol, 15.0 eq) and DCM (1 mL) were added and the solution was stirred at ambient temperature for 24 h. The crude was purified by RP chromatography with a gradient of 10-60% MeCN/H₂O

+ 0.1% TFA to yield the di-TFA salt of **2bG** (89 mg, 106 μmol , 78% o2s) as a white powder. ¹H NMR (400 MHz, Methanol-*d*4) 7.60 (d, *J* = 8.0 Hz, 4H), 7.38 (d, *J* = 8.0 Hz, 4H), 3.64 – 3.54 (m, 2H), 3.44 (d, *J* = 14.4 Hz, 2H), 3.39 (d, *J* = 14.4 Hz, 2H), 3.21 (dt, *J* = 9.2, 7.0 Hz, 4H), 2.70 (t, *J* = 6.9 Hz, 2H), 1.99 – 1.90 (m, 2H), 1.38 – 1.26 (m, 4H). ¹³C NMR (101 MHz, Methanol-*d*4) δ 175.2 (2C), 158.3, 140.4 (2C), 131.8 (4C), 126.4 (q, *J* = 3.8 Hz, 4C), 72.8, 41.3 (2C), 40.2, 40.0, 39.4, 36.4, 29.6, 28.3. CF₃ carbon and the neighboring carbon were not observed due to too low intensity. HRMS (ESI): calcd for C₂₇H₃₃F₆N₈O₂⁺ [M+H]⁺ 615.2625, found 615.2626. SFC: >99.0%.

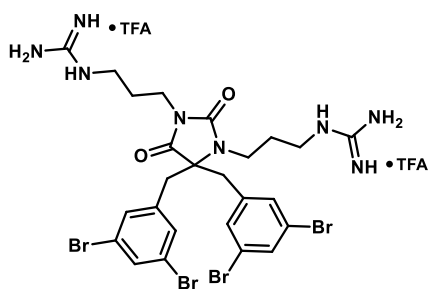


1,1'-((4,4-bis(4-bromo-3-chlorobenzyl)-2,5-dioxoimidazolidine-1,3-diyl)bis(propane-3,1-diyl))diguanidine **2cG**.

2cA (57 mg, 68 μmol , 1.0 eq), *N,N'*-Di-Boc-1*H*-pyrazole-1-carboxamidine (53 mg, 170 μmol , 2.50 eq), DIPEA (47 μL , 272 μmol , 4.00 eq) and THF (1 mL) were stirred at 45 °C for 2.0 h. The crude was purified with a gradient of 10-52% EtOAc in heptane to yield impure Boc-**2cG** (120 mg, 109 μmol , 159%) as a white foam.

TFA (78 μL , 102 mmol, 15.0 eq) and DCM (1 mL) were added and the solution was stirred at ambient temperature for 24 h. The crude was purified by RP chromatography with a gradient of 10-60% MeCN/H₂O + 0.1% TFA to yield the di-TFA salt of **2cG** (44 mg, 47 μmol , 69%

o2s) as a white powder. ¹H NMR (400 MHz, Methanol-*d*4) δ 7.60 (d, *J* = 8.3 Hz, 2H), 7.33 (d, *J* = 2.1 Hz, 2H), 7.03 (dd, *J* = 8.3, 2.1 Hz, 2H), 3.59 – 3.50 (m, 2H), 3.29 – 3.20 (m, 8H), 2.78 (t, *J* = 7.0 Hz, 2H), 1.95 (qn, *J* = 7.1 Hz, 2H), 1.39 (qn, *J* = 7.1 Hz, 2H). ¹³C NMR (101 MHz, Methanol-*d*4) δ 175.2, 158.7, 158.6, 158.0, 137.2 (2C), 135.4 (2C), 135.0 (2C), 132.9 (2C), 131.1 (2C), 122.4 (2C), 72.6, 40.4 (2C), 40.2, 40.0, 39.4, 37.8, 36.4, 29.7, 28.6. HRMS (ESI): calcd for C₂₅H₃₁Br₂Cl₂N₈O₂⁺ [M+H]⁺ 703.0308, found 703.0312. SFC: >99.0%.

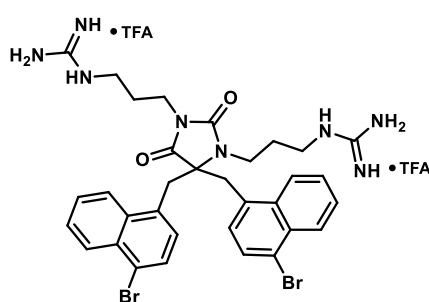


1,1'-((4,4-bis(3,5-dibromobenzyl)-2,5-dioxoimidazolidine-1,3-diyl)bis(propane-3,1-diyl))diguanidine 2dG.

2dA (53 mg, 57 μ mol, 1.0 eq), *N,N'*-Di-Boc-1*H*-pyrazole-1-carboxamide (44 mg, 141 μ mol, 2.50 eq), DIPEA (39 μ L, 226 μ mol, 4.00 eq) and THF (1 mL) were stirred at 45 °C for 2.0 h. The crude was purified with a gradient of 10-52% EtOAc in heptane to yield Boc-**2dG** (60 mg, 50 μ mol, 89%) as a white foam.

TFA (65 μ L, 848 μ mol, 15.0 eq) and DCM (1 mL) were added and the solution was stirred at ambient temperature for 24 h. The crude was purified by RP chromatography with a gradient of 10-60% MeCN/H₂O +

0.1% TFA to yield the di-TFA salt of **2dG** (50 mg, 49 μ mol, 87% o2s) as a white powder. ¹H NMR (400 MHz, Methanol-*d*4) δ 7.66 (t, *J* = 1.7 Hz, 2H), 7.34 (d, *J* = 1.8 Hz, 4H), 3.57 – 3.46 (m, 2H), 3.30 – 3.22 (m, 8H), 2.87 (t, *J* = 7.0 Hz, 2H), 2.01 – 1.90 (m, 2H), 1.46 (qn, *J* = 7.1 Hz, 2H). ¹³C NMR (101 MHz, Methanol-*d*4) δ 175.1, 158.7, 158.6, 157.9, 140.1 (2C), 134.2 (2C), 133.0 (4C), 123.9 (4C), 72.7, 40.4 (2C), 40.2, 40.0, 39.5, 36.5, 29.7, 28.8. HRMS (ESI): calcd for C₂₅H₃₁Br₄N₈O₂⁺ [M+H]⁺ 790.9309, found 790.9310. SFC: >99.0%.

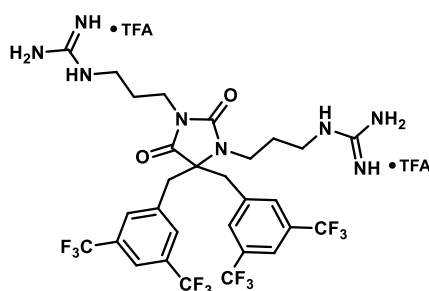


1,1'-((4,4-bis((4-bromonaphthalen-1-yl)methyl)-2,5-dioxoimidazolidine-1,3-diyl)bis(propane-3,1-diyl))diguanidine 2eG.

2eA (27 mg, 31 μ mol, 1.0 eq), *N,N'*-Di-Boc-1*H*-pyrazole-1-carboxamide (24 mg, 77 μ mol, 2.50 eq), DIPEA (21 μ L, 123 μ mol, 4.00 eq) and THF (1 mL) were stirred at 45 °C for 2.0 h. The crude was purified with a gradient of 10-45% EtOAc in heptane to yield Boc-**2eG** (27 mg, 24 μ mol, 77%) as a clear liquid.

TFA (35 μ L, 460 μ mol, 15.0 eq) and DCM (1 mL) were added and the solution was stirred at ambient temperature for 24 h. The crude was purified by RP chromatography with a gradient of 10-55% MeCN/H₂O + 0.1% TFA to yield the di-TFA salt of **2eG** (20 mg, 21 μ mol, 68%

o2s) as a white powder. ¹H NMR (400 MHz, Methanol-*d*4) δ 8.28 (ddt, *J* = 7.7, 4.6, 2.2 Hz, 4H), 7.74 (d, *J* = 7.8 Hz, 2H), 7.70 – 7.60 (m, 4H), 7.16 (d, *J* = 7.8 Hz, 2H), 4.06 (d, *J* = 15.4 Hz, 2H), 3.85 (d, *J* = 15.3 Hz, 2H), 3.71 – 3.59 (m, 2H), 3.04 (dt, *J* = 10.4, 6.9 Hz, 4H), 2.32 (t, *J* = 7.0 Hz, 2H), 1.47 (qn, *J* = 7.0 Hz, 2H), 0.72 (qn, *J* = 7.0 Hz, 2H). ¹³C NMR (101 MHz, Methanol-*d*4) δ 175.7, 158.5, 158.3, 158.0, 135.0 (2C), 133.5 (2C), 132.7 (2C), 130.4 (2C), 129.0 (2C), 128.7 (2C), 128.6 (2C), 128.2 (2C), 126.1 (2C), 123.7 (2C), 71.7, 40.1, 40.1, 39.0, 37.0 (2C), 36.2, 29.2, 28.1. HRMS (ESI): calcd for C₃₃H₃₇Br₂N₈O₂⁺ [M+H]⁺ 735.1401, found 735.1393. SFC: >99.0%.



1,1'-((4,4-bis(3,5-bis(trifluoromethyl)benzyl)-2,5-dioxoimidazolidine-1,3-diyl)bis(propane-3,1-diyl))diguanidine 2fG.

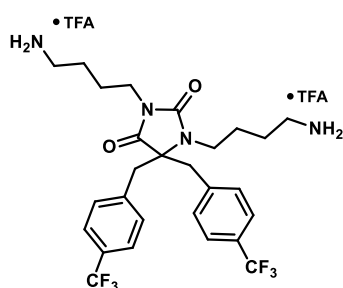
2fA (83 mg, 93 μ mol, 1.0 eq), *N,N'*-Di-Boc-1*H*-pyrazole-1-carboxamide (72 mg, 232 μ mol, 2.50 eq), DIPEA (65 μ L, 371 μ mol, 4.00 eq) and THF (1 mL) were stirred at 45 °C for 2.0 h. The crude was purified with a gradient of 10-50% EtOAc in heptane to yield Boc-**2fG** (48 mg, 42 μ mol, 45%) as a clear liquid.

TFA (107 μ L, 1.39 mmol, 15.0 eq) and DCM (1 mL) were added and the solution was stirred at ambient temperature for 24 h. The crude was purified by RP chromatography with a gradient of 15-55% MeCN/H₂O

+ 0.1% TFA to yield the di-TFA salt of **2fG** (30 mg, 31 μ mol, 33% o2s) as a white powder. ¹H NMR (400 MHz, Methanol-*d*4) δ 7.94 – 7.89 (m, 2H), 7.83 – 7.76 (m, 4H), 3.67 – 3.60 (m, 2H), 3.57 (d, *J* = 14.3 Hz, 2H), 3.50 (d, *J* = 14.3 Hz, 2H), 3.30 (t, *J* = 6.8 Hz, 2H), 3.20 – 3.12 (m, 2H), 2.80 (t, *J* = 6.9 Hz, 2H), 2.07 – 1.96 (m, 2H), 1.34 – 1.19 (m, 2H). ¹³C NMR (101 MHz, Methanol-*d*4) δ 174.7, 158.8, 158.6, 157.5, 138.9 (2C), 132.8 (q, *J* = 33.3 Hz, 4C), 132.0 – 131.7 (m, 4C), 124.7 (q, *J* = 272.0 Hz, 4C), 122.6 – 122.4 (m, 2C), 72.3, 40.4 (2C), 40.2, 40.0, 39.2, 36.4, 29.8, 28.5. HRMS (ESI): calcd for C₂₉H₃₁F₁₂N₈O₂⁺ [M+H]⁺ 751.2373, found 751.2375. SFC: >99.0%.

3.4.5 Synthesis of *N,N'*-dialkylated hydantoin 6A

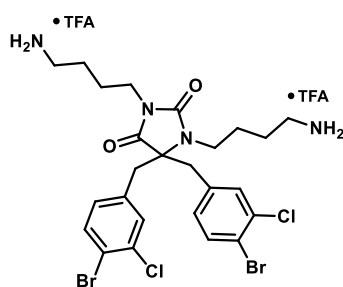
The following compounds were prepared according to General Procedure C:



1,3-bis(4-aminobutyl)-5,5-bis(4-(trifluoromethyl)benzyl)imidazolidine-2,4-dione 6bA.

9b (69 mg, 166 μmol , 1.0 eq), *tert*-butyl (4-bromobutyl)carbamate **S8** (104 mg, 414 μmol , 2.5 eq), Cs_2CO_3 (189 mg, 580 μmol , 3.5 eq), TBAI (6.1 mg, 17 μmol , 0.1 eq) and acetone (2.0 mL) were stirred at 75 $^\circ\text{C}$ for 72 h. Purification by column chromatography on silica gel with a gradient of 15-50% EtOAc in heptane delivered the impure intermediate Boc-**6bA** (110 mg, 145 μmol , 88%) as a colorless solid.

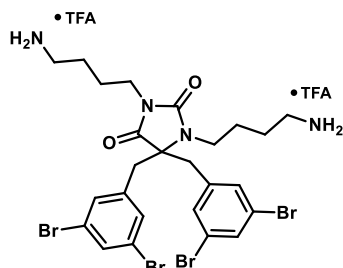
TFA (127 μL , 1.66 mmol, 10.0 eq) and DCM (1.5 mL) were added and the solution was stirred at ambient temperature for 24 h. The crude was purified by RP chromatography with a gradient of 15-55% MeCN/ H_2O + 0.1% TFA to yield the di-TFA salt of **6bA** (64 mg, 81 μmol , 49% o2s) as a white solid. $^1\text{H NMR}$ (400 MHz, Methanol-*d*4) δ 7.60 (d, J = 8.0 Hz, 4H), 7.38 (d, J = 8.0 Hz, 4H), 3.58 – 3.49 (m, 2H), 3.39 (s, 4H), 3.12 (t, J = 7.3 Hz, 2H), 2.97 (t, J = 7.2 Hz, 2H), 2.74 (t, J = 7.7 Hz, 2H), 1.82 – 1.64 (m, 4H), 1.31 – 1.18 (m, 2H), 1.05 (h, J = 7.4, 6.8 Hz, 2H). $^{13}\text{C NMR}$ (101 MHz, Methanol-*d*4) δ 175.1, 157.8, 140.5 – 140.4 (m, 2H), 131.9 (4C), 130.7 (q, J = 32.3 Hz, 2C), 126.3 (q, J = 3.9 Hz, 4C), 125.6 (q, J = 271.2 Hz, 2C), 72.5, 42.0, 41.3 (2C), 40.2, 39.7, 38.2, 27.2, 26.3, 25.6, 25.4. **HRMS** (ESI): calcd for $\text{C}_{27}\text{H}_{33}\text{F}_6\text{N}_4\text{O}_2^+$ $[\text{M}+\text{H}]^+$ 559.2502, found 559.2503. **SFC**: 96.6%.



1,3-bis(4-aminobutyl)-5,5-bis(4-bromo-3-chlorobenzyl)imidazolidine-2,4-dione 6cA.

9c (73 mg, 144 μmol , 1.0 eq), *tert*-butyl (4-bromobutyl)carbamate **S8** (91 mg, 360 μmol , 2.5 eq), Cs_2CO_3 (164 mg, 504 μmol , 3.5 eq), TBAI (5.3 mg, 14 μmol , 0.1 eq) and acetone (2.0 mL) were stirred at 75 $^\circ\text{C}$ for 72 h. Purification by column chromatography on silica gel with a gradient of 15-50% EtOAc in heptane delivered the impure intermediate Boc-**6cA** (92 mg, 108 μmol , 75%) as a colorless solid.

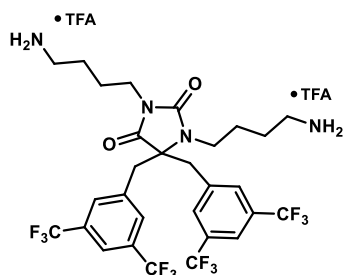
TFA (111 μL , 1.44 mmol, 10.0 eq) and DCM (1.5 mL) were added and the solution was stirred at ambient temperature for 24 h. The crude was purified by RP chromatography with a gradient of 15-55% MeCN/ H_2O + 0.1% TFA to yield the di-TFA salt of **6cA** (71 mg, 81 μmol , 56% o2s) as a white solid. $^1\text{H NMR}$ (400 MHz, Methanol-*d*4) δ 7.60 (d, J = 8.3 Hz, 2H), 7.34 (d, J = 2.1 Hz, 2H), 7.03 (dd, J = 8.3, 2.1 Hz, 2H), 3.48 (t, J = 7.5 Hz, 2H), 3.25 (s, 4H), 3.19 (t, J = 7.2 Hz, 2H), 2.98 (t, J = 7.2 Hz, 2H), 2.81 (t, J = 7.6 Hz, 2H), 1.81 – 1.65 (m, 4H), 1.35 – 1.23 (m, 2H), 1.20 – 1.08 (m, 2H). $^{13}\text{C NMR}$ (101 MHz, Methanol-*d*4) δ 175.1, 157.8, 137.2 (2C), 135.2 (2C), 135.0 (2C), 133.1 (2C), 131.2 (2C), 122.2 (2C), 72.4, 41.9, 40.4 (2C), 40.2, 40.1, 38.3, 27.3, 26.2, 26.0, 25.5. **HRMS** (ESI): calcd for $\text{C}_{25}\text{H}_{31}\text{Br}_2\text{Cl}_2\text{N}_4\text{O}_2^+$ $[\text{M}+\text{H}]^+$ 647.0185, found 647.0192. **SFC**: 97.3%.



1,3-bis(4-aminobutyl)-5,5-bis(3,5-dibromobenzyl)imidazolidine-2,4-dione 6dA.

9d (73 mg, 123 μmol , 1.0 eq), *tert*-butyl (4-bromobutyl)carbamate **S8** (77 mg, 306 μmol , 2.5 eq), Cs_2CO_3 (140 mg, 429 μmol , 3.5 eq), TBAI (4.5 mg, 12 μmol , 0.1 eq) and acetone (2.5 mL) were stirred at 75 $^\circ\text{C}$ for 72 h. Purification by column chromatography on silica gel with a gradient of 15-50% EtOAc in heptane delivered the impure intermediate Boc-**6dA** (91 mg, 97 μmol , 79%) as a colorless solid.

TFA (94 μL , 1.23 mmol, 10.0 eq) and DCM (1.5 mL) were added and the solution was stirred at ambient temperature for 24 h. The crude was purified by RP chromatography with a gradient of 15-55% MeCN/ H_2O + 0.1% TFA to yield the di-TFA salt of **6dA** (73 mg, 76 μmol , 62% o2s) as a white solid. $^1\text{H NMR}$ (400 MHz, Methanol-*d*4) δ 7.66 (t, J = 1.7 Hz, 2H), 7.34 (d, J = 1.7 Hz, 4H), 3.49 – 3.41 (m, 2H), 3.29 – 3.24 (m, 4H), 3.22 (d, J = 7.4 Hz, 2H), 3.02 – 2.95 (m, 2H), 2.87 (t, J = 7.6 Hz, 2H), 1.72 (qn, J = 3.6 Hz, 4H), 1.40 (qn, J = 7.4 Hz, 2H), 1.34 – 1.23 (m, 2H). $^{13}\text{C NMR}$ (101 MHz, Methanol-*d*4) δ 175.1, 157.6, 140.2 (2C), 134.2 (2C), 133.1 (4C), 123.9 (4C), 72.6, 42.0, 40.5 (2C), 40.3, 40.0, 38.5, 27.2, 26.2, 26.2, 25.6. **HRMS** (ESI): calcd for $\text{C}_{25}\text{H}_{31}\text{Br}_4\text{N}_4\text{O}_2^+$ $[\text{M}+\text{H}]^+$ 734.9175, found 734.9179. **SFC**: 96.1%.



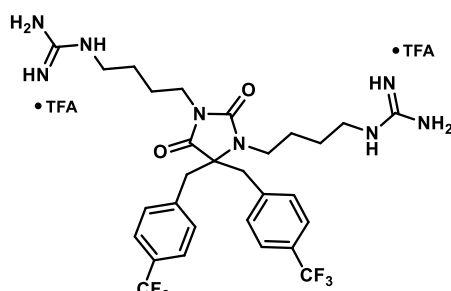
1,3-bis(4-aminobutyl)-5,5-bis(3,5-bis(trifluoromethyl)benzyl)imidazolidine-2,4-dione 6fA.

9f (72 mg, 130 μmol , 1.0 eq), *tert*-butyl (4-bromobutyl)carbamate **S8** (82 mg, 326 μmol , 2.5 eq), Cs_2CO_3 (149 mg, 456 μmol , 3.5 eq), TBAI (4.8 mg, 13 μmol , 0.1 eq) and acetone (2.0 mL) were stirred at 75 $^\circ\text{C}$ for 72 h. Purification by column chromatography on silica gel with a gradient of 15-50% EtOAc in heptane delivered the impure intermediate Boc-**6fA** (103 mg, 115 μmol , 88%) as a colorless solid.

TFA (100 μL , 1.30 mmol, 10.0 eq) and DCM (1.5 mL) were added and the solution was stirred at ambient temperature for 24 h. The crude was purified by RP chromatography with a gradient of 8-48% MeCN/ H_2O + 0.1% TFA to yield the di-TFA salt of **6fA** (96 mg, 104 μmol , 80% o2s) as a white solid. $^1\text{H NMR}$ (400 MHz, Methanol-*d*4) δ 7.92 (d, J = 2.0 Hz, 2H), 7.81 – 7.77 (m, 4H), 3.59 – 3.53 (m, 2H), 3.54 (d, J = 14.3 Hz, 2H), 3.49 (d, J = 14.3 Hz, 2H), 3.10 (dd, J = 8.4, 6.7 Hz, 2H), 2.96 (t, J = 6.8 Hz, 2H), 2.79 – 2.69 (m, 2H), 1.76 (qn, J = 3.3 Hz, 4H), 1.37 – 1.25 (m, 2H), 1.08 (tt, J = 9.4, 6.5 Hz, 2H). $^{13}\text{C NMR}$ (101 MHz, Methanol-*d*4) δ 174.7, 157.2, 139.0 (2C), 132.7 (q, J = 33.2 Hz, 4C), 132.0 – 1.31.7 (m, 4C), 124.7 (q, J = 272.0 Hz, 4C), 122.6 – 122.4 (m, 2C), 72.2, 42.0, 40.5 (2C), 40.2, 39.7, 38.3, 27.4, 26.2, 25.7, 25.3. **HRMS** (ESI): calcd for $\text{C}_{29}\text{H}_{31}\text{F}_{12}\text{N}_4\text{O}_2^+$ [M+H] $^+$ 695.2250, found 695.2254. **SFC**: 95.5%.

3.4.6 Synthesis of *N,N'*-dialkylated hydantoinins **6G**

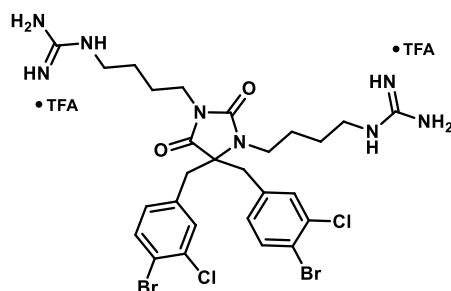
The following compounds were prepared according to General Procedure D:



1,1'-((2,5-dioxo-4,4-bis(4-(trifluoromethyl)benzyl)imidazolidine-1,3-diyl)bis(butane-4,1-diyl))diguanidine 6bG.

6bA (29 mg, 37 μmol , 1.0 eq), *N,N'*-Di-Boc-1*H*-pyrazole-1-carboximidine (29 mg, 92 μmol , 2.50 eq), DIPEA (26 μL , 148 μmol , 4.0 eq) and THF (0.75 mL) were stirred at 45 $^\circ\text{C}$ for 2.5 h. The crude was purified with a gradient of 20-55% EtOAc in heptane to yield pure Boc-**6bG** (38 mg, 36 μmol , 99%) as a clear solid.

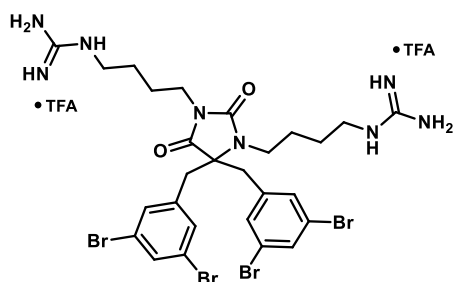
TFA (85 μL , 1.11 mmol, 30.0 eq) and DCM (0.75 mL) were added and the solution was stirred at ambient temperature for 44 h. The crude was purified by RP chromatography with a gradient of 20-60% MeCN/ H_2O + 0.1% TFA to yield the di-TFA salt of **6bG** (25 mg, 29 μmol , 78% o2s) as a white powder. $^1\text{H NMR}$ (400 MHz, Methanol-*d*4) δ 7.59 (d, J = 8.1 Hz, 4H), 7.38 (d, J = 8.0 Hz, 4H), 3.54 (dd, J = 9.1, 6.7 Hz, 2H), 3.39 (s, 4H), 3.22 (t, J = 7.1 Hz, 2H), 3.14 (t, J = 6.5 Hz, 2H), 3.00 (t, J = 6.9 Hz, 2H), 1.82 – 1.69 (m, 2H), 1.69 – 1.58 (m, 2H), 1.15 – 1.02 (m, 4H). $^{13}\text{C NMR}$ (101 MHz, Methanol-*d*4) δ 175.3, 158.7, 158.6, 158.0, 140.5 (2C), 131.9 (4C), 130.8 (q, J = 32.3 Hz, 2C), 126.3 (q, J = 3.9 Hz, 4C), 125.6 (q, J = 271.4 Hz, 2C), 72.5, 42.2, 42.0, 41.5, 41.4 (2C), 38.4, 27.5 (2C), 26.5, 25.8. **HRMS** (ESI): calcd for $\text{C}_{29}\text{H}_{37}\text{F}_6\text{N}_8\text{O}_2^+$ [M+H] $^+$ 643.2938, found 643.2936. **SFC**: >99%.



1,1'-((4,4-bis(4-bromo-3-chlorobenzyl)-2,5-dioxoimidazolidine-1,3-diyl)bis(butane-4,1-diyl))diguanidine 6cG.

6cA (28 mg, 32 μmol , 1.0 eq), *N,N'*-Di-Boc-1*H*-pyrazole-1-carboximidine (25 mg, 80 μmol , 2.50 eq), DIPEA (22 μL , 128 μmol , 4.0 eq) and THF (0.75 mL) were stirred at 45 $^\circ\text{C}$ for 2.5 h. The crude was purified with a gradient of 20-55% EtOAc in heptane to yield pure Boc-**6cG** (35 mg, 31 μmol , 97%) as a clear solid.

TFA (74 μL , 0.96 mmol, 30.0 eq) and DCM (0.75 mL) were added and the solution was stirred at ambient temperature for 44 h. The crude was purified by RP chromatography with a gradient of 20-60% MeCN/ H_2O + 0.1% TFA to yield the di-TFA salt of **6cG** (28 mg, 29 μmol , 91% o2s) as a white powder. $^1\text{H NMR}$ (400 MHz, Methanol-*d*4) δ 7.59 (d, J = 8.2 Hz, 2H), 7.33 (d, J = 2.1 Hz, 2H), 7.03 (dd, J = 8.3, 2.1 Hz, 2H), 3.53 – 3.44 (m, 2H), 3.27 – 3.16 (m, 8H), 3.06 (t, J = 7.1 Hz, 2H), 1.81 – 1.69 (m, 2H), 1.69 – 1.58 (m, 2H), 1.25 – 1.06 (m, 4H). $^{13}\text{C NMR}$ (101 MHz, Methanol-*d*4) δ 175.2, 158.7, 158.6, 158.0, 137.3 (2C), 135.3 (2C), 134.9 (2C), 133.0 (2C), 131.2 (2C), 122.3 (2C), 72.4, 42.2, 42.1, 41.8, 40.5 (2C), 38.5, 27.6, 27.5, 26.5, 26.1. **HRMS** (ESI): calcd for $\text{C}_{27}\text{H}_{35}\text{Br}_2\text{Cl}_2\text{N}_8\text{O}_2^+$ [M+H] $^+$ 731.0621, found 731.0630. **SFC**: >99%.

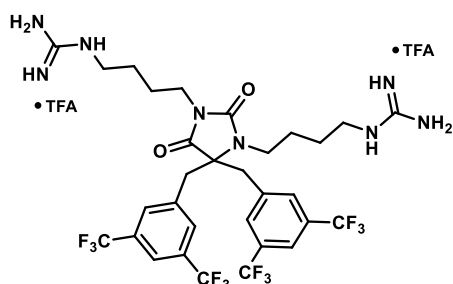


1,1'-((4,4-bis(3,5-dibromobenzyl)-2,5-dioximidazolidine-1,3-diyl)bis(butane-4,1-diyl)diguanidine **6dG**.

6dA (31 mg, 32 μmol , 1.0 eq), *N,N'*-Di-Boc-1*H*-pyrazole-1-carboximidine (25 mg, 80 μmol , 2.50 eq), DIPEA (22 μL , 129 μmol , 4.0 eq) and THF (0.75 mL) were stirred at 45 °C for 2.5 h. The crude was purified with a gradient of 20-55% EtOAc in heptane to yield pure Boc-**6dG** (36 mg, 29 μmol , 92%) as a clear solid.

TFA (74 μL , 963 μmol , 30.0 eq) and DCM (0.75 mL) were added and the solution was stirred at ambient temperature for 44 h. The crude was purified by RP chromatography with a gradient of 10-45%

MeCN/H₂O + 0.1% TFA to yield the di-TFA salt of **6dG** (25 mg, 24 μmol , 74% o2s) as a white powder. ¹H NMR (400 MHz, Methanol-*d*4) δ 7.65 (t, *J* = 1.7 Hz, 2H), 7.34 (d, *J* = 1.7 Hz, 4H), 3.45 (t, *J* = 7.7 Hz, 2H), 3.28 – 3.19 (m, 8H), 3.11 (t, *J* = 6.8 Hz, 2H), 1.79 – 1.57 (m, 2H), 1.34 – 1.17 (m, 4H). ¹³C NMR (101 MHz, Methanol-*d*4) δ 175.1, 158.7, 158.6, 157.8, 140.2 (2C), 134.1 (2C), 133.1 (4C), 123.9 (4C), 72.6, 42.2 (2C), 41.9, 40.5 (2C), 38.7, 27.5 (2C), 26.7, 26.4. HRMS (ESI): calcd for C₂₇H₃₅Br₄N₈O₂⁺ [M+H]⁺ 818.9611, found 818.9613. SFC: >99%.



1,1'-((4,4-bis(3,5-bis(trifluoromethyl)benzyl)-2,5-dioximidazolidine-1,3-diyl)bis(butane-4,1-diyl)diguanidine **6fG**.

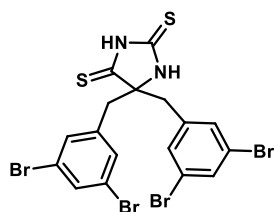
6fA (33 mg, 36 μmol , 1.0 eq), *N,N'*-Di-Boc-1*H*-pyrazole-1-carboximidine (28 mg, 89 μmol , 2.50 eq), DIPEA (25 μL , 143 μmol , 4.0 eq) and THF (0.75 mL) were stirred at 45 °C for 2.5 h. The crude was purified with a gradient of 20-55% EtOAc in heptane to yield pure Boc-**6fG** (40 mg, 34 μmol , 95%) as a clear solid.

TFA (82 μL , 1.07 mmol, 30.0 eq) and DCM (0.75 mL) were added and the solution was stirred at ambient temperature for 44 h. The crude was purified by RP chromatography with a gradient of 20-60%

MeCN/H₂O + 0.1% TFA to yield the di-TFA salt of **6fG** (31 mg, 31 μmol , 86% o2s) as a white powder. ¹H NMR (400 MHz, Methanol-*d*4) δ 7.91 (s, 2H), 7.81 – 7.77 (m, 4H), 3.60 – 3.52 (m, 2H), 3.55 (d, *J* = 14.3 Hz, 2H), 3.49 (d, *J* = 14.3 Hz, 2H), 3.23 (t, *J* = 7.0 Hz, 2H), 3.10 (t, *J* = 6.8 Hz, 2H), 3.00 (t, *J* = 6.8 Hz, 2H), 1.78 (q, *J* = 8.4, 7.7 Hz, 2H), 1.74 – 1.63 (m, 2H), 1.17 – 1.04 (m, 4H). ¹³C NMR (101 MHz, Methanol-*d*4) δ 174.8, 158.7, 158.6, 157.5, 139.0 (2C), 132.7 (q, *J* = 33.3 Hz, 4C), 132.0 – 131.7 (m, 4C), 124.7 (q, *J* = 272.1 Hz, 4C), 122.6 – 122.3 (m, 2C), 72.2, 42.2, 42.0, 41.5, 40.5 (2C), 38.5, 27.7, 27.5, 26.5, 25.9. HRMS (ESI): calcd for C₃₁H₃₅F₁₂N₈O₂⁺ [M+H]⁺ 779.2686, found 779.2689. SFC: >99%.

3.5 Synthesis of different core structures 3-5 and 15

3.5.1 2,4-Dithiohydantoin

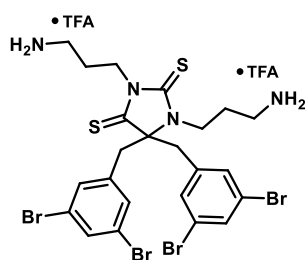


5,5-bis(3,5-dibromobenzyl)imidazolidine-2,4-dithione **16**.

Hydantoin **9d** (175 mg, 294 μmol , 1.0 eq) was mixed with anhydrous 1,4-dioxane (2.5 mL) in an oven dried vial under inert atmosphere. Lawesson's reagent (475 mg, 1.17 mmol, 4.0 eq) was added and the solution was stirred at 115 °C for 40 h. The mixture became yellow and clear at elevated temperature. The mixture was allowed to cool to ambient temperature and the solvent was removed under reduced pressure.

Purification by column chromatography on silica gel with a gradient of 10-15 % EtOAc in heptane and subsequent lyophilization delivered **16** (152 mg, 242 μmol , 82%) as a yellow solid.

¹H NMR (400 MHz, DMSO-*d*6) δ 12.91 (s, 1H), 10.97 (d, *J* = 1.7 Hz, 1H), 7.72 (t, *J* = 1.8 Hz, 2H), 7.37 (d, *J* = 1.8 Hz, 4H), 3.17 (d, *J* = 13.5 Hz, 2H), 3.10 (d, *J* = 13.5 Hz, 2H). ¹³C NMR (101 MHz, DMSO-*d*6) δ 206.5, 180.4, 138.5 (2C), 132.3 (4C), 132.2 (2C), 121.9 (4C), 80.6, 43.5. HRMS (ESI): calcd for C₁₇H₁₁Br₄N₂S₂⁻ [M-H]⁻ 622.7103, found: 622.7109.



1,3-bis(3-aminopropyl)-5,5-bis(3,5-dibromobenzyl)imidazolidine-2,4-dithione **4A**.

2,4-dithiohydantoin **16** (75 mg, 119 μmol , 1.0 eq), *tert*-butyl (3-bromopropyl)carbamate **S7** (92 mg, 388 μmol , 3.25 eq), Cs₂CO₃ (97 mg, 0.299 μmol , 2.5 eq), TBAI (8.8 mg, 24 μmol , 0.2 eq) and acetone (2.0 mL) were stirred at 55 °C for 72 h. The mixture was allowed to cool to ambient temperature before water and EtOAc were added. The layers were separated, and the aqueous layer was extracted with EtOAc twice. The combined organics were dried over MgSO₄, filtered and the solvent was removed under reduced pressure. Purification by automated flash column chromatography on silica gel with a

removed under reduced pressure. Purification by automated flash column chromatography on silica gel with a

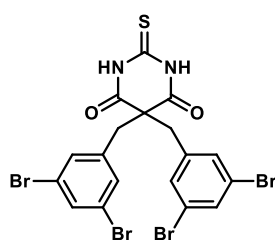
gradient of 10-45% EtOAc in heptane delivered the impure intermediate Boc-**4A** (169 mg, 159 μ mol, 74%) as a yellow foam.

Boc-**4A**, TFA (138 μ L, 1.79 mmol, 15.0 eq) and DCM (1.0 mL) were combined, and the mixture stirred for 24 h at ambient temperature. The solvent was removed and the crude purified by RP chromatography with a gradient of 20-60% MeCN/H₂O + 0.1% TFA to yield the di-TFA salt of **4A** (65 mg, 67 μ mol, 56% o2s) as a white solid.

Note: Peaks in the NMR that are not accounted for are likely to be the S-alkylated isomers.

¹H NMR (400 MHz, Methanol-*d*₄) δ 7.56 (t, *J* = 1.8 Hz, 2H), 7.31 (d, *J* = 1.8 Hz, 4H), 3.61 – 3.55 (m, 2H), 3.37 (t, *J* = 7.2 Hz, 2H), 3.36 (d, *J* = 13.0 Hz, 2H), 3.26 (d, *J* = 12.9 Hz, 2H), 3.17 (t, *J* = 7.2 Hz, 2H), 2.74 (t, *J* = 7.3 Hz, 2H), 2.25 (qn, *J* = 7.2 Hz, 2H), 1.56 – 1.43 (m, 2H). ¹³C NMR *not obtained*. HRMS (ESI): calcd for C₂₃H₂₇Br₄N₄S₂⁺ [M+H]⁺ 738.8405, found: 738.8405. SFC: *not obtained*.

3.5.2 Thiobarbituric acid

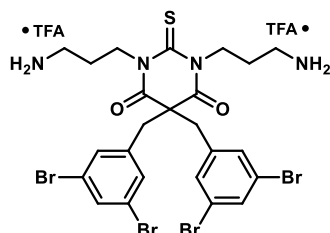


5,5-bis(3,5-dibromobenzyl)-2-thioxodihydropyrimidine-4,6(1H,5H)-dione 18.

Diethyl 2,2-bis(3,5-dibromobenzyl)malonate^[11] (1.10 g, 1.67 mmol, 1.0 eq) was dissolved in 15 mL of anhydrous THF:DMF (2:1) under inert atmosphere and cooled to 0 °C. Thiourea (1.27 g, 16.7 mmol, 10.0 eq) and NaH (201 mg, 5.02 mmol, 3.0 eq, 60% in mineral oil) were added and the mixture was stirred at that temperature for 30 min. The suspension was then heated to 65 °C for 5 days, cooled to ambient temperature and EtOAc was added. The organic layer was washed with 5% LiCl_(aq) solution thrice, dried over MgSO₄, filtered and the solvent was removed under reduced pressure. The crude solids were purified by column chromatography on silica gel with 5% EtOAc in heptane to yield **18** (261 mg, 408 μ mol, 24%) as a yellow foam.

¹H NMR (400 MHz, Chloroform-*d*) δ 9.20 (s, 2H), 7.58 (t, *J* = 1.8 Hz, 2H), 7.23 (d, *J* = 1.8 Hz, 4H), 3.33 (s, 4H). ¹³C NMR (101 MHz, Chloroform-*d*) δ 174.0, 168.4, 137.6 (2C), 134.2 (2C), 131.6 (4C), 123.6 (4C), 59.9, 43.3 (2C). HRMS (ESI): calcd for C₁₈H₁₁Br₄N₂O₂S⁻ [M-H]⁻ 634.7280, found: 634.7275.

The following compound was synthesized according to General procedure C:



1,3-bis(3-aminopropyl)-5,5-bis(3,5-dibromobenzyl)-2-thioxodihydropyrimidine-4,6(1H,5H)-dione 5A.

2-Thiobarbituric acid **18** (106 mg, 166 μ mol, 1.0 eq), *tert*-butyl (3-bromopropyl)carbamate **S7** (118 mg, 497 μ mol, 3.0 eq), Cs₂CO₃ (119 mg, 364 μ mol, 2.2 eq), TBAI (12 mg, 33 μ mol, 0.2 eq) and acetone (1.5 mL) were stirred at 70 °C for 87 h. Purification by automated column chromatography on silica with a gradient of 5-45% EtOAc in heptane delivered the impure intermediate Boc-**5A** (83 mg, 87 μ mol, 53%) as a yellow solid.

TFA (102 μ L, 1.33 mmol, 8.0 eq) and DCM (1.0 mL) were added and the solution was stirred at ambient temperature for 17 h. The crude was purified by RP chromatography with a gradient of 20-60% MeCN/H₂O + 0.1% TFA to yield two batches of a mixture of desulfurized (**1A**) and thionylated product (**5A**) as their di-TFA salts. Yield adjusted to pure **5A** (15 mg, 15 μ mol, 9% o2s) Analytical data is only referring to the thionylated product. *Note: De-sulfurization has taken place.*

Mixture 1: white solid, 2-thiobarbituric acid **5A** : barbituric acid **1A** 2.4:1.0^a,

Mixture 2: slightly yellow solid, 2-thiobarbituric acid **5A** : barbituric acid **1A** 1.0:1.7^a

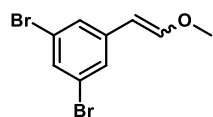
Analytical data for the 2-thiobarbituric acid derivative **5A**:

¹H NMR (400 MHz, Methanol-*d*₄) δ 7.65 (t, *J* = 1.7 Hz, 2H), 7.25 (d, *J* = 1.7 Hz, 4H), 4.26 – 4.18 (m, 4H), 3.48 (s, 4H), 2.94 (t, *J* = 7.3 Hz, 4H), 1.93 – 1.81 (m, 4H). ¹³C NMR (101 MHz, Methanol-*d*₄) δ 179.1, 169.8, 140.3 (2C), 134.7 (2C), 132.6 (4C), 124.2 (4C), 61.9, 46.5 (2C), 45.1 (2C), 38.3 (2C), 26.6 (2C). HRMS (ESI): calcd for C₂₄H₂₇Br₄N₄O₂S⁺ [M+H]⁺ 750.8583, found: 750.8592. SFC: *not obtained*.

Analytical data for desulfurized derivative was identical to the data obtained previously.^[12]

^a Ratio was determined by NMR

3.5.3 4-imidazolidin-2-one and its constitutional isomers

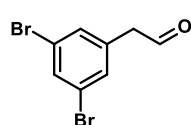


(E)/(Z)-1,3-dibromo-5-(2-methoxyvinyl)benzene **S9**.

(Methoxymethyl)triphenylphosphonium chloride (7.27 g, 21.2 mmol, 1.6 eq) was taken up in dry THF (40 mL) under inert atmosphere and cooled to -78 °C. NaHMDS (21.2 mL, 21.2 mmol, 1.6 eq; 1.0 M in THF) was added slowly and the resulting mixture was stirred at 0 °C for 30 min. The mixture was re-cooled to -78 °C and 3,5-dibromobenzaldehyde **10** (3.50 g, 13.2 mmol, 1.0 eq) was added slowly. Stirring was continued at -78 °C for 30 min and then at ambient temperature for another 2 h. Water and EtOAc were added and the layers were separated. The aqueous layer was extracted with EtOAc twice and the combined organics were dried over MgSO₄, filtered and the solvent was removed under reduced pressure. Heptane was added to the crude solids, and the suspension was sonicated for 5 min. The organic layer was decanted, and the procedure was repeated 3 times. The organic layers were combined, and the solvent was removed under reduced pressure. The crude product was purified by column chromatography on silica gel with 0-5% EtOAc in heptane to yield **S9** (3.54 g, 12.1, 91%) as a slightly yellow liquid. A 1.5 : 1.0 mixture of the *(E)*:*(Z)* isomers was obtained. **HRMS** (ESI): calcd for C₉H₉Br₂O⁺ [M+H]⁺ 290.9015 found: *not found*.

Cis-**ABML444**: ¹H NMR (400 MHz, Chloroform-*d*) δ 7.64 (d, *J* = 1.7 Hz, 2H), 7.41 (t, *J* = 1.8 Hz, 1H), 6.20 (d, *J* = 7.0 Hz, 1H), 5.08 (d, *J* = 7.0 Hz, 1H), 3.82 (s, 3H). ¹³C NMR (101 MHz, Chloroform-*d*) δ 150.3, 139.6, 130.9, 129.6 (2C), 122.7 (2C), 103.3, 57.0.

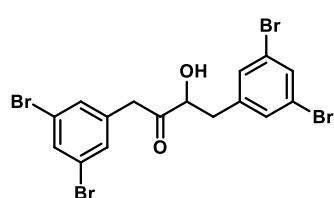
Trans-**ABML444**: ¹H NMR (400 MHz, Chloroform-*d*) δ 7.40 (t, *J* = 1.7 Hz, 1H), 7.28 (d, *J* = 1.8 Hz, 2H), 7.04 (d, *J* = 12.9 Hz, 1H), 5.65 (d, *J* = 12.9 Hz, 1H), 3.69 (s, 3H). ¹³C NMR (101 MHz, Chloroform-*d*) δ 151.0, 140.4, 130.9, 126.7 (2C), 123.2 (2C), 102.9, 57.0.



2-(3,5-dibromophenyl)acetaldehyde **11**.

The mixture of *(E)/(Z)*-**S9** (2.87 g, 9.83 mmol, 1.0 eq) was taken up in anhydrous MeCN (197 mL, *c* = 0.05 M) and NaI (3.09, 20.6 mmol, 2.1 eq) was added. To the vigorously stirring mixture TMSCl (2.63 mL, 20.6 mmol, 2.1 eq) was added and the suspension was stirred at ambient temperature for 110 min. A 0.5 M Na₂SO_{3(aq)} solution was added and the layers were separated. The aqueous layer was extracted with Et₂O thrice and the combined organics were dried over MgSO₄, filtered and the solvent was removed under reduced pressure. The crude solids were taken up in CCl₄, filtered and the solvent was removed under reduced pressure. The crude orange solids were quickly filtered over a short silica plug to yield aldehyde **11** (1.63 g, 5.68 mmol, 60%) as a white solid. *Note: The product decomposes on silica upon extended exposure.*

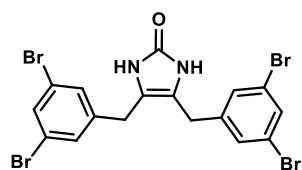
¹H NMR (400 MHz, Chloroform-*d*) δ 9.75 (t, *J* = 1.9 Hz, 1H), 7.62 (t, *J* = 1.8 Hz, 1H), 7.32 (d, *J* = 1.8 Hz, 2H), 3.67 (d, *J* = 1.9 Hz, 2H). ¹³C NMR (101 MHz, Chloroform-*d*) δ 197.5, 135.7, 133.4, 131.6 (2C), 123.5 (2C), 49.5. **HRMS** (ESI): calcd for C₈H₇Br₂O⁺ [M+H]⁺ 276.8858, found: *not found*.



1,4-bis(3,5-dibromophenyl)-3-hydroxybutan-2-one **12**.

Aldehyde **11** (1.63 g, 5.86 mmol, 1.0 eq) and 3-benzyl-5-(2-hydroxyethyl)-4-methylthiazolium chloride (119 mg, 440 μmol, 0.07 eq) were mixed with anhydrous PEG-400 (18 mL) under inert atmosphere. Triethylamine (409 μL, 2.93 mmol, 0.50 eq) was added and the resulting mixture was stirred at 80 °C for 5 h. The oil bath was removed ice-water was added and stirring was continued for 1.0 h. Water and BRINE were added and the aqueous layer was extracted with Et₂O thrice. The combined organics were washed with water twice, dried over MgSO₄, filtered and the solvent was removed under reduced pressure. The crude product was purified by column chromatography on silica gel with 10% EtOAc in heptane to yield **12** (635 mg, 1.14 mmol, 39%) as a yellow solid.

¹H NMR (400 MHz, Chloroform-*d*) δ 7.60 (t, *J* = 1.8 Hz, 1H), 7.57 (t, *J* = 1.8 Hz, 1H), 7.31 (d, *J* = 1.8 Hz, 2H), 7.24 (d, *J* = 1.8 Hz, 2H), 4.49 – 4.40 (m, 1H), 3.78 (d, *J* = 16.5 Hz, 1H), 3.72 (d, *J* = 16.4 Hz, 1H), 3.16 (s, 1H), 3.10 (dd, *J* = 14.2, 4.2 Hz, 1H), 2.79 (dd, *J* = 14.2, 7.7 Hz, 1H). ¹³C NMR (101 MHz, Chloroform-*d*) δ 207.0, 140.1, 136.2, 133.2, 132.9, 131.4 (2C), 131.2 (2C), 123.2 (2C), 123.1 (2C), 76.6, 44.3, 39.2. *Note: Residual EtOAc and heptane were observed.* **LRMS** (ESI): calcd for C₁₆H₁₁Br₄O₂⁻ [M-H]⁻ 550.7, found 550.7.



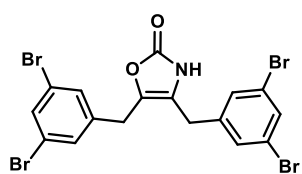
4,5-bis(3,5-dibromobenzyl)-1,3-dihydro-2H-imidazol-2-one **14**.

Acyloin **12** (543 mg, 0.98 mmol, 1.0 eq) was mixed with dry urea (205 mg, 3.42 mmol, 3.5 eq) in a heat dried flask. Glacial acetic acid (2 mL) and anhydrous PEG-400 (2 mL) were added and the mixture was heated to 130 °C for 110 min. After cooling to ambient temperature water was added and a white solid formed. The suspension was stirred for 45 min at ambient temperature, before the solids were filtered off. The residue was washed with water twice. The crude solids were purified by automated flash

column chromatography on silica gel with a gradient of 60-80% EtOAc/heptane + 2.5% MeOH. The title compound **14** (221 mg, 381 μ mol, 39%) was obtained as a white solid.

$^1\text{H NMR}$ (400 MHz, DMSO-*d*₆) δ 9.78 (s, 2H), 7.65 (t, *J* = 1.8 Hz, 2H), 7.39 (d, *J* = 1.8 Hz, 4H), 3.69 (s, 4H). *Note: Residual MeOH was observed at δ 4.10 (q, *J* = 5.3 Hz), 3.17 (d, *J* = 5.2 Hz).* $^{13}\text{C NMR}$ (101 MHz, DMSO-*d*₆) δ 154.2, 144.3 (2C), 131.2 (2C), 130.3 (4C), 122.4 (4C), 115.5 (2C), 28.4. *Residual MeOH was observed at 48.6.* **HRMS** (ESI): calcd for C₁₇H₁₃Br₄N₂O⁺ [M+H]⁺ 576.7756, found: 576.7756.

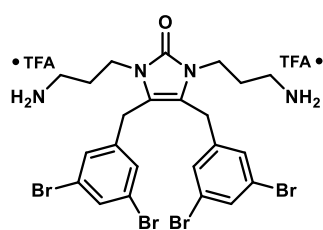
The following constitutional isomer was obtained from the reaction mixture of compound **14**:



4,5-bis(3,5-dibromobenzyl)oxazol-2(3H)-imine 13.

Same chemicals and procedure as for **14**. The title compound **13** (100 mg, 172 μ mol, 18%) was obtained as a white solid.

$^1\text{H NMR}$ (400 MHz, DMSO-*d*₆) δ 10.61 (s, 1H), 7.72 (t, *J* = 1.7 Hz, 1H), 7.71 (t, *J* = 1.8 Hz, 1H), 7.49 (d, *J* = 1.8 Hz, 2H), 7.41 (d, *J* = 1.7 Hz, 2H), 3.89 (s, 2H), 3.77 (s, 2H). $^{13}\text{C NMR}$ (101 MHz, DMSO-*d*₆) δ 155.0, 142.5 (2C), 133.5, 131.7, 131.7, 130.5 (2C), 130.4 (2C), 122.6 (2C), 122.5 (2C), 120.2, 28.5, 27.5. *Note: Residual CDCl₃ was observed at 79.3, 79.0, 78.6.* **LRMS** (ESI): calcd for C₁₇H₁₀Br₄NO₂⁻ [M-H]⁻ 575.9, found 575.7.



1,3-bis(3-aminopropyl)-4,5-bis(3,5-dibromobenzyl)-1,3-dihydro-2H-imidazol-2-one 3A.

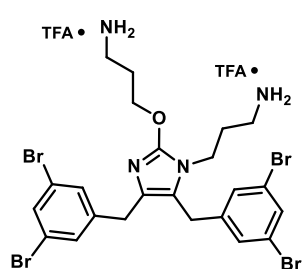
4-imidazolidin-2-one **14** (100 mg, 172 μ mol, 1.0 eq), *tert*-butyl (3-bromopropyl)carbamate **S7** (329 mg, 1.38 mmol, 8.0 eq), K₂CO₃ (135 mg, 0.98 mmol, 5.7 eq) and (*n*-hexadecyl)tri-*n*-butylphosphonium bromide (88 mg, 172 μ mol, 1.0 eq) were mixed with toluene (0.5 mL) and water (0.5 mL). The resulting mixture was heated under microwave irradiation to 130 °C for 90 min and then to 150 °C for 60 min. After cooling to ambient temperature, water was added and

the aqueous layer was extracted with toluene thrice. The combined organics were dried over MgSO₄, filtered and the solvent was removed. The crude yellow solid was purified by automated column chromatography on silica gel with a gradient of 15-45% EtOAc/heptane + 2.5% MeOH. Boc-**3A** (35 mg, 39 μ mol, 23%) was obtained as a slightly yellow solid.

Boc-**3A** (35 mg, 39 μ mol, 1.0 eq) was taken up in DCM (500 μ L) and TFA (75 μ L, 0.98 mmol, 25 eq) was added. The solution was stirred at ambient temperature for 20 h before removal of the solvent. The crude amine was purified by RP chromatography with a gradient of 20-55% MeCN/H₂O + 0.1% TFA. The title compound **3A** (30 mg, 33 μ mol, 19% o2s) was obtained as a white di-TFA salt.

$^1\text{H NMR}$ (400 MHz, Methanol-*d*₄) δ 7.60 (t, *J* = 1.8 Hz, 2H), 7.27 (d, *J* = 1.8 Hz, 4H), 3.99 (s, 4H), 3.72 (t, *J* = 6.8 Hz, 4H), 2.89 (t, *J* = 7.1 Hz, 4H), 1.77 (qn, *J* = 6.9 Hz, 4H). $^{13}\text{C NMR}$ (101 MHz, Methanol-*d*₄) δ 155.5, 143.7 (2C), 133.7 (2C), 131.1 (4C), 124.4 (4C), 119.7 (2C), 39.2 (2C), 37.7 (2C), 28.6, 28.4 (2C). **HRMS** (ESI): calcd for C₂₃H₂₇Br₄N₄O₁⁺ [M+H]⁺ 690.8913 found 690.8924. **SFC**: >99%.

The constitutional isomer **15A** was obtained from the reaction mixture of **3A**:



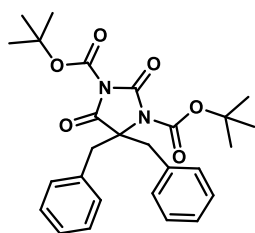
3-(2-(3-aminopropoxy)-4,5-bis(3,5-dibromobenzyl)-1H-imidazol-1-yl)propan-1-amine 15A.

Chemicals and procedure as stated above for **3A**. Boc-**15A** was obtained impure as a yellow foam (no yield determined).

After TFA treatment and purification by RP chromatography with a gradient of 20-60% MeCN/H₂O + 0.1% TFA, the di-TFA salt of **15A** (27 mg, 29 μ mol 17% o2s) was obtained as a white solid.

$^1\text{H NMR}$ (400 MHz, Methanol-*d*₄) δ 7.58 (t, *J* = 1.8 Hz, 1H), 7.54 (t, *J* = 1.8 Hz, 1H), 7.31 (d, *J* = 1.7 Hz, 2H), 7.17 (d, *J* = 1.8 Hz, 2H), 4.62 – 4.54 (m, 2H), 4.07 (s, 2H), 3.90 (s, 2H), 3.87 – 3.80 (m, 2H), 3.18 (t, *J* = 7.4 Hz, 2H), 2.91 (t, *J* = 7.9 Hz, 2H), 2.24 (qn, *J* = 6.5 Hz, 2H), 1.90 (qn, *J* = 7.8 Hz, 2H). $^{13}\text{C NMR}$ (101 MHz, Methanol-*d*₄) δ 151.4, 144.1, 143.1, 133.9, 133.4, 131.5 (2C), 131.1 (2C), 128.0 124.4 (2C), 124.1 (2C), 123.3, 70.6, 41.2, 37.9, 37.6, 31.3, 28.4 (2C), 28.0. **HRMS** (ESI): calcd for C₂₃H₂₇Br₄N₄O₁⁺ [M+H]⁺ 690.8913, found 690.8907. **SFC**: 96.5%.

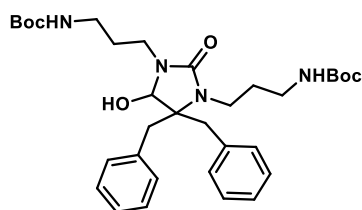
3.5.4 4-imidazolidin-2-one via *N*-acyliminium ion rearrangement



Di-tert-butyl 4,4-dibenzyl-2,5-dioxoimidazolidine-1,3-dicarboxylate Boc-9a.

5,5-disubstituted hydantoin **9a** (100 mg, 357 μmol , 1.0 eq) was taken up in THF (2.0 mL) and cooled to 0 °C. 4-DMAP (3.3 mg, 27 μmol , 0.1 eq) and Boc₂O (234 mg, 1.07 mmol, 3.0 eq) were added the cooling bath was removed and the resulting solution was stirred at 45 °C for 20 h. The solution was allowed to cool to ambient temperature and DCM was added. The organic layer was washed with 0.1 M HCl_(aq) thrice, dried over MgSO₄, filtered and the solvent was removed. The crude was purified by automated column chromatography on silica gel with a gradient of 10-38% EtOAc in heptane to yield Boc-**9a** (156 mg, 325 μmol , 91%) as a white solid.

¹H NMR (400 MHz, Chloroform-*d*) δ 7.29 – 7.20 (m, 6H), 7.15 – 7.09 (m, 4H), 3.69 (d, *J* = 13.7 Hz, 2H), 3.38 (d, *J* = 13.6 Hz, 2H), 1.63 (s, 9H), 1.43 (s, 9H). ¹³C NMR (101 MHz, Chloroform-*d*) δ 170.1, 149.4, 146.9, 144.5, 133.9 (2C), 129.6 (4C), 128.8 (4C), 127.8 (2C), 85.9, 84.5, 71.8, 40.8 (2C), 28.1 (3C), 27.6 (3C). HRMS (ESI): calcd for C₂₇H₃₂N₂O₆Na⁺ [M+Na]⁺ 503.2153, found: 503.2155.

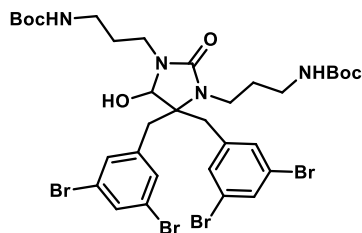


Di-tert-butyl ((4,4-dibenzyl-5-hydroxy-2-oxoimidazolidine-1,3-diyl)bis(propane-3,1-diyl))dicarbamate S2

Boc-**2aA** (226 mg, 380 μmol , 1.0 eq) was dissolved in anhydrous DCM (2.5 mL) under inert atmosphere and cooled to -78 °C. DIBAL-H (1 M in DCM, 570 μL , 570 μmol , 1.5 eq) was added and the resulting mixture was stirred at -78 °C for 3h. 10% Rochelle's salt_(aq) solution was added and the suspension was stirred at ambient temperature for 30 min. The aqueous layer was extracted with Et₂O thrice and the combined organics were washed twice

with 10% Rochelle's salt_(aq) solution, dried over MgSO₄, filtered and the solvent was removed under reduced pressure. The crude was purified by automated column chromatography on silica gel with a gradient of 15-60% EtOAc in heptane to yield **S2** (126 mg, 211 μmol , 56%) as a colorless solid.

¹H NMR (400 MHz, Chloroform-*d*) δ 7.53 – 7.45 (m, 2H), 7.37 – 7.23 (m, 3H), 7.22 – 7.12 (m, 3H), 6.95 – 6.81 (m, 2H), 5.60 (t, *J* = 6.9 Hz, 1H), 5.04 (d, *J* = 6.7 Hz, 1H), 4.73 (d, *J* = 6.8 Hz, 1H), 4.59 (s, 1H), 3.81 – 3.66 (m, 1H), 3.50 (d, *J* = 13.5 Hz, 1H), 3.43 – 3.31 (m, 1H), 3.26 – 3.14 (m, 1H), 3.10 – 2.98 (m, 1H), 2.84 (d, *J* = 14.1 Hz, 1H), 2.80 (d, *J* = 13.5 Hz, 1H), 2.80 – 2.58 (m, 4H), 2.48 (d, *J* = 14.1 Hz, 1H), 1.86 – 1.64 (m, 2H), 1.44 (s, 9H), 1.41 (s, 9H), 1.24 – 1.19 (m, 2H). Residual DCM (5.29, s), EtOAc (4.14 (q, *J* = 7.2 Hz), 2.06 (s), 1.27 (t, *J* = 7.1 Hz)) and heptane (0.93 – 0.86 (m, 1H)) were observed. ¹³C NMR (101 MHz, Chloroform-*d*) δ 159.8, 156.7, 156.4, 136.9 (2C), 135.8 (2C), 131.1 (2C), 129.8 (2C), 128.6 (2C), 128.5 (2C), 127.0 (2C), 126.9 (2C), 84.2, 79.3, 79.2, 67.4, 40.6, 39.9, 37.7, 37.5, 37.3, 31.7, 29.5, 28.6 (3C), 28.6 (3C). Residual EtOAc (171.3, 60.5, 21.2, 14.2), heptane (32.0, 22.8, 14.3) and "grease" (29.1) were observed. HRMS (ESI): calcd for C₃₃H₄₉N₄O₆⁺ [M+H]⁺ 597.3647, found: 597.3647.

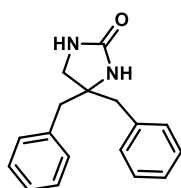


Di-tert-butyl ((4,4-bis(3,5-dibromobenzyl)-5-hydroxy-2-oxoimidazolidine-1,3-diyl)bis(propane-3,1-diyl))dicarbamate S3.

Boc-**2dA** (131 mg, 144 μmol , 1.0 eq) was dissolved in anhydrous DCM under inert atmosphere and cooled to -78 °C. DIBAL-H (432 μL , 432 μmol , 3.0 eq) was added and the resulting mixture was allowed to warm to 0 °C and stirred for 3h. 10% Rochelle's salt_(aq) solution was added and after stirring at ambient temperature for 60 min, the aqueous layer was extracted with DCM thrice.

The combined organics were washed twice with 10% Rochelle's salt_(aq) solution, dried over MgSO₄, filtered and the solvent was removed under reduced pressure. The crude was purified by automated column chromatography on silica gel with a gradient of 50-85% EtOAc in heptane to yield **S3** (92 mg, 101 μmol , 70%) as a white solid.

¹H NMR (400 MHz, Chloroform-*d*) δ 7.62 (d, *J* = 1.8 Hz, 2H), 7.59 (t, *J* = 1.7 Hz, 1H), 7.50 (t, *J* = 1.7 Hz, 1H), 7.01 (d, *J* = 1.7 Hz, 2H), 5.58 (s, 1H), 5.50 (s, 1H), 4.93 (t, *J* = 6.7 Hz, 1H), 4.75 (d, *J* = 6.3 Hz, 1H), 3.80 – 3.64 (m, 2H), 3.46 (d, *J* = 13.3 Hz, 1H), 3.42 – 3.31 (m, 1H), 3.19 – 3.09 (m, 2H), 3.09 – 2.80 (m, 5H), 2.77 (d, *J* = 14.0 Hz, 1H), 2.70 (d, *J* = 13.4 Hz, 1H), 2.40 (d, *J* = 14.0 Hz, 1H), 1.86 – 1.73 (m, 2H), 1.73 – 1.61 (m, 2H), 1.45 (s, 9H), 1.44 (s, 9H), 1.24 – 1.18 (m, 2H). Residual heptane was observed at 1.33 – 1.22 (m) and 0.90 – 0.85 (m). ¹³C NMR (101 MHz, Chloroform-*d*) δ 159.5, 157.3, 156.4, 140.6, 139.5, 133.0 (3C), 132.7, 131.5 (2C), 123.1 (2C), 122.9 (2C), 83.7, 80.5, 79.4, 67.0, 40.5, 39.2, 37.8 (2C), 37.6, 37.4 31.8, 30.5, 28.6 (6C). Residual heptane was observed at 32.0, 29.2, 22.8, 14.3. HRMS (ESI): calcd for C₃₃H₄₄Br₄N₄O₆Na⁺ [M+Na]⁺ 930.9887, found: 930.9886.



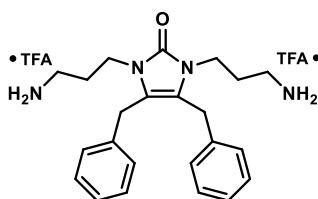
4,4-dibenzylimidazolidin-2-one S4.

Boc-**9a** (156 mg, 325 μmol , 1.0 eq) was dissolved in EtOH, NaBH_4 (61 mg, 1.62 mmol, 5.0 eq) was added and the mixture was stirred at ambient temperature for 16 h. 0.1 M HCl was added to destroy residual NaBH_4 , followed by the addition of water. The aqueous layer was extracted with Et_2O thrice. The combined organics were dried over MgSO_4 , filtered and the solvent was removed under reduced pressure. The crude was purified by automated column chromatography on silica gel with a gradient of 15-55% EtOAc in heptane to yield impure-**S1** (16 mg,

33 μmol , 10%) as a white solid. **S1** was obtained as a mixture of compounds having between zero to two Boc groups and was used without further purification.

S1 (16 mg, 33 μmol , 1.0 eq) was dissolved in anhydrous toluene (0.75 mL) in an oven dried flask under inert atmosphere and *p*-TsOH (1.6 mg, 8.3 μmol , 0.25 eq) was added. The resulting mixture was heated to 120 $^\circ\text{C}$ for 24 h. The mixture was allowed to cool to ambient temperature and the solvent was removed. To the resulting crude DCM (0.75 mL) and TFA (64 μL , 828 μmol , 25 eq) were added and the resulting solution was stirred at ambient temperature for 20 h. The solvent was removed and the crude product was purified by automated column chromatography on silica gel with a gradient of 15-55% EtOAc in heptane to yield impure **S4** (3 mg, 11 μmol , 24%) as a white solid.

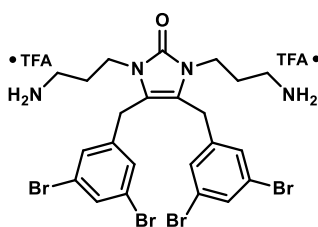
$^1\text{H NMR}$ (400 MHz, Methanol-*d4*) δ 7.37 – 7.20 (m, 10H), 4.19 (s, 2H), 2.97 (d, $J = 13.8$ Hz, 2H), 2.89 (d, $J = 13.8$ Hz, 2H). $^{13}\text{C NMR}$ (101 MHz, Methanol-*d4*) δ 161.8, 137.0 (2C), 131.7 (4C), 129.5 (4C), 128.1 (2C), 72.1, 62.6, 45.9 (2C). **LRMS** (ESI): calcd for $\text{C}_{17}\text{H}_{18}\text{N}_2\text{O}^+$ $[\text{M}+\text{H}]^+$ 267.1, found 267.1.



1,3-bis(3-aminopropyl)-4,5-dibenzyl-1,3-dihydro-2H-imidazol-2-one S5.

S2 (18 mg, 30 μmol , 1.0 eq) was dissolved in DCM (750 μL) and TFA (46 μL , 603 μmol , 20.0 eq) was added. The resulting clear solution was stirred at ambient temperature for 18 h. The solvent was removed under reduced pressure and the crude was purified by RP column chromatography with a gradient of 10-45% MeCN/ H_2O + 0.1% TFA to yield the impure di-TFA salt of **S5** (15 mg, 25 μmol , 82%) as a slightly yellow solid.

$^1\text{H NMR}$ (400 MHz, Methanol-*d4*) δ 8.09 (s, 6H), 7.34 – 7.26 (m, 4H), 7.26 – 7.19 (m, 4H), 7.10 (d, $J = 7.3$ Hz, 4H), 3.86 (s, 4H), 3.64 (s, 4H), 2.71 (s, 4H), 1.48 (s, 4H). $^{13}\text{C NMR}$ (101 MHz, Methanol-*d4*) δ 154.9, 137.0 (2C), 129.3 (4C), 127.9 (4C), 127.5 (2C), 119.3 (2C), 37.6 (2C), 36.2 (2C), 29.2 (2C), 26.5 (2C). **HRMS** (ESI): calcd for $\text{C}_{23}\text{H}_{31}\text{N}_4\text{O}^+$ $[\text{M}+\text{H}]^+$ 379.2492, found: 379.2499.



1,3-bis(3-aminopropyl)-4,5-bis(3,5-dibromobenzyl)-1,3-dihydro-2H-imidazol-2-one 3A.

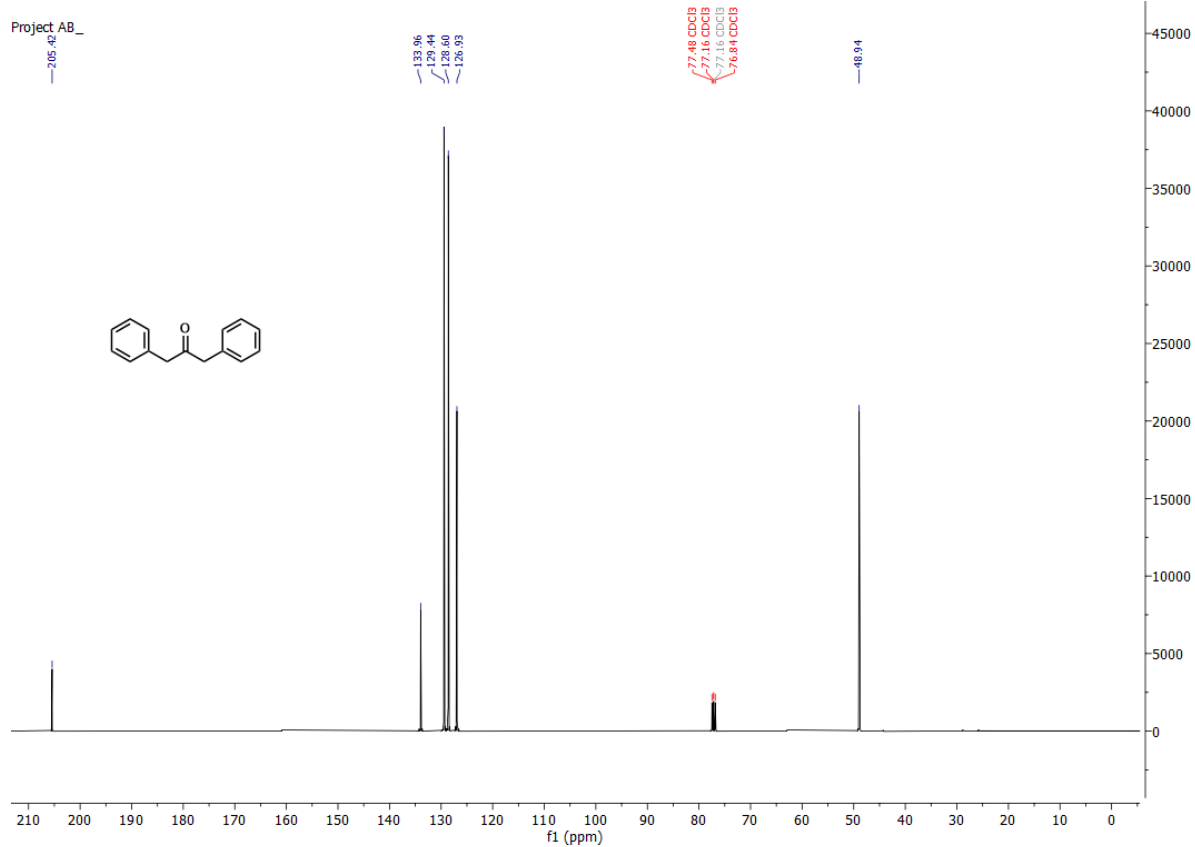
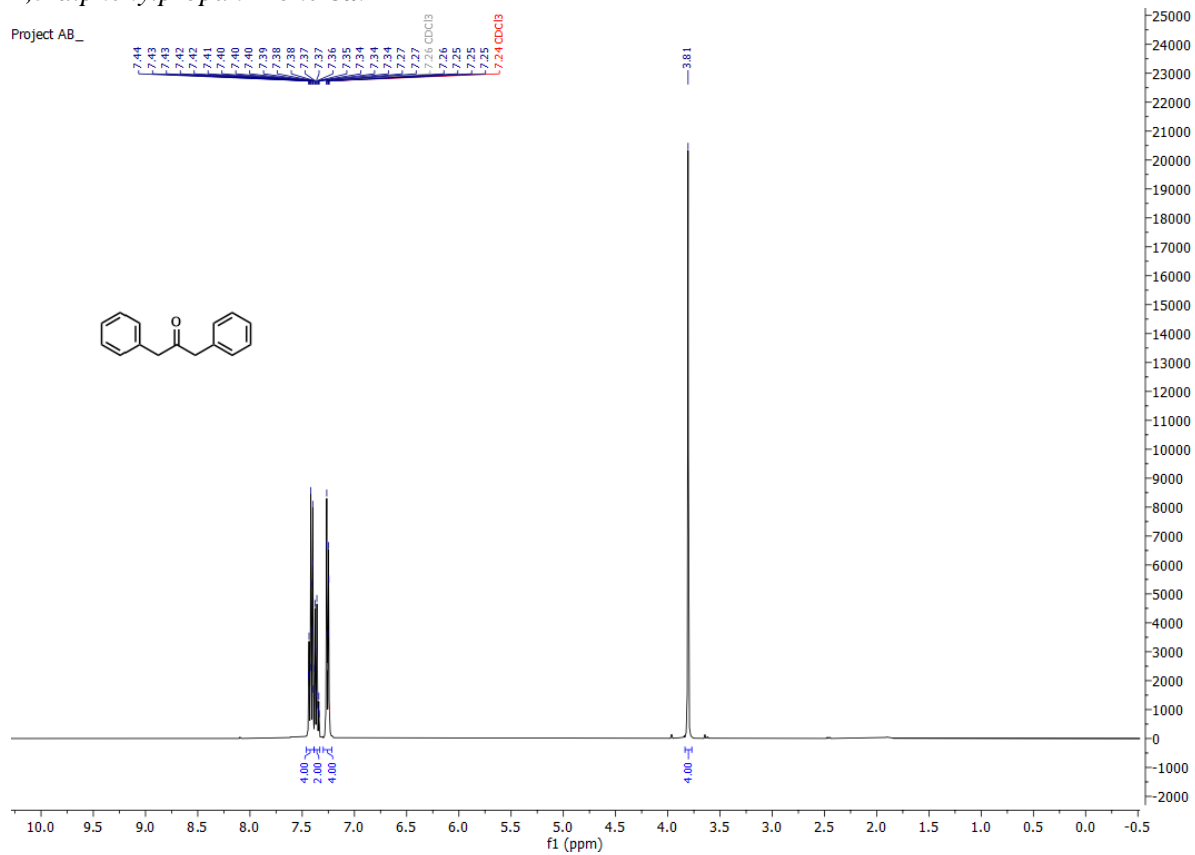
S3 (92 mg, 101 μmol , 1.0 eq) was dissolved in DCM (1 mL) and TFA (116 μL , 1.51 mL, 15.0 eq) was added. The mixture was stirred at ambient temperature for 22 h. A second portion of TFA (116 μL , 1.51 mL, 15.0 eq) was added and the mixture was heated to 45 $^\circ\text{C}$ for 20 h. The solution was allowed to cool to ambient temperature after a total of 42 h and the solvent was removed. The crude was purified by RP column chromatography with a gradient of 10-55% MeCN/ H_2O +

0.1% TFA to yield the impure di-TFA salt of **3A** (40 mg, 43 μmol , 43%) as a slightly yellow solid. The spectroscopic data was identical to the ones reported (*vide supra*).

4. NMR spectra

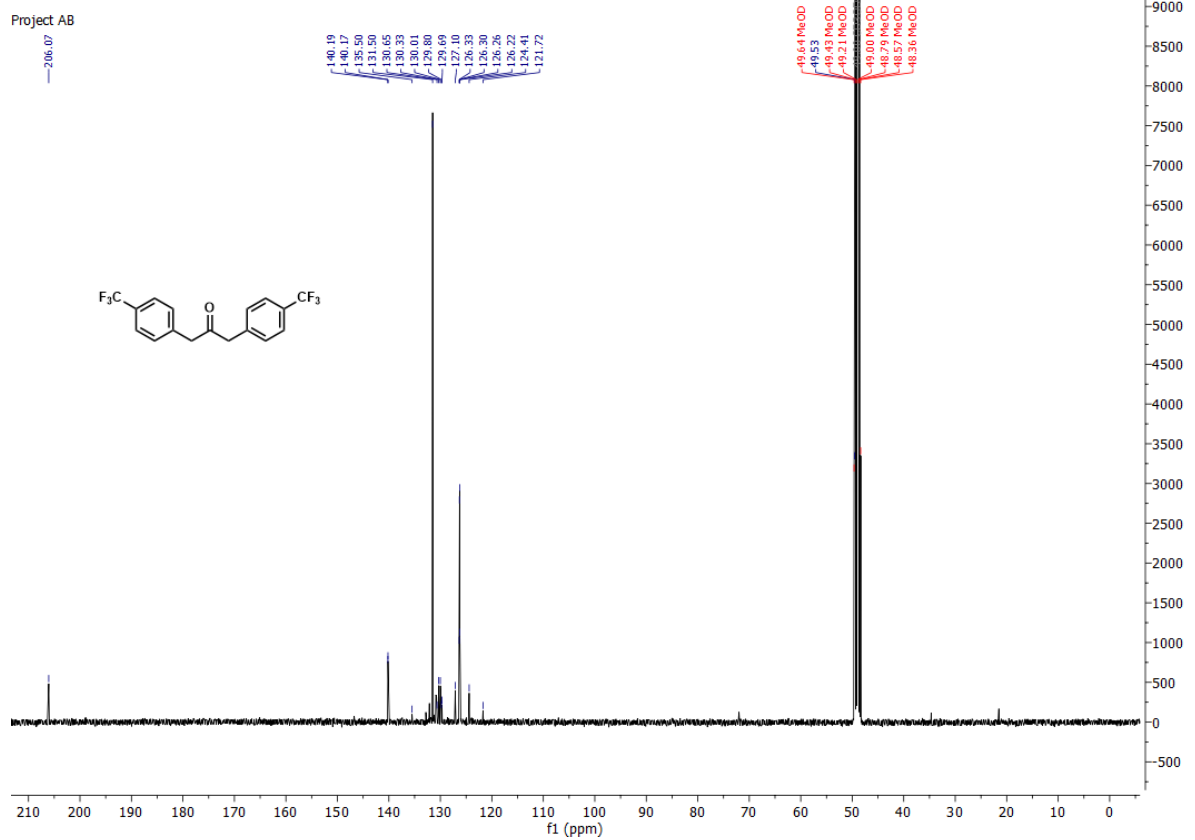
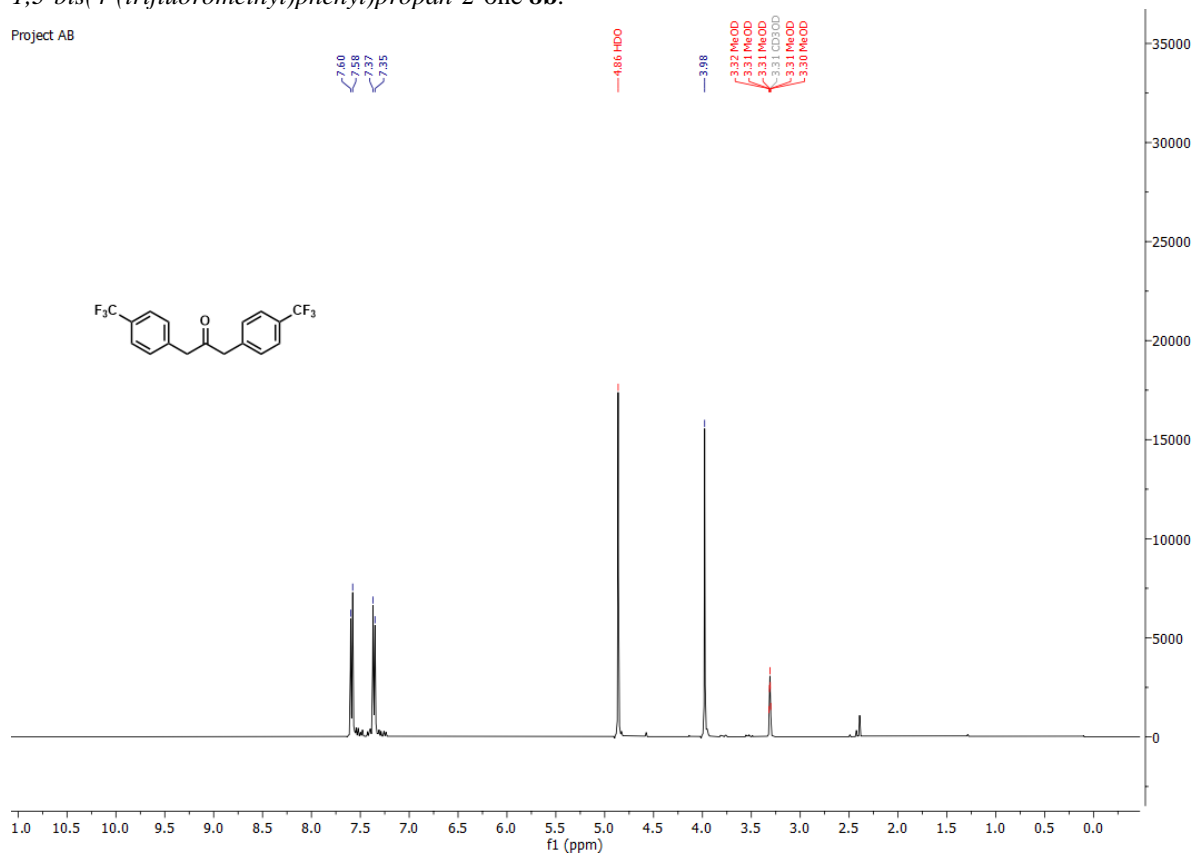
4.1 Symmetrical ketones 8

1,3-diphenylpropan-2-one **8a**.



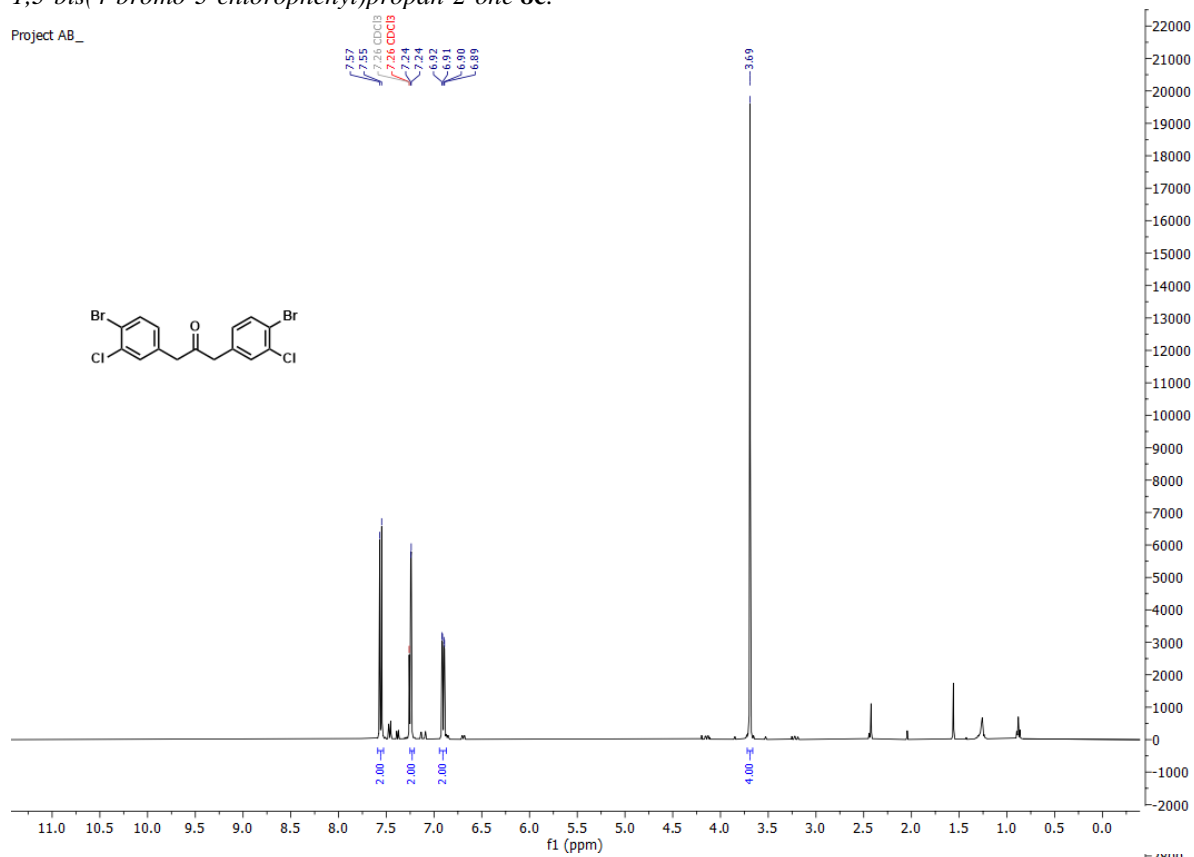
1,3-bis(4-(trifluoromethyl)phenyl)propan-2-one **8b**.

Project AB

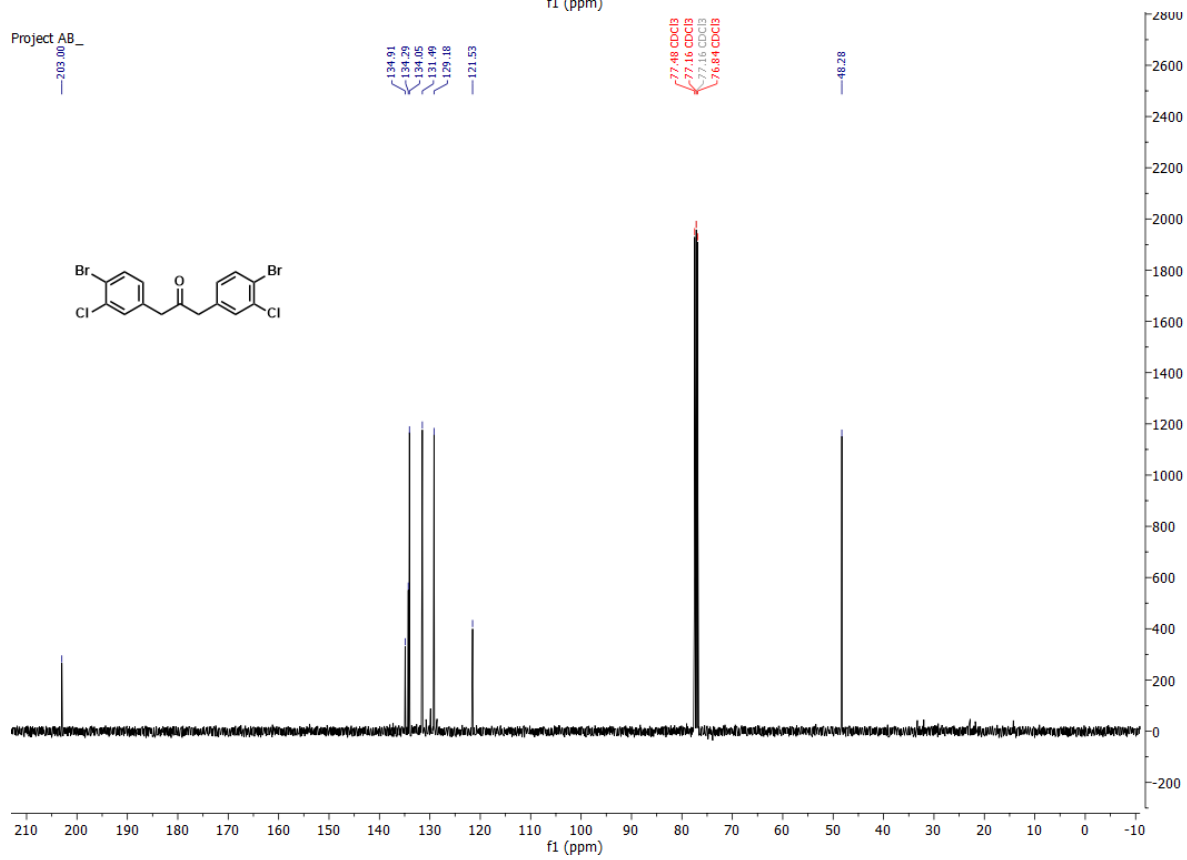


1,3-bis(4-bromo-3-chlorophenyl)propan-2-one **8c**.

Project AB_

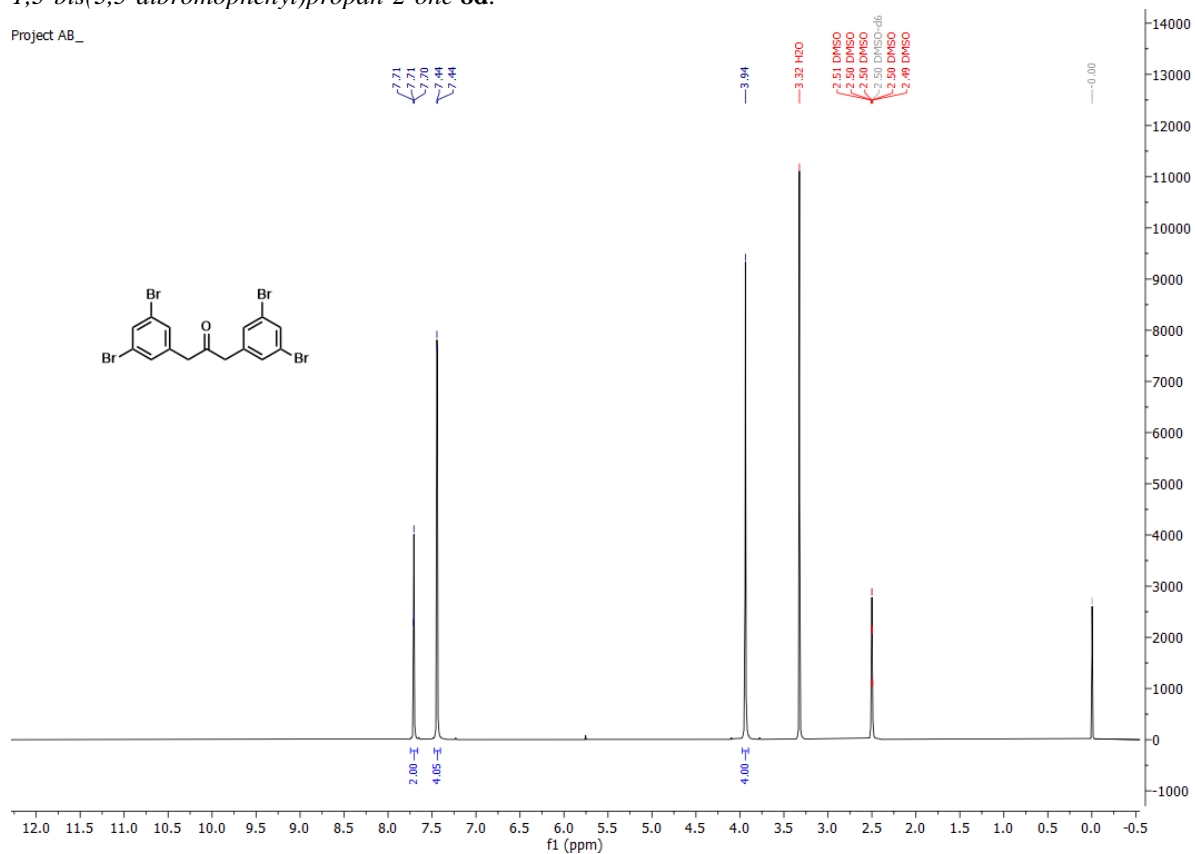


Project AB_

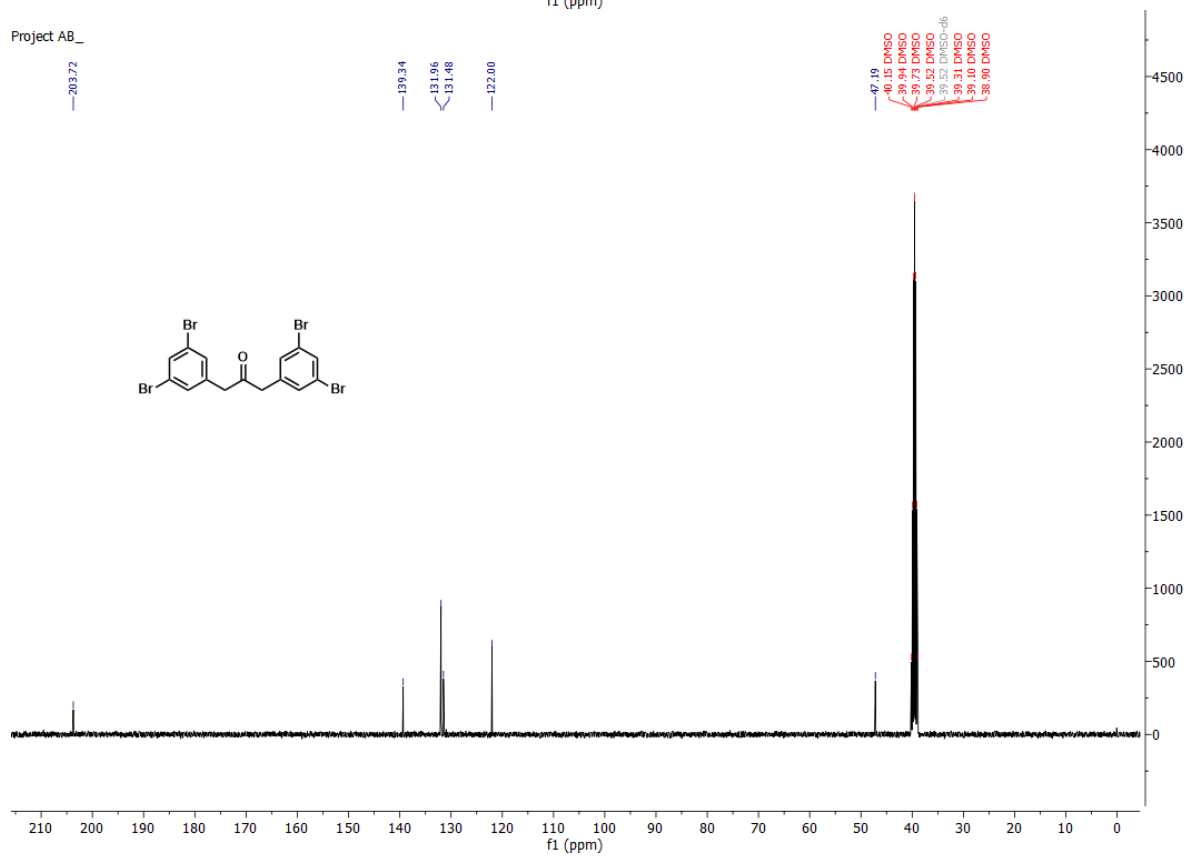


1,3-bis(3,5-dibromophenyl)propan-2-one **8d**.

Project AB_

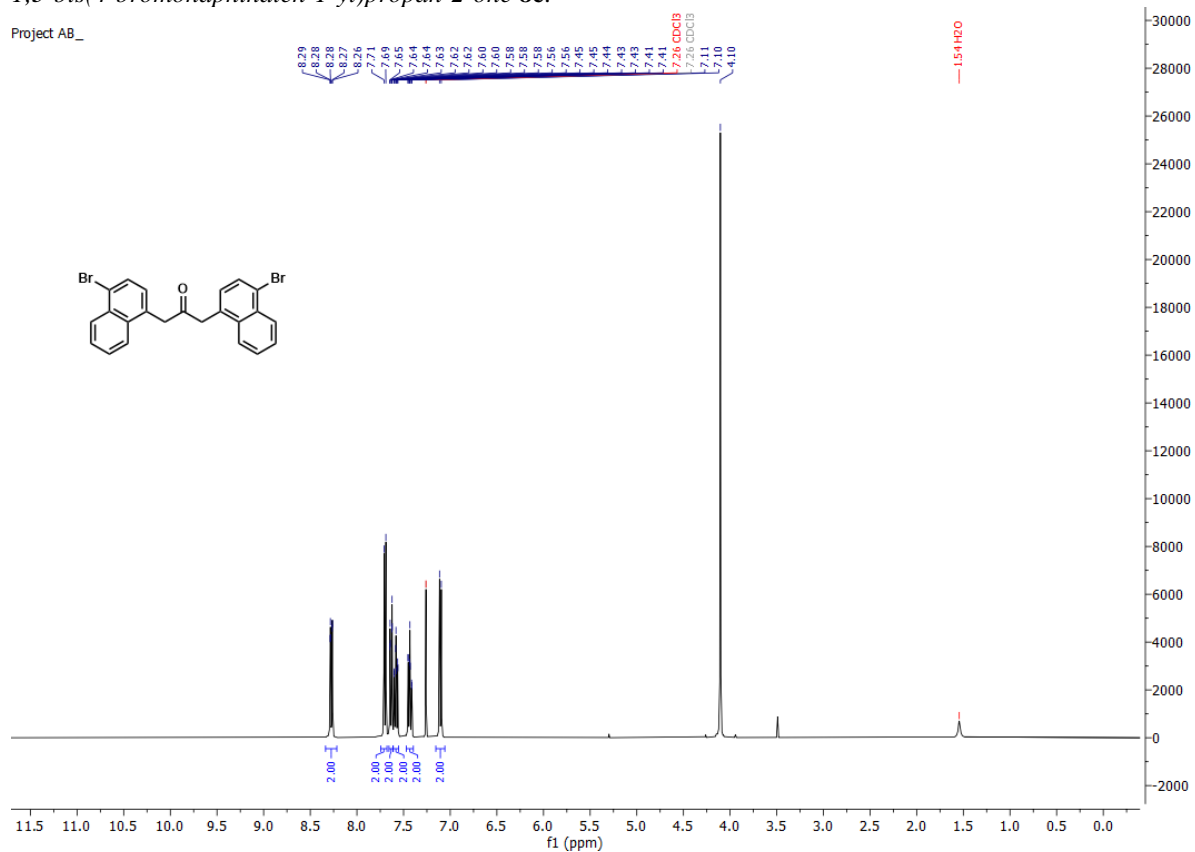


Project AB_

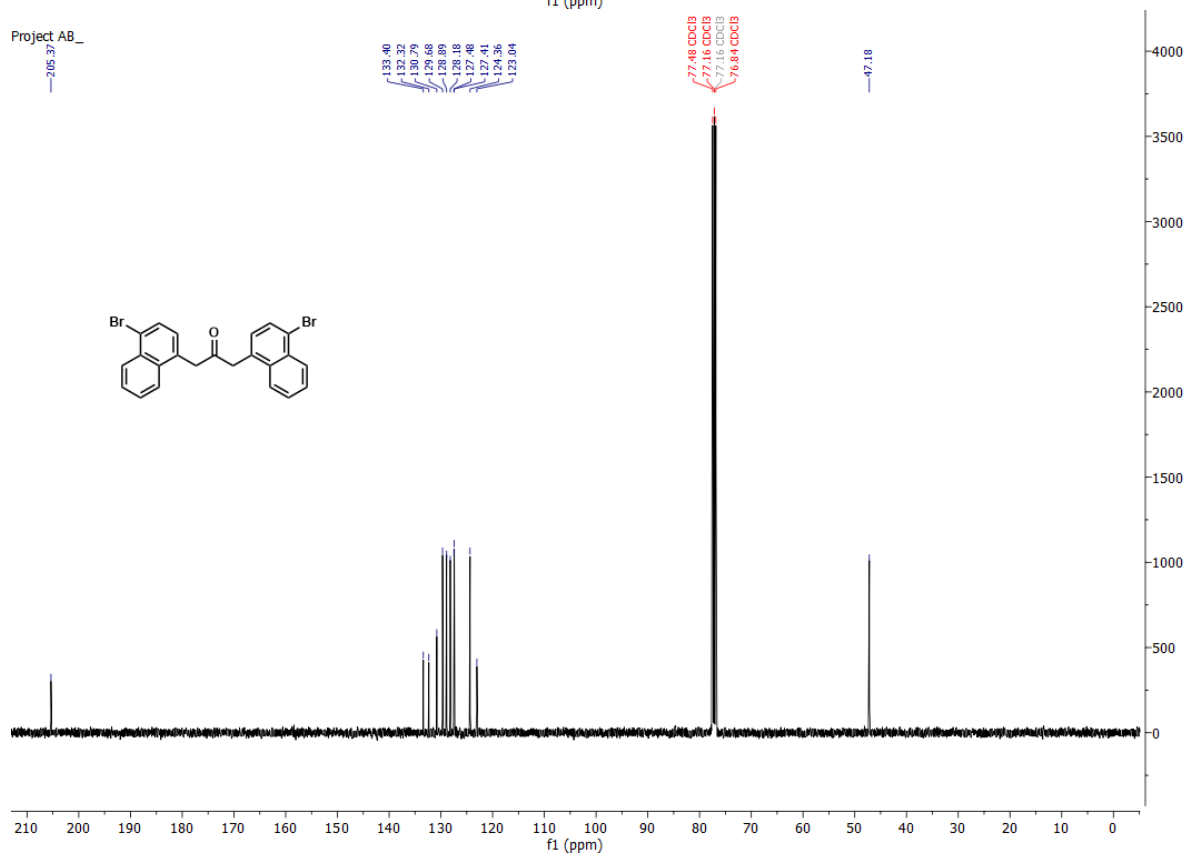


1,3-bis(4-bromonaphthalen-1-yl)propan-2-one **8e**.

Project AB_

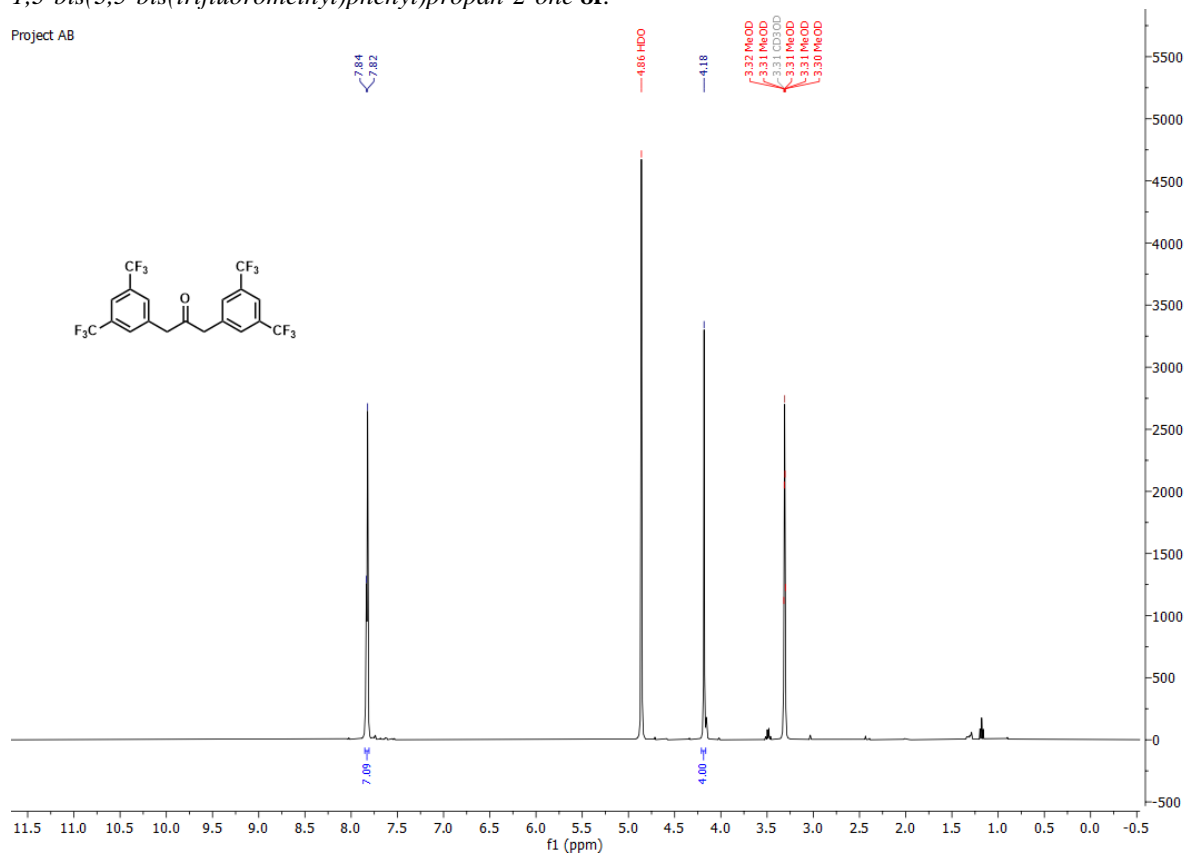


Project AB_

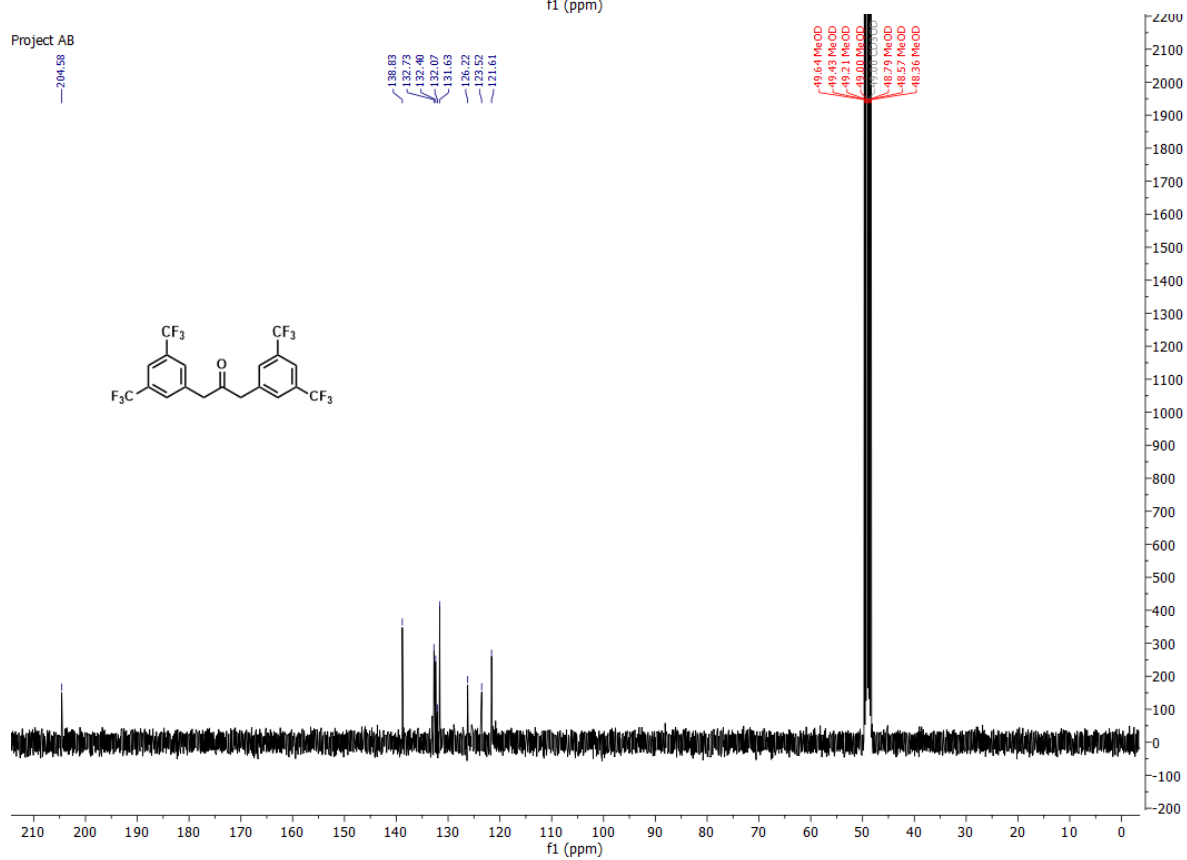


1,3-bis(3,5-bis(trifluoromethyl)phenyl)propan-2-one **8f**.

Project AB



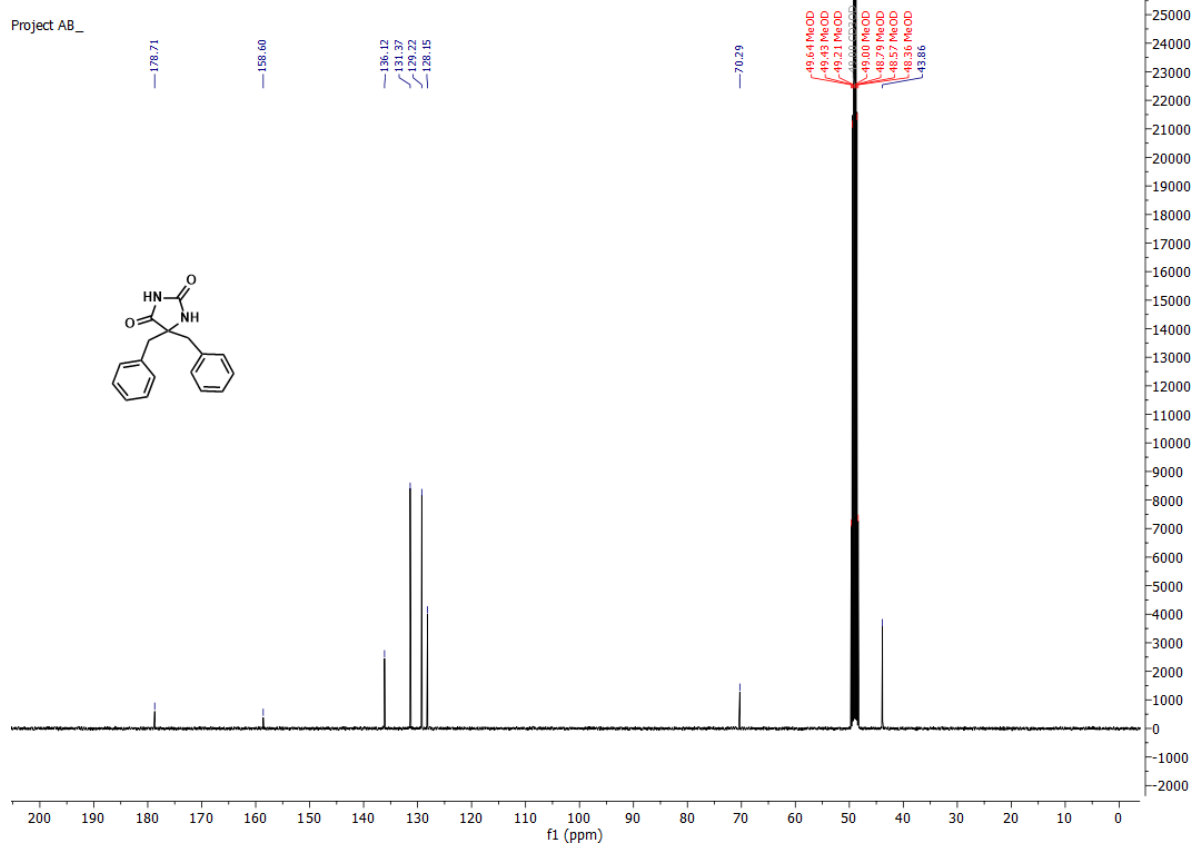
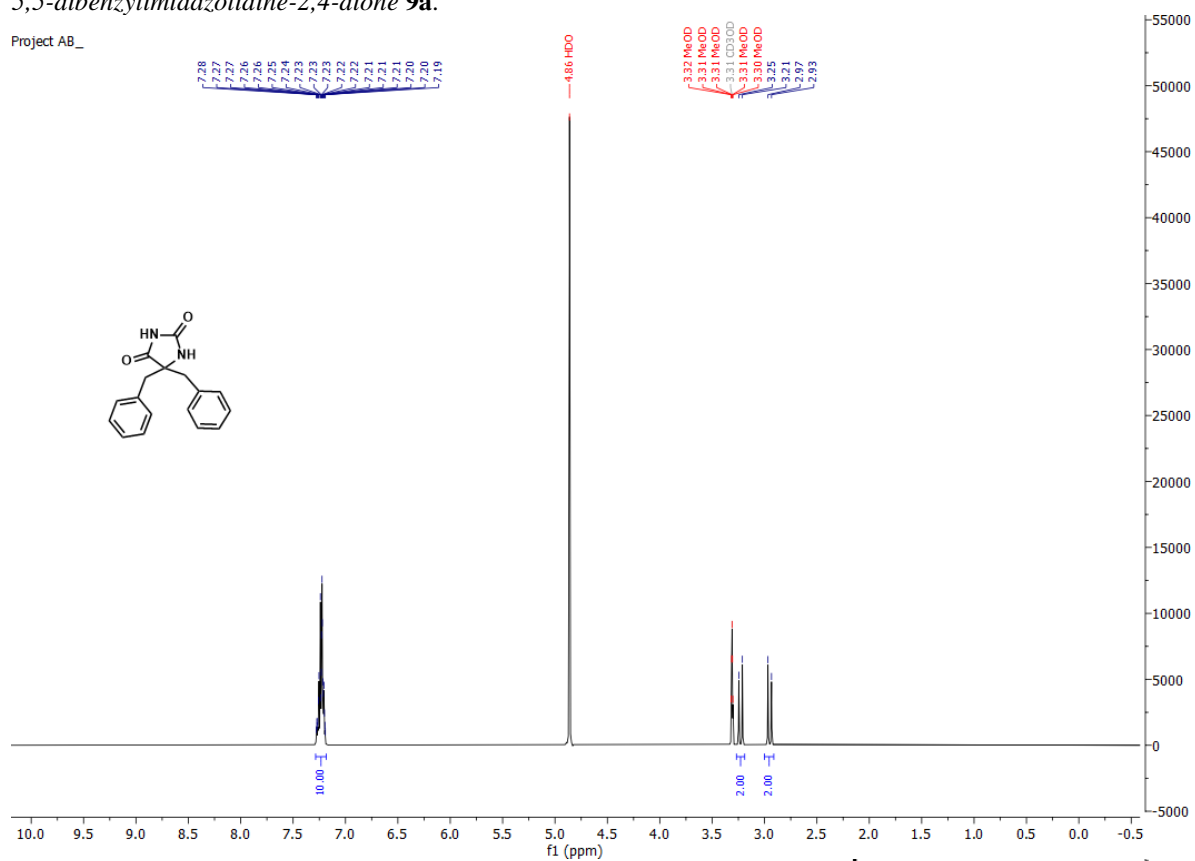
Project AB



4.2 Hydantoin 9

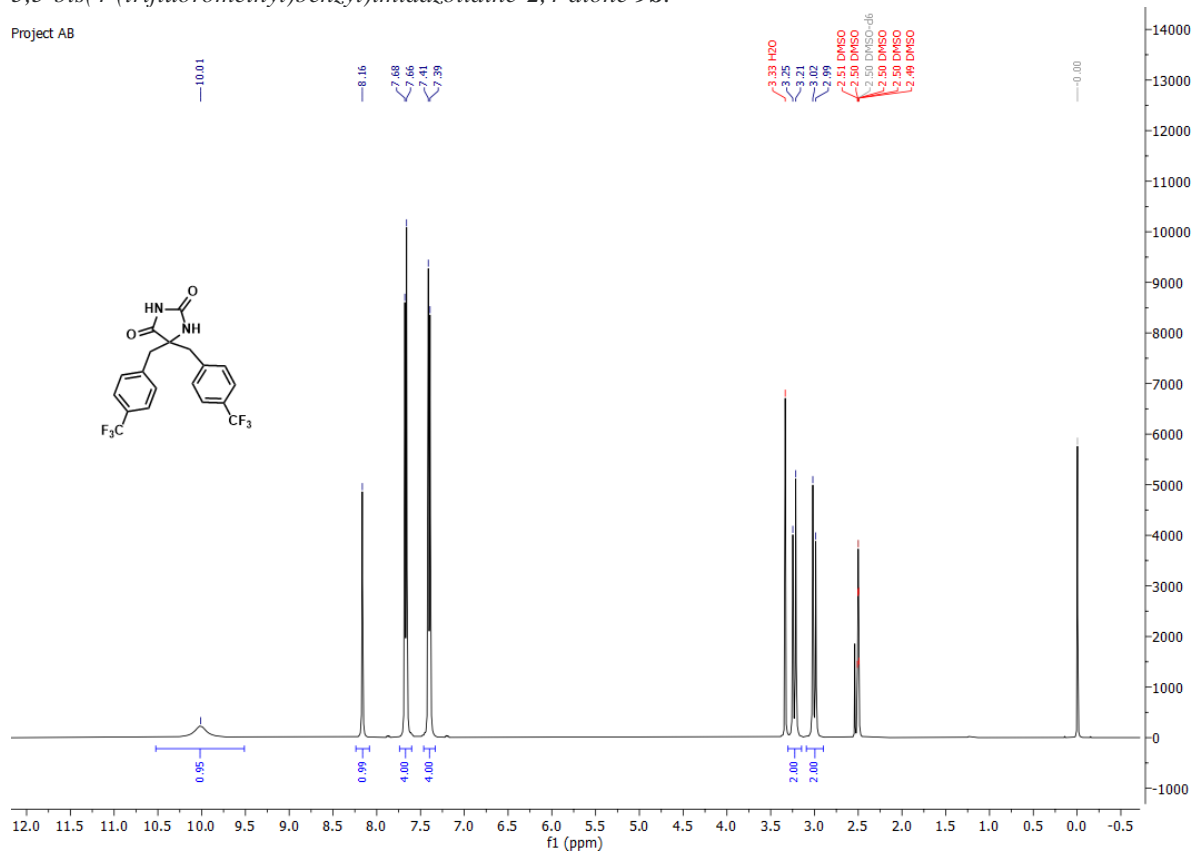
5,5-dibenzylimidazolidine-2,4-dione **9a**.

Project AB_

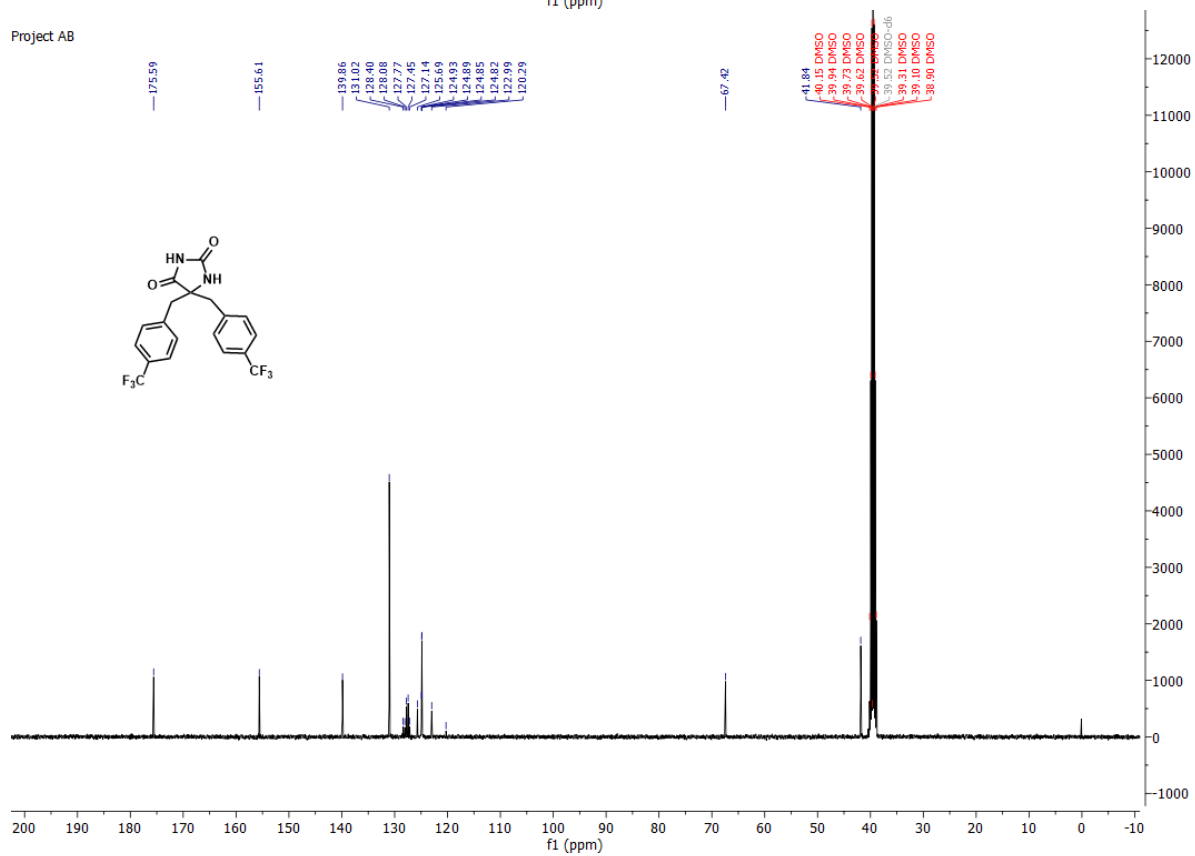


5,5-bis(4-(trifluoromethyl)benzyl)imidazolidine-2,4-dione **9b**.

Project AB

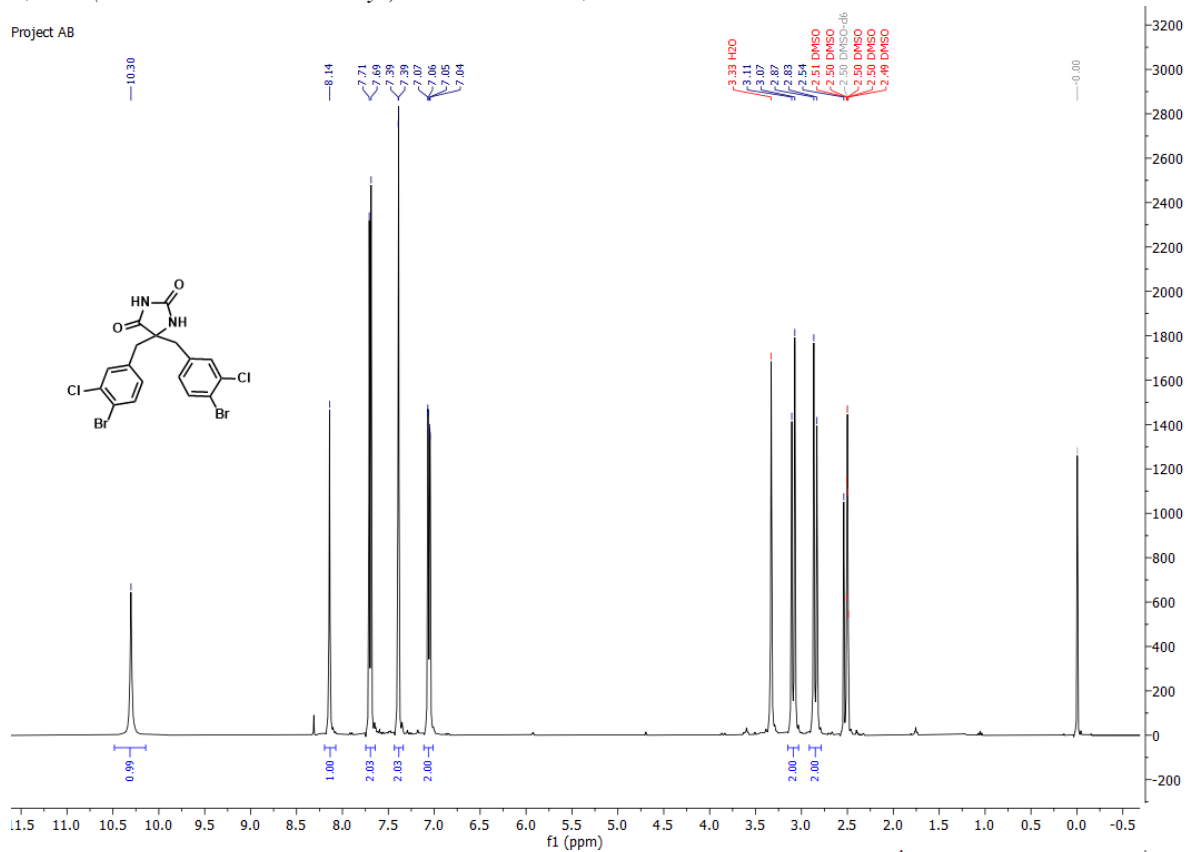


Project AB

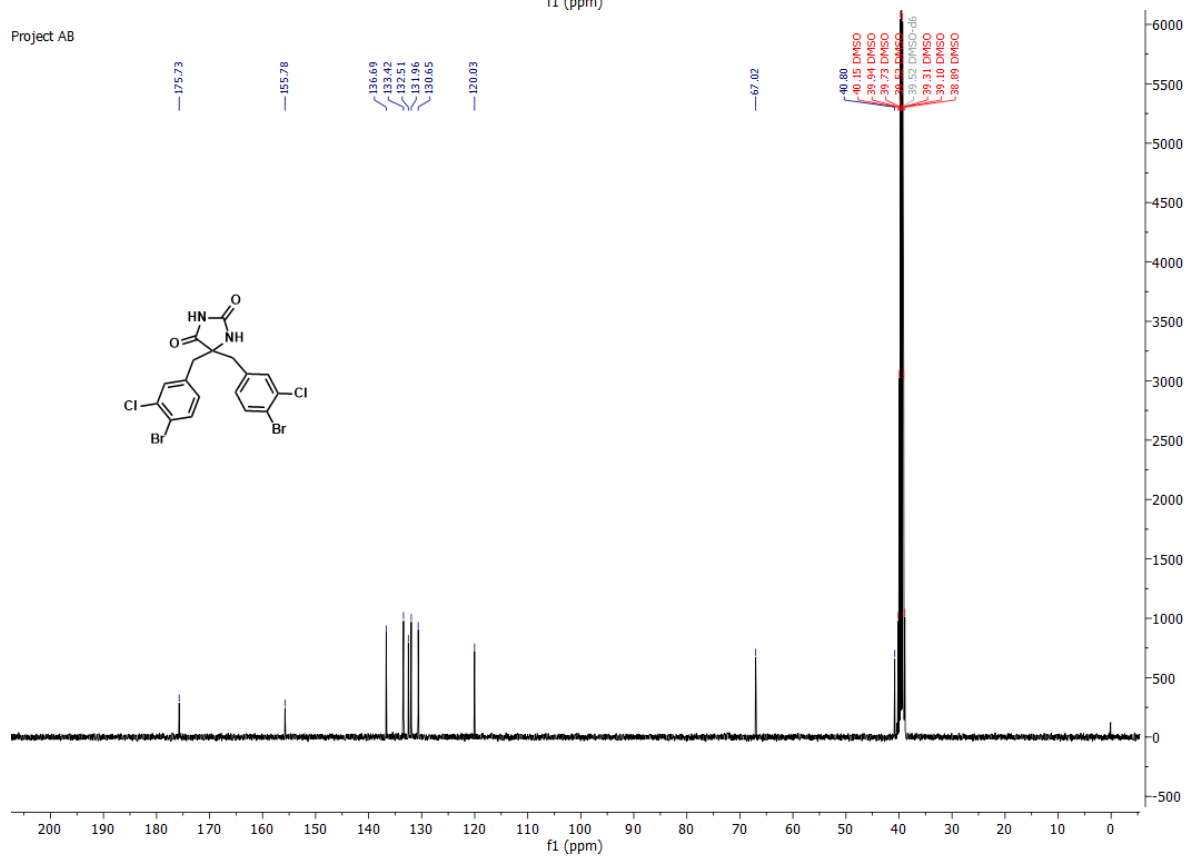


5,5-bis(4-bromo-3-chlorobenzyl)imidazolidine-2,4-dione **9c**.

Project AB

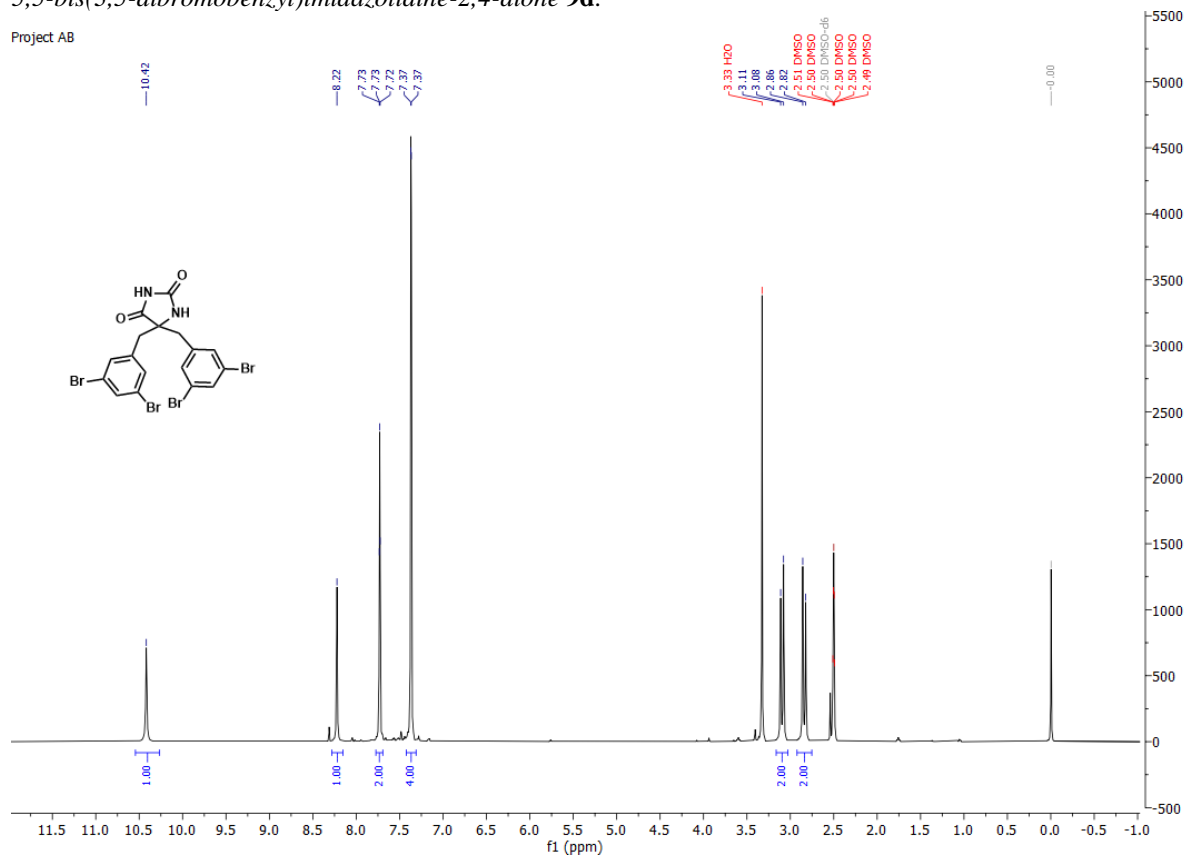


Project AB

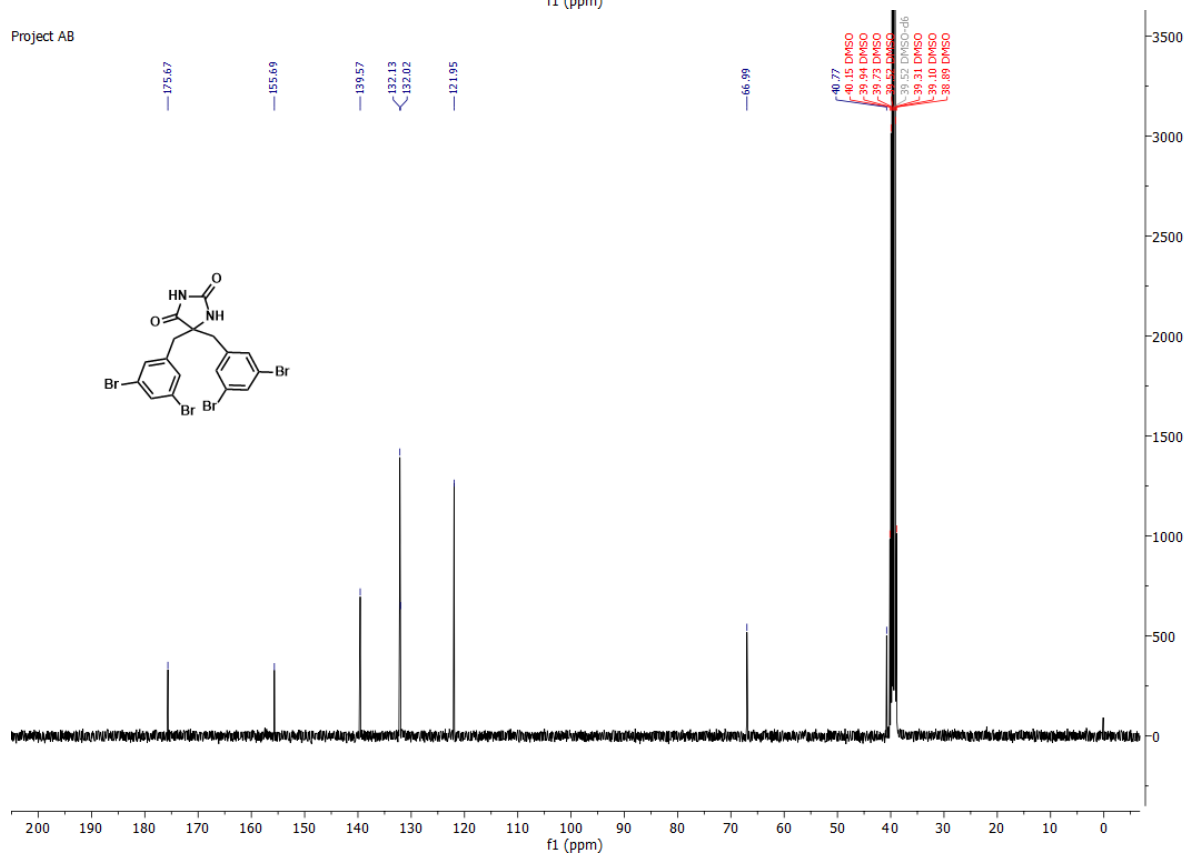


5,5-bis(3,5-dibromobenzyl)imidazolidine-2,4-dione **9d**.

Project AB

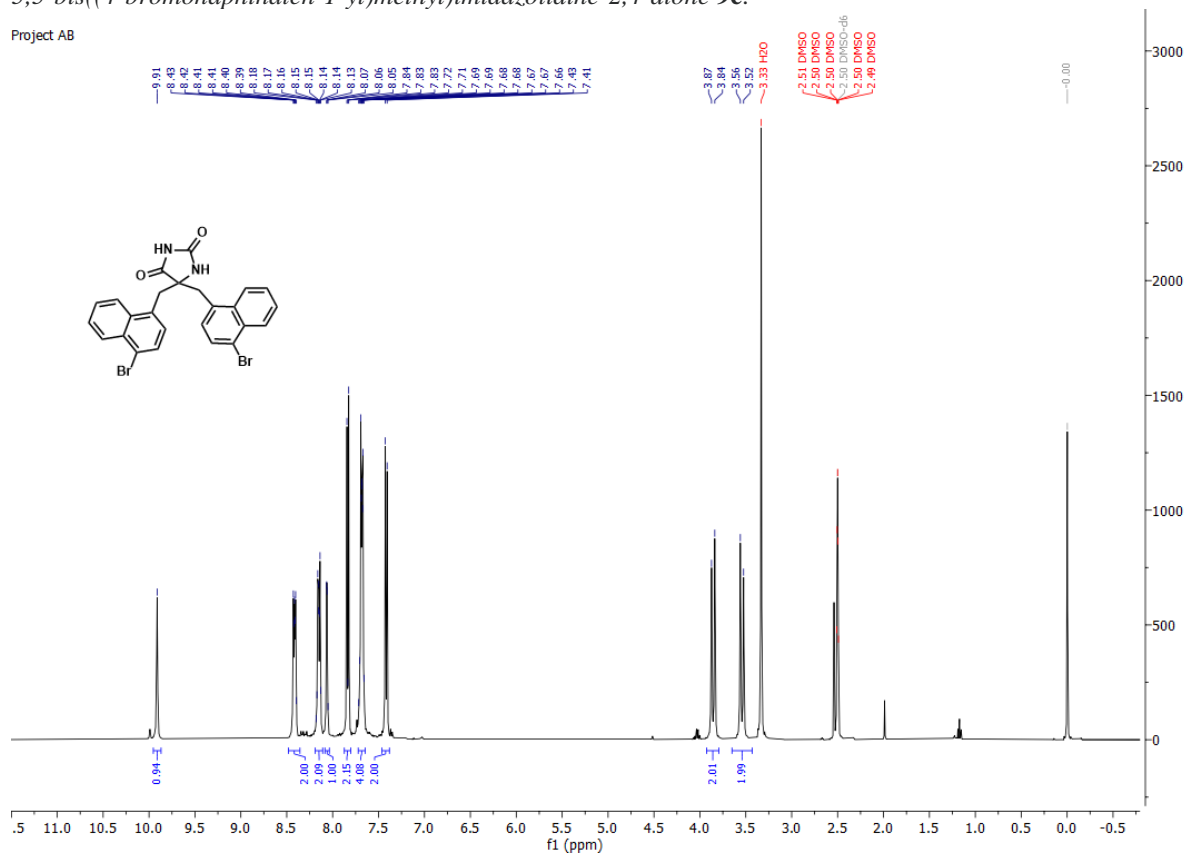


Project AB

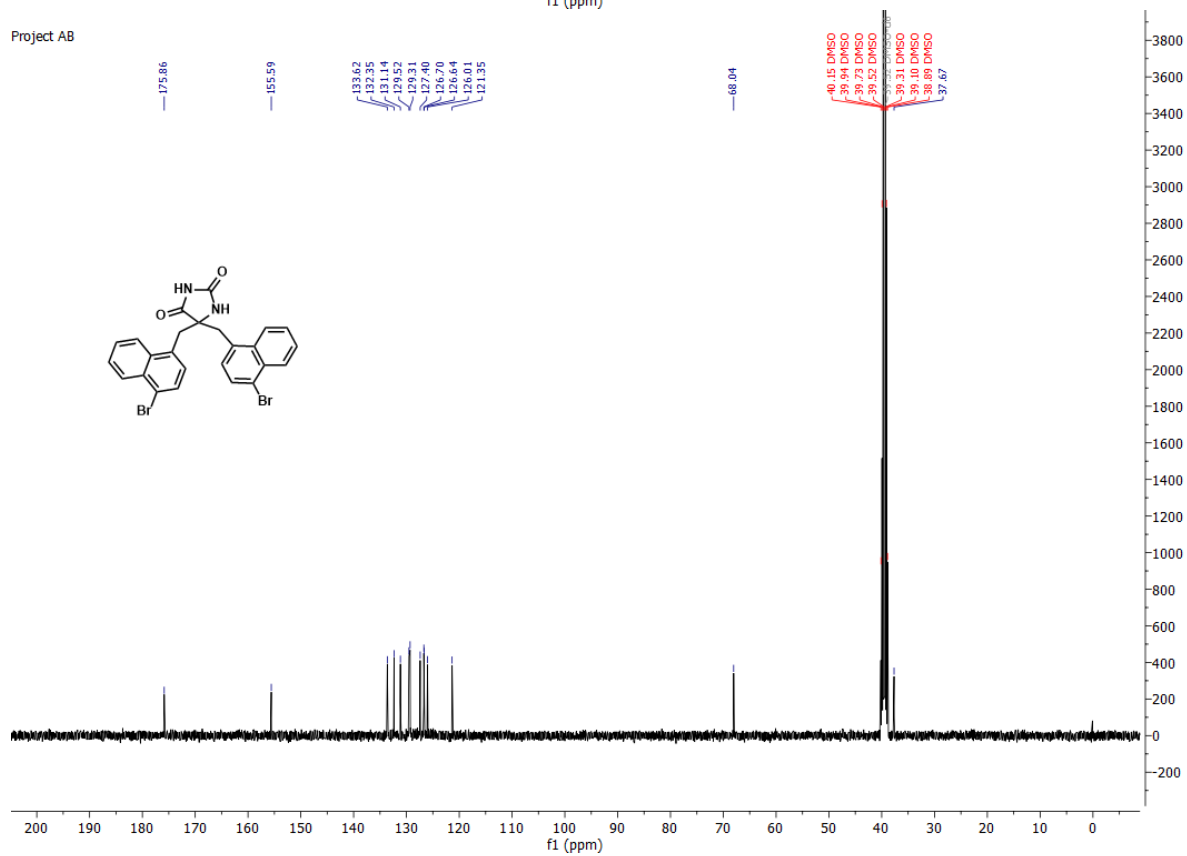


5,5-bis((4-bromonaphthalen-1-yl)methyl)imidazolidine-2,4-dione **9e**.

Project AB

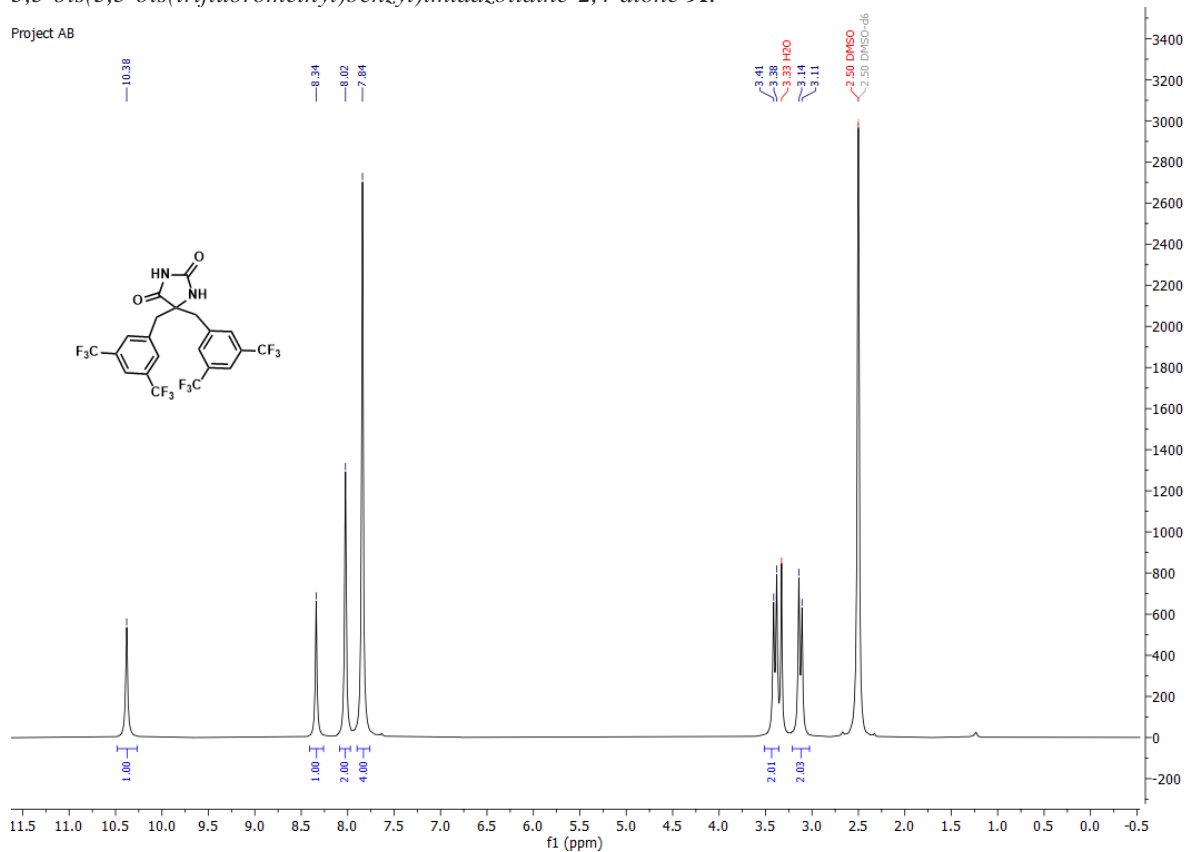


Project AB

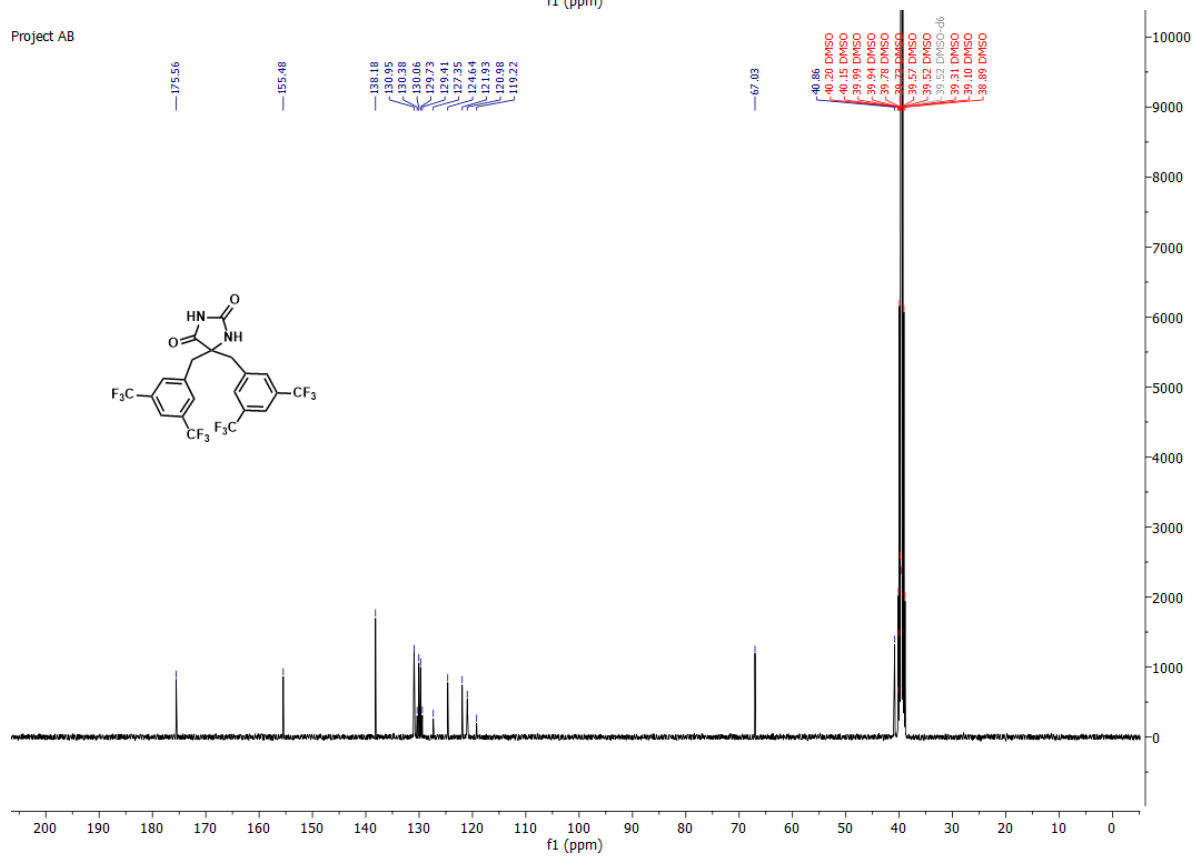


5,5-bis(3,5-bis(trifluoromethyl)benzyl)imidazolidine-2,4-dione **9f**.

Project AB



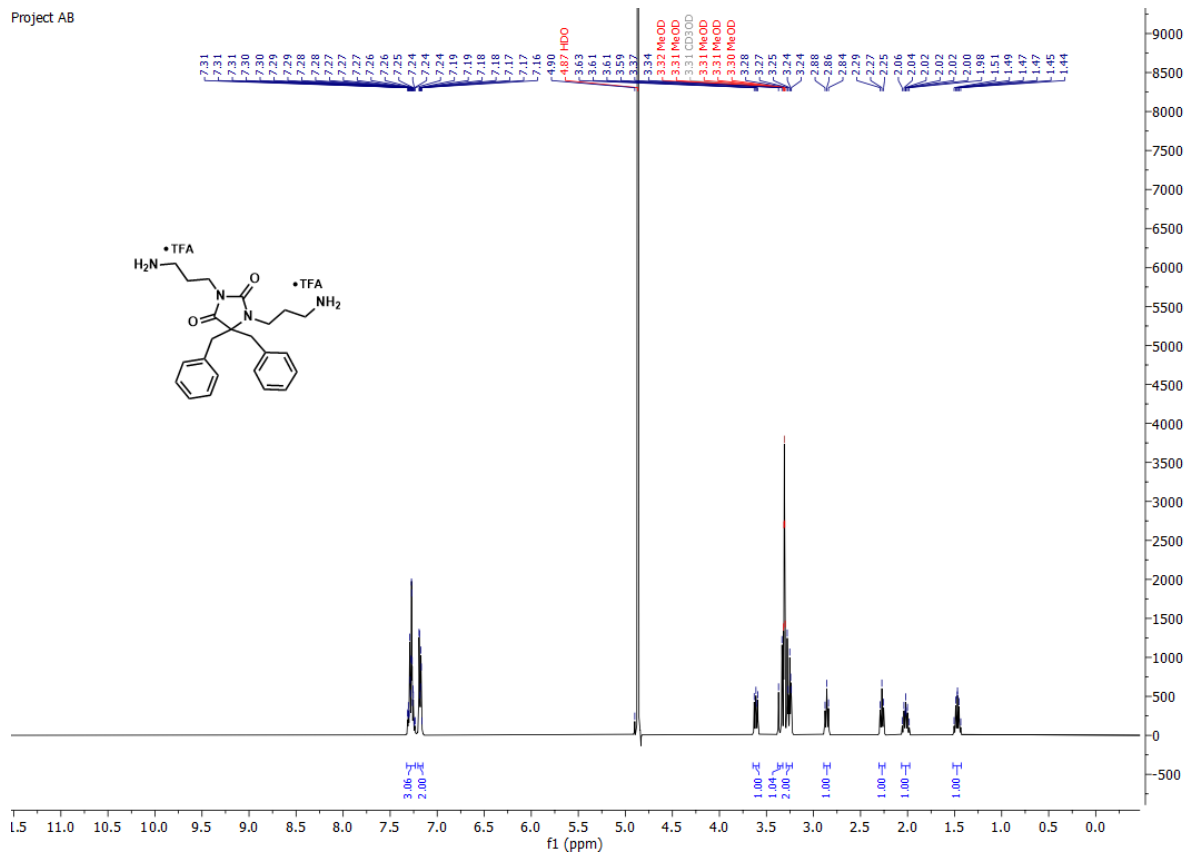
Project AB



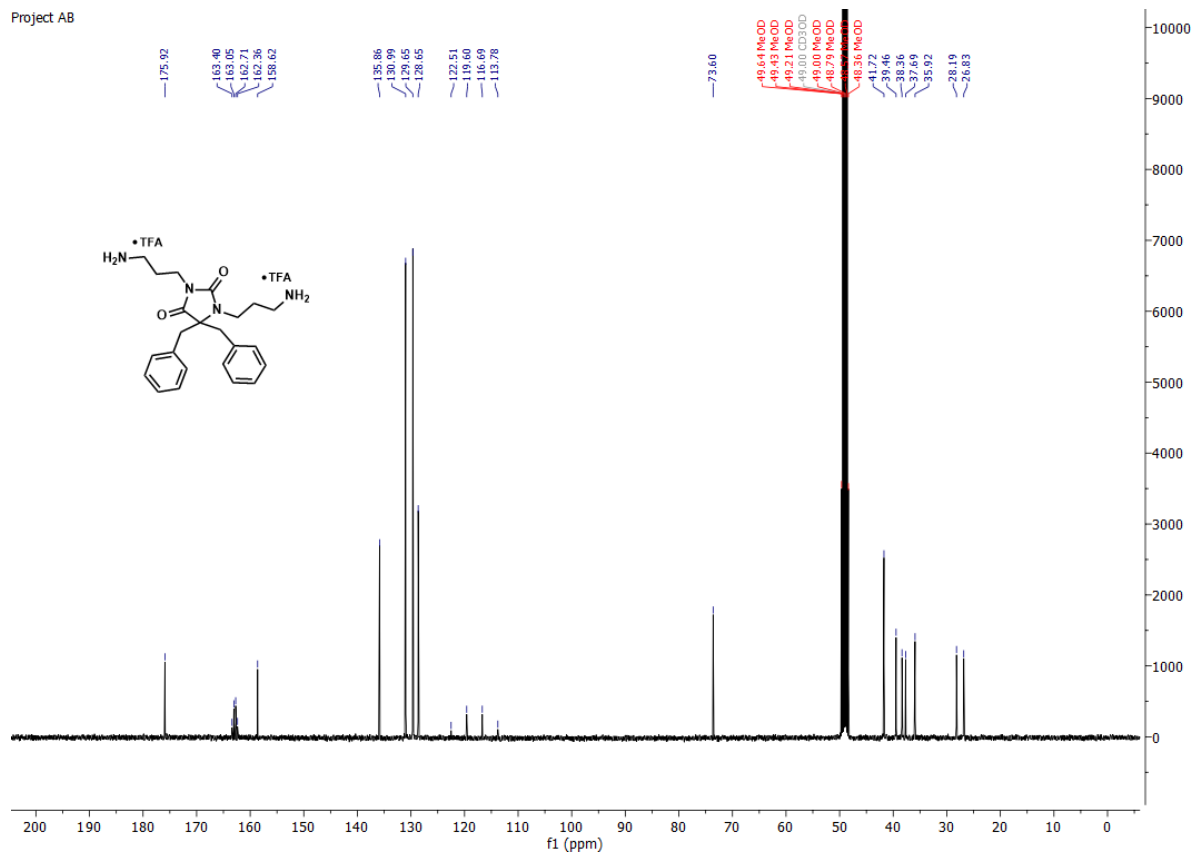
4.3 *N,N'*-dialkylated hydantoin 2A

1,3-bis(3-aminopropyl)-5,5-dibenzylimidazolidine-2,4-dione **2aA**.

Project AB

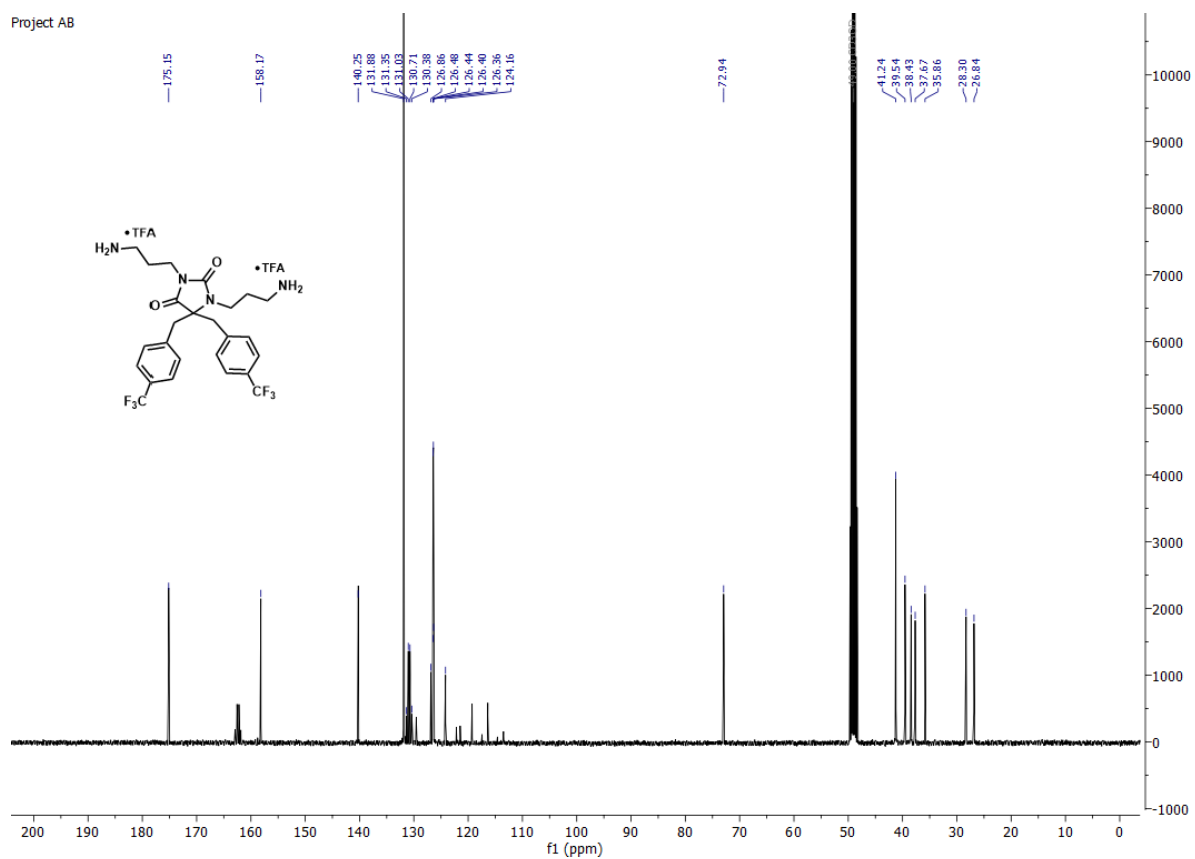
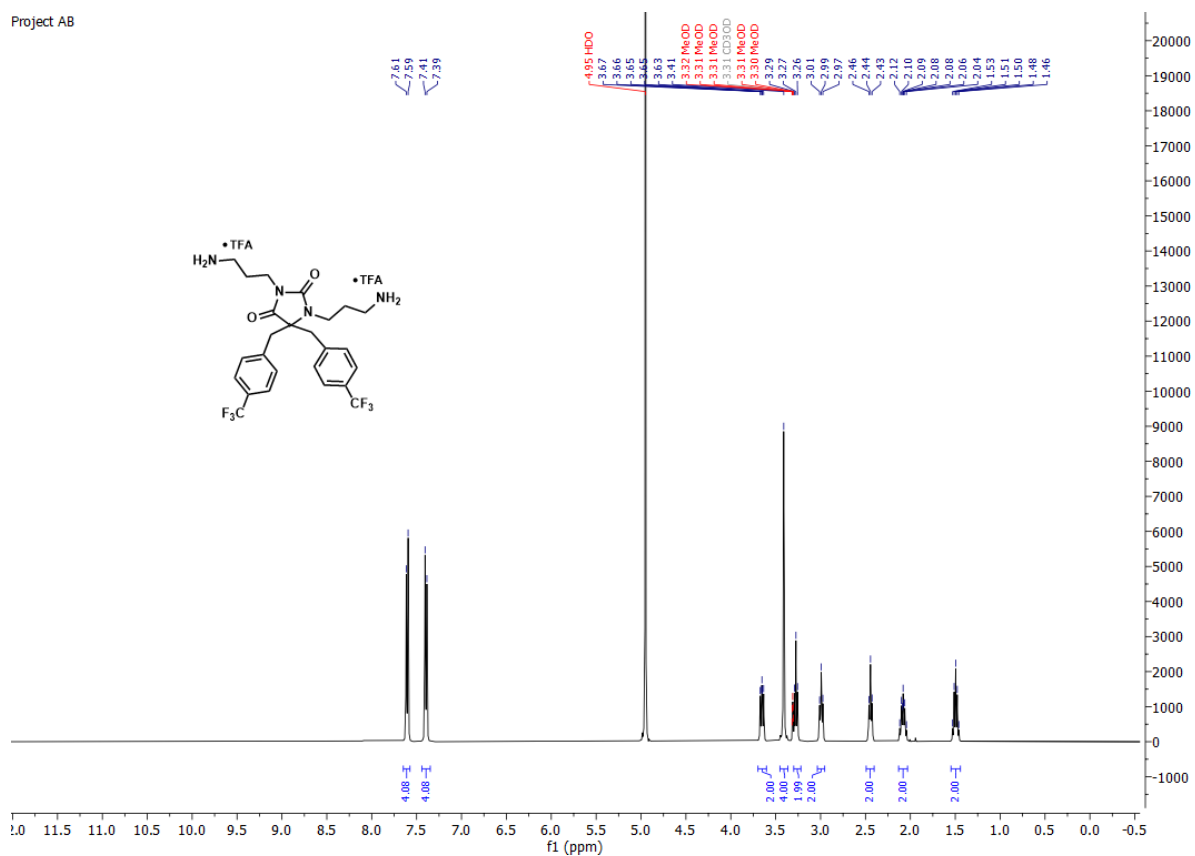


Project AB



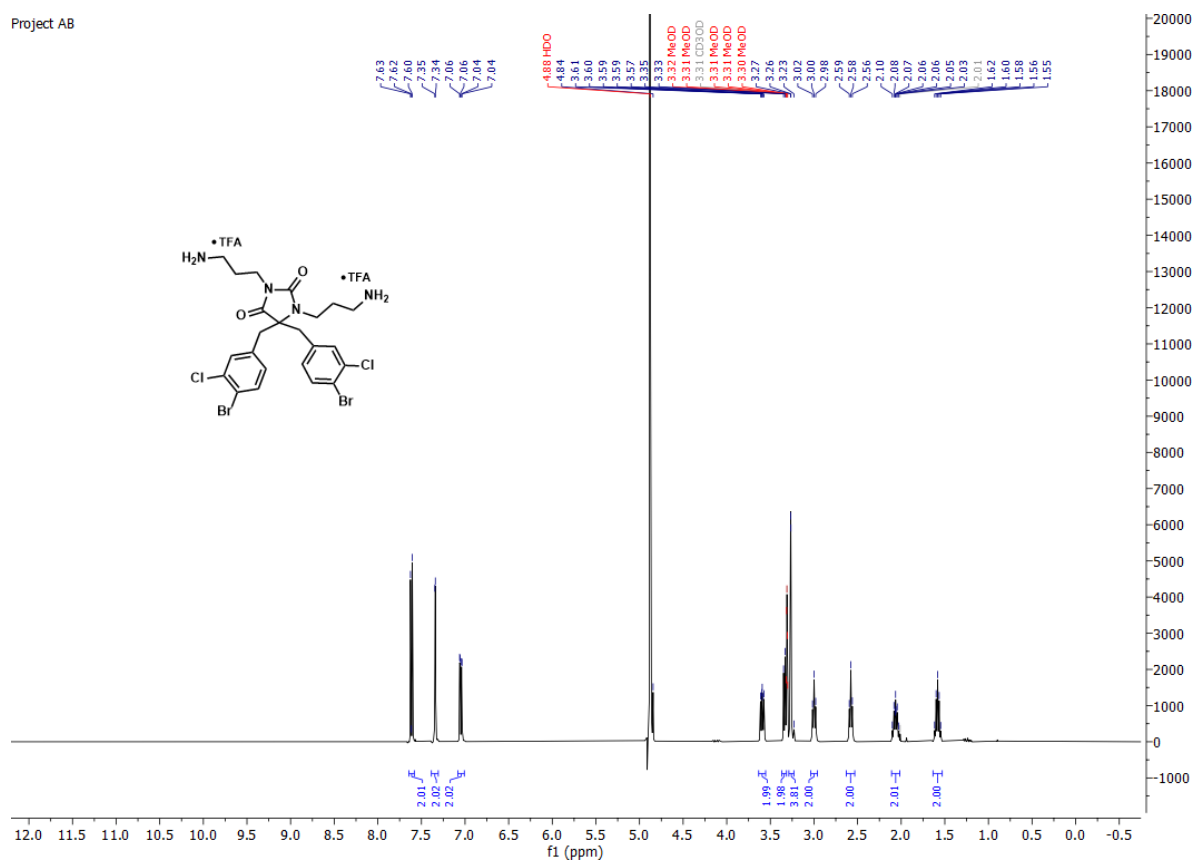
1,3-bis(3-aminopropyl)-5,5-bis(4-(trifluoromethyl)benzyl)imidazolidine-2,4-dione **2bA**.

Project AB

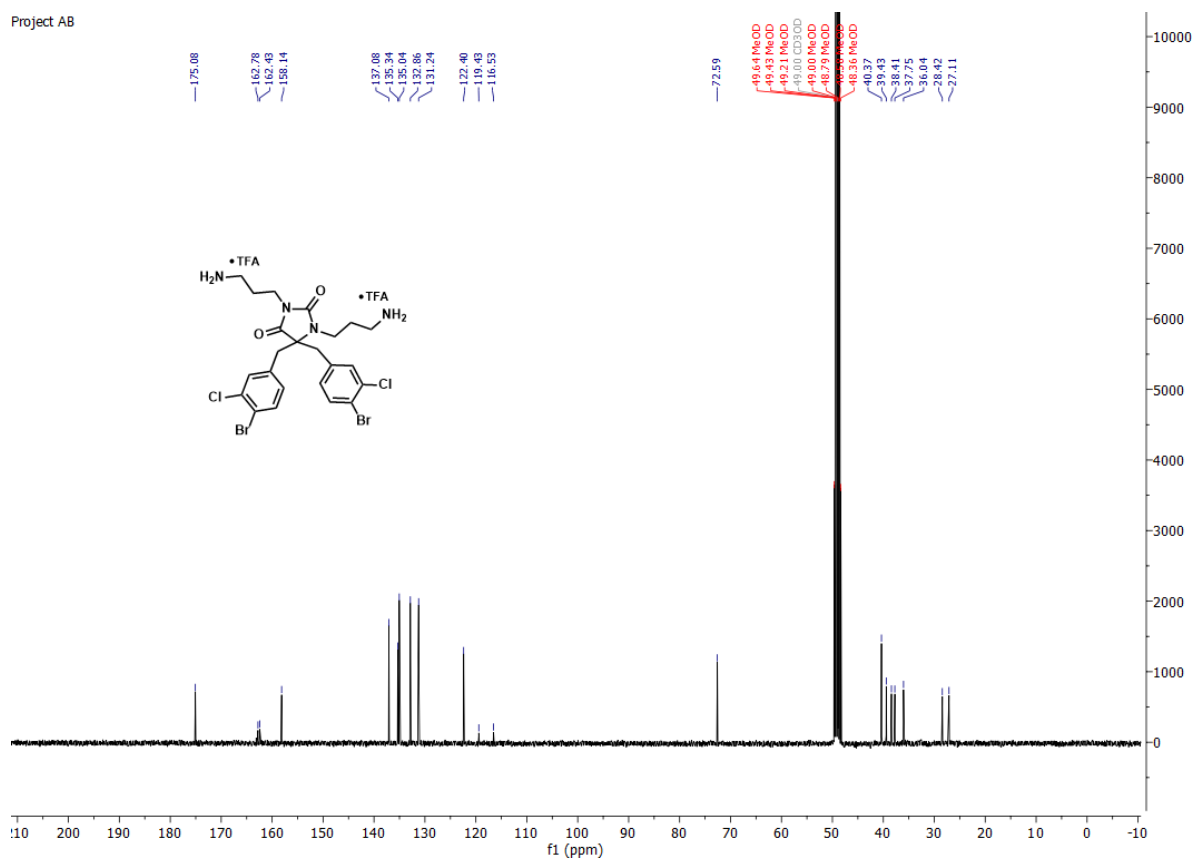


1,3-bis(3-aminopropyl)-5,5-bis(4-bromo-3-chlorobenzyl)imidazolidine-2,4-dione **2cA**.

Project AB

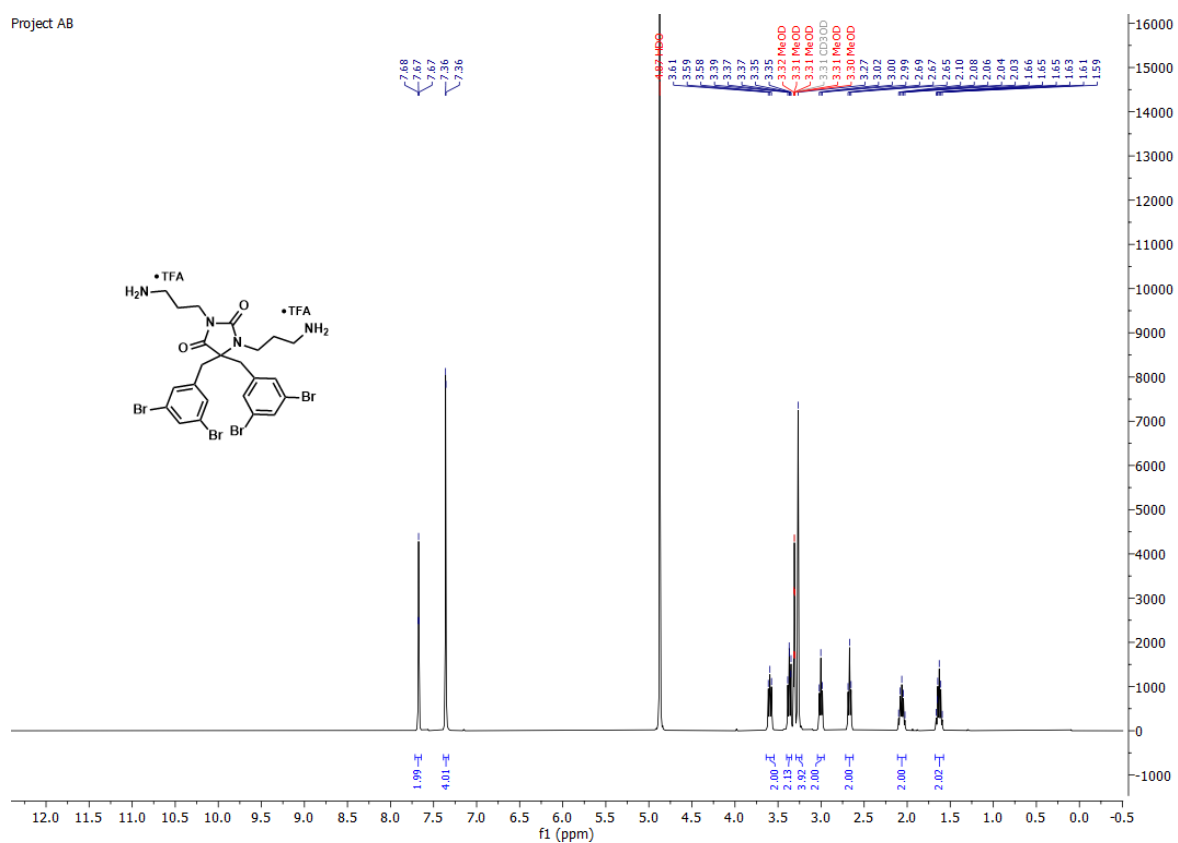


Project AB

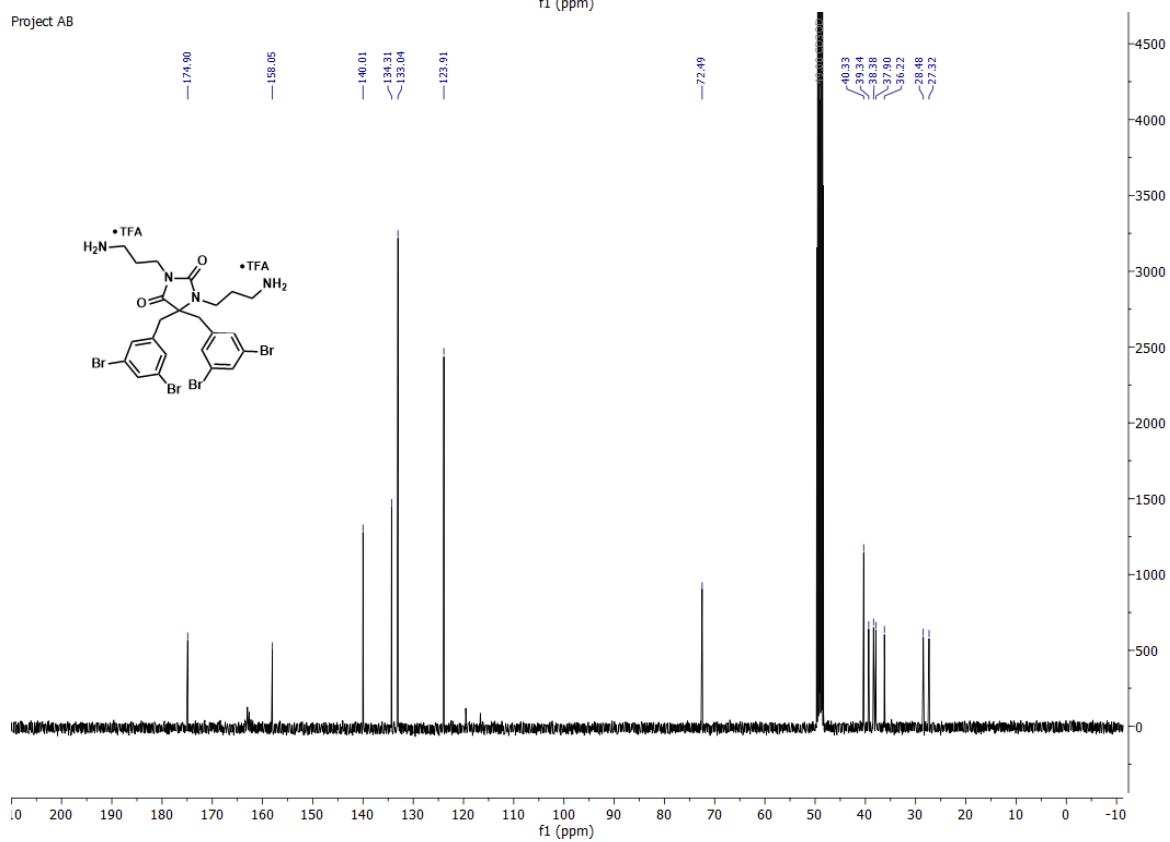


1,3-bis(3-aminopropyl)-5,5-bis(3,5-dibromobenzyl)imidazolidine-2,4-dione 2dA.

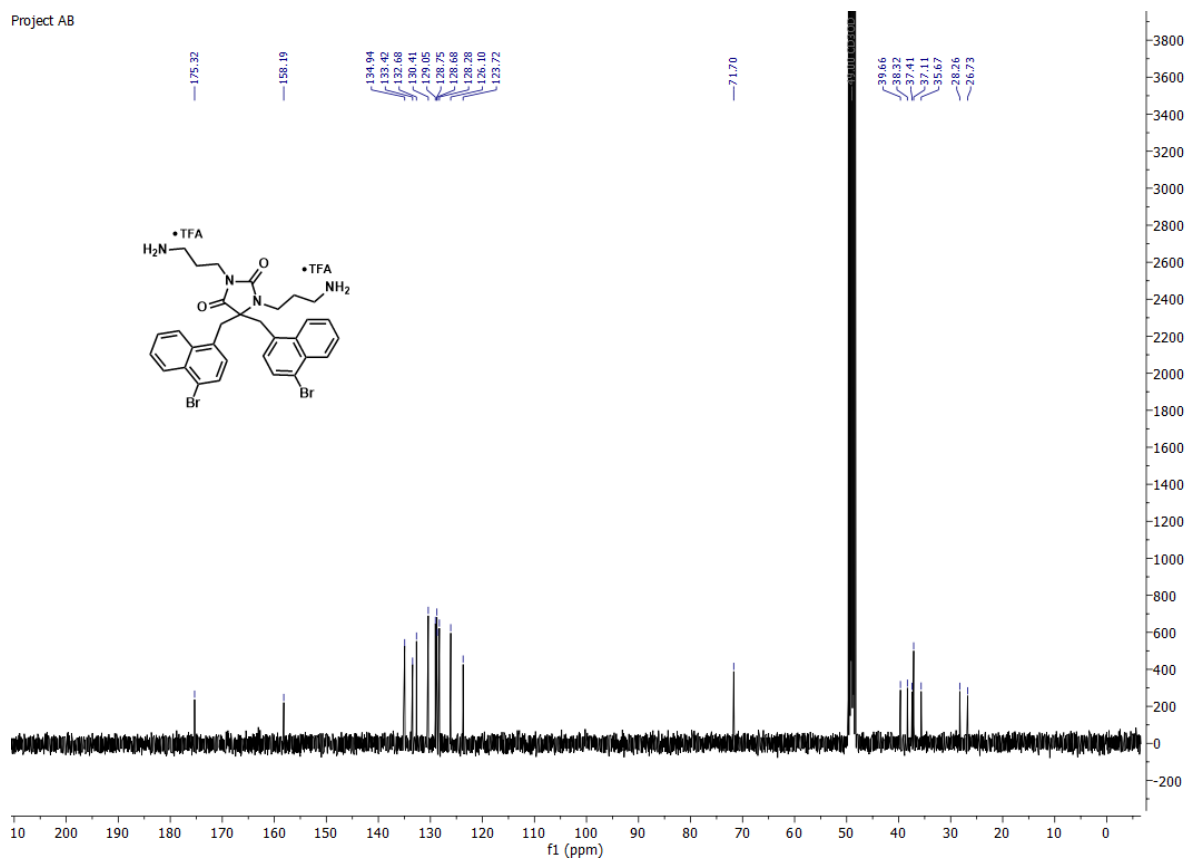
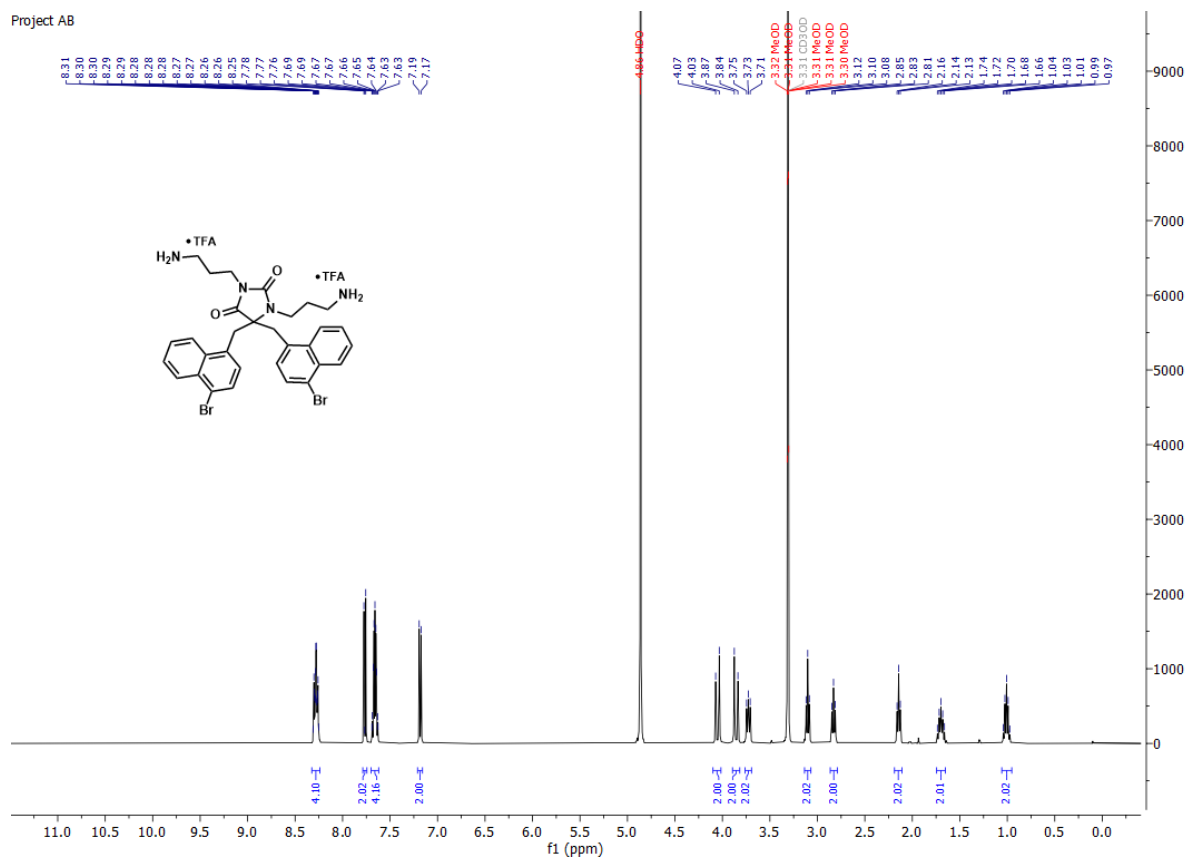
Project AB



Project AB

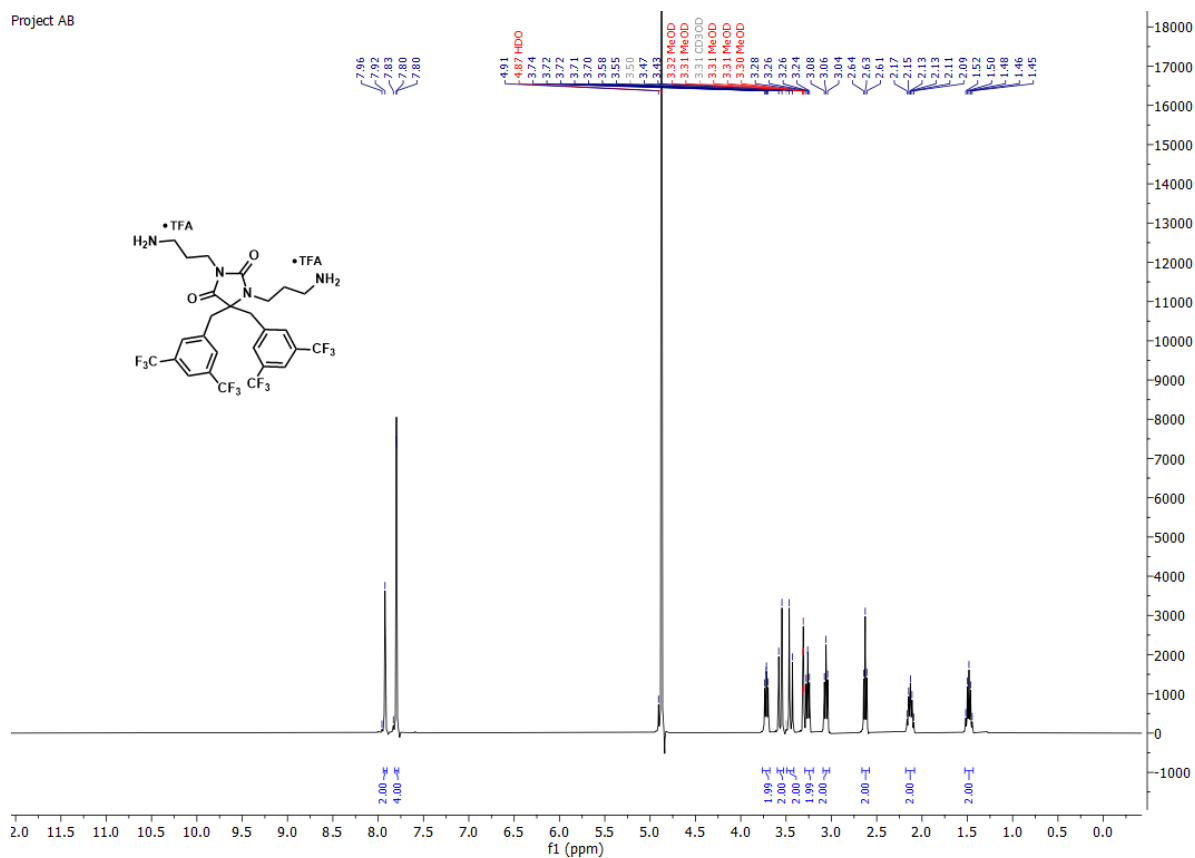


1,3-bis(3-aminopropyl)-5,5-bis((4-bromonaphthalen-1-yl)methyl)imidazolidine-2,4-dione **2eA**.

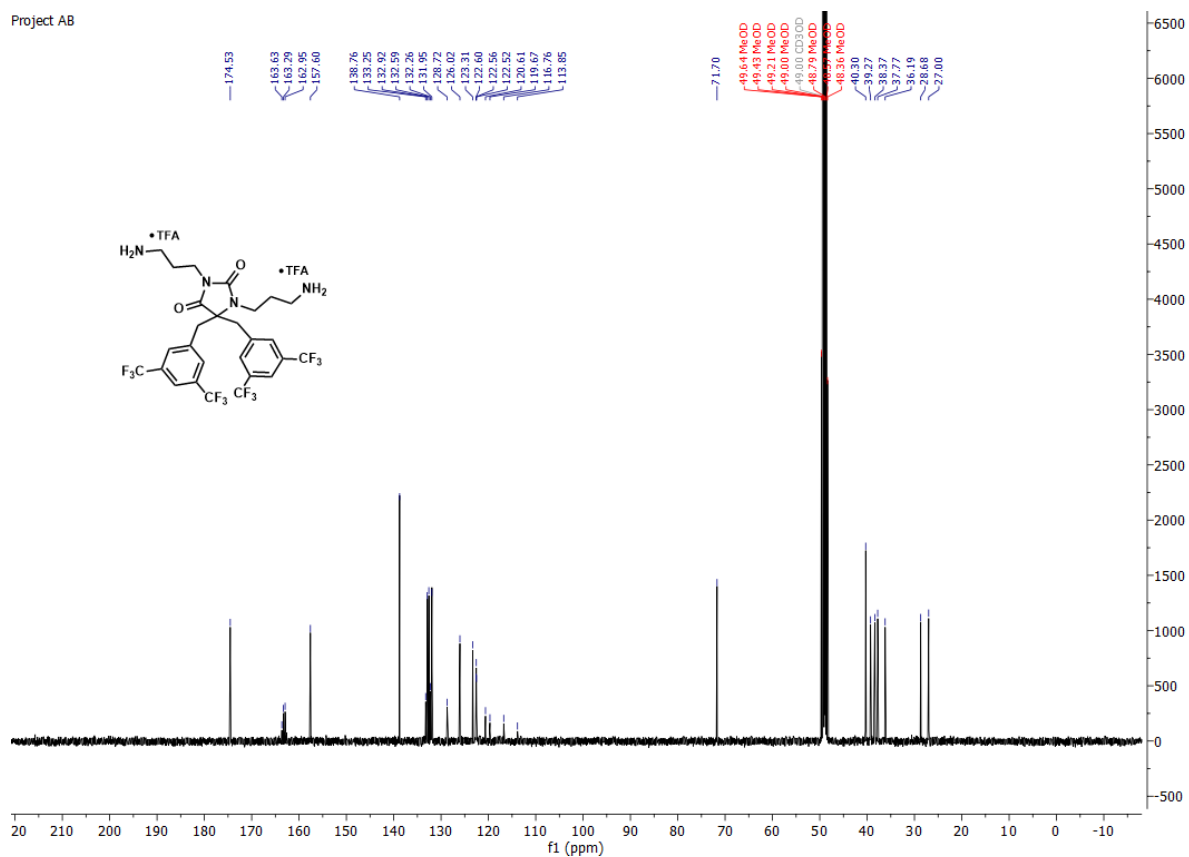


1,3-bis(3-aminopropyl)-5,5-bis(3,5-bis(trifluoromethyl)benzyl)imidazolidine-2,4-dione **2fA**.

Project AB



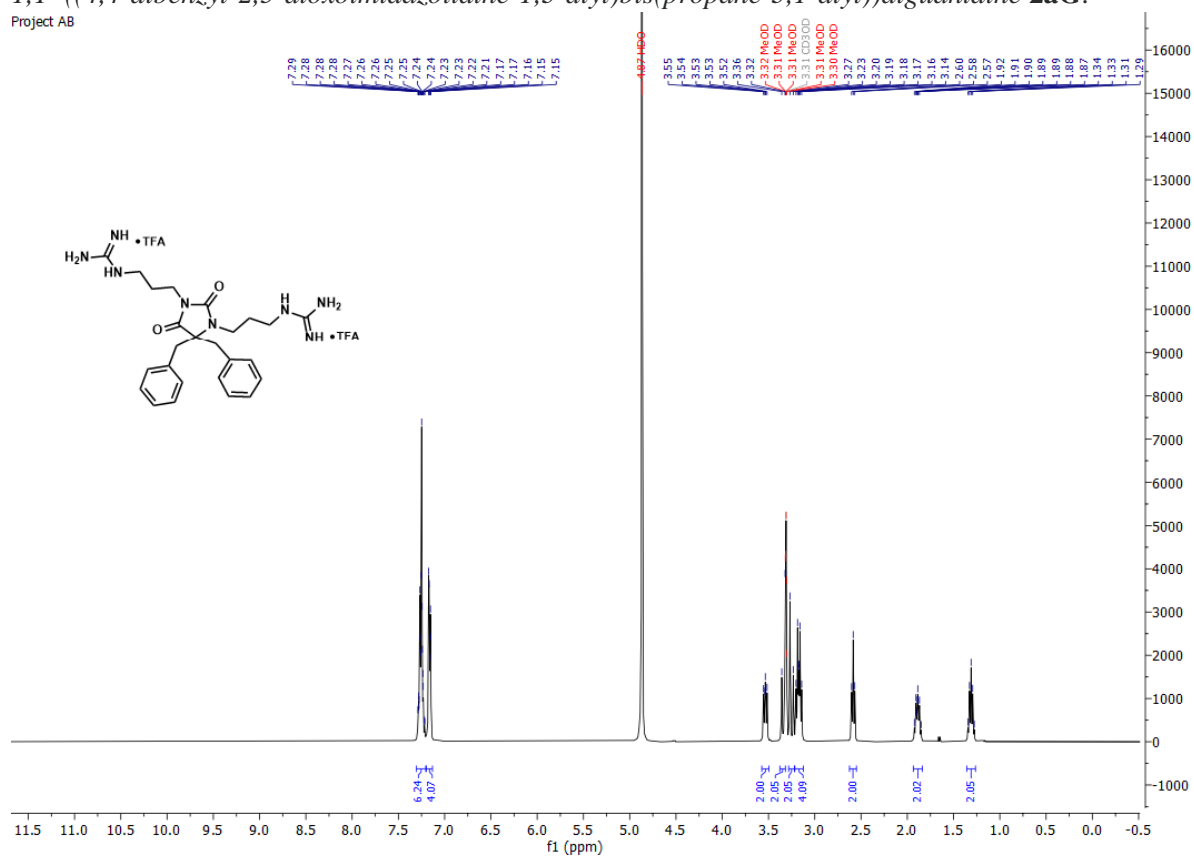
Project AB



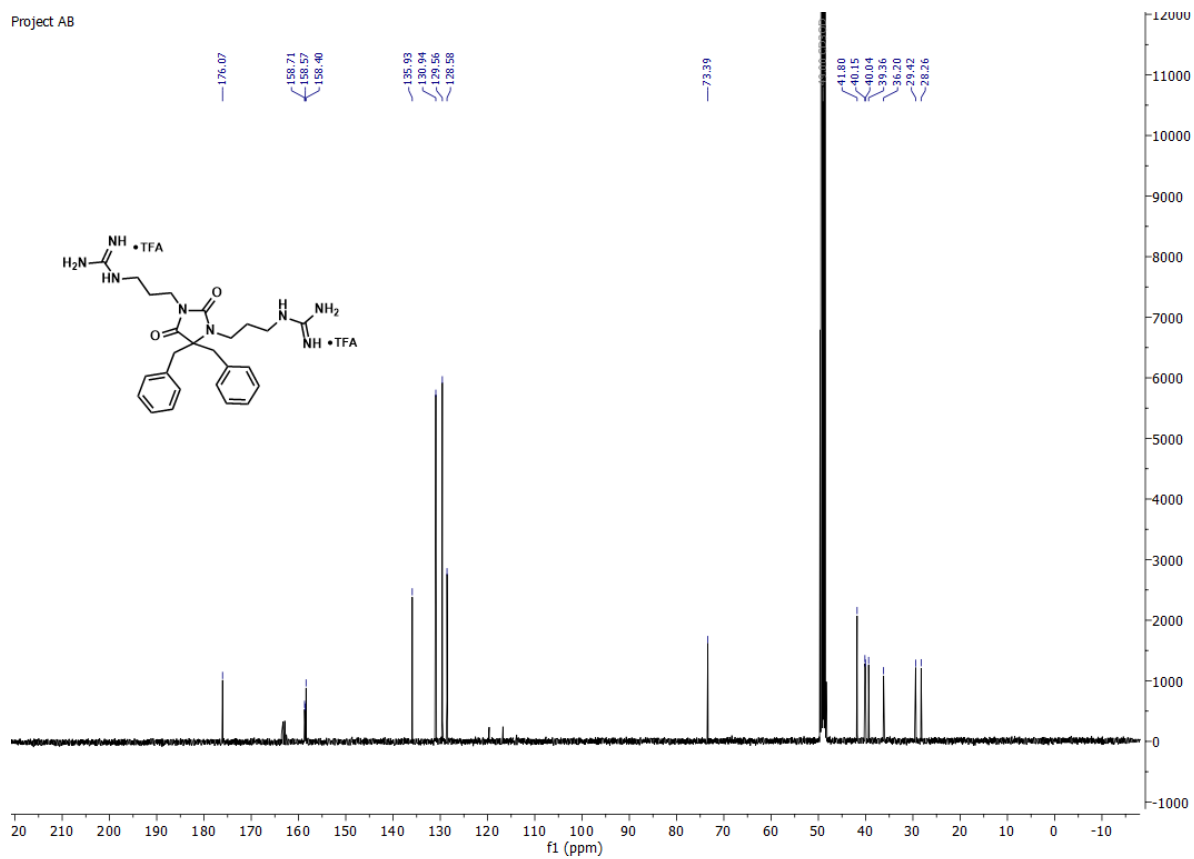
4.4 *N,N'*-dialkylated hydantoin 2G

1,1'-((4,4-dibenzyl-2,5-dioximidazolidine-1,3-diyl)bis(propane-3,1-diyl))diguanidine **2aG**.

Project AB

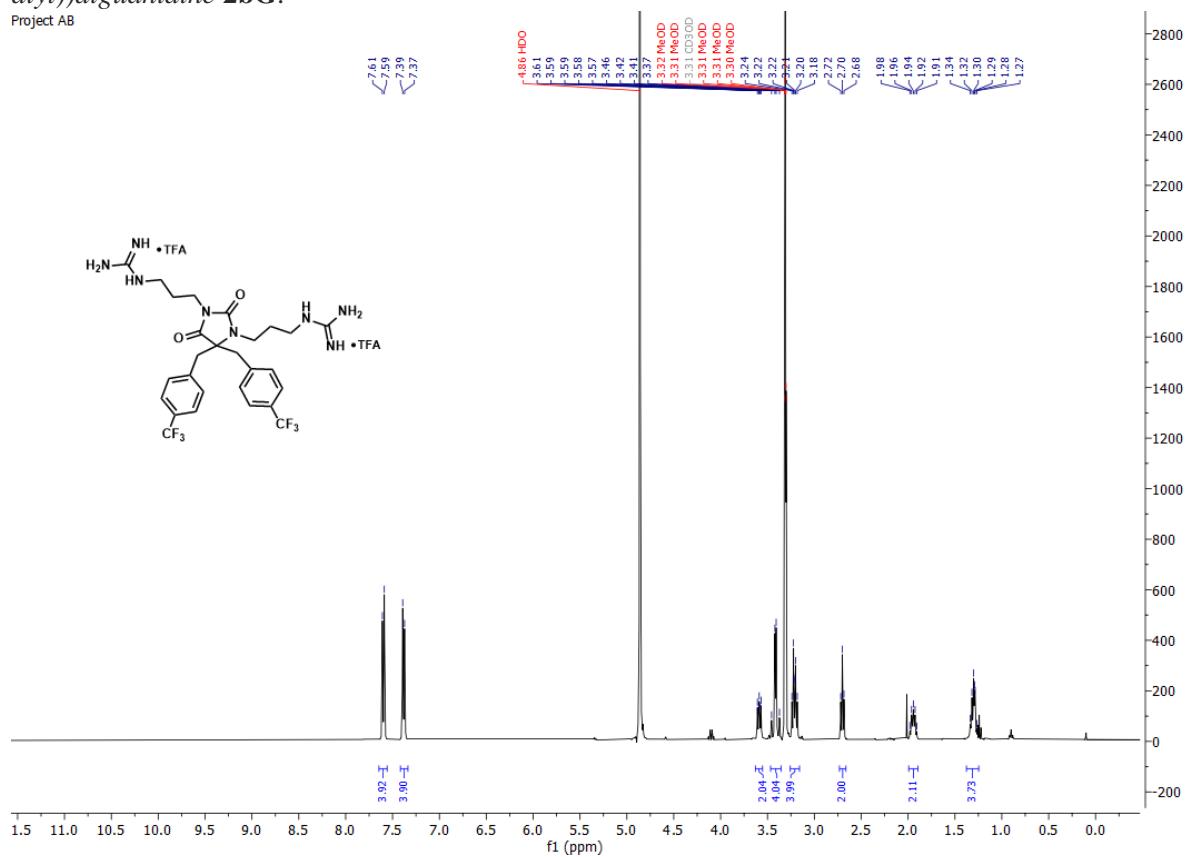


Project AB

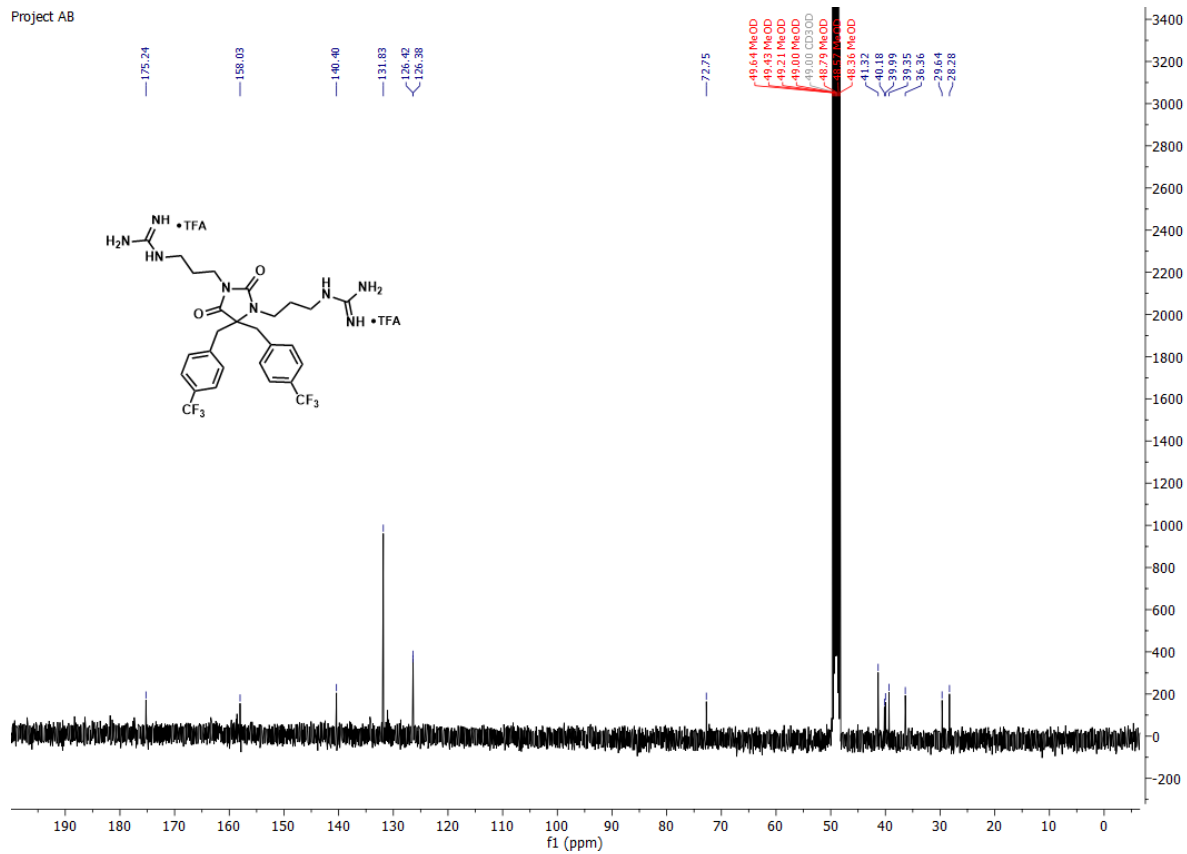


1,1'-((2,5-dioxo-4,4-bis(4-(trifluoromethyl)benzyl)imidazolidine-1,3-diyl)bis(propane-3,1-diyl))diguanidine **2bG**.

Project AB

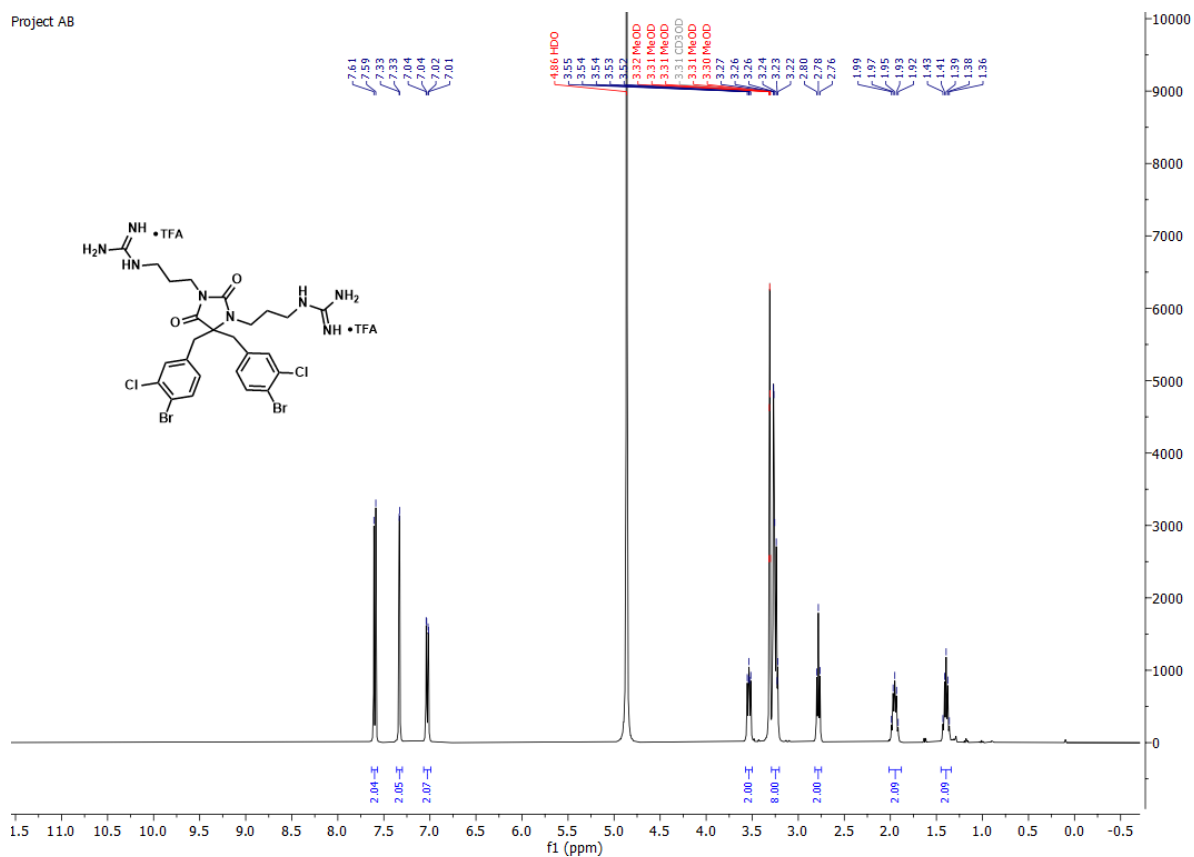


Project AB

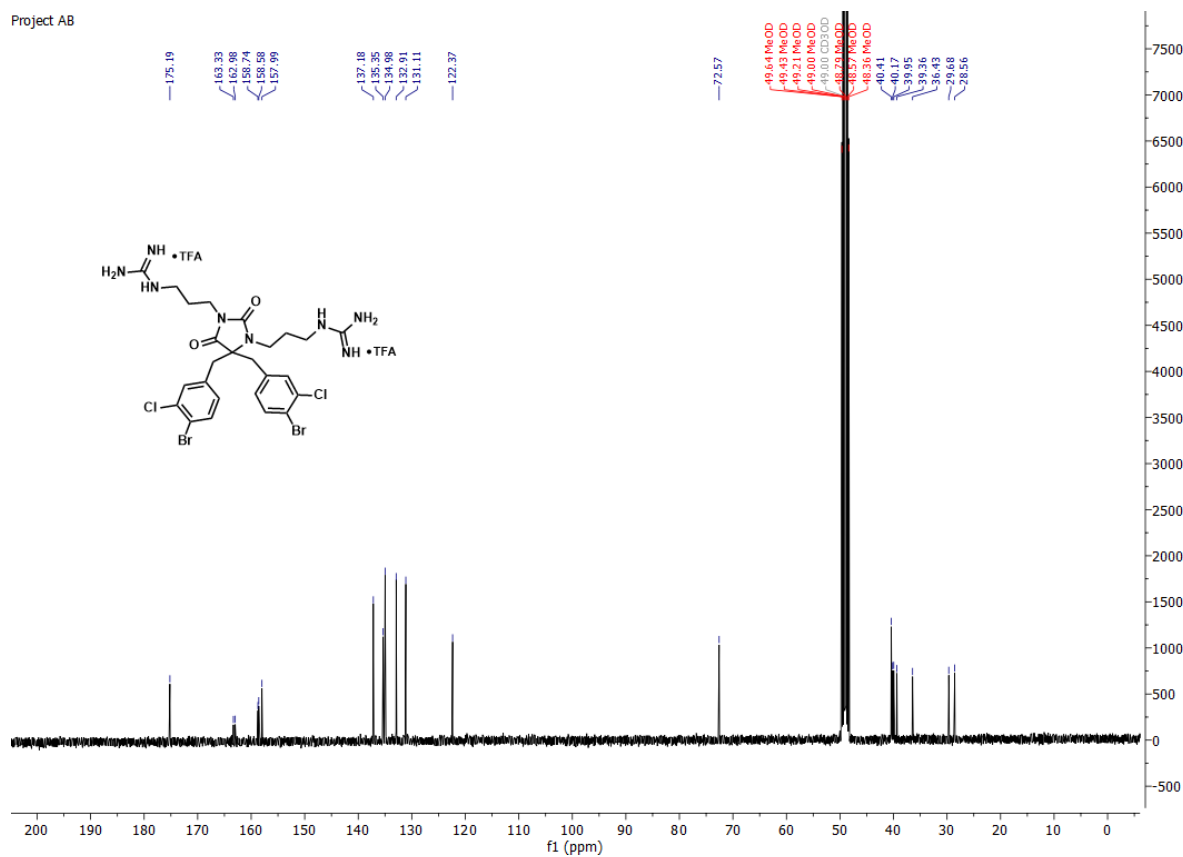


1,1'-((4,4-bis(4-bromo-3-chlorobenzyl)-2,5-dioximidazolidine-1,3-diyl)bis(propane-3,1-diyl))diguanidine **2cG**.

Project AB

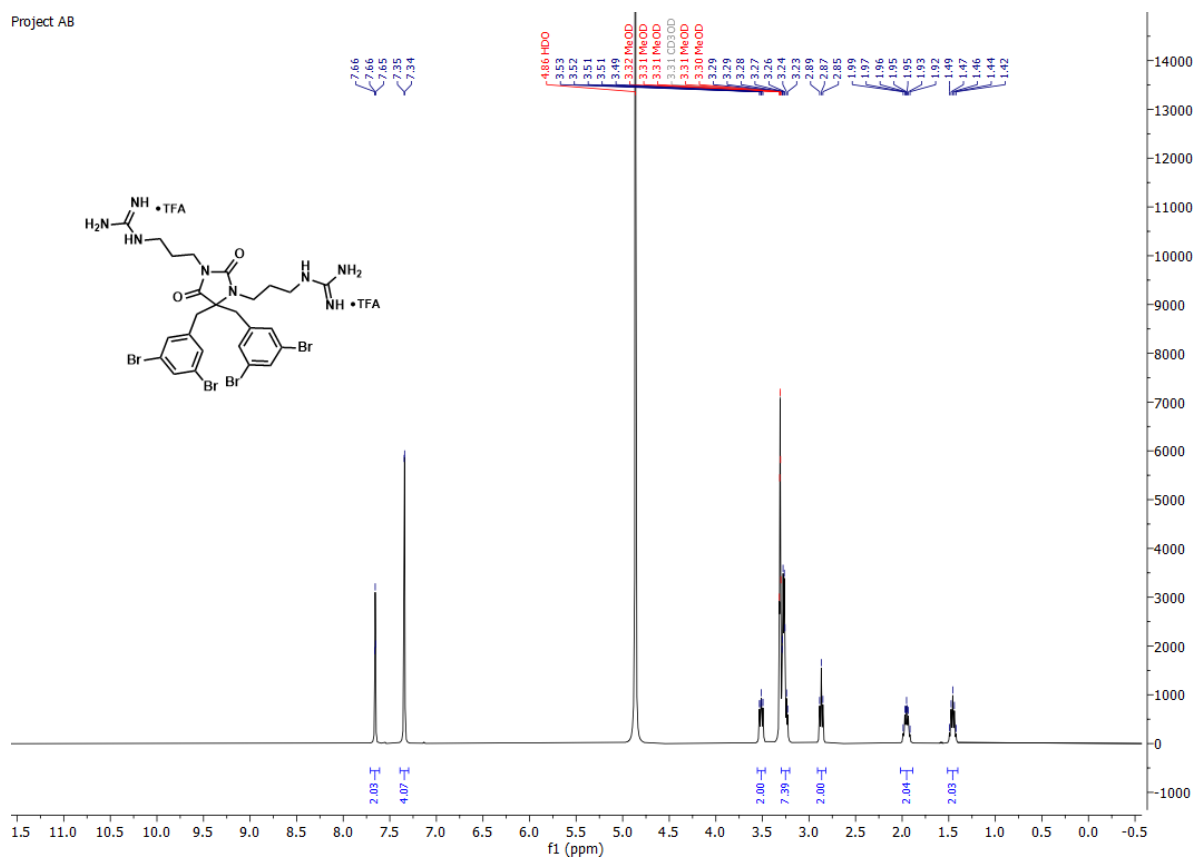


Project AB

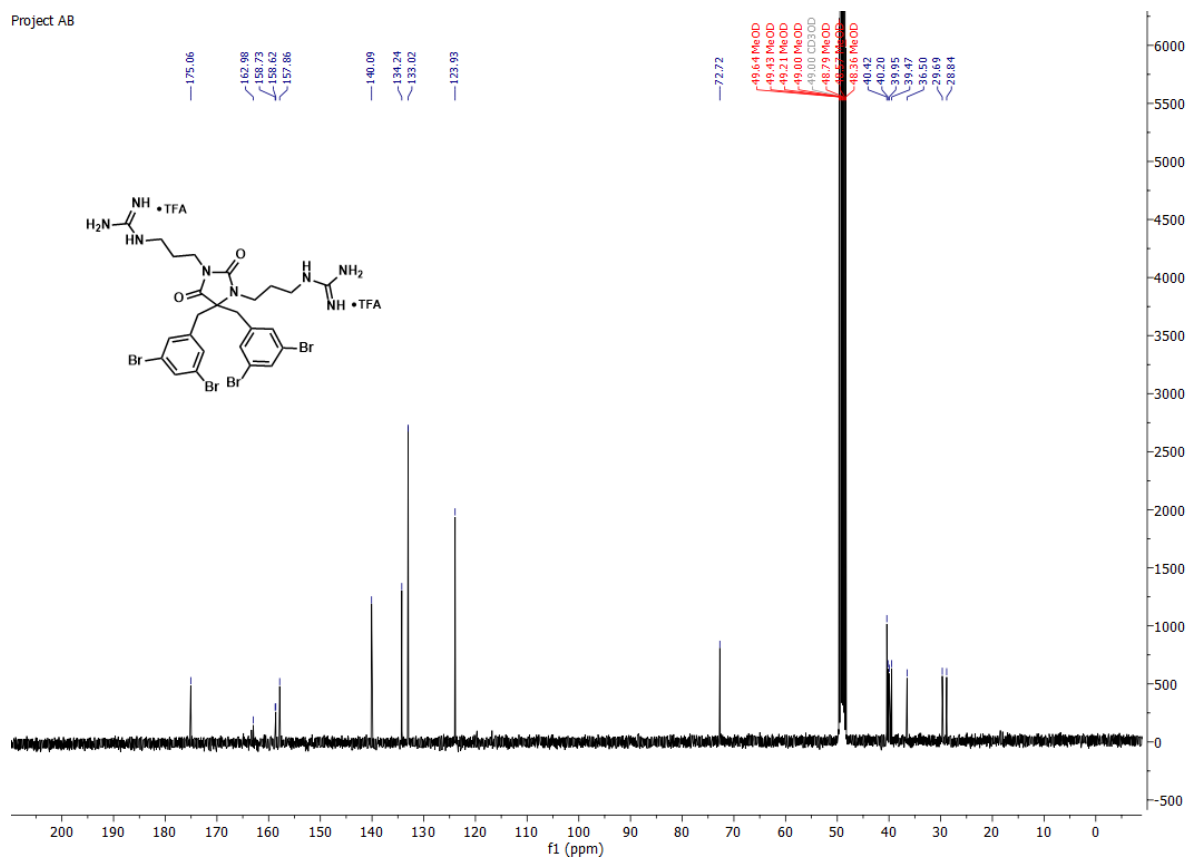


1,1'-((4,4-bis(3,5-dibromobenzyl)-2,5-dioximidazolidine-1,3-diyl)bis(propane-3,1-diyl)diguandine 2dG.

Project AB

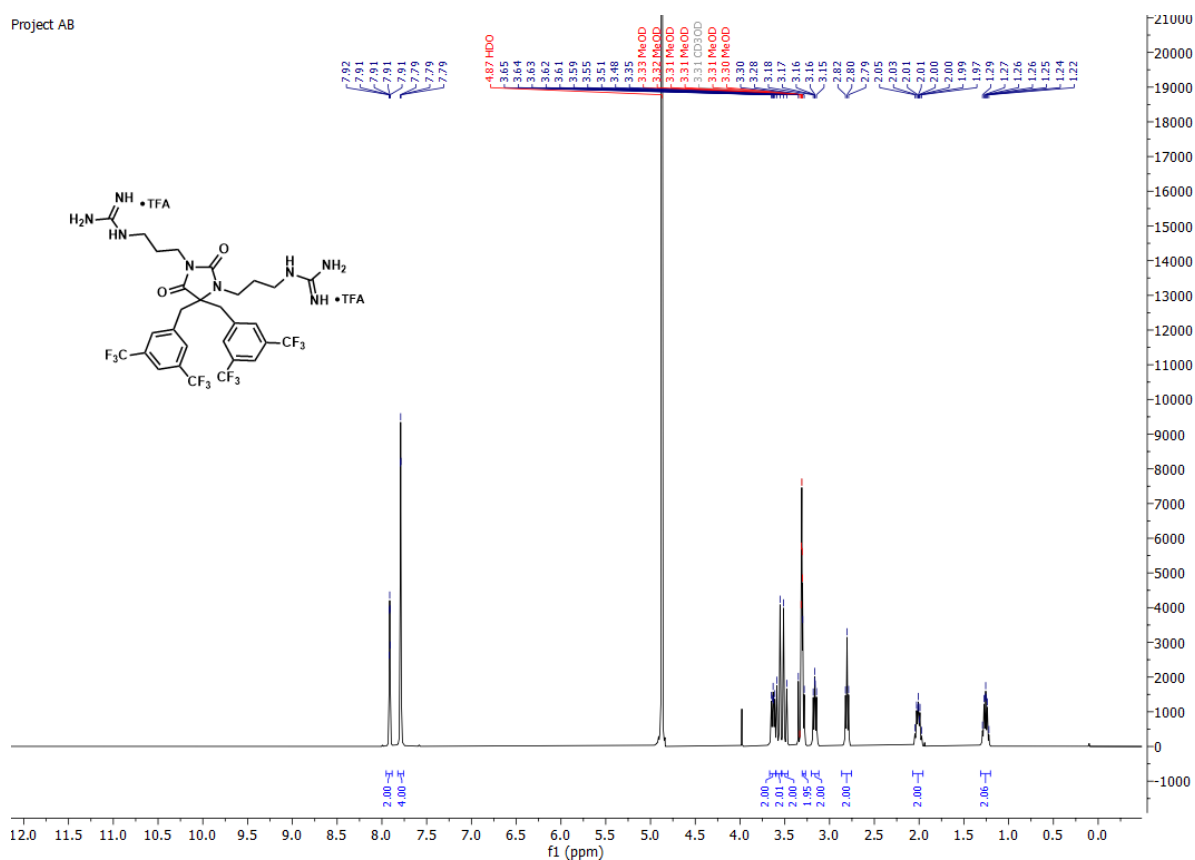


Project AB

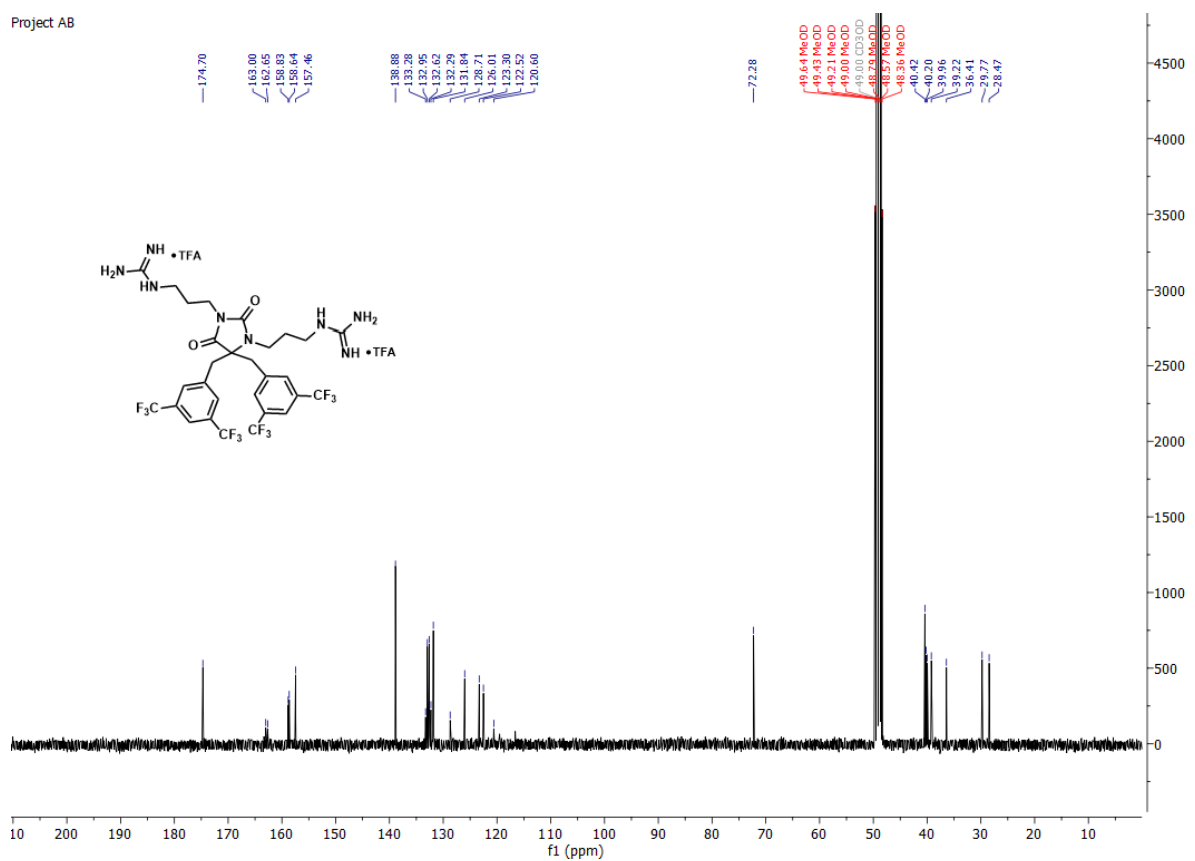


1,1'-((4,4-bis(3,5-bis(trifluoromethyl)benzyl)-2,5-dioximidazolidine-1,3-diyl)bis(propane-3,1-diyl))diguanidine **2fG**.

Project AB



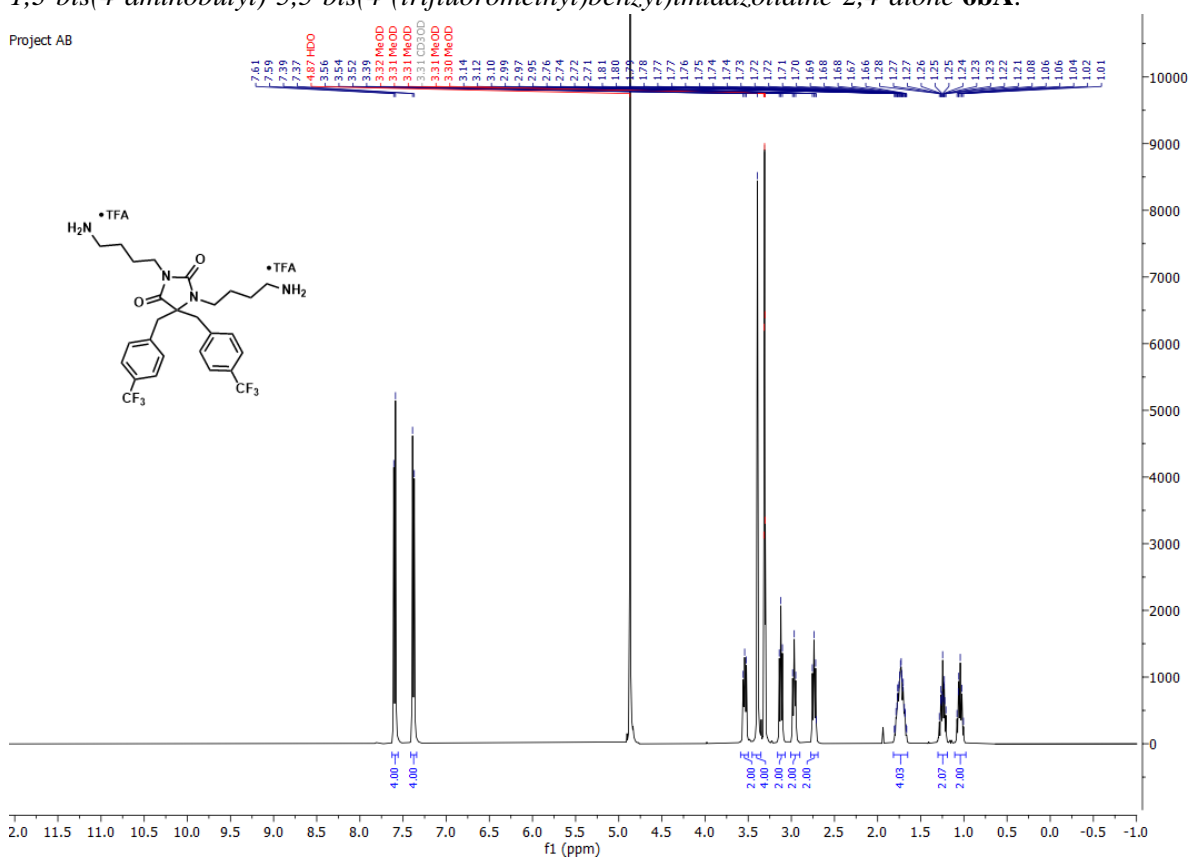
Project AB



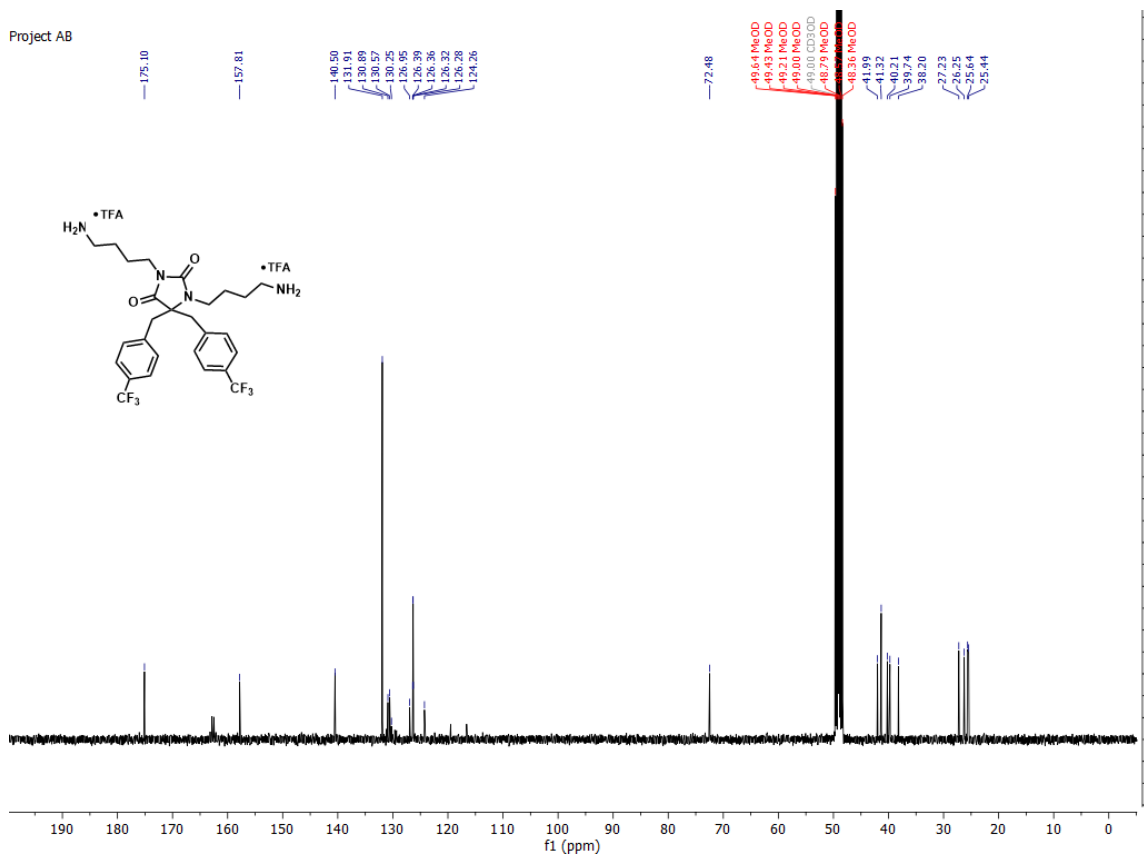
4.5 *N,N'*-dialkylated hydantoin 6A

1,3-bis(4-aminobutyl)-5,5-bis(4-(trifluoromethyl)benzyl)imidazolidine-2,4-dione **6aA**.

Project AB

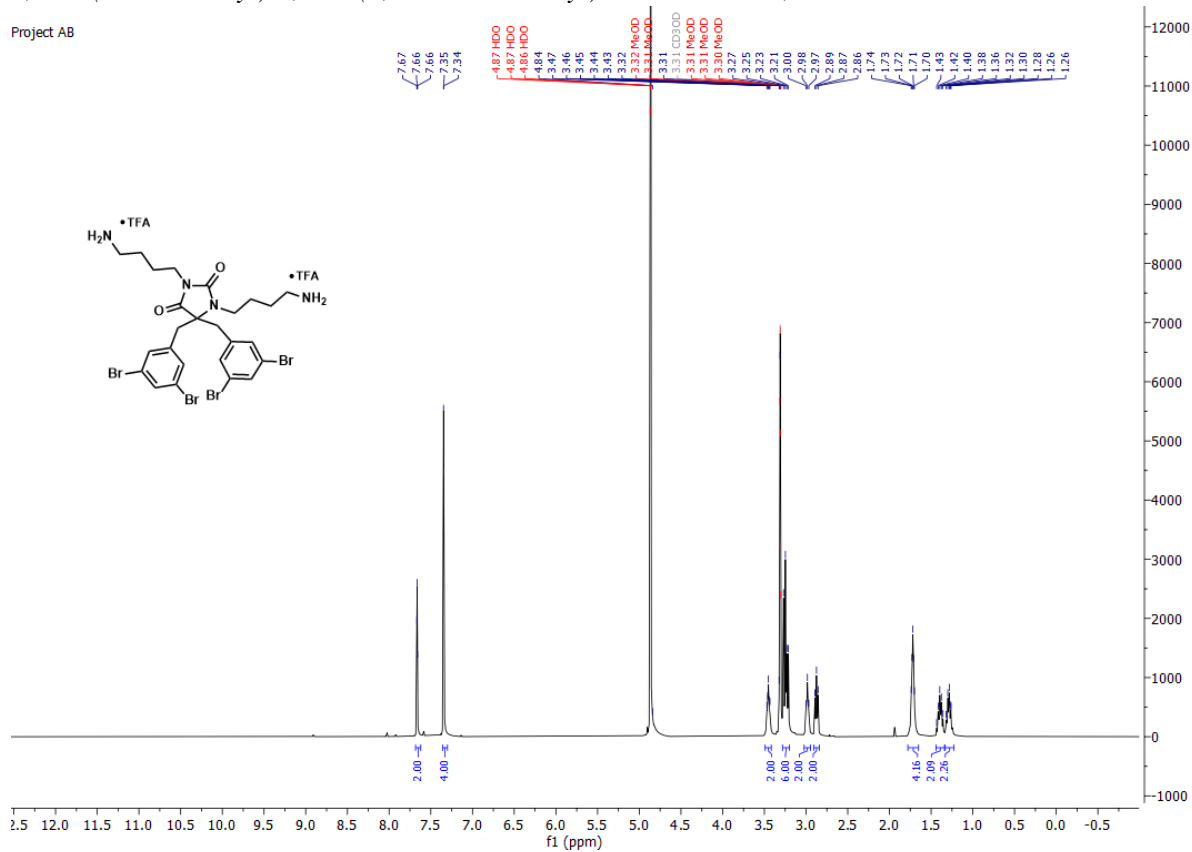


Project AB

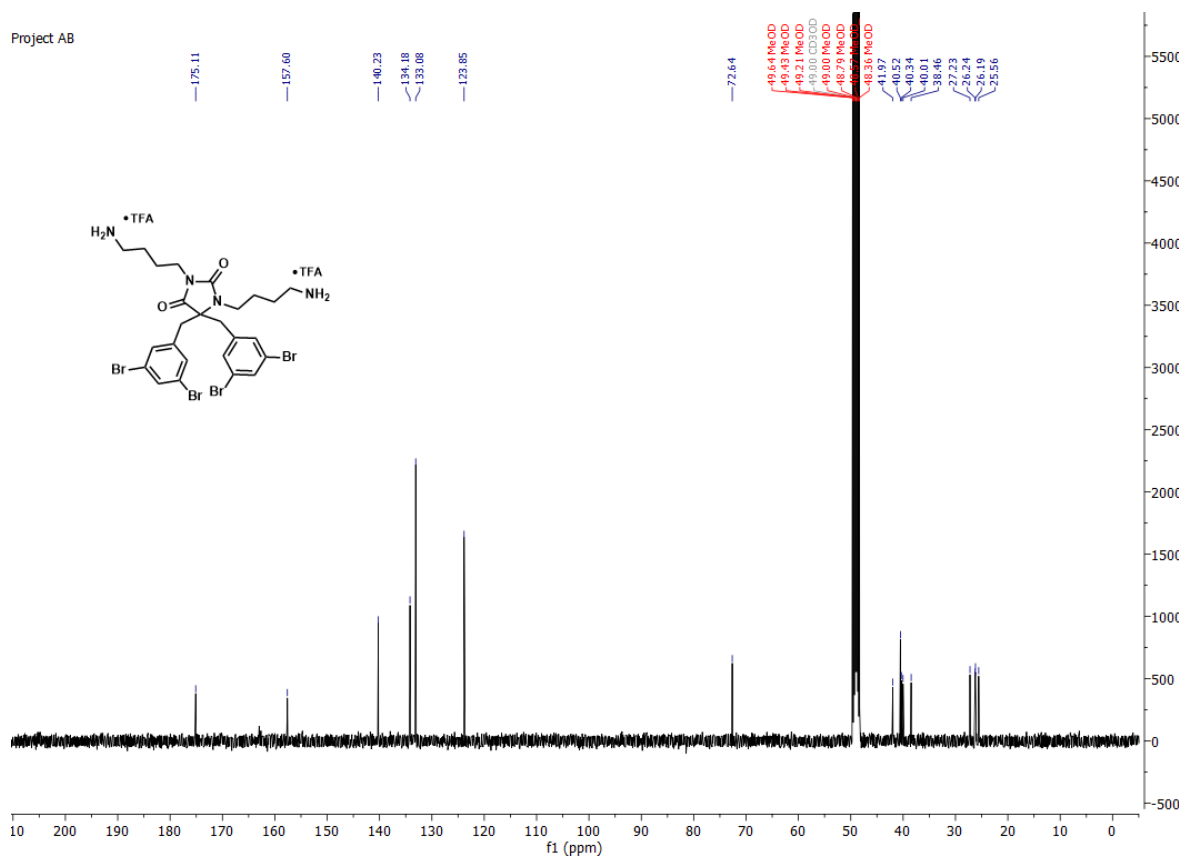


1,3-bis(4-aminobutyl)-5,5-bis(3,5-dibromobenzyl)imidazolidine-2,4-dion 6dA.

Project AB

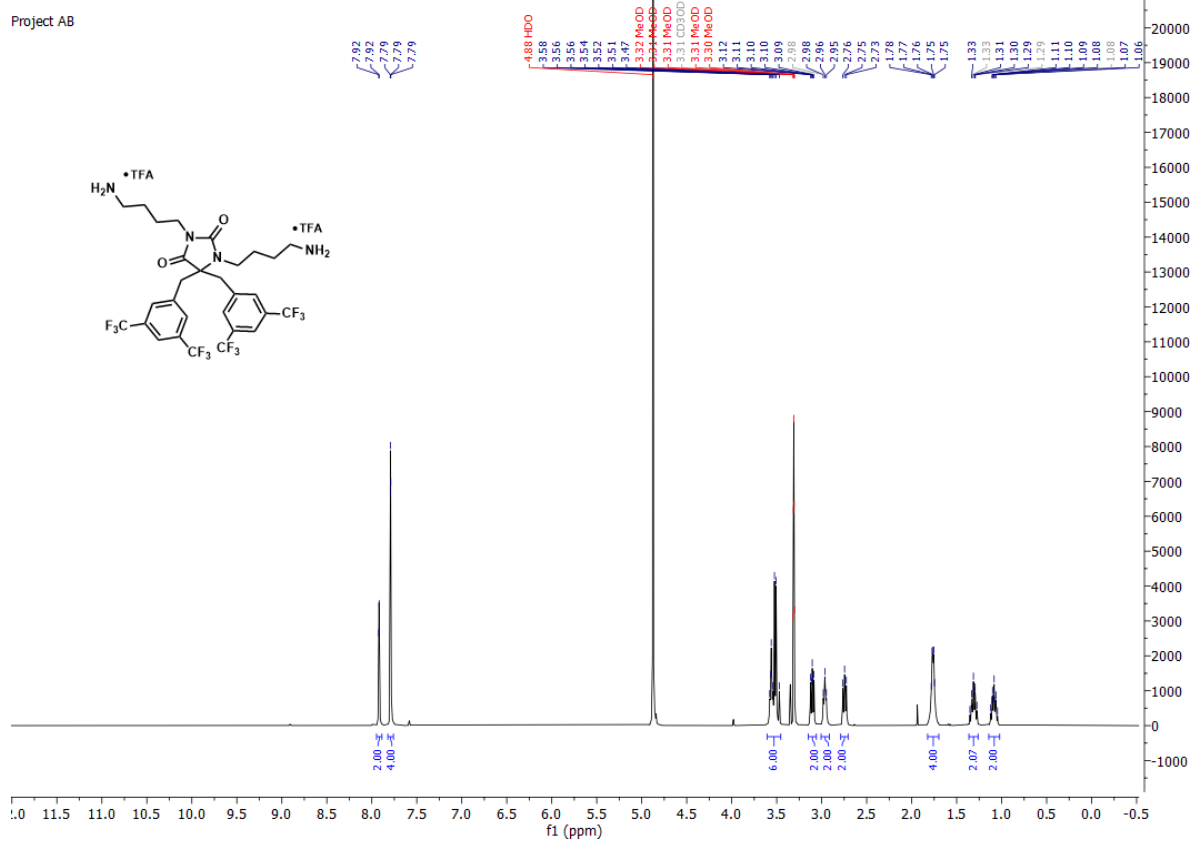


Project AB

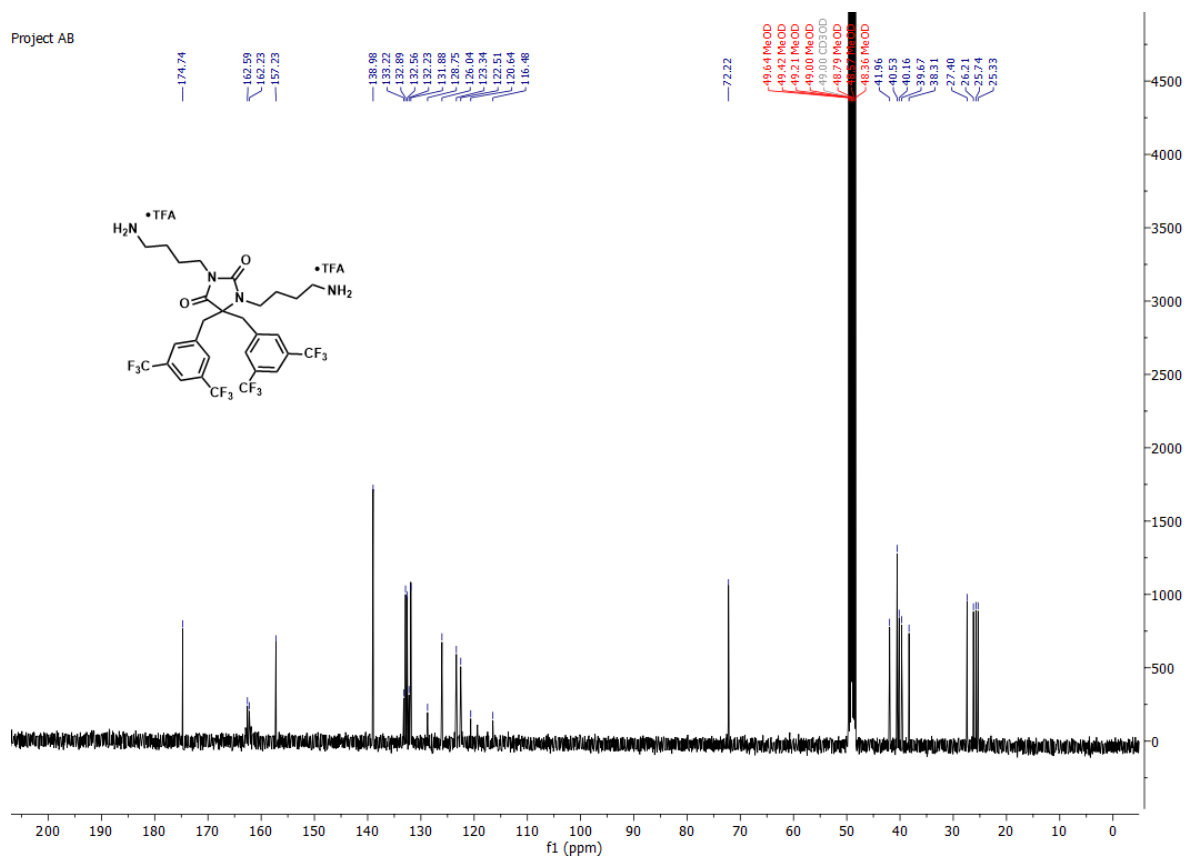


1,3-bis(4-aminobutyl)-5,5-bis(3,5-bis(trifluoromethyl)benzyl)imidazolidine-2,4-dione **6fA**.

Project AB



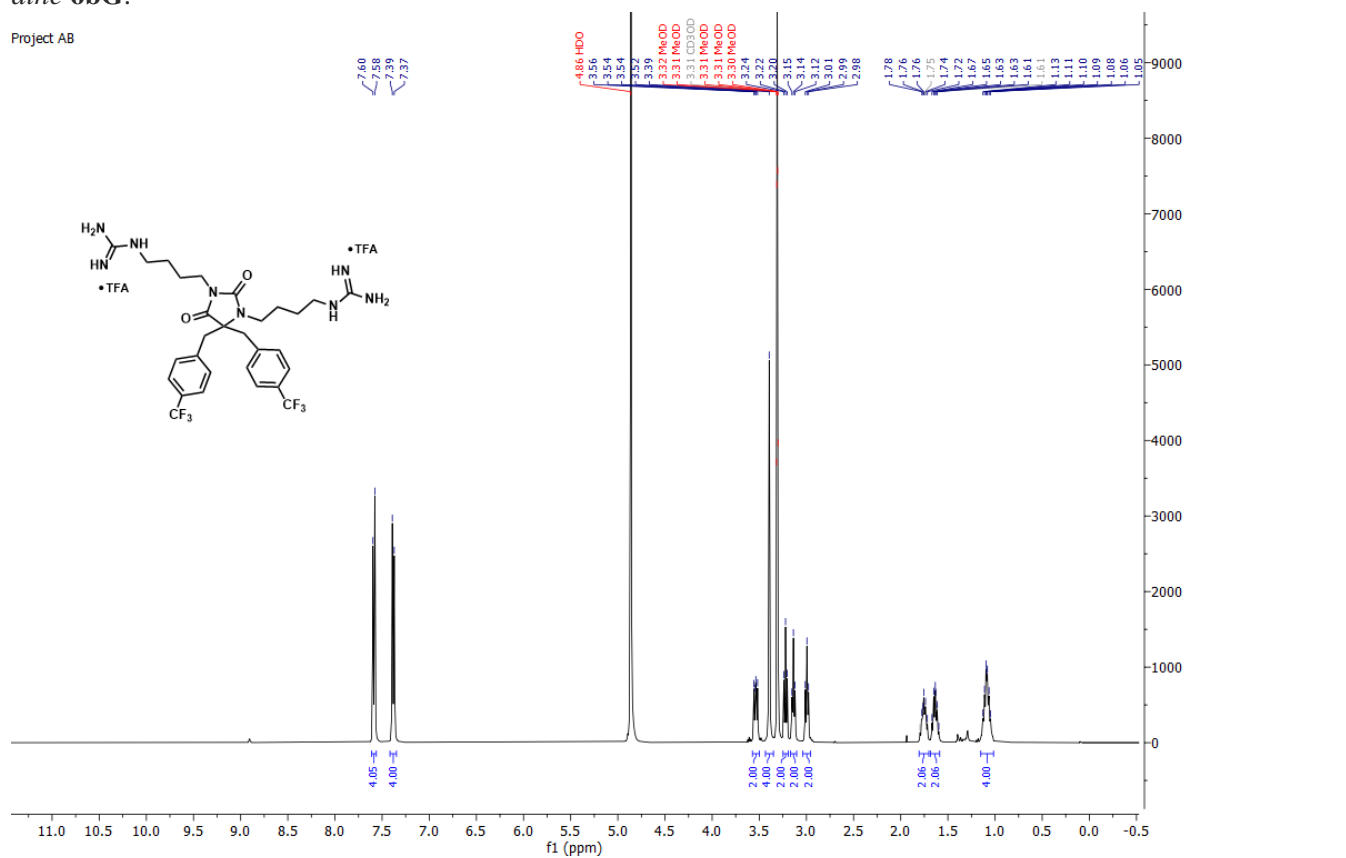
Project AB



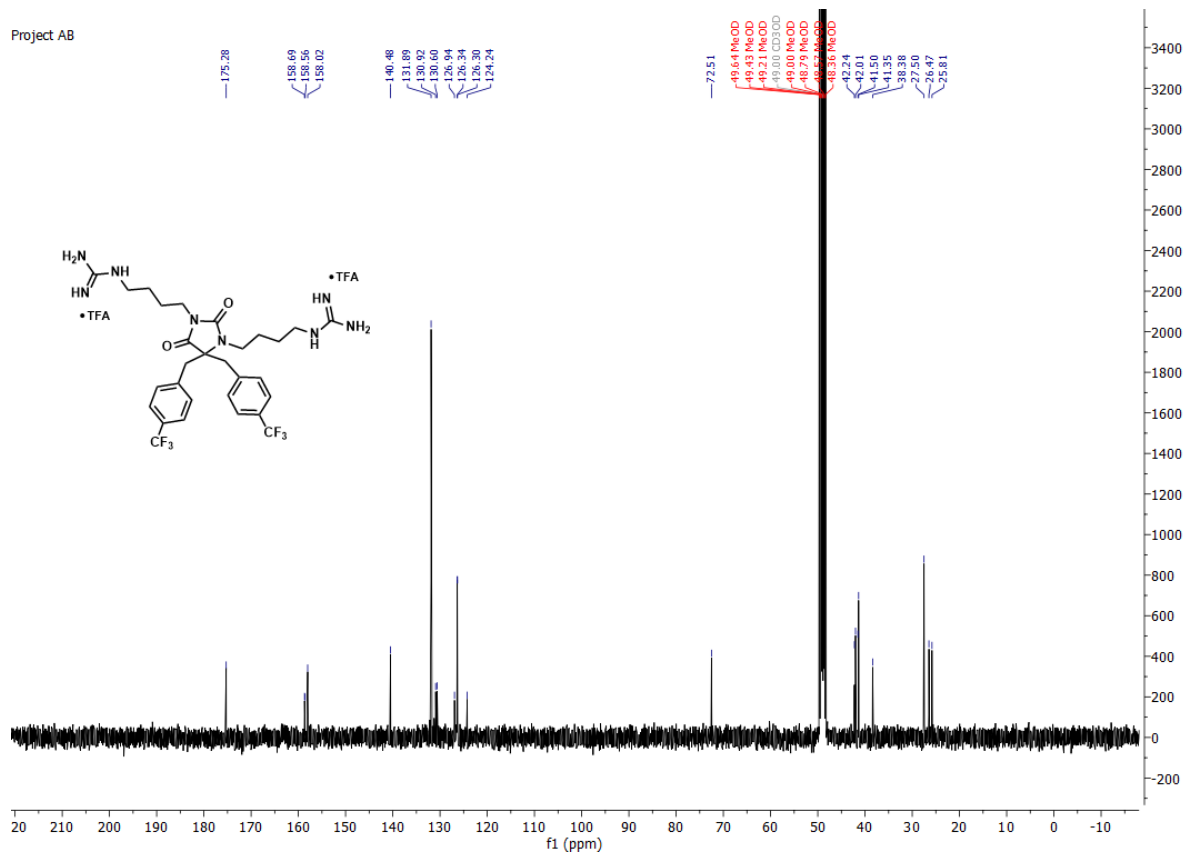
4.6 *N,N'*-dialkylated hydantoin 6G

1,1'-((2,5-dioxo-4,4-bis(4-(trifluoromethyl)benzyl)imidazolidine-1,3-diyl)bis(butane-4,1-diyl))diguanidine 6bG.

Project AB

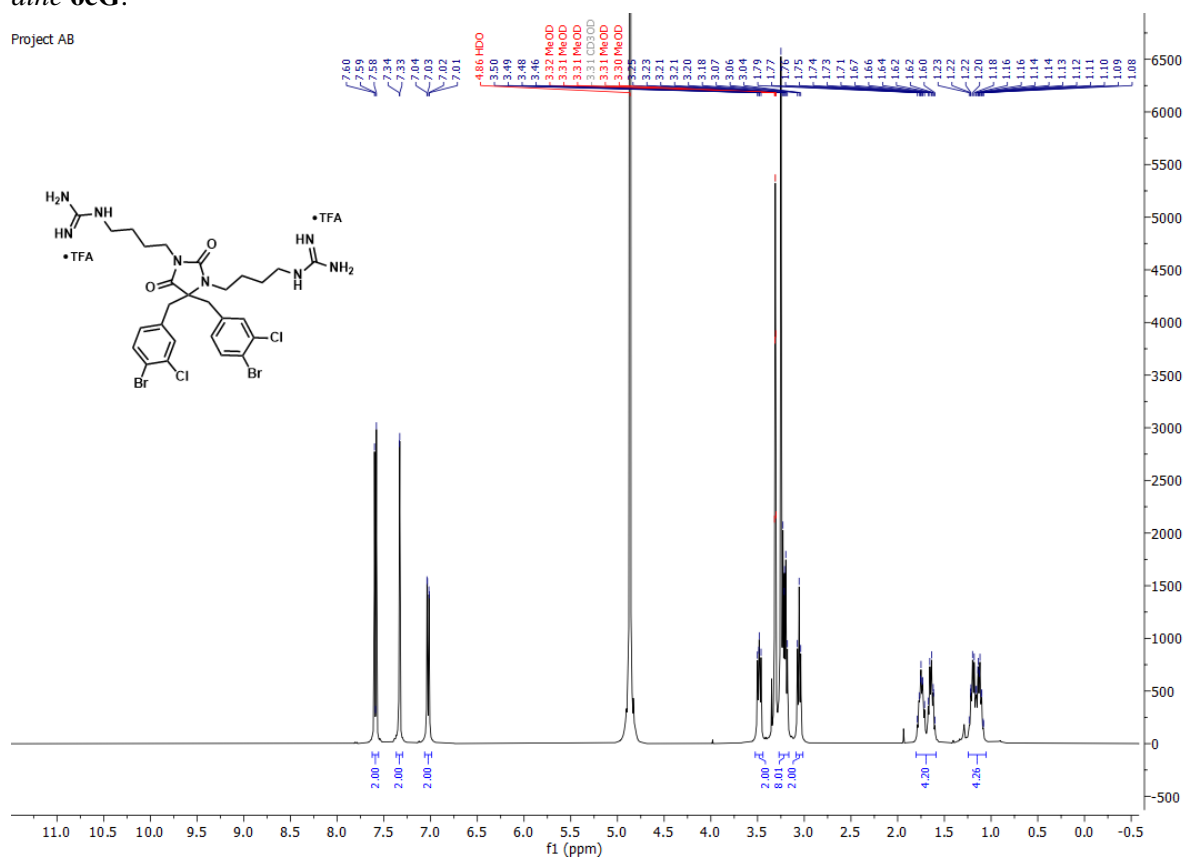


Project AB

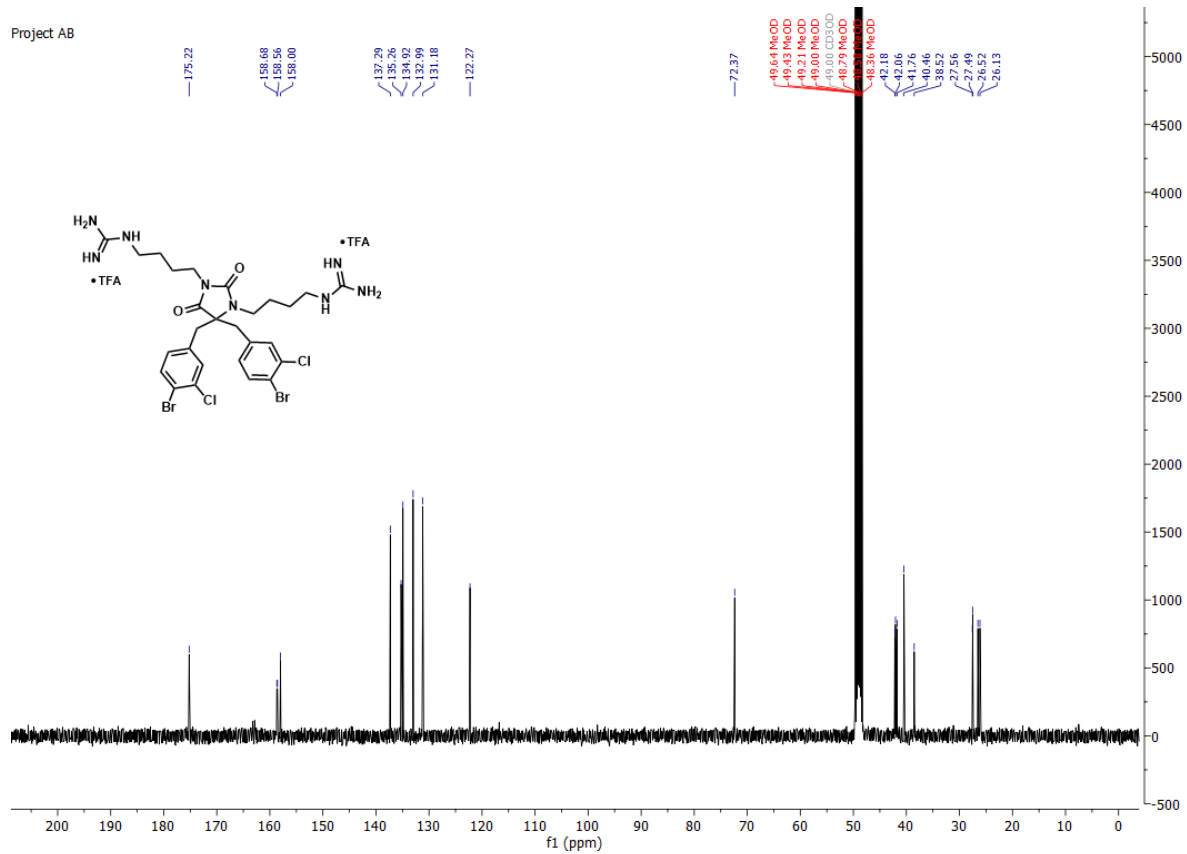


*1,1'-((4,4-bis(4-bromo-3-chlorobenzyl)-2,5-dioximidazolidine-1,3-diyl)bis(butane-4,1-diyl)diguani-
dine 6cG.*

Project AB

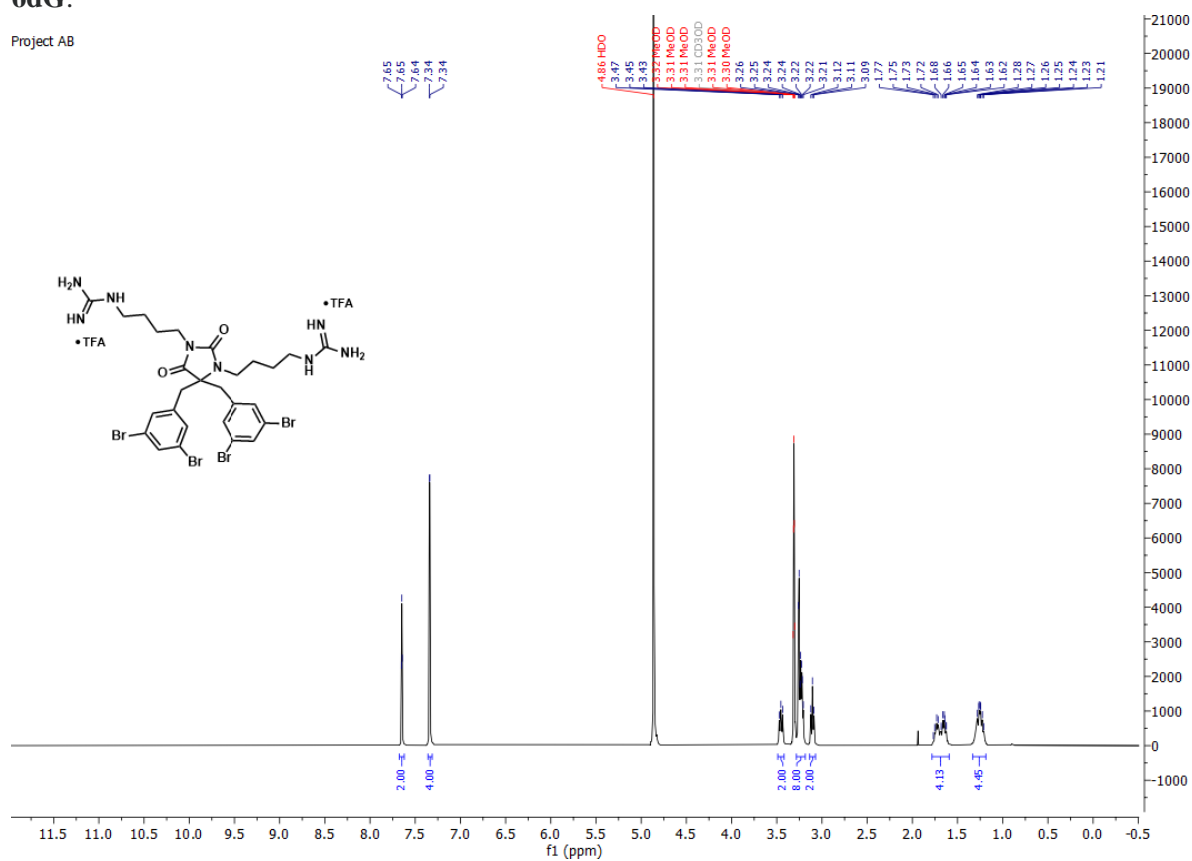


Project AB

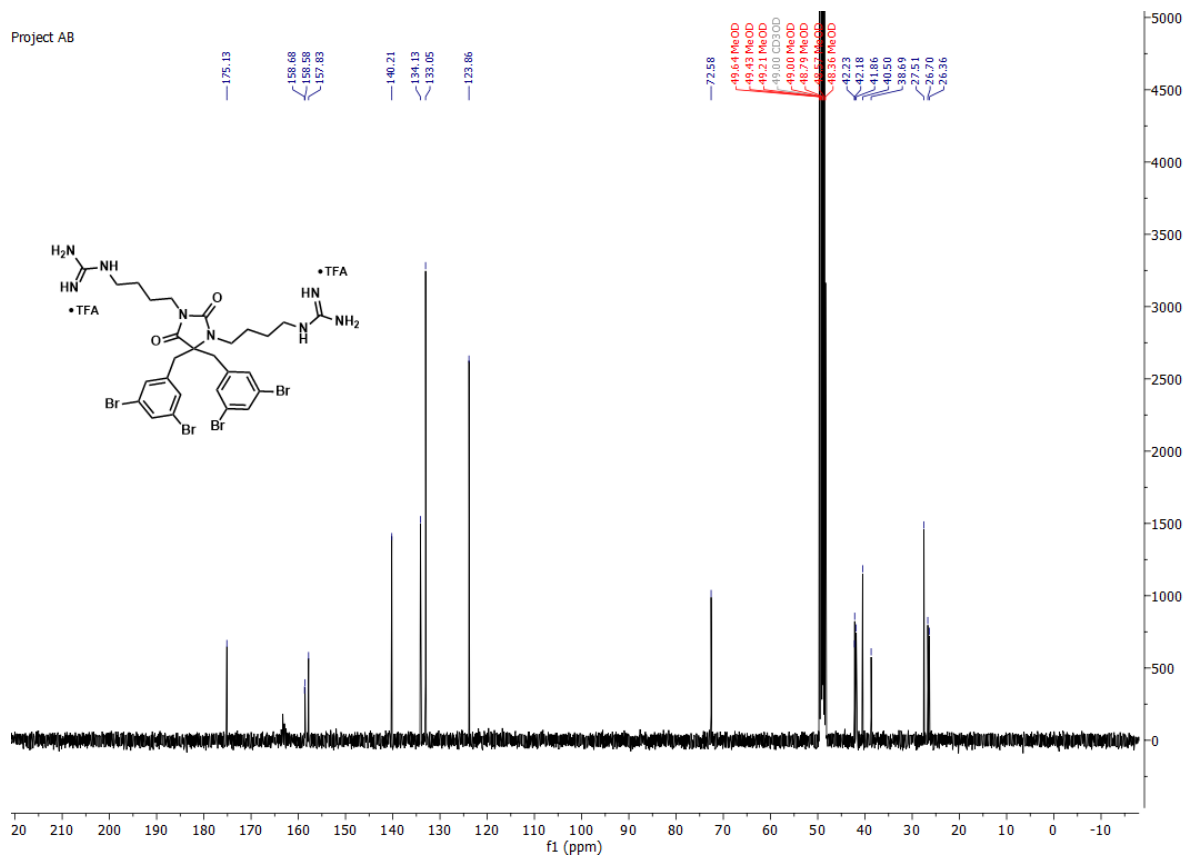


1,1'-(4,4-bis(3,5-dibromobenzyl)-2,5-dioximidazolidine-1,3-diyl)bis(butane-4,1-diyl)diguandine
6dG.

Project AB

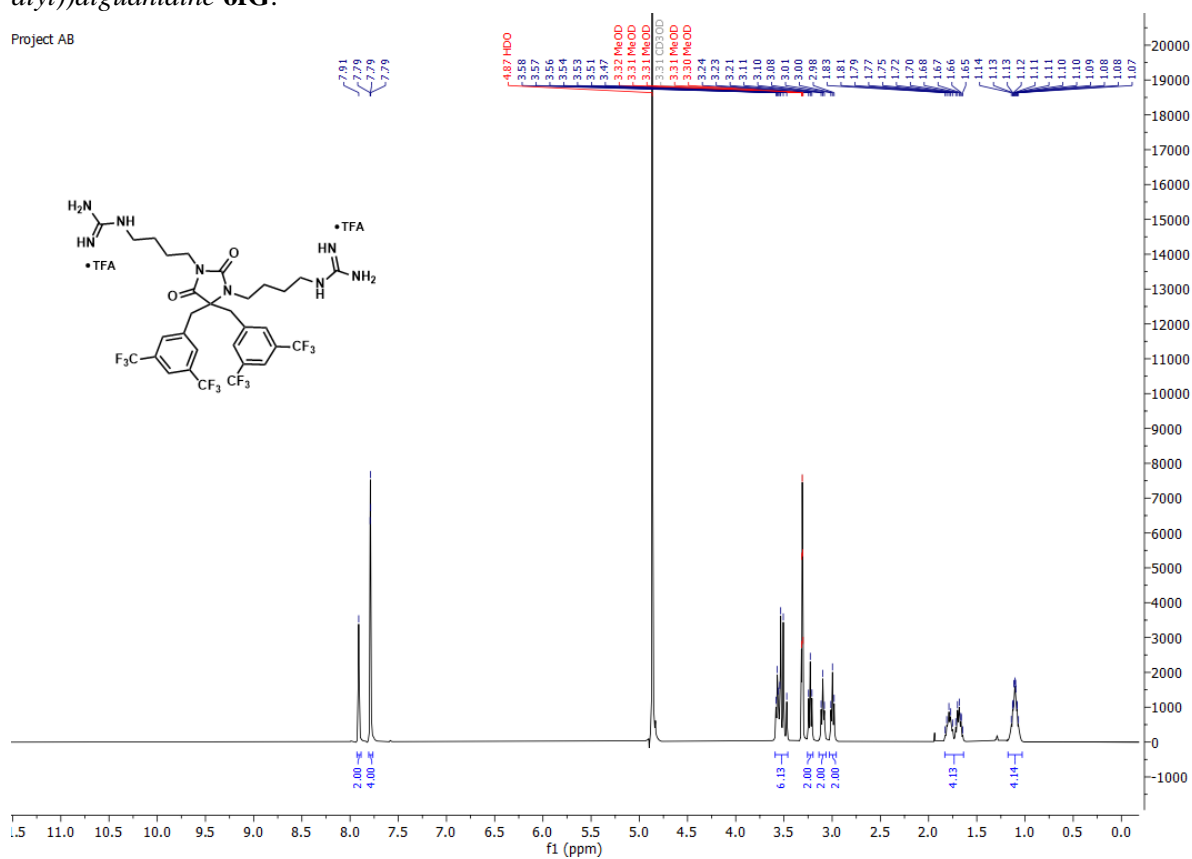


Project AB

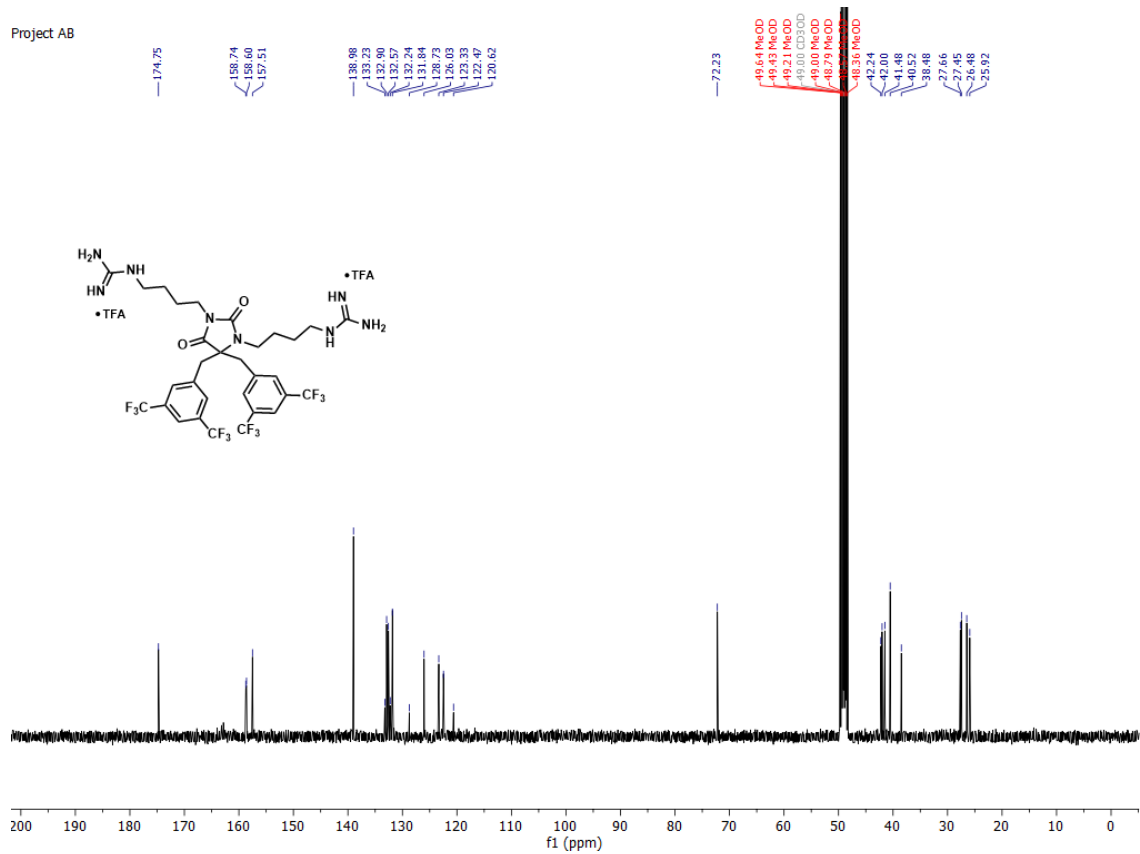


1,1'-((4,4-bis(3,5-bis(trifluoromethyl)benzyl)-2,5-dioximidazolidine-1,3-diyl)bis(butane-4,1-diyl))diguanidine 6fG.

Project AB



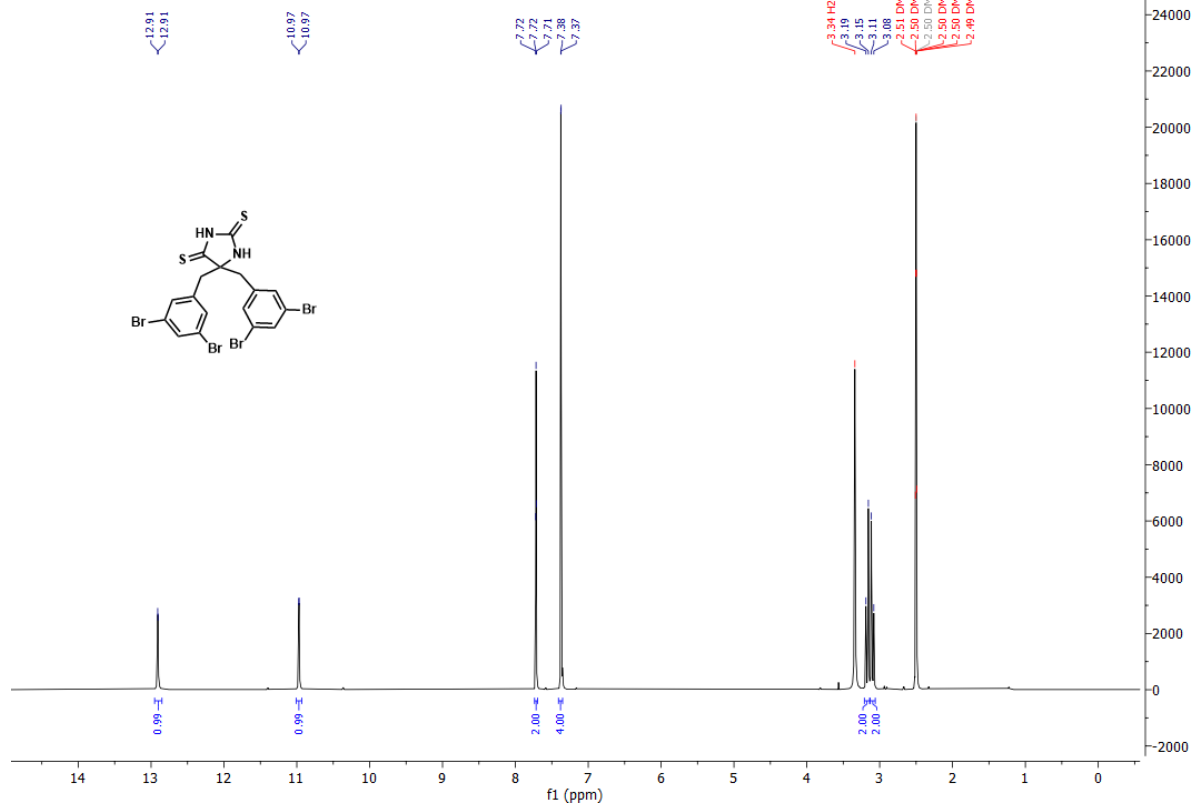
Project AB



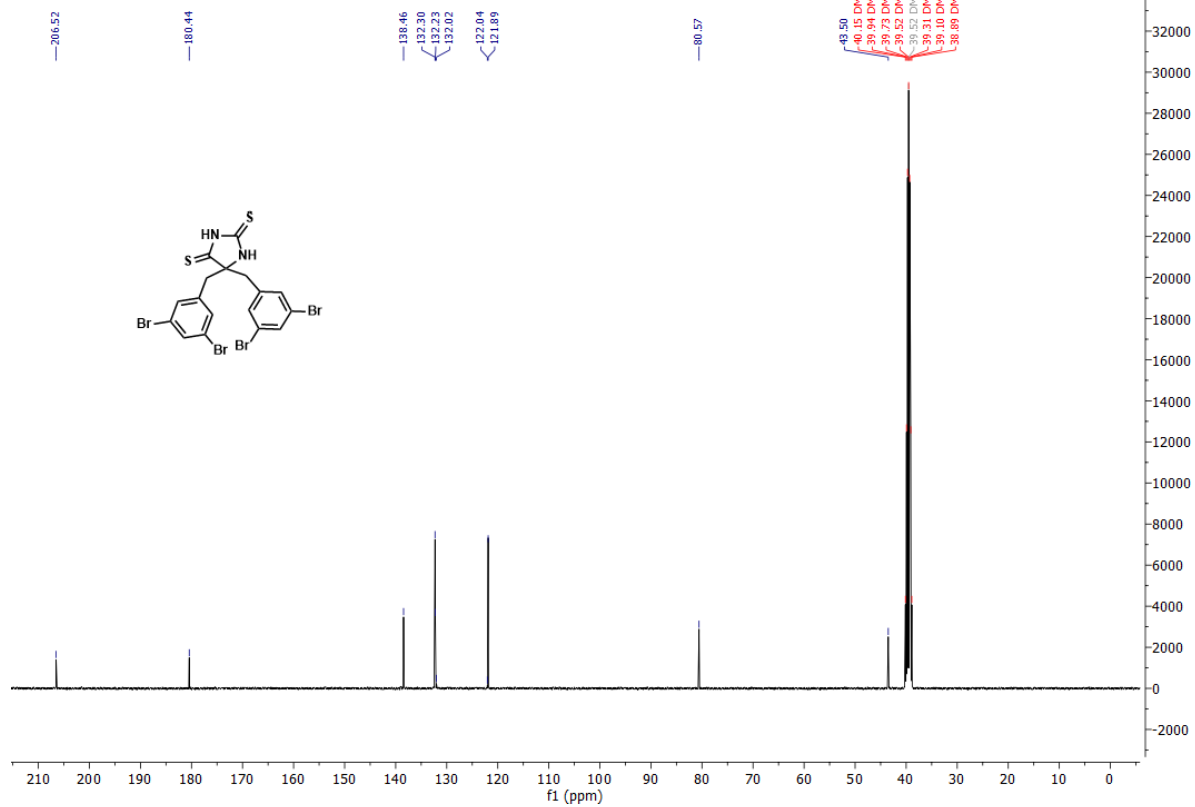
4.7 2,4-Dithiohydantoin core

5,5-bis(3,5-dibromobenzyl)imidazolidine-2,4-dithione **16**.

Project AB

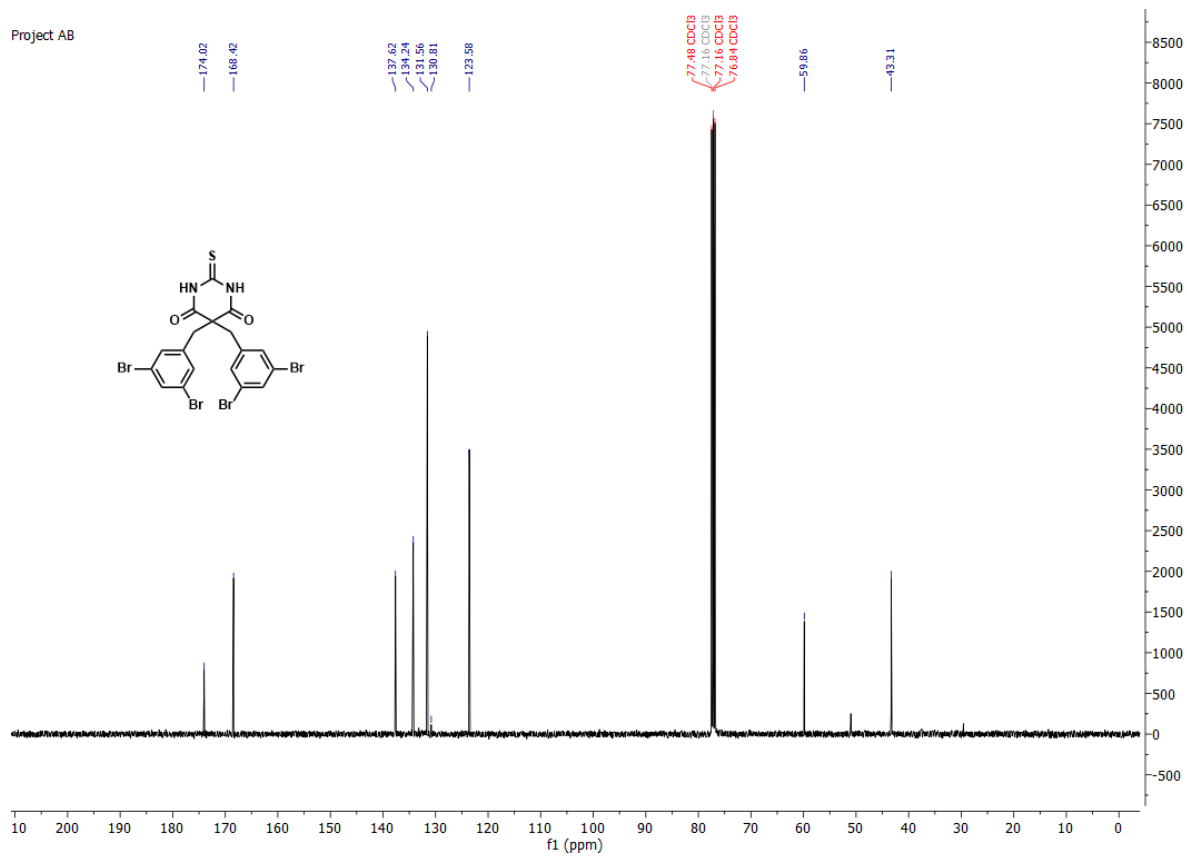
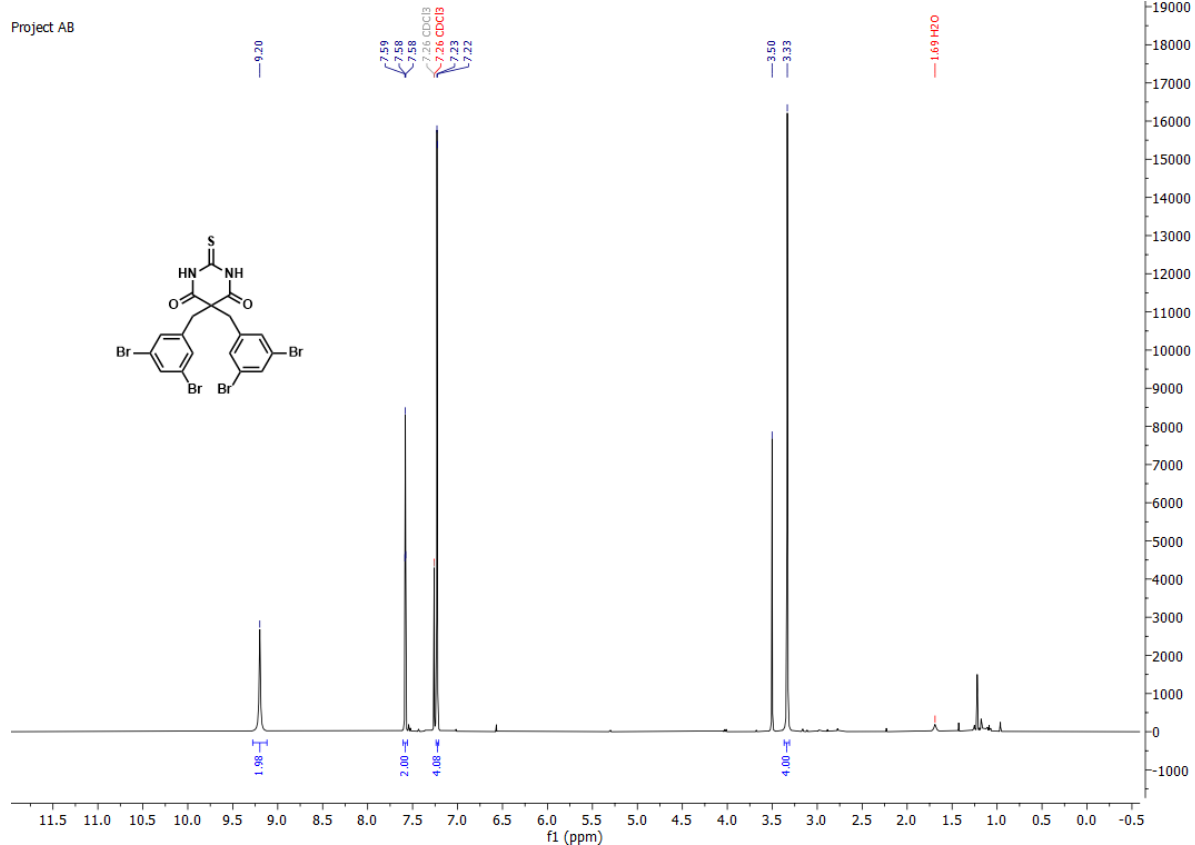


Project AB



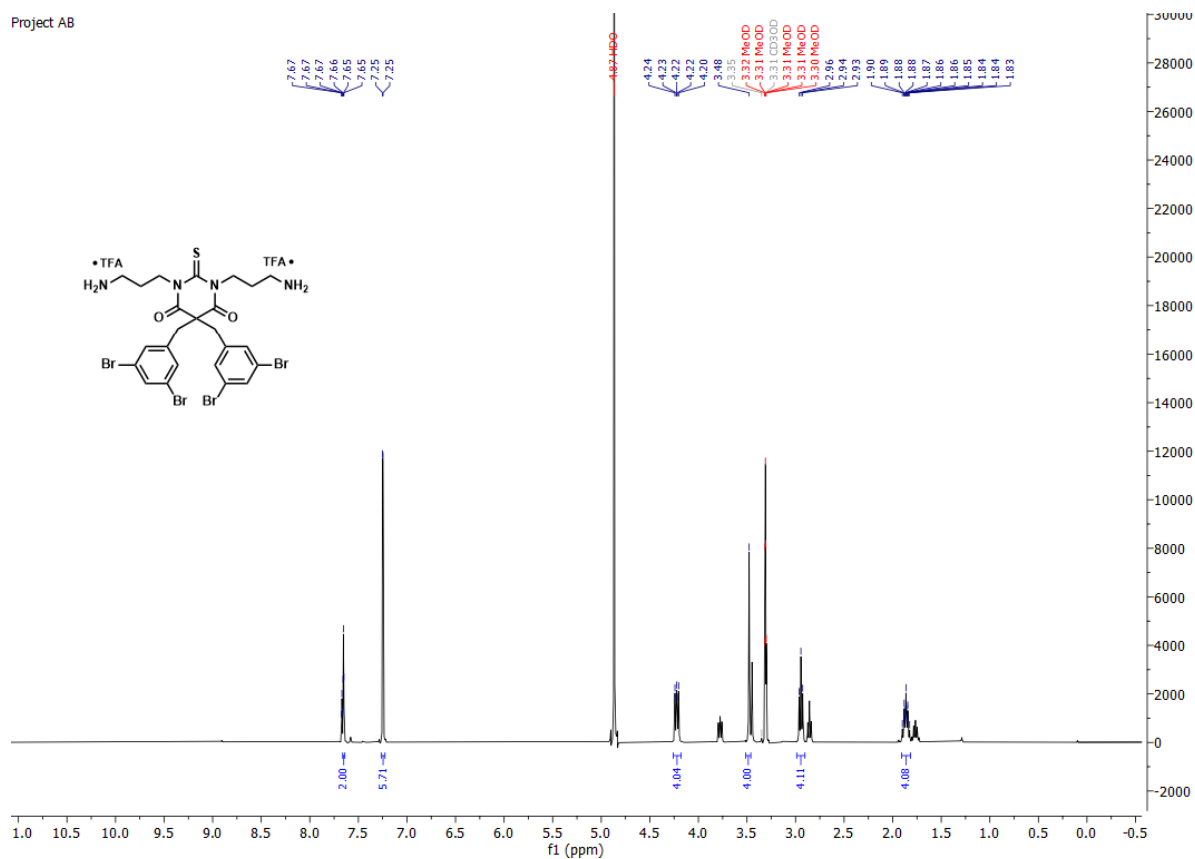
4.8 2-Thiobarbituric acid core

5,5-bis(3,5-dibromobenzyl)-2-thioxodihydropyrimidine-4,6(1H,5H)-dione **18**.

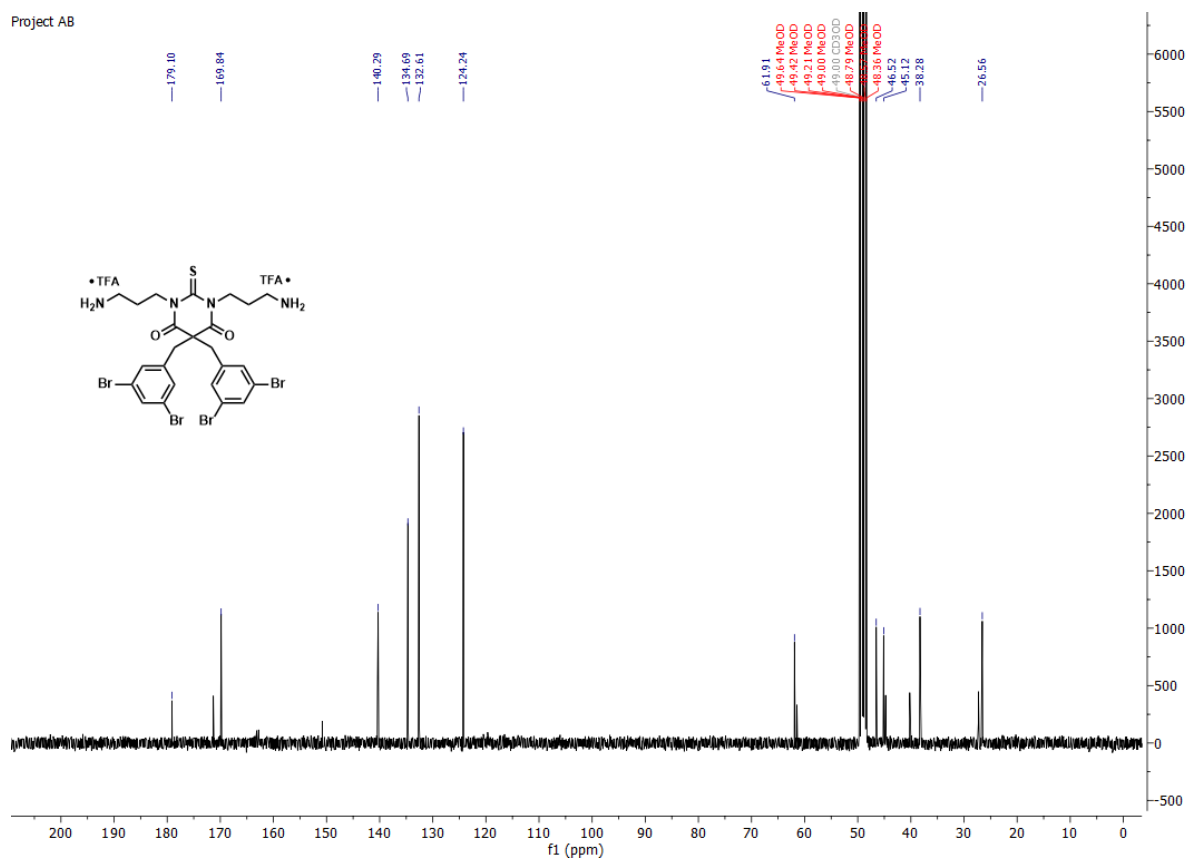


1,3-bis(3-aminopropyl)-5,5-bis(3,5-dibromobenzyl)-2-thioxodihydropyrimidine-4,6(1H,5H)-dione **5A**.

Project AB

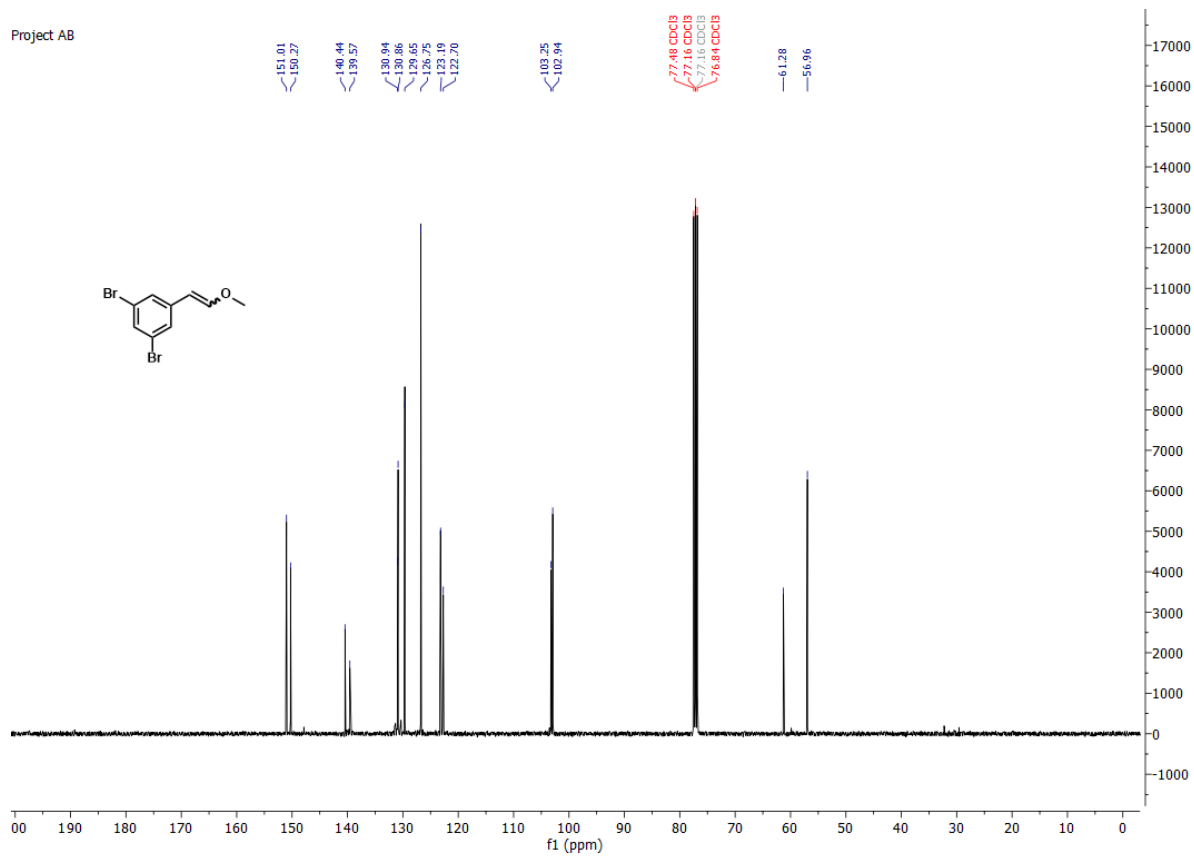
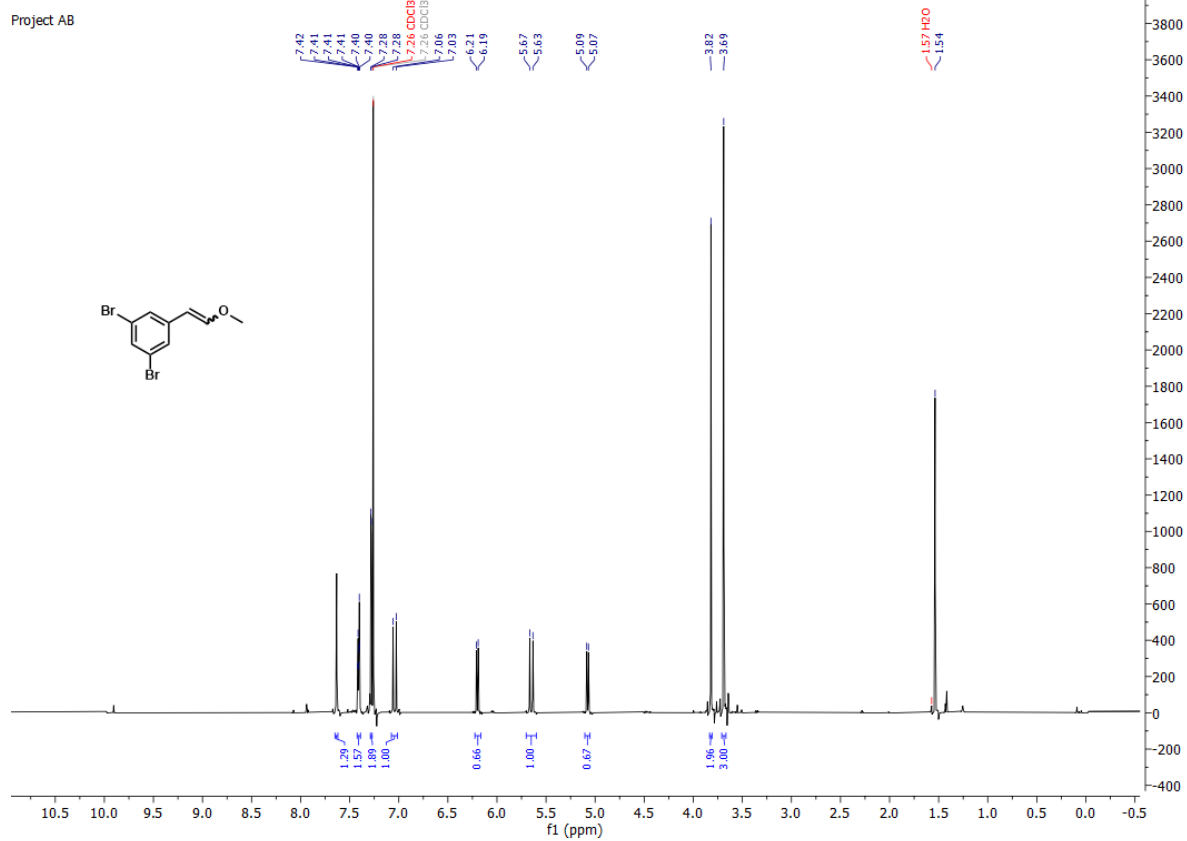


Project AB



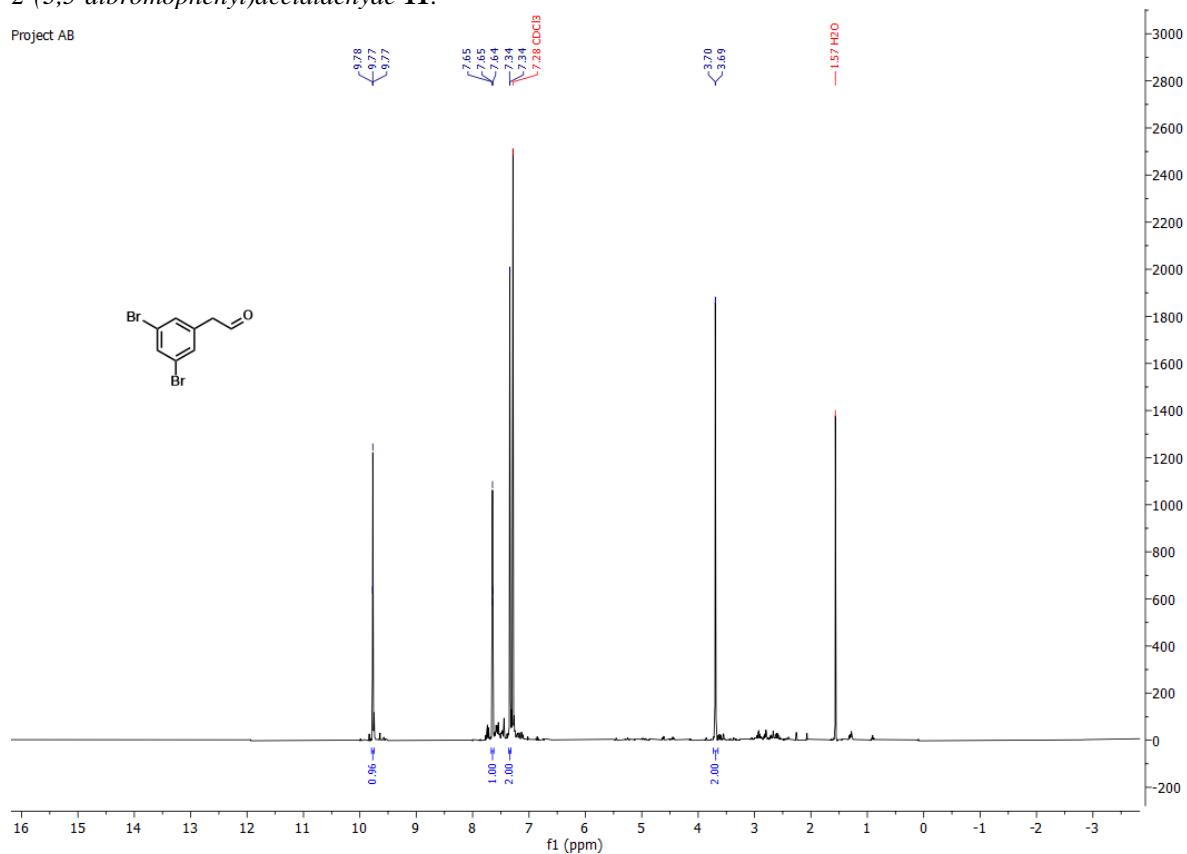
4.9 4-imidazolidin-2-one and its constitutional isomers

(E)/(Z)-1,3-dibromo-5-(2-methoxyvinyl)benzene **S9**.

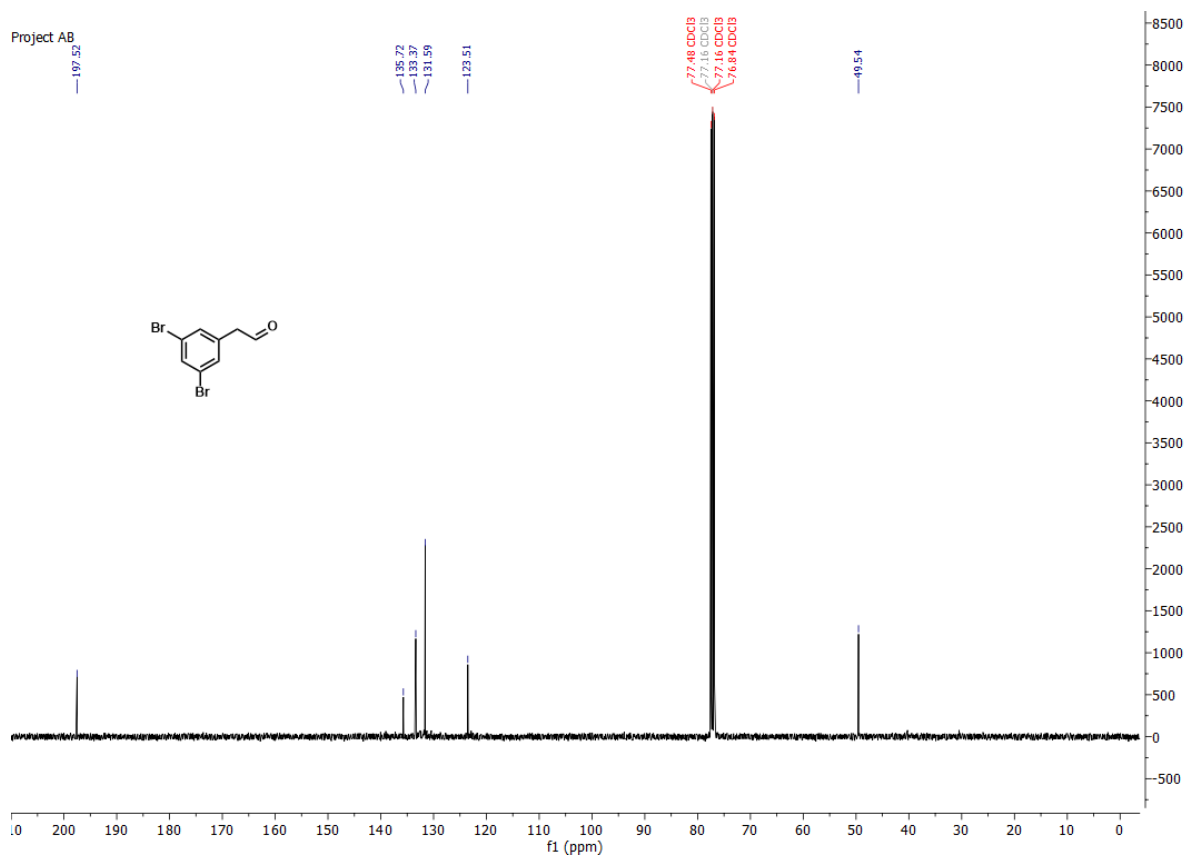


2-(3,5-dibromophenyl)acetaldehyde **11**.

Project AB

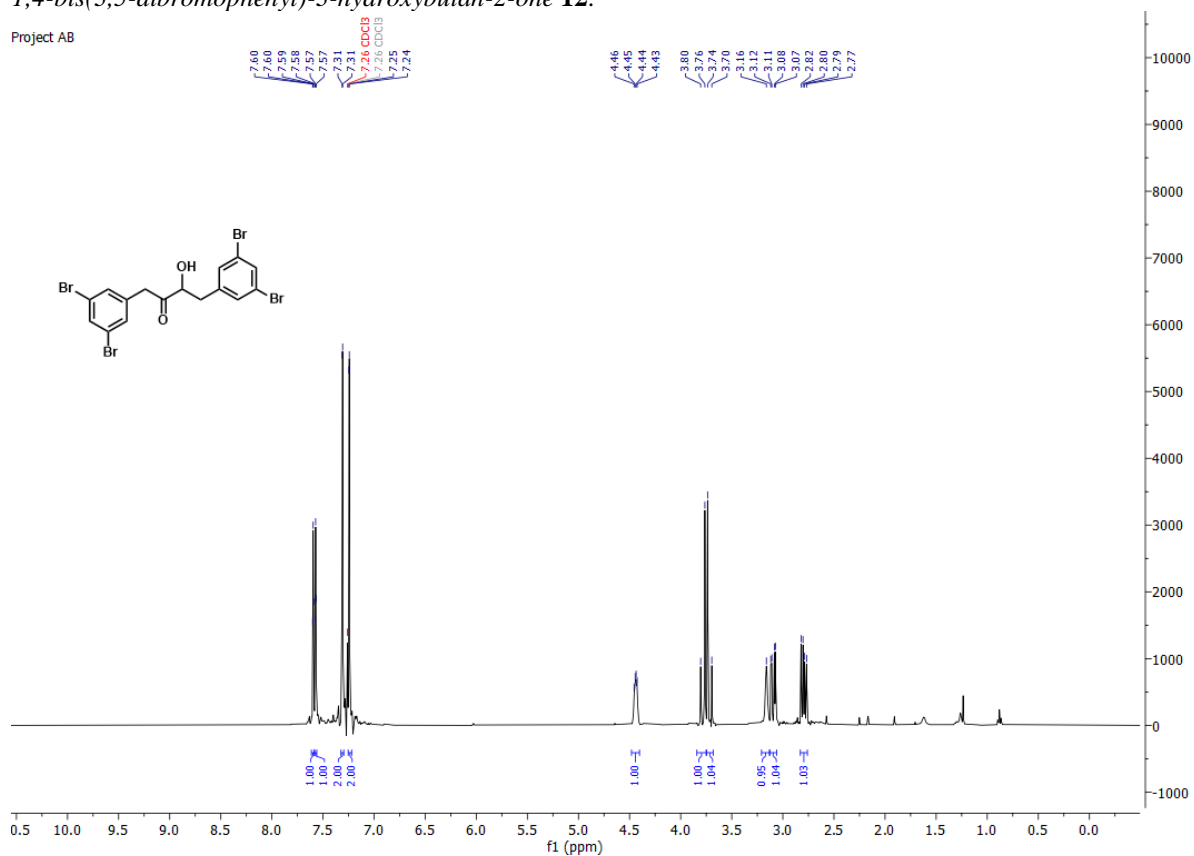


Project AB

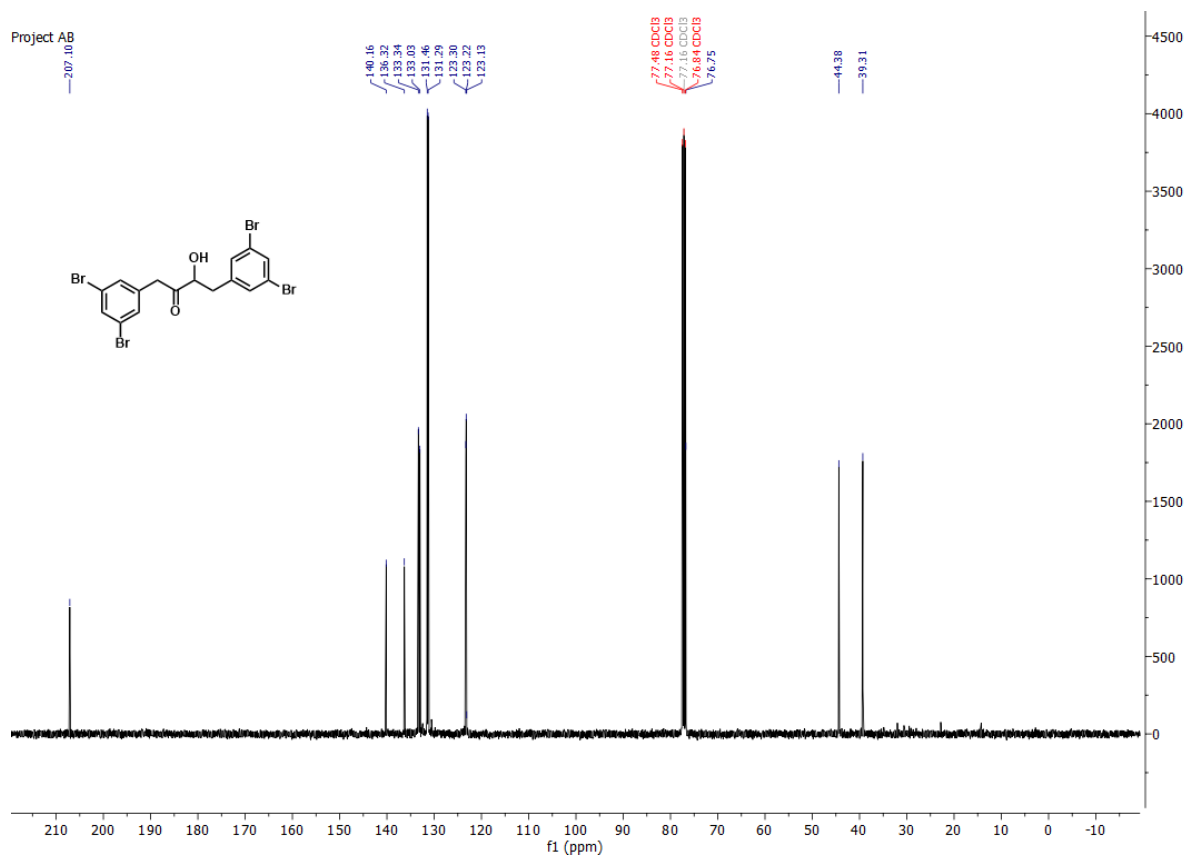


1,4-bis(3,5-dibromophenyl)-3-hydroxybutan-2-one **12**.

Project AB

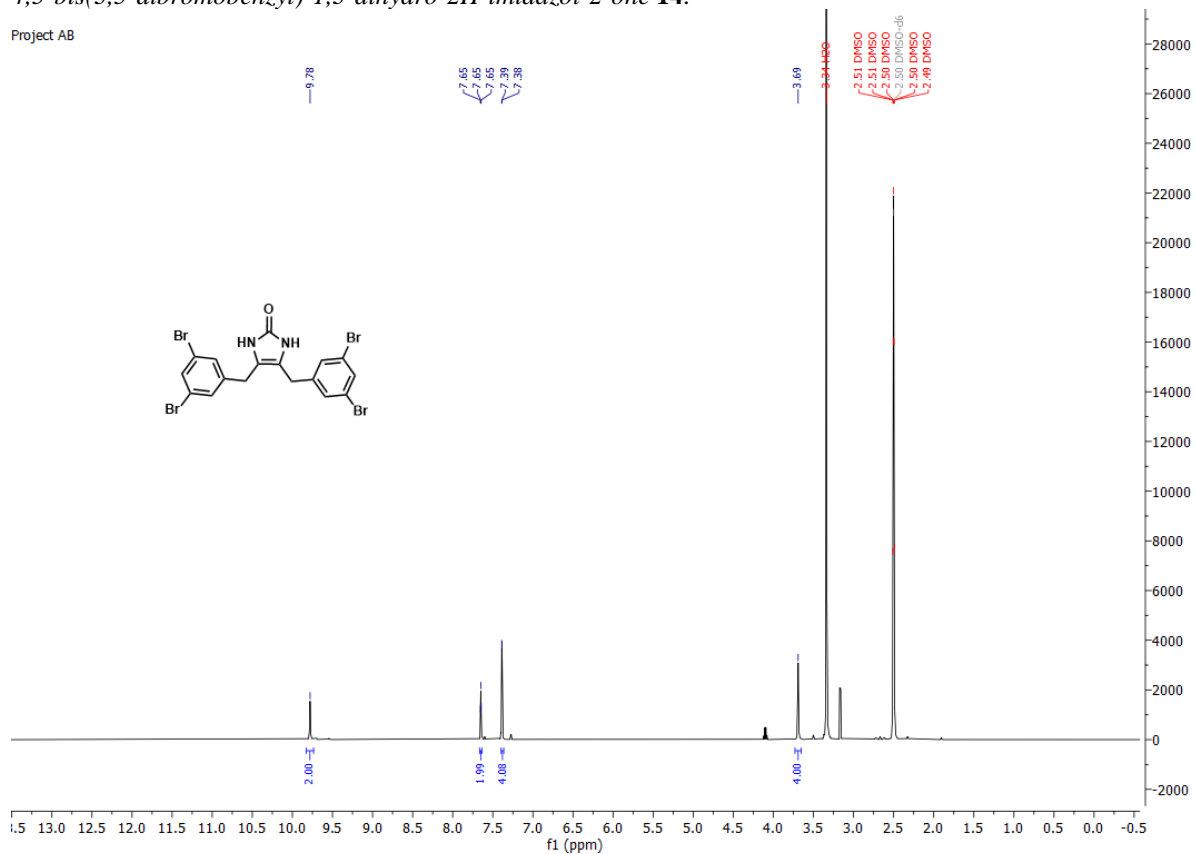


Project AB

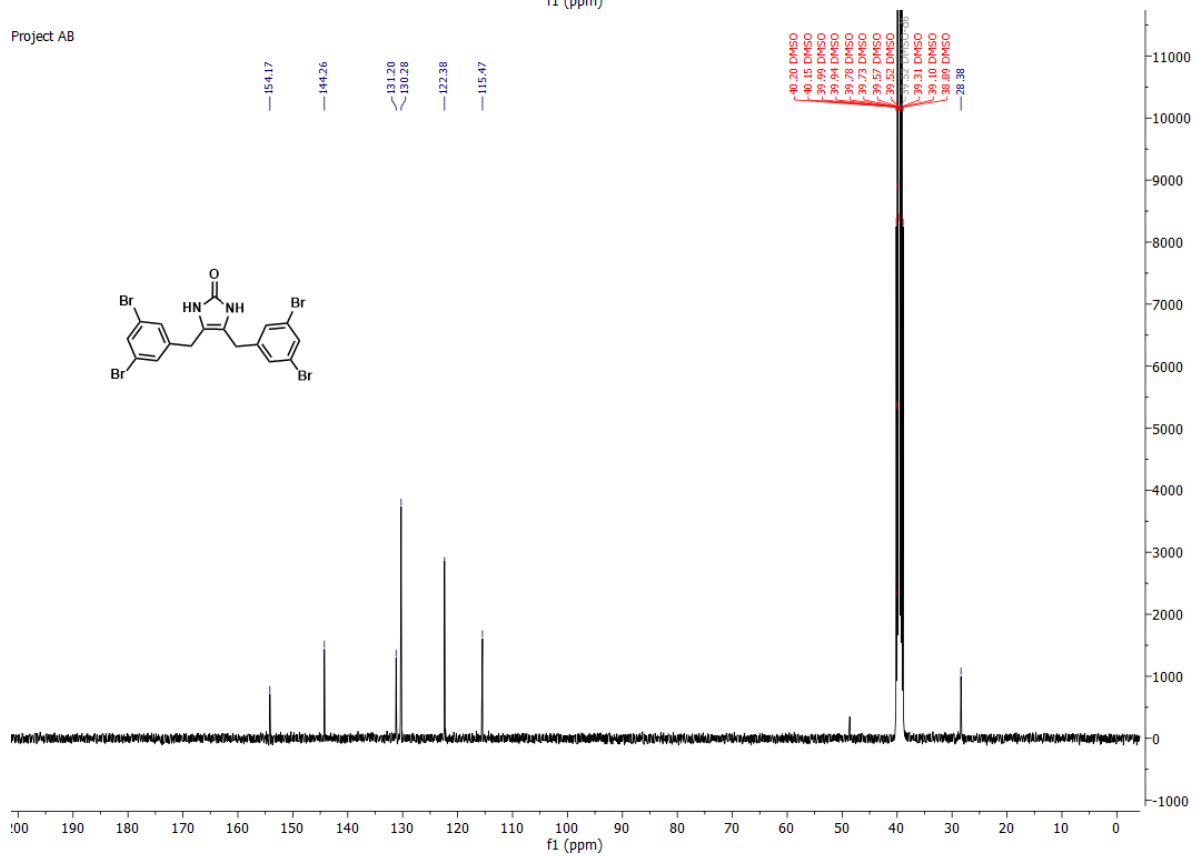


4,5-bis(3,5-dibromobenzyl)-1,3-dihydro-2H-imidazol-2-one **14**.

Project AB

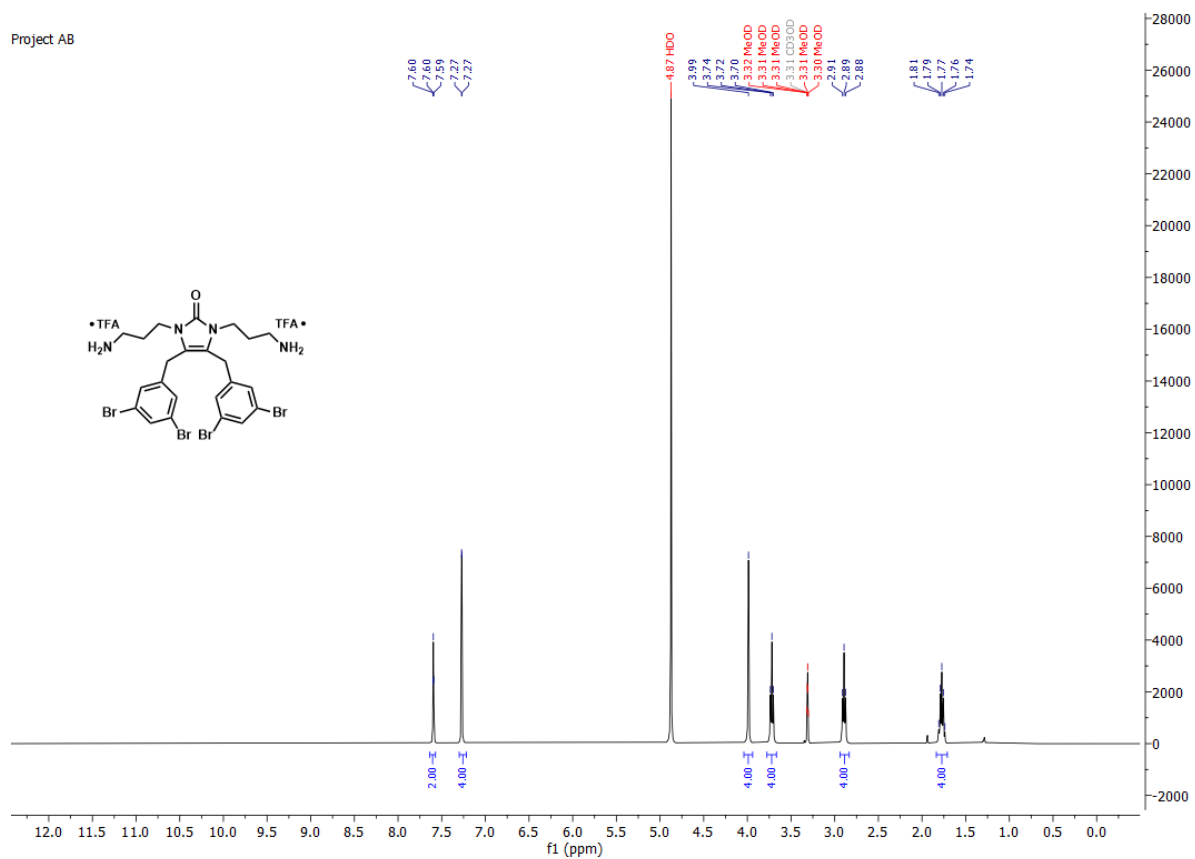


Project AB

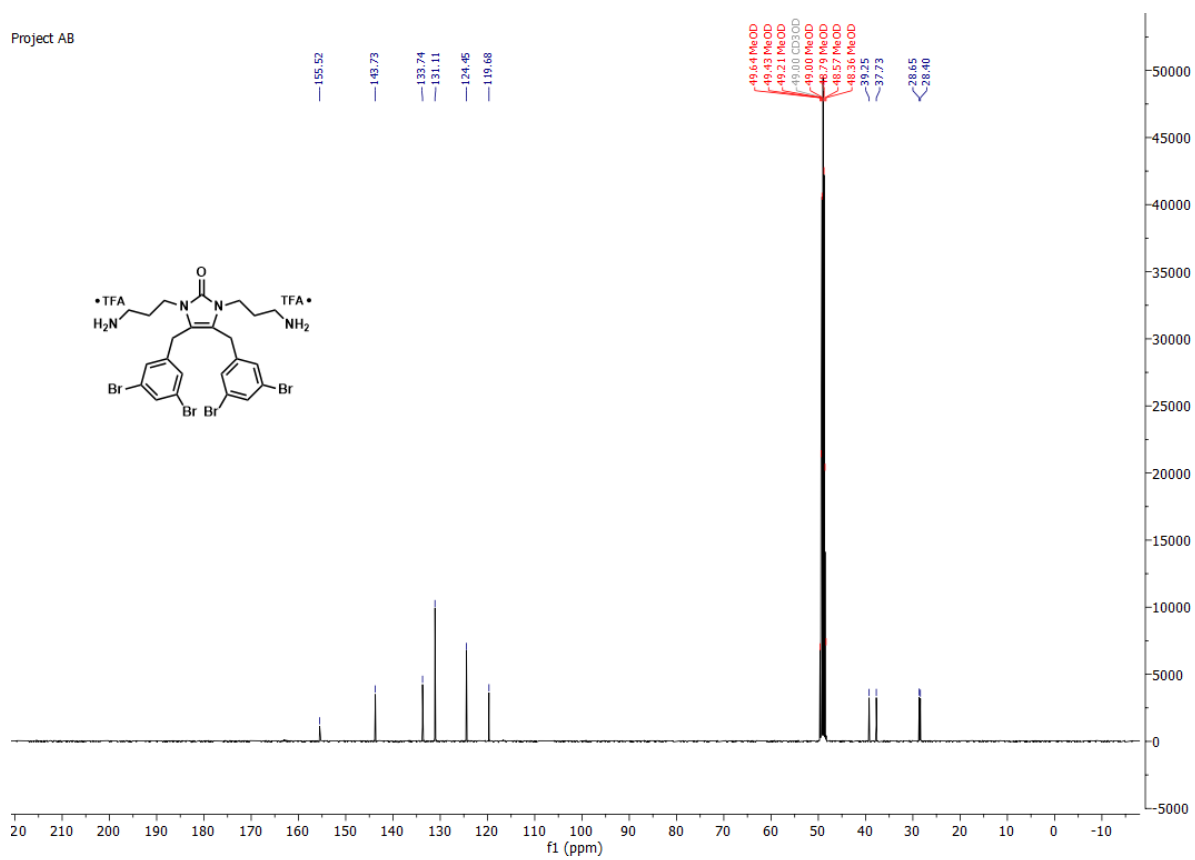


1,3-bis(3-aminopropyl)-4,5-bis(3,5-dibromobenzyl)-1,3-dihydro-2H-imidazol-2-one **3A**.

Project AB

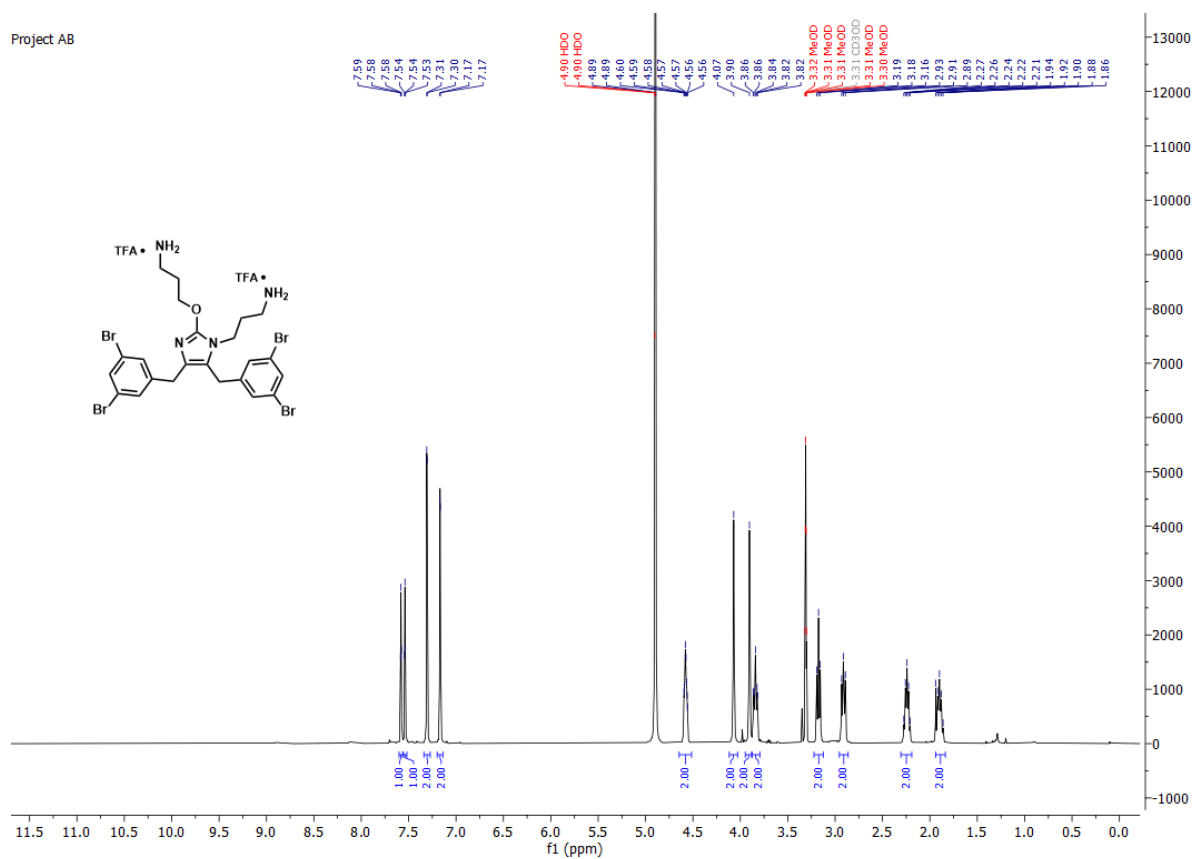


Project AB

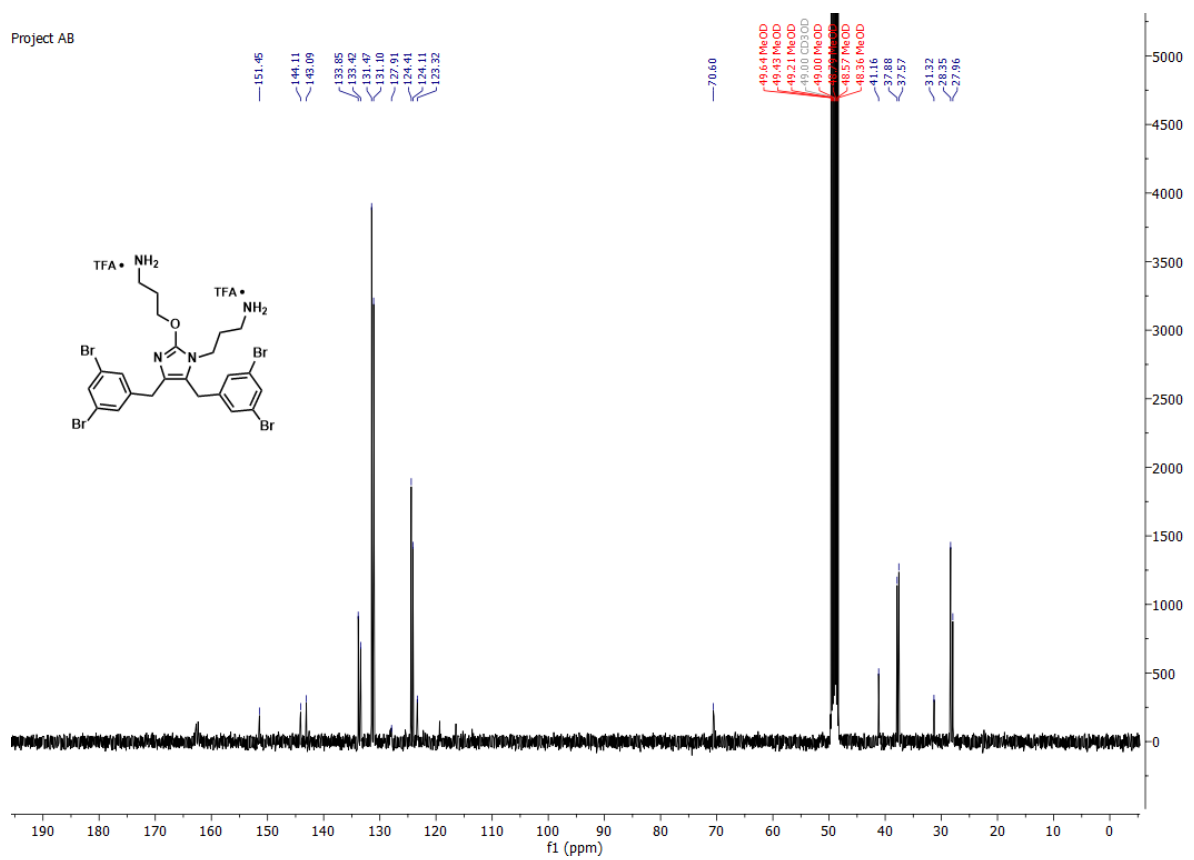


3-(2-(3-aminopropoxy)-4,5-bis(3,5-dibromobenzyl)-1H-imidazol-1-yl)propan-1-amine **15A**.

Project AB

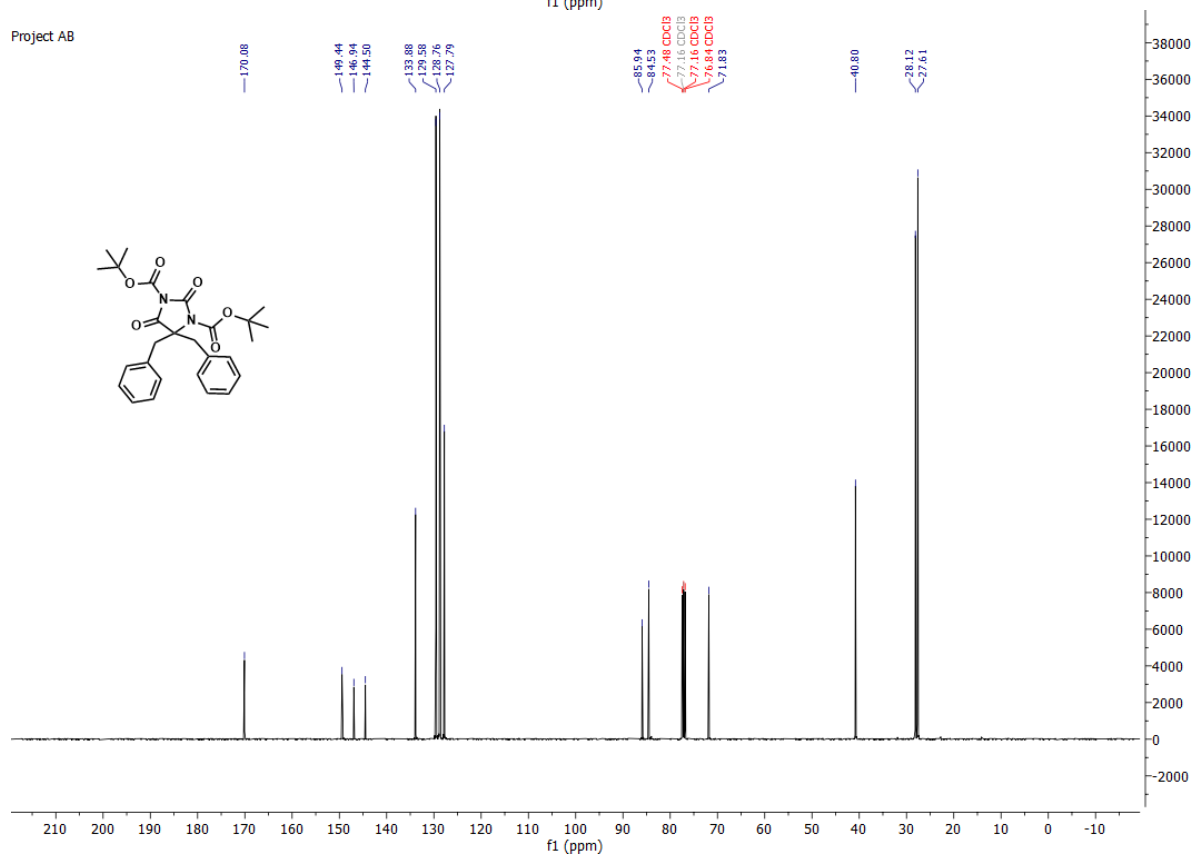
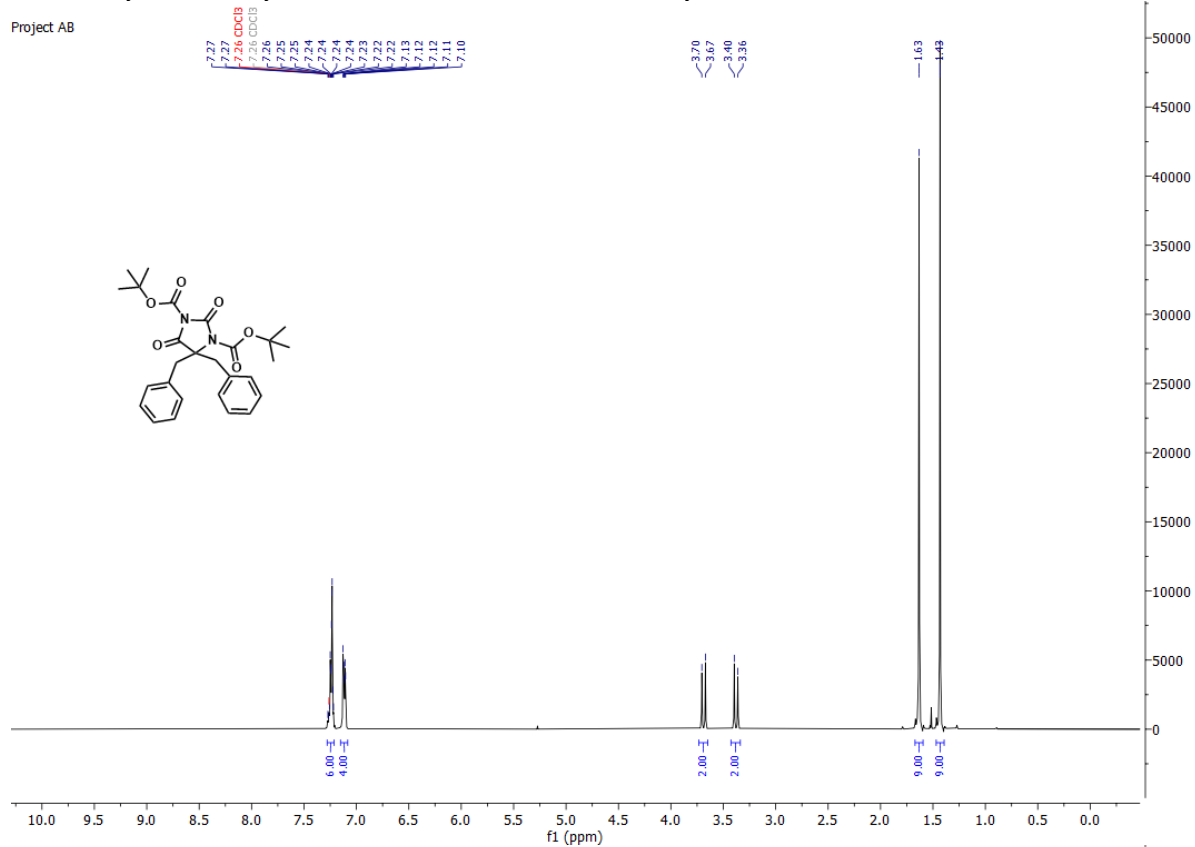


Project AB

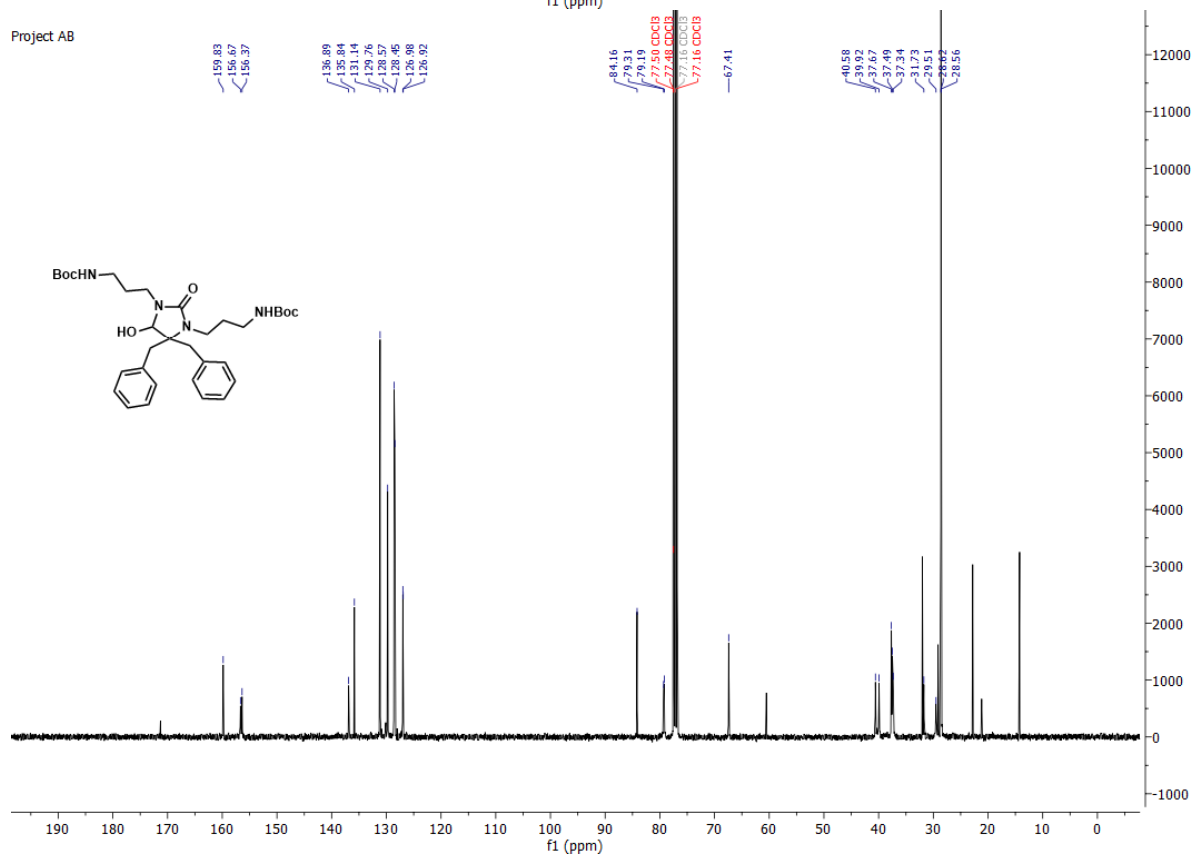
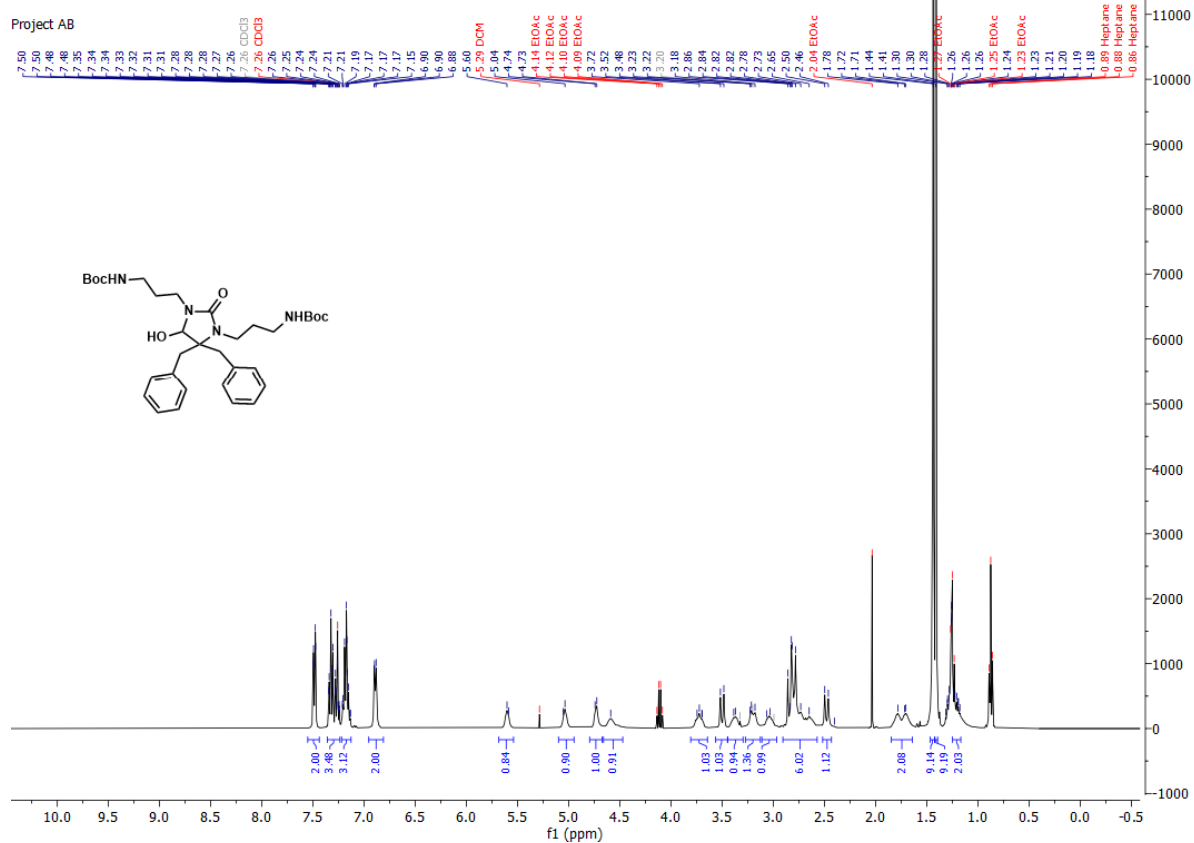


4.10 4-imidazolidin-2-one via *N*-acyliminium ion rearrangement

Di-tert-butyl 4,4-dibenzyl-2,5-dioxoimidazolidine-1,3-dicarboxylate Boc-**9a**.

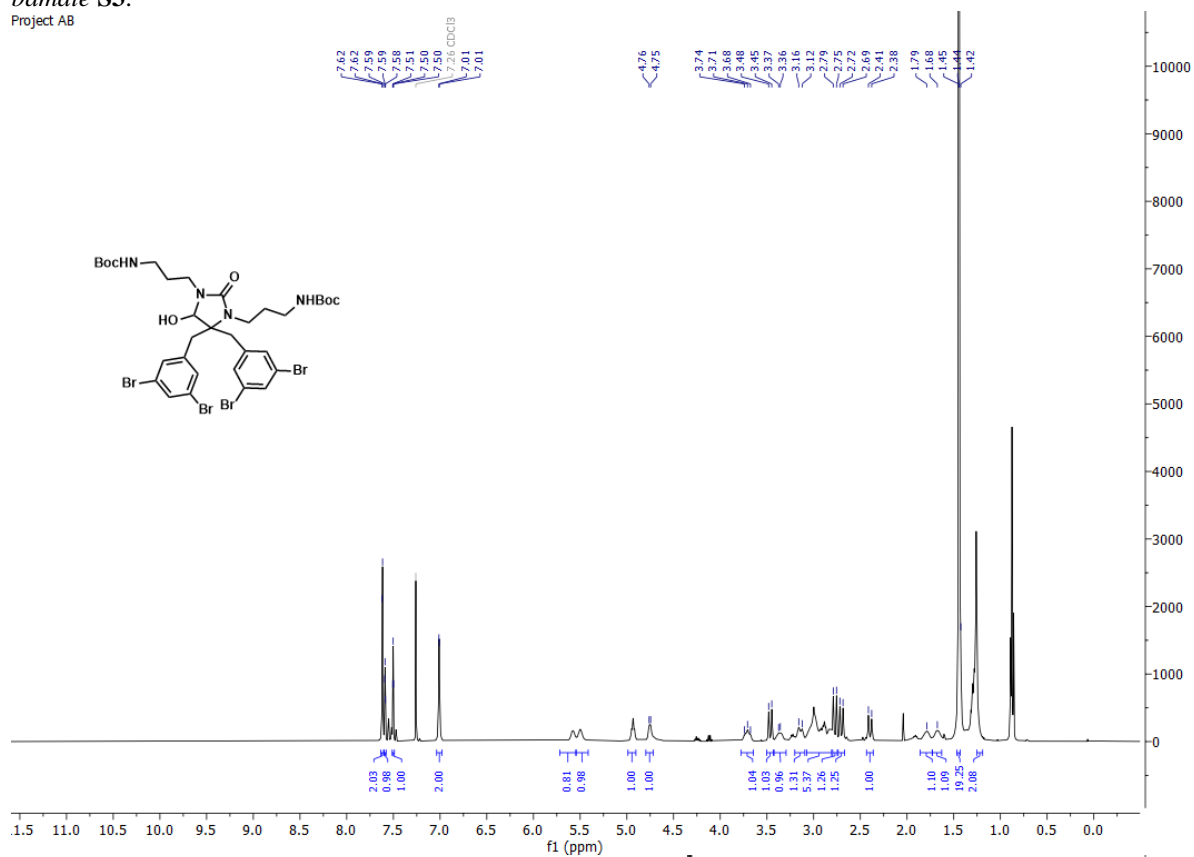


Di-tert-butyl ((4,4-dibenzyl-5-hydroxy-2-oxoimidazolidine-1,3-diyl)bis(propane-3,1-diyl)dicarbamate S2.

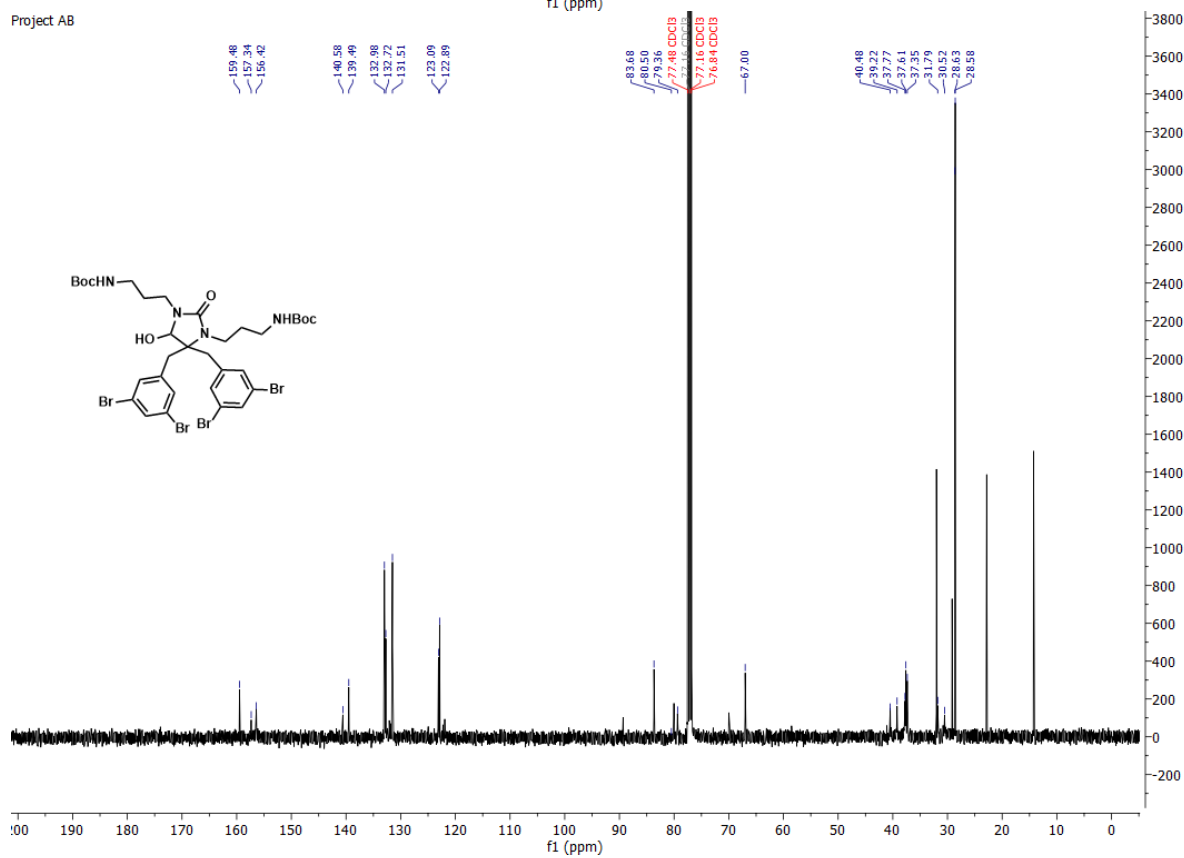


Di-tert-butyl ((4,4-bis(3,5-dibromobenzyl)-5-hydroxy-2-oximidazolidine-1,3-diyl)bis(propane-3,1-diyl)dicarbamate S3.

Project AB

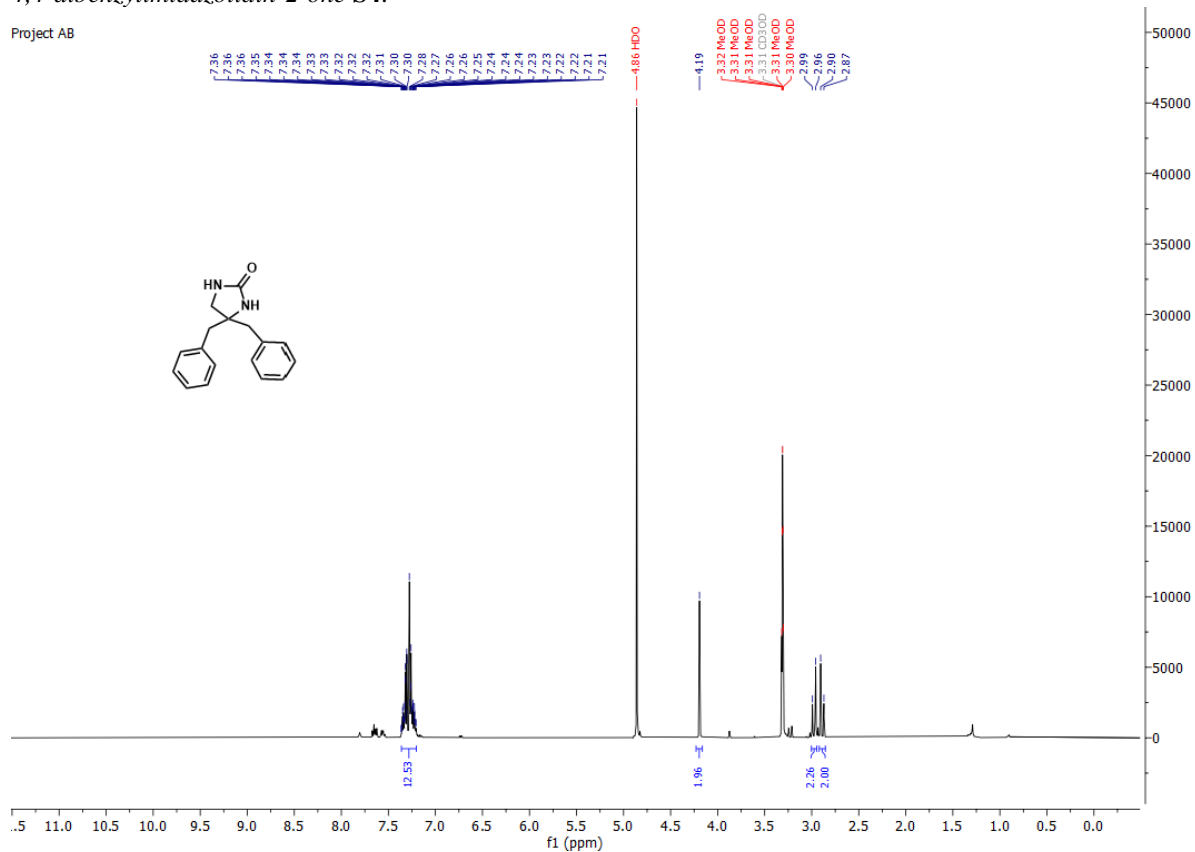


Project AB

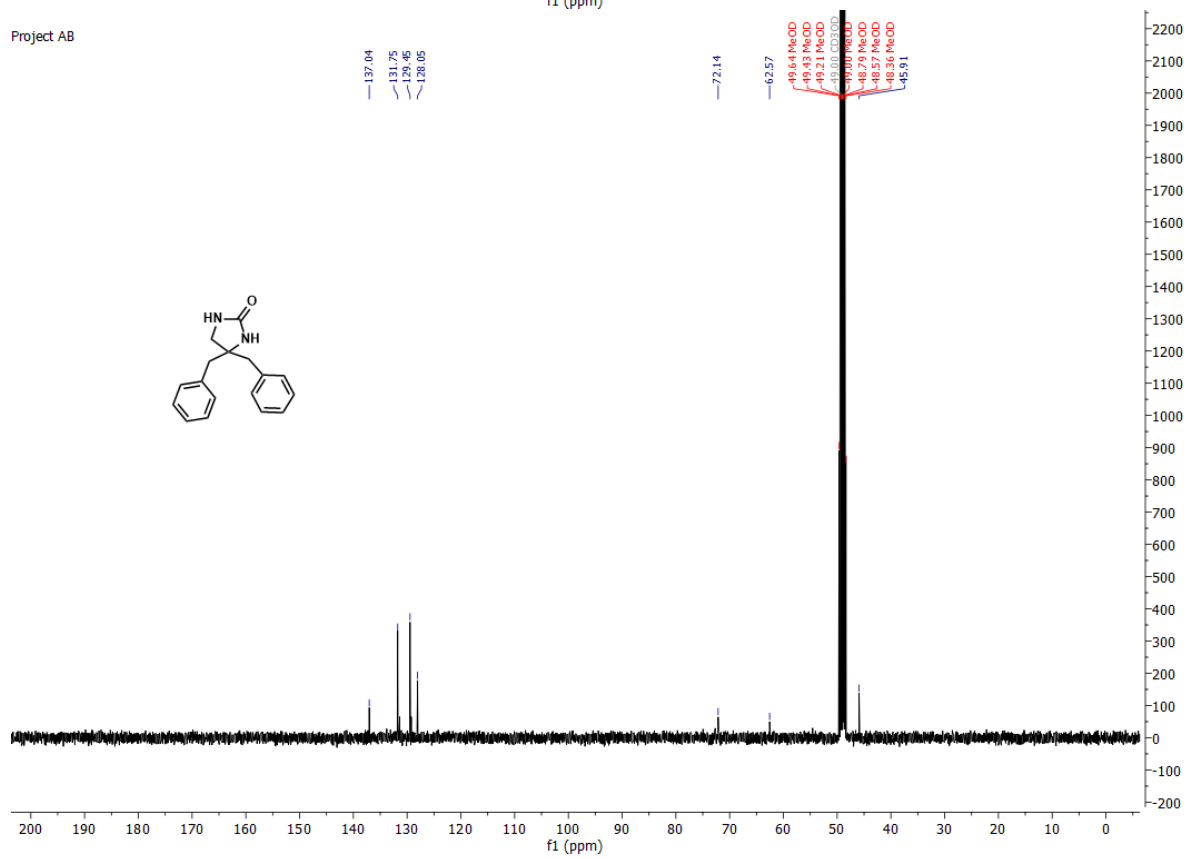


4,4-dibenzylimidazolidin-2-one S4.

Project AB

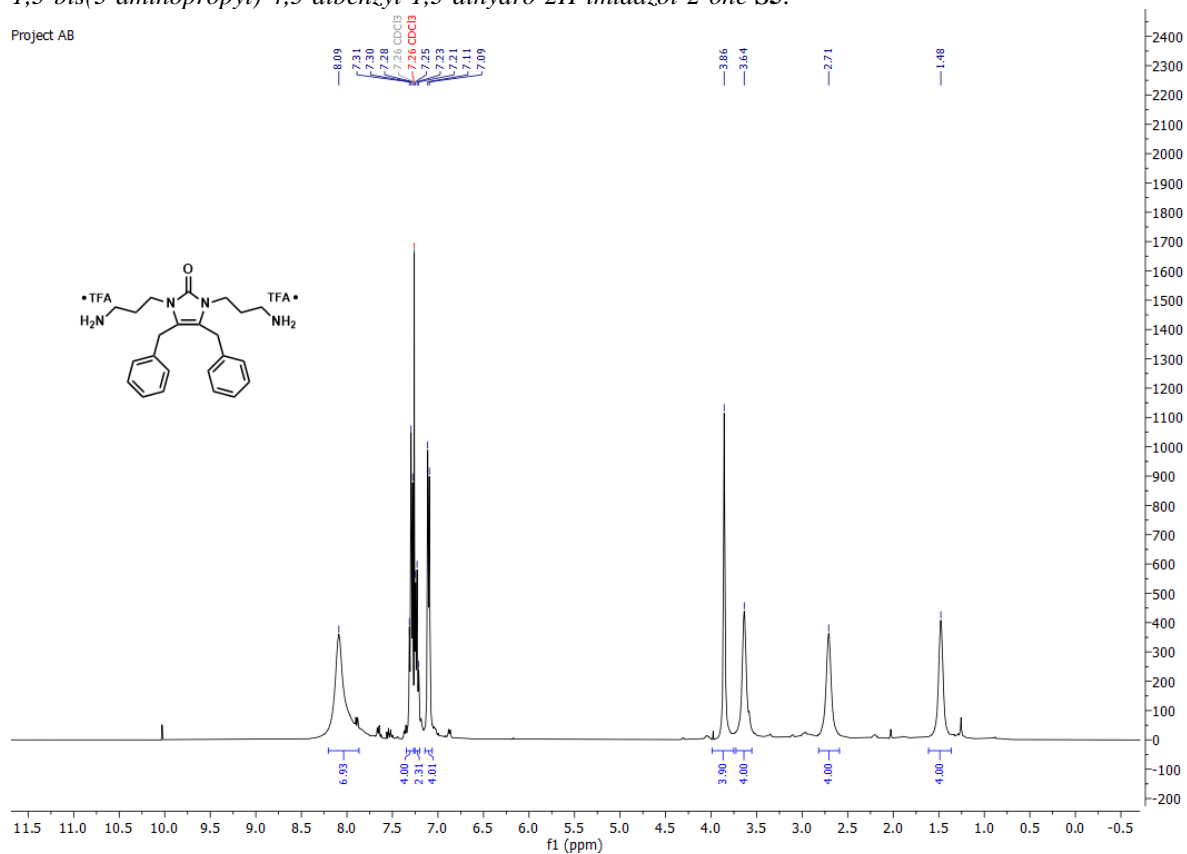


Project AB

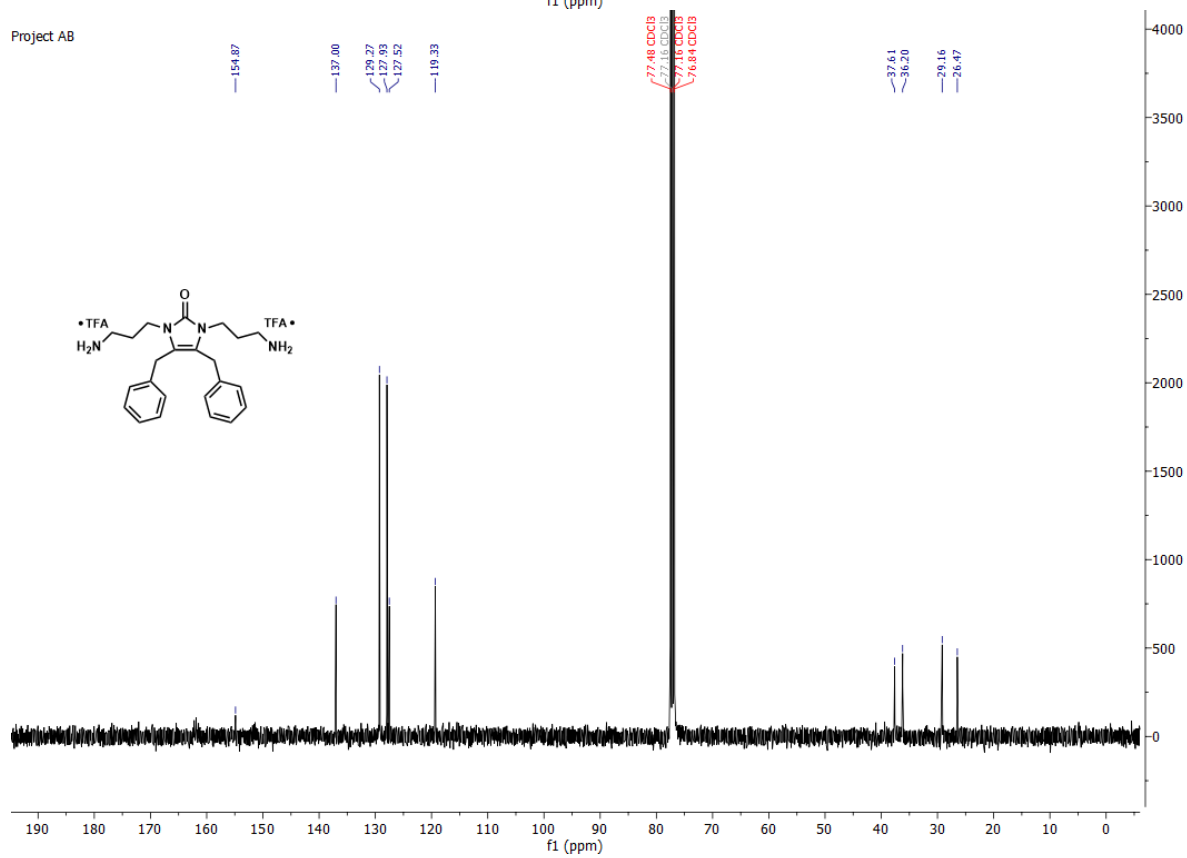


1,3-bis(3-aminopropyl)-4,5-dibenzyl-1,3-dihydro-2H-imidazol-2-one S5.

Project AB



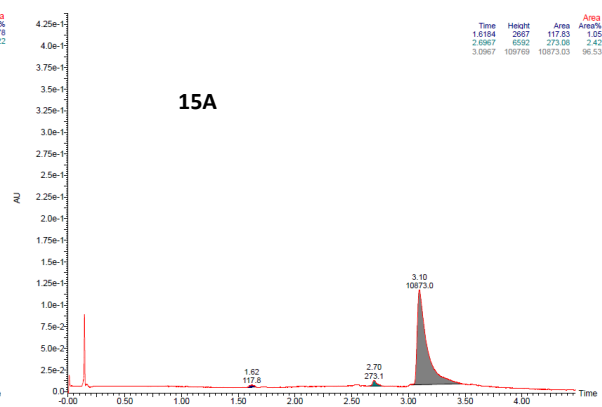
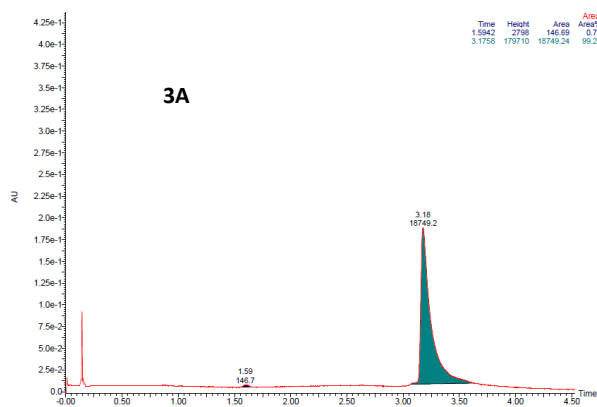
Project AB



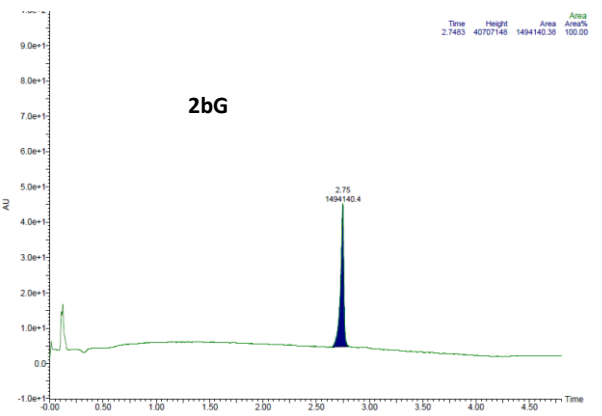
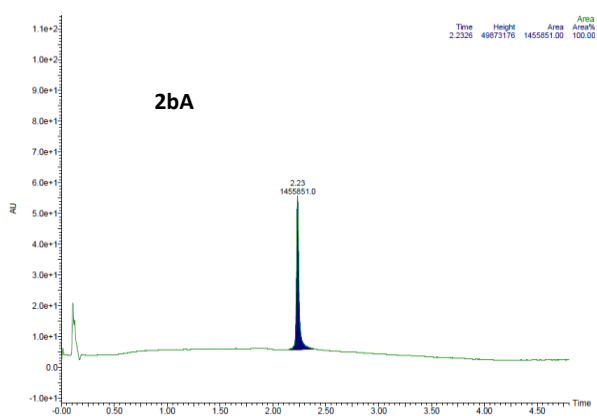
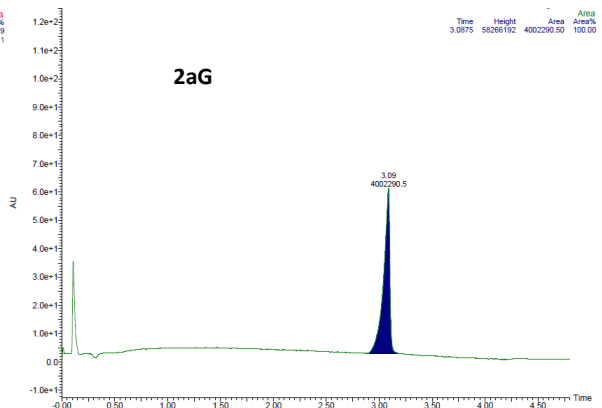
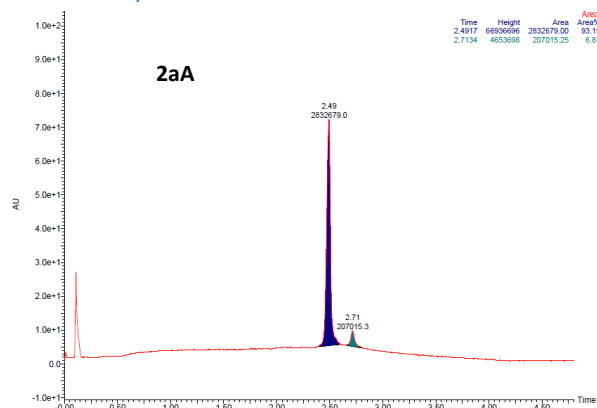
5. SFC traces

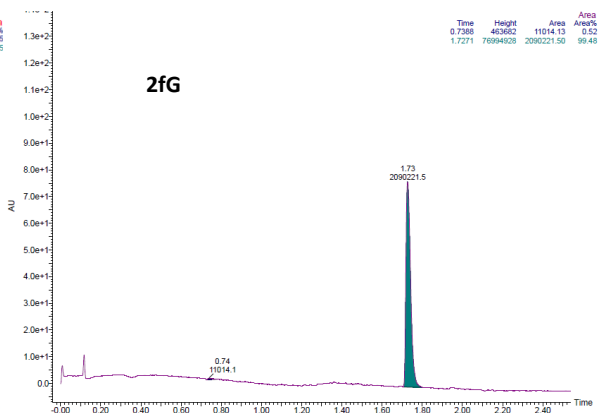
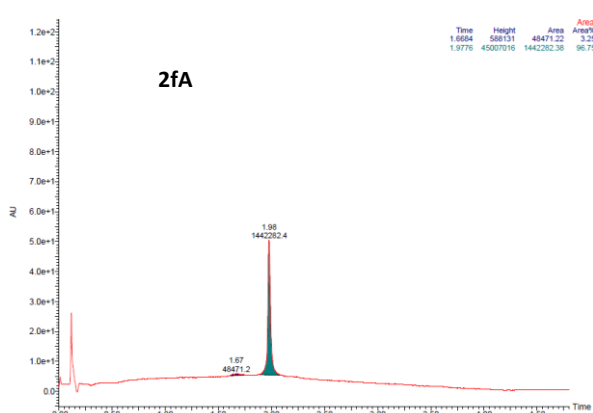
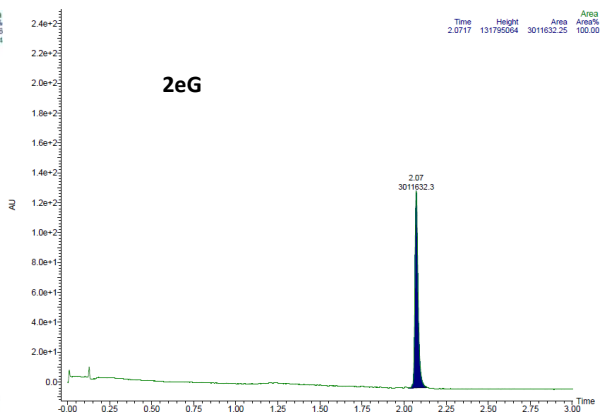
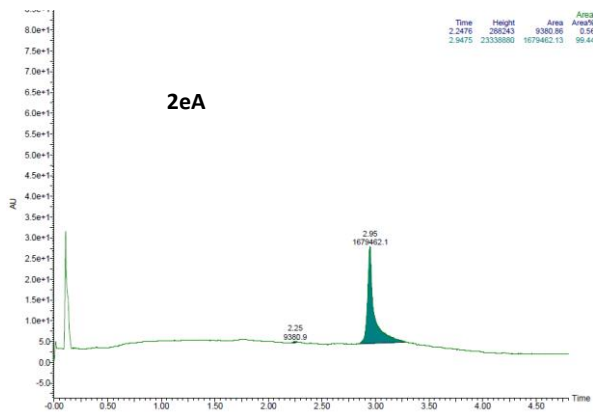
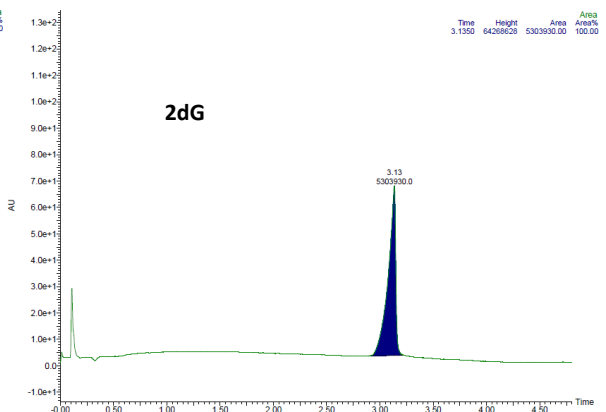
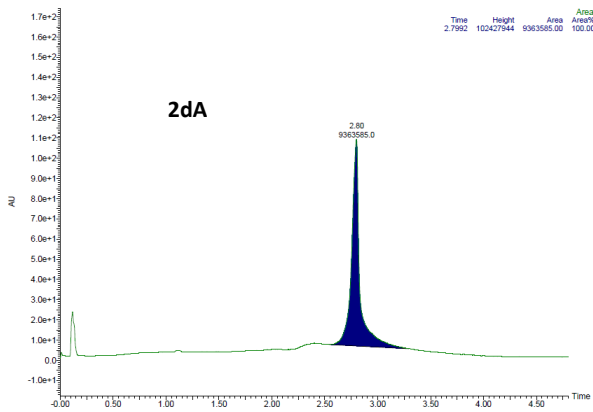
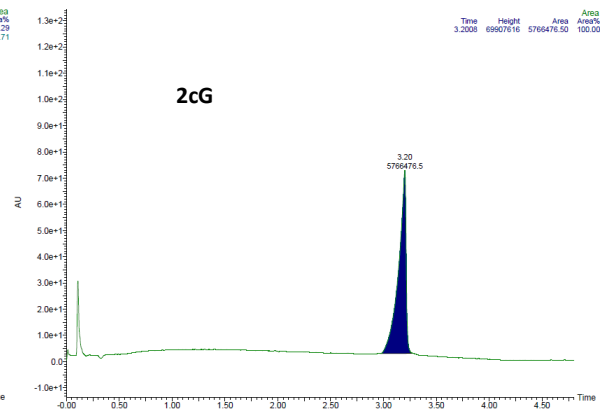
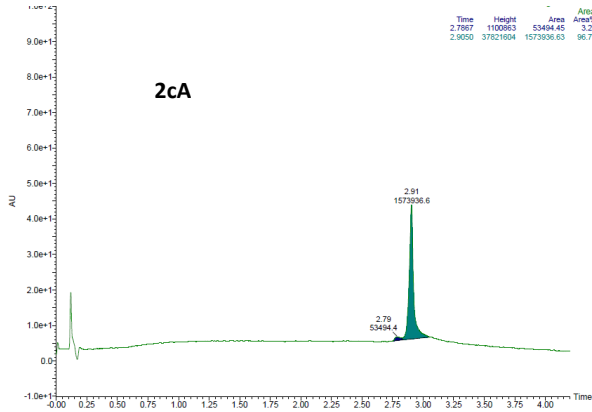
5.1 Scaffolds 3A, 4A, 5A and 15A

For compounds **4A** and **5A** no SFC traces were obtained.

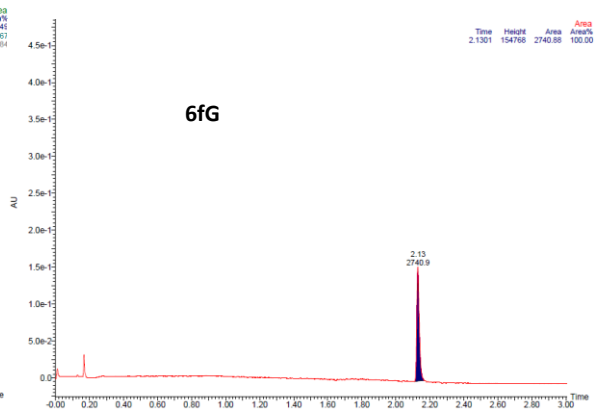
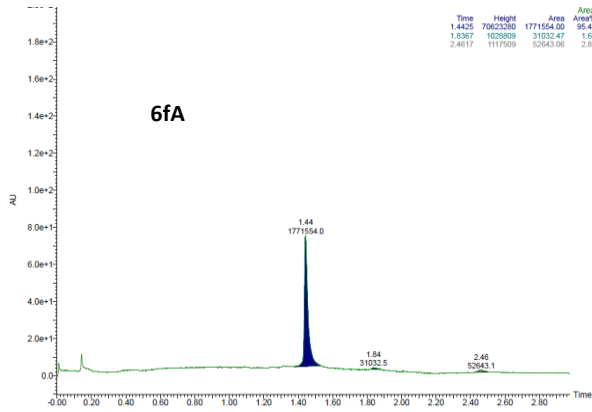
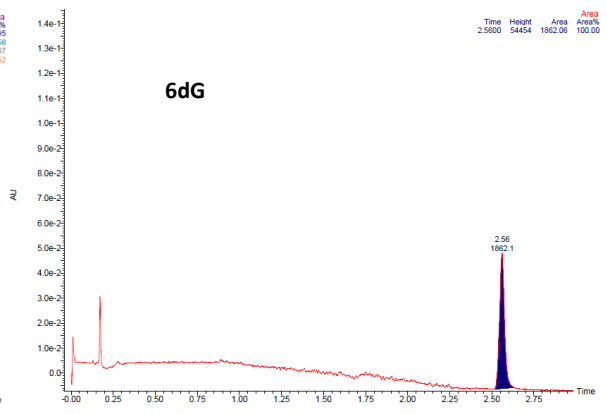
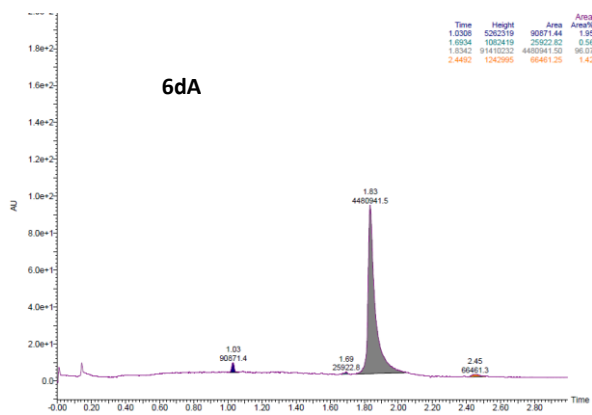
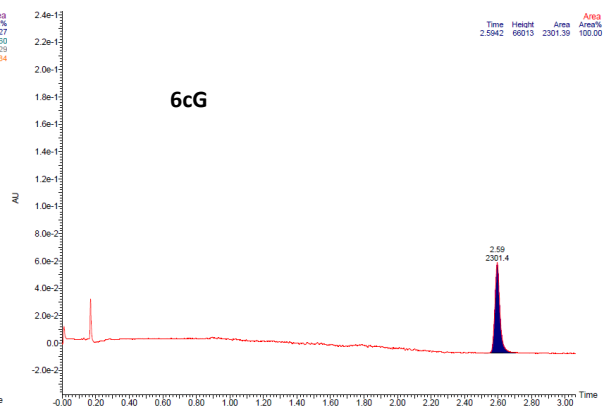
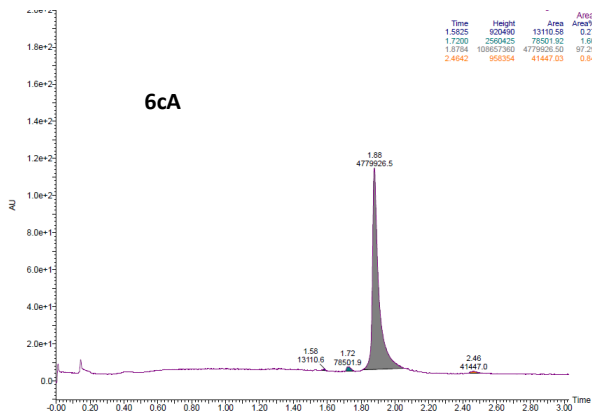
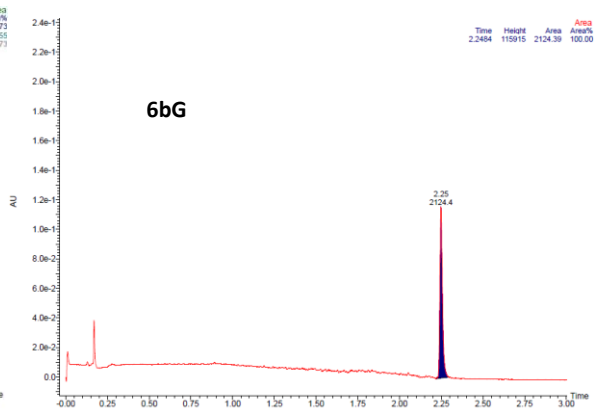
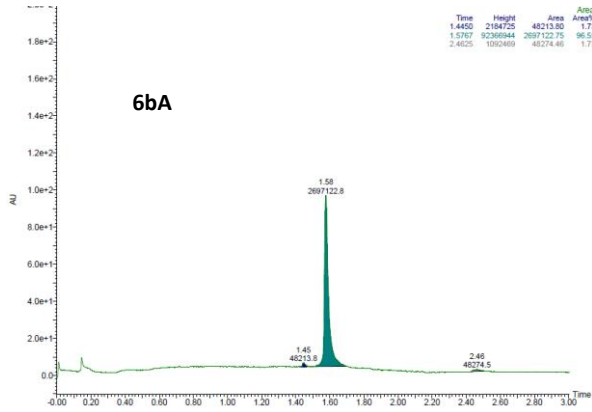


5.2 Hydantoins 2A and 2G





5.3 Hydantoin 6A and 6G



6. Full selectivity index table

Table S3. Selectivity index (SI) of all compounds towards all bacterial strains tested. EC₅₀ values are given in [µg/mL].

Code	Core	ClogP ^b	SI (MIC/EC ₅₀)				EC ₅₀ ^c
			S. a	B. s	E. c	P. a	
2dA	Hydantoin	-1.69	43	86	22	43	344
4A	2,4-dithiohydantoin	-1.22	48	48	24	–	385
3A	4-imidazolidin-2-one	-0.47	24	48	24	6	48
15A	2-(hydroxy)-1 <i>H</i> -imidazol	0.26	22	22	11	11	44
Mix 1	2-thiobarbituric acid	-0.10	38	76	39	19	305
Mix 2	2-thiobarbituric acid	-0.10	23	46	23	23	182
1A	Barbituric acid	-1.44	25	25	12	12	99

Code	Ar	Y	ClogP ^b	SI (MIC/EC ₅₀)				EC ₅₀ ^c	Code	SI (MIC/EC ₅₀)				
				S. a	B. s	E. c	P. a			S. a	B. s	E. c	P. a	EC ₅₀ ^c
2aA	(Ph)	<i>n</i> -propyl	2.64	–	–	–	–	>311	2aG	–	–	–	–	>353
2bA	(4-CF ₃ Ph)	<i>n</i> -propyl	3.52	–	>24	–	–	>379	2bG	>26	>65	–	–	>421
2cA	(3-Cl, 4-BrPh)	<i>n</i> -propyl	4.08	46	92	–	–	368	2cG	>234	>234	–	–	>467
2dA	(3,5-di-BrPh)	<i>n</i> -propyl	4.38	43	86	22	43	344	2dG	243	122	30	–	486
2eA	(4-Br-1-Nal)	<i>n</i> -propyl	4.68	17	17	6	6	69	2eG	103	103	26	–	206
2fA	(3,5-di-CF ₃ Ph)	<i>n</i> -propyl	5.03	25	50	25	25	399	2fG	>122	>245	–	–	>489

Code	Ar	Y	ClogP ^b	SI (MIC/EC ₅₀)				EC ₅₀ ^c	Code	SI (MIC/EC ₅₀)				
				S. a	B. s	E. c	P. a			S. a	B. s	E. c	P. a	EC ₅₀ ^c
6bA	(4-CF ₃ Ph)	<i>n</i> -butyl	3.52	–	>25	–	–	>393	6bG	>126	>126	–	–	>503
6cA	(3-Cl, 4-BrPh)	<i>n</i> -butyl	4.08	>55	>110	–	–	>439	6cG	347	347	43	–	347
6dA	(3,5-di-BrPh)	<i>n</i> -butyl	4.38	46	182	–	–	364	6dG	206	206	52	13	206
6fA	(3,5-di-CF ₃ Ph)	<i>n</i> -butyl	5.03	>29	>115	–	–	>461	6fG	192	192	48	–	384

Bacterial reference strains: S. a – *Staphylococcus aureus* ATCC 9144, B.s – *Bacillus subtilis* 168, E. c – *Escherichia coli* ATCC 25922, and P. a – *Pseudomonas aeruginosa* ATCC 27853. ^a –: No SI was calculated if MIC was >16 µg/mL.

7. Biological Methods

7.1 Minimum inhibitory concentration (MIC) assay

Based on the CLSI M07-A9 protocol,^[13] a modified broth microdilution sensitivity test^[14] was used to determine the minimum inhibitory concentration (MIC). Initially, a stock solution of water-soluble compounds was prepared by dissolving it in ultrapure water (Milli-Q H₂O, Millipore, MA, United States). Before being further diluted with ultrapure water, the less water-soluble compounds were first dissolved in 25 - 50 μ L 100% DMSO. The concentration of DMSO is always less than 1% in each compound's working concentration. The test components were then two-fold diluted with ultrapure water in polystyrene microplates with 96 wells of flat bottom (NUNC, Roskilde, Denmark). The bacterial inoculum was diluted into Mueller-Hinton broth (MHB, Difco Laboratories, USA) at $2.5 - 3 \times 10^4$ cells / ml and added to the different diluted compounds in a 1:1 ratio. In each experiment, positive control (ciprofloxacin, Sigma-Aldrich, USA), negative control (bacteria + water), and medium control (media + water) were included. The microplates were incubated in EnVision microplate readers at 35 °C for 48 hours (Perkin-Elmer, Turku, Finland). The lowest concentration of compounds that did not cause bacterial growth was defined as MIC by optical density measurements (OD600). All components have been tested in 3 technical repetitions.

7.2 Membrane integrity assay

7.2.1 Inner membrane

Bacillus subtilis 168 (ATCC 23857) and *Escherichia coli* K12 (ATCC MC1061) were used as test strains to perform the inner membrane integrity assay in real time. Both strains were transformed with the reporter plasmid pCSS962 containing the gene encoding eukaryotic luciferase (*lucGR* gene).^[15] D-luciferin, which was added externally, was used as a substrate for luciferase to detect light emissions. MH media supplemented with 5 μ g/mL chloramphenicol (Merck KGaA, Darmstadt, Germany) and a mixture of 20 μ g/mL chloramphenicol and 100 μ g/mL ampicillin (Sigma-Aldrich, USA), respectively, were used to suspend *B. subtilis* and *E. coli* colonies and grown overnight at RT. The overnight culture was further diluted and grown at RT for 2-3 hours until OD600 = 0.1. A final concentration of 1 mM of D-luciferin potassium salt (Synchem Inc., Elk Grove Village, IL, USA) was added to the bacterial cultures and the background light is measured before the actual tests. Black microtiter plates (96 wells, round-bottom; Nunc, Roskilde, Denmark) were prepared with a twofold series of dilutions of compounds (10 μ L per well) at final concentrations of 51.2 to 1.6 μ g/mL. MQ-H₂O and chlorhexidine acetate (Fresenius Kabi, Halden, Norway) were used as negative and positive control, respectively. The bacterial suspension was primed before loading the assay plate into the Synergy H1 Hybrid Plate Reader (BioTek, Winowski, VT, USA). The 90 μ L bacterial inoculum with D-luciferin was injected sequentially (well by well) by automated injection into test wells. Light emission (luminescence) due to bacterial membrane disturbance was monitored every second for 3 minutes. Each study was conducted at least three times independently and the figures show a representative set.

7.2.2 Outer membrane

The integrity testing of the outer membrane was carried out in real time using *E. coli*, the integrity same strain used in the testing of the integrity of the inner membrane. 1-N-phenyl-naphthylamine (NPN), which was added externally, was used as a substrate for fluorescent detection. The MH medium was used to suspend *E. coli* colonies and grown overnight at RT. The overnight cultures were further diluted and grown in RT for 2-3 hours until OD600 = 0.1. NPN (Sigma-Aldrich, USA) was added to bacterial cultures at a final concentration of 20 μ M in glucose hepes buffer (5mM). Background fluorescence was measured before the actual assay. Black 96-well microtiter plates (round bottom) are prepared with a two-fold series of compounds (10 μ L per well) diluted at final concentrations between 51.2 and 1.6 μ g/mL. MQ-H₂O and chlorhexidine acetate were used as negative and positive control. The bacterial suspension was primed before the assay plate was loaded into the Synergy H1 hybrid plate reader. Bacterial inoculum (aliquots of 90 μ L) with NPN was sequentially (well by well) injected into the test wells by an automated injector. As a result of bacterial outer membrane disruption, light (fluorescence) emission was monitored every second for 3 minutes. Each study has been carried out independently at least three times and the figures show a representative set.

7.3 Viability assay

B. subtilis 168 and *E. coli* K12, the same strains used in the inner membrane integrity assay, were used to perform the bacterial viability assay in real time. However, *E. coli* K12 was transformed with the reporter plasmid pCGLS-

1 and *B. subtilis* 168 has a constitutively expressed lux operon as a chromosomal integration at the sacA locus (P_{liaG}).^[16] MH medium supplemented with 5 µg/mL chloramphenicol and a mixture of 20 µg/mL chloramphenicol and 100 µg/mL ampicillin, respectively, were used to culture *B. subtilis* and *E. coli*, the same way as the membrane integrity assay. The respective injector was primed with bacterial suspension and continuous light production by these biosensors was monitored in the Synergy H1 hybrid reader. 10 µL of each compound at the final concentration ranging from 51.2 to 1.6 µg/mL (two-fold dilutions) was prepared in black round-bottom 96-well microtiter plates. Chlorhexidine was used as a positive control and MQ-H₂O as a negative control. The automated injector added bacterial suspension (aliquot of 90 µL) consequently. Due to changes in bacterial viability, the reduction of light emission was monitored every second for 3 minutes. Each study was carried out at least three times individually and the figures show a representative set.

7.4 Red Blood Cell Haemolysis Assay

The protocol was adapted from Paulsen et al.^[11] Haemolysis was determined using a heparinized fraction (10 IU/mL) of freshly drawn blood. The blood collected in ethylenediaminetetraacetic acid-containing test tubes (Vacutest, KIMA, Arzergrande, Italy) was used for the determination of the hematocrit (hct). The heparinized blood was washed 3× with pre-warmed phosphate-buffered saline (PBS) and adjusted to a final hct of 4%. Derivatives in DMSO (50 mM) were added to a 96-well polypropylene V-bottom plate (NUNC, Fisher Scientific, Oslo, Norway) and serially diluted. The test concentration range was 500–4 µM with DMSO contents ≤1%. A solution of 1% triton X-100 was used as a positive control for 100% haemolysis. As a negative control, a solution of 1% DMSO in PBS was included. No signs of DMSO toxicity were detected. RBCs (1% v/v final concentration) were added to the well plate and incubated at 37 °C and 800 rpm for 1 h. After centrifugation (5 min, 3000g), 100 µL of each well was transferred to a 96-well flat-bottomed microtiter plate, and absorbance was measured at 545 nm with a microplate reader (VersaMax™, Molecular Devices, Sunnyvale, CA, USA). The percentage of haemolysis was calculated as the ratio of the absorbance in the derivative-treated and surfactant-treated samples, corrected for the PBS background. Three independent experiments were performed, and EC₅₀ values are presented as averages.

8. Membrane integrity and viability assay

Table S4. Summary of the membrane integrity and viability assay against *B. subtilis* 168.

Code	MIC ¹ (μg/mL, 24h)	MIA (activity and speed) ²	VA (effects) ³
	B. s		
2bG	8	–	–
2cA	4	++	+
2cG	2	+++	++
2dA	4	++	+
2dG	4	++++	++
2eG	2	++++	+++
2fG	2	+++	++
6bG	4	++	++
6cA	4	++	+
6cG	1	++++	+++
6dA	2	++	+
6dG	1	++++	+++
6fG	2	+++	+++
CHX	1.5	++++	+++

B. s: *Bacillus subtilis* 168

¹MIC assay was also performed in biosensor assay, and the value was similar.

²For membrane integrity assay: High active, fast speed (++++), Medium active, Intermediate speed (+++), Medium active, Slow speed (++) , Low active, Slow speed (+) and Not active (–).

³For viability assay: High effect (+++), Medium effect (++) , Low effect (+) and No effect (–). The highest concentration (51.2 μg/mL) was used to compare and evaluate the membrane integrity and viability assay results.

Table S5. Summary of the membrane integrity and viability assay against *E. coli* K12.

Code	MIC ¹ (μg/mL, 24h)	MIA (activity and speed) ²	VA (effects) ³
	E. c		
2dA	16	+	+
2dG	16	+	+
2eG	8	+	+
6cG	8	+	+
6dG	4	+	+
6fG	8	+	+
CHX	1.5	++++	+++

E. c: *Escherichia coli* K12

¹MIC assay was also performed in biosensor assay, and the value was similar.

²For membrane integrity assay: High active, fast speed (++++), Medium active, Intermediate speed (+++), Medium active, Slow speed (++) , Low active, Slow speed (+) and Not active (–).

³For viability assay: High effect (+++), Medium effect (++) , Low effect (+) and No effect (–). The highest concentration (51.2 μg/mL) was used to compare and evaluate the membrane integrity and viability assay results.

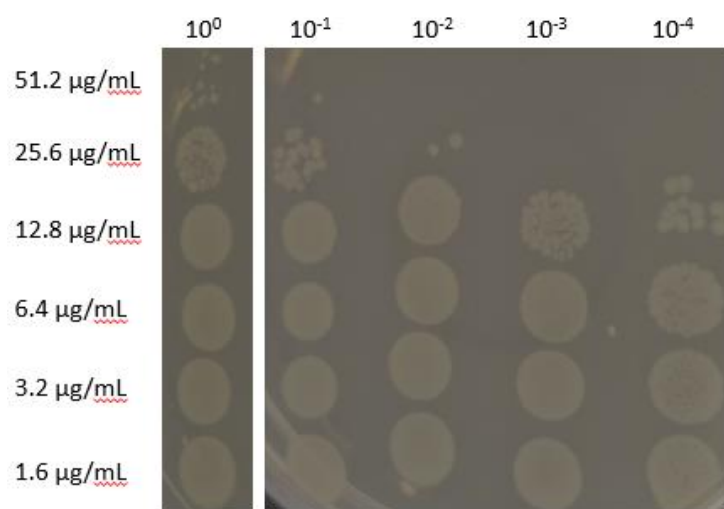


Figure S1. Bactericidal effect of hydantoin **6cG** against *E. coli* K12 after the outer membrane study with NPN. Horizontal: Dilution of the bacterial load.

9. Literature

- [1] J. Dijkink, H. E. Schoemaker, W. N. Speckamp, *Tetrahedron Lett.* **1975**, *16*, 4043-4046.
- [2] H. Hiemstra, W. N. Speckamp, in *Alkaloids Chem. Biol.*, Vol. 32 (Ed.: A. Brossi), Academic Press, **1988**, pp. 271-339.
- [3] aD. J. Hart, T. K. Yang, *J. Org. Chem.* **1985**, *50*, 235-242; bH. Ent, H. De Koning, W. N. Speckamp, *J. Org. Chem.* **1986**, *51*, 1687-1691.
- [4] H. Kohn, Z. K. Liao, *J. Org. Chem.* **1982**, *47*, 2787-2789.
- [5] aD. Gupta, D. Bhatia, V. Dave, V. Sutariya, S. Varghese Gupta, *Molecules (Basel, Switzerland)* **2018**, *23*, 1719; bA. T. M. Serajuddin, *Adv. Drug Del. Rev.* **2007**, *59*, 603-616.
- [6] P. L. Gould, *Int. J. Pharm.* **1986**, *33*, 201-217.
- [7] C. Huixiong, L. Jean-Philippe, G. Nohad, G. Christiane, *Eur. J. Org. Chem.* **2006**, *2006*, 2329-2335.
- [8] M. Donnier-Maréchal, P. Carato, P.-E. Larchanché, S. Ravez, R. Boulahjar, A. Barczyk, B. Oxombre, P. Vermersch, P. Melnyk, *Eur. J. Med. Chem.* **2017**, *138*, 964-978.
- [9] J. Simonin, S. K. V. Vernekar, A. J. Thompson, J. D. Hothersall, C. N. Connolly, S. C. R. Lummis, M. Lochner, *Bioorg Med Chem Lett* **2012**, *22*, 1151-1155.
- [10] L. Tao, F. Luoyi, G. Hao, X. Zeming, Z. Yanpeng, J. Nianqiang, J. Long, L. Gaofeng, L. Yang, W. Jiaobing, *Angew. Chem. Int. Ed.* **2017**, *56*, 9473-9477.
- [11] M. H. Paulsen, M. Engqvist, D. Ausbacher, T. Anderssen, M. K. Langer, T. Haug, G. R. Morello, L. E. Liikanen, H.-M. Blencke, J. Isaksson, E. Juskewitz, A. Bayer, M. B. Strøm, *J. Med. Chem.* **2021**.
- [12] M. K. Langer, Rahman, A.; Dey, H.; Anderssen, T.; Zilioli, F.; Haug, T.; Blencke, H.-M.; Stensvåg, K.; Strøm, M. B.; Bayer, A., (*submitted Manuscript*) **2022**.
- [13] F. R. Cockerill, 9th ed. (Ed.: C. a. L. S. Institut), Wayne, Pa : Clinical and Laboratory Standards Institut, **2012**.
- [14] E. M. Igumnova, E. Mishchenko, T. Haug, H.-M. Blencke, J. U. E. Sollid, E. G. A. Fredheim, S. Lauksund, K. Stensvåg, M. B. Strøm, *Biorg. Med. Chem.* **2016**, *24*, 5884-5894.
- [15] M. Virta, K. E. O. Åkerman, P. Saviranta, C. Oker-Blom, M. T. Karp, *J. Antimicrob. Chemother.* **1995**, *36*, 303-315.
- [16] aJ. Radeck, K. Kraft, J. Bartels, T. Cikovic, F. Dürr, J. Emenegger, S. Kelterborn, C. Sauer, G. Fritz, S. Gebhard, T. Mascher, *J. Biol. Eng.* **2013**, *7*, 29; bS. Frackman, M. Anhalt, K. H. Nealson, *J. Bacteriol.* **1990**, *172*, 5767-5773.

Paper III

Peptidomimetic tetrasubstituted barbiturates and hydantoins: Investigation of their antibiofilm, *in vivo* toxicity and antimicrobial activity

Ataur Rahman¹, Manuel Karl Langer², Bartosz Michno⁵, Gabriela Żyłka⁵, Jonathan Hira³, Hege Devold¹, Ida Kristine Østnes Hansen¹, Ekaterina Mishchenko³, Johanna U Ericson³, Morten B. Strøm⁴, Annette Bayer², Tomasz Prajsnar⁵, Klara Stensvåg¹

¹ The Norwegian College of Fishery Science, Faculty of Biosciences, Fisheries and Economics, UiT The Arctic University of Norway, NO-9037 Tromsø, Norway. ² Department of Chemistry, Faculty of Science and Technology, UiT The Arctic University of Norway, NO-9037 Tromsø, Norway. ³ Department of Medical Biology, Faculty of Health Sciences, UiT The Arctic University of Norway, NO-9037 Tromsø, Norway. ⁴ Department of Pharmacy, Faculty of Health Sciences, UiT The Arctic University of Norway, NO-9037 Tromsø, Norway. ⁵ Department of Evolutionary Immunology, Institute of Zoology and Biomedical Research, Faculty of Biology, Jagiellonian University, 30-387 Krakow, Poland. # corresponding author. Email: klara.stensvag@uit.no

Abstract

Antimicrobial resistance (AMR) is a growing concern in public health and has drawn considerable attention due to its potential effects on global health. Increasing concerns about antimicrobial resistance highlight the urgent need for new antimicrobial agents. However, the search for discovering and developing these unspecific new treatments is still an unknown territory. Inspired by a family of marine natural products, the eusynstyelamides, we have reported barbituric acid and hydantoin derivatives as peptidomimetics of AMPs. We investigated the antibiofilm (inhibition and eradication) potential of these two classes of compounds and their antimicrobial activity against antimicrobial-resistant clinical isolates. *In vivo* toxicity and antimicrobial activity were also evaluated using the zebrafish model. 13iA and 2cA were considered the most promising lead compounds and showed broad-spectrum and narrow-spectrum antimicrobial activity, respectively. Both showed outstanding biofilm inhibition at sub-MIC (1/2 MIC) and eradication potential at 5x MIC levels. Both also showed moderate antimicrobial activity against antimicrobial-resistant clinical isolates. When injected into zebrafish embryos up to 16 mg/kg, both compounds did not show toxicity or immunogenic response. Both compounds can recover infected zebrafish with *in vivo* antimicrobial potential. These findings indicate that these lead compounds can potentially be a source of new antibiotics to combat AMR.

Keywords: AMR, AMP, barbituric acid, hydantoin, antimicrobial, antibiofilm, *in vivo*, zebrafish

Introduction

Antimicrobial resistance (AMR) is an increasingly pressing concern within public health, drawing significant attention due to its potential global health implications^{1,2}. AMR arises from the remarkable ability of microorganisms to adapt and develop mechanisms to render antimicrobial drugs ineffective^{3,4}. The rise in AMR can be attributed to many factors, including the excessive and inappropriate use of antimicrobials in medical settings, agriculture, and livestock production, along with a lack of public awareness of appropriate drug utilization². Furthermore, the unregulated availability of antimicrobials has contributed substantially to the emergence and spread of AMR². Consequently, the efficacy of commonly used antibiotics and other antimicrobials has diminished, resulting in increased mortality and morbidity from previously treatable infections². In light of this, it becomes imperative to accelerate the development of alternative antibiotics at a rate that exceeds the ability of microorganisms to develop resistance, thus addressing the increasing threat of AMR².

The increasing concern about antimicrobial resistance underscores the urgent need for new antimicrobial agents⁵. However, the quest to discover and develop these new treatments remains unresolved territory. Given the increasing prevalence of antimicrobial-resistant microorganisms, investing in forthcoming research efforts to discover new antimicrobial compounds is imperative. Without these new agents, many existing therapies may lose their efficacy, even against common infections, in the days ahead. However, the development of antimicrobial medications to combat Gram-negative resistant pathogens has proven a formidable challenge, leading to a decline in interest and investment from major pharmaceutical companies^{5,6}. Smaller companies attempt to fill this void, but limited resources hinder the introduction of new antibiotics to the market^{5,6}. The existence of these antimicrobial gaps underscores the ongoing need for relentless research and development in the realm of antimicrobial technology, aiming to tackle the increasing threat of antimicrobial resistance and improve public health outcomes⁵.

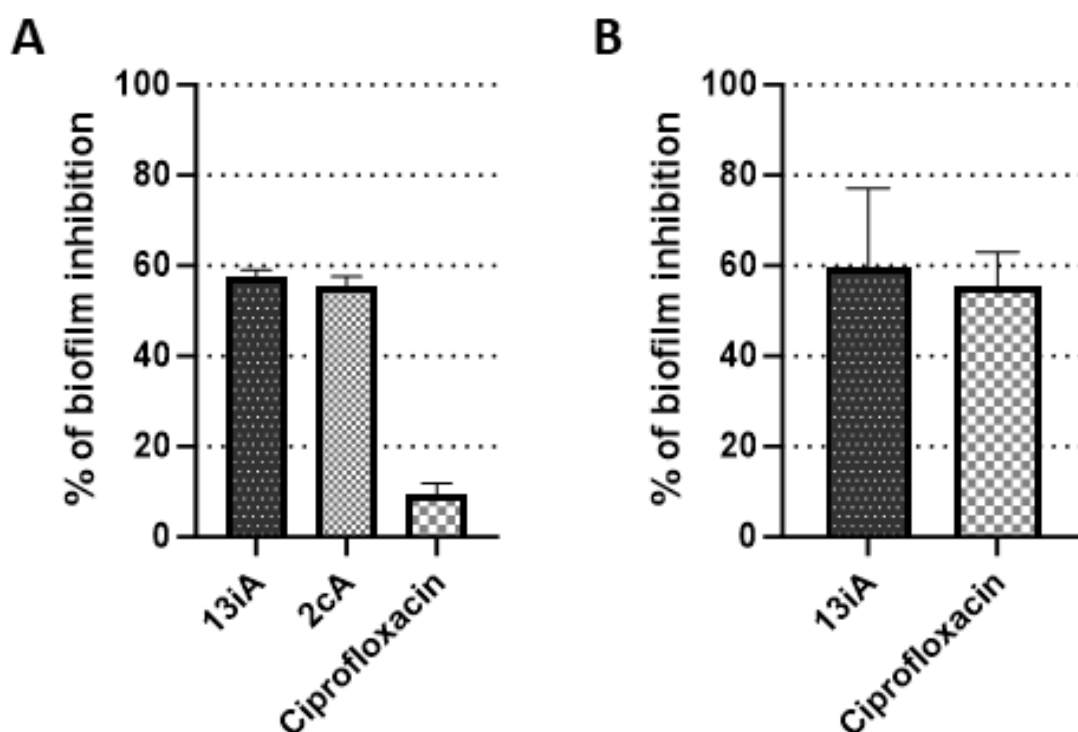
Various alternative approaches have been explored⁷⁻¹⁴. From them, short cationic antimicrobial peptides (AMPs) are an intriguing type of compound. They are the first line of defence for most eukaryotic organisms, including plants, mammals, and insects¹⁵. Inspired by a family of marine natural products, eusynstyelamides^{16,17}, we have recently reported substituted barbituric acid derivatives^{18,19} as peptidomimetics of AMP. In that second study¹⁹, we described a detailed SAR study to improve the potency and selectivity of these peptidomimetics. Several series of amphipathic barbiturates have been designed and synthesised with systematically different substituents, and their antimicrobial potential has been investigated along with their mode of action¹⁹. In another work, we first investigated five heterocyclic scaffolds²⁰, which would allow for the same substitution pattern of two lipophilic side chains and two cationic chains, as demonstrated by barbituric acid 1^{18,19}. Subsequently, we built a small library based on the most promising scaffold, hydantoin 2, and evaluated the effect of different lipophilic and cationic side chains.

In this study, we initially investigated the antibiofilm (inhibition and eradication) potential of these two classes of compounds against both Gram-positive and Gram-negative biofilm-forming human pathogen-related bacteria. Then, their antimicrobial activity was tested against antimicrobial-resistant clinical isolates. Finally, *in vivo* toxicity and antimicrobial activity were evaluated using the zebrafish model.

Results

Inhibition of biofilm formation

Based on structural alterations, MIC values, haemolytic activity, and selectivity index (SI), out of a total of 82 synthesised compounds, 31 compounds from the barbiturates class and 13 compounds from the hydantoins class were chosen to perform membrane integrity assays and viability assays as described in previous studies^{19,20}. The same 44 compounds of those two classes were used to perform the biofilm inhibition potential (Table S1). Two Gram-positive (*Staphylococcus epidermidis* RP62A, and *Staphylococcus epidermidis* 5179-R1) and one Gram-negative (*Pseudomonas aeruginosa* PAO1) strain were used as human pathogen relative of biofilm-forming bacteria (Table S2). Six compounds among 44 showed biofilm inhibition above 50 per cent against the *S. epidermidis* RP62A strain when treated at sub-MIC (1/2 MIC) level (Table S1). Based on the biofilm inhibition potential against *S. epidermidis* RP62A, 15 compounds (both active against Gram-positive and -negative) were chosen for biofilm inhibition studies against *S. epidermidis* 5179-R1 and ten compounds (only active against Gram-negative) against *P. aeruginosa* PAO1 (Table S1). Among the set of 15 compounds, only 13jA showed biofilm inhibition potential against *S. epidermidis* 5179-R1 at sub-MIC (1/2 MIC) level, approximately 34% (Table S1). Conversely, three of the ten selected compounds showed biofilm inhibition potential (above 50 per cent inhibition) against *P. aeruginosa* PAO1 at sub-MIC (1/2 MIC) level (Table S1). Taking into account all preliminary results, 13iA and 2cA were considered the most promising lead compounds, showing broad-spectrum and narrow-spectrum activity, respectively. Both compounds exhibited an outstanding biofilm inhibition potential at sub-MIC (1/2 MIC) level against *S. epidermidis* (RP62A) of approximately 60% (Figure 1A). Having broad-spectrum activity, 13iA also showed an excellent biofilm inhibition potential at sub-MIC (1/2 MIC) level, around 60 % against *P. aeruginosa* PAO1 (Figure 1B). Both showed dose-dependent biofilm inhibition against *S. epidermidis* RP62A (Figure 1C), *S. epidermidis* 5179-R1, and *P. aeruginosa* PAO1 (data not shown).



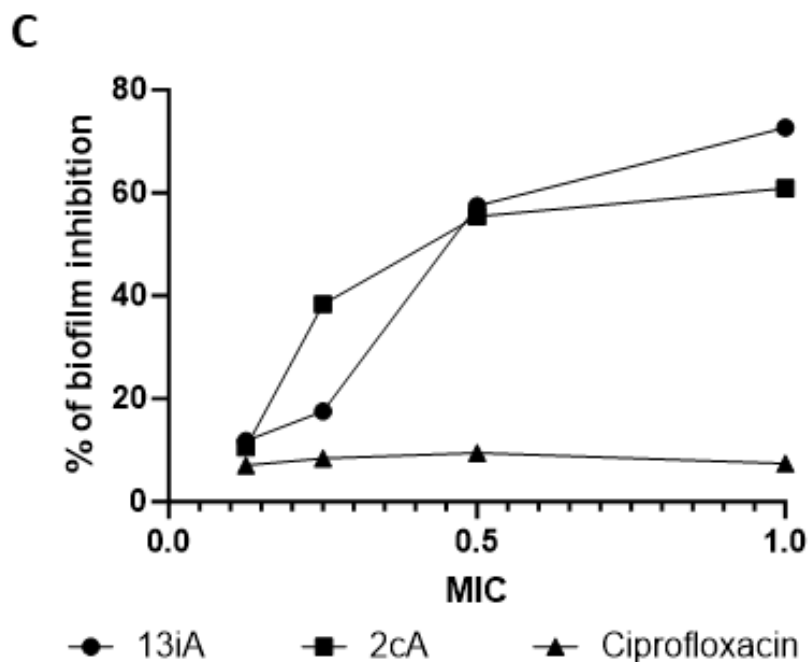


Figure 1. Biofilm inhibition potential of two promising compounds, 13iA and 2cA. A) at sub-MIC (1/2 MIC) level against *S. epidermidis* RP62A. B) at sub-MIC (1/2 MIC) level against *P. aeruginosa* PAO1. C) dose-dependent biofilm inhibition against *S. epidermidis* RP62A.

Eradicate of pre-formed biofilm

Based on the biofilm inhibition potential of the previously discussed 44 compounds against *S. epidermidis* RP62A, 11 compounds were chosen for the biofilm eradication study against *S. epidermidis* RP62A, seven against *S. epidermidis* 5179-R1 and ten against *P. aeruginosa* PAO1 (Table S1). Seven compounds among 11 showed biofilm eradication of more than 80% against the *S. epidermidis* RP62A strain when treated with 5x MIC (Table S1). For *S. epidermidis* 5179-R1, two out of seven and *P. aeruginosa* PAO1, four out of ten compounds showed biofilm eradication potential (Table S1). Lead compounds 13iA and 2cA showed an outstanding biofilm eradication potential at 5x MIC, more than 80 % against *S. epidermidis* RP62A (Figure 2A). Compound 13iA also showed excellent biofilm eradication potential (more than 90%) against *P. aeruginosa* PAO1 (Figure 2B) at 5x MIC. Both showed dose-dependent biofilm eradication against *S. epidermidis* RP62A (Figure 2C), *S. epidermidis* 5179-R1, and *P. aeruginosa* PAO1 (data not shown).

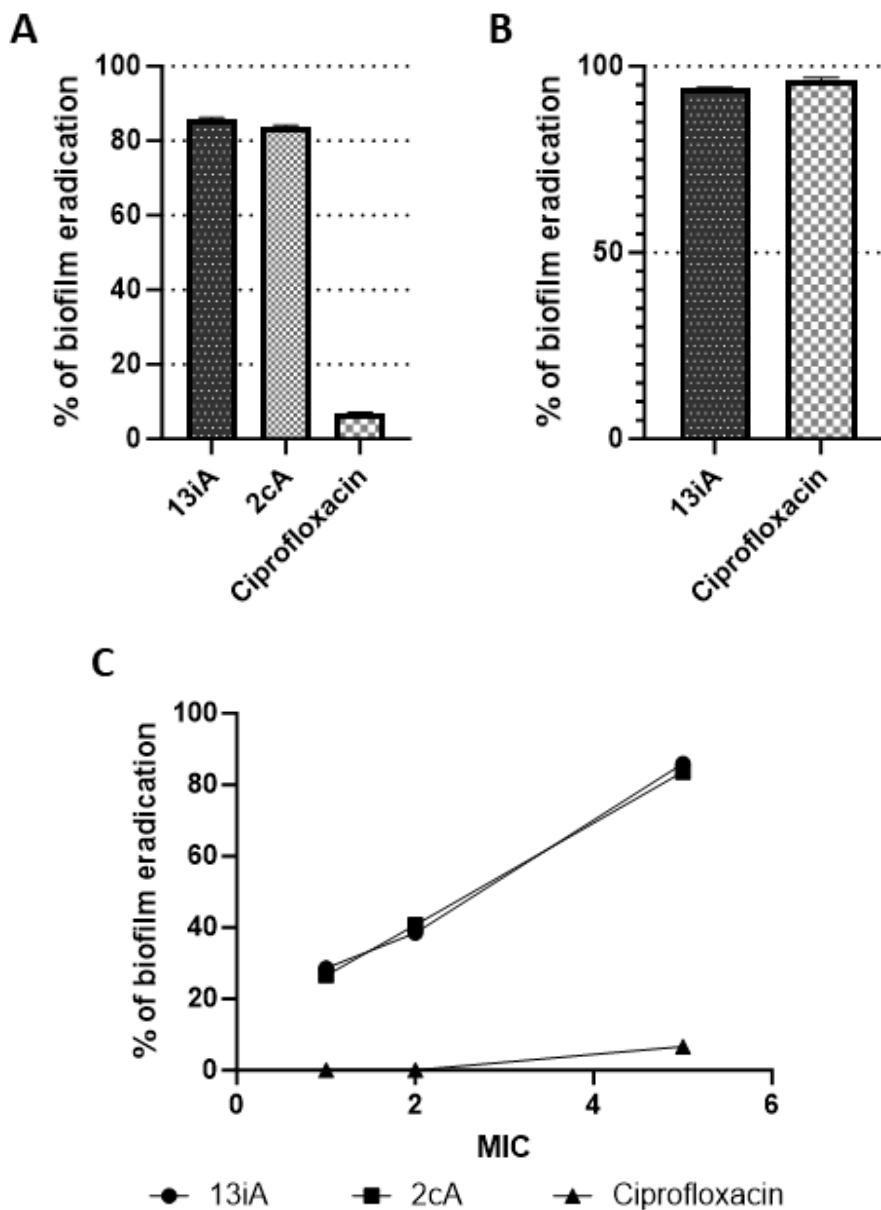


Figure 2. Biofilm eradication potential of two promising compounds, 13iA and 2cA. A) against *S. epidermidis* RP62A at 5x MIC. B) against *P. aeruginosa* PAO1 at 5x MIC. C) dose-dependent biofilm eradication against *S. epidermidis* RP62A.

Antimicrobial activity against antibiotic-resistant clinical isolates

Based on the biofilm inhibition and eradication potential along with all the parameters we have tested earlier¹⁹, 14 compounds (4 narrow-spectrum and 10 broad-spectrum) were chosen to perform antimicrobial susceptibility tests against a panel of resistant clinical isolates (Table S3). 12 of them had a MIC value <2-16 against vancomycin-resistant *Enterococcus faecium* and methicillin-resistant *Staphylococcus aureus* (MRSA) (Table 1). On the other hand, two compounds had a MIC value <2-16 against all three resistant Gram-negative strains (*Acinetobacter baumannii*, *Klebsiella pneumoniae*, and *Pseudomonas aeruginosa*) (Table 1). 13iA and 2cA showed the same activity against antibiotic susceptible *Staphylococcus aureus* and MRSA. However, activity against drug-resistant *P. aeruginosa* (VIM-2) was four times higher than against the susceptible *P. aeruginosa* (ATCC 27853) strain.

Table 1. Antimicrobial activity (MIC in µg/mL) against bacterial reference strains and antibiotic-resistant clinical isolates.

Type	Comp. ID.	Antimicrobial activity against reference bacteria (µg/mL, 24h)						Antimicrobial activity against clinical isolates (µg/mL, 24h)				
		Gram+				Gram-		Gram+		Gram-		
		<i>B. s</i> ^a	<i>S. a</i> ^a	<i>S. e</i> (RP62A)	<i>S. e</i> (5179-R1)	<i>E. c</i> ^a	<i>P. a</i> ^a	<i>E. f</i> (VRE)	<i>S. a</i> (MRSA)	<i>A. b</i> (OXA-23)	<i>K. p</i> (KPC-2)	<i>P. a</i> (VIM-2)
Barbiturates	10dG	2	2	1	1	4	16	2	<2	64	32	32
	11IA	8	16	8	8	32	64	8	8	-	-	-
	11nA	4	4	4	4	16	16	4	4	64	64	32
	11oA	2	8	4	4	8	8	4	8	64	32	32
	12aG	2	2	0.5	0.5	4	16	<2	<2	16	16	16
	13aG	2	2	0.5	0.5	4	8	2	<2	8	16	8
	13iA	4	8	8	4	8	16	8	8	32	64	64
	13jA	4	8	8	8	8	8	4	8	32	32	32
	13pA	2	4	4	4	8	8	4	8	32	32	64
	13pG	1	1	1	0.5	2	16	<2	<2	8	16	32
Hydantoin	2dA	4	8	8	4	16	8	4	8	128	128	16
	2cA	4	8	8	4	32	32	16	8	-	-	-
	6dA	2	8	8	4	32	32	32	16	-	-	-
	6cA	4	8	4	4	64	64	32	16	-	-	-
Reference antibiotics	Ciprofloxacin	-	0.06	0.03	0.062	-	0.25	42	>42	>42	>42	21
	Polymyxin B	-	8	4	4	-	0.5	>256	16	256	16	0.5
	Vancomycin	-	0.5	1	1	-	256	512	0.5	>256	>256	>256
	Rifampicin	-	<0.125	<0.125	>16	-	16	-	-	<2	32	-
	Gentamicin	-	<0.125	2	8	-	<0.125	-	-	>256	<2	>256

Bacterial reference strains: *B. s* - *Bacillus subtilis* 168, *S. a* - *Staphylococcus aureus* (ATCC 9144), *S. e* (RP62A) - *Staphylococcus epidermidis* RP62A (ATCC 35984), *S. e* (5179-R1) - *Staphylococcus epidermidis* 5179-R1, *E. c* - *Escherichia coli* (ATCC 25922), and *P. a* - *Pseudomonas aeruginosa* (ATCC 27853).

Bacterial clinical Isolates: *E. f* (VRE) - *Enterococcus faecium* (VRE), *S. a* (MRSA) - *Staphylococcus aureus* (MRSA), *A. b* (OXA-23) - *Acinetobacter baumannii* (OXA-23), *K. p* (KPC-2) - *Klebsiella pneumoniae* (KPC-2), and *P. a* (VIM-2) - *Pseudomonas aeruginosa* (VIM-2).

^a Values were taken from the previous work^{19,20}.

Blue- narrow spectrum. Green- broad spectrum. “-“ means not tested.

In vivo toxicity in zebrafish embryos

Initially, one set of eight compounds was selected based on their antimicrobial activity against resistant clinical isolates to investigate their *in vivo* toxicity in zebrafish embryos using the immersion method. However, all eight compounds showed toxicity above MIC or 2x MIC values (Table S4). Compounds 13iA and 2cA showed toxicity at higher concentrations than their MIC value against Gram-positive bacteria, which is 8 µg/mL (**Figure 3A**, **Figure 3B**, and Table S4). Based on structural alterations and haemolytic activity, an additional two sets comprising 23 compounds were selected to perform the *in vivo* toxicity analysis in zebrafish embryos using the immersion method, and their toxicity was also similar as seen with the first set of compounds (Table S5 and S6). Nevertheless, compounds 6bG, 9, and 8 were only toxic at considerably higher concentrations compared to their MIC values, and their safe concentrations were 40, 50, and 100 µg/mL, respectively (**Figure 3C**, **Figure 3D**, **Figure 3E**, Table S5 and Table S6).

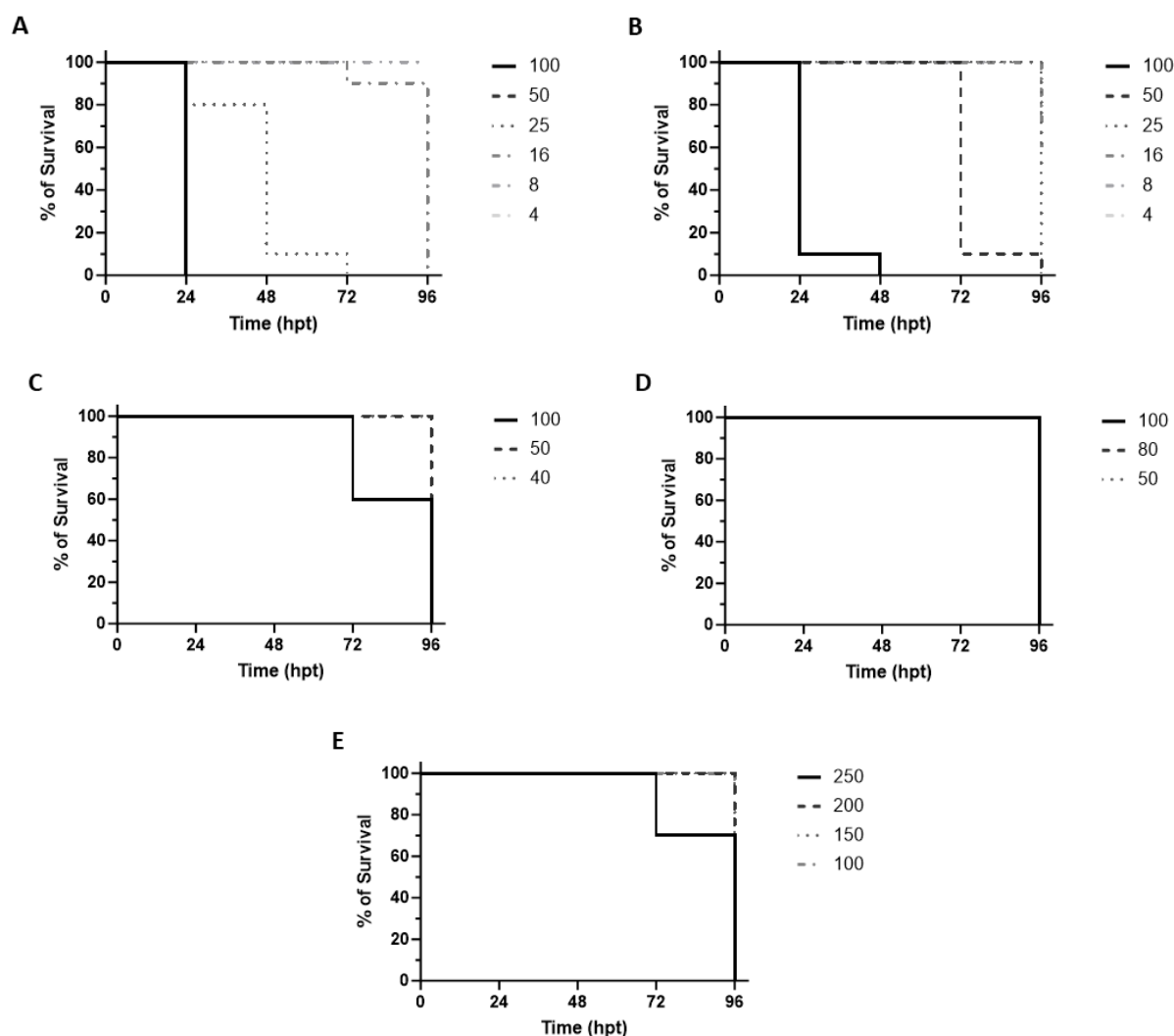


Figure 3. In vivo toxicity evaluation of five compounds in zebrafish embryos using the immersion technique. A) 13iA, B) 2cA, C) 6bG, D) 9, and E) 8.

The toxicity varied between the different age groups of the zebrafish embryos. When treated with compounds 13iA and 2cA, older embryos (3 days old) died faster than the younger embryos (1 day old) (S4).

Reasoning that the immersion method might not be a suitable model for the application of these compounds, intrayolk (IY) microinjection was used as an alternative method to further investigate the toxicity profile of the shortlisted compounds (Table S7). Here, 2 mg/kg (preclinical dose in the zebrafish model) was used as the lowest injection dose and 16 mg/kg as the highest dose. No toxicity was observed for all five compounds tested in the IY microinjection method up to a 8 mg/kg dose (Table S7). Compounds 13iA and 2cA did not show toxicity at a 16 mg/kg dose, similar to the positive control, tetracycline (**Figure 4** and Table S7).

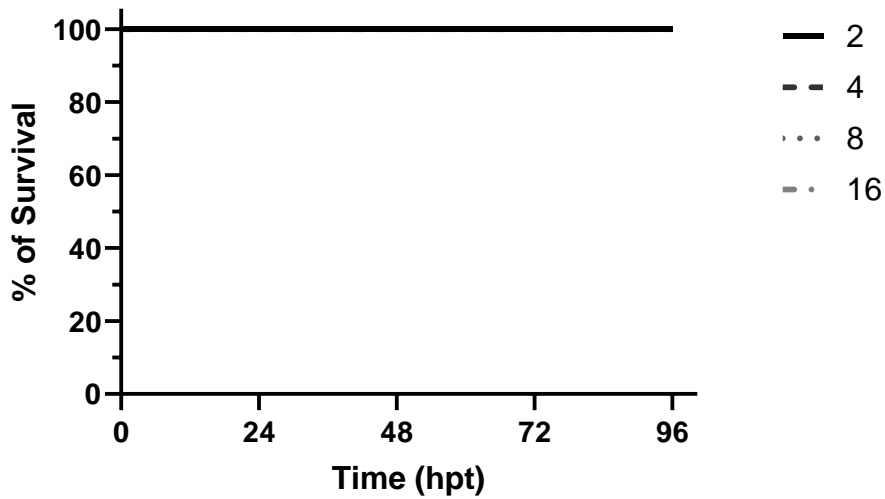


Figure 4. In vivo toxicity evaluation of compounds 13iA and 2cA in zebrafish embryos using the intrayolk (IY) microinjection technique. Both compounds did not show toxicity up to a 16 mg/kg dose, like the positive control, tetracycline.

The selected compounds did not exhibit an immunogenic response when injected through IY in the zebrafish transgenic line (Tg(mpx:GFP; mpeg1:mCherry-F)) after 48 hours post fertilisation (hpf), showing macrophages in red and neutrophils in green (Figure 5). There was no significant difference in total body neutrophils between the compounds, the negative control (DMSO) and the positive control (tetracycline) (Figure 5D).

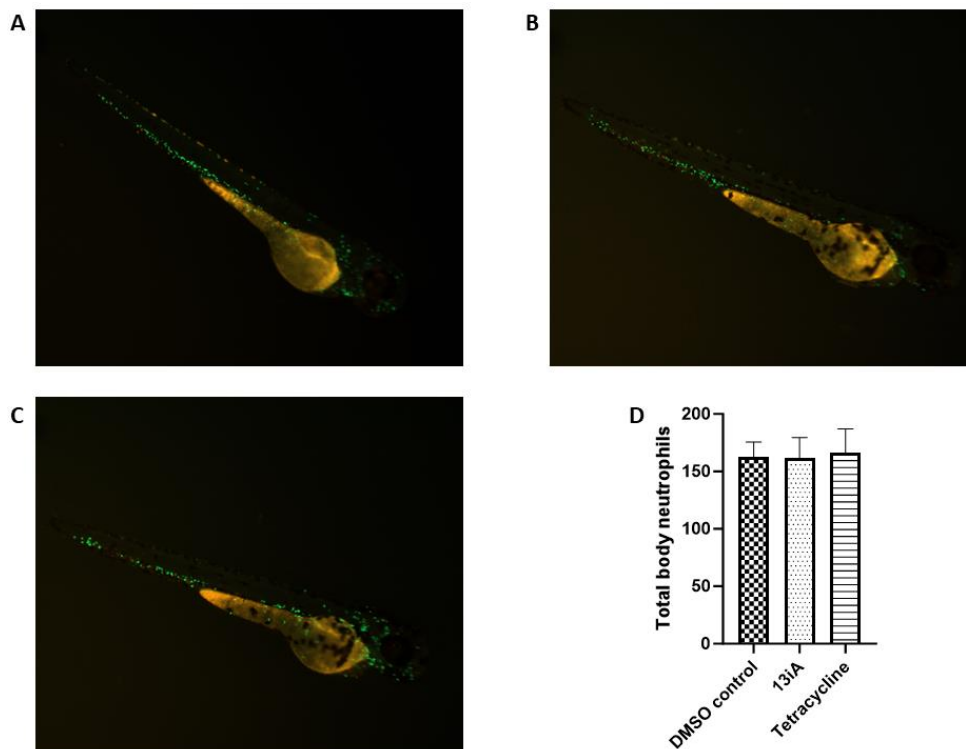


Figure 5. No immunogenic response to selected five compounds. A) compound 13iA, B) negative control, DMSO, C) positive control, tetracycline, and D) quantified neutrophils.

In vivo antibacterial activity in zebrafish embryos

The five compounds (13iA, 2cA, 9, 8, and 6bG) that were tested for toxicity using the IY microinjection method were used to treat the embryos after infecting them with *Staphylococcus aureus* SH1000, *S. epidermidis* RP62A, *Streptococcus pneumoniae* D39, *Escherichia coli* 25922, *P. aeruginosa* PAO1, and *Porphyromonas gingivalis* W83 (Table S8). There was no significant *in vivo* antibacterial activity of the selected compounds against Gram-negative bacteria, except for compound 8, which exhibited some antibacterial activity against *P. gingivalis* W83 (Table S9). On the other hand, selected compounds showed significant antibacterial activity *in vivo* against Gram-positive bacteria, especially against *S. aureus* SH1000 and *S. epidermidis* RP62A (Table S9). Compound 13iA was the most effective against *S. epidermidis* RP62A (Figure 6A) and compound 2cA against *S. aureus* SH1000 (Figure 6B), both outperforming the positive control tetracycline (Figure 6 and Table S9).

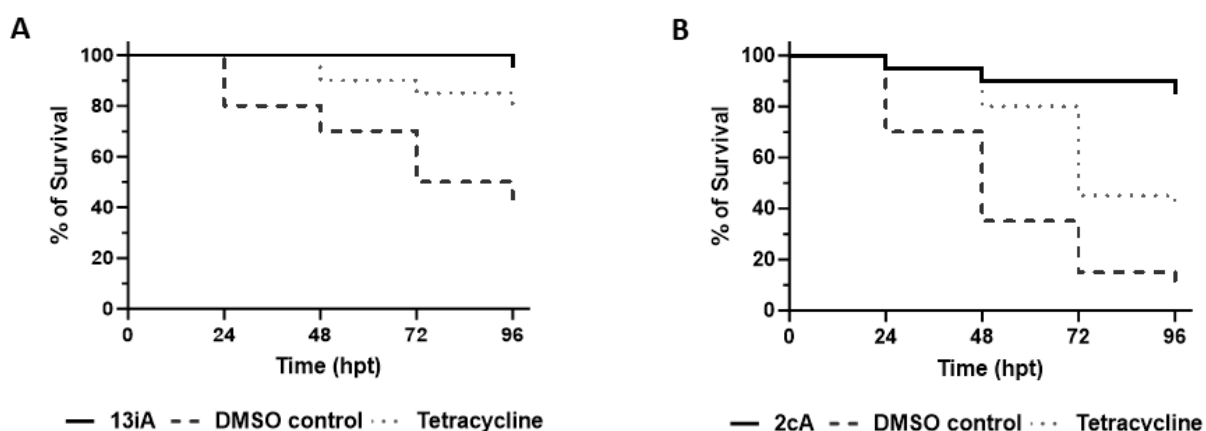


Figure 6. Antimicrobial activity of the compounds in zebrafish embryos. A) 13iA against *S. epidermidis* RP62A. B) 2cA against *S. aureus* SH1000.

Compounds 13iA and 9 had some antimicrobial protection for up to 24 hours. Therefore, we wanted to check whether administering repeated doses could further improve antimicrobial activity and found that it did when using compound 9 (Figure 7). As shown in Figure 7, there was an improvement in antibacterial activity of compound 9 against *S. aureus* SH1000 when administered in repeated daily doses through IY (same amount each day, in total 3 times higher than a single dose).

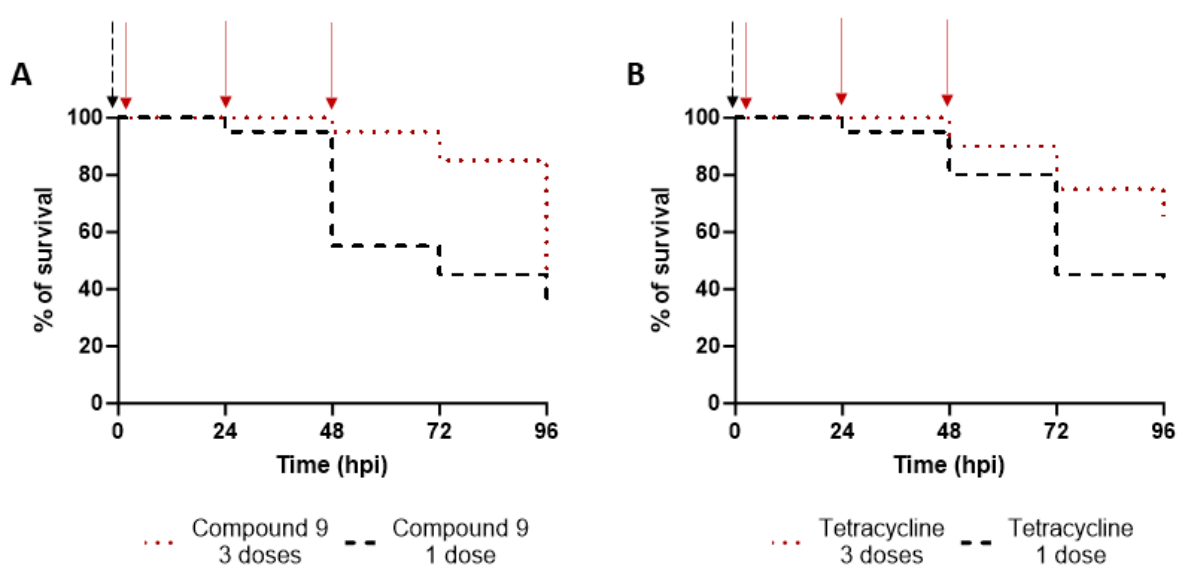


Figure 7. Improved antibacterial activity against *S. aureus* SH1000 when administered in repeated doses daily through IY. A) Compound 9. B) Positive control, tetracycline.

Discussion

A promising group of antibiotics are naturally produced cationic antimicrobial peptides (AMPs)²¹. In past years, we have focused on the development of synthetic AMP analogues that meet and work within the limits of the pharmacophore model for AMPs^{18,22-26}. Recently, we constructed and expanded libraries based on two scaffold structures, barbituric acid¹⁹ and hydantoin²⁰. Several barbituric acid and hydantoin derivatives showed excellent antibiofilm potential in inhibiting biofilm formation and eradicating formed biofilm. These compounds showed dose-dependent inhibition and eradication of biofilms against *S. epidermidis* RP62A (Figure 1C and Figure 2C), *S. epidermidis* 5179-R1, and *P. aeruginosa* PAO1. However, there were some inconsistencies against *P. aeruginosa* PAO1, which was expected, as it is challenging to obtain homogeneous biofilm between the different concentrations and between the replicates. On the other hand, *S. epidermidis* RP62A and *S. epidermidis* 5179-R1 gave consistent results between the different concentrations and replicates. *S. epidermidis* RP62A forms a polysaccharide-based biofilm²⁷, whereas *S. epidermidis* 5179-R1 forms a proteinaceous biofilm²⁸. Most of the compounds were mainly effective against polysaccharide-based biofilms formed by *S. epidermidis* RP62A.

Since antibiotics have been introduced as antimicrobials, the minimum inhibitor concentration (MIC) baselines for many commonly used antibiotics have increased considerably. Examples of this "MIC creep" include ciprofloxacin (120-times MIC increase in 19 years), erythromycin (250-times MIC increase in 5 years), tobramycin (8-times MIC increase in 17 years), and vancomycin (60-times MIC increase in 16 years)²⁹. Most of the selected compounds showed promising results against antibiotic-resistant Gram-positive bacteria, exhibiting almost the same MIC values as against antibiotic susceptible reference strains (Table 1). However, against antibiotic-resistant Gram-negative bacteria, the MIC values were the same or 2-4 times higher than for susceptible reference bacteria (Table 1).

Although most of the tested compounds were toxic in a zebrafish model using the immersion method (Table S4, S5, and S6), IY microinjection of five selected compounds did not show any toxicity at the dose of 2-8 mg/kg (Table S7), with 2 mg/kg being the preclinical dose in the zebrafish model³⁰. There is one study in which they compiled a set of 700 compounds that were reported in the literature to be active in zebrafish assays³¹. They assessed their properties and compared them with those obtained from a set of historical and recently approved oral drugs³¹. They concluded that zebrafish-absorbed molecules tend to be more lipophilic than known drugs, and in most cases, their physiochemical properties fall within a narrow range of values compared to the Lipinski rules³¹. Although the physiochemical properties of these compounds do not fall within a narrow range of values compared to the Lipinski rules (Table S10), the amphipathic nature of these compounds could hamper gaseous exchange, which could suffocate the fish, thus explaining the observed toxicity in the immersion method. This circumstance led us to use the IY microinjection method to conduct further toxicity and antibacterial activity studies *in vivo*³⁰.

Zebrafish possess toll-like receptors (TLRs) with high homology to their counterparts in other vertebrates, including humans^{32,33}, and bacterial and viral infections upregulate these TLRs^{33,34}, making zebrafish an excellent infection model. Compounds 13iA and 9 showed excellent *in vivo* antibacterial activity against *S. epidermidis* RP62A (Figure 6A and Table S9), while compound 2cA showed very good *in vivo* antibacterial activity against *S. aureus* SH1000 (Figure 6B and Table S9). However, repeated daily doses of compounds are needed to control infection in the zebrafish model, as exemplified by the improved survival of zebrafish infected with *S. aureus* SH1000 upon repeated daily treatment with compound 9 (Figure 7).

This work provides antibacterial lead compounds with an improved understanding of their toxicity profile and antimicrobial activity obtained in the *in vivo* zebrafish model. This finding can act as an arsenal to combat drug-resistant bad bugs.

Methods

Bacterial strains and growth conditions

Supplementary Tables 2, 3, and 8 list the bacteria used in this work. If not mentioned otherwise, the bacteria were grown in Mueller Hinton medium (MHB) at 37 °C.

Antibiofilm testing.

Biofilm inhibition assay

The selected compounds were screened for inhibition of biofilm formation. The test strains were the Gram-positive strain *S. epidermidis* RP62A and *S. epidermidis* 5179-R1, and the Gram-negative strain *P. aeruginosa* PAO1. Briefly, overnight cultures were grown and diluted to 6×10^6 cells/mL in TSB containing 1% glucose for *S. epidermidis* RP62A and *S. epidermidis* 5179-R1, 6×10^8 cells/mL in MHB for *P. aeruginosa*. A volume of 50 μ L of the respective bacterial inoculum was added to the serially diluted compounds and controls in a 1:1 ratio. For *P. aeruginosa*, the microplate lid was swiped with a lid containing pegs. After incubation for 24 h at 37 °C without shaking, the bacterial suspension was discarded. The wells were washed with tap water (3x) and incubated for 1 hour at 55 °C to fix the biofilm. To stain the adhered biofilm, a volume of 150 μ L of 0.1% crystal violet was added to each well and plates were incubated for 5 min at room temperature. The wells were again washed (3x) with tap water, and the biofilm-bound dye was solubilised by adding 200 μ L of 70% ethanol to each well. The plates were shaken at 250 rpm for 15 min, and the OD600 was measured. The percentage of inhibition of biofilm formation of each compound was calculated using the formula: $[100 - \{(OD600 \text{ extract}/OD600 \text{ negative control}) \times 100\}]$, where the negative control was bacteria + water. All samples were tested in 3 technical replicates.

Biofilm eradication assay

Selected compounds were screened for the eradication of the formed biofilm. The same bacterial strains and procedure were followed as mentioned in the biofilm inhibition assay, except that no compounds were added with the bacterial inoculum. Here, only bacterial inoculum was added without any compounds and after incubation for 24 h at 37 °C without shaking, the bacterial suspension was discarded. Then, the serially diluted compounds and controls were added to the respective well. After incubation for 24 h at 37 °C without shaking, the bacterial suspension was discarded, and the rest of the steps were followed as mentioned in the biofilm inhibition assay. The percentage of biofilm eradication of each compound was calculated using the formula: $[100 - \{(OD600 \text{ extract}/OD600 \text{ negative control}) \times 100\}]$, where the negative control was bacteria + water. All samples were tested in 3 technical replicates.

Antimicrobial-susceptibility testing

A modified broth microdilution susceptibility test, based on the CLSI M07-A9 protocol²⁵, was used to determine the minimal inhibitory concentrations (MIC). The resistant bacterial strains (Gram-positive and Gram-negative bacteria) that were used are listed in Supporting Information Table S3. The bacteria were grown overnight in Mueller-Hinton broth (MHB, Difco Laboratories, USA) at 35 °C.

The compounds were dissolved in Milli-Q water at a concentration of 1024 μ g/mL, and a series of two-fold dilutions (50 μ L) of the compounds were prepared in 96-well flat-bottom polystyrene microplates (Thermo Fisher Scientific, Denmark). A suspension of actively growing bacteria was diluted in Mueller-Hinton broth to approximately $2.5\text{--}3 \times 10^4$ cells/mL. A volume of 50 μ L of the respective bacterial inoculum was added to the diluted compounds in a 1:1 ratio. The positive control (ciprofloxacin, Sigma-Aldrich, USA), the negative control (bacteria + water), and the medium control (media + water) were included in each experiment. The microplates were incubated for 48 h at 35 °C in an EnVision microplate reader (PerkinElmer, Turku, Finland). The lowest concentration of extract that resulted in no

bacterial growth, as determined by OD600 measurements, was defined as the minimal inhibitory concentration (MIC) value. All samples were tested in 3 technical replicates.

In vivo toxicity in zebrafish larvae

Zebrafish lines and maintenance

The adult and embryos of zebrafish were treated in accordance with local animal welfare regulations and maintained according to standard protocols (zfin.org) following the international guidelines of the EU Animal Protection Directive 2010/63/EU. Wild-type (AB/TL) and transgenic zebrafish line (Tg(mpx:GFP; mpeg1:mCherry-F)) were used for the experiments. The embryos were incubated and maintained in E3 medium (5 mM NaCl, 0.17 mM KCl, 0.33 mM CaCl₂, 0.33 mM MgSO₄) at 28.5°C according to standard protocols.

Immersion

The wild-type (AB/TL) zebrafish line was used for this toxicity experiment using the immersion method. 24 (Day 1), 48 (Day 2) and 72 (Day 3) hours post fertilisation (hpf) embryos were used for the toxicity study of the compounds. Dechoriation was performed for 24 and 48 hpf embryos before treating them with compounds. The compounds were diluted at different concentrations (200 - 4 µg/mL) in E3 medium, and 10 embryos were used per concentration in each well of 12 well plates. Tetracycline was used as a positive control, and DMSO was used as a negative control. Embryos were observed every 24 hours up to 120 hpf, and the number of dead embryos was recorded at each time.

Intrayolk (IY) microinjection

The wild-type zebrafish (AB/TL) line was used for this toxicity experiment. 24 and 48 hpf embryos were used for the toxicity study of compounds using the IY microinjection method. Dechoriation was performed for 24 and 48 hpf embryos before injection with compounds. The compounds were diluted at different concentrations (0.5 and 2 mg/mL) in PBS to have the dose (2, 4, 8, 16 mg/kg), and 15 embryos were injected into the yolk sack per dose and placed in each well of six-well plates. Tetracycline was used as a positive control, and DMSO was used as a negative control. Embryos were observed every 24 hours up to 120 hpf, and the number of dead embryos was recorded at each time.

Microscopic observations

The transgenic zebrafish line (Tg(mpx:GFP; mpeg1:mCherry-F)) was used for the experiments, where green (GFP) was neutrophils and red (mCherry) was macrophage. The embryo dechoriation was performed at 24 hpf before injecting the compounds into intrayolk. The compounds were diluted to 2 mg/mL in PBS to have the safe dose determined in the IY microinjection method. Twenty embryos were injected into the yolk sack per compound and placed in Petri plates. Tetracycline was used as a positive control, and DMSO was used as a negative control. The image was taken 48 hours post fertilisation (hpf) using an inverted fluorescence microscope (Zeiss, SteREO, Discovery. V12) with a Zeiss camera (Plan S, 1.0x, FWD 81mm). Image acquisition and processing were performed with ZEN (version 3.2).

In vivo infection in zebrafish larvae

Bacterial cultures

S. aureus SH1000 and *S. epidermidis* RP62A were cultured in tryptic soy broth (TSB) medium at 37 °C with shaking at 200-250 rpm. Inoculum for injection (OD 7.0) was prepared from the active culture when the OD reached 0.8-1.0. *S. pneumoniae* D39 was cultured in Todd-Hewitt broth (THY) medium at 37 °C without shaking³⁵. The inoculum for injection (OD 4.5) was prepared from the active culture when the OD reached 0.3-0.5. *E. coli* 25922 was also cultured in TSB medium at 37 °C with shaking at 200-250 rpm. Inoculum for injection (OD 0.5) was prepared from the overnight culture. *P. aeruginosa* PAO1 was also cultured in TSB medium at 37 °C with shaking at 200-250 rpm. Inoculum for injection (OD 1.5) was prepared from the active culture when the OD reached 0.6-0.7. *P. gingivalis* W83 was cultured in TSB containing supplements (0.5 mg/L menadione sodium bisulfate, 0.25 g/L L-cysteine-HCl, 5 mg/L

hemin, 5% (v/v) defibrinated horse blood)³⁶. The plate was placed in an anaerobic bag with a gas pack and incubated at 37 °C without shaking. The inoculum for injection (OD 5.0) was prepared from the overnight culture.

Microinjection of bacteria into zebrafish embryos

Zebrafish embryos were dechorionated at 26 hpf for *S. aureus* SH1000, *S. epidermidis* RP62A, and *P. gingivalis* W83. However, dechlorination was performed at 50 hpf for *S. pneumoniae* D39, *E. coli* 25922, and *P. aeruginosa* PAO1. The embryos were anaesthetised by immersion in 0.02% w/v buffered tricaine (Sigma) and embedded in 3% w/v methylcellulose (Sigma, M7027). The embryos were then individually injected using microcapillary pipettes (WPI, TW100-4) filled with the known concentration of bacterial suspension. To confirm the CFU, injections were collected and plated at the beginning and end of the injection. Plates were incubated at 37 °C overnight, counted the colony, and calculated the CFU.

Microinjection of compounds onto yolk sack of zebrafish embryos

Compounds were injected into the yolk sac at a concentration that was found to be safe during the IY microinjection method. Tetracycline was used as a positive control, and DMSO was used as a negative control. Embryos were observed every 24 hours up to 120 hpf, and the number of dead embryos was recorded at each time.

Statistical analysis

The survival rate was evaluated using the Kaplan–Meier method. The analysis was performed with GraphPad Prism (version 10). The statistical significance was expected with a P value below 0.05.

References

- 1 Reynoso, E. C., Laschi, S., Palchetti, I. & Torres, E. Advances in antimicrobial resistance monitoring using sensors and biosensors: A review. *Chemosensors* **9**, 232 (2021).
- 2 Santajit, S. & Indrawattana, N. Mechanisms of antimicrobial resistance in ESKAPE pathogens. *BioMed research international* (2016).
- 3 Tenover, F. C. Mechanisms of antimicrobial resistance in bacteria. *The American journal of medicine* **119**, S3-S10 (2006).
- 4 Abebe, M., Tadesse, S., Meseret, G. & Derbie, A. Type of bacterial isolates and antimicrobial resistance profile from different clinical samples at a Referral Hospital, Northwest Ethiopia: five years data analysis. *BMC research notes* **12**, 1-6 (2019).
- 5 Slama, T. G. Gram-negative antibiotic resistance: there is a price to pay. *Critical Care* **12**, 1-7 (2008).
- 6 Palmer, M. E., Andrews, L. J., Abbey, T. C., Dahlquist, A. E. & Wenzler, E. The importance of pharmacokinetics and pharmacodynamics in antimicrobial drug development and their influence on the success of agents developed to combat resistant gram negative pathogens: A review. *Frontiers in Pharmacology* **13**, 888079 (2022).
- 7 Tamma, P. D., Cosgrove, S. E. & Maragakis, L. L. Combination therapy for treatment of infections with gram-negative bacteria. *Clinical microbiology reviews* **25**, 450-470 (2012).
- 8 Laws, M., Shaaban, A. & Rahman, K. M. Antibiotic resistance breakers: current approaches and future directions. *FEMS microbiology reviews* **43**, 490-516 (2019).
- 9 Mandal, S. M., Roy, A., Ghosh, A. K., Hazra, T. K., Basak, A. & Franco, O. L. Challenges and future prospects of antibiotic therapy: from peptides to phages utilization. *Frontiers in pharmacology* **5**, 105 (2014).
- 10 Hamblin, M. R. & Hasan, T. Photodynamic therapy: a new antimicrobial approach to infectious disease? *Photochemical & Photobiological Sciences* **3**, 436-450 (2004).
- 11 DiGiandomenico, A. & Sellman, B. R. Antibacterial monoclonal antibodies: the next generation? *Current opinion in microbiology* **27**, 78-85 (2015).

- 12 Beyth, N., Hourı-Haddad, Y., Domb, A., Khan, W. & Hazan, R. Alternative antimicrobial approach: nano-antimicrobial materials. *Evidence-based complementary and alternative medicine* (2015).
- 13 Mulani, M. S., Kamble, E. E., Kumkar, S. N., Tawre, M. S. & Pardesi, K. R. Emerging strategies to combat ESKAPE pathogens in the era of antimicrobial resistance: a review. *Frontiers in microbiology* **10**, 539 (2019).
- 14 Hancock, R. & Patrzykat, A. Clinical development of cationic antimicrobial peptides: from natural to novel antibiotics. *Current drug targets-Infectious disorders* **2**, 79-83 (2002).
- 15 Mahlapuu, M., Håkansson, J., Ringstad, L. & Björn, C. Antimicrobial peptides: an emerging category of therapeutic agents. *Frontiers in cellular and infection microbiology*, 194 (2016).
- 16 Tapiolas, D. M., Bowden, B. F., Abou-Mansour, E., Willis, R. H., Doyle, J. R., Muirhead, A. N., Liptrot, C., Llewellyn, L. E., Wolff, C. W. & Wright, A. D. Eusynstyelamides A, B, and C, nNOS inhibitors, from the ascidian *Eusynstyela latericius*. *Journal of natural products* **72**, 1115-1120 (2009).
- 17 Tadesse, M., Tabudravu, J. N., Jaspars, M., Strøm, M. B., Hansen, E., Andersen, J. H., Kristiansen, P. E. & Haug, T. The antibacterial ent-eusynstyelamide B and eusynstyelamides D, E, and F from the Arctic bryozoan *Tegella cf. spitzbergensis*. *Journal of natural products* **74**, 837-841 (2011).
- 18 Paulsen, M. H., Engqvist, M., Ausbacher, D., Anderssen, T., Langer, M. K., Haug, T., Morello, G. R., Liikanen, L. E., Blencke, H.-M. & Isaksson, J. Amphipathic barbiturates as mimics of antimicrobial peptides and the marine natural products eusynstyelamides with activity against multi-resistant clinical isolates. *Journal of Medicinal Chemistry* **64**, 11395-11417 (2021).
- 19 Langer, M. K., Rahman, A., Dey, H., Anderssen, T., Zilioli, F., Haug, T., Blencke, H.-M., Stensvåg, K., Strøm, M. B. & Bayer, A. A concise SAR-analysis of antimicrobial cationic amphipathic barbiturates for an improved activity-toxicity profile. *European Journal of Medicinal Chemistry* **241**, 114632 (2022).
- 20 Langer, M. K., Rahman, A., Dey, H., Anderssen, T., Blencke, H.-M., Haug, T., Stensvåg, K., Strøm, M. B. & Bayer, A. Investigation of tetrasubstituted heterocycles reveals hydantoins as a promising scaffold for development of novel antimicrobials with membranolytic properties. *European Journal of Medicinal Chemistry* **249**, 115147 (2023).
- 21 Pasupuleti, M., Schmidtchen, A. & Malmsten, M. Antimicrobial peptides: key components of the innate immune system. *Critical reviews in biotechnology* **32**, 143-171 (2012).
- 22 Strøm, M. B., Haug, B. E., Skar, M. L., Stensen, W., Stiberg, T. & Svendsen, J. S. The pharmacophore of short cationic antibacterial peptides. *Journal of medicinal chemistry* **46**, 1567-1570 (2003).
- 23 Hansen, T., Alst, T., Havelkova, M. & Strøm, M. B. Antimicrobial activity of small β -peptidomimetics based on the pharmacophore model of short cationic antimicrobial peptides. *Journal of medicinal chemistry* **53**, 595-606 (2010).
- 24 Paulsen, M. H., Ausbacher, D., Bayer, A., Engqvist, M., Hansen, T., Haug, T., Anderssen, T., Andersen, J. H., Sollid, J. U. E. & Strøm, M. B. Antimicrobial activity of amphipathic α , α -disubstituted β -amino amide derivatives against ESBL-CARBA producing multi-resistant bacteria; effect of halogenation, lipophilicity and cationic character. *European journal of medicinal chemistry* **183**, 111671 (2019).
- 25 Igumnova, E. M., Mishchenko, E., Haug, T., Blencke, H.-M., Sollid, J. U. E., Fredheim, E. G. A., Lauksund, S., Stensvåg, K. & Strøm, M. B. Synthesis and antimicrobial activity of small cationic amphipathic aminobenzamide marine natural product mimics and evaluation of relevance against clinical isolates including ESBL-CARBA producing multi-resistant bacteria. *Bioorganic & Medicinal Chemistry* **24**, 5884-5894 (2016).
- 26 Bakka, T. A., Strøm, M. B., Andersen, J. H. & Gautun, O. R. Synthesis and antimicrobial evaluation of cationic low molecular weight amphipathic 1, 2, 3-triazoles. *Bioorganic & Medicinal Chemistry Letters* **27**, 1119-1123 (2017).
- 27 Sadovskaya, I., Vinogradov, E., Flahaut, S., Kogan, G. & Jabbouri, S. d. Extracellular carbohydrate-containing polymers of a model biofilm-producing strain, *Staphylococcus epidermidis* RP62A. *Infection and immunity* **73**, 3007-3017 (2005).

- 28 Rohde, H., Burdelski, C., Bartscht, K., Hussain, M., Buck, F., Horstkotte, M. A., Knobloch, J. K. M., Heilmann, C., Herrmann, M. & Mack, D. Induction of *Staphylococcus epidermidis* biofilm formation via proteolytic processing of the accumulation-associated protein by staphylococcal and host proteases. *Molecular microbiology* **55**, 1883-1895 (2005).
- 29 Fernández, L., Breidenstein, E. B. & Hancock, R. E. Creeping baselines and adaptive resistance to antibiotics. *Drug Resistance Updates* **14**, 1-21 (2011).
- 30 Guarin, M., Ny, A., De Croze, N., Maes, J., Léonard, M., Annaert, P. & de Witte, P. A. Pharmacokinetics in zebrafish embryos (Zfe) following immersion and intrayolk administration: A fluorescence-based analysis. *Pharmaceuticals* **14**, 576 (2021).
- 31 Long, K., Kostman, S. J., Fernandez, C., Burnett, J. C. & Huryn, D. M. Do zebrafish obey lipinski rules? *ACS Medicinal Chemistry Letters* **10**, 1002-1006 (2019).
- 32 Jault, C., Pichon, L. & Chluba, J. Toll-like receptor gene family and TIR-domain adapters in *Danio rerio*. *Molecular immunology* **40**, 759-771 (2004).
- 33 Meijer, A. H., Krens, S. G., Rodriguez, I. A. M., He, S., Bitter, W., Snaar-Jagalska, B. E. & Spaik, H. P. Expression analysis of the Toll-like receptor and TIR domain adaptor families of zebrafish. *Molecular immunology* **40**, 773-783 (2004).
- 34 Phelan, P. E., Mellon, M. T. & Kim, C. H. Functional characterization of full-length TLR3, IRAK-4, and TRAF6 in zebrafish (*Danio rerio*). *Molecular immunology* **42**, 1057-1071 (2005).
- 35 Prajsnar, T. K., Michno, B. J., Pooranachandran, N., Fenton, A. K., Mitchell, T. J., Dockrell, D. H. & Renshaw, S. A. Phagosomal Acidification Is Required to Kill *Streptococcus pneumoniae* in a Zebrafish Model. *Cellular Microbiology* **2022** (2022).
- 36 Widziolek, M., Prajsnar, T. K., Tazzyman, S., Stafford, G. P., Potempa, J. & Murdoch, C. Zebrafish as a new model to study effects of periodontal pathogens on cardiovascular diseases. *Scientific reports* **6**, 36023 (2016).

Supporting Information
for
Peptidomimetic Tetrasubstituted Barbiturates and Hydantoins: Investigation of their antibiofilm and in vivo antimicrobial activity

Ataur Rahman¹, Manuel Karl Langer², Bartosz Michno⁵, Gabriela Żyłka⁵, Jonathan Hira³, Hege Devold¹, Ida Kristine Østnes Hansen¹, Ekaterina Mishchenko³, Johanna U Ericson³, Morten B. Strøm⁴, Annette Bayer², Tomasz Prajsnar⁵, Klara Stensvåg¹

¹ The Norwegian College of Fishery Science, Faculty of Biosciences, Fisheries and Economics, UiT The Arctic University of Norway, NO-9037 Tromsø, Norway. ² Department of Chemistry, Faculty of Science and Technology, UiT The Arctic University of Norway, NO-9037 Tromsø, Norway. ³ Department of Medical Biology, Faculty of Health Sciences, UiT The Arctic University of Norway, NO-9037 Tromsø, Norway. ⁴ Department of Pharmacy, Faculty of Health Sciences, UiT The Arctic University of Norway, NO-9037 Tromsø, Norway. ⁵ Department of Evolutionary Immunology, Institute of Zoology and Biomedical Research, Faculty of Biology, Jagiellonian University, 30-387 Krakow, Poland. # corresponding author. Email: klara.stensvag@uit.no

List of Tables

Table S1. List of compounds from barbiturates and hydantoins derivatives, which undergo antibiofilm testing and their antibiofilm potential.	2
Table S2. List of biofilm-forming bacteria that were used to screen antibiofilm activity.	5
Table S3. List of antibiotic resistance clinical isolates.	5
Table S4. Toxicity of the compounds (first set with 8 compounds) in zebrafish embryos using the immersion method.	6
Table S5. Toxicity of the compounds (second set with 9 compounds) in zebrafish embryos using immersion method.	9
Table S6. Toxicity of the compounds (third set with 14 compounds) in zebrafish embryos using immersion method.	11
Table S7. Toxicity of the compounds in zebrafish embryos using the intrayolk (IY) microinjection method.	15
Table S8. List of bacteria that were used in in vivo antibacterial activity study.	16
Table S9. Antimicrobial activity of the compounds in zebrafish embryos using the intrayolk (IY) microinjection method.	17
Table S10. The compounds' physicochemical properties (molecular descriptors) compared to the Lipinski rules.	18

Table S1. List of compounds from barbiturates and hydantoin derivatives, which undergo antibiofilm testing and their antibiofilm potential.

Sl. No.	Compound ID	Type of compounds (Paper)	MIA (B. s) ^a	VIA (B. s) ^a	BIA (S. e-RP62A)		BEA (S. e-RP62A)		BIA (S. e-5179-R1)		BEA (S. e-5179-R1)		BIA (P. a-PA01)		BEA (P.a-PA01)		MIA (E. c) ^a	VIA (E. c) ^a	
			A&S	Effects	1/2MIC	1/4MIC	5xMIC	2xMIC	1/2MIC	1/4MIC	5xMIC	2xMIC	1/2MIC	1/4MIC	5xMIC	2xMIC	A&S	Effects	
1	7	Barbiturates ¹	+++	+	37	28													
2	8		-	-	16	3													
3	9		+	+	0	0													
4	10cA		++	+	20	6	58	32	0	0									
5	10cG		++	++	9	7													
6	10dG		++++	++	35	5			0	0			92	39	88	86	+++	++	
7	11kG		+++	++	3	0												++	++
8	11IA		+++	+	19	3	87	30	15	1									
9	11IG		++++	++	0	0												++	++
10	11nA		+++	+	31	8			0	0				36	28	69	34		
11	11nG		++++	++	12	16												+++	++
12	11oA		++++	++	72	55	84	74	0	0	83	0	0	0	0	50	49	++	++
13	11oG		++++	++	37	25												++	++
14	11pA		++++	++	31	28													
15	11pG		++++	+++	8	9												++	++
16	12aA		+++	++	23	5												++++	++
17	12aG		++++	+++	3	3			0	0			87	21	83	83			
18	13aA		+++	+++	44	18												++	+
19	13aG		++++	+++	0	0	2	2	0	0	4	2	28	29	56	0	+++	++	
20	13cG		++	+	0	0													
21	13eG		+++	+++	3	3												+	++
22	13hG		-	+	23	7													
23	13iA		++	+	58	18	86	38	4	0	58	24	60	70	94	67			

Sl. No.	Compound ID	Type of compounds (Paper)	MIA (B. s) ^a	VIA (B. s) ^a	BIA (S. e-RP62A)		BEA (S. e-RP62A)		BIA (S. e-5179-R1)		BEA (S. e-5179-R1)		BIA (P. a-PA01)		BEA (P. a-PA01)		MIA (E. c) ^a	VIA (E. c) ^a
			A&S	Effects	1/2MIC	1/4MIC	5xMIC	2xMIC	1/2MIC	1/4MIC	5xMIC	2xMIC	1/2MIC	1/4MIC	5xMIC	2xMIC	A&S	Effects
24	13iG	Hydantoin ²	++++	++	2	3												
25	13jA		+++	+	3	0	85	11	34	0	51	4	35	19	78	0	++	++
26	13jG		+++	+	45	0											+++	++
27	13lG		++++	++	24	8											+	+
28	13pA		+++	++	53	25	76	21	6	0	90	19	15	11	71	54		
29	13pG		++++	+++	3	1			0	0			0	39	80	55		
30	16aG		++	+++	4	4											+	++
31	17aA		++	++	28	19											++	++
32	2bG		-	-	22	6												
33	2cA		++	+	55	38	84	41	4	0	24	22						
34	2cG		+++	++	3	9											+	+
35	2dA	++	+	53	20	84	32	2	0			0	0	74	20	+	+	
36	2dG	++++	++	0	7											+	+	
37	2eG	++++	+++	22	6											+	+	
38	2fG	+++	++	20	4													
39	6bG	++	++	15	12													
40	6cA	++	+	46	18	46	10	3	0									
41	6cG	++++	+++	8	0											+	+	
42	6dA	++	+	57	36	88	32	2	0	38	0							
43	6dG	++++	+++	5	0											+	+	
44	6fG	+++	+++	8	0											+	+	
45	Ciprofloxacin	Reference antibiotics			2	7	3		1	0	5	16	96	51	96	96		
46	Clorhexidine		++++	+++			4	2			1	0	0	0	84	56	++++	+++
47	Polymixin B				10	6					42	0	95	24				

Sl. No.	Compound ID	Type of compounds (Paper)	MIA (B. s) ^a	VIA (B. s) ^a	BIA (S. e-RP62A)		BEA (S. e-RP62A)		BIA (S. e-5179-R1)		BEA (S. e-5179-R1)		BIA (P. a-PA01)		BEA (P.a-PA01)		MIA (E. c) ^a	VIA (E. c) ^a		
			A&S	Effects	1/2MIC	1/4MIC	5xMIC	2xMIC	1/2MIC	1/4MIC	5xMIC	2xMIC	1/2MIC	1/4MIC	5xMIC	2xMIC	A&S	Effects		
48	Vancomycin				0	3														
49	Daptomycin																			
50	Ampicillin																			
51	Erythromycin						0	0												
52	Rifampicin												24	19						
53	Tetracycline				18	14														
54	Gentamicin				1	3														
55	Streptomycin																			
56	Chloramphenicol																			

Bacterial reference strains: B. s - *Bacillus subtilis* 168, S. a - *Staphylococcus aureus* (ATCC 9144), S. e (RP62A) - *Staphylococcus epidermidis* RP62A (ATCC 35984), S. e (5179-R1) - *Staphylococcus epidermidis* 5179-R1, E. c - *Escherichia coli* (ATCC 25922), and P. a - *Pseudomonas aeruginosa* PAO1.

MIC - minimum inhibitory concentration, MIA - membrane integrity assay, VIA - viability assay, BIA - biofilm inhibition assay.

^a Values were taken from our previous work^{1,2}.

Blue - narrow spectrum, green - broad spectrum.

Dark orange - most active as antibiofilm agent, light orange - moderate active as antibiofilm agent.

Table S2. List of biofilm-forming bacteria that were used to screen antibiofilm activity.

Sl. No.	Genus and species	Abbreviation	Strain	Gram +/-
1	<i>Staphylococcus epidermidis</i>	S. e	RP62A	+
2	<i>Staphylococcus epidermidis</i>	S. e	5179-R1	+
3	<i>Pseudomonas aeruginosa</i>	P. a	PAO1	-

Table S3. List of antibiotic resistance clinical isolates.

Sl. No.	Antibiotic-resistant clinical isolate	Resistance	Abbreviation	Gram +/-
1	<i>Enterococcus faecium</i> I-H-4	VRE	E. f	+
2	<i>Staphylococcus aureus</i> 42-74	MRSA	S. a	+
3	<i>Acinetobacter baumannii</i> K47-42	OXA-23, oxacillinase	A. b	-
4	<i>Klebsiella pneumoniae</i> K47-25	KPC-2, K. pneumoniae carbapenemase	K. p	-
5	<i>Pseudomonas aeruginosa</i> K34-7	VIM-2, verona integron-encoded metallo- β -lactamase	P. a	-

Table S4. Toxicity of the compounds (first set with 8 compounds) in zebrafish embryos using the immersion method.

Sl. No.	Compound ID	In vitro toxicity	MIC against S. a/S. e	In vivo toxicity_Zebrafish embryo (mortality)											
		Conc. At 50% hemolysis (µg/mL)		Concentration (µg/mL)	Day 1 Embryo (% of mortality)				Day 2 Embryo (% of mortality)			Day 3 Embryo (% of mortality)			
					24 hr	48 hr	72 hr	96 hr	24 hr	48 hr	72 hr	24 hr	48 hr		
1	13iA	322.8	8	200	100					-	-		-	-	
				100	100					100			100		
				50	100					100			100		
				25	20	90	100			90	100		100		
				25	0	30	100			90	100				
				16	0	0	10	100	0	0	100				
				8	0	0	0	0	0	0	0				
				4	0	0	0	0	0	0	0				
2	6f ³	177.8	16	200	100					-	-		-	-	
				100	100					100					
				50	100					100					
				25	40	90	100			50	100				
				25	0	0	0	100			20	100			
				16	0	0	0	80			0	0	60		
				8	0	0	0	0	0	0	0				
				4	0	0	0	0	0	0	0				
3	2cA	367.7	8	100	90	100				100			100		
				50	0	0	90	100			80	100		100	
				25	0	0	0	100			0	0	100	60	100
				25	0	0	10	100			0	0	100		
				16	0	0	0	40			0	0	20		
				8	0	0	0	0	0	0	0	0	0		

Sl. No.	Compound ID	In vitro toxicity		In vivo toxicity_Zebrafish embryo (mortality)									
		Conc. At 50% hemolysis (µg/mL)	MIC against S. a/S. e	Concentration (µg/mL)	Day 1 Embryo (% of mortality)				Day 2 Embryo (% of mortality)			Day 3 Embryo (% of mortality)	
					24 hr	48 hr	72 hr	96 hr	24 hr	48 hr	72 hr	24 hr	48 hr
				4	0	0	0	0	0	0	0		
4	6dA	364	8	100	100				100			100	
				50	0	40	100		100			100	
				25	0	0	0	100	0	0	100	90	100
				25	0	0	0	100	0	0	100		
				16	0	0	0	70	0	0	0		
				8	0	0	0	0	0	0	0		
				4	0	0	0	0	0	0	0		
5	11A	341.9	16/8	100	100				100				
				50	100				100				
				25	0	0	0	100	80	100			
				25	0	0	0	100	100				
				16	0	0	0	100	0	0	100		
				8	0	0	0	0	0	0	0		
				4	0	0	0	0	0	0	0		
6	13aG	169.1	2/0.5	100	100				100				
				50	100				100				
				25	100				100				
				25	100				100				
				16	50	80	100		100				
				8	0	0	0	100	100				
				4	0	0	0	0	0	0	10		
7	12aG	154.6	2/0.5	100	100				100				
				50	100				100				

Sl. No.	Compound ID	In vitro toxicity		In vivo toxicity_Zebrafish embryo (mortality)										
		Conc. At 50% hemolysis (µg/mL)	MIC against S. a/S. e	Concentration (µg/mL)	Day 1 Embryo (% of mortality)				Day 2 Embryo (% of mortality)			Day 3 Embryo (% of mortality)		
					24 hr	48 hr	72 hr	96 hr	24 hr	48 hr	72 hr	24 hr	48 hr	
				25	100					100				
				25	60	90	100			100				
				16	0	0	80	100		100				
				8	0	0	0	20		0	0	40		
				4	0	0	0	0		0	0	0		
8	13pA	163.9	4	100	100					100				
				50	100					100				
				25	80	100				100				
				25	90	100				100				
				16	20	80	100			100				
				8	0	0	0	100		0	100			
				4	0	0	0	0		0	0	0		
9	Tetracyclin	nt	0.25	100	0	0	0	0		0	0	0		
				50	0	0	0	0		0	0	0		
				25	0	0	0	0		0	0	0		
				16	0	0	0	0		0	0	0		
				8	0	0	0	0		0	0	0		
				4	0	0	0	0		0	0	0		
10	DMSO Ctrl	NA	NA	5.00%	0	100				100				
				4.00%	0	0	80	100		0	90	100		
				3.00%	0	0	0	0		0	0	0		
				2.00%	0	0	0	0		0	0	0		
				1.00%	0	0	0	0		0	0	0		

S. a - *Staphylococcus aureus* (ATCC 9144) and S. e - *Staphylococcus epidermidis* RP62A (ATCC 35984). MIC - minimum inhibitory concentration, blue - narrow spectrum, light green - broad spectrum, dark green - safe concentration.

Table S5. Toxicity of the compounds (second set with 9 compounds) in zebrafish embryos using immersion method.

Sl. No.	Compound ID	In vitro toxicity	MIC against S. a/S. e	In vivo toxicity_Zebrafish embryo (mortality)								
		Conc. at 50% haemolysis (µg/mL)		Concentration (µg/mL)	Day 1 Embryo (% of mortality)				Day 2 Embryo (% of mortality)			
					24 hr	48 hr	72 hr	96 hr	24 hr	48 hr	72 hr	
1	2dA	359.3	8	100	100					100		
				50	0	100			100			
				25	0	0	0	100	0	100		
				16	0	0	0	100	0	0	100	
				8	0	0	0	0	0	0	0	
2	10cA	432.4	16	100	0	0	100			100		
				50	0	10	10	90	10	100		
				25	0	0	0	10	0	20	20	
				32	0	0	0	0	0	0	40	
				24	0	0	0	0	0	0	60	
				16	0	0	0	0	0	0	30	
3	6cA	439	8	100	0	100			80	100		
				50	0	0	0	100	10	100		
				25	0	0	0	10	0	0	60	
				32	0	0	0	0	0	0	100	
				24	0	0	0	40	0	0	80	
				16	0	0	0	0	0	0	10	
4	9	>525.2	4	100	0	0	0	100	0	0	100	
				80	0	0	0	90	0	0	100	
				60	0	0	0	0	0	0	10	
				50	0	0	0	0	0	0	0	
				25	0	0	0	0	0	0	0	
5	8	>525.2	8	250	0	0	30	100	0	0	100	

Sl. No.	Compound ID	In vitro toxicity		In vivo toxicity_Zebrafish embryo (mortality)							
		Conc. at 50% haemolysis (µg/mL)	MIC against S. a/S. e	Concentration (µg/mL)	Day 1 Embryo (% of mortality)				Day 2 Embryo (% of mortality)		
					24 hr	48 hr	72 hr	96 hr	24 hr	48 hr	72 hr
				200	0	0	0	100	0	0	100
				150	0	0	0	70	0	0	100
				100	0	0	0	0	0	0	0
				50	0	0	0	0	0	0	0
				25	0	0	0	0	0	0	0
6	13cG	500	8	100	0	0	70	100	60	100	
				50	0	0	0	30	0	0	100
				40	0	0	0	0	0	0	90
				32	0	0	0	0	0	0	20
				25	0	0	0	0	0	0	0
7	13IG	500	4	100	100				100		
				50	40	100			100		
				25	0	0	0	100	50	100	
				16	0	0	0	30	0	0	100
				8	0	0	0	0	0	0	0
				4	0	0	0	0	0	0	0
8	13hG	>574.3	8	100	0	0	80	100	0	100	
				50	0	0	0	10	0	0	100
				40	0	0	0	0	0	0	30
				32	0	0	0	0	0	0	10
				25	0	0	0	0	0	0	0
9	2dG	>516.6	2	100	100				100		
				50	60	100			100		
				25	0	10	100		100		

Sl. No.	Compound ID	In vitro toxicity		In vivo toxicity_Zebrafish embryo (mortality)							
		Conc. at 50% haemolysis (µg/mL)	MIC against S. a/S. e	Concentration (µg/mL)	Day 1 Embryo (% of mortality)				Day 2 Embryo (% of mortality)		
					24 hr	48 hr	72 hr	96 hr	24 hr	48 hr	72 hr
				16	0	0	0	80	0	60	100
				8	0	0	0	0	0	0	0
				4	0	0	0	0	0	0	0

S. a - *Staphylococcus aureus* (ATCC 9144) and S. e - *Staphylococcus epidermidis* RP62A (ATCC 35984). MIC - minimum inhibitory concentration, blue - narrow spectrum, light green - broad spectrum, dark green - safe concentration.

Table S6. Toxicity of the compounds (third set with 14 compounds) in zebrafish embryos using immersion method.

Sl. No.	Compound ID	In vitro toxicity		In vivo toxicity_Zebrafish embryo (mortality)							
		Conc. at 50% hemolysis (µg/mL)	MIC against S. a/S. e	Concentration (µg/mL)	Day 1 Embryo (% of mortality)				Day 2 Embryo (% of mortality)		
					24 hr	48 hr	72 hr	96 hr	24 hr	48 hr	72 hr
1	11qG	31.9	2	100	100				100		
				50	100				100		
				25	100				100		
				16	100				100		
				8	90	90	90	100	100		
				4	0	40	90	90	100		
2	11kG	449.8	2	100	100				100		
				50	10	100			100		
				25	0	60	100		70	100	
				16	0	0	90	100	0	100	
				8	0	0	0	50	0	0	0
				4	0	0	0	0	0	0	0
3	13jG	439.1	4	100	100				100		

Sl. No.	Compound ID	In vitro toxicity		In vivo toxicity_Zebrafish embryo (mortality)								
		Conc. at 50% hemolysis (µg/mL)	MIC against S. a/S. e	Concentration (µg/mL)	Day 1 Embryo (% of mortality)				Day 2 Embryo (% of mortality)			
					24 hr	48 hr	72 hr	96 hr	24 hr	48 hr	72 hr	
				50	100					100		
				25	100					100		
				16	90	100				100		
				8	0	0	0	40	0	100		
				4	0	0	0	0	0	0	0	0
4	2bG	444.9	16	100	0	0	0	10	0	0	0	0
				96	0	0	0	10	0	0	0	0
				80	0	0	0	0	0	0	0	0
				64	0	0	0	0	0	0	0	0
				50	0	0	0	0	0	0	0	0
				25	0	0	0	0	0	0	0	0
5	2cG	>466.7	2	100	100				100			
				50	10	100			100			
				25	0	0	90	100	90	100		
				16	0	0	0	60	0	0	90	
				8	0	0	0	0	0	0	0	
				4	0	0	0	0	0	0	0	
6	2fA	356.9	16	100	100				100			
				50	0	30	100		100			
				25	0	0	0	100	0	0	100	
				16	0	0	0	80	0	0	100	
				8	0	0	0	0	0	0	0	
				4	0	0	0	0	0	0	0	
7	10cG	441	2	100	100				100			

Sl. No.	Compound ID	In vitro toxicity		In vivo toxicity_Zebrafish embryo (mortality)								
		Conc. at 50% hemolysis (µg/mL)	MIC against S. a/S. e	Concentration (µg/mL)	Day 1 Embryo (% of mortality)				Day 2 Embryo (% of mortality)			
					24 hr	48 hr	72 hr	96 hr	24 hr	48 hr	72 hr	
				50	0	90	100			100		
				25	0	0	10	100		0	100	
				16	0	0	0	60		0	0	100
				8	0	0	0	0		0	0	0
				4	0	0	0	0		0	0	0
8	2fG	>489.3	4	100	10	100				100		
				50	0	0	100		0	40	100	
				25	0	0	0	100	0	0	10	
				16	0	0	0	0	0	0	0	
				8	0	0	0	0	0	0	0	
				4	0	0	0	0	0	0	0	
9	6dG	195	1	100	100				100			
				50	100				100			
				25	70	100			100			
				16	10	90	100		90	100		
				8	0	0	0	100	0	0	100	
				4	0	0	0	0	0	0	0	
10	6fG	384	2	100	100				100			
				50	60	100			100			
				25	0	0	100		0	80	100	
				16	0	0	0	0	0	0	100	
				8	0	0	0	0	0	0	0	
				4	0	0	0	0	0	0	0	
11	6bG	435	4	100	0	0	40	100	30	100		

Sl. No.	Compound ID	In vitro toxicity		In vivo toxicity_Zebrafish embryo (mortality)							
		Conc. at 50% hemolysis (µg/mL)	MIC against S. a/S. e	Concentration (µg/mL)	Day 1 Embryo (% of mortality)				Day 2 Embryo (% of mortality)		
					24 hr	48 hr	72 hr	96 hr	24 hr	48 hr	72 hr
				50	0	0	0	100	0	0	100
				40	0	0	0	0	0	0	0
				32	0	0	0	0	0	0	0
				28	0	0	0	0	0	0	0
				25	0	0	0	0	0	0	0
				100	100				100		
				50	100				100		
12	6cG	347	1	25	0	100			100		
				16	0	0	80	100	10	100	
				8	0	0	0	90	0	0	100
				4	0	0	0	0	0	0	0
				100	100				100		
				50	100				100		
13	11oA	148.6	8	25	90	100			100		
				16	40	90	100		100		
				8	0	0	0	90	0	0	100
				4	0	0	0	0	0	0	0
				100	100				100		
				50	100				100		
14	13eA	22.7	2	25	100				100		
				16	90	100			100		
				8	40	80	90	100	100		
				4	0	0	0	60	0	60	60
				100	100				100		
				50	100				100		

S. a - *Staphylococcus aureus* (ATCC 9144) and S. e - *Staphylococcus epidermidis* RP62A (ATCC 35984). MIC - minimum inhibitory concentration, blue - narrow spectrum, light green - broad spectrum, dark green - safe concentration.

Table S7. Toxicity of the compounds in zebrafish embryos using the intrayolk (IY) microinjection method.

Comp. ID	In vitro toxicity		In vivo toxicity (IY injection) using zebrafish embryo									
	Conc. at 50% hemolysis (µg/mL)	MIC against S. a/ S. e	Safe conc. (µg/mL) in immersion	IY injection dose (mg/kg)	Amount injected (ng)	Day 1 embryo (% of mortality)				Day 2 embryo (% of mortality)		
						24 hr	48 hr	72 hr	96 hr	24 hr	48 hr	72 hr
13iA	322.8	8	8	2	0.5	0	0	0	0	0	0	0
				4	1	0	0	0	0	0	0	0
				8	2	0	0	0	0	0	0	0
				16	4	0	0	0	0	0	0	0
2cA	367.7	8	8	2	0.5	0	0	0	0	0	0	0
				4	1	0	0	0	0	0	0	0
				8	2	0	0	0	0	0	0	0
				16	4	0	0	0	0	0	0	0
9	>525.2	4	50	2	0.5	0	0	0	0	0	0	0
				4	1	0	0	0	0	0	0	0
				8	2	0	0	0	0	0	0	0
				16	4	0	7	13	13	0	0	0
8	>525.2	8	100	2	0.5	0	0	0	0	0	0	0
				4	1	0	0	0	0	0	0	0
				8	2	0	0	0	0	0	0	0
				16	4	0	7	7	33	0	0	0
6bG	435	4	40	2	0.5	0	0	0	0	0	0	0
				4	1	0	0	0	0	0	0	0
				8	2	0	0	0	0	0	0	0
				16	4	7	7	7	7	0	0	0
Tetracycline Ctrl	nt	0.25	100	2	0.5	0	0	0	0	0	0	0
				4	1	0	0	0	0	0	0	0
				8	2	0	0	0	0	0	0	0
				16	4	0	0	0	0	0	0	0

Comp. ID	<i>In vitro</i> toxicity		<i>In vivo</i> toxicity (IY injection) using zebrafish embryo									
	Conc. at 50% hemolysis (µg/mL)	MIC against <i>S. a</i> / <i>S. e</i>	Safe conc. (µg/mL) in immersion	IY injection dose (mg/kg)	Amount injected (ng)	Day 1 embryo (% of mortality)				Day 2 embryo (% of mortality)		
						24 hr	48 hr	72 hr	96 hr	24 hr	48 hr	72 hr
DMSO Ctrl	NA	NA	1%	NA	0.000004%	0	0	0	0	0	0	0
				NA	0.000008%	0	0	0	0	0	0	0

S. a - *Staphylococcus aureus* (ATCC 9144) and *S. e* - *Staphylococcus epidermidis* RP62A (ATCC 35984). MIC - minimum inhibitory concentration, nt - not tested, NA - not applicable.

Table S8. List of bacteria that were used in *in vivo* antibacterial activity study.

Sl. No.	Genus and species	Abbreviation	Strain	Gram +/-
1	<i>Staphylococcus aureus</i>	<i>S. a</i>	SH1000	+
2	<i>Staphylococcus epidermidis</i>	<i>S. e</i>	RP62A (ATCC 35984)	+
3	<i>Streptococcus pneumoniae</i>	<i>S. p</i>	D39	+
4	<i>Escherichia coli</i>	<i>E. c</i>	ATCC 25922	-
5	<i>Pseudomonas aeruginosa</i>	<i>P. a</i>	PAO1 (DSM 22644)	-
6	<i>Porphyromonas gingivalis</i>	<i>P. g</i>	W83	-

Table S9. Antimicrobial activity of the compounds in zebrafish embryos using the intrayolk (IY) microinjection method.

Treatment (Comp. ID)	In vitro toxicity		In vivo activity using Zebrafish embryo									
	Conc. at 50% hemolysis (µg/mL)	MIC against S. a/ S. e	Safe conc. (µg/mL) in immersion	Safe IY injection dose (mg/kg)	Activity against	Day 1 embryo (% of mortality)				Day 2 embryo (% of mortality)		
						24 hr	48 hr	72 hr	96 hr	24 hr	48 hr	72 hr
DMSO Ctrl	NA	NA	1.00%	0.00001%	S. a	30	65	85	90			
					S. e	20	30	50	60			
					S. p					75	100	
					E. c					40	55	55
					P. g	45	80	80	90			
13iA	322.8	8	8	16	S. a	0	15	35	55			
					S. e	0	0	0	5			
					S. p					75	100	
					E. c					50	75	80
2cA	367.7	8	8	16	S. a	5	10	10	15			
					S. e	0	25	25	40			
					S. p					90	95	95
9	>525.2	4	50	8	S. a	5	45	55	65			
					S. e	0	0	0	5			
					S. p					45	100	
					E. c					40	70	75
					P. g	50	80	80	90			
8	>525.2	8	100	8	S. a	40	60	70	70			
					S. e	0	30	40	50			
					S. p					85	100	
					P. g	30	65	65	75			
6bG	435	4	40	8	S. a	30	50	65	90			
					S. e	0	5	15	25			

Treatment (Comp. ID)	In vitro toxicity		In vivo activity using Zebrafish embryo									
	Conc. at 50% hemolysis (µg/mL)	MIC against S. a/ S. e	Safe conc. (µg/mL) in immersion	Safe IY injection dose (mg/kg)	Activity against	Day 1 embryo (% of mortality)				Day 2 embryo (% of mortality)		
						24 hr	48 hr	72 hr	96 hr	24 hr	48 hr	72 hr
Tetracycline Ctrl	nt	0.25	100	8	S. p					85	100	
					P. g	45	75	80	85			
					S. a	5	20	55	60			
					S. e	0	10	15	20			
					S. p					30	75	100
					E. c					10	35	50

S. a - *Staphylococcus aureus* (ATCC 9144), S. e - *Staphylococcus epidermidis* RP62A (ATCC 35984), S. p - *Streptococcus pneumoniae* D39, E. c - *Escherichia coli* (ATCC 25922), P. a - *Pseudomonas aeruginosa* PAO1 (DSM 22644), and P. g - *Porphyromonas gingivalis* W83. MIC - minimum inhibitory concentration, nt - not tested, NA - not applicable.

Table S10. The compounds' physicochemical properties (molecular descriptors) compared to the Lipinski rules.

Set of compounds	Sl. No.	Compound ID	Narrower Lipinski/Veber guidelines for Zebrafish						Molar Refractivity (≤ 130)	Bioavailability Score	Druglikeness (Lipinski)	Leadlikeness
			Mol. Wt. (≤ 500)	clogP (≤ 5.3)	HBD (≤ 3)	HBA (≤ 7)	rotatable bonds (≤ 9)	tPSA (≤ 124 Å)				
1st set	1	6c	950.6223	4.84	2	25	18	193.23	182.06	0.17	No	No
	2	13aG	1050.2414	2.59	6	17	16	264.99	205.64	0.17	No	No
	3	11IA	904.4196	3.15	2	16	15	193.23	182.45	0.17	No	No
	4	13pA	864.4754	2.53	2	13	13	193.23	187.11	0.17	No	No
	5	13iA	877.2514	2.34	2	13	12	193.23	177.86	0.17	No	No
	6	2cA	849.2414	2.55	2	12	12	176.16	173.15	0.55	Yes	No
	7	6dA	948.5574	3.63	6	13	17	265.23	208.33	0.17	No	No
	8	12aG	1022.1874	2.96	6	13	14	265.23	194.84	0.17	No	No
2nd set	9	10cA	938.52	2.55	2	15	14	219.01	208.05	0.17	No	No
	10	6cA	877.30	3.17	2	12	14	176.16	182.76	0.55	Yes	No

Set of compounds	Sl. No.	Compound ID	Narrower Lipinski/Veber guidelines for Zebrafish						Molar Refractivity (≤ 130)	Bioavailability Score	Druglikeness (Lipinski)	Leadlikeness
			Mol. Wt. (≤ 500)	clogP (≤ 5.3)	HBD (≤ 3)	HBA (≤ 7)	rotatable bonds (≤ 9)	tPSA (≤ 124 Å)				
	11	2dA	938.15	2.64	2	12	12	176.16	178.53	0.55	Yes	No
	12	8	1078.38	1.93	0	13	16	137.95	218.51	0.17	No	No
	13	9	1118.36	4.21	0	13	16	145.71	231.14	0.17	No	No
	14	13cG	994.55	3	6	15	16	291.01	219.66	0.17	No	No
	15	13hG	870.65	2.3	6	23	18	264.99	184.84	0.17	No	No
	16	13IG	960.45	3.57	6	16	17	265.23	194.06	0.17	No	No
	17	2dG	867.10	0.65	6	6	14	167.66	189.14	0.17	No	No
3rd set	18	11qG	965.3774	3.43	6	17	18	264.99	225.06	0.17	No	No
	19	11kG	816.421	0.15	6	8	16	197.62	203.36	0.17	No	No
	20	13jG	851.5198	2.24	6	19	18	184.73	183.05	0.17	No	No
	21	2bG	842.6438	2.41	6	22	18	247.92	180.13	0.17	No	No
	22	2cG	778.193	0.53	6	6	14	167.66	183.76	0.17	No	No
	23	2fA	894.5583	4.45	2	24	16	176.16	167.74	0.55	Yes	No
	24	10cG	1022.5994	3.57	6	15	18	291.01	229.27	0.17	No	No
	25	2fG	978.6403	5.58	6	24	20	248.16	188.96	0.17	No	No
	26	6dG	1050.2854	4.45	6	12	18	248.16	209.36	0.17	No	No
	27	6fG	1006.6943	5.87	6	24	22	248.16	198.57	0.17	No	No
	28	6bG	870.6978	4.2	6	18	20	248.16	188.57	0.17	No	No
	29	6cG	961.3774	4.24	6	12	18	248.16	203.98	0.17	No	No
	30	11oA	972.4178	4.17	2	19	16	193.23	187.45	0.17	No	No
	31	13eA	908.4874	3.02	2	13	12	193.23	202.85	0.17	No	No

HBD - hydrogen bond donor, HBA - hydrogen bond acceptor, tPSA - topological polar surface area. Blue - narrow spectrum, and light green - broad spectrum.

Reference

- 1 Langer, M. K., Rahman, A., Dey, H., Anderssen, T., Zilioli, F., Haug, T., Blencke, H.-M., Stensvåg, K., Strøm, M. B. & Bayer, A. A concise SAR-analysis of antimicrobial cationic amphipathic barbiturates for an improved activity-toxicity profile. *European Journal of Medicinal Chemistry* **241**, 114632 (2022).
- 2 Langer, M. K., Rahman, A., Dey, H., Anderssen, T., Blencke, H.-M., Haug, T., Stensvåg, K., Strøm, M. B. & Bayer, A. Investigation of tetrasubstituted heterocycles reveals hydantoins as a promising scaffold for development of novel antimicrobials with membranolytic properties. *European Journal of Medicinal Chemistry* **249**, 115147 (2023).
- 3 Paulsen, M. H., Ausbacher, D., Bayer, A., Engqvist, M., Hansen, T., Haug, T., Anderssen, T., Andersen, J. H., Sollid, J. U. E. & Strøm, M. B. Antimicrobial activity of amphipathic α , α -disubstituted β -amino amide derivatives against ESBL–CARBA producing multi-resistant bacteria; effect of halogenation, lipophilicity and cationic character. *European journal of medicinal chemistry* **183**, 111671 (2019).

Paper IV

Antimicrobial potential of marine bacteria from the Arctic and sub-Arctic regions

Ataur Rahman*, Andrea Iselin Elvheim*, Christoffer Ågnes, Ida Kristine Østnes Hansen, Hege Devold, Frode Jacobsen Øyen, Gabriel Magno de Freitas Almeida, Hans-Matti Blencke, Bjarne Landfald, Tor Haug, Klara Stensvåg#

Norwegian College of Fishery Science, Faculty of Life Sciences, Fisheries and Economics, UiT The Arctic University of Norway, 9019 Tromsø, Norway

** Authors contributed equally; # corresponding author*

Abstract

Progressively, more concerns about antimicrobial resistance (AMR) highlight the urgent need for new antimicrobials, and researchers are exploring alternative sources to develop new antibiotics. The potential source of increasing attention is the secondary metabolites produced by marine bacteria, which are little studied and thus represent an undiscovered unique source. This study aimed to isolate, screen, and characterise Arctic marine bacterial isolates from the under-floating ice, planktonic, marine invertebrates, and sediments of the ocean floor collected from north of Tromsø, Norway, to the edge of the ice of the north pole. One hundred and fifty-eight marine bacterial isolates were cultured, isolated, stored, and screened for antibacterial activity using co-culture and the presence of potential biosynthetic gene clusters (BGCs), nonribosomal peptide synthetases (NRPS), and polyketide synthases (PKS), using PCR screening. Sixty-five marine bacterial isolates showed antibacterial activity against a panel of Gram-positive and Gram-negative human pathogen relative of bacteria and Gram-negative marine biofilm-forming bacteria. Thirty-seven marine bacterial isolates confirmed the presence of BGC of NRPS or PKS. Seven isolates showed activity against bacteria related to Gram-positive and Gram-negative human pathogens and have NRPS or PKS BGCs. Genome sequencing and mining revealed the presence of several BGCs, which could be a potential source of antimicrobial activity. These findings suggest that the secondary metabolites of Arctic marine bacteria could be a potential source of new antibiotics to fight against AMR.

Keywords: Bioprospecting, Arctic, marine bacteria, BGCs, antibiotics, AMR, PKS

Introduction

Due to the growing threat of antibiotic resistance in pathogens, researchers are exploring alternative sources to develop new antibiotics. A potential source that is increasingly attracting attention is secondary metabolites produced by marine bacteria. Marine bacteria are known to inhabit a variety of ecological niches, including extreme environments such as deep-sea hydrothermal vents and polar regions¹. These stressful environments offer unique conditions that stimulate marine bacteria to produce bioactive compounds for potential pharmaceutical applications. In recent years, interest in the discovery of new antibiotic-producing bacteria has moved from terrestrial strains to marine strains². There are several reasons why secondary metabolites of marine bacteria can be a source of new antibiotics. Firstly, marine environments are considered to be a resource of microbial biodiversity that has not yet been explored. This means that there is a high probability of discovering new bioactive compounds from unidentified marine bacteria. Second, the stressful environment of the marine ecosystem causes marine bacteria to produce metabolites that are different from those produced by terrestrial bacteria. These metabolites may have distinctive chemical structures and biological activities, making them potentially effective against drug-resistant pathogens. Furthermore, the development of bioprospecting technology has made it easier to collect samples from various marine environments, including deep sea, thermal vents, and polar regions. These advances have expanded our ability to access and study the different microorganisms present in these environments and increased our chance of discovering new antibiotic-producing marine bacteria that might produce secondary metabolites with novel, interesting structures and new mechanisms of action towards antibiotic-resistant pathogenic bacteria.

Marine bacteria, especially those associated with marine sponges and octocorals, have been found to have a variety of secondary metabolite biosynthesis potentials and antimicrobial activity. Metagenomic studies revealed the presence of genes encoding polyketide synthase (PKS) in the microbiome of marine sponges, indicating the potential for the production of polyketide with antimicrobial properties³. Furthermore, clusters of nonribosomal peptide synthetase (NRPS) genes have been reported in the microbiomes of octocorals, indicating the production of nonribosomal peptides with antimicrobial activity³. Furthermore, bacteria isolated from marine sponges have been shown to inhibit the growth of methicillin-resistant *Staphylococcus aureus* (MRSA) and highlight its potential as a source of antimicrobial components³. However, it should be noted that biosynthetic gene clusters (BGCs), including PKS and NRPS, are not limited to the microbiome of marine invertebrates. PKS, NRPS, and their derivatives are now the basis for many life-saving drugs for various acute and chronic diseases⁴. Among the notable antibiotics are nonribosomal penicillin and polyketide erythromycin A⁴. This realisation prompted efforts to unravel the machinery of these systems, aiming to grasp why and how nature employs large proteins to synthesise small molecules⁴. Additionally, this understanding facilitates the genetic engineering of these enzymes to modify their products, creating potentially valuable analogs⁴. In conclusion, BGCs, including PKS and NRPS-associated genes from marine bacteria, can be a fruitful search strategy to discover small molecules with antimicrobial activity.

In this study, we isolated, cultured, and evaluated the antimicrobial potential of marine bacteria collected at seven different collection points in Arctic regions. We used co-culture-based screening for bioactive marine bacteria and PCR-based screening in conjunction with genome sequencing to evaluate the potential biosynthetic gene cluster for activity.

Results

Marine bacteria from the Arctic

Marine bacteria were cultured from four different types of samples (benthic invertebrates, sediment from the ocean floor, zooplankton, and biomass from under the sea ice) collected at seven different collection points in the Arctic regions during a July 2019 research cruise (*Figure 9*, *Figure S1*, and *Table S1*). In total, 158 marine bacterial isolates were kept for further analysis. Of these, 65 isolates originated from zooplankton, 39 from sediment, 28 from marine invertebrates, and 26 from under-ice material. The growth temperature was assessed at different temperatures (4, 10, 15, 20, and 25 °C). All isolates were able to grow at 4 °C, but a decreasing fraction showed growth when rising the temperature, i.e., 130 (82%) at 10 °C, 98 (62%) at 15 °C, 83 (53%) at 20 °C and 36 (23%) at 25 °C (*Table S2*).

Taxonomic classification

We used matrix-assisted laser desorption ionisation-time-of-flight mass spectrometry (MALDI-TOF MS) data to construct an accurate and reliable in-house MS library. This technology has become a prevailing tool for rapid and reliable microbial identification. *Figure 1* shows the phylogenetic tree based on ribosomal proteins from the MALDI-TOF MS spectra of 91 strains, as those were culturable during the experiment. The purpose of this library was to characterise and dereplicate marine bacteria from Arctic regions.

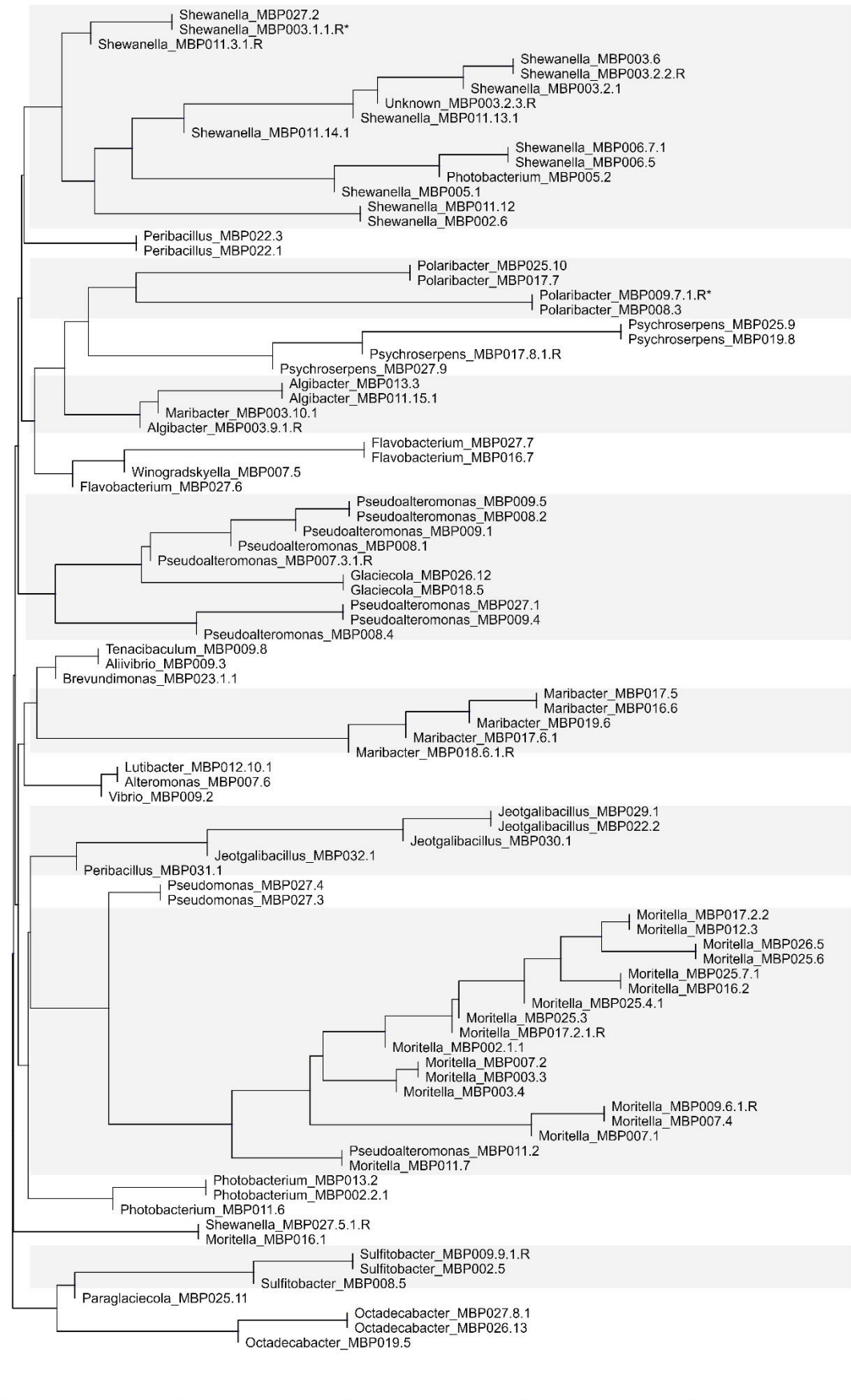


Figure 1. Phylogenetic tree based on the spectra of microbial ribosomal proteins from MALDI-TOF MS, which was combined with the genus of each marine bacterial isolate from 16S rRNA sequencing.

From the 158 marine bacterial isolates, 155 were successfully sequenced for their 16S rRNA, and their taxonomic classification was shown in Table S2 and Figure 2a. However, only *Moritella* (30), *Psychromonas* (27), and *Shewanella* (19) cover almost half (total 76, Figure 2b) of the identified genus.

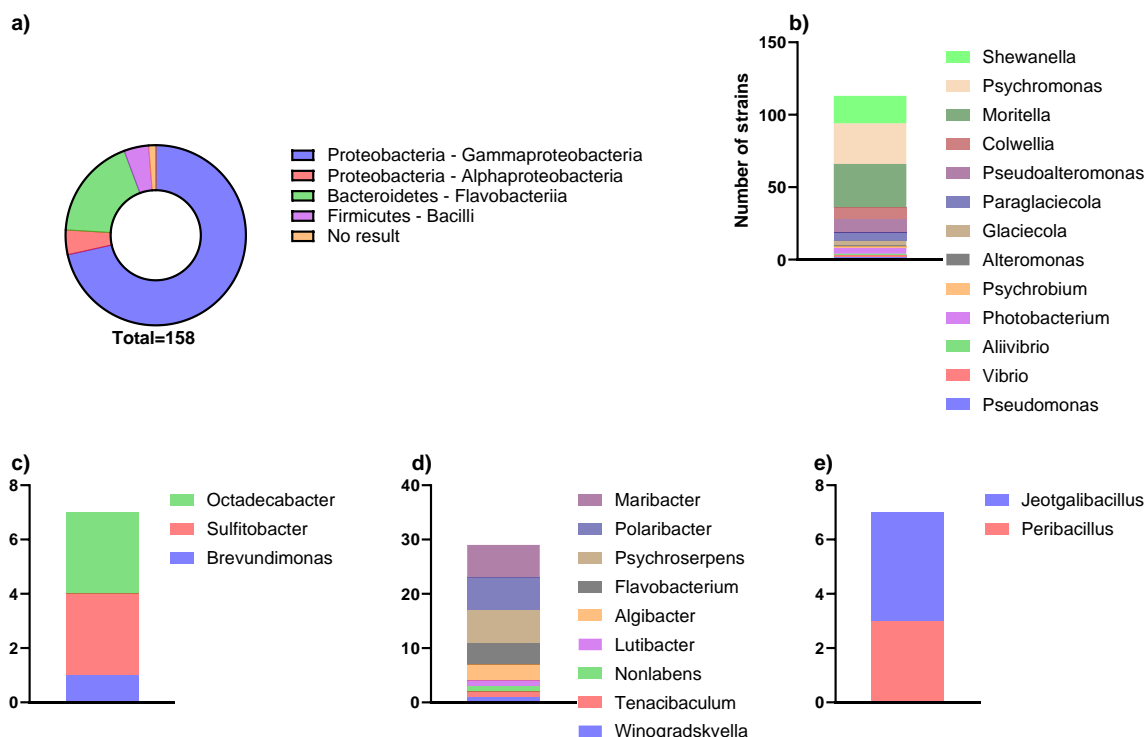


Figure 2. Taxonomic distribution of marine bacteria from the 2019 bioprospecting cruise based on 16S rRNA sequencing. a) Distribution of phyla and classes b) genus of Gammaproteobacterial strains c) genus of Alphaproteobacteria strains d) genus of Bacteroidetes strains e) genus of Firmicutes strains.

Antimicrobial activity and presence of NRPS and PKS domains

Marine bacteria were screened for their antimicrobial bioactivity using a co-culture approach. Among the 158 isolates, 65 (Table 1) showed antimicrobial activity as a zone of inhibition against at least one strain from the panel of 5 Gram-positive and 5 Gram-negative human pathogen relatives (Table S3) and 5 Gram-negative biofilm-forming marine bacteria (Table S4). Only 2 biofilm-forming bacteria are included in Table 1 and Table S2. ESKAPE pathogen relatives (Table S3) were included in this panel of human pathogen relatives. Most bioactive antimicrobial activity was found against *Bacillus subtilis*, *Enterococcus raffinosus*, and *Klebsiella aerogenes*. The representative results of the antimicrobial activity (zone of inhibition) against *B. subtilis* are shown in

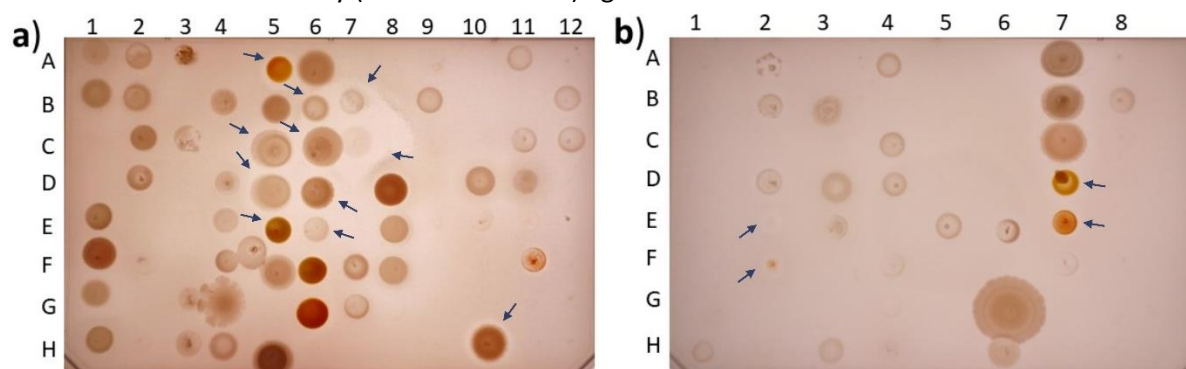


Figure 3. Most potential marine bacterial isolates were pointed out with the black arrows.

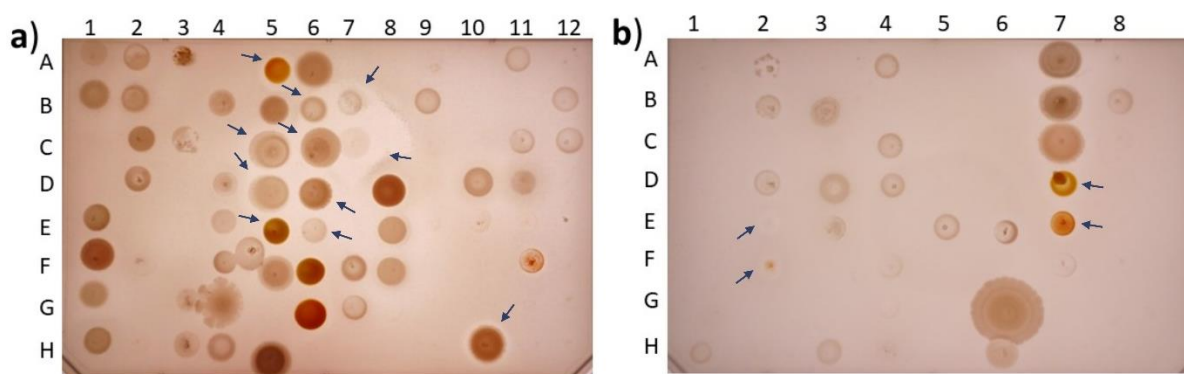


Figure 3. Antimicrobial activity (zone of inhibition) of marine bacteria against *Bacillus subtilis*. a) plate 1, and b) plate 2. The most promising ones are shown with black arrows.

The collection of isolates was screened for the presence of NRPS or PKS gene clusters using a selection of PCR primers from the literature (Table S5). From the collection of 158 marine bacterial isolates, 37 isolates resulted in PCR products of the expected size (Table 1 and Table S2).

Table 1. Results from screening using a co-culture approach for the bioactivity and PCR for detection of NRPS and PKS domains. The marine bacteria were collected from a bioprospecting cruise in the Arctic.

Code (culture)	Genus	PCR-screening			Gram +					Gram -					Marine (Gram -)	
		NRPS	PKS 1	PKS 2	Bs	Cg	Er	Sa	Se	Ab	Ec	Eh	Ka	Pa	Ha	PsyA
MBP002.1.1	Moritella	-	-	-	-	-	+	-	-	-	-	-	-	-	-	-
MBP002.2.1	Photobacterium	-	-	-	++	-	+	-	-	+	-	-	+	-	-	-
MBP002.5	Sulfitobacter	Y	-	-	++	-	-	-	-	-	-	-	-	-	-	-
MBP002.6	Shewanella	-	-	-	++	+	-	-	-	+	-	+	+	-	-	-
MBP003.1.1.R*	Shewanella	-	-	-	+++	-	-	-	-	-	++	-	-	-	++	++
MBP003.2.1	Shewanella	Y	-	-	-	+	-	-	-	-	-	-	-	-	-	-
MBP003.2.2.R	Shewanella	Y	-	-	++	-	+	-	-	-	-	-	-	-	-	-
MBP003.2.3.R	Unknown	-	-	-	-	-	+	-	-	-	-	-	-	-	-	-
MBP003.6	Shewanella	Y	-	-	-	-	+	-	-	-	-	-	-	-	-	-
MBP003.10.1	Maribacter	-	-	-	++	-	-	-	-	-	-	-	-	-	-	-
MBP005.1	Shewanella	Y	-	-	-	-	-	-	-	-	-	-	-	-	-	-
MBP005.2	Photobacterium	-	-	-	-	-	-	-	-	+	-	+	+	-	-	-
MBP006.2	Shewanella	-	-	-	-	-	-	-	-	-	-	+	+	-	-	-
MBP006.3	Shewanella	-	-	-	-	+	-	-	-	+	-	+	+	-	-	-
MBP006.5	Shewanella	-	-	-	-	+	-	-	-	+	-	+	+	-	-	-
MBP006.7.1	Shewanella	-	-	-	-	-	-	-	-	-	-	+	-	-	-	-
MBP007.3.1.R	Pseudoalteromonas	-	-	-	++	-	+	-	-	-	-	-	+	+	-	-
MBP007.4	Moritella	-	-	-	-	-	+	-	-	-	-	-	-	-	-	-
MBP007.5	Winogradskyella	-	-	-	+++	-	-	-	-	-	-	-	-	-	-	-
MBP007.6	Alteromonas	-	-	-	-	-	-	-	-	-	-	+	+	-	-	-
MBP008.1	Pseudoalteromonas	-	-	-	+++	-	+	-	-	-	-	-	-	-	-	-

Code (culture)	Genus	PCR-screening			Gram +					Gram -					Marine (Gram -)	
		NRPS	PKS 1	PKS 2	Bs	Cg	Er	Sa	Se	Ab	Ec	Eh	Ka	Pa	Ha	PsyA
MBP008.2	Pseudoalteromonas	-	-	-	+++	-	+	-	-	-	-	-	-	-	-	-
MBP008.3	Polaribacter	Y	-	-	++	-	+	-	-	-	-	-	-	-	-	-
MBP008.4	Pseudoalteromonas	-	-	-	++	-	+	-	-	-	-	+	-	-	-	-
MBP008.5	Sulfitobacter	Y	Y	-	-	-	-	-	-	-	-	-	-	-	-	-
MBP009.1	Pseudoalteromonas	Y	-	-	+++	-	+	-	-	+	-	+	+	-	-	-
MBP009.2	Vibrio	-	-	-	-	-	+	-	-	+	-	-	-	-	-	-
MBP009.3	Aliivibrio	-	-	-	++	-	+	-	-	-	-	-	-	-	-	-
MBP009.4	Pseudoalteromonas	-	-	-	++	-	+	-	-	-	-	-	+	-	-	-
MBP009.5	Pseudoalteromonas	-	-	-	++	-	+	-	-	-	-	-	-	-	-	-
MBP009.6.1.R	Moritella	-	-	-	++	-	+	-	-	-	-	-	-	-	-	-
MBP009.7.1.R*	Polaribacter	-	-	-	++	-	-	-	-	-	-	-	+	-	-	-
MBP009.8	Tenacibaculum	-	-	-	++	-	-	-	-	+	-	-	+	-	-	-
MBP009.9.1.R	Sulfitobacter	-	-	-	-	-	-	-	-	-	-	-	+	-	-	-
MBP011.1	Unknown	Y	-	-	-	-	-	-	-	-	-	-	-	-	-	-
MBP011.2	Pseudoalteromonas	-	-	-	++	-	+	-	-	-	-	-	-	-	-	-
MBP011.3.1.R	Shewanella	Y	-	-	++	-	+	-	-	-	+++	-	-	-	++	-
MBP011.4	Psychromonas	-	-	-	-	-	+	-	-	-	-	-	-	-	-	-
MBP011.5	Psychromonas	-	-	-	-	-	+	-	-	-	-	-	-	-	-	-
MBP011.6	Photobacterium	-	-	-	-	-	+	-	-	-	-	-	+	-	-	-
MBP011.10	Psychromonas	-	-	-	++	-	-	-	-	-	-	-	-	-	-	-
MBP011.12	Shewanella	-	-	-	+	+	-	-	-	+	-	+	+	+	-	-
MBP011.13.1	Shewanella	Y	-	-	-	-	-	-	+++	+	-	-	-	-	+++	-
MBP011.14.1	Shewanella	Y	-	-	-	-	-	-	-	+	-	-	+	-	+++	-
MBP012.4.1	Psychromonas	-	-	-	-	-	+	-	-	-	-	-	-	-	-	-
MBP012.6	Psychromonas	-	-	-	-	-	+	-	-	-	-	-	-	-	-	-
MBP012.7	Psychromonas	-	-	-	-	-	+	-	-	-	-	-	-	-	-	-
MBP012.13	Psychromonas	-	-	-	-	-	-	-	-	-	-	+	-	-	-	-
MBP013.1	Psychromonas	-	-	-	-	-	+	-	-	-	-	-	-	-	-	-
MBP013.2	Photobacterium	-	-	-	-	+	-	-	-	+	-	-	+	-	-	-
MBP013.3	Algibacter	Y	-	-	-	-	-	-	-	-	-	-	-	-	-	-
MBP016.1	Moritella	-	-	-	+++	+	-	-	-	+	+	-	+	+	-	-
MBP016.5.1	Paraglaeicola	-	-	-	-	+	-	-	-	+	+	-	+	+	-	-
MBP016.7	Flavobacterium	-	-	-	+	-	-	-	-	-	-	-	-	-	-	-
MBP016.9	Psychroserpens	Y	-	-	-	-	-	-	-	-	-	-	-	-	-	-
MBP017.4	Glaciecola	-	-	-	-	-	-	-	-	-	-	+	-	-	-	-
MBP019.3	Moritella	Y	-	-	-	-	-	-	-	-	-	-	-	-	-	-
MBP019.5	Octadecabacter	-	-	-	++	-	-	-	-	-	-	-	-	-	-	-
MBP019.6	Maribacter	-	-	-	++	-	-	-	-	-	-	-	-	-	-	-
MBP019.7	Flavobacterium	Y	-	-	-	-	-	-	-	-	-	-	-	-	-	-
MBP019.8	Psychroserpens	Y	-	-	-	-	-	-	-	-	-	-	-	-	-	-
MBP022.1	Peribacillus	-	-	-	-	+	-	-	-	-	-	-	+	-	-	-

Code (culture)	Genus	PCR-screening			Gram +					Gram -					Marine (Gram -)	
		NRPS	PKS 1	PKS 2	Bs	Cg	Er	Sa	Se	Ab	Ec	Eh	Ka	Pa	Ha	PsyA
MBP022.2	Jeotgalibacillus	Y	-	-	-	-	-	-	-	-	-	-	-	-	-	-
MBP023.1.1	Brevundimonas	Y	-	-	-	-	-	-	-	-	-	-	-	-	-	-
MBP025.6	Moritella	Y	-	-	-	-	-	-	-	-	-	-	-	-	-	-
MBP025.7.1	Moritella	Y	-	-	-	-	-	-	-	-	-	-	-	-	-	-
MBP025.9	Psychroserpens	Y	-	-	-	-	-	-	-	-	-	-	-	-	-	-
MBP025.11	Paraglaciecola	Y	Y	-	-	+	-	-	-	+	-	-	+	-	-	-
MBP026.4	Colwellia	Y	-	-	-	-	-	-	-	-	-	-	-	-	-	-
MBP026.7	Psychromonas	Y	Y	-	-	-	-	-	-	-	-	-	-	-	-	-
MBP026.9	Psychromonas	Y	-	-	-	-	-	-	-	-	-	-	-	-	-	-
MBP026.13	Octadecabacter	Y	Y	-	++	-	-	-	-	-	-	-	-	-	-	-
MBP026.15	Polaribacter	-	-	-	-	-	-	+	-	-	-	-	-	-	-	-
MBP027.1	Pseudoalteromonas	Y	Y	-	-	-	-	-	-	-	-	+	+	+	-	-
MBP027.2	Shewanella	Y	-	-	-	+	-	-	-	+	-	-	+	-	+	-
MBP027.3	Pseudomonas	Y	-	-	+++	-	+	-	-	-	-	+	-	-	-	-
MBP027.4	Pseudomonas	Y	-	-	+++	+	+	-	-	+	-	-	+	+	-	-
MBP027.5.1.R	Shewanella	-	-	-	+++	+	-	-	-	+	-	-	+	+	-	-
MBP027.6	Flavobacterium	-	-	-	+++	+	-	-	-	+	-	-	+	+	-	-
MBP027.7	Flavobacterium	-	-	-	++	-	-	-	-	-	-	-	-	-	+	-
MBP027.8.1	Octadecabacter	-	Y	Y	-	-	-	-	-	-	-	-	-	-	+	-
MBP027.9	Psychroserpens	Y	-	-	-	-	-	-	-	-	-	-	-	-	-	-
MBP027.11	Paraglaciecola	Y	Y	-	-	-	-	-	-	-	-	-	-	-	-	-
MBP029.1	Jeotgalibacillus	Y	-	-	-	-	-	-	-	-	-	-	-	-	-	-
MBP030.1	Jeotgalibacillus	Y	-	-	-	-	-	-	-	-	-	-	-	-	-	-
MBP032.1	Jeotgalibacillus	Y	Y	-	-	-	-	-	-	-	-	-	-	-	-	-

Y – yes, - - negative, +/+/+/+ - antibacterial activity, NRPS - nonribosomal peptide synthetases, PKS - polyketide synthases, Bs - *Bacillus subtilis*, Cg - *Corynebacterium glutamicum*, Er - *Enterococcus raffinosus*, Sa - *Staphylococcus aureus*, Se - *Staphylococcus epidermidis*, Ab - *Acinetobacter baylyi*, Ec - *Escherichia coli*, Eh - *Enterobacter hormaechei*, Ka - *Klebsiella aerogenes*, Pa - *Pseudomonas aeruginosa*, Ha - *Halomonas aquamarina*, PsyA- *Psychromonas arctica*.

Among 37 BGC-positive marine bacterial isolates, 36 isolates generated PCR products by NRPS primers, 8 by PKS 1 primers, and 1 by PKS 2 primers (Table 1).

The Venn diagram (Figure 5) shows that among the 158 marine bacterial isolates, 22 were positive in the PCR screening but did not show any antimicrobial activity. Seven and 23 marine bacterial isolates had antibacterial activity against Gram-negative and Gram-positive human pathogen relatives' bacteria, respectively, but were not positive in the PCR screening. Among the bacterial strains positive in the PCR screening, 2 showed activity against Gram-negative human pathogen relatives and 6 against Gram-positive. On the other hand, 19 marine bacterial isolates showed activity against both Gram-negative and Gram-positive human pathogen relatives' bacteria but were not positive in PCR screening. Seven marine bacterial isolates showed activity against both Gram-negative and Gram-positive human pathogen relatives' bacteria and could also have NRPS or PKS BGCs.

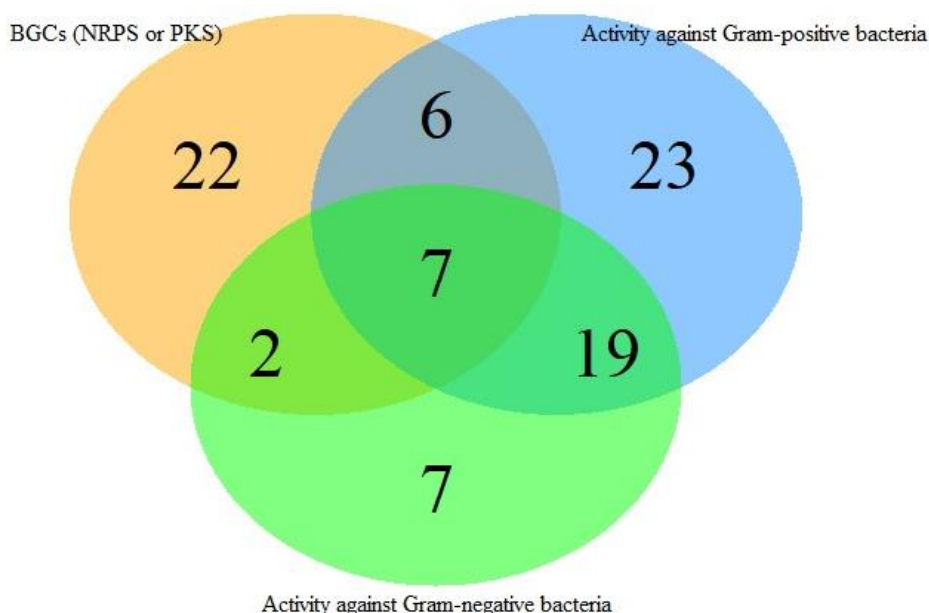


Figure 4. Venn diagram showing the NRPS or PKS positive BGCs (orange) with links to bioactivity against either Gram-negative (green) or Gram-positive (blue) human pathogen relative bacteria.

Whole genome sequencing of selected strains

Based on the co-culturing and PCR screening results, 37 marine bacterial isolates were selected for whole genome sequencing using Nanopore technology. The yield from the sequencing runs varied from 39 Mb to 1,1 Gb (Table S6). The DNA of some strains was fragmented, resulting in read N50 values down to 1 kb, while the DNA of other strains was of better quality, with read N50 values up to 20 kb. The reads were assembled and annotated into draft genomes. One assembly had 151 fragments, two had between 100 and 40 fragments, four had between 20 and 10 fragments, seven had from 9 to 5 fragments, six had three fragments, five had two fragments, and twelve had only one fragment. The assembly with 151 fragments had an N50 of 473530; otherwise, the N50 ranged from 1483162 to 8166020. Assembly statistics are available in Table S6.

Some of the marine bacterial isolates that clustered together in the phylogenetic tree prepared from the MALDI-TOF MS spectra (Figure 1) were genome sequenced to validate the potential for dereplication. Table 2 shows the strains classified as the same species based on average nucleotide identity (ANI). Figure 5 shows the summary of clusters from Figure 1 prepared using spectra of MALDI-TOF MS.

Table 2: Strains of the same species based on average nucleotide identity (ANI) (cut off 95%).

Strain 1	Strain 2	ANI
MBP009.7.1.R* - Polaribacter	MBP008.3 - Polaribacter	99.9674
MBP029.1 - Jeotgalibacillus	MBP022.2 - Jeotgalibacillus	98.6104
MBP029.1 - Jeotgalibacillus	MBP030.1 - Jeotgalibacillus	98.428
MBP029.1 - Jeotgalibacillus	MBP032.1 - Jeotgalibacillus	95.5518
MBP030.1 - Jeotgalibacillus	MBP022.2 - Jeotgalibacillus	99.3304
MBP030.1 - Jeotgalibacillus	MBP032.1 - Jeotgalibacillus	95.5818
MBP032.1 - Jeotgalibacillus	MBP022.2 - Jeotgalibacillus	95.6078
MBP026.13 - Octadecabacter	MBP027.8.1 - Octadecabacter	98.9786

MBP008.4 - <i>Pseudoalteromonas</i>	MBP009.4 - <i>Pseudoalteromonas</i>	98.0173
MBP011.13.1 - <i>Shewanella</i>	MBP011.14.1 - <i>Shewanella</i>	99.9653
MBP005.1 - <i>Shewanella</i>	MBP006.5 - <i>Shewanella</i>	98.5219
MBP005.1 - <i>Shewanella</i>	MBP006.7.1 - <i>Shewanella</i>	98.5142
MBP006.5 - <i>Shewanella</i>	MBP006.7.1 - <i>Shewanella</i>	98.9401
MBP019.8 - <i>Psychroserpens</i>	MBP027.9 - <i>Psychroserpens</i>	99.3784

For example, MBP009.7.1.R* and MBP008.3 had 99.9674 % average nucleotide identity based on genome sequence (Table 2), and they also fall into the same cluster of phylogenetic tree prepared from MALDI-TOF MS (Figure 1 and Figure 5a). The same was observed for MBP022.2, MBP029.1, MBP030.1, and MBP032.1 (Table 2 and Figure 5b) and MBP026.13 and MBP027.8.1 (Table 2 and Figure 5c).

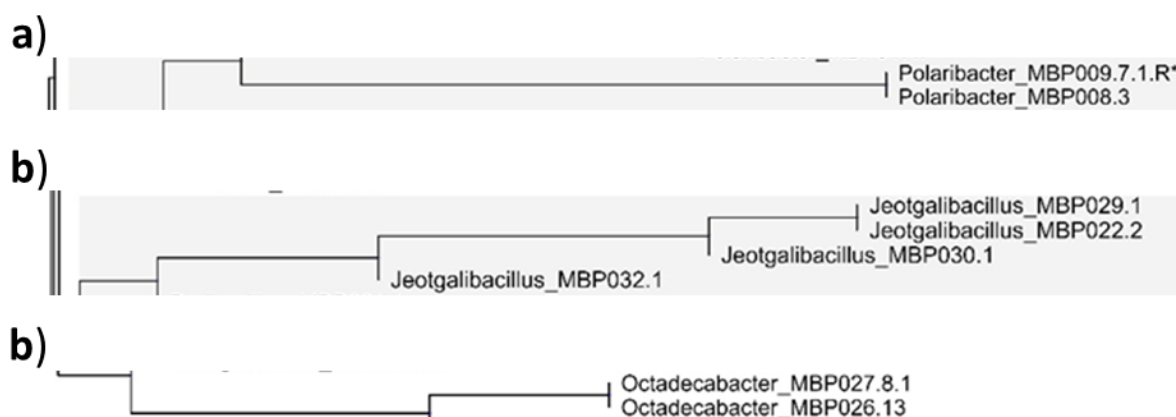


Figure 5. Strains of the same species fall into the same cluster based on ribosomal protein spectra using MALDI-TOF MS and verified by genome sequence.

BGCs were predicted in the 37 sequenced genomes (Figure 6 and Table S7) by antiSMASH. These genomes contained 1-15 BGCs. The *Shewanella sp.* MBP003.1.1.R genome had the highest number of BGCs (15). On the other hand, the genomes of *Pseudoalteromonas sp.* MBP009.5, *Jeotgalibacillus sp.* MBP022.2, *Brevundimonas sp.* MBP023.1.1 and *Jeotgalibacillus sp.* MBP029.1 contained only one BGC. The most promising marine bacterial isolates, which had antimicrobial activity and were positive for NRPS or PKS were *Shewanella sp.* MBP011.13.1 and *Pseudomonas sp.* MBP027.3 and MBP027.4 (Table 3). They contained several BGCs of different types. Most of the strains selected by the indication of present NRPS and PKS modules had NRPS or PKS1 BGCs predicted by antiSMASH (Figure 7). For these strains, 7 out of 23 did not have NRPS or PKS1 BGCs predicted by AntiSMASH. These could either have modules outside of the BGCs predicted by AntiSMASH or be false positives where the PCR products are caused by similar sequences. Not all the primers performed equally well; a summary of the results for each primer is presented in Table S8.

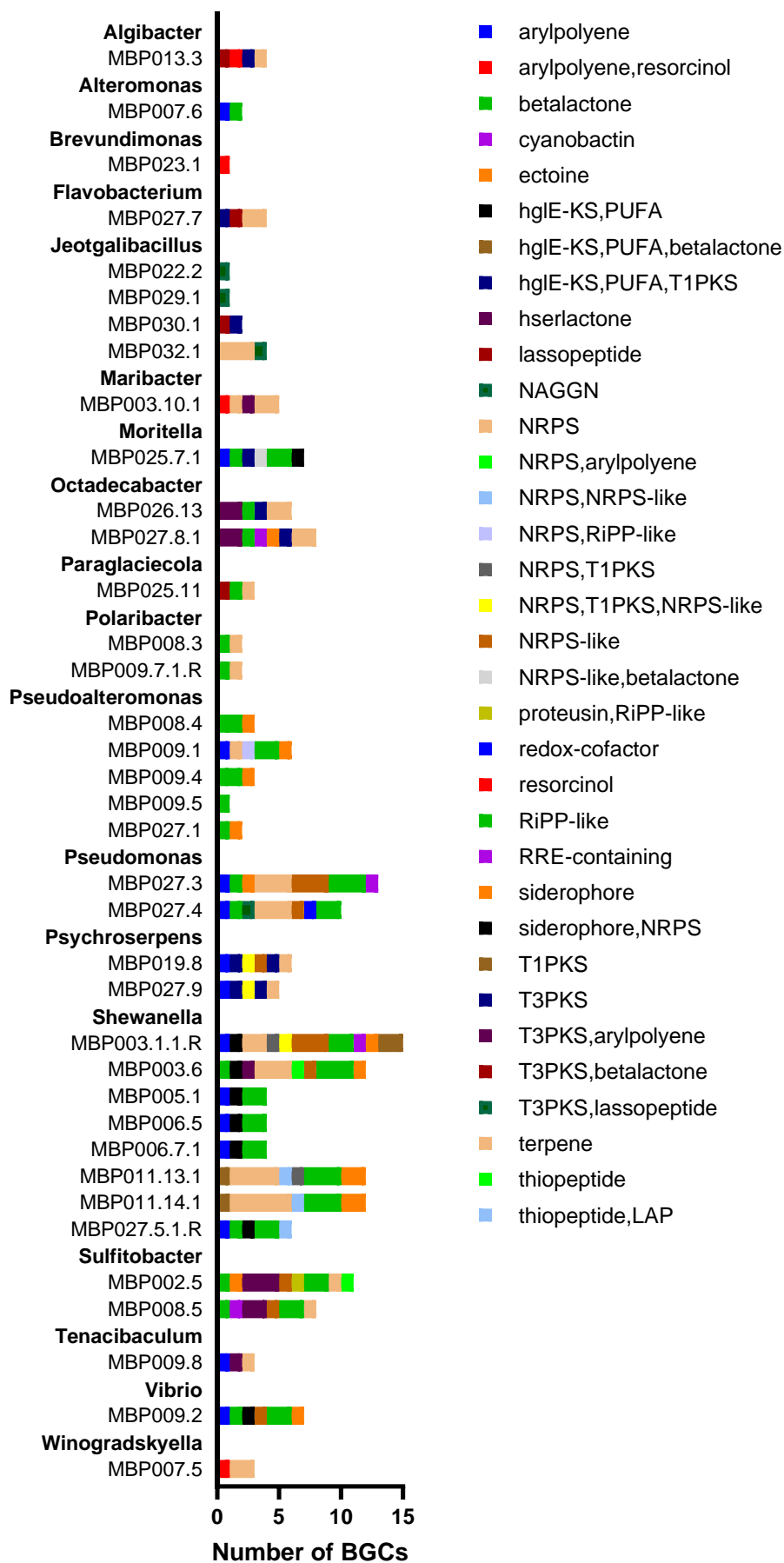


Figure 6: The number and class of BGCs in each bacterial strain.

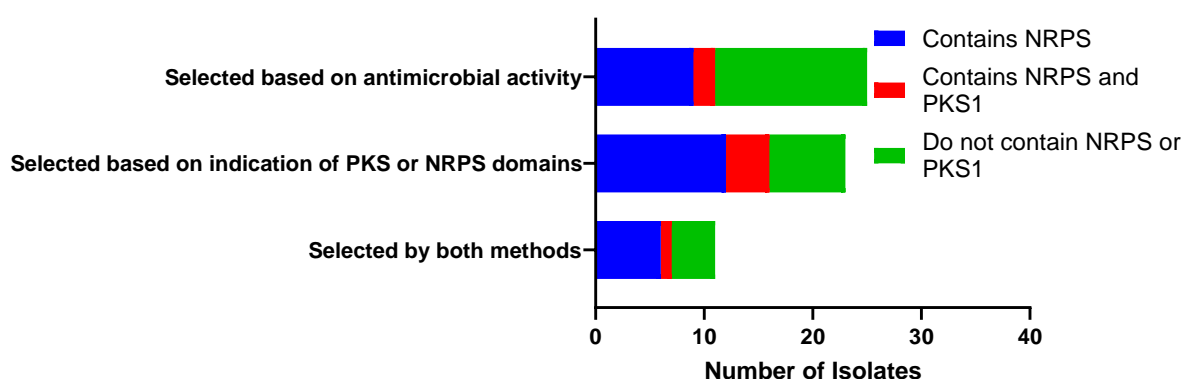


Figure 7: The number of bacterial isolates with NRPS and PKS1 BGCs predicted by AntiSMASH. All strains with PKS1 clusters also contained NRPS clusters. The strains selected by both methods are counted in all three categories.

The seven most promising marine bacteria were identified based on the indication of presence of NRPS or PKS clusters and bioactivity against both Gram-negative and Gram-positive bacteria from human pathogen relatives (Figure 4 and Table 3). Three of them are from the genus *Shewanella*, two are from *Pseudomonas*, and one of each is from *Paraglaciecola* and *Pseudoaltermonas*.

Table 3. The most promising marine bacteria with NRPS or PKS-positive BGC and bioactivity against both Gram-negative or Gram-positive human pathogen relatives bacteria.

Marine bacteria (ID)	Genus	BGCs (using PCR)	BGCs based on the whole genome using antiSMASH	Activity against Gram-positive bacteria	Activity against Gram-negative bacteria
MBP009.1	<i>Pseudoaltermonas</i>	NRPS	NRPS, RiPP-like; RiPP-like; RiPP-like; NRPS; arylpolyene; siderophore	Bs, Er	Ab, Eh, Ka
MBP011.3.1.R	<i>Shewanella</i>	NRPS	Sequencing is in progress	Bs, Er	Ec, Ha
MBP011.13.1	<i>Shewanella</i>	NRPS	RiPP-like; hglE-KS,PUFA,betalactone; RiPP-like; NRPS; NRPS; NRPS, T1PKS; RiPP-like; siderophore; siderophore; NRPS; NRPS; NRPS-like, NRPS	Se	Ab, Ha
MBP025.11	<i>Paraglaciecola</i>	NRPS, PKS 1	RiPP-like; lassopeptide,RRE-containing; terpene	Cg	Ab, Ka
MBP027.2	<i>Shewanella</i>	NRPS	Sequencing is in progress	Cg	Ab, Ka, Ha
MBP027.3	<i>Pseudomonas</i>	NRPS	NRPS; betalactone; NRPS; RiPP-like; ectoine; NRPS-like; RiPP-like; NRPS-like; arylpolyene; NRPS-like; RiPP-like; RRE-containing; NRPS	Bs, Er	Ka
MBP027.4	<i>Pseudomonas</i>	NRPS	RiPP-like; NRPS-like; arylpolyene; NRPS; NAGGN; betalactone; NRPS; NRPS; RiPP-like; redox-cofactor	Bs, Cg, Er	Ka, Pa

BGCs - biosynthetic gene clusters, NRPS - nonribosomal peptide synthetases, PKS - polyketide synthases, Bs - *Bacillus subtilis*, Cg - *Corynebacterium glutamicum*, Er - *Enterococcus raffinosus*, Se - *Staphylococcus epidermidis*, Ab - *Acinetobacter baylyi*, Ec - *Escherichia coli*, Eh - *Enterobacter hormaechei*, Ka - *Klebsiella aerogenes*, Pa - *Pseudomonas aeruginosa*, Ha - *Halomonas aquamarina*.

These seven bacterial isolates were analysed for their specialised metabolite production using MALDI-TOF MS (Figure 8). *Pseudoaltermonas* sp. MBP009.1 and *Pseudomonas* sp. MBP027.4 demonstrated that they have their most distinct metabolites. On the other hand, *Shewanella* sp. MBP027.2 did not exhibit any distinct metabolites.

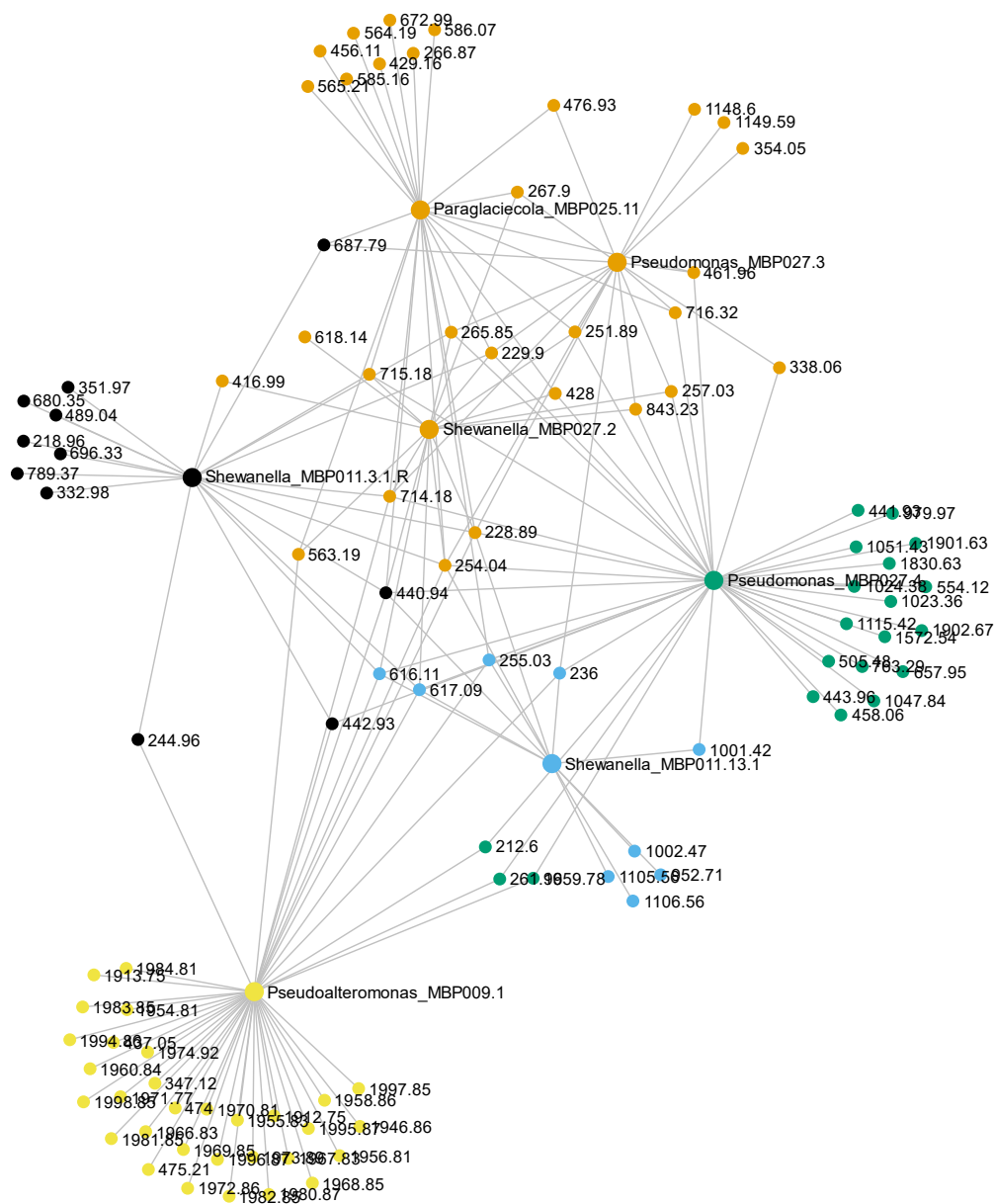


Figure 8. Selected seven marine bacterial isolates showed differential production of specialised metabolites.

Solid phase extraction from the co-culture of *Shewanella* sp. MBP011.13.1

Solid phase extraction (SPE) of compounds was performed using 10, 40, and 80 % acetonitrile (ACN) both from the monoculture of *Shewanella* sp. MBP011.13.1 and co-culture with *Staphylococcus epidermidis* RP62A based on the initial co-culture results. 80 % ACN extract of both monoculture and co-culture showed activity against mainly *B. subtilis*, *Corynebacterium glutamicum*, and *S. aureus* Gram-positive bacteria (Table S9). On the other hand, 10, and 40 % ACN extract showed activity against *S. aureus* (data not shown). Peak fractionation of 10 % ACN extract showed several fractions from co-culture have activity against *C. glutamicum* compared to the monoculture (Figure S2). Further purification followed by structure elucidation with bioactivity testing is necessary to conclude.

Discussion

The Arctic marine bacterial isolates capable of showing antimicrobial activity against a panel of Gram-positive and negative bacteria, including ESKAPE pathogen relatives, were from all four types of habitats. In our study, *Moritella* (30), *Psychromonas* (27), and *Shewanella* (19) were the most dominant genera (total 76, Figure 2b), and all of them from Gammaproteobacteria class, distributed in all four types of samples except deep water sediments. Some previous research has examined sediment communities in Arctic and sub-Arctic regions⁵⁻⁸, where diverse microbial communities were found in the Arctic marine sediments except deep water sediment⁹, which were similar to our findings. The microbial diversity of Arctic pelagic communities has been studied in some previous research⁵⁻⁸. Others observed that Proteobacteria, including SAR11 and Bacteroidetes, are prominent in the surface waters of the Arctic^{7,8} and that Deltaproteobacteria are abundant in deeper waters⁷.

An in-house MS library was prepared to discriminate the different marine bacteria using MALDI-TOF MS, as it has become a prevalent tool for rapid and reliable microbial identification^{10,11}. A phylogenetic tree was initially prepared and combined with 16S rRNA sequencing data. To validate the MS library using MALDI-TOF MS, the same cluster from the phylogenetic tree of marine bacterial isolates was genome sequenced, and their average nucleotide identity (ANI) was calculated. Table 2 and Figure 5 show the validation of our prediction, and in the future, we can use this in-house MS library to remove duplication of the marine bacterial isolates at the beginning of our bioprospecting pipeline before using it in the screening and genome sequencing steps. This in-house library was built as an early contribution to establish a database for Arctic marine bacteria.

Most marine bacterial isolates could grow at both 4°C (100%) and 10°C (82%). However, almost half (38-47 %) were sensitive to 15-20 °C, which means that they had a distinctly psychrophilic growth characteristic (commonly defined as those not growing at >20 degC, separating them from psychrotrophs, with a wider temperature range). Around one-fourth of the marine bacterial isolates were able to grow at 25°C (Table S2). Most of the marine bacterial isolates (16 out of 20) from zooplankton were flexible to all temperatures tested. On the other hand, 5 of 26 marine bacterial isolates from the under-ice sample grew at all the temperatures tested. Identifying marine bacteria with antibacterial activity against human pathogen relatives through co-culture was challenging because most marine bacterial isolates thrive at suboptimal temperatures for human pathogen relatives, typically around 10°C. Therefore, it revealed a principal problem when doing this kind of challenge test with psychrotrophs/-philes. Marine ecosystems are characterised by complex interactions among microorganisms, forming dynamic ecological networks through material, energy, and information exchange¹². Challenges arise in constructing marine-derived microbial co-culture models and tracking their processes and outcomes¹². These challenges involve understanding marine microbial ecological networks, the roles of paired strains, and key bioactive metabolites¹². During fermentation, issues include adjusting strain growth rates, balancing nutritional requirements, regulating temperature, mitigating dominant strain overgrowth, and ensuring repeatability and scalability¹². Complete co-culture models remain elusive, and many co-culture induction strategies still rely on serendipity.

Maximum isolates with antimicrobial activity were from two marine invertebrates (Porifera), zooplankton, under ice and sediment from 452 m. Almost no bioactive isolates were found in seaweed from puddles on floating ice and sediment from 3895 and 3999 meters. *E. raffinosus* (37), *B. subtilis* (29), and *K. aerogenes* (29) were the most susceptible targets for marine bacterial isolates to create a zone of inhibition to show antimicrobial activity. *E. raffinosus* and

K. aerogenes are members of the ESKAPE pathogen relatives, as the Infectious Disease Society of America recognises them as the bacteria posing the most significant risk to public health in the United States¹³.

Based on the PCR screening for NRPS and PKS, 37 marine bacterial isolates showed positive outcomes (Table 1). Additionally, genome sequencing of some of the marine bacterial isolates (Figure 6 and Table S7) showed the presence not only NRPS and PKS but also other potential BGCs, which could be a potential source of antimicrobial activity.

Antimicrobial screening of SPE eluates from *Shewanella* sp. MBP011.13.1 and *S. epidermidis* RP62A co-culture showed that 10, 40, and 80% ACN fractions exhibited the highest activity. The 10% ACN fraction underwent further fractionation using preparative RP-HPLC, monitored by DAD at 220 and 280 nm. Active fractions, identified in tests and shown in Figure S2, were analysed using UHPLC-QTOF-MS. Although several fractions demonstrated antibacterial properties, extensive purification via RP-HPLC is required for structural elucidation and further activity studies.

Conclusion

This bioprospecting study of Arctic marine bacterial isolates demonstrates how co-culture and genome mining can be used to identify bioactive marine bacteria as a potential source of antimicrobial compounds. Marine bacterial isolates of zooplankton have good growth at all tested temperatures. However, two marine invertebrates (Porifera), zooplankton, under the ice, and sediments of 452 m were the source of the isolates with the highest production of active compound according to these methods. Genome mining also facilitated the identification of potential BGCs that could be the cause of antimicrobial activity. *Shewanella* sp. MBP011.13.1 and *S. epidermidis* RP62A co-culture showed promising potential to find antimicrobial compounds. Further investigation will be required to isolate the bioactive compounds and their link to BGCs, which could help identify potential lead compounds towards discovering new antimicrobials with novel mechanisms of action to fight infection and AMR bacterial strains.

Materials and methods

Sample collection

All marine samples were collected during a research cruise with R/V Kronprins Haakon in the Barents Sea and Arctic Ocean from 4-13 July 2019. The sampling extended from the northern coast of the Norwegian mainland to well within the melting Arctic seasonal ice cover at 84.4 degrees N (Figure 1 and Table S1). We collected marine invertebrates by dredge and bottom trawl, sediment from the ocean floor by box corer, zooplankton by plankton net, and heterogeneous biological material from beneath the sea ice by a vacuum suction device.



Figure 9. The locations during a bioprospecting cruise in 2019 in the Arctic region.

Culturing marine bacterial isolate

The invertebrates were initially sorted, washed with sterile seawater, dissected (both internal and external tissue separately), chopped, and homogenised in sterile plastic bags. Portions of the homogenised organisms were then filter sterilised, and 50 μL volumes were spread onto the FMAP (modified marine broth with 5 % yeast extract) plates intended for cultivating bacteria from the same source material. A dilution series of the homogenates was spread on these enriched FMAP plates, which were subsequently incubated at 4 °C.

The top 10 cm gradients of sediment were collected from the boxcorer using a 50 mL (10 cm) falcon tube, which was then divided into four layers, each measuring 2.5 cm. Different dilutions were prepared from each layer and plated onto FMAP media.

For zooplankton and under-ice samples, several dilutions (10^{-1} , 10^{-2} , 10^{-3}) were prepared from the collected sample as mentioned in the sample collection steps and plated onto FMAP medium.

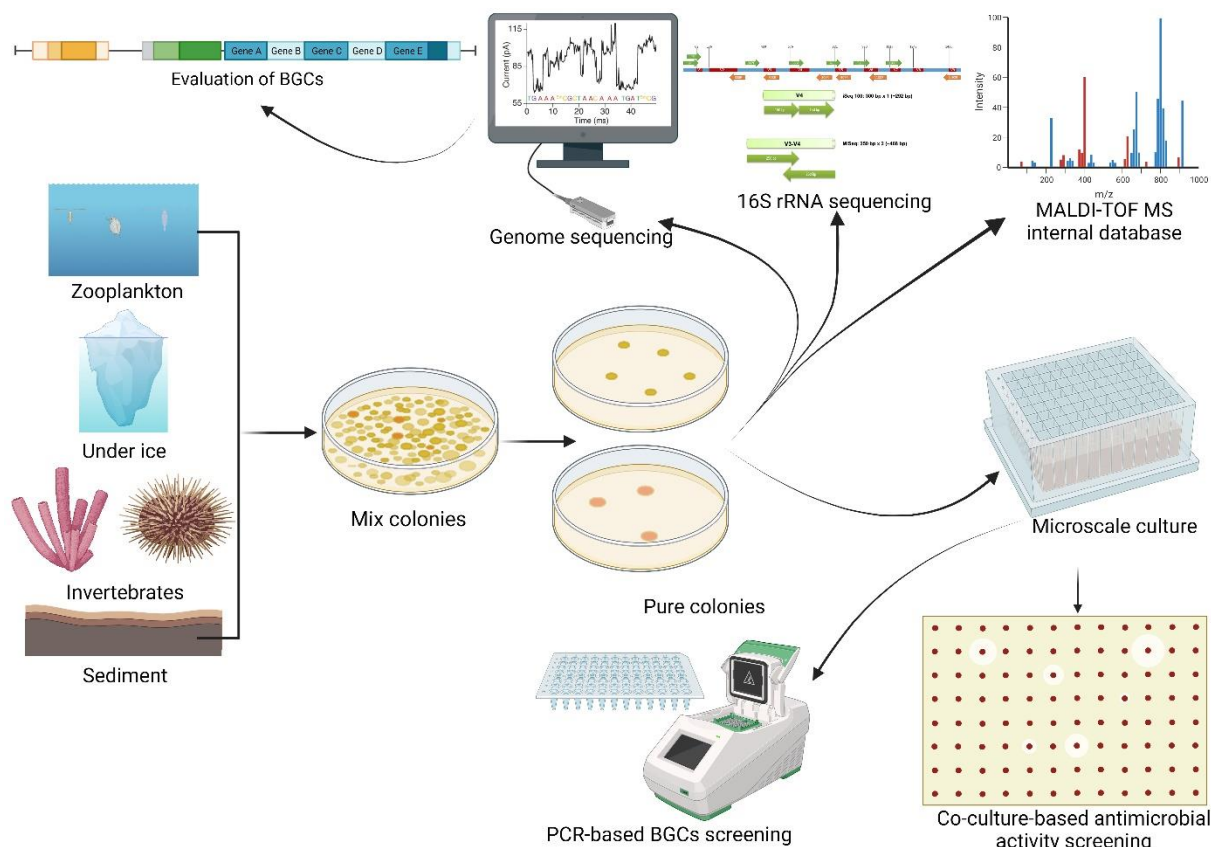


Figure 10. Overview of the marine bioprospecting workflow.

Evaluating the growth of Arctic isolates at different temperatures

Liquid cultures were prepared from the marine bacteria isolates in 96 deep-well plates containing FMAP media. Subsequently, 5 μL of each bacterial culture was transferred as a drop on tray plates (Nunc OmniTray, Single-Well Plate, Catalog number- 140156, Thermo Scientific) containing FMAP agar medium. These plates were incubated at various temperatures (4, 10, 15, 20, and 25 $^{\circ}\text{C}$) and monitored daily for growth.

Analysis of microbial protein (dereplication) using MALDI-TOF

Liquid culture was prepared from marine bacteria in a culture tube containing FMAP media. The overnight culture was then centrifuged, the supernatant was removed, and the pellet was washed with 70% ethanol before being dried. Formic acid (70%) and acetonitrile (100%) were added to the pellet, thoroughly mixed, and then centrifuged. The protein-containing supernatant was collected and stored at -80°C for further analysis.

For acquisition, 1 μL of the supernatant from each bacterial preparation was added to a 96-spot MALDI plate (MSP 96 target polished steel, Bruker). After drying at room temperature for a few minutes, 1 μL of matrix (α -Cyano-4-hydroxycinnamic acid, C2020, Sigma-Aldrich) was added to the dried supernatant. Data acquisition for each sample was carried out in the mass range of 2000-20000 Da using a MALDI Biotyper instrument (Bruker). The acquired data were then analysed using an open-source MALDI TOF-MS IDBac pipeline.

Taxonomic classification using 16S rRNA sequencing

Bacterial cells were harvested from 1 mL of culture, and DNA was extracted for PCR. The Bio-On-Magnetic-Beads (BOMB) DNA extraction protocol was used in a 96-well format¹⁴, together with the Sera-MagTM SpeedBeadsTM magnetic carboxylate modified particles (Cytiva). Before use, the beads were washed in TE buffer (pH 7.5) and then diluted at 1:50.

The taxonomic affiliations of the bacterial strains were inferred by sequencing PCR amplicons covering the larger part of the 16S rRNA gene. The PCR was set according to the manufacturer's protocol for Platinum™ II Hot-Start Green PCR Master Mix (2X) (Invitrogen). The 16S rRNA region was amplified with primers B27F/U1492R. The PCR products were inspected on a 1% (v/w) agarose gel and then purified using the BOMB protocol for the clean-up and size exclusion of PCR products. Cycle sequencing reactions were set up with the BigDye™ Terminator v3.1 Cycle Sequencing Kit (Applied Biosystems™), and the samples were sequenced at The University Hospital of North Norway sequencing facility. Mainly, the region was sequenced in the forward direction, but in some cases where B27F repeatedly yielded poor-quality sequences, 1457R was used instead.

Screening of bioactivity using co-culture

Liquid cultures of marine bacteria were prepared in 96 deep-well plates containing FMAP media, while liquid cultures of the reference human pathogen relative bacteria were prepared in a culture tube containing Mueller-Hinton (MH, Difco Laboratories, USA) medium. Subsequently, overnight cultures of each reference bacterium were mixed with FMAP medium containing 0.7% agar and poured into an Omni-tray plate. Next, 5 µL of each bacterial culture was transferred as a droplet onto Omni-tray plates for each reference bacterium. The plates were allowed to air dry and then incubated in a 10 °C incubator, except for the plate with *Psychromonas arctica* strain. The co-culture plates were observed daily, and any changes, zone of inhibition (ZI), or other notable characteristics were noted. After 3-5 days, the plates were transferred to 15 °C, and this procedure was repeated at 20 °C and 25 °C, except for the plate with the *Psychromonas arctica* strain.

Evaluation of secondary metabolites using MALDI-TOF

For acquisition, a colony from each bacterium was spread on a 96-spot MALDI plate (MSP 96 target polished steel, Bruker) using a sterile toothpick. Subsequently, 1 µL of the matrix was added to the spread bacterial colony. Data acquisition for each sample was performed in the mass range of 200-2000 Da using a MALDI Biotyper instrument (Bruker). The acquired data were then analysed using an open-source MALDI TOF-MS IDBac pipeline.

PCR screening for BGCs

PCRs to identify bacterial strains with NRPS and PKS domains were set up with Platinum™ II Hot-Start Green PCR Master Mix (2X) (Invitrogen), according to the manufacturer's protocol, using 1 µL of extracted DNA as a template. The reactions were run with a panel of primers from the literature targeting the C-domain in NRPS BGCs and the KS-domains in PKS type I and type II PKS BGCs. The list of primers is shown in supporting information, Table S5. The products were inspected on a 1% (v/w) agarose gel and characterised based on the number and size of the fragments. Strains resulting in a fragment of the correct size were considered positives.

Genome sequencing and assembly

Strains were selected for whole genome sequencing with Nanopore technology based on the outcomes of the antimicrobial activity and BGC screenings. DNA was extracted with the BOMB protocol for DNA extraction¹⁴. The extraction was performed in 1.5 mL tubes to allow individual control of each sample and increase DNA yields, quality, and purity. For two *Shewanella* strains where the BOMB DNA extraction did not yield sufficient amounts of DNA (MBP003.6 and MBP006.7.1), the Qiagen Blood and Tissue kit was used instead. The culture volumes used to harvest cells were adjusted based on the cell density and trial and error for individual strains. For Gram-positive *Jeotgalibacillus* strains (MBP0022.2, MBP0029.1,

MBP0030.1, and MBP0032.1), the samples were treated with lysozyme before adding lysis buffer. Two initial samples (MBP0025.11 (*Paraglaciecola*) and MBP0027.3 (*Pseudomonas*)) were sequenced on Flongle flow cells after library preparation with the Nanopore Rapid Sequencing kit. The remaining samples were sequenced at Genomics Support Center Tromsø (GSCT), on a MinION flow cell using the ligation sequencing kit.

The Nanopore reads were assembled by Flye¹⁵ and annotated by Prokka¹⁶. The contamination and completion of the draft genomes were estimated by CheckM¹⁷, resulting in completeness of >93.15 % and contamination of <2.95 %. GTDB-Tk¹⁸ was used for the taxonomical classification of the whole genomes (Table S10). Two Alphaproteobacteria strains were classified as *Sulfitobacter* based on the 16S rRNA sequence but were classified as *Asciidiaceihabitans*, a closely related genus, based on its whole genome. Out of 37, 15 strains were assigned to a species. ANI values were calculated with fastANI. The resulting draft genomes were analysed with AntiSMASH (v.6.1.0)¹⁹ for the prediction of BGCs and to assess the biosynthetic potential of the strains.

Solid phase extraction from the co-culture of *Shewanella* sp. MBP011.13.1

Shewanella sp. MBP011.13.1 was inoculated from a glycerol stock onto FMAP plate and incubated at 10° C for 96 hours. *Shewanella* sp. MBP011.13.1 liquid seed culture was prepared by transferring a colony into 25 mL FMAP liquid media, incubating for 72 hours at 10° C and 400 rpm. *S. epidermidis* RP62A was cultured from glycerol stock on an MH plate incubated overnight at 37° C. 7 mL of *Shewanella* sp. MBP011.13.1 seed culture (OD₆₀₀ 2.4) was added to 100 mL FMAP liquid media in two 500 mL flasks - one for *Shewanella* sp. MBP011.13.1 monoculture and one for co-culture with *S. epidermidis*. The flasks were incubated for 24 hours at 10° C, 200 rpm. *S. epidermidis* was inoculated in 5 mL MH liquid media and incubated for 24 hours at 37° C, 400 rpm. 350 µL of *S. epidermidis* (OD₆₀₀ 4.8) was added to both co-culture and *S. epidermidis* monoculture flasks. All flasks were incubated for 5 days at 10° C, 200 rpm, then at 15° C for 2 days, and finally at room temperature for 3 days, maintaining 200 rpm throughout.

Each culture was aliquoted to 15 mL and combined with another 15 mL of ACN (HPLC-grade, Sigma-Aldrich, Steinheim, Germany) containing 0.1% trifluoroacetic acid (TFA; Sigma-Aldrich) in a 50 ml falcon tube. The tube was incubated for an hour at RT with shaking at 90 rpm. The mixture was dried in a ScanSpeed 40 vacuum centrifuge (LabogeneApS, Denmark) and resuspended with 30 mL Milli-Q water. The tube was incubated for an hour at RT with shaking at 90 rpm. Salt was removed by SPE, as previously described²⁰. In brief, the extracts were applied to C18 35cc Sep-Pak Vac cartridges (Waters, MA, USA), pre-conditioned with 0.05% TFA in water. They were washed with acidified water and eluted sequentially using ACN solutions (10, 40, and 80% v/v) with 0.05% TFA. The solid-phase extraction (SPE) eluates were dried using a ScanSpeed 40 vacuum centrifuge.

Screening for antibacterial activity

A modified broth microdilution susceptibility test, based on the CLSI M07-A9 protocol, was used to determine minimal inhibitory concentrations (MIC) of the obtained extracts. The Gram-positive bacteria *C. glutamicum* (ATCC 13032), *S. aureus* (ATCC 9144) and *S. epidermidis* RP62A (ATCC 35984) and the Gram-negative bacteria *Escherichia coli* (ATCC 25922), and *Pseudomonas aeruginosa* (ATCC 27853) were used as test strains. The bacteria were grown overnight in MH broth at 35 °C.

Dried ACN-extracts and SPE-fractions were dissolved in Milli-Q water to a concentration of 10 mg/mL (5 mg/mL if a limited amount of material), and a series of two-fold dilutions (50 μ L) of the extracts were prepared in 96-well flat-bottom polystyrene microplates (Thermo Fisher Scientific, Denmark). A suspension of actively growing bacteria was diluted in appropriate media to approximately $2.5\text{--}3 \times 10^4$ cells/mL. A volume of 50 μ L of the respective bacterial inoculum was added to the diluted extracts in a 1:1 ratio. The positive control (ciprofloxacin, Sigma-Aldrich, USA), the negative control (bacteria + water), and the medium control (media + water) were included in each experiment. The microplates were incubated for 48 h at 35 °C in an EnVision microplate reader (PerkinElmer, Turku, Finland). The lowest concentration of extract that resulted in no bacterial growth, as determined by OD600 measurements, was defined as the minimal inhibitory concentration (MIC) value. All samples were tested in 3 technical replicates.

Statistical analysis

The phylogenetic tree and molecular network (MAN) was prepared using an open-source MALDI TOF-MS IDBac pipeline¹¹. This dendrogram was created by analysing 91 samples and retaining peaks with a signal-to-noise ratio above 4 and occurring in greater than 70 % of replicate spectra. Peaks occurring below 2000 m/z or above 20000 m/z were removed from the analyses. For clustering spectra, distance and algorithms were used. This MAN was created by analysing 7 samples, subtracting a matrix blank, retaining peaks with a signal-to-noise ratio above 4, and occurring in greater than 70 % of replicate spectra. Peaks occurring below 200 m/z or above 2000 m/z were removed from the analysis. Graphs were prepared using GraphPad Prism (version 10). R program was used to make the Venn diagram.

References

- 1 Kristoffersen, V. *et al.* Two novel lyso-ornithine lipids isolated from an Arctic marine *Lacinutrix* sp. bacterium. *Molecules* **26**, 5295 (2021).
- 2 Wibowo, J. T. *et al.* Secondary Metabolites from Marine-Derived Bacteria with Antibiotic and Antibiofilm Activities against Drug-Resistant Pathogens. *Marine Drugs* **21**, 50 (2023).
- 3 Almeida, J. F. *et al.* Marine sponge and octocoral-associated bacteria show versatile secondary metabolite biosynthesis potential and antimicrobial activities against human pathogens. *Marine Drugs* **21**, 34 (2022).
- 4 Weissman, K. J. The structural biology of biosynthetic megaenzymes. *Nature Chemical Biology* **11**, 660-670, doi:10.1038/nchembio.1883 (2015).
- 5 Bano, N., Ruffin, S., Ransom, B. & Hollibaugh, J. T. Phylogenetic composition of Arctic Ocean archaeal assemblages and comparison with Antarctic assemblages. *Applied and Environmental Microbiology* **70**, 781-789 (2004).
- 6 Galand, P. E., Casamayor, E. O., Kirchman, D. L., Potvin, M. & Lovejoy, C. Unique archaeal assemblages in the Arctic Ocean unveiled by massively parallel tag sequencing. *The ISME journal* **3**, 860-869 (2009).
- 7 Galand, P. E., Potvin, M., Casamayor, E. O. & Lovejoy, C. Hydrography shapes bacterial biogeography of the deep Arctic Ocean. *The ISME journal* **4**, 564-576 (2010).
- 8 Kirchman, D. L., Cottrell, M. T. & Lovejoy, C. The structure of bacterial communities in the western Arctic Ocean as revealed by pyrosequencing of 16S rRNA genes. *Environmental microbiology* **12**, 1132-1143 (2010).
- 9 Kurdy, W., Yakovleva, G. & Ilinskaya, O. Structure and Functional Potential of Arctic Sea Sediment Microbiota. *The Journal of General and Applied Microbiology* **69**, 24-33 (2023).
- 10 Freiwald, A. & Sauer, S. Phylogenetic classification and identification of bacteria by mass spectrometry. *Nature protocols* **4**, 732-742 (2009).

- 11 Clark, C. M. *et al.* Using the open-source MALDI TOF-MS IDBac pipeline for analysis of microbial protein and specialised metabolite data. *JoVE (Journal of Visualized Experiments)*, e59219 (2019).
- 12 Li, X., Xu, H., Li, Y., Liao, S. & Liu, Y. Exploring Diverse Bioactive Secondary Metabolites from Marine Microorganisms Using Co-Culture Strategy. *Molecules* **28**, 6371 (2023).
- 13 Boucher, H. W. *et al.* Bad bugs, no drugs: no ESKAPE! An update from the Infectious Diseases Society of America. *Clinical infectious diseases* **48**, 1-12 (2009).
- 14 Oberacker, P. *et al.* Bio-On-Magnetic-Beads (BOMB): Open platform for high-throughput nucleic acid extraction and manipulation. *PLoS biology* **17**, e3000107 (2019).
- 15 Kolmogorov, M., Yuan, J., Lin, Y. & Pevzner, P. A. Assembly of long, error-prone reads using repeat graphs. *Nature Biotechnology* **37**, 540+, doi:10.1038/s41587-019-0072-8 (2019).
- 16 Seemann, T. Prokka: rapid prokaryotic genome annotation. *Bioinformatics* **30**, 2068-2069, doi:10.1093/bioinformatics/btu153 (2014).
- 17 Parks, D. H., Imelfort, M., Skennerton, C. T., Hugenholtz, P. & Tyson, G. W. CheckM: assessing the quality of microbial genomes recovered from isolates, single cells, and metagenomes. *Genome research* **25**, 1043-1055, doi:10.1101/gr.186072.114 (2015).
- 18 Chaumeil, P.-A., Mussig, A. J., Hugenholtz, P. & Parks, D. H. GTDB-Tk v2: memory friendly classification with the genome taxonomy database. *Bioinformatics* **38**, 5315-5316, doi:10.1093/bioinformatics/btac672 (2022).
- 19 Blin, K. *et al.* antiSMASH 6.0: improving cluster detection and comparison capabilities. *Nucleic acids research* **49**, W29-W35, doi:10.1093/nar/gkab335 (2021).
- 20 Haug, T., Kjuul, A. K., Stensvåg, K., Sandsdalen, E. & Styrvold, O. B. Antibacterial activity in four marine crustacean decapods. *Fish & shellfish immunology* **12**, 371-385 (2002).

Supporting Information for Antimicrobial potential of marine bacteria from the Arctic and sub- Arctic regions

Ataur Rahman*, Andrea Iselin Elvheim*, Christoffer Ågnes, Ida Kristine Østnes Hansen, Hege Devold, Frode Jacobsen Øyen, Gabriel Magno de Freitas Almeida, Hans-Matti Blencke, Bjarne Landfald, Tor Haug, Klara Stensvåg#

Norwegian College of Fishery Science, Faculty of Life Sciences, Fisheries and Economics, UiT The Arctic University of Norway, 9019 Tromsø, Norway

** Authors contributed equally; # corresponding author*

List of Figures

Figure S1. Marine invertebrates were used to isolate bacteria. (Photo: Klara Stensvåg and Bjarne Landfald).....	3
Figure S2. Disk diffusion assay to test the activity of different fractions of 10 % ACN extract against <i>C. glutamicum</i>. a) <i>Shewanella</i> sp. MBP011.13.1 monoculture. b) co-culture of <i>Shewanella</i> sp. MBP011.13.1 with <i>S. epidermidis</i> RP62A. Red dashed circles are the active fraction.....	19

List of Tables

Table S1. The sample types with the location coordinates and depths.....	2
Table S2. A list of marine bacteria collected from a bioprospecting cruise in the Arctic, along with growth observation at different temperatures, taxonomic distribution, BGCs screening using PCR, and bioactive marine bacteria identified using co-culture.....	4
Table S3. List of human pathogen relative bacteria used to screen bioactive (antimicrobial) marine bacteria.....	11
Table S4. List of biofilm-forming marine bacteria to screen bioactive (antimicrobial) marine bacteria.	11
Table S5. List of PCR primers used to screen NRPS and PKS modules.	11
Table S6. Summary of results from Nanopore sequencing and genome assembly with Flye.....	13
Table S7. BGCs of marine bacterial strains, predicted by antiSMASH.....	14
Table S8. The bacterial strains that yielded PCR products of the expected size, for each primer pair, together with the BGCs predicted by AntiSMASH, for the whole genome sequenced strains.....	15
Table S9. Minimum inhibitory concentration (MIC) of solid phase extracted samples from both monoculture and co-culture in µg/mL.	18
Table S10. Taxonomic classification of draft genomes by GTDB-Tk.	20

Table S1. The sample types with the location coordinates and depths.

Sample ID	Sample type	Date	Latitude		Longitude		Depth	
			From	To	From	To	From	To
MBP001	<i>Echinus acutus</i>	040719	7141.589 N	7143.31 N	02640.26 E	02644.72 E	364.81	359.93
MBP002	<i>Thenea muricata</i>	050719	7400.19 N	7528.58 N	02710.47 E	02743.50 E	415.01	253.08
MBP003	<i>Polymastia grimaldii</i>							
MBP004	<i>Molpadia borealis</i>							
MBP005	<i>Brada inhabilis</i>	060719	7528.59 N	7528.52 N	02743.50 E	02749.91 E	253	251.01
MBP006	<i>Phascolian strombus</i>							
MBP007	Zooplankton (Tangential flow, 5mL - 20 mL)	070719	8057.61 N	8120.41 N	03449.94 E	03415.10 E	450.45	452.05
MBP008	Zooplankton (Tangential flow, 5mL - 20 mL)							
MBP009	Zooplankton (Tangential flow, 5mL - 20 mL)							
MBP010	Box coreer, Sediment, Gradient 10 cm							
MBP011	Box coreer, Sediment, Gradient 0-2.5 cm							
MBP012	Box coreer, Sediment, Gradient 2.5 - 5.0 cm							
MBP013	Box coreer, Sediment, Gradient 5.0 - 7.5 cm							
MBP014	Box coreer, Sediment, Gradient 0.75-10.0 cm							
MBP016	Zooplankton 1 from a puddle on ice	110719	8412.15 N	8410.25 N	02846.02 E	02910.58 E	0	3948.87
MBP017	Zooplankton 2 from a puddle on ice							
MBP018	Zooplankton 3 from a puddle on ice							
MBP019	Zooplankton 4 from a puddle on ice							
MBP020	Box coreer, Sediment, Gradient 10 cm	120719	8413.52 N	8415.86 N	02931.10 E	02926.43 E	0	3894.92
MBP021	Box coreer, Sediment, Gradient 0-2.5 cm							
MBP022	Box coreer, Sediment, Gradient 2.5 - 5.0 cm							
MBP023	Box coreer, Sediment, Gradient 5.0 - 7.5 cm							
MBP024	Box coreer, Sediment, Gradient 0.75-10.0 cm							
MBP025	Seaweed from puddle on ice (12 ml)	130719	8441.03 N	8439.79 N	02846.02 E	02843.92 E	3998.23	3998.78
MBP026	Vacum cleaner material from under the ice 400 ul							
MBP027	Vacum cleaner material from under the ice 45 ml							
MBP028	Box coreer, Sediment, Gradient 10 cm							
MBP029	Box coreer, Sediment, Gradient 0-2.5 cm							
MBP030	Box coreer, Sediment, Gradient 2.5 - 5.0 cm							
MBP031	Box coreer, Sediment, Gradient 5.0 - 7.5 cm							
MBP032	Box coreer, Sediment, Gradient 0.75-10.0 cm							



MBP001
Echinus acutus



MBP002
Thenea muricata



MBP003
Polymastia grimaldii



MBP004
Molpadia borealis



MBP005
Brada inhabilis



MBP006
Phascolian strombus

Figure S1. Marine invertebrates were used to isolate bacteria. (Photo: Klara Stensvåg and Bjarne Landfald)

Table S2. A list of marine bacteria collected from a bioprospecting cruise in the Arctic, along with growth observation at different temperatures, taxonomic distribution, BGCs screening using PCR, and bioactive marine bacteria identified using co-culture.

Marine bacterial isolates (ID)	Habitat	Closest match	Identity (%)	Accession no	BGCs			Gram +					Gram -					Marine (Gram -)		Growth in different temperature (°C)				
					NRPS	PKS 1	PKS 2	Bs	Cg	Er	Sa	Se	Ab	Ec	Eh	Ka	Pa	Ha	PsyA	5	10	15	20	25
MBP002.1.1	Thenea muricata (Fungus, Porifera)	Moritella dasanensis ArB 0140	98.49	NR_044156.1	-	-	-	-	-	+	-	-	-	-	-	-	-	-	-	✓	✓	✓	✓	x
MBP002.2.1		Photobacterium frigidiphilum	98.76	NR_042964.1	-	-	-	++	-	+	-	-	+	-	-	+	-	-	-	✓	✓	✓	✓	✓
MBP002.3		Colwellia psychrerythraea	98.98	NR_037047.1	-	-	-	-	-	-	-	-	-	-	-	-	-	-	-	✓	x	x	x	x
MBP002.4		Psychromonas hadalis	97.89	NR_040949.1	-	-	-	-	-	-	-	-	-	-	-	-	-	-	-	✓	x	x	x	x
MBP002.5		Sulfitobacter sabulilitoris	96.95	NR_169477.1	Y	-	-	++	-	-	-	-	-	-	-	-	-	-	-	✓	✓	✓	✓	✓
MBP002.6		Shewanella pealeana	98.34	NR_074821.1	-	-	-	++	+	-	-	-	+	-	+	+	-	-	-	✓	✓	✓	✓	✓
MBP003.1.1.R*	Polymastia grimaldii (Fungus, Porifera)	Shewanella surugensis	98.13	NR_040950.1	-	-	-	+++	-	-	-	-	-	++	-	-	-	++	++	✓	✓	✓	✓	✓
MBP003.2.1		Shewanella sediminis HAW-EB3	97.01	NR_074819.1	Y	-	-	-	+	-	-	-	-	-	-	-	-	-	-	✓	✓	✓	✓	✓
MBP003.2.2.R		Shewanella canadensis	93.91	NR_042994.1	Y	-	-	++	-	+	-	-	-	-	-	-	-	-	-	✓	✓	✓	✓	✓
MBP003.2.3.R		Unknown	NA	NA	-	-	-	-	-	+	-	-	-	-	-	-	-	-	-	✓	✓	✓	✓	✓
MBP003.3		Moritella marina ATCC 15381	97.57	NR_040842.1	-	-	-	-	-	-	-	-	-	-	-	-	-	-	-	✓	✓	✓	✓	x
MBP003.4		Moritella marina ATCC 15381	98.95	NR_040842.1	-	-	-	-	-	-	-	-	-	-	-	-	-	-	-	✓	✓	✓	✓	x
MBP003.5.1		Paraglaciecola psychrophila	98.89	NR_043463.1	-	-	-	-	-	-	-	-	-	-	-	-	-	-	-	✓	x	x	x	x
MBP003.6		Shewanella woodyi ATCC 51908	97.46	NR_114412.1	Y	-	-	-	-	+	-	-	-	-	-	-	-	-	-	✓	x	x	x	x
MBP003.8.1		Colwellia maris	97.26	NR_024635.1	-	-	-	-	-	-	-	-	-	-	-	-	-	-	-	✓	x	x	x	x
MBP003.9.1.R		Algibacter psychrophilus	99.56	NR_135863.1	-	-	-	-	-	-	-	-	-	-	-	-	-	-	-	✓	✓	✓	✓	x
MBP003.10.1		Maribacter antarcticus	97.47	NR_044515.1	-	-	-	++	-	-	-	-	-	-	-	-	-	-	-	✓	✓	✓	✓	✓
MBP005.1		Brada inabilis (Polychaetes, Bristle worms)	Shewanella sediminis HAW-EB3	98.56	NR_074819.1	Y	-	-	-	-	-	-	-	-	-	-	-	-	-	✓	x	x	x	x
MBP005.2			Photobacterium frigidiphilum	98.34	NR_042964.1	-	-	-	-	-	-	-	-	+	-	+	+	-	-	-	✓	✓	✓	x
MBP005.3	Psychromonas hadalis		97.28	NR_040949.1	-	-	-	-	-	-	-	-	-	-	-	-	-	-	-	✓	x	x	x	x
MBP005.4	Shewanella woodyi		97.51	NR_074846.1	-	-	-	-	-	-	-	-	-	-	-	-	-	-	-	✓	x	x	x	x
MBP006.1		Shewanella woodyi ATCC 51908	94.44	NR_114412.1	-	-	-	-	-	-	-	-	-	-	-	-	-	-	✓	✓	x	x	x	
MBP006.2		Shewanella canadensis	97.51	NR_042994.1	-	-	-	-	-	-	-	-	-	-	+	+	-	-	✓	✓	✓	x	x	

Marine bacterial isolates (ID)	Habitat	Closest match	Identity (%)	Accession no	BGCs			Gram +					Gram -					Marine (Gram -)		Growth in different temperature (°C)					
					NRPS	PKS 1	PKS 2	Bs	Cg	Er	Sa	Se	Ab	Ec	Eh	Ka	Pa	Ha	PsyA	5	10	15	20	25	
MBP006.3	Phascolian strombus (Snail star worm)	Shewanella woodyi	97.57	NR_074846.1	-	-	-	-	+	-	-	-	+	-	+	+	-	-	-	✓	✓	✓	✓	x	
MBP006.4		Shewanella woodyi	97.90	NR_074846.1	-	-	-	-	-	-	-	-	-	-	-	-	-	-	-	-	✓	x	x	x	x
MBP006.5		Shewanella sediminis HAW-EB3	97.83	NR_074819.1	-	-	-	-	+	-	-	-	+	-	+	+	-	-	-	-	✓	✓	✓	✓	x
MBP006.6.1.R		Psychromonas hadalis	97.95	NR_040949.1	-	-	-	-	-	-	-	-	-	-	-	-	-	-	-	-	✓	x	x	x	x
MBP006.7.1		Shewanella sediminis HAW-EB3	98.22	NR_074819.1	-	-	-	-	-	-	-	-	-	-	+	-	-	-	-	-	✓	✓	✓	✓	x
MBP007.1	Zooplankton	Moritella marina ATCC 15381	99.48	NR_040842.1	-	-	-	-	-	-	-	-	-	-	-	-	-	-	-	✓	✓	✓	✓	✓	
MBP007.2		Moritella marina ATCC 15381	99.68	NR_040842.1	-	-	-	-	-	-	-	-	-	-	-	-	-	-	-	-	✓	✓	✓	✓	✓
MBP007.3.1.R		Pseudoalteromonas neustonica	97.94	NR_151996.1	-	-	-	++	-	+	-	-	-	-	-	+	+	-	-	-	✓	✓	✓	✓	✓
MBP007.4		Moritella marina	99.48	NR_119143.1	-	-	-	-	-	+	-	-	-	-	-	-	-	-	-	-	✓	✓	✓	✓	x
MBP007.5		Winogradskyella eximia	99.46	NR_025804.1	-	-	-	+++	-	-	-	-	-	-	-	-	-	-	-	-	✓	✓	✓	✓	✓
MBP007.6		Alteromonas naphthalenivorans	99.25	NR_145589.1	-	-	-	-	-	-	-	-	-	-	+	+	-	-	-	-	✓	✓	✓	✓	✓
MBP008.1		Pseudoalteromonas nigrifaciens	98.97	NR_114188.1	-	-	-	+++	-	+	-	-	-	-	-	-	-	-	-	-	✓	✓	✓	✓	✓
MBP008.2		Pseudoalteromonas distincta	99.04	NR_114436.1	-	-	-	+++	-	+	-	-	-	-	-	-	-	-	-	-	✓	✓	✓	✓	✓
MBP008.3		Polaribacter sejongensis	98.22	NR_109324.1	Y	-	-	++	-	+	-	-	-	-	-	-	-	-	-	-	✓	✓	✓	✓	✓
MBP008.4		Pseudoalteromonas tetraodonis GFC	99.69	NR_114187.1	-	-	-	++	-	+	-	-	-	-	-	+	-	-	-	-	✓	✓	✓	✓	✓
MBP008.5		Sulfitobacter brevis	96.91	NR_029346.1	Y	Y	-	-	-	-	-	-	-	-	-	-	-	-	-	-	✓	x	x	x	x
MBP009.1		Pseudoalteromonas aliena	99.78	NR_025775.1	Y	-	-	+++	-	+	-	-	+	-	+	+	-	-	-	-	✓	✓	✓	✓	✓
MBP009.2		Vibrio splendidus	99.15	NR_109668.1	-	-	-	-	-	+	-	-	+	-	-	-	-	-	-	-	✓	✓	✓	✓	✓
MBP009.3		Aliivibrio sifiae	99.55	NR_112824.1	-	-	-	++	-	+	-	-	-	-	-	-	-	-	-	-	✓	✓	✓	✓	✓
MBP009.4		Pseudoalteromonas tetraodonis GFC	99.47	NR_114187.1	-	-	-	++	-	+	-	-	-	-	-	+	-	-	-	-	✓	✓	✓	✓	✓
MBP009.5		Pseudoalteromonas marina	99.70	NR_042981.1	-	-	-	++	-	+	-	-	-	-	-	-	-	-	-	-	✓	✓	✓	✓	✓
MBP009.6.1.R		Moritella marina ATCC 15381	99.68	NR_040842.1	-	-	-	++	-	+	-	-	-	-	-	-	-	-	-	-	✓	✓	✓	✓	x
MBP009.7.1.R*		Polaribacter sejongensis	98.23	NR_109324.1	-	-	-	++	-	-	-	-	-	-	-	+	-	-	-	-	✓	✓	✓	✓	✓
MBP009.8		Tenacibaculum haliotis	98.05	NR_158003.1	-	-	-	++	-	-	-	-	+	-	-	+	-	-	-	-	✓	✓	✓	✓	✓
MBP009.9.1.R		Sulfitobacter brevis	96.90	NR_029346.1	-	-	-	-	-	-	-	-	-	-	-	+	-	-	-	-	✓	x	x	x	x

Marine bacterial isolates (ID)	Habitat	Closest match	Identity (%)	Accession no	BGCs			Gram +					Gram -					Marine (Gram -)		Growth in different temperature (°C)				
					NRPS	PKS 1	PKS 2	Bs	Cg	Er	Sa	Se	Ab	Ec	Eh	Ka	Pa	Ha	PsyA	5	10	15	20	25
MBP011.1	Sediment (452 m)	Unknown	NA	NA	Y	-	-	-	-	-	-	-	-	-	-	-	-	-	✓	x	x	x	x	
MBP011.2		<i>Pseudoalteromonas neustonica</i>	94.36	NR_151996.1	-	-	-	++	-	+	-	-	-	-	-	-	-	-	-	✓	✓	✓	x	x
MBP011.3.1.R		<i>Shewanella surugensis</i>	99.02	NR_040950.1	Y	-	-	++	-	+	-	-	-	+++	-	-	-	++	-	✓	✓	✓	✓	x
MBP011.4		<i>Psychromonas macrocephali</i>	97.77	NR_041605.1	-	-	-	-	-	+	-	-	-	-	-	-	-	-	-	✓	x	x	x	x
MBP011.5		<i>Psychromonas japonica</i>	97.97	NR_041603.1	-	-	-	-	-	+	-	-	-	-	-	-	-	-	-	✓	x	x	x	x
MBP011.6		<i>Photobacterium frigidophilum</i>	100.00	NR_042964.1	-	-	-	-	-	+	-	-	-	-	-	+	-	-	-	✓	✓	✓	✓	✓
MBP011.7		<i>Moritella marina</i> ATCC 15381	98.29	NR_040842.1	-	-	-	-	-	-	-	-	-	-	-	-	-	-	-	✓	✓	✓	✓	x
MBP011.8		<i>Psychromonas ingrahamii</i>	96.94	NR_074862.1	-	-	-	-	-	-	-	-	-	-	-	-	-	-	-	✓	x	x	x	x
MBP011.9		<i>Psychromonas macrocephali</i>	97.83	NR_041605.1	-	-	-	-	-	-	-	-	-	-	-	-	-	-	-	✓	x	x	x	x
MBP011.10		<i>Psychromonas ossibalaenae</i>	98.95	NR_041606.1	-	-	-	++	-	-	-	-	-	-	-	-	-	-	-	✓	x	x	x	x
MBP011.11		<i>Psychromonas macrocephali</i>	97.59	NR_041605.1	-	-	-	-	-	-	-	-	-	-	-	-	-	-	-	✓	x	x	x	x
MBP011.12		<i>Shewanella gelidimarina</i>	99.38	NR_026058.1	-	-	-	+	+	-	-	-	+	-	+	+	+	-	-	✓	✓	✓	✓	x
MBP011.13.1		<i>Shewanella woodyi</i> ATCC 51908	98.48	NR_114412.1	Y	-	-	-	-	-	-	-	+++	+	-	-	-	+++	-	✓	✓	✓	✓	x
MBP011.14.1		<i>Shewanella woodyi</i> ATCC 51908	97.84	NR_114412.1	Y	-	-	-	-	-	-	-	+	-	-	+	-	+++	-	✓	✓	✓	✓	x
MBP011.15.1		<i>Algibacter psychrophilus</i>	99.35	NR_135863.1	-	-	-	-	-	-	-	-	-	-	-	-	-	-	-	✓	x	x	x	x
MBP012.1		<i>Psychromonas japonica</i>	98.01	NR_041603.1	-	-	-	-	-	-	-	-	-	-	-	-	-	-	-	✓	x	x	x	x
MBP012.2		<i>Psychromonas macrocephali</i>	98.11	NR_041605.1	-	-	-	-	-	-	-	-	-	-	-	-	-	-	-	✓	✓	✓	x	x
MBP012.3		<i>Moritella dasanensis</i> ArB 0140	99.56	NR_044156.1	-	-	-	-	-	-	-	-	-	-	-	-	-	-	-	✓	✓	✓	✓	x
MBP012.4.1		<i>Psychromonas japonica</i>	97.20	NR_041603.1	-	-	-	-	-	+	-	-	-	-	-	-	-	-	-	✓	✓	✓	✓	x
MBP012.6		<i>Psychromonas kaikoae</i> ATCC BAA-353	97.07	NR_028003.1	-	-	-	-	-	+	-	-	-	-	-	-	-	-	-	✓	✓	✓	x	x
MBP012.7	<i>Psychromonas kaikoae</i> ATCC BAA-353	97.13	NR_028003.1	-	-	-	-	-	+	-	-	-	-	-	-	-	-	-	✓	✓	x	x	x	
MBP012.8	<i>Psychromonas japonica</i>	97.13	NR_041603.1	-	-	-	-	-	-	-	-	-	-	-	-	-	-	-	✓	x	x	x	x	
MBP012.9	<i>Psychromonas kaikoae</i> ATCC BAA-353	97.07	NR_028003.1	-	-	-	-	-	-	-	-	-	-	-	-	-	-	-	✓	x	x	x	x	
MBP012.10.1	<i>Lutibacter oceani</i>	98.25	NR_146841.1	-	-	-	-	-	-	-	-	-	-	-	-	-	-	-	✓	x	x	x	x	
MBP012.11.1	<i>Psychromonas</i> sp. FS11-3	87.07	JQ799970.1	-	-	-	-	-	-	-	-	-	-	-	-	-	-	-	✓	✓	✓	x	x	

Marine bacterial isolates (ID)	Habitat	Closest match	Identity (%)	Accession no	BGCs			Gram +					Gram -					Marine (Gram -)		Growth in different temperature (°C)						
					NRPS	PKS 1	PKS 2	Bs	Cg	Er	Sa	Se	Ab	Ec	Eh	Ka	Pa	Ha	PsyA	5	10	15	20	25		
MBP012.13	Zooplankton (puddle on ice)	<i>Psychromonas macrocephali</i>	97.29	NR_041605.1	-	-	-	-	-	-	-	-	-	-	-	+	-	-	-	-	✓	✓	✓	✓	x	
MBP013.1		<i>Psychromonas japonica</i>	97.42	NR_041603.1	-	-	-	-	-	+	-	-	-	-	-	-	-	-	-	-	-	✓	✓	✓	✓	x
MBP013.2		<i>Photobacterium frigidiphilum</i>	98.40	NR_042964.1	-	-	-	-	+	-	-	-	+	-	-	+	-	-	-	-	-	✓	✓	✓	✓	x
MBP013.3		<i>Algibacter psychrophilus</i>	99.44	NR_135863.1	Y	-	-	-	-	-	-	-	-	-	-	-	-	-	-	-	-	✓	✓	✓	✓	x
MBP014.1		<i>Psychromonas macrocephali</i>	97.66	NR_041605.1	-	-	-	-	-	-	-	-	-	-	-	-	-	-	-	-	-	✓	✓	✓	x	x
MBP014.2		<i>Psychromonas macrocephali</i>	97.87	NR_041605.1	-	-	-	-	-	-	-	-	-	-	-	-	-	-	-	-	-	✓	✓	✓	x	x
MBP016.1		<i>Moritella dasanensis</i> ArB 0140	98.43	NR_044156.1	-	-	-	+++	+	-	-	-	+	+	-	+	+	-	-	-	-	✓	✓	✓	✓	✓
MBP016.2		<i>Moritella dasanensis</i> ArB 0140	99.68	NR_044156.1	-	-	-	-	-	-	-	-	-	-	-	-	-	-	-	-	-	✓	✓	✓	✓	x
MBP016.3		<i>Moritella profunda</i>	99.15	NR_025381.1	-	-	-	-	-	-	-	-	-	-	-	-	-	-	-	-	-	✓	x	x	x	x
MBP016.4		<i>Moritella dasanensis</i> ArB 0140	99.78	NR_044156.1	-	-	-	-	-	-	-	-	-	-	-	-	-	-	-	-	-	✓	✓	✓	✓	x
MBP016.5.1		<i>Paraglaciecola psychrophila</i>	97.93	NR_043463.1	-	-	-	-	+	-	-	-	+	+	-	+	+	-	-	-	-	✓	✓	✓	✓	x
MBP016.6		<i>Maribacter antarcticus</i>	99.56	NR_044515.1	-	-	-	-	-	-	-	-	-	-	-	-	-	-	-	-	-	✓	✓	✓	✓	x
MBP016.7		<i>Flavobacterium frigoris</i>	99.15	NR_025597.1	-	-	-	+	-	-	-	-	-	-	-	-	-	-	-	-	-	✓	✓	✓	✓	x
MBP016.8		<i>Polaribacter litorisediminis</i>	98.31	NR_156971.1	-	-	-	-	-	-	-	-	-	-	-	-	-	-	-	-	-	✓	x	x	x	x
MBP016.9		<i>Psychroserpens damuponensis</i>	98.46	NR_109097.1	Y	-	-	-	-	-	-	-	-	-	-	-	-	-	-	-	-	✓	x	x	x	x
MBP017.1		<i>Moritella dasanensis</i> ArB 0140	99.77	NR_044156.1	-	-	-	-	-	-	-	-	-	-	-	-	-	-	-	-	-	✓	✓	✓	✓	x
MBP017.2.1.R		<i>Moritella dasanensis</i> ArB 0140	99.57	NR_044156.1	-	-	-	-	-	-	-	-	-	-	-	-	-	-	-	-	-	✓	✓	✓	✓	x
MBP017.2.2		<i>Moritella dasanensis</i> ArB 0140	99.79	NR_044156.1	-	-	-	-	-	-	-	-	-	-	-	-	-	-	-	-	-	✓	✓	✓	✓	x
MBP017.3		<i>Moritella dasanensis</i> ArB 0140	99.65	NR_044156.1	-	-	-	-	-	-	-	-	-	-	-	-	-	-	-	-	-	✓	x	x	x	x
MBP017.4		<i>Glaciecola punicea</i>	96.53	NR_036866.1	-	-	-	-	-	-	-	-	-	-	-	+	-	-	-	-	-	✓	✓	x	x	x
MBP017.5		<i>Maribacter antarcticus</i>	99.45	NR_044515.1	-	-	-	-	-	-	-	-	-	-	-	-	-	-	-	-	-	✓	x	x	x	x
MBP017.6.1		<i>Maribacter antarcticus</i>	99.58	NR_044515.1	-	-	-	-	-	-	-	-	-	-	-	-	-	-	-	-	-	✓	✓	✓	x	x
MBP017.7		<i>Polaribacter litorisediminis</i>	98.01	NR_156971.1	-	-	-	-	-	-	-	-	-	-	-	-	-	-	-	-	-	✓	✓	✓	x	x
MBP017.8.1.R		<i>Psychroserpens damuponensis</i>	98.00	NR_109097.1	-	-	-	-	-	-	-	-	-	-	-	-	-	-	-	-	-	✓	✓	x	x	x
MBP018.1		<i>Moritella dasanensis</i> ArB 0140	98.39	NR_044156.1	-	-	-	-	-	-	-	-	-	-	-	-	-	-	-	-	-	✓	✓	x	x	x

Marine bacterial isolates (ID)	Habitat	Closest match	Identity (%)	Accession no	BGCs			Gram +					Gram -					Marine (Gram -)		Growth in different temperature (°C)				
					NRPS	PKS 1	PKS 2	Bs	Cg	Er	Sa	Se	Ab	Ec	Eh	Ka	Pa	Ha	PsyA	5	10	15	20	25
MBP018.2		Moritella dasanensis ArB 0140	99.58	NR_044156.1	-	-	-	-	-	-	-	-	-	-	-	-	-	-	✓	✓	x	x	x	
MBP018.3		Moritella dasanensis ArB 0140	99.36	NR_044156.1	-	-	-	-	-	-	-	-	-	-	-	-	-	-	✓	✓	x	x	x	
MBP018.4		Moritella dasanensis ArB 0140	99.89	NR_044156.1	-	-	-	-	-	-	-	-	-	-	-	-	-	-	✓	✓	x	x	x	
MBP018.5		Glaciecola punicea	95.14	NR_036866.1	-	-	-	-	-	-	-	-	-	-	-	-	-	-	✓	✓	x	x	x	
MBP018.6.1.R		Maribacter antarcticus	99.59	NR_044515.1	-	-	-	-	-	-	-	-	-	-	-	-	-	-	✓	✓	✓	✓	x	
MBP018.7.1.R		Psychroserpens damuponensis	98.49	NR_109097.1	-	-	-	-	-	-	-	-	-	-	-	-	-	-	✓	✓	x	x	x	
MBP019.1		Moritella dasanensis ArB 0140	99.68	NR_044156.1	-	-	-	-	-	-	-	-	-	-	-	-	-	-	✓	✓	✓	✓	x	
MBP019.2		Moritella dasanensis ArB 0140	99.68	NR_044156.1	-	-	-	-	-	-	-	-	-	-	-	-	-	-	✓	✓	✓	✓	x	
MBP019.3		Moritella dasanensis ArB 0140	99.67	NR_044156.1	Y	-	-	-	-	-	-	-	-	-	-	-	-	-	✓	✓	x	x	x	
MBP019.4		Moritella dasanensis ArB 0140	99.79	NR_044156.1	-	-	-	-	-	-	-	-	-	-	-	-	-	-	✓	✓	✓	✓	x	
MBP019.5		Octadecabacter arcticus	99.79	NR_102905.1	-	-	-	++	-	-	-	-	-	-	-	-	-	-	✓	✓	✓	✓	x	
MBP019.6		Maribacter antarcticus	99.07	NR_044515.1	-	-	-	++	-	-	-	-	-	-	-	-	-	-	✓	✓	✓	✓	x	
MBP019.7		Flavobacterium frigoris	99.02	NR_025597.1	Y	-	-	-	-	-	-	-	-	-	-	-	-	-	✓	✓	x	x	x	
MBP019.8		Psychroserpens damuponensis	98.54	NR_109097.1	Y	-	-	-	-	-	-	-	-	-	-	-	-	-	✓	✓	✓	x	x	
MBP019.9		Psychromonas profunda	98.71	NR_025506.1	-	-	-	-	-	-	-	-	-	-	-	-	-	-	✓	✓	✓	x	x	
MBP022.1	Sediment (3895 m)	Peribacillus simplex	99.26	NR_114919.1	-	-	-	-	+	-	-	-	-	-	-	-	-	-	✓	✓	✓	✓	✓	
MBP022.2		Jeotgalibacillus marinus	98.21	NR_112057.1	Y	-	-	-	-	-	-	-	-	-	-	-	-	-	✓	✓	✓	x	x	
MBP022.3		Peribacillus simplex NBRC 15720 = DSM 1321	99.65	NR_042136.1	-	-	-	-	-	-	-	-	-	-	-	-	-	-	✓	✓	✓	✓	✓	
MBP023.1.1		Brevundimonas staleyii	98.24	NR_114710.1	Y	-	-	-	-	-	-	-	-	-	-	-	-	-	✓	✓	✓	✓	✓	
MBP025.1	Seaweed from puddle on ice	Psychromonas kaikoeae ATCC BAA-353	98.87	NR_028003.1	-	-	-	-	-	-	-	-	-	-	-	-	-	-	✓	✓	x	x	x	
MBP025.2		Psychromonas kaikoeae ATCC BAA-353	98.51	NR_028003.1	-	-	-	-	-	-	-	-	-	-	-	-	-	-	✓	✓	✓	x	x	
MBP025.3		Moritella dasanensis ArB 0140	99.47	NR_044156.1	-	-	-	-	-	-	-	-	-	-	-	-	-	-	✓	✓	✓	✓	x	
MBP025.4.1		Moritella dasanensis ArB 0140	99.37	NR_044156.1	-	-	-	-	-	-	-	-	-	-	-	-	-	-	✓	✓	✓	✓	✓	
MBP025.5		Psychromonas kaikoeae ATCC BAA-353	98.96	NR_028003.1	-	-	-	-	-	-	-	-	-	-	-	-	-	-	-	✓	✓	x	x	x
MBP025.6		Moritella dasanensis ArB 0140	98.89	NR_044156.1	Y	-	-	-	-	-	-	-	-	-	-	-	-	-	-	✓	✓	✓	✓	x

Marine bacterial isolates (ID)	Habitat	Closest match	Identity (%)	Accession no	BGCs			Gram +					Gram -					Marine (Gram -)		Growth in different temperature (°C)				
					NRPS	PKS 1	PKS 2	Bs	Cg	Er	Sa	Se	Ab	Ec	Eh	Ka	Pa	Ha	PsyA	5	10	15	20	25
MBP025.7.1		Moritella dasanensis ArB 0140	99.89	NR_044156.1	Y	-	-	-	-	-	-	-	-	-	-	-	-	-	✓	✓	✓	✓	x	
MBP025.8		Paraglaciecola psychrophila	94.35	NR_043463.1	-	-	-	-	-	-	-	-	-	-	-	-	-	-	✓	✓	x	x	x	
MBP025.9		Psychroserpens damuponensis	98.50	NR_109097.1	Y	-	-	-	-	-	-	-	-	-	-	-	-	-	✓	✓	x	x	x	
MBP025.10		Polaribacter litorisediminis	98.63	NR_156971.1	-	-	-	-	-	-	-	-	-	-	-	-	-	-	✓	✓	✓	✓	x	
MBP025.11		Paraglaciecola psychrophila	99.22	NR_043463.1	Y	Y	-	-	+	-	-	-	+	-	-	+	-	-	✓	✓	✓	✓	x	
MBP026.1	Under ice	Colwellia rossensis	99.04	NR_025957.1	-	-	-	-	-	-	-	-	-	-	-	-	-	-	✓	✓	x	x	x	
MBP026.2		Colwellia rossensis	98.55	NR_025957.1	-	-	-	-	-	-	-	-	-	-	-	-	-	-	✓	✓	x	x	x	
MBP026.3		Psychrobium conchae	97.82	NR_134146.1	-	-	-	-	-	-	-	-	-	-	-	-	-	-	✓	✓	x	x	x	
MBP026.4		Colwellia hornerae	99.68	NR_104941.1	Y	-	-	-	-	-	-	-	-	-	-	-	-	-	✓	✓	x	x	x	
MBP026.5		Moritella dasanensis ArB 0140	99.47	NR_044156.1	-	-	-	-	-	-	-	-	-	-	-	-	-	-	✓	✓	✓	✓	x	
MBP026.6		Psychromonas kaikoae ATCC BAA-353	95.30	NR_028003.1	-	-	-	-	-	-	-	-	-	-	-	-	-	-	✓	✓	x	x	x	
MBP026.7		Psychromonas profunda	99.13	NR_025506.1	Y	Y	-	-	-	-	-	-	-	-	-	-	-	-	✓	✓	x	x	x	
MBP026.8		Colwellia rossensis	98.84	NR_025957.1	-	-	-	-	-	-	-	-	-	-	-	-	-	-	✓	✓	x	x	x	
MBP026.9		Psychromonas kaikoae ATCC BAA-353	98.92	NR_028003.1	Y	-	-	-	-	-	-	-	-	-	-	-	-	-	✓	✓	x	x	x	
MBP026.10		Colwellia maris	98.49	NR_024635.1	-	-	-	-	-	-	-	-	-	-	-	-	-	-	✓	✓	x	x	x	
MBP026.11		Colwellia maris	98.51	NR_024635.1	-	-	-	-	-	-	-	-	-	-	-	-	-	-	✓	✓	x	x	x	
MBP026.12		Glaciecola punicea	96.47	NR_036866.1	-	-	-	-	-	-	-	-	-	-	-	-	-	-	✓	✓	x	x	x	
MBP026.13		Octadecabacter arcticus	99.77	NR_102905.1	Y	Y	-	++	-	-	-	-	-	-	-	-	-	-	✓	✓	✓	✓	x	
MBP026.15		Polaribacter litorisediminis	98.20	NR_156971.1	-	-	-	-	-	-	+	-	-	-	-	-	-	-	✓	✓	x	x	x	
MBP027.1		Pseudoalteromonas carrageenovora	99.37	NR_113605.1	Y	Y	-	-	-	-	-	-	-	-	-	+	+	+	✓	✓	✓	✓	✓	
MBP027.2		Shewanella hanedai	98.43	NR_114050.1	Y	-	-	-	+	-	-	-	+	-	-	+	-	+	✓	✓	✓	✓	x	
MBP027.3		Pseudomonas brenneri	99.58	NR_025103.1	Y	-	-	+++	-	+	-	-	-	-	-	+	-	-	✓	✓	✓	✓	x	
MBP027.4		Pseudomonas rhodesiae	99.79	NR_112074.1	Y	-	-	+++	+	+	-	-	+	-	-	+	+	-	✓	✓	✓	✓	x	
MBP027.5.1.R		Shewanella vesiculosa	98.97	NR_042710.1	-	-	-	+++	+	-	-	-	+	-	-	+	+	-	✓	✓	✓	✓	✓	
MBP027.6		Flavobacterium ponti	98.93	NR_104505.1	-	-	-	+++	+	-	-	-	+	-	-	+	+	-	✓	✓	✓	✓	✓	

Marine bacterial isolates (ID)	Habitat	Closest match	Identity (%)	Accession no	BGCs			Gram +					Gram -					Marine (Gram -)		Growth in different temperature (°C)					
					NRPS	PKS 1	PKS 2	Bs	Cg	Er	Sa	Se	Ab	Ec	Eh	Ka	Pa	Ha	PsyA	5	10	15	20	25	
MBP027.7		Flavobacterium frigidis	99.03	NR_025597.1	-	-	-	++	-	-	-	-	-	-	-	-	-	+	-	✓	✓	✓	✓	✓	
MBP027.8.1		Octadecabacter arcticus	100.00	NR_102905.1	-	Y	Y	-	-	-	-	-	-	-	-	-	-	+	-	✓	✓	✓	✓	✓	
MBP027.9		Psychroserpens damponensis	97.87	NR_109097.1	Y	-	-	-	-	-	-	-	-	-	-	-	-	-	-	-	✓	✓	x	x	x
MBP027.10		Nonlabens dokdonensis DSW-6	98.25	NR_043471.1	-	-	-	-	-	-	-	-	-	-	-	-	-	-	-	-	✓	✓	x	x	x
MBP027.11		Paraglaciecola psychrophila	97.96	NR_043463.1	Y	Y	-	-	-	-	-	-	-	-	-	-	-	-	-	-	✓	✓	x	x	x
MBP027.12		Paraglaciecola psychrophila	98.21	NR_043463.1	-	-	-	-	-	-	-	-	-	-	-	-	-	-	-	-	✓	✓	x	x	x
MBP029.1		Sediment (3999 m)	Jeotgalibacillus marinus	99.15	NR_112057.1	Y	-	-	-	-	-	-	-	-	-	-	-	-	-	-	✓	✓	✓	✓	✓
MBP030.1	Jeotgalibacillus marinus		99.20	NR_112057.1	Y	-	-	-	-	-	-	-	-	-	-	-	-	-	-	-	✓	✓	✓	x	x
MBP031.1	Peribacillus simplex		96.59	NR_114919.1	-	-	-	-	-	-	-	-	-	-	-	-	-	-	-	-	✓	✓	✓	✓	x
MBP032.1	Jeotgalibacillus marinus		99.13	NR_112057.1	Y	Y	-	-	-	-	-	-	-	-	-	-	-	-	-	-	✓	✓	✓	✓	x

Y – yes, - - negative, +/+/+/+ - antibacterial activity, ✓ - growth, x - no growth, BGCs - biosynthetic gene clusters, NRPS - nonribosomal peptide synthetases, PKS - polyketide synthases, Bs - *Bacillus subtilis*, Cg - *Corynebacterium glutamicum*, Er - *Enterococcus raffinosus*, Sa - *Staphylococcus aureus*, Se - *Staphylococcus epidermidis*, Ab - *Acinetobacter baylyi*, Ec - *Escherichia coli*, Eh - *Enterobacter hormaechei*, Ka - *Klebsiella aerogenes*, Pa - *Pseudomonas aeruginosa*, Ha - *Halomonas aquamarina*, PsyA- *Psychromonas arctica*.

Table S3. List of human pathogen relative bacteria used to screen bioactive (antimicrobial) marine bacteria.

Sl. No.	Genus and species	Abbreviation	Strain	Gram +/-	ESKAPE Safe Relatives
1	<i>Bacillus subtilis</i>	Bs	168	+	other
2	<i>Corynebacterium glutamicum</i>	Cg	ATCC13032	+	other
3	<i>Enterococcus raffinosus</i>	Er	ATCC 49464	+	E, safe relative of <i>Enterococcus faecium</i>
4	<i>Staphylococcus aureus</i>	Sa	ATCC 9144	+	S
5	<i>Staphylococcus epidermidis</i>	Se	RP62A	+	or S, safe relative of <i>Staphylococcus aureus</i>
6	<i>Escherichia coli</i>	Ec	ATCC 25922	-	K, safe relative of <i>Escherichia coli</i>
7	<i>Acinetobacter baylyi</i>	Ab	DSM 24193	-	A, safe relative of <i>Acinetobacter baumannii</i>
8	<i>Pseudomonas aeruginosa</i>	Pa	ATCC 27853	-	P
9	<i>Klebsiella aerogenes</i>	Ka	ATCC 51697	-	E
10	<i>Enterobacter hormaechei</i>	Eh	ATCC 700323	-	or E

Table S4. List of biofilm-forming marine bacteria to screen bioactive (antimicrobial) marine bacteria.

Sl. No.	Genus and species	Abbreviation	Strain	Gram +/-	Temp. for optimum growth
1	<i>Alteromonas macleodii</i>	Am	DSM 100460/LMG 2843	-	RT/25 °C
2	<i>Halomonas aquamarina</i>	Ha	LMG 2853 / DSM 30161 (IK-MB3)	-	RT/25 °C
3	<i>Phaeobacter inhibens</i>	Pi	DSM 24588 (2.10)	-	RT/25 °C
4	<i>Pseudoalteromonas antarctica</i>	PseA	LMG 18002 (NF3)	-	RT/25 °C
5	<i>Psychromonas arctica</i>	PsyA	DSM 14288	-	4-10 °C

Table S5. List of PCR primers used to screen NRPS and PKS modules.

Target	Primer	Sequence (5'-3')	T (°C)	Product size (bp)	Ref.
PKS1	K1F	TSAAGTCSAACATCGGBCA	55	1200-1500	1
	M6R	CGCAGGTTSCSGTACCAGTA			
NRPS	A3F	GCSTACSYSATSTACACSTCSGG	59	700	1
	A7R	SASGTCVCCSGTSCGGTAS			
PKS2	KSaF	TSGCSTGCTTGGAYGCSATC	55	600	2
	KSaR	TGGAANCCGCCGAABCCGCT			
NRPS	MTF2	GCNNGGYGGYGCNTAYGTNCC	55	1000	3
	MTR	CCNCGDATYTTNACYTG			
PKS1	MDPQQR f	RTRGAYCCNCAGCAICG	55	690	4
	HGTGT r	VGTNCCNGTGCCRTG			
NRPS	A2f/A2gamF	AAG GCN GGC GSB GCS TAY STG CC	60	200-300	5
	A3r/A3gamR	TTG GGB IKB CCG GTS GIN CCS GAG GTG			
PKS1	KSDPQQF	MGNGARGCENNWSMNATGGAYCCNCARCANMG	55	700	6

Target	Primer	Sequence (5'-3')	T (°C)	Product size (bp)	Ref.
	KSHGTGR	GGRTCNCCNARNSWNGTNCNGTNC CRTG			
PKS1	degKS2.i F	GCIATGGAYCCICARCMGIVT	55	700	7
	degKS5.i R	GTICCI GTIC CRTGISCYTCIAC			
NRPS	degNRPS-1F	AARDSIGGIGSIGSITAYBICC	40	1000	8
	degNRPS-4R	CKRWAICCICKIAIYTTIAYYTG			
PKS2	540F	GGITGCACSTCIGGIMTSGAC	60	550	9
	1100R	CCGATSGCICCSAGIGAGTG			
PKS2	ARO-PKS-F	GGCAGCGGITTGGCGGITTCCAG	64	490-630	10
	ARO-PKS-R	CGITGTTIACIGCGTAGAACCAGGCG			
NRPS	NRPS F (F2)	CGCGCGCATGTACTGGACNNGNGAYYT	63	480	11
	NRPS R	GGAGTGGCCGCCCARNYBRAARAA			
PKS1	PKS F	GGCAACGCCTACCACATGCANGGNYT	61	350	11
	PKS R	GGTCCGCGGGACGTARTCNARRTC			

Table S6. Summary of results from Nanopore sequencing and genome assembly with Flye.

Sample	Genus	Total read length	Reads N50	Total length	Fragments	Largest fragment	N50	Mean coverage
MBP002.5	Sulfitobacter	251245208	1743	4519418	6	4177302	4177302	47
MBP003.1.1.R*	Shewanella	699587102	4221	6254918	61	3437859	3437859	111
MBP003.6	Shewanella	1051451396	2166	6899090	151	1161671	473530	140
MBP003.10.1	Maribacter	63897369	17577	4569335	1	4569335	4569335	13
MBP005.1	Shewanella	376182570	4829	5426441	2	5335621	5335621	63
MBP006.5	Shewanella	488120157	3089	5330485	1	5330485	5330485	85
MBP006.7.1	Shewanella	212092111	10474	5350320	1	5350320	5350320	38
MBP007.5	Winogradskyella	46678889	5981	4334739	15	2260064	2260064	9
MBP007.6	Alteromonas	459225876	10596	5044372	1	5044372	5044372	90
MBP008.3	Polariibacter	427269503	5415	3290287	1	3290287	3290287	127
MBP008.4	Pseudoalteromonas	595448667	9697	4296592	3	3482629	3482629	137
MBP008.5	Sulfitobacter	430170799	4676	4380755	6	4238962	4238962	93
MBP009.1	Pseudoalteromonas	330344499	8591	4652415	3	3839906	3839906	70
MBP009.2	Vibrio	474455956	3262	5543582	3	3575859	3575859	79
MBP009.4	Pseudoalteromonas	237738538	7833	4139938	2	3409186	3409186	56
MBP009.5	Pseudoalteromonas	340062465	5953	4118362	2	3392668	3392668	79
MBP009.7.1.R*	Polariibacter	400634337	5301	3289337	1	3289337	3289337	116
MBP009.8	Tenacibaculum	512249193	4967	2876188	2	2869679	2869679	173
MBP011.13.1	Shewanella	462539977	7390	6448403	17	2864692	1483162	70
MBP011.14.1	Shewanella	410355066	2443	6436307	41	3286266	3286266	59
MBP013.3	Algibacter	100078819	14823	4524804	1	4524804	4524804	21
MBP019.8	Psychroserpens	307458161	10184	4852464	1	4852464	4852464	63
MBP022.2	Jeotgalibacillus	111967143	19533	3657128	3	3572374	3572374	30
MBP023.1	Brevundimonas	39216923	18239	3226709	1	3226709	3226709	11
MBP025.7.1	Moritella	380007866	8051	5236099	5	5124969	5124969	71
MBP026.13	Octadecabacter	58970902	9267	4769119	9	3906596	3906596	11
MBP027.1	Pseudoalteromonas	119609981	11418	4119112	3	3398235	3398235	28
MBP027.4	Pseudomonas	242230938	2937	7016740	11	6943160	6943160	29
MBP027.5.1.R	Shewanella	865078660	1076	5042915	3	4959705	4959705	147
MBP027.7	Flavobacterium	297523759	2322	3642903	1	3642903	3642903	75
MBP027.8.1	Octadecabacter	102027480	8107	4853320	17	4798061	4798061	19
MBP027.9	Psychroserpens	165552181	10380	4861569	1	4861569	4861569	33
MBP029.1	Jeotgalibacillus	79796610	9162	3793847	6	3691675	3691675	19
MBP030.1	Jeotgalibacillus	81029975	17431	3644092	5	3541157	3541157	21
MBP032.1	Jeotgalibacillus	112122819	15561	3601628	6	3483524	3483524	29
MBP025.11	Paraglaciecola	299547803	19827	6186559	1	6186559	6186559	48
MBP027.3	Pseudomonas	517441322	19884	8472547	2	8166020	8166020	61

Table S7. BGCs of marine bacterial strains, predicted by antiSMASH.

Marine bacterial isolates (ID)	Genus	No. of BGCs	Types of BGCs
MBP002.5	Sulfitobacter	11	hserlactone; RiPP-like; NRPS-like; hserlactone; RiPP-like; ectoine; betalactone; proteusin, RiPP-like; thiopeptide; terpene; hserlactone
MBP003.1.1.R*	Shewanella	15	NRPS-like; NRPS-like; RiPP-like; siderophore; RiPP-like; T1PKS; arylpolyene; NRPS; NRPS; NRPS-like; T1PKS; PUFA, hglE-KS; NRPS-like, T1PKS, NRPS; RRE-containing; NRPS, T1PKS
MBP003.10.1	Maribacter	5	terpene; arylpolyene, resorcinol; terpene; T3PKS, arylpolyene; NRPS
MBP003.6	Shewanella	12	RiPP-like; siderophore; NRPS, arylpolyene; NRPS; NRPS; RiPP-like; betalactone; PUFA, hglE-KS; RiPP-like; hserlactone; NRPS; NRPS-like
MBP005.1	Shewanella	4	arylpolyene; RiPP-like; PUFA, hglE-KS; RiPP-like
MBP006.5	Shewanella	4	PUFA, hglE-KS; RiPP-like; arylpolyene; RiPP-like
MBP006.7.1	Shewanella	4	PUFA, hglE-KS; RiPP-like; arylpolyene; RiPP-like
MBP007.5	Winogradskyella	3	arylpolyene, resorcinol; terpene; terpene
MBP007.6	Alteromonas	2	redox-cofactor; RiPP-like
MBP008.3	Polaribacter	2	betalactone; terpene
MBP008.4	Pseudoalteromonas	3	betalactone; RiPP-like; siderophore
MBP008.5	Sulfitobacter	8	hserlactone; RiPP-like; betalactone; RiPP-like; hserlactone; NRPS-like; cyanobactin; terpene
MBP009.1	Pseudoalteromonas	6	NRPS, RiPP-like; RiPP-like; RiPP-like; NRPS; arylpolyene; siderophore
MBP009.2	Vibrio	7	siderophore; NRPS-like; RiPP-like; betalactone; arylpolyene; PUFA, hglE-KS; RiPP-like
MBP009.4	Pseudoalteromonas	3	RiPP-like; betalactone; siderophore
MBP009.5	Pseudoalteromonas	1	RiPP-like
MBP009.7.1.R*	Polaribacter	2	terpene; betalactone
MBP009.8	Tenacibaculum	3	arylpolyene, T3PKS; arylpolyene; terpene
MBP011.13.1	Shewanella	12	RiPP-like; hglE-KS, PUFA, betalactone; RiPP-like; NRPS; NRPS; NRPS, T1PKS; RiPP-like; siderophore; siderophore; NRPS; NRPS; NRPS-like, NRPS
MBP011.14.1	Shewanella	12	NRPS; siderophore; siderophore; RiPP-like; NRPS; NRPS, NRPS-like; RiPP-like; hglE-KS, PUFA, betalactone; RiPP-like; NRPS; NRPS; NRPS
MBP013.3	Algibacter	4	resorcinol; T3PKS; lassopeptide; terpene
MBP019.8	Psychroserpens	6	T3PKS; arylpolyene; T1PKS, NRPS-like, NRPS; NRPS-like; terpene; T1PKS, PUFA, hglE-KS
MBP022.2	Jeotgalibacillus	1	T3PKS, lassopeptide
MBP023.1.1	Brevundimonas	1	resorcinol
MBP025.7.1	Moritella	7	betalactone; siderophore, NRPS; RiPP-like; RiPP-like; PUFA, T1PKS, hglE-KS; NRPS-like, betalactone; arylpolyene
MBP026.13	Octadecabacter	6	RiPP-like; T3PKS; terpene; hserlactone; terpene; hserlactone

Marine bacterial isolates (ID)	Genus	No. of BGCs	Types of BGCs
MBP027.1	Pseudoalteromonas	2	RiPP-like; siderophore
MBP027.4	Pseudomonas	10	RiPP-like; NRPS-like; arylpolyene; NRPS; NAGGN; betalactone; NRPS; NRPS; RiPP-like; redox-cofactor
MBP027.5.1.R	Shewanella	6	arylpolyene; hglE-KS, PUFA; RiPP-like; betalactone; RiPP-like; thiopeptide, LAP
MBP027.7	Flavobacterium	4	terpene; terpene; T3PKS, betalactone; T3PKS
MBP027.8.1	Octadecabacter	8	terpene; RRE-containing; hserlactone; RiPP-like; siderophore; T3PKS; terpene; hserlactone
MBP027.9	Psychroserpens	5	T3PKS; arylpolyene; hglE-KS, PUFA, T1PKS; terpene; NRPS, T1PKS, NRPS-like
MBP029.1	Jeotgalibacillus	1	T3PKS, lassopeptide
MBP030.1	Jeotgalibacillus	2	T3PKS; lassopeptide
MBP032.1	Jeotgalibacillus	4	NRPS; NRPS; T3PKS, lassopeptide; NRPS
MBP0025.11	Paraglaciecola	3	RiPP-like; lassopeptide, RRE-containing; terpene
MBP0027.3	Pseudomonas	13	NRPS; betalactone; NRPS; RiPP-like; ectoine; NRPS-like; RiPP-like; NRPS-like; arylpolyene; NRPS-like; RiPP-like; RRE-containing; NRPS

Table S8. The bacterial strains that yielded PCR products of the expected size, for each primer pair, together with the BGCs predicted by AntiSMASH, for the whole genome sequenced strains.

Primer pair	Genus	Strain	AntiSMASH
A2gamF/A3gamR (NRPS)	Brevundimonas	MBP023.1.1	resorcinol
	Polaribacter	MBP008.3	betalactone; terpene
	Pseudomonas	MBP027.3	NRPS; betalactone; NRPS; RiPP-like; ectoine; NRPS-like; RiPP-like; NRPS-like; arylpolyene; NRPS-like; RiPP-like; RRE-containing; NRPS
		MBP027.4	RiPP-like; NRPS-like; arylpolyene; NRPS; NAGGN; betalactone; NRPS; NRPS; RiPP-like; redox-cofactor
	Shewanella	MBP003.2.1	-
		MBP003.2.2	-
		MBP003.6	RiPP-like; siderophore; NRPS, arylpolyene; NRPS; NRPS; RiPP-like; betalactone; PUFA, hglE-KS; RiPP-like; hserlactone; NRPS; NRPS-like
		MBP011.13.1	RiPP-like; hglE-KS, PUFA, betalactone; RiPP-like; NRPS; NRPS; NRPS, T1PKS; RiPP-like; siderophore; siderophore; NRPS; NRPS; NRPS-like, NRPS
		MBP011.14.1	NRPS; siderophore; siderophore; RiPP-like; NRPS; NRPS, NRPS-like; RiPP-like; hglE-KS, PUFA, betalactone; RiPP-like; NRPS; NRPS; NRPS
		MBP011.3.1.R	-
MBP027.2		-	

	Sulfitobacter	MBP002.5	hserlactone; RiPP-like; NRPS-like; hserlactone; RiPP-like; ectoine; betalactone; proteusin, RiPP-like; thiopeptide; terpene; hserlactone
		MBP008.5	hserlactone; RiPP-like; betalactone; RiPP-like; hserlactone; NRPS-like; cyanobactin; terpene
	Unknown	MBP011.1	-
degNRPS-1F/4R (NRPS)	Algibacter	MBP013.3	resorcinol; T3PKS; lassopeptide; terpene
	Colwellia	MBP026.4	-
	Jeotgalibacillus	MBP022.2	T3PKS, lassopeptide
		MBP029.1	T3PKS, lassopeptide
		MBP030.1	T3PKS; lassopeptide
	Moritella	MBP025.6	-
		MBP025.7	betalactone; siderophore, NRPS; RiPP-like; RiPP-like; PUFA, T1PKS, hglE-KS; NRPS-like, betalactone; arylpolyene
	Octadecabacter	MBP026.13	RiPP-like; T3PKS; terpene; hserlactone; terpene; hserlactone
	Paraglaciecola	MBP025.11	RiPP-like; lassopeptide, RRE-containing; terpene
MBP027.11		-	
Shewanella	MBP005.1	arylpolyene; RiPP-like; PUFA, hglE-KS; RiPP-like	
K1F/M6R (PKS1)	Octadecabacter	MBP027.8.1	terpene; RRE-containing; hserlactone; RiPP-like; siderophore; T3PKS; terpene; hserlactone
	Paraglaciecola	MBP025.11	RiPP-like; lassopeptide, RRE-containing; terpene
	Sulfitobacter	MBP008.5	hserlactone; RiPP-like; betalactone; RiPP-like; hserlactone; NRPS-like; cyanobactin; terpene
MDPQQRf f/HGTGT r (PKS1)	Jeotgalibacillus	MBP032.1	NRPS; NRPS; T3PKS, lassopeptide; NRPS
	Octadecabacter	MBP026.13	RiPP-like; T3PKS; terpene; hserlactone; terpene; hserlactone
		MBP027.8.1	terpene; RRE-containing; hserlactone; RiPP-like; siderophore; T3PKS; terpene; hserlactone
	Pseudoalteromonas	MBP027.1	RiPP-like; siderophore
Psychromonas	MBP026.7	-	
degKS2.i F/degKS5.i R (PKS1)	Octadecabacter	MBP027.8.1	terpene; RRE-containing; hserlactone; RiPP-like; siderophore; T3PKS; terpene; hserlactone
	Paraglaciecola	MBP027.11	-
K α F/R (PKS2)	Octadecabacter	MBP027.8.1	terpene; RRE-containing; hserlactone; RiPP-like; siderophore; T3PKS; terpene; hserlactone
NRPS F/R (NRPS)	Brevundimonas	MBP023.1.1	resorcinol
	Flavobacterium	MBP019.7	-
	Jeotgalibacillus	MBP029.1	T3PKS, lassopeptide
		MBP032.1	NRPS; NRPS; T3PKS, lassopeptide; NRPS

	Moritella	MBP019.3	-
		MBP025.6	-
		MBP025.7	betalactone; siderophore, NRPS; RiPP-like; RiPP-like; PUFA, T1PKS, hglE-KS; NRPS-like, betalactone; arylpolyene
	Paraglaciecola	MBP025.11	RiPP-like; lassopeptide, RRE-containing; terpene
		MBP027.11	-
	Pseudoalteromonas	MBP009.1	NRPS, RiPP-like; RiPP-like; RiPP-like; NRPS; arylpolyene; siderophore
		MBP027.1	RiPP-like; siderophore
	Pseudomonas	MBP027.3	NRPS; betalactone; NRPS; RiPP-like; ectoine; NRPS-like; RiPP-like; NRPS-like; arylpolyene; NRPS-like; RiPP-like; RRE-containing; NRPS
		MBP027.4	RiPP-like; NRPS-like; arylpolyene; NRPS; NAGGN; betalactone; NRPS; NRPS; RiPP-like; redox-cofactor
	Psychromonas	MBP026.7	-
		MBP026.9	-
	Psychroserpens	MBP016.9	-
		MBP019.8	T3PKS; arylpolyene; T1PKS, NRPS-like, NRPS; NRPS-like; terpene; T1PKS, PUFA, hglE-KS
		MBP025.9	-
		MBP027.9	T3PKS; arylpolyene; hglE-KS, PUFA, T1PKS; terpene; NRPS, T1PKS, NRPS-like
Shewanella	MBP027.2	-	
Sulfitobacter	MBP008.5	hserlactone; RiPP-like; betalactone; RiPP-like; hserlactone; NRPS-like; cyanobactin; terpene	
A3F/A7R (NRPS)	Pseudomonas	MBP027.3	NRPS; betalactone; NRPS; RiPP-like; ectoine; NRPS-like; RiPP-like; NRPS-like; arylpolyene; NRPS-like; RiPP-like; RRE-containing; NRPS

All the strains listed here are PCR positive and “-“ means not genome sequenced.

Table S9. Minimum inhibitory concentration (MIC) of solid phase extracted samples from both monoculture and co-culture in µg/mL.

Sample type (SPE of 80% ACN)	Minimum inhibitory concentration (MIC), µg/mL					
	Bs	Cg	Sa	Se	Ec	Pa
FMAP media	1250	625	1250	1250	>1250	1250
Se monoculture	1250	625	1250	625	>1250	1250
S monoculture	625	312	625	625	1250	1250
Se+S co-culture	625	312	625	625	1250	1250

SPE - solid phase extraction, ACN - Acetonitrile, S - *Shewanella* sp. MBP011.13.1, Bs - *Bacillus subtilis*, Cg - *Corynebacterium glutamicum*, Sa - *Staphylococcus aureus*, Se - *Staphylococcus epidermidis*, Ec - *Escherichia coli*, Pa - *Pseudomonas aeruginosa*.

a)



b)

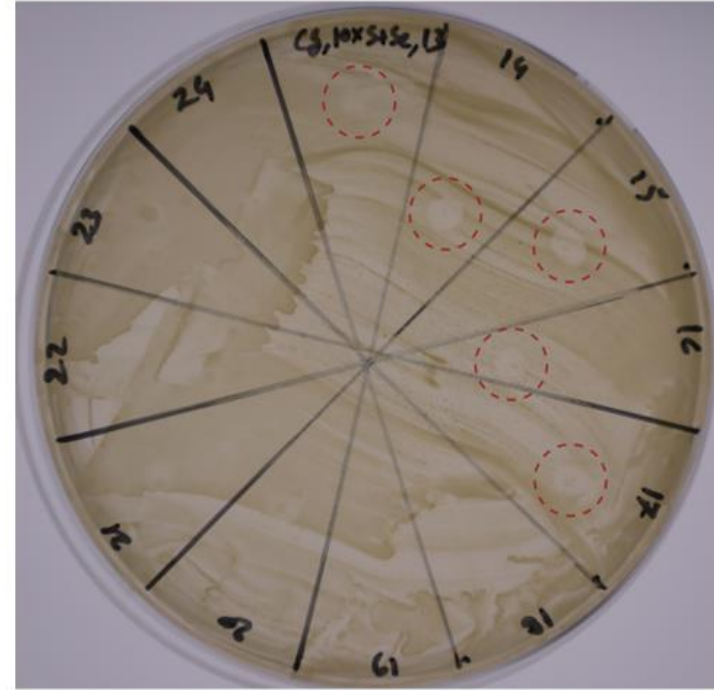


Figure S2. Disk diffusion assay to test the activity of different fractions of 10 % ACN extract against *C. glutamicum*. a) *Shewanella* sp. MBP011.13.1 monoculture. b) co-culture of *Shewanella* sp. MBP011.13.1 with *S. epidermidis* RP62A. Red dashed circles are the active fraction.

Table S10. Taxonomic classification of draft genomes by GTDB-Tk.

Strain	Genus (based on 16S rRNA gene)	Classification based on whole genome					
		Phylum	Class	Order	Family	Genus	Species
MBP002.5	Sulfitobacter	Proteobacteria	Alphaproteobacteria	Rhodobacterales	Rhodobacteraceae	Asciidiaceihabitans	
MBP003.1.1.R*	Shewanella	Proteobacteria	Gammaproteobacteria	Enterobacterales	Shewanellaceae	Shewanella	
MBP003.10.1	Maribacter	Bacteroidota	Bacteroidia	Flavobacteriales	Flavobacteriaceae	RZ26 (Maribacter)	
MBP003.6	Shewanella	Proteobacteria	Gammaproteobacteria	Enterobacterales	Shewanellaceae	Shewanella	
MBP005.1	Shewanella	Proteobacteria	Gammaproteobacteria	Enterobacterales	Shewanellaceae	Shewanella	
MBP006.5	Shewanella	Proteobacteria	Gammaproteobacteria	Enterobacterales	Shewanellaceae	Shewanella	
MBP006.7.1	Shewanella	Proteobacteria	Gammaproteobacteria	Enterobacterales	Shewanellaceae	Shewanella	
MBP007.5	Winogradskyella	Bacteroidota	Bacteroidia	Flavobacteriales	Flavobacteriaceae	Winogradskyella	Winogradskyella eximia
MBP007.6	Alteromonas	Proteobacteria	Gammaproteobacteria	Enterobacterales	Alteromonadaceae	Alteromonas	Alteromonas naphthalenivorans
MBP008.3	Polaribacter	Bacteroidota	Bacteroidia	Flavobacteriales	Flavobacteriaceae	Polaribacter	
MBP008.4	Pseudoalteromonas	Proteobacteria	Gammaproteobacteria	Enterobacterales	Alteromonadaceae	Pseudoalteromonas	Pseudoalteromonas undina
MBP008.5	Sulfitobacter	Proteobacteria	Alphaproteobacteria	Rhodobacterales	Rhodobacteraceae	Asciidiaceihabitans	
MBP009.1	Pseudoalteromonas	Proteobacteria	Gammaproteobacteria	Enterobacterales	Alteromonadaceae	Pseudoalteromonas	Pseudoalteromonas aliena
MBP009.2	Vibrio	Proteobacteria	Gammaproteobacteria	Enterobacterales	Vibrionaceae	Vibrio	Vibrio splendidus
MBP009.4	Pseudoalteromonas	Proteobacteria	Gammaproteobacteria	Enterobacterales	Alteromonadaceae	Pseudoalteromonas	Pseudoalteromonas undina
MBP009.5	Pseudoalteromonas	Proteobacteria	Gammaproteobacteria	Enterobacterales	Alteromonadaceae	Pseudoalteromonas	Pseudoalteromonas marina
MBP009.7.1.R*	Polaribacter	Bacteroidota	Bacteroidia	Flavobacteriales	Flavobacteriaceae	Polaribacter	
MBP009.8	Tenacibaculum	Bacteroidota	Bacteroidia	Flavobacteriales	Flavobacteriaceae	Tenacibaculum	
MBP011.13.1	Shewanella	Proteobacteria	Gammaproteobacteria	Enterobacterales	Shewanellaceae	Shewanella	
MBP011.14.1	Shewanella	Proteobacteria	Gammaproteobacteria	Enterobacterales	Shewanellaceae	Shewanella	
MBP013.3	Algibacter	Bacteroidota	Bacteroidia	Flavobacteriales	Flavobacteriaceae	Algibacter	
MBP019.8	Psychroserpens	Bacteroidota	Bacteroidia	Flavobacteriales	Flavobacteriaceae	Psychroserpens	
MBP022.2	Jeotgalibacillus	Firmicutes	Bacilli	Bacillales	Jeotgalibacillaceae	Jeotgalibacillus	

MBP023.1.1	Brevundimonas	Proteobacteria	Alphaproteobacteria	Caulobacterales	Caulobacteraceae	Brevundimonas	
MBP0025.11	Paraglaciecola	Proteobacteria	Gammaproteobacteria	Enterobacterales	Alteromonadaceae	Paraglaciecola	
MBP025.7.1	Moritella	Proteobacteria	Gammaproteobacteria	Enterobacterales	Moritellaceae	Moritella	Moritella dasanensis
MBP026.13	Octadecabacter	Proteobacteria	Alphaproteobacteria	Rhodobacterales	Rhodobacteraceae	Octadecabacter	Octadecabacter arcticus
MBP027.1	Pseudoalteromonas	Proteobacteria	Gammaproteobacteria	Enterobacterales	Alteromonadaceae	Pseudoalteromonas	Pseudoalteromonas sp001974855
MBP0027.3	Pseudomonas	Proteobacteria	Gammaproteobacteria	Pseudomonadales	Pseudomonadaceae	Pseudomonas	Pseudomonas sp002874965
MBP027.4	Pseudomonas	Proteobacteria	Gammaproteobacteria	Pseudomonadales	Pseudomonadaceae	Pseudomonas	Pseudomonas rhodesiae
MBP027.5.1.R	Shewanella	Proteobacteria	Gammaproteobacteria	Enterobacterales	Shewanellaceae	Shewanella	Shewanella sp002836315
MBP027.7	Flavobacterium	Bacteroidota	Bacteroidia	Flavobacteriales	Flavobacteriaceae	Flavobacterium	Flavobacterium sp002836475
MBP027.8.1	Octadecabacter	Proteobacteria	Alphaproteobacteria	Rhodobacterales	Rhodobacteraceae	Octadecabacter	Octadecabacter arcticus
MBP027.9	Psychroserpens	Bacteroidota	Bacteroidia	Flavobacteriales	Flavobacteriaceae	Psychroserpens	
MBP029.1	Jeotgalibacillus	Firmicutes	Bacilli	Bacillales	Jeotgalibacillaceae	Jeotgalibacillus	
MBP030.1	Jeotgalibacillus	Firmicutes	Bacilli	Bacillales	Jeotgalibacillaceae	Jeotgalibacillus	
MBP032.1	Jeotgalibacillus	Firmicutes	Bacilli	Bacillales	Jeotgalibacillaceae	Jeotgalibacillus	

Reference

- 1 Ayuso-Sacido, A. & Genilloud, O. New PCR primers for the screening of NRPS and PKS-I systems in actinomycetes: detection and distribution of these biosynthetic gene sequences in major taxonomic groups. *Microb Ecol* **49**, 10-24 (2005). <https://doi.org/10.1007/s00248-004-0249-6>
- 2 Metsä-Ketelä, M., Salo, V., Halo, L., Hautala, A., Hakala, J., Mäntsälä, P. & Ylihonko, K. An efficient approach for screening minimal PKS genes from *Streptomyces*. *FEMS Microbiology Letters* **180**, 1-6 (1999). <https://doi.org/10.1111/j.1574-6968.1999.tb08770.x>
- 3 Neilan, B. A., Dittmann, E., Rouhiainen, L., Bass, R. A., Schaub, V., Sivonen, K. & Börner, T. Nonribosomal Peptide Synthesis and Toxicogenicity of Cyanobacteria. *Journal of Bacteriology* **181**, 4089-4097 (1999). <https://doi.org/10.1128/jb.181.13.4089-4097.1999>
- 4 Kim, T. K., Garson, M. J. & Fuerst, J. A. Marine actinomycetes related to the 'Salinospora' group from the Great Barrier Reef sponge *Pseudoceratina clavata*. *Environmental Microbiology* **7**, 509-518 (2005). <https://doi.org/10.1111/j.1462-2920.2005.00716.x>
- 5 Martens, T., Gram, L., Grossart, H.-P., Kessler, D., Müller, R., Simon, M., Wenzel, S. C. & Brinkhoff, T. Bacteria of the Roseobacter Clade Show Potential for Secondary Metabolite Production. *Microbial Ecology* **54**, 31-42 (2007). <https://doi.org/10.1007/s00248-006-9165-2>
- 6 Piel, J. A polyketide synthase-peptide synthetase gene cluster from an uncultured bacterial symbiont of *Paederus* beetles. *Proceedings of the National Academy of Sciences* **99**, 14002-14007 (2002). <https://doi.org/10.1073/pnas.222481399>
- 7 Schirmer, A., Gadkari, R., Reeves, C. D., Ibrahim, F., DeLong, E. F. & Hutchinson, C. R. Metagenomic Analysis Reveals Diverse Polyketide Synthase Gene Clusters in Microorganisms Associated with the Marine Sponge *Discodermia dissoluta*. *Applied and Environmental Microbiology* **71**, 4840-4849 (2005). <https://doi.org/10.1128/aem.71.8.4840-4849.2005>
- 8 Bukelskis, D., Dabkeviciene, D., Lukoseviciute, L., Bucelis, A., Kriauciūnas, I., Lebedeva, J. & Kuisiene, N. Screening and Transcriptional Analysis of Polyketide Synthases and Non-ribosomal Peptide Synthetases in Bacterial Strains From Krubera–Voronja Cave. *Frontiers in Microbiology* **10** (2019). <https://doi.org/10.3389/fmicb.2019.02149>
- 9 Wawrik, B., Kerkhof, L., Zylstra, G. J. & Kukor, J. J. Identification of unique type II polyketide synthase genes in soil. *Applied and environmental microbiology* **71**, 2232-2238 (2005). <https://doi.org/10.1128/AEM.71.5.2232-2238.2005>
- 10 Wood, S. A., Kirby, B. M., Goodwin, C. M., Le Roes, M. & Meyers, P. R. PCR screening reveals unexpected antibiotic biosynthetic potential in *Amycolatopsis* sp. strain UM16. *J Appl Microbiol* **102**, 245-253 (2007). <https://doi.org/10.1111/j.1365-2672.2006.03043.x>
- 11 Amos, G. C. A., Borsetto, C., Laskaris, P., Krsek, M., Berry, A. E., Newsham, K. K., Calvo-Bado, L., Pearce, D. A., Vallin, C. & Wellington, E. M. H. Designing and Implementing an Assay for the Detection of Rare and Divergent NRPS and PKS Clones in European, Antarctic and Cuban Soils. *PLOS ONE* **10**, e0138327 (2015). <https://doi.org/10.1371/journal.pone.0138327>

